National Library of Canada
Bibliothèque nationale du Canada

Acquisitions and Bibliographic Services Branch
Direction des acquisitions et des services bibliographiques

395 Wellington Street
Ottawa, Ontario
K1A 0N4

395, rue Wellington
Ottawa (Ontario)
K1A 0N4

Your file Votre référence

Our file Notre référence

NOTICE

The quality of this microform is heavily dependent upon the quality of the original thesis submitted for microfilming. Every effort has been made to ensure the highest quality of reproduction possible.

If pages are missing, contact the university which granted the degree.

Some pages may have indistinct print especially if the original pages were typed with a poor typewriter ribbon or if the university sent us an inferior photocopy.

Reproduction in full or in part of this microform is governed by the Canadian Copyright Act, R.S.C. 1970, c. C-30, and subsequent amendments.

AVIS

La qualité de cette microforme dépend grandement de la qualité de la thèse soumise au microfilmage. Nous avons tout fait pour assurer une qualité supérieure de reproduction.

S'il manque des pages, veuillez communiquer avec l'université qui a conféré le grade.

La qualité d'impression de certaines pages peut laisser à désirer, surtout si les pages originales ont été dactylographiées à l'aide d'un ruban usé ou si l'université nous a fait parvenir une photocopie de qualité inférieure.

La reproduction, même partielle, de cette microforme est soumise à la Loi canadienne sur le droit d'auteur, SRC 1970, c. C-30, et ses amendements subséquents.

Canada

UNIVERSITY OF ALBERTA

NUMERICAL STRUCTURAL ANALYSIS OF BURIED PIPELINES

by

ZHILONG ZHOU

©

A THESIS

SUBMITTED TO THE FACULTY OF GRADUATE STUDIES AND RESEARCH

IN PARTIAL FULFILLMENT OF THE REQUIREMENTS FOR THE DEGREE OF

DOCTOR OF PHILOSOPHY

DEPARTMENT OF CIVIL ENGINEERING

EDMONTON, ALBERTA

SPRING, 1993

National Library of Canada
Bibliothèque nationale du Canada

Acquisitions and Bibliographic Services Branch
Direction des acquisitions et des services bibliographiques

395 Wellington Street
Ottawa, Ontario
K1A 0N4

395, rue Wellington
Ottawa (Ontario)
K1A 0N4

Your file Votre référence

Our file Notre référence

The author has granted an irrevocable non-exclusive licence allowing the National Library of Canada to reproduce, loan, distribute or sell copies of his/her thesis by any means and in any form or format, making this thesis available to interested persons.

L'auteur a accordé une licence irrévocable et non exclusive permettant à la Bibliothèque nationale du Canada de reproduire, prêter, distribuer ou vendre des copies de sa thèse de quelque manière et sous quelque forme que ce soit pour mettre des exemplaires de cette thèse à la disposition des personnes intéressées.

The author retains ownership of the copyright in his/her thesis. Neither the thesis nor substantial extracts from it may be printed or otherwise reproduced without his/her permission.

L'auteur conserve la propriété du droit d'auteur qui protège sa thèse. Ni la thèse ni des extraits substantiels de celle-ci ne doivent être imprimés ou autrement reproduits sans son autorisation.

ISBN 0-315-81978-2

Canada

UNIVERSITY OF ALBERTA

RELEASE FORM

NAME OF AUTHOR :	ZHILONG ZHOU
TITLE OF THESIS :	NUMERICAL STRUCTURAL ANALYSIS OF BURIED PIPELINES
DEGREE :	DOCTOR OF PHILOSOPHY
YEAR THIS DEGREE GRANTED :	SPRING 1993

Permission is hereby granted to the University of Alberta Library to reproduce single copies of this thesis and to lend or sell such copies for private, scholarly or scientific research purposes only.

The author reserves other publication rights, and neither the thesis nor extensive extracts from it may be printed or otherwise reproduced without the author's written permission.

(signed) _____

PERMANENT ADDRESS :

c/o D.W. Murray
Dept. of Civil Engineering
University of Alberta
Edmonton, Canada T6G 2G7

Date : February 5th, 1993

UNIVERSITY OF ALBERTA

FACULTY OF GRADUATE STUDIES AND RESEARCH

The undersigned certify that they have read, and recommend to the Faculty of Graduate Studies and Research, a thesis entitled NUMERICAL STRUCTURAL ANALYSIS OF BURIED PIPELINES submitted by ZHILONG ZHOU in partial fulfillment of the requirements for the degree of DOCTOR OF PHILOSOPHY.

Dr. D.W. Murray (Supervisor)

Dr. A.E. Elwi

Dr. J.J. Cheng

Dr. N.R. Morgenstern

Dr. D.J. Steigmann

Dr. M. Epstein (External)

Date : Feb. 17, 1993

ABSTRACT

Buried pipelines for transportations of oil and gas function in complex environments, such as Arctic and sub-Arctic regions. In addition to the normal operational loading conditions, for example, the internal pressure, buried pipelines are subject to various types of imposed deformations. The objectives of this work are to develop a predictive approach for the behavior of pipelines under imposed deformations and to establish associated criteria for design, maintenance and assessment of pipelines. The standard procedure for analysis of buried pipelines at the present time, which has been developed by industry, is based on an elastic-plastic beam model for the pipeline, combined with elastic-plastic soil springs for the surrounding soil. A design criterion commonly used is the buckling strain criterion. This criterion has been demonstrated to be overly conservative, in general, by both experimental and analytical studies.

The predictive approach developed in this study is based on the fact that local buckling of pipe walls interacts with overall response of the line of pipe. A two-step predictive approach has been developed. These are denoted as segment analysis and line analysis. The segment analysis is based on a three-dimensional shell model simulating a pipe segment. The line analysis models the pipeline by using a pipeline-beam element, developed in this study, acting interactively with the soil. To integrate the local behavior into the overall behavior, representative cross-sectional stiffness is abstracted from the segment analysis and is then fed into the line analysis.

For the segment analysis, a solution technique based on an improved arc-length controlled equilibrium iterative method is developed. A solution procedure based on a direct search technique is explored as an alternative. The results of segment analyses demonstrated the softening behavior in postbuckling regions. Two basic buckling modes, referred to as diamond and bulging modes, and significant cross-sectional distortions have been predicted.

A program ABP has been developed for the line analysis. It is based on the ISPDR and RMDI techniques, defined herein, which include and exclude the effects of local buckling, respectively. Responses of lines of pipe, characterized by localization of deformation, have been predicted and analyzed. Results demonstrate great influence for effects of local buckling and the strengths of bearing and uplifting springs.

Based on the predicted behavior, criteria for design and assessment of pipelines are proposed on a more rational basis. The procedures for establishment and application of these criteria have been illustrated.

ACKNOWLEDGEMENTS

This study was carried out in the Structural Division of the Department of Civil Engineering in the University of Alberta. The author wishes to thank all the Professors for their excellent lectures and his fellow graduate students for their friendly advice.

The author wishes to express his special thanks and deep appreciation to Professor D.W. Murray for his supervision, thoughtful advice, encouragement, extreme patience and care during the time of this study.

The author wishes to thank C-FER (Center of Frontier Engineering Research) for providing financial support for more than three years, particularly, to Mr. Tom Zimmerman for his role in committing this support. The financial support of Pao Yu-kong and Pao Zao-long Scholarship, China, for the first year of author's Ph.D. program is also greatly appreciated.

Finally, I would like to thank my parents and my wife for their encouragement and understanding.

TABLE OF CONTENTS

LIST OF TABLES

LIST OF FIGURES

LIST OF SYMBOLS

SCALARS AND TENSORS

• LATIN CHARACTERS

a	thickness of shell in the direction normal to the mid-surface of a shell structure
C	segment cross-sectional stiffness property (amplification factor)
$C_{\theta x}$	ratio between the circumferential strain and the longitudinal strain for RMDI technique
C_{rx}	ratio between the radial strain and the longitudinal strain for RMDI technique
C^{EP}	elastic-plastic modulus for RMDI technique
C_{ijkl}	elastic-plastic material tensor
C^{EPS}_{ijkl}	elastic-plastic material tensor for shell structures
${}^{t}d$	current gap width between pipe and soil springs
D	diameter of a cylindrical shell
D_{max}	maximum diameter of a deformed cross-section
D_{min}	minimum diameter of a deformed cross-section
D_{in}	diameter of a cross-section in the bending plane of the pipe segment
D_{out}	diameter of a cross-section out of the bending plane of the pipe segment
D_{diff}	diametric differential
D_{exp}	diametric expansion
e	distance from the elastic stiffness centroid to the tangent stiffness centroid of a cross-section
E	modulus of elasticity
e_{ij}	small strain tensor in nonlinear formulation
F_i	components of body force as external loads
F	axial force
${}^{t}F_{eq}$	energy equivalent axial force in RMDI technique
F_y	yield axial force
${}_{t}F_{BS}$	incremental force of bearing soil spring
${}_{t}F_{US}$	incremental force of uplift soil spring
${}_{t}F_{LS}$	incremental force of longitudinal soil spring
F_{BY}	yield force of bearing spring
F_{UY}	yield force of uplift spring

F_{LY}	yield force of longitudinal spring
G	shear modulus
H'	equivalent hardening constant for multi-axial stress states
${}^{t}H_i$	finite element interpolation functions
K_1	beam cross-sectional stiffness coeffcient (axial)
K_2	beam cross-sectional stiffness coeffcient (flexural)
K_3	beam cross-sectional stiffness coeffcient (coupling)
K_a	segment cross-sectional stiffness property (axial)
K_b	segment cross-sectional stiffness property (flexural)
${}^{t}K_{BS}$	current stiffness of bearing soil spring
${}^{t}K_{US}$	current stiffness of uplift soil spring
${}^{t}K_{LS}$	current stiffness of longitudinal soil spring
L	length of cylindrical shells
${}^{t}L$	current length of pipeline-beam element
L_{PW}	principal wavelength
L_{TR}	half length of the transition zone of the ground profile
Δl	reference arc-length
m	wave number in longitudinal direction of cylindrical shells
M	moment
${}^{t}M_{eq}$	energy equivalent moment in RMDI technique
M_y	yield moment
n	wave number in circumferential direction of cylindrical shells
N_b	force intensity on the buckling strip
p	internal pressure
p_y	yield internal pressure
r, s, t	coordinates of the natural coordinate system for shell structures
$\bar{r}, \bar{s}, t$	coordinates of the Cartesian shell-aligned coordinate system for shell structures
R	radius of cylindrical shells
R_{diff}	radius differential
${}^{t}s_{ij}$	deviator tensor of the second Piola-Kirchhoff stress tensor
${}^{t}S_{ij}$	second Piola-Kirchhoff stress tensor
$\bar{S}$	effective stress
${}^{t}S_Y$	current yield strength
${}^{t}S_\theta$	constant circumferential stress
t	thickness of a cylindrical shell

T_i	components of surface traction as external load
u, v	displacements in the local x, y coordinate system for the beam formulation
$\tilde{u}$, $\tilde{v}$	displacements in the global $\tilde{x}$ $\tilde{y}$ coordinate system for the beam formulation
u_i	displacements in the glob[illegible]inate system of shell structures
$\|\mathbf{U}\|$	norm of unbalanced forces
V_{3i}	components of vector normal to the mid-surface of a shell structure
$\bar{v}_c$	segment cross-sectional stiffness property (location of the elastic stiffness centroid of the cross-section)
x, y	local coordinate system for beam formulation
$\tilde{x}$, $\tilde{y}$	global coordinate system for beam formulation
x_i	coordinates in the global coordinate system for shell structures
${}^{t}_{0}x_{i,m}$	components of deformation gradient tensor
$\bar{y}_s$	segment cross-sectional stiffness property (location of the tangent stiffness centroid of the cross-section)
Z	Batdorf parameter

- GREEK CHARACTERS

α	rotation angle of the normal vector, $\mathbf{V}_3$, about vector $\mathbf{V}_1$
α	angle of orientation of beam elements
α_1, α_2	roots of quadratic arc-length constraint equations
β	the angle of rotation of the normal vector, $\mathbf{V}_3$, about vector $\mathbf{V}_2$
β	relaxation factor in the improved arc-length constraint equation
β_{max}	maximum permissible value of relaxation factor
δ	differential settlement
${}_t\Delta_{BS}$	incremental deformation of bearing soil spring
${}_t\Delta_{US}$	incremental deformation of uplift soil spring
${}_t\Delta_{LS}$	incremental deformation of longitudinal soil spring
ε_{cr}	critical (buckling) strain
$d\bar{\varepsilon}^P$	incremental effective plastic strain
$\bar{\varepsilon}^P$	accumulated effective plastic strain
ε_L	local strain defined on the buckling segment
ε_o	overall strain defined on the pipe segment
${}^t\varepsilon_o$	longitudinal strain at the centroid for the beam formulation
${}_t\varepsilon_o$	increment of longitudinal strain at the centroid for the beam formulation

${}_t\varepsilon^P$	incremental effective plastic strain
${}_t\varepsilon_\theta^P$	incremental plastic strain component in the circumferential direction
${}_t\varepsilon_r^P$	incremental plastic strain component in the radial direction
${}_t\varepsilon_x^P$	incremental plastic strain component in the longitudinal direction
ε_w	wrinkling strain
${}^t\varepsilon_x$	longitudinal strain for the beam formulation
${}_t\varepsilon_x$	increment of longitudinal strain for the beam formulation
ε_y	yield strain
ε_{ij}	strain tensor in linear formulation for shell structures
${}^t\varepsilon_{ij}$	Green-Lagrange strain tensor with respect to the current configuration
${}_0^t\varepsilon_{ij}$	Green-Lagrange strain tensor with respect to the original configuration
ϕ	curvature
ϕ_L	local curvature defined on the buckling segment
ϕ_o	overall curvature defined on the pipe segment
ϕ_y	yield curvature
$\Delta\lambda$	accumulated increment of load factor
$d\lambda$	increment of load factor
${}_o\eta_{ij}$	nonlinear component of incremental strain tensor with respect to the original configuration
${}_t\eta_{ij}$	nonlinear component of incremental strain tensor with respect to the current configuration
ψ_s	ratio between the elastic modulus and secant modulus
ψ_t	ratio between the elastic modulus and tangent modulus
ρ	mass density
σ_{cr}	critical (buckling) stress
σ_s	circumferential stress
σ_x	longitudinal stress
σ_y	yield strength
σ_Y	yield strength
${}^t\tau_{mn}$	Cauchy stress tensor
ν	Poisson ratio
ξ_d	tolerance for displacement increments
ξ_f	tolerance for unbalanced forces
ζ	a constant balancing the relative magnitudes of the displacement increments and load increments

VECTORS AND MATRICES

$[\mathbf{B}_L]$ linear strain-displacement matrix for shell structures

$[\mathbf{B}_{NL}]$ nonlinear strain-displacement matrix for shell structures

$[{}^t\mathbf{B}^L]$ linear strain-displacement matrix for pipeline-beam element

$[{}^t\mathbf{B}_1^{NL}]$ non-linear strain-displacement matrix for pipeline-beam element

$[{}^t\mathbf{B}_2^{NL}]$ non-linear strain-displacement matrix for pipeline-beam element

$[{}^t\mathbf{B}^s]$ strain-displacement matrix for soil springs

$[\mathbf{C}_e]$ elastic material matrix in the Cartesian shell-aligned coordinate system

$[\mathbf{C}_{sh}]$ elastic material matrix for a shell in the global coordinate system

$[{}^t\mathbf{D}^p]$ cross-sectional material property matrix for pipe

$[{}^t\mathbf{D}^s]$ material property matrix for soil springs

$[{}^t\mathbf{F}]$ matrix of axial force

$[{}^t\mathbf{H}]$ interpolation function matrix

$\mathbf{J}$ Jacobian operator

$[\mathbf{K}]$ stiffness matrix

$[\mathbf{K}_E]$ elastic stiffness matrix

$[\mathbf{K}_{EP}]$ elastic-plastic stiffness matrix

$[\mathbf{K}_G]$ geometric stiffness matrix

$[\mathbf{K}_S]$ soil stiffness matrix

$[{}^t\mathbf{M}]$ matrix of moment

$\{\mathbf{P}\}$ total external load vector

$\{\Delta\mathbf{P}\}$ incremental external load vector

$\{\hat{\mathbf{P}}\}$ reference load vector

$\{\mathbf{Q}\}$ equlibrating force vector

$[\mathbf{Q}_{sh}]$ transformation matrix

$[{}^t\mathbf{T}]$ transformation matrix

$\{\mathbf{u}\}$ total displacement vector

$\{d\mathbf{u}\}$	displacement increment associated with an iteration
$\{\Delta\mathbf{u}\}$	accumulated displacement associated with an increment
$\mathbf{V}_1$	a directional vector perpendicular to directions $\mathbf{V}_3$ and $\mathbf{e}_2$
$\mathbf{V}_2$	a directional vector perpendicular to directions $\mathbf{V}_3$ and $\mathbf{V}_1$
$\mathbf{V}_3$	vector normal to the mid-surface of a shell structure
$[\mathbf{W}]$	weight matrix for constraint equation of indirect displacement control
${}^t_0\mathbf{X}$	deformation gradient tensor

$\{\alpha\}$	incremental vector of reduced (generalized) displacements
$\{\varepsilon\}$	strain vector in the global coordinate system
$\{\varepsilon_e\}$	strain vector in the Cartesian shell-aligned coordinate system
$\{\phi_i\}$	base vector in reduction method
$[\Phi]$	reduced base in reduction method
$[\Lambda]$	reduced (generalized) stiffness matrix
$\{\gamma\}$	reduced (generalized) unbalanced force vector
$\{\sigma\}$	stress vector
$\{\Delta\sigma\}$	incremental stress vector
$\{\tau\}$	stress vector in the global coordinate system
$\{\tau_e\}$	stress vector in the Cartesian shell-aligned coordinate system
Γ	configuration of structure

CHAPTER 1 INTRODUCTION

Buried pipelines as a means of transportation of oil and gas have become more and more important to the oil and gas industries in the last few decades. As the resource exploration moves to remote frontiers such as the Arctic and sub-Arctic, pipelines have been extended into new and more challenging environments. Consequently, there is a great need to have better understanding of pipeline behavior and a refined design procedure to meet the requirements imposed by the new working conditions. This project was proposed based principally on this fact. The thesis as a whole will present the research work carried out by the author between 1989 and 1992, and summarize the findings and suggestions achieved. The first chapter presents the objectives of the project in Sect. 1.1 followed by a brief literature review on relevant subjects in Sect. 1.2. A general discussion on conceptual approach to the analysis of pipelines subjected to imposed deformation is presented in Sect. 1.3. The chapter ends with a brief description of the content of subsequent chapters.

Pipelines subjected to imposed deformation are often forced to deform into the elastic-plastic region of the pipe steel. Due to the self-limiting nature of the deformation imposed loads, the load carrying capacity is not the major concern. Fundamentally, failure of pipelines should be defined in terms of two conditions, namely, leaking and excessive deformation. Leaking of the pipe wall starts from fracture initiation and propagates into through-thickness cracks which leads to loss of containment integrity. Predictions of fracture initiation and propagation requires a fracture mechanics approach and is not the primary objective of this project. Excessive deformation may be associated with local buckling which can be produced by various types of imposed deformation. Predictions of pipeline behavior under imposed deformation and the study of limit states associated with excessive deformations are the objective of this project, as is detailed in the following section.

1.1 OBJECTIVES

The general objective of this project is to analyze deformational behavior of pipelines and to contribute to the rationalization of the design criteria based on limit states design principles. To elaborate this general objective, the specific objectives are :

(1) to develop a robust solution technique which is able to trace various types of equilibrium paths for shell structures.

(2) to carry out nonlinear large deformation analysis and analyze the postbuckling

behavior of cylindrical shell segments, and determine the effects of loading conditions and geometric parameters, such as, diameter and wall thickness on the postbuckling behavior.

(3) to develop a procedure of buckling analysis, especially for cylindrical shells subjected to combined loads, and carry out buckling analyses to identify the onset of buckling. This onset is the phenomenon on which the current design criteria used in the pipeline industry, for imposed deformation loading conditions on pipelines, are based.

(4) to examine the effects of loading conditions and geometric parameters on the onset of buckling.

(5) to develop an analytical model for buried pipelines which can account for both the characteristics of a pipeline as a shell structure and as a long line structure.

(6) to determine the interaction between the pipeline and surrounding soil.

(7) Based on the behavioral understanding obtained from analysis of buckling and postbuckling of pipe segments and the integrated pipeline, propose a procedure on which more rational limit states design for imposed deformation can be established.

1.2 LITERATURE REVIEW

Pipelines are a type of structure which must function in complex environments. The behavior of pipelines is complicated by such factors as local shell buckling, soil-structure interaction, and combinations of externally applied loads and imposed deformations.

Despite the complex behavior and conditions imposed on pipelines, the design procedure specified by the current Canadian design code (CAN/CSA-Z183,1989), hereinafter referred to as 'the code', is based on linear elastic stress analysis and working stress design principles which can't be considered as a completely rational approach for pipeline design problems. This is particularly true for the conditions of imposed deformation where significant local yielding, local buckling, and large deformation may occur. A rational nonlinear deformation analysis should be employed to analyze this highly nonlinear response and to design pipelines safely and economically. Recognizing the inadequacy of the design procedure in the code and the need for more rational design criteria, a substantial effort has been made herein to improve the knowledge and understanding of pipeline behavior. In the remainder of Sect. 1.2, a review of the subjects related to the behavior and design of buried pipelines subjected to imposed deformations is

presented. This focuses on the design procedure in the code, on complementary design criteria and procedures used in the oil and gas industries, and on the critical buckling strain of pipes subjected to combined axial load, bending load and internal pressure.

1.2.1 Design Procedure in the Code

The code for oil pipeline systems in Canada, CAN/CSA-Z183 (Canadian Standard Association,1989), is based on linear elastic stress analysis and accumulated experience with the design loads of pressure, temperature differential, and sustained forces. The design specifications, as stated in Clause 5.6.1.1 of the code, are the following requirements : (a) design wall thickness, (b) maximum allowable temperature differential in restrained sections, (c) maximum allowable freely supported spans for axially restrained sections, (d) minimum required flexibility in partially or fully unrestrained sections, (e) maximum allowable support spacings for stress design of unrestrained sections, and, (f) maximum allowable cold-sprung reactions on equipment attached to flexible piping.

The code recognizes design conditions other than the basic conditions of pressure, temperature and sustained forces, such as slope movements, fault movements, seismic related earth movements, thaw settlements and frost heave. These are imposed deformations with regard to pipelines and would normally result in a locally nonlinear response which is not covered by the design procedure in the code. The code does not provide design requirements for conditions arising from imposed deformations. As stated in Clause 5.1.4 the designer is required to determine what supplemental design criteria are necessary for these effects. Clause 5.2.1.3 states that the designer is responsible for determining supplemental local design criteria for structural limits for denting, wrinkling, secondary tensile loading and structural stability.

1.2.2 Design Criteria Currently Used in Industry

As stated in the previous section, the current design code does not provide any guidance on design criteria for conditions of imposed deformations. Consequently, designers of pipelines must develop their own supplemental design criteria. Longitudinal strain has been chosen as a quantity upon which to establish the governing criteria for loads imposed by deformations for the following reasons.

First, the loads arising from imposed deformations are self-limiting in nature, because they are developed by the constraints of adjacent materials or by self-constraint of the structure itself. That is, stresses arise to satisfy strain-displacement compatibility within

the structure or between the structure and its supporting medium. The magnitudes of these loads depend on the imposed deformation, and more importantly, on the stiffness of the structure. Deformations or strains, rather than the loads, are the dominant quantities which control the response of the structure under these conditions.

Second, the amount of displacement involved in slope movements, fault movements, thaw settlements and frost heave, are usually large enough to force pipelines to deform into the elastic-plastic range of the material. Because the typical stress-strain curve for pipeline metal is very flat in the elastic-plastic range, strain is a far more sensitive quantity than stress with regard to the equilibrium state of pipeline.

Third, the longitudinal strain is used because local buckling of the pipe wall depends mainly on its (compressive) magnitude. In addition, in the case of tensile longitudinal strain, the total inelastic behavior is bounded by limiting the longitudinal strain provided that the circumferential stress due to internal pressure is limited to a value below yield strength of the material.

The strain criteria are intended to prevent the failure of pipelines. Pipelines may fail because of leaking, which is the result of crack initiation and propagation, or because of excessive deformation associated with local buckling. A criterion in terms of the maximum tensile strain in the longitudinal direction is used to prevent crack initiation and propagation. This has been commonly set at 0.5 percent (CANUCK Engineering Ltd., 1983). Studies (Price, 1990) show that this is, in general, a conservative criterion. Although much work is currently under way to develop rational criteria for the conditions of crack initiation and propagation, this aspect is not the principal interest of this project.

The maximum acceptable value of compressive longitudinal strain is normally set at the onset of local buckling in the pipe wall. The rationale for this is based on the fact that thin cylindrical shells have unstable postbuckling behavior. Load carrying capability of such a shell usually drops dramatically upon the initiation of local buckling and deformation of the postbuckling pattern, either axisymmetric or non-axisymmetric, grows rapidly after buckling occurs. To preserve load carrying capability and prevent excessive deformation and cross-sectional distortion, it appears to be natural to avoid local buckling completely. However, for a buried pipeline subjected to imposed deformation, the load carrying capability of the pipeline is not not significance and large additional deformation can be accommodated by the pipeline without affecting its capacity to carry the internal pressure. This behavior will be further developed in subsequent sections since it is one of the major

concerns of this research.

Because local buckling of shells is such a complicated phenomenon, as will be discussed in detail in Chapter 2, great efforts have been made to evaluate the strain at the onset of buckling both experimentally and analytically. This will be elaborated on in the next section. A typical value for maximum compressive strain in the current design procedures is 0.5 percent. A derivation of this value for a pipeline with outer-diameter of 12.75 inches and wall thickness of 0.25 inches was given by Workman (1981).

The common design procedure for pipelines appears to be to design the preliminary wall thickness for internal pressure according to stress criteria and then check for given imposed deformations. If the maximum permissible strain is exceeded, the wall thickness is adjusted or other measures, such as soft padding beneath the pipeline, are introduced to improve the geotechnical performance, so that the strain criteria are satisfied.

1.2.3 Experimental Studies of Buckling Strain

Many testing programs have been carried out in the past to study the buckling behavior of cylinders under various load combinations. However, most of them focused on buckling strength instead of buckling strain because buckling strength has much more engineering significance if the principal function of the cylinder is to carry loads. Consequently, only a handful of testing programs on buckling strain were conducted and reported (Bouwkamp and Stephen, 1973, 1974, 1975; Korol, 1979; Reddy, 1979; Jirsa *et al*, 1972; and Sherman, 1976). Some of these tests were carried out deep into the postbuckling ranges, but little measurement on postbuckling behavior has been reported up to present time. The testing programs and their results are briefly reviewed in the following subsections.

1.2.3.1 Tests of Bouwkamp and Stephen

Bouwkamp and Stephen carried out a series of tests at the University of California-Berkeley, in 1973, for pipes to be used on the Trans-Alaska pipeline. Eight tests on seven specimens were conducted. The specimens were fabricated from nominal 48 inch (1219 mm) diameter longitudinally seam-welded pipe. The test sections, except for one specimen, were fabricated from X60 pipe with a nominal wall thickness 0.462 inches (11.7 mm) and an yield strength of 60 ksi (413.7 MPa). The loading conditions were increasing bending moment combined with constant internal pressure and constant axial load. The internal pressure was set at two levels, high pressure at about 950 and 150 psi (6.55 and 1.03

MPa) and low pressure at 25 psi (0.17 MPa). The axial load was also set at two levels which correspond to temperature differentials of 135° and 90° F (57.2° and 32.2° C). The measured thickness and loading conditions are listed in Table 1.1.

The primary objective of the test series was to investigate the strain at the onset of buckling under various load combinations and loading sequences. After the results from the first test showed that the operational integrity of the line would not be impaired by development of buckling , the subsequent tests were continued into their postbuckling region to assess the postbuckling strength and deformation capability. Unfortunately, only minimum measurements were taken. However, the postbuckling deformation patterns from these tests are probably the best available information up to the present time. The buckling strains and radii of buckling curvatures are listed in Table 1.1.

The primary conclusions from this test series are summarized in the following. Failure, which occurred only at the end of the postbuckling phase, resulted from excessive local deformations except for one case of tearing of the pipe wall. When the pipes buckled at relatively low curvature values, the cross-sectional distortions were small enough not to affect the flow-through capacity of the pipeline. Following buckling the pipe is capable of undergoing further deformations which are twenty to thirty times those observed at buckling. The buckling mode has two basic forms : (1) For the pipes with middle to high pressure (150-950 psi) initial buckling develops as an outward buckling of the pipe wall over a substantial portion (up to 75%) of the pipe circumference; and, (2) For pipes with low pressure (25 psi), the buckled wall takes on a diamond like in-and-outward type of deformation pattern. On the sections other than the buckled sections, the distributions of longitudinal strain are basically linear up to a load level close to the buckling load, and only departs slightly from linearity afterward.

1.2.3.2 Tests of Reddy

Reddy (1979) performed a series of tests on stainless steel and aluminium alloy to investigate the plastic buckling behavior of pipes which had D/t from 35 to 80. It was realized that curvature is a much more satisfactory measure of buckling processes than bending moment, or equivalently, that extreme fiber compressive strain is a better measure than the corresponding stress. This is so because the shape of a typical moment-curvature response is very flat in the plastic range. Consequently, the strains at the onset of buckling were taken as the major measurements. Ten steel specimens and nine aluminium alloy specimens were tested. The specimens had a nominal diameter of 25 mm and were tested

under pure bending loading conditions. The thickness and buckling strains are listed in Table 1.2.

An important observation from Reddy's tests is the presence of wave-like ripples on the compression sides of the specimens before collapse took place. These ripples were found to remain after unloading at the end of test. They were non-uniformly distributed along the extreme compression side and had a principal ripple which was significant larger than the others in some cases. The average wavelengths of the ripples are smaller than the one of the plastic axisymmetric buckling of axially compressed cylinders. It was concluded that the ripples, rather than the small amount of ovalization, were the primary cause of collapses. This implied that the tubes behaved as imperfect cylinders, the imperfections of which gave rise to a steady growth of these ripple which eventually led to collapse.

The strain data in Table 1.2 was not directly available in the paper given by Reddy (1979). They have been retrieved from the plots in the published paper. Consequently, some errors may be expected. The reported buckling strains were defined at the limit points where collapses occurred.

1.2.3.3 Tests of Korol and Jirsa

Korol (1979) carried out a series of 11 tests on single and double span circular hollow tubular beams to compare with inelastic bending and axial compression theories of buckling. The main purpose of this series of tests was to investigate the D/t limit for tubular sections which can be used in plastic design. The test sections were loaded in uniform moments. The geometric properties of specimens, buckling strains at the onset of bifurcation which are observed visually, and strains at limit points are listed in Table 1.3.

Jirsa et. al (1972) conducted tests on six pipes to study the influence of ovaling on the flexural behavior of pipelines stressed beyond the elastic limit. The diameters of pipes range from 10.75 to 20 inches (273 and 508 mm) and D/t ratio from 30 to 80. Four of the pipes tested were uncoated and two were coated with concrete. The test sections were loaded in uniform moments. Geometric properties of specimens and buckling curvatures are listed in Table 1.4. The stress-strain curve was reported for each of the specimens. The buckling curvatures were recorded at the limit points. The values of buckling curvature are retrieved from plots in the published paper. One conclusion about the effects of ovaling from this test series is that the influence of ovaling on the moment capacity is relatively small in general, and local buckling occurred before large reductions in moment capacity

were observed. Therefore, local buckling, rather than ovaling is the principal cause of pipe failure.

1.2.3.4 Tests of Sherman

Sherman (1976) carried out a series of tests to determine the moment redistribution capabilities of round tubes and to determine if the plastic design principle could be applied to tubes subjected to flexure. Eighteen specimens were tested with nominal diameter of 10.75 inches and diameter-to thickness ratio ranging from 18 to 102. Three arrangements of support conditions were included in testing. They were simple supports at both ends, fixed supports at both ends and a cantilever. The fixed ends were welded to heavy end plates which allowed no distortion of the cross-section. The properties of the specimens are listed in Table 1.5 where simple, fixed, and cantilever are designated for boundary conditions mentioned above, respectively. The test results for those which failed by buckling are also listed in Table 1.5, where the buckling curvature was defined as that at which a diameter change of 0.05 inches occurred or was visually evident.

The following are some conclusions and observations obtained from this series of tests. Members with D/t of 35 or less could develop a plastic moment and sustain sufficient rotation to fully redistribute the moments. Ovalization at the hinge was slight and buckling did not occur. The section with D/t of 102 buckled in the elastic-plastic range. A deep buckle with single wave formed suddenly and the moment could not be maintained. The presence of a moment gradient and a stiffened end caused the initial buckle to occur at higher strains than when there was a constant moment region. For the heavier sections, the buckle formed slowly. The same or an increased load was sustained after the initiation of buckling, and the load started to drop at larger curvatures.

1.2.3.5 Tests in Progress

Two independent test programs in progress at the present time are being carried out at the University of Alberta (U of A) and at the Center for Frontier Engineering Research (C-FER). The objectives of these two test programs are to determine the strain at the onset of buckling and study the postbuckling behavior of pipe segments subjected to combined axial load, internal pressure and bending moment. The test program at U of A includes 7 specimens where 4 of them have a diameter of 20 inches (508 mm) and the other three have a diameter of 12.75 inches (324 mm). These tests have been completed at this moment. However, the data reduction is yet to be carried out. The test program at C-FER may

include 6 to 10 specimens which have a diameter of 24 inches (610 mm). The tests have yet to be completed. It is believed that the results from these test programs will be an important contribution to the knowledge of buckling and postbuckling behavior of pipe segments.

1.2.4 Analytical Studies of Buckling Strain

Predicting the buckling strain by an analytical approach or by numerical analysis is a research subject which has attracted the attention of many researchers. Similar to the experimental studies carried out in the past, most analytical studies were directed at the buckling loads instead of the buckling strains. Therefore, only relatively few studies are closely related to the current subject. These will be reviewed in the following subsections. They are grouped into closed-form solutions based on differential equations and numerical solutions based on finite element procedures.

1.2.4.1 Solutions Based on Differential Equations

Solutions based on differential equations are largely for axially compressed cylinders because the uniform membrane stress state existing in the prebuckling cylinder is easier to treat theoretically. The classical elastic buckling strain of an axially compressed cylinder has been studied by many researchers and reported in many references. These are summarized in the book by Brush and Almroth (1975). For cylinders of intermediate length, the elastic buckling strain can be expressed as

$$\varepsilon_{cr} = 1.21 \frac{t}{D} \tag{1.1}$$

1.2.4.1.1 Analysis of Batterman

Batterman (1965) used a procedure similar to that for elastic buckling for plastic buckling. Starting with an incremental differential equation of equilibrium, Batterman employed an elastic-plastic stress-strain relation to evaluate stress increments according to either the incremental theory or the deformation theory of plasticity. Great efforts were made to examine the differences in solutions because of the controversy that existed, which is, that incremental theory is essential for a proper description of irreversible plastic behavior. Nevertheless, the experimentally obtained loads are in good agreement with predictions of deformation theory. In analogy with the tangent modulus theory for columns it was assumed that the entire thickness of the shell wall is loading at buckling. The elastic-plastic buckling strains were expressed as

$$\varepsilon_{cr} = A \frac{t}{D} \tag{1.2}$$

where
$$A = \frac{4\,\psi_s}{\sqrt{3\,((5-4\nu)\psi_t - (1-2\nu)^2)}} \tag{1.3}$$

for the incremental theory of plasticity and

$$A = \frac{4\,\psi_s}{\sqrt{(3\psi_s+2-4\nu)\psi_t - (1-2\nu)^2}} \tag{1.4}$$

for the deformation theory. In Eqs. (1.3) and (1.4), ν is Poisson ratio, and ψ_t and ψ_s are the ratios of the elastic modulus to tangent modulus and elastic modulus to secant modulus, respectively. If unloading was allowed, as in the reduced modulus theory for columns, solutions were obtained with much more complex forms which are not presented here. It should be pointed out that the coefficient A in Eq. (1.2) which is defined by Eqs. (1.3) and (1.4) is dependent on the strain states because the tangent modulus and secant modulus have to be properly evaluated at the current strain state. Consequently, an iterative procedure is needed to determine the value of the buckling strain. This is usually a numerical procedure.

1.2.4.1.2 Analysis of Workman

Workman (1981) did an analysis for the Norman Wells pipeline. Despite the fact that the pipeline goes through the sub-arctic environment and might be subject to a complex combination of internal pressure, axial loads and bending moment, Workman idealized the problem of determining the buckling strain of such a pipeline to the relatively simple problem of finding the buckling strain of an axially compressed cylinder with internal pressure. The assumption employed was that the buckling strain of the pipe subjected to internal pressure and axial load is equal to or less than the buckling strain of the same pipe subjected to internal pressure, axial and bending loads. By employing deformation theory of plasticity and a Ramberg-Osgood curvilinear material representation, and assuming sine waves in both the longitudinal and hoop directions, a characteristic equation was obtained for a given material description and pipe size. This equation is

$$\phi\,(\,\sigma_x, \sigma_s, m, n\,) = 0 \tag{1.5}$$

where σ_x and σ_s are stresses, while m and n are wave numbers, in the longitudinal and

hoop directions, respectively. The lowest possible longitudinal stress state was identified as the buckling stress. This was determined by a numerical procedure in which the hoop stress was assumed to be constant and the buckling stress was obtained by search through the various wave numbers. Since the deformation theory of plasticity was employed, the buckling strain was determined from the buckling stress.

1.2.4.1.3 Analysis of Popov

The theoretical study by Popov (1973, 1974) proposed a methodology for determining the buckling strain of pipelines when subjected to the combined loading of pressure, axial and bending loads. His procedure had two steps.

The pipe was first subjected to internal pressure and axial load. It was modelled as an inelastic axisymmetric shell by finite element. An isotropic strain hardening material model with a curvilinear stress-strain relationship was used. From the axisymmetric model, an average stress-strain relationship representing the axisymmetric buckling characteristics was obtained by an incremental solution approach, which then served as a material constitutive law to be used in the bending problem.

In the second step, bending was introduced and the cross section was assumed to remain circular throughout the deformation history. A theory which formulates the behavior of a membrane tube under internal pressure, axial and bending loads was developed. The bulging effects were introduced by using the stress-strain relation derived from the axisymmetric model instead of the actual material properties on the compressive face of the pipe. Failure of the pipe due to wrinkling was then defined as the point at which the strain in the compression side reached the average axial strain at bulging in the axisymmetric problem. The proposed methodology was supported by good agreement between the predicted curvatures at which the wrinkle formed and the test results of Bouwkamp (1973).

1.2.4.2 Solutions Based on Finite Element Procedure

Finite element procedures have been used extensively to determine the buckling strain of cylinders. In general, three types of finite element model can be employed for buckling of a cylinder. The first is a model based on general shell elements which are available in many general-purpose programs on the market today. This model is the most general and capable in the sense that it can model any geometry of the shell and any type of deformation pattern. The second is based on the so-called 'elbow element' such as the one in ABAQUS (Hibbit, 1984). Elbow elements have polynomial interpolation between the

nodes in the longitudinal direction and Fourier interpolation around the circumference. Due to the nature of the interpolation, elbow elements have relatively limited capability of modelling deformation. The third is the axisymmetric model based on axisymmetric elements. This model has great advantages of efficiency, but can only model axisymmetric geometry and deformation.

1.2.4.2.1 Solutions of Row

Row *et al* (1983a) did a numerical study, in which he employed a similar methodology to Popov (1973, 1974). For the pipe subjected to internal pressure and axial load, the pipe wall was modeled using a 8-node axisymmetric solid finite element. A general multilinear stress-strain relationship with a kinematic hardening model was adopted, and an axisymmetric imperfection was introduced to represent thickness variation and/or offset at circumferential welds. With the axisymmetric model, the average stress-strain curve and the critical strain at which wrinkling or buckling occurs were obtained. The bending problem was modelled using an inelastic large deformation three dimensional shell element. Both the actual stress-strain curve and the average stress-strain curve were used in bending analysis. The results of the analyses indicated that, if the critical extreme fiber strains were defined at limit point in both bending and axisymmetric analyses, the critical extreme fiber strains in a bending analysis were substantially larger than those in an axisymmetric analysis because of the strain gradient in the bending case. A similar conclusion for curvatures corresponding to the extreme fiber strains was also valid. The use of the average stress-strain curve resulted in some difference in the moment-curvature response from the solution using actual material properties. This difference is significantly increased in the post-buckling softening range.

1.2.4.2.2 Solutions of Lara

P.F. Lara (1987) is probably the first one who studied the post-buckling behavior of pipe and tried to validate the strain criteria which are commonly used at the present time. The pipe was modeled by elbow elements, available, for example, in ABAQUS (Hibbit,1984). The cross sectional deformation is incorporated by Fourier interpolation. The wrinkle formation and wrinkle growth in pipes under combined loading were studied.

The results indicated that, for the low pressure cases which had the 'diamond shaped' wrinkle, a rapid wrinkle growth followed wrinkle formation. However, for high pressure cases, rapid wrinkle growth happened much later than when the wrinkle first

formed. It was concluded that the strain criterion based on wrinkle onset is adequate for low pressure cases, and too conservative for high pressure cases.

The strain at which rapid wrinkle growth begins was proposed as a more rational failure criterion. Sensitivity analysis of wrinkle growth was carried out to understand how the failure criteria would vary qualitatively when the design parameters, such as pressure, operating temperature, material properties, and wall thickness, were changed. Outward wrinkle formation was determined to be mildly sensitive to pressure effects, while inward wrinkle formation was a strong function of pressure. The pressure had a favorable effect in delaying wrinkle growth, and its influence was very significant for inward wrinkle growth. The operating temperature, or the compressive load had secondary effect on wrinkle growth. Increase in wall thickness could slightly delay the wrinkle growth. But thicker wall tended to revert the buckling mode from the outward bulging mode to the inward diamond mode, and consequently reduced the critical failure strain significantly. With regard to the material properties, wrinkle growth was found to be mainly dependent on the plastic properties.

1.2.4.2.3 Solutions of Bushnell

Bushnell published a series of papers (Bushnell, 1974,1976, 1981 and 1984) and a comprehensive book (Bushnell, 1985) on numerical buckling analysis of shells with a good portion of them devoted to cylindrical shells. In his works, an axisymmetric model for buckling analysis of shells of revolution was established and a program for this purpose, BOSOR5, was developed. With this tool, buckling behavior of various types of shells of revolution were analyzed for various loading and boundary conditions. The bifurcation analysis was based on eigen-value analysis, and an incremental solution approach was employed for nonlinear path analysis. The focus has been on determining the bifurcation load or limit load rather than the post-buckling behavior, although initial post-buckling behavior was one of the topics in his works. The prebuckling behavior is found to have a significant influence on imperfection sensitive shell buckling.

1.2.4.3 Comment on Previous Analytical Studies

A few comments will be made with regard to previous studies reviewed in this section.

First, there does not appear to be a firm basis for the assumption that the critical longitudinal buckling strain from axisymmetric conditions is applicable to general

conditions. This assumption is based upon the observation that the elastic buckling stress of a cylindrical shell subjected to axial load is about equal to or less than that of a cylindrical shell subjected to bending moment (Seide, 1961). Even though the elastic buckling stresses are close for the two load cases, there is no indication that the elastic-plastic buckling loads will be close, and even less support for elastic-plastic buckling strains to be close. It is well known that the buckling of the pipe with particular geometries of interest in buried oil pipeline design occurs after the initiation of elastic-plastic behavior, and therefore the strains could be much different while the stresses are reasonably close. Therefore, this fundamental assumption, which has been used directly by Workman (1981), and indirectly by Popov (1973) and Row (1983a), does not appear to have a sound theoretical basis. Furthermore, the axisymmetric model is not sufficient because it can only predict axisymmetric buckling modes, while tests (Bouwkamp, 1973) indicated that the buckling mode at low internal pressure was of the inward diamond shape which was obviously non-axisymmetric.

Second, the assumption that the cross-section remains circular does not appear to be satisfactory for predicting behavior in the post-buckling range. For shell type local buckling, cross sectional distortion, which results from both ovalization and local buckling, has a significant effect on post-buckling structural behavior, and should be included. The circular assumption was used by Popov (1973).

Third, only limited test results for pipes, in terms of buckling strain and buckling curvature are available. The test results from Berkeley are probably the best available. However, because the objective of these tests was to establish design criteria based on the onset of local buckling, there is no data with regard to post-buckling, even though the tests were carried on into the final collapse stage. For the range of practically used geometry and material properties, the post-buckling behavior is virtually unknown and more study is necessary.

Finally, the rationality of the practice of defining the pipe failure condition at the point of wrinkle onset is in question. As observed in Bouwkamp's tests (1973), the cross-sectional changes were small after the initiation of buckling occurred and the pipe appeared to remain in a condition which would permit it to be fully operational. Row (1987) indicated that wrinkle initiation is one of the damage conditions but not a failure condition, and a certain amount of wrinkling could be allowed. Lara (1987) showed that the criteria based on the initial buckling strains are very conservative for pipe with high internal pressure.

In view of the research work related to the buckling strain limits, design criteria currently employed are, in general, very conservative and the basis for them is neither rational nor complete. In the present study, by predicting the behavior of pipe, particularly the post-buckling behavior, through a rational and general numerical analysis, an attempt is being made to establish a firmer basis for more rational and complete design criteria for deformation imposed loads.

1.2.5 Analysis of Pipeline Subjected to Settlement

Within the past decade, analysis of soil support and stress distribution in buried pipelines has evolved from simple approximations using closed form solutions (Yen *et al*, 1981) to the use of sophisticated analytical methods which incorporate plastic analysis of steel and nonlinear soil behavior (Row *et al*, 1983b). One of the reasons for this development is the need for pipelines in adverse environments, such as buried pipelines in the arctic and pipelines under deep water. Buried arctic pipelines have to be designed for adequate restraint against thermal loading as well as to maintain integrity against thaw settlement and frost heave. Analysis of pipelines when subject to differential thaw settlement has two fundamental roles which are : (a) determining the acceptable design of a pipeline for a given differential settlement; and, (b) determining the allowable differential settlement for a given pipeline.

The model for analysis of pipelines subjected to differential settlement should cover several important issues. Soil settlement induces deformation of the pipeline which disturbs the distribution of strains and stresses existing in the line prior to the settlement. The magnitude and pattern of this disturbance depends on the structural response of the pipeline to the imposed deformation from soil settlement. Pipeline-soil interaction is an important feature. Because of the interaction, both the pipeline as a structure and the soil as a supporting medium have to be properly modelled. This usually leads to a complicated analytical model.

Depending on the major interest of the investigator, one could have a combination of a relatively simple model for soil and a relatively elegant model for pipeline or vice versa. In settlement analysis, more interest may be directed at the redistribution of the strains and stresses over the length than at the local cross-sectional deformation. Consequently, the analytical model has to cover sufficient length of the pipeline in order to properly evaluate this overall response. This usually results in a large scale model

depending on the particular discretization technique employed. Because of the large scale involved, full scale experimental studies of pipelines subjected to differential settlement are rare, and those that exist are questionable. Therefore, most studies reported on this subject were based on numerical and theoretical models.

1.2.5.1 Interaction Model

There are, in general, two types of analytical models for two different purposes. One is the pipe-soil interaction model which includes a segment of pipe and surrounding soil. The purpose of this model is to analyze the interaction between the pipe and the soil with the focus on the resistance provided by the soil. Consequently, a simple model for the pipe and relatively accurate model for the soil are usually employed. Examples of this type of analysis are studies carried out by Selvadurai (1983), Selig (1988), and Wagner (1989) where the proper soil parameters used for design of buried pipelines are the main concern. Because the scale of the model to determine the soil parameters is relatively small, experimental studies (Sultanov, 1986 and Wagner, 1989) were carried out to support and establish the analytical model. Detailed discussion is beyond the scope of this project. However, some discussion on the model, and results obtained, will be presented in Ch. 6.

The second type of analytical model is the pipeline-soil interaction model which includes a sufficient long pipeline and supporting soil. The purpose of this model is to analyze the response of the pipeline when it is subjected to imposed deformation that is applied through the interaction between the pipeline and soil. As the main interest is on the behavior of the pipeline, it is natural to have a relatively complicated model for pipeline that may include both geometric and material nonlinearities and a reasonable model for soil such as elastic-plastic soil springs. Because of the long length of pipeline that has to be covered in this type of study and the surrounding soil which is difficult to model, experimental study is difficult to carry out with a few exceptions. Two of them that can be mentioned here are tests on the effects of thermal loading (Iimura and Nishio, 1986) where only axial deformation needs to be considered; and tests on effects of frost heave (Williams, 1992). For the same reason, pipelines would normally be discretized by beam-type elements in numerical models, although other options, such as elbow elements and shell elements are possible.

Because of the great number of degrees of freedom introduced by discrete models of pipelines based on elbow elements and shell elements, the analysis becomes very expensive in terms of computer resources and, therefore, unrealistic for practical

application of pipeline design. Several models proposed for settlement analysis are reviewed in the following.

1.2.5.2 Model of Nyman

Nyman (1983) carried out a study on thaw settlement analysis for buried pipelines. After discussing the classification of thaw settlement configurations and mechanisms, a beam-on-elastic foundation model was proposed. In his model, the pipeline was modelled by an elastic beam element which is governed by maximum allowable stress. The soil loading and support conditions were represented as soil springs attached to the pipeline.

Each soil spring had a load-displacement relationship which is, typically, in the form of an elastic-perfectly plastic curve represented by the ultimate value of soil restraint and the corresponding yielding displacement. There are three aspects of soil effects needed to be modelled by soil springs. These are, soil overburden loading above the pipeline, bearing support below the pipeline and the longitudinal friction along the pipeline. Three types of soil springs were designated for these soil effects. These are, uplift springs, bearing springs and longitudinal springs, respectively. Equations to determine the ultimate soil resistance and yield displacement for each type of soil spring were proposed for both the settlement zone and the transition zone. The computations were carried out by using a public domain program which can model the pipeline as a beam-on-elastic foundation and predict settlement subject to a governing criterion of maximum allowable stress.

1.2.5.3 Model in Program PIPLIN-III

A more elegant model was proposed by Row *et al* (1983b) who was associated with the development of the specialized computer program for stress and deformation analysis of pipelines, PIPLIN-III (Structural Software Development, Inc., 1989). The model presented in his paper summarized the theoretical basis for the program PIPLIN-III. Since this program has been on the market for more than a decade and is extensively used by the pipeline industry, this particular model reflects the state-of-art in the field of pipeline analysis. The pipeline was modelled as a series of inelastic beam-type finite elements in a plane.

The pipeline material was represented by a material model proposed by Mroz (1967) which could consider yield under biaxial stress (hoop and longitudinal), nonlinear strain hardening and arbitrary cycling loading. The pipe cross-section was assumed to remain circular which means the cross-sectional ovaling is neglected. The local buckling of

the pipe wall was not directly modelled; instead, the strain at the onset of buckling was used to be the governing failure criterion. The buckling strain was required to be determined by separate theoretical and experimental studies.

The soil was modelled as a nonlinear Winkler foundation, i.e. a series of uncoupled nonlinear springs. The transverse soil spring consisted of four components. These were : the inelastic spring which models the basic nonlinear behavior; and, a spring and two dashpots which are used to model the creep effects. The inelastic spring component was assigned properties which accounted for nonlinear behavior, including : initial loading; inelastic unloading; development of gaps between the soil and pipeline under reversed loading; and, seasonal variation of uplift resistance. The longitudinal spring was a nonlinear spring similar to the transverse spring except that it was not dependent on the direction of the axial movement of the pipeline.

1.2.5.4 Model of Selvadurai

A interesting model was proposed by Selvadurai (1985) where elastic beam elements were used to model the pipeline and boundary elements were used to model the surrounding soil. The advantage of this model was that the soil was modelled as a three-dimensional continuous elastic medium rather than a series of uncoupled soil springs. Consequently, the effects of surrounding soil were more accurately simulated. The price paid for this is that the soil had to be two-dimensionally discretized on the exterior surface and the interface between the pipeline and elastic medium, which resulted in larger scale system. Therefore, its application in practical problems was limited. It is interesting to notice, however, that the three-dimensional medium can be modelled by a two-dimensional mesh through the use of the boundary element technique.

1.3 CONCEPTUAL APPROACH TO DEFORMATION ANALYSIS

The analysis of a pipeline subjected to imposed deformations is a complex problem due to the effects of material non-linearity, geometrical non-linearity, local buckling, and soil-structural interaction. A pipeline is a type of shell structure, and a three-dimensional shell model is necessary to properly examine its buckling and post-buckling behavior and to evaluate the nonlinear effects, both material and geometric. Considering the size of the problem, in terms of the length of pipeline which has to be covered in order to properly model the interactive soil-structural response when subjected to differential soil settlement, a three-dimensional shell model, which is theoretically possible, is intractable. Therefore, a

beam-type of line element has been employed. The settlement analysis of the pipeline is, then, divided into two phases, which are discussed in the following.

In the first phase, a three-dimensional shell model is used to represent a short segment of pipeline, which is free from soil support, in order to study buckling and postbuckling behavior. This includes the effects of material nonlinearity, geometrical nonlinearity, and geometric parameters, such as, diameter and wall thickness, and load combinations of axial load, internal pressure and bending moment. In this phase, the initiation of local buckling can be identified, and postbuckling response can be examined. The characteristics of the response include moment capacity vs. average strain history, where this latter term includes average curvature and average axial strain, cross-sectional deformation and distortion, and the development of wrinkling. With this model, parametric studies relative to the onset of local buckling and post-buckling behavior can be carried out. In addition, a variety of incremental stiffness properties can be determined and more rational criteria for serviceability deformation limit states can be established, based on the post-buckling prediction of the cross-sectional distortion. This type of analysis will be called a *segment analysis* and is the basis for boxes with A to F linkages in the flow chart of Fig. 1.1.

In the second phase, beam-type elements are used to model a pipeline of sufficient length for the settlement analysis. The effects of soil-structural interaction, differential temperature, lateral load and supports are included in this phase. Stiffness properties determined from the first phase are available to simulate the response of beam elements. Several aspects of the response of the pipeline can be examined from such an analysis. The results include the distribution of the curvature, axial strain, moment, and axial force along the pipeline length for any given settlement. For a given design and failure criteria, the allowable settlement can be determined. The sensitivity of the pipeline response to the various soil parameters can be studied. Rational criteria for deformation limit states in terms of critical curvature or compressive strain can be related to the settlement. This type of analysis will be called a *line analysis* and is the basis for the boxes with G to N linkages in the flow chart of Fig. 1.1.

All approaches to solutions will be discussed conceptually in the following sub-sections and are summarized in the flow chart shown in Fig. 1.1.

1.3.1 Shell Model Analysis of Segments

In the shell model analysis of pipeline segments, i.e. the segment analysis, the local buckling behavior and postbuckling behavior are of main interest. In order to numerically simulate these aspects of behavior, a robust solution technique which is able to account for the effects of nonlinear material properties and large displacements, and to trace various types of equilibrium paths which may include snap-back and snap-through types of behavior, is essential. In addition to robust solution techniques, a finite element model must be developed which can properly model the loading and boundary conditions, and deformation patterns anticipated. With such a finite element model and solution technique, the incremental nonlinear analysis of pipeline segments can be carried out to trace the equilibrium path up to any required degree.

The objective of buckling analysis is to identify the onset of buckling. Because the strain at the onset of buckling is currently used for many applications as the governing design criteria for excessive deformation when pipelines are subject to deformation imposed load, buckling analysis becomes an important part of the analysis, in spite of the fact that design criteria based on buckling strain cannot be totally rationalized. Detailed discussion on the rationality will be presented in Ch. 8. Depending on the definition and understanding of the buckling phenomenon, different approaches can be employed to determine the onset of buckling. For a pipeline segment subjected to a combined loading condition, a procedure based on incremental nonlinear analysis is developed and employed. With buckling strains predicted from this procedure, comparison with experimental data can be made which would be able to verify this procedure. Parametric study on the sensitivity of the buckling strain with respect to geometric, loading and material parameters can be carried out to expand the data base of buckling strains and the understanding of buckling behavior. Buckling analysis is confined to the path joining boxes with linkages B and C in Fig. 1.1.

The objective of postbuckling analysis is to study the structural response after buckling occurs. Since it is probable that pipelines can operate normally in the postbuckling range as implied by Bouwkamp and Stephen (1973), Row *et al* (1987) and Lara (1987), it is natural and reasonable to extend the acceptable design conditions into the postbuckling range. Consequently, understanding of postbuckling behavior is necessary. Postbuckling analysis of pipeline segments, which can be considered as imperfect shell structures because of imperfections from various sources, is essentially incremental nonlinear analysis

which covers the entire equilibrium path. With such postbuckling analyses, deformation history in terms of strains, cross-sectional deformation, and development of wrinkling and buckling patterns can be established. This solution path is represented by the shortest path with links from A to E in Fig. 1.1. Here, the effects of geometric, loading and material parameters can be studied. In addition, postbuckling analysis can also generate the Stiffness-Property-Deformation relationships used in beam models as generalized stress-strain relationships that define the incremental force-strain relations on the cross-section of the beam. This is a way to summarize and synthesize local buckling dominated behavior obtained from shell model analysis in such a way that it is suitable for input into the beam model, where it is impossible to directly simulate the local effects. This function is illustrated by linkage F in the flow chart of fig. 1.1.

For this work, segment analysis is carried out using a modified version of the NISA program developed by Stegmuller and Ramm (1984).

1.3.2 Beam Model Analysis of Pipelines

In the phase of beam model analysis of pipelines, i.e. the line analysis, the major concerns are the pipeline-soil interaction and the resulting distribution of forces and strains along the pipeline, when it is subject to imposed deformation. The pipeline is modelled by using inelastic pipeline elements. This is discussed further in the following, for cases with and without local buckling, respectively.

The soil is modelled as an inelastic Winkler foundation, which is a series of uncoupled soil springs. Uplift, bearing and longitudinal soil springs are used to simulate the soil resistance to uplift, soil support and longitudinal friction. The soil springs can model inelastic behavior and develop gaps between the pipeline and soil. Since the beam model line analysis is used for settlement analysis which involves long segments of pipelines and surrounding soil, it is economically prohibitive to use more elegant models for the pipeline and soil. It is believed that the current line model can capture all the essential features of behavior for the anticipated problem.

1.3.2.1 Response of the Pipeline without Buckling

Considering a pipeline with elastic-plastic strain-hardening material, the response of the pipeline, in general, can be characterized by a hardening moment-curvature relationship, providing that local buckling does not occur. The elastic-plastic prediction of the response, that is appropriate to be applied in this case, is discussed in the following.

For any specified path of loading in deformation space (ie.-ϕ-ε space), and any elastic-plastic material stress strain curve, the values of P and M for the pipe can be determined to within any prescribed tolerance (providing, again, that local buckling does not occur), by integrating along the deformation path. In general, the stress resultants can be determined from the integration of the final stresses over the cross-section which remains circular. The stresses may be evaluated by using incremental hardening elastic-plastic stress-strain relations with proper loading and unloading control associated with the loading function at each integration point on the cross-section. The resulting technique can properly follow strain reversals as they occur across any part of the cross-section. For reliable results stresses should be determined using a subincrement technique. In the absence of local buckling, this direct integration technique gives the correct solution. It will be referred to subsequently as the *reduced modulus direct integration* (RMDI) technique and is contained in Fig. 1.1 as the path along links from G to M.

When applied to a line of pipe the RMDI technique suffers from the deficiency that it is extremely demanding on storage, because strain-history information must be retained at each integration point of each cross-section which is associated with the longitudinal integration of the pipeline solution. It is also numerically intensive since, in addition to the incremental evaluation of the stresses, the equilibrium equations must be iterated to achieve an equilibrium position. This latter characteristic is, however, common to all techniques for solving nonlinear beam or pipeline problems.

1.3.2.2 Response of the Pipeline Including Local Buckling

At least two motivations exist to induce the analyst to discard the RMDI technique. First, if the objective is to investigate pipeline behavior including the effects of local buckling, it is not possible to handle this effect by direct integration techniques. This is because stress is no longer related to apparent compressive strain through a material law. Second, because of the amount of numerical computation involved, the direct integration techniques may be inefficient even for simple loading paths. Consequently, one looks for alternative methods.

The first consideration in the paragraph above is, of course, the predominant consideration for this study. Popov (1973, 1974) developed a methodology to analyze pipe segments subjected to combined load. This has been reviewed in Sect. 1.2.4.1. Following the same principal idea, the methods developed for the study of the pipe problem have been

based on the generation and application of generalized stress-generalized strain relationships. For a pipeline these relationships are the moment-curvature relationship, the axial stiffness-curvature relationship and some other relevant relationships giving strain dependent cross-sectional properties. We can refer to these relationships as cross sectional *stiffness-property-deformation* relationships (SPD relationships), and will refer to the solution methods employing them as *integration of stiffness-property-deformation relationship* (ISPDR) methods. The ISPDR technique is illustrated by the path along the links from G to K in Fig. 1.1, and the SPD relationships are required through the link F.

An ISPDR method has two separate steps. The first step is to construct the SPD relationships utilizing a three-dimensional shell model of a pipeline segment under selected loading and support conditions. The second step is to apply the SPD relationships as generalized-stress generalized-strain relationships to the soil-structure interactive beam model and analyze the response and behavior of the pipeline subjected to imposed deformation. The verification procedure to establish the applicability of this approach to settlement analysis, is discussed in following section.

The response of the pipeline with local buckling can be characterized by a post-buckling softening moment-curvature relationship. The hardening and softening moment-curvature relationships lead to very different response of the pipeline when it is subject to imposed deformation. When subject to actions beyond the yield point, the pipeline with a hardening moment-curvature relationship forms plastic hinges and may be expected to redistribute internal forces because of the resulting variations of stiffness along the length of the pipeline. If the moment-curvature relationship softens, the moment at the point of maximum curvature begins to decrease with increasing rotation. As a result of this, moments in segments adjacent to the developing 'hinge' also decrease and these segments unload elastically. The effect of the unloading in adjacent segments is to concentrate the curvature into the softening segment rather than to distribute it along the length of the beam. This effect leads to curvatures which are much greater locally than would be expected from settlements of a pipe with hardening in its moment-curvature curve.

Because local buckling results in softening of the moment-curvature curve, which leads to curvature concentration within a particular pipe segment, its effect is that all aspects of local buckling deformations are accentuated in this critical segment. Consequently, any limit state criterion based on local buckling is directly influenced by the concentration. This implies that analyses which do not include softening produce results that are non-conservative with respect to limit state deformation criteria for post-buckling regions.

1.3.2.3 Verification of ISPDR Technique

The ISPDR technique to analyze a line of pipe is a technique based on the construction and application of SPD relationships. Comparing the RMDI technique of Sect. 1.3.2.1 with the ISPDR technique of Sect. 1.3.2.2, the fundamental difference can be found in the integration process. In the RMDI technique, the integration over the volume of the pipeline material is carried out in a continuous operation by first integrating over the cross-section and then over the length. In the ISPDR technique, however, the volume integration over the pipeline material is broken into two separate processes carried out at different times, namely, the *generation procedure* for properties, and, the *solution procedure* for the pipeline.

The generated SPD relationships are used to define cross-sectional stiffness properties on which the incremental-stress incremental-generalized-strain relationship is based. The generation procedure can be considered as equivalent to the integration over the cross-section in the RMDI technique. At some later time, during the solution procedure using the SPD relationships, the element stiffness matrix is evaluated by integrating the cross-sectional stiffness over the element length. The question about the validity of ISPDR technique arises from the fact that the deformation paths in the generation and in the solution procedures may be different. These deformation paths will be referred to in subsequent discussion as the *generating deformation path* and *actual deformation path*, respectively.

A verification procedure is proposed here to establish the validity of ISPDR technique or to determine the boundary of its applicability. In the absence of local buckling the applicability of ISPDR technique can be verified by comparing the behavior it predicts with that obtained from the RMDI technique of Sect. 1.3.2.1, which gives the 'correct' answer under stated conditions. The comparisons between the ISPDR technique and RMDI technique can be made for various material models. In particular, they can be made for an elastic-plastic hardening (EPH) material and for an elastic-plastic softening (EPS) material. If a (fictitious) EPS material stress-strain relation can be evaluated, which simulates the softening moment-curvature curve produced by the effect of local buckling, the validity of the ISPDR technique for this type of characteristic behavior can also be inferred. This verification procedure is indicated by links L and O to the common box in Fig. 1.1.

Additional verification can be extended to comparisons with results obtained by

program PIPLIN (Structural Software Development, Inc., 1989). However, these analyses will not include the effects of local buckling because, to the writers' knowledge, PIPLIN does not have a rational solution procedure to evaluate these effects, although it permits the input of properties for a user supplied "wrinkling element". Nevertheless, the comparisons will establish the reliability of the programs developed in association with this project to produce the correct results associated with standard pipeline behavioral characteristics.

For this work, line analyses are carried out using the program Analysis of Buried Pipelines (ABP) developed by the writer.

1.4 SCOPE OF FOLLOWING CHAPTERS

The remainder of this work develops in detail the method of deformation analysis which has been described conceptually in Sect. 1.3. The major subjects and content presented in each of the following chapters may be summarized as follows.

Chapter 2 reviews the formulations for analysis of shell structures in the form of continuum mechanics equations and finite element equations. This provides the theoretical background for the numerical analyses carried out in this work. A relatively detailed discussion on behavioral characteristics of the shell structures is also presented with the focus on buckling and postbuckling behavior of cylindrical shells. This serves as a general guideline for buckling and postbuckling analyses of pipeline segments that are discussed in Chs. 4 and 5.

Chapter 3 presents the solution technique developed in this work for incremental nonlinear analysis of three-dimensional shell structures, which is shown in the box below link A of Fig. 1.1. The solution technique includes two independent procedures which can be employed either independently or in combination. One is the equilibrium iteration procedure with modified arc-length control, loading and convergence criteria. The other is a subspace searching technique which is particularly efficient for postbuckling analysis of certain shell structures. This procedure is developed based on the algorithms commonly used for optimization problems and the fact that there are only a few displacement modes dominating the deformation. Maximum efficiency can be achieved by using a proper combination of these two procedures.

Chapter 4 focus on postbuckling analysis and behavior of pipeline segments. A shell model is established with proper discretization, loading and boundary conditions. A discussion on buckling modes, deformation history, and effects of loading is presented.

The characteristics of the postbuckling behavior are summarized. It describes the developments required in the box at the end of link D in Fig. 1.1.

Chapter 5 is about buckling analysis and behavior of pipeline segments. It starts with a review of approaches for buckling analysis. Based on the understanding of the problem of pipeline segments subjected to combined loading conditions, a procedure for buckling analysis based on incremental nonlinear analysis is proposed. Comparisons between predicted buckling strains and corresponding test data are carried out to verify this procedure. Significant factors relative to buckling strain, and their influences, are also discussed. Chapter 5 contains the development for the boxes at the ends of links B and C of Fig. 1.1.

Chapter 6 presents the formulation of the pipeline beam element developed in this project for settlement analysis of pipelines. The formulation includes the following aspects :

(a) strain-displacement relationships that account for large displacements;

(b) stress-strain relationships for the RMDI technique which consider yielding under biaxial stress (hoop and longitudinal) and mixed hardening rules;

(c) stiffness-property-deformation relationships for the ISPDR technique, and their generation procedure, which can account for the effects of local buckling and cross-sectional distortion; and,

(d) pipeline-soil interaction modelling where the soil is modelled as a series of uncoupled inelastic springs.

Finite element discretization and interpolation schemes are then applied to this formulation. Development and verification of the program Analysis of Buried Pipelines (ABP) which implements this formulation and provides a solution tool for settlement analysis of pipelines are also discussed. Chapter 6, therefore, covers details of the subjects contained in the boxes at the ends of links G, H, L, M and O of Fig. 1.1.

Chapter 7 focuses on the analysis and behavior of pipelines subjected to imposed deformation. First a model for analysis is established which includes finite element discretization, stress-strain relationship, generated stiffness-property-deformation relationships and proper soil parameters. With the solution based on this model, behavior of such a pipeline is summarized. Parametric studies are carried out to examine the sensitivity of the pipeline behavior to soil parameters. The contents of boxes at the ends of links J and N of Fig. 1.1 are, therefore, contained in Ch. 7.

Chapter 8 discusses the design criteria for imposed deformations. It is believed that

the criterion based on buckling strain is not a rational one. The rational design criteria that are proposed are based either on the service limit states, characterized by cross-sectional distortion, or on the pipeline behavior represented by the rapid growth of the curvature or strain. Although the criteria are not able to be completely established due to the limited data base available at present time, the procedure proposed here appears to be more rational than present practices.

Chapter 9 draws the conclusions from previous chapters.

specimen	nominal thickness	measured thickness	internal pressure	ΔT	comp. axial load	comp. buckling strain	tensile buckling strain	buckling curvature radii
	(in)	(in)	(psi)	(°F)	(kip)	(in/in%)	(in/in%)	(ft)
1	0.462	0.495	942	135	2580	-0.5735	0.0795	627
2	0.462	0.485	917	135	2520	-0.4726	0.0796	608
3	0.462	0.490	25	135	1920	-0.2694	0.0796	779
4	0.462	0.487	950	90	1920	-0.8196	0.1816	436
5	0.462	0.487	150	90	1373	-0.2797	0.1265	900
5A	0.462	0.487	950	90	1920	-0.4088*	0.1136*	780*
6	0.562	0.585	150	90	1630	-0.5705	0.2678	486
7	0.462	0.467	150	90	1322	-0.2333	0.1431	920

* values at pressure drop, not the onset of buckling

Table 1.1 Specimen Properties and Test Results of Bouwkamp's Tests

Steel Specimens				Aluminium Alloy Specimens			
specimen	D/t	t	buckling strain	specimen	D/t	t	buckling strain
		(mm)	(mm/mm%)			(mm)	(mm/mm%)
1	76.50	0.3543	0.75	A1	55.42	0.4511	0.77
2	79.80	0.3133	0.77	A2	57.12	0.4377	0.70
3	66.80	0.3743	0.93	A3	45.94	0.5442	1.01
4	61.46	0.4068	0.90	A4	46.10	0.5423	1.11
5	51.34	0.4869	1.58	A5	36.92	0.6771	1.35
6	51.42	0.4862	1.32	A6	36.92	0.6771	1.98
7	46.22	0.5409	1.32	A7	34.72	0.7200	1.09
8	46.28	0.5402	1.58	A8	34.72	0.7200	1.39
9	46.28	0.5402	1.32	A9	34.72	0.7200	1.49
10	42.18	0.5927	1.76				

Table 1.2 Specimen Properties and Results of Reddy's Tests

specimen	diameter D	thickness t	D/t	σ_y	buckling strain	E_T at buckling	strain at limit point
	(in)	(in)		(ksi)	(%)	(ksi)	(%)
1	4.50	0.156	28.9	44.8	0.82	380	-
2	6.63	0.156	42.5	44.2	0.59	560	-
3	6.63	0.188	35.2	53.5	0.72	500	1.00
4	20.0	0.25	80.0	54.4	0.17	~100000	-
5	10.75	0.219	49.1	44.4	0.49	690	0.97
6	12.75	0.25	51.0	54.5	0.52	740	-
7	14.00	0.25	56.0	43.2	0.44	810	-
8	16.00	0.25	64.0	44.8	0.46	750	0.66
9	4.50	0.156	28.9	44.8	-	-	-
10	10.75	0.219	49.1	44.4	-	-	-
11	20.0	0.25	80.0	52.3	0.43	1000	-

Table 1.3 Specimen Properties and Results of Korol's Tests

specimen	diameter D	thickness t	D/t	coating thickness	buckling curvature	buckling strain
	(in)	(in)		(in)	(10^{-4}/in)	(%)
10a	10.75	0.233	46.14	0	25.00	1.345
10b	10.75	0.350	30.71	0	-	-
16a	16.00	0.260	61.54	0	10.00	0.800
20a	20.00	0.255	78.43	0	3.75	0.375
12a	12.80	0.260	49.23	1.45	19.00	1.216
16b	16.10	0.260	61.92	1.70	6.00	0.483

Note : the buckling strain is calculated from buckling curvature by multiplying the nominal radius

Table 1.4 Specimen Properties and Results of Jirsa's Tests

specimen	average diameter	average thickness	yield strength	D/t	length	boundary condition	buckling curvature	ϕ/ϕ_y	buckling strain
	(in)	(in)	(kis)		(in)		(10^{-4}/in)		(%)
7	10.785	0.221	58.6	48.6	12	simple	12.54	3.3	0.676
8	10.785	0.221	58.6	48.6	20	fixed	22.73	6.0	1.226
9	10.785	0.221	58.6	48.6	10	cantilever	32.04	8.5	1.728
10	10.752	0.194	61.1	55.4	12	simple	7.52	1.9	0.404
11	10.752	0.194	61.1	55.4	20	fixed	12.70	3.2	0.683
12	10.752	0.194	61.1	55.4	10	cantilever	32.55	8.3	1.750
13	10.751	0.139	41.8	77.3	12	simple	6.10	2.3	0.328
14	10.751	0.139	41.8	77.3	20	fixed	5.83	2.2	0.313
15	10.751	0.139	41.8	77.3	10	cantilever	18.76	7.0	1.008
16	10.746	0.097	44.9	110.7	12	simple	8.30	2.9	0.446
17	10.762	0.105	44.9	102.5	20	fixed	15.46	5.4	0.831

Note : the buckling strain is calculated from buckling curvature by multiplying the nominal radius

Table 1.5 Specimen Properties and Results of Sherman's Tests

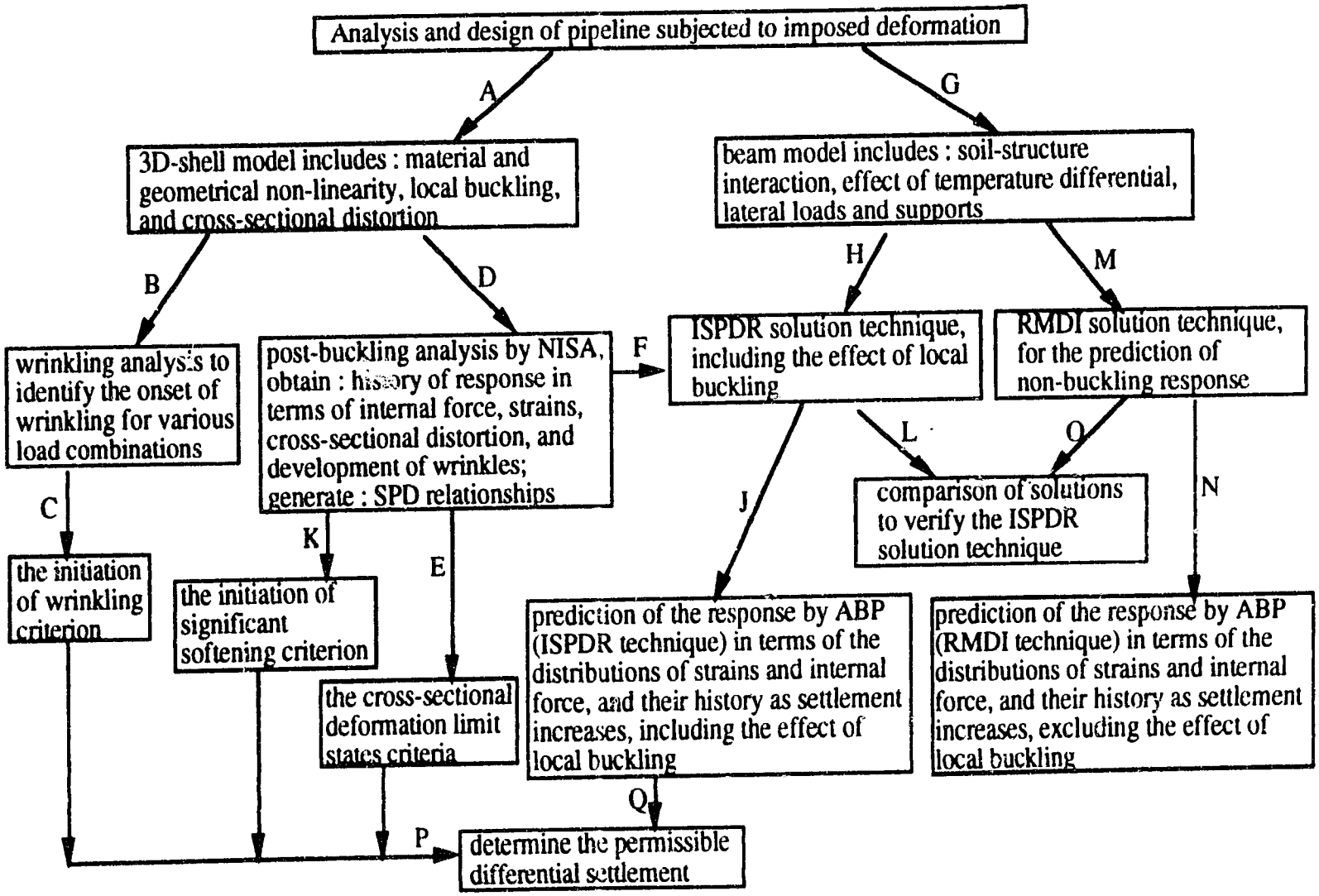

Fig. 1.1 Flow Chart of Solution Procedures

CHAPTER 2 SHELL STRUCTURE FORMULATIONS AND BEHAVIOR : A REVIEW

Shell structures have been used extensively in various engineering fields because of their superior load carrying capacity and adaptive geometry. Pipelines represent one type of shell structure that has become a very important means to transport oil, gas, water and other types of fluid. Before pipeline behavior and its prediction are discussed, the formulations and behavior of general shell structures are described systematically in this chapter. The formulations for analysis of shell structures are reviewed in Sect. 2.1 and this serves as a framework for analytical procedures which are referenced in later chapters. The behavior discussed in Sect. 2.2 will serve as a general guideline for the discussion of pipeline behavior.

2.1 FORMULATION

Shell structure analysis can be formulated in linear and nonlinear form dependent on whether or not the nonlinear effects of geometry and materials are included. The linear formulation involves only linear relationships for equilibrium, displacement and strain, and the stress-strain material relationship. These restrictions make the linear formulation relatively simple but, at the same time, limit its application to analyses with small displacements and linear elastic materials. Nonlinear formulations may include both large displacements and nonlinear material behavior. Therefore, it is applicable to general analysis of shell structures. The complexity of the geometrical relationships is one of the characteristics of shell structures, and has to be simplified by assumptions introduced by analyst according to his purpose and understanding. Different assumptions will eventually result in formulations which are different from each other in detail (Bathe, 1982; Ramm and Matzenmiller, 1986; Basar and Kratzig, 1990; and, Onate *et al*, 1990). In this section, representative linear and nonlinear formulations will be reviewed. Finite element discretization, in which the definitions of various stiffness matrices and load vectors will be discussed afterward.

2.1.1 Linear Formulation

In linear formulations of shell structures, differences are few because of the simplicity in the strain-displacement and stress-strain relations. However, description of the geometry of a shell can be different from one formulation to another by utilizing some special features of shell structures such as shells of revolution and shallow shells. The

formulation presented in the following is for general shell structures and based upon Bathe's work (1982).

2.1.1.1 Geometrical Relations

An element of a shell structure is shown in Fig. 2.1 where three coordinate systems are defined. They are the global Cartesian coordinate system x_1, x_2, and x_3, the Cartesian shell-aligned coordinate system $\bar{r}$, $\bar{s}$, and t, and the curvilinear natural coordinate system r, s, and t. The global Cartesian coordinate system is a reference system in which equilibrium equations are assembled. The natural coordinate system is defined by the element such that each of r, s, t vary from -1 to +1 within the element. The natural coordinate system is, in general, not an orthogonal system. The Cartesian shell-aligned coordinate system is an orthogonal system with unit vectors defined in terms of unit vectors of natural coordinate system as

$$\mathbf{e}_{\bar{r}} = \frac{\mathbf{e}_s \times \mathbf{e}_t}{|\mathbf{e}_s \times \mathbf{e}_t|} \tag{2.1a}$$

$$\mathbf{e}_{\bar{s}} = \mathbf{e}_t \times \mathbf{e}_{\bar{r}} \tag{2.1b}$$

where $\mathbf{e}_r$, $\mathbf{e}_s$, $\mathbf{e}_t$ and $\mathbf{e}_{\bar{r}}$, $\mathbf{e}_{\bar{s}}$, $\mathbf{e}_t$ are the unit vectors for the natural coordinate system and the Cartesian shell-aligned coordinate system, respectively.

A direction normal to the mid-surface of the shell element in the undeformed configuration is introduced where its unit vector is denoted as ${}^0\mathbf{V}_3$ in Fig. 2.1. The Cartesian coordinates of any point in the shell can be expressed in terms of the Cartesian coordinates of a corresponding point on the mid-surface and a unit vector in the normal direction as

$${}^m x_i(r,s,t) = {}^m x_i(r,s) + \frac{a}{2} t \, {}^m V_{3i} \qquad i = 1, 2, 3 \tag{2.2}$$

where ${}^m x_i(r,s,t)$ = Cartesian coordinates of any point in the element,

${}^m x_i(r,s)$ = Cartesian coordinates of any point on the mid-surface,

a = Thickness of shell in t direction at point r,s,

${}^m V_{3i}$ = Cartesian components of normal unit vector ${}^m\mathbf{V}_3$.

The left superscript m denotes the configuration of the shell element; i.e. m = 0 and 1 denote the original and final configuration of the shell element.

2.1.1.2 Deformation Relations

In order to introduce two-dimensional displacement variables, the following assumptions are made, i.e. the straight line in the normal direction remains straight and normal during deformation and no change of the length occurs in normal direction. Based on these assumptions, the displacements can be expressed in terms of the displacements on the mid-surface of shell element and the incremental vector of the unit normal vector as following,

$$u_i\,(r,s,t) = u_i(r,s) + \frac{a}{2}\,t\,V_{3i} \qquad i = 1, 2, 3 \tag{2.3}$$

where $u_i\,(r,s,t)$ = displacement components at any point in the shell element,
$u_i(r,s)$ = displacement components at any point on the mid-surface,
V_{3i} = components of incremental vector of unit normal vector.

The incremental vector of the unit normal vector can be written as

$$\mathbf{V}_3 = {}^1\mathbf{V}_3 - {}^0\mathbf{V}_3 \tag{2.4}$$

The components of $\mathbf{V}_3$ should be expressed in terms of rotations at the point on the mid-surface, so that all the displacement variables can be located on the mid-surface of the shell element. One way of doing this is to introduce two unit vectors ${}^0\mathbf{V}_1$ and ${}^0\mathbf{V}_2$ which are orthogonal to ${}^0\mathbf{V}_3$ as well as to each other as shown in Fig. 2.1. The first unit vector is defined as

$${}^0\mathbf{V}_1 = \frac{\mathbf{e}_2 \times {}^0\mathbf{V}_3}{|\mathbf{e}_2 \times {}^0\mathbf{V}_3|} \tag{2.5}$$

where $\mathbf{e}_2$ is a unit vector in the direction of x_2-axis. For the special case where ${}^0\mathbf{V}_3$ parallels to $\mathbf{e}_2$ and Eq. (2.5) fails to define a non-zero vector, ${}^0\mathbf{V}_1$ can be set to equal to $\mathbf{e}_3$ as an alternative. The other unit vector can be defined as

$${}^0\mathbf{V}_2 = {}^0\mathbf{V}_3 \times {}^0\mathbf{V}_1 \tag{2.6}$$

Let α and β be the rotations of the normal vector ${}^0\mathbf{V}_3$ about the vectors ${}^0\mathbf{V}_1$ and ${}^0\mathbf{V}_2$. Considering the fact that α and β are small angles, the increment vector of the normal unit vector can be expressed as follows and demonstrated in Fig. 2.2.

$$\mathbf{V}_3 = -{}^0\mathbf{V}_2\,\alpha + {}^0\mathbf{V}_1\,\beta \tag{2.7}$$

Substituting Eq. (2.7) into Eq. (2.3), it becomes

$$u_i\,(r,s,t) = u_i\,(r,s) + \frac{a}{2}\,t\,(-{}^0V_{2i}\,\alpha + {}^0V_{1i}\,\beta) \tag{2.8}$$

With the assumption of small displacement, the strain-displacement relations can be defined as

$$\varepsilon_{ij} = \frac{1}{2}\left(\frac{\partial u_i}{\partial x_j} + \frac{\partial u_j}{\partial x_i}\right) \qquad i, j = 1, 2, 3 \tag{2.9}$$

Since the displacements and global Cartesian coordinates are defined in terms of natural coordinates as shown in Eqs. (2.8) and (2.2), the differential operators with respect to Cartesian coordinates in Eq. (2.9) have to be expressed in terms of differential operators with respect to natural coordinates. By the chain rule, following relation can be obtained

$$\begin{Bmatrix} \dfrac{\partial}{\partial r} \\ \dfrac{\partial}{\partial s} \\ \dfrac{\partial}{\partial t} \end{Bmatrix} = \begin{bmatrix} \dfrac{\partial x_1}{\partial r} & \dfrac{\partial x_2}{\partial r} & \dfrac{\partial x_3}{\partial r} \\ \dfrac{\partial x_1}{\partial s} & \dfrac{\partial x_2}{\partial s} & \dfrac{\partial x_3}{\partial s} \\ \dfrac{\partial x_1}{\partial t} & \dfrac{\partial x_2}{\partial t} & \dfrac{\partial x_3}{\partial t} \end{bmatrix} \begin{Bmatrix} \dfrac{\partial}{\partial x_1} \\ \dfrac{\partial}{\partial x_2} \\ \dfrac{\partial}{\partial x_3} \end{Bmatrix} \tag{2.10}$$

or, in matrix notation

$$\frac{\partial}{\partial \mathbf{r}} = \mathbf{J}\frac{\partial}{\partial \mathbf{x}} \tag{2.11}$$

where **r** and **x** are position vectors in the natural and global Cartesian coordinate system, respectively, and **J** is the Jacobian operator relating derivatives with respect to the natural coordinate to those with respect to the Cartesian coordinates. The entries of **J** can be easily evaluated from Eq. (2.2). The differential operator with respect to Cartesian coordinates can be expressed from Eq. (2.11) as

$$\frac{\partial}{\partial \mathbf{x}} = \mathbf{J}^{-1}\frac{\partial}{\partial \mathbf{r}} \tag{2.12}$$

which requires that the inverse of **J** exists. This inverse exists provided that there is a one-to-one correspondence between the natural and the Cartesian coordinates of the shell element. The general explicit expression for the inverse of **J** is difficult to obtain, therefore it is usually evaluated at each integration point by numerical procedures.

With the differential operator and displacement defined in Eqs. (2.12) and (2.8), the derivative in Eq. (2.9) can be obtained and consequently the strain-displacement relation is established.

2.1.1.3 Constitutive Relation

For the linear formulation, the material behavior is assumed to be linear elastic. In the Cartesian shell-aligned coordinate system, the general Hook's law has the following form after introducing the shell assumption that the stress normal to the mid-surface of the shell element is zero.

$$\tau_e = \mathbf{C}_e \varepsilon_e \tag{2.13}$$

where

$$\tau_e^T = [\tau_{\bar{r}\bar{r}}\ \tau_{\bar{s}\bar{s}}\ \tau_{tt}\ \tau_{\bar{r}\bar{s}}\ \tau_{\bar{s}t}\ \tau_{t\bar{r}}]$$

$$\varepsilon_e^T = [\varepsilon_{\bar{r}\bar{r}}\ \varepsilon_{\bar{s}\bar{s}}\ \varepsilon_{tt}\ 2\varepsilon_{\bar{r}\bar{s}}\ 2\varepsilon_{\bar{s}t}\ 2\varepsilon_{t\bar{r}}]$$

$$\mathbf{C}_e = \frac{E}{1-\nu^2}\begin{bmatrix} 1 & \nu & 0 & 0 & 0 & 0 \\ & 1 & 0 & 0 & 0 & 0 \\ & & 0 & 0 & 0 & 0 \\ & & & \frac{1-\nu}{2} & 0 & 0 \\ & \text{symmetrical} & & & \frac{1-\nu}{2} & 0 \\ & & & & & \frac{1-\nu}{2} \end{bmatrix} \tag{2.14}$$

To transform the constitutive relation defined in Eq. (2.13) from the shell-aligned coordinate system $\bar{r}$, $\bar{s}$, t into global Cartesian coordinate system x_1, x_2 and x_3, a

transformation matrix $\mathbf{Q}_{sh}$ is introduced. The entries of the matrix $\mathbf{Q}_{sh}$ are obtained from the direction cosines of the $\bar{r}$, $\bar{s}$, t coordinate axes measured in the x_1, x_2 and x_3, coordinate directions. The matrix $\mathbf{Q}_{sh}$ can be expressed as (Bathe, 1982)

$$\mathbf{Q}_{sh} = \begin{bmatrix} l_1^2 & m_1^2 & n_1^2 & l_1m_1 & m_1n_1 & n_1l_1 \\ l_2^2 & m_2^2 & n_2^2 & l_2m_2 & m_2n_2 & n_2l_2 \\ l_3^2 & m_3^2 & n_3^2 & l_3m_3 & m_3n_3 & n_3l_3 \\ 2l_1l_2 & 2m_1m_2 & 2n_1n_2 & l_1m_2+l_2m_1 & m_1n_2+m_2n_1 & n_1l_2+n_2l_1 \\ 2l_2l_3 & 2m_2m_3 & 2n_2n_3 & l_2m_3+l_3m_2 & m_2n_3+m_3n_2 & n_2l_3+n_3l_2 \\ 2l_3l_1 & 2m_3m_1 & 2n_3n_1 & l_3m_1+l_1m_3 & m_3n_1+m_1n_3 & n_3l_1+n_1l_3 \end{bmatrix} \tag{2.15}$$

where

$$\begin{aligned} l_1 &= \mathbf{e}_1\,\mathbf{e}_{\bar{r}}\,; & m_1 &= \mathbf{e}_2\,\mathbf{e}_{\bar{r}}\,; & n_1 &= \mathbf{e}_3\,\mathbf{e}_{\bar{r}} \\ l_2 &= \mathbf{e}_1\,\mathbf{e}_{\bar{s}}\,; & m_2 &= \mathbf{e}_2\,\mathbf{e}_{\bar{s}}\,; & n_2 &= \mathbf{e}_3\,\mathbf{e}_{\bar{s}} \\ l_3 &= \mathbf{e}_1\,\mathbf{e}_t\,; & m_3 &= \mathbf{e}_2\,\mathbf{e}_t\,; & n_3 &= \mathbf{e}_3\,\mathbf{e}_t \end{aligned}$$

The constitutive relation in the global Cartesian coordinate system becomes

$$\tau = \mathbf{C}_{sh}\,\varepsilon \tag{2.16}$$

where

$$\tau^T = [\tau_{11}\ \tau_{22}\ \tau_{33}\ \tau_{12}\ \tau_{23}\ \tau_{13}]$$

$$\varepsilon^T = [\varepsilon_{11}\ \varepsilon_{22}\ \varepsilon_{33}\ 2\varepsilon_{12}\ 2\varepsilon_{23}\ 2\varepsilon_{13}]$$

$$\mathbf{C}_{sh} = \mathbf{Q}_{sh}^T\,\mathbf{C}_e\,\mathbf{Q}_{sh} \tag{2.17}$$

2.1.1.4 Virtual Work Equations

The virtual work principle can be stated as following : for any kinematically compatible deformation field (δu, $\delta\varepsilon$), the external virtual work, with consistent body forces and surface tractions, must equal to the internal virtual work. Expressing the virtual work principle in the form of an equation, the virtual work equation is

$$\int_v \tau^T\,\delta\varepsilon\,dV = \int_v \mathbf{F}^T\,\delta\mathbf{u}\,dV + \int_s \mathbf{T}^T\,\delta\mathbf{u}\ dS \tag{2.18}$$

This virtual work equation is valid for any constitutive relation provided that the virtual deformation field is small.

Substituting Eq. (2.16) into Eq. (2.18), a form of virtual work equation which is the basis of a linear formulation of the finite element method for shell structures is obtained as

$$\int_V \varepsilon^T \mathbf{C}_{sh}\, \delta\varepsilon\, dV = \int_V \mathbf{F}^T \delta\mathbf{u}\, dV + \int_S \mathbf{T}^T \delta\mathbf{u}\, dS \tag{2.19}$$

2.1.2 Nonlinear Formulation

2.1.2.1 Introduction

Linear formulations are based on the assumptions of small displacements, linear elastic constitutive relationships, and unchanging nature of the boundary conditions, as discussed in Sect. 2.1.1. If any of these assumptions is not satisfied, nonlinear effects will be introduced and a nonlinear formulation should be used for analysis. Depending on the sources from which the nonlinear effects are introduced, nonlinear analysis can be categorized into following four types.

(1) Material-nonlinear-only. In this type of nonlinear analysis, displacements and strains are assumed to be small, and only the stress-strain relation is nonlinear.

(2) Large displacement, large rotations, but small strains. In this type of nonlinear analysis, displacements and rotations of fibers may be large, but fiber extension and angle changes between fibers are small. The stress-strain relation may be linear or nonlinear.

(3) Large displacements, large rotations and large strains. In this type of nonlinear analysis, displacements and rotations of fibers may be large. Fiber extension and angle changes between fibers may also be large. The stress-strain relation may be linear or nonlinear.

(4) Contact Problems. In this type of nonlinear analysis, the boundary conditions change during the motion of the body under consideration. The displacements and rotations may be small or large, and the stress-strain relation may be linear and nonlinear.

For the purpose of analyzing a structure made from common structural materials, such as steel and concrete, the second type of nonlinear analysis is considered to be the

most appropriate formulation. In this section, a nonlinear formulation based on the assumptions of large displacements, large rotations, small strains and a nonlinear elastic-plastic stress-strain relationship is presented.

There are two fundamental approaches to describe the motion of material in a nonlinear analysis, i.e. Lagrangian (or material) formulation and Eulerian formulation. In a Lagrangian formulation, all particles of the body are followed in their motion, from the original to the final configuration of the body (Fung, 1965). In an Eulerian formulation, attention is focused on the motion of the material through a stationary control volume. Considering the analysis of solids and structures, a Lagrangian formulation usually represents a more natural and effective analytical approach than an Eulerian formulation.

In general, it is necessary to employ an incremental formulation for nonlinear analysis, because the equilibrium of the body under consideration must be established in the current configuration based on the fact that the strains and stress-strain relation are dependent on the current configuration. The motion of a general body in a stationary Cartesian coordinate system is shown in Fig. 2.3, and large displacements and rotations and nonlinear stress-strain relation are assumed to occur. The aim of incremental solution procedures is to evaluate the equilibrium configurations at the discrete time points 0, Δt, $2\Delta t$, $3\Delta t$, $\cdots$, to cover entire equilibrium path, where Δt is an increment in time.

For an effective use and understanding of notation, a convention is employed as follows (Bathe, 1982). In the stationary Cartesian coordinate system in Fig. 2.3, the coordinates of a generic point P in the body are (${}^0x_1$, ${}^0x_2$, ${}^0x_3$), (${}^tx_1$, ${}^tx_2$, ${}^tx_3$) and (${}^{t+\Delta t}x_1$, ${}^{t+\Delta t}x_2$, ${}^{t+\Delta t}x_3$) at times 0, t and t + Δt, respectively, where the left superscripts indicate the configurations of the body and the subscripts refer to the coordinate axes. For quantities such as strain and stress, a left subscript will be used to indicate the configuration with respect to which the quantities are measured.

2.1.2.2 Geometrical Relations and Displacements

The geometrical relations and displacement expressions are essentially the same as those in the linear formulation discussed in Sect. 2.1.1.1 and 2.1.1.2. In tensor notation, the coordinates and displacements at time t can be expressed as

$$ {}^tx_i(r,s,t) = {}^tx_i(r,s) + \frac{a}{2} t\, {}^tV_{3i} \qquad i = 1, 2, 3 \tag{2.20} $$

$$ {}^{t}u_i(r,s,t) = {}^{t}u_i(r,s) + \frac{a}{2} t \left({}^{t}V_{3i} - {}^{0}V_{3i} \right) \qquad i = 1, 2, 3 \tag{2.21} $$

The incremental displacements are defined as

$$ u_i(r,s,t) = {}^{t+\Delta t}u_i(r,s,t) - {}^{t}u_i(r,s,t) = u_i(r,s) + \frac{a}{2} t\, V_{3i} \qquad i = 1, 2, 3 \tag{2.22a} $$

or in terms of incremental rotations about two vectors which are orthogonal to ${}^{t}\mathbf{V}_3$ as

$$ u_i(r,s,t) = u_i(r,s) + \frac{a}{2} t \left(- {}^{t}V_{2i}\, \alpha + {}^{t}V_{1i}\, \beta \right) \qquad i = 1, 2, 3 \tag{2.22b} $$

where the vectors are defined in a similar manner to the linear formulation

$$ {}^{t}\mathbf{V}_1 = \frac{\mathbf{e}_2 \times {}^{t}\mathbf{V}_3}{|\mathbf{e}_2 \times {}^{t}\mathbf{V}_3|} \tag{2.23a} $$

$$ {}^{t}\mathbf{V}_2 = {}^{t}\mathbf{V}_3 \times {}^{t}\mathbf{V}_1 \tag{2.23b} $$

and α and β are measured with respect to configuration ${}^{t}\Gamma$.

The assumption activated in Sect. 2.1.1.2, which is that the straight line in the normal direction remains straight and normal and no change of length occurs, is also valid in the nonlinear formulation of shell structures. Therefore, thickness "a" in Eqs. (2.21) to (2.22) is considered as constant.

2.1.2.3 Stress and Strain Tensors

In nonlinear analysis including large displacements and rotations, special attention must be given to the fact that the configuration of the shell is changing continuously. This change in configuration can be dealt with in an elegant and effective manner by defining auxiliary stress and strain measures. In this section, stresses and strains are defined which are deemed to be most effective in an incremental formulation by the virtual work principle. They can be found in the book by Bathe (1982).

The Cauchy stress and its increment, denoted by ${}^{t}\tau_{mn}$ (or ${}^{t}_{t}\tau_{mn}$) and τ_{mn} (or ${}_{t}\tau_{mn}$) respectively, are the current stress and stress increment referred to the current configuration. From the Cauchy stress, a stress measure which is used most extensively, the 2nd Piola-Kirchhoff stress tensor, can be defined. At time t the 2nd Piola-Kirchhoff stress referred to the configuration at time 0 is defined as

$$ {}^{t}_{0}S_{ij} = \frac{{}^{0}\rho}{{}^{t}\rho} \, {}^{0}_{t}x_{i,m} \, {}^{t}\tau_{mn} \, {}^{0}_{t}x_{j,n} \tag{2.24} $$

where ${}^{0}\rho$ / ${}^{t}\rho$ represents the ratio of the mass densities at time 0 and time t, and

$$ {}^{0}_{t}x_{i,m} = \frac{\partial {}^{0}x_i}{\partial {}^{t}x_m} \tag{2.25} $$

Alternatively, the following relation is equally valid

$$ {}^{t}\tau_{mn} = \frac{{}^{t}\rho}{{}^{0}\rho} \, {}^{t}_{0}x_{m,i} \, {}^{t}_{0}S_{ij} \, {}^{t}_{0}x_{n,j} \tag{2.26} $$

where ${}^{t}_{0}x_{m,i}$ is now a entry of the deformation gradient tensor ${}^{t}_{0}\mathbf{X}$, which can be defined as following

$$ {}^{t}_{0}\mathbf{X} = \begin{bmatrix} \frac{\partial {}^{t}x_1}{\partial {}^{0}x_1} & \frac{\partial {}^{t}x_1}{\partial {}^{0}x_2} & \frac{\partial {}^{t}x_1}{\partial {}^{0}x_3} \\ \frac{\partial {}^{t}x_2}{\partial {}^{0}x_1} & \frac{\partial {}^{t}x_2}{\partial {}^{0}x_2} & \frac{\partial {}^{t}x_2}{\partial {}^{0}x_3} \\ \frac{\partial {}^{t}x_3}{\partial {}^{0}x_1} & \frac{\partial {}^{t}x_3}{\partial {}^{0}x_2} & \frac{\partial {}^{t}x_3}{\partial {}^{0}x_3} \end{bmatrix} \tag{2.27} $$

In the incremental form, the Eqs. (2.24) and (2.26) become

$$ {}_{0}S_{ij} = \frac{{}^{0}\rho}{{}^{t}\rho} \, {}^{0}_{t}x_{i,m} \, \tau_{mn} \, {}^{0}_{t}x_{j,n} \tag{2.28} $$

$$ \tau_{mn} = \frac{{}^{t}\rho}{{}^{0}\rho} \, {}^{t}_{0}x_{m,i} \, {}_{0}S_{ij} \, {}^{t}_{0}x_{n,j} \tag{2.29} $$

The mass density ratio in Eqs. (2.24) and (2.26) can be evaluated by applying the mass conservation law to the material under consideration which is

$$ \int_{{}^{t}V} {}^{t}\rho \, d{}^{t}x_1 \, d{}^{t}x_2 \, d{}^{t}x_3 = \int_{{}^{0}V} {}^{0}\rho \, d{}^{0}x_1 \, d{}^{0}x_2 \, d{}^{0}x_3 \tag{2.30} $$

Considering the definition of the deformation gradient tensor in Eq. (2.27), the following equation can be obtained

$$d^t x_1 \, d^t x_2 \, d^t x_3 = (\det {}_0^t\mathbf{X}) \, d^0 x_1 \, d^0 x_2 \, d^0 x_3 \tag{2.31}$$

Substituting Eq.(2.31) into Eq. (2.30), and since the relation in Eq. (2.30) must hold for any arbitrary volume, the relation of mass densities is obtained as

$${}^0\rho = (\det {}_0^t\mathbf{X}) \, {}^t\rho \tag{2.32}$$

The 2nd Piola-Kirchhoff stress tensor is symmetrical, and most importantly, its components are invariant under a rigid body rotation of the material. It should be also recognized that the 2nd Piola-Kirchhoff stresses have little physical meaning, and they do not represent the stress physically existing in the body. In practice, Cauchy stresses must be calculated in order to properly interpret the physical state in the material under consideration.

Having stress tensors defined, two strain tensors, the small strain and the Green-Lagrange Strain tensors, will be defined in the following. The small strain tensor is the same as the strain defined in Eq. (2.9) in the linear formulation except that it is defined with respect to ${}^t\Gamma$, which can be expressed in tensor notation as

$${}^t e_{ij} = \frac{1}{2} \left(\frac{\partial {}^t u_i}{\partial {}^t x_j} + \frac{\partial {}^t u_j}{\partial {}^t x_i} \right) \tag{2.33}$$

In the nonlinear formulation, the small strain tensor is normally used in the incremental form or variational form such as

$${}_t e_{ij} = \frac{1}{2} \left(\frac{\partial u_i}{\partial {}^t x_j} + \frac{\partial u_j}{\partial {}^t x_i} \right) \tag{2.34}$$

The Green-Lagrange strain tensor and its increment with respect to ${}^0\Gamma$ are defined as

$${}_0^t\varepsilon_{ij} = \frac{1}{2} \left(\frac{\partial {}^t u_i}{\partial {}^0 x_j} + \frac{\partial {}^t u_j}{\partial {}^0 x_i} + \frac{\partial {}^t u_k}{\partial {}^0 x_i} \frac{\partial {}^t u_k}{\partial {}^0 x_j} \right) \tag{2.35a}$$

$$ {}_0\varepsilon_{ij} = \frac{1}{2}\left(\frac{\partial u_i}{\partial {}^0x_j} + \frac{\partial u_j}{\partial {}^0x_i} + \frac{\partial {}^tu_k}{\partial {}^0x_i}\frac{\partial u_k}{\partial {}^0x_j} + \frac{\partial u_k}{\partial {}^0x_i}\frac{\partial {}^tu_k}{\partial {}^0x_j} + \frac{\partial u_k}{\partial {}^0x_i}\frac{\partial u_k}{\partial {}^0x_j} \right) \quad (2.35b) $$

These become the following if ${}^t\Gamma$ is taken as reference configuration

$$ {}^t\varepsilon_{ij} = \frac{1}{2}\left(\frac{\partial {}^tu_i}{\partial {}^tx_j} + \frac{\partial {}^tu_j}{\partial {}^tx_i} + \frac{\partial {}^tu_k}{\partial {}^tx_i}\frac{\partial {}^tu_k}{\partial {}^tx_j} \right) \quad (2.36a) $$

$$ {}_t\varepsilon_{ij} = \frac{1}{2}\left(\frac{\partial u_i}{\partial {}^tx_j} + \frac{\partial u_j}{\partial {}^tx_i} + \frac{\partial u_k}{\partial {}^tx_i}\frac{\partial u_k}{\partial {}^tx_j} \right) \quad (2.36b) $$

The Green-Lagrange strain tensor is symmetrical and its components are invariant under a rigid body rotation of the material. In addition, the incremental small strain tensor in Eq. (2.34), and the incremental Green-Lagrange strain tensors in Eqs. (2.35b) and (2.36b) are energetically conjugate to the Cauchy stress and 2nd Piola-Kirchhoff stress increment tensors, respectively. In other words, $\tau_{ij}\,\delta_t e_{ij}$ represents incremental virtual work at time t per unit current volume, and ${}_0S_{ij}\,\delta_0\varepsilon_{ij}$ represents incremental virtual work at time t per unit original volume. Hence, the total incremental internal virtual work can be calculated using either the Cauchy stress or 2nd Piola-Kirchhoff stress tensors as stress measures provided that the energetically conjugate strain tensors are employed and the integrations are performed over the current and original volume, respectively.

2.1.2.4 Nonlinear Constitutive Relation

As discussed in Sect. 2.1.2.1, the constitutive relation for nonlinear analysis may be linear or nonlinear. Since the linear-elastic constitutive relation has been defined in Eq. (2.13), only the nonlinear elastic-plastic constitutive relation in incremental form is discussed in this section.

The general incremental form of stress-strain relationship in terms of incremental Cauchy stresses and incremental small strains can be expressed as

$$ \tau_{ij} = {}_tC_{ijkl}\,({}_te_{kl} - {}_te^P_{kl}) \quad (2.37) $$

and also in terms of incremental 2nd Piola-Kirchhoff stresses and incremental Green-Lagrange strains as

$$ {}_0S_{ij} = {}_0C_{ijkl}\,({}_0\varepsilon_{kl} - {}_0\varepsilon^P_{kl}) \quad (2.38a) $$

$$ {}_tS_{ij} = {}_tC_{ijkl} ({}_t\varepsilon_{kl} - {}_t\varepsilon^P_{kl}) \tag{2.38b} $$

with ${}^0\Gamma$ and ${}^t\Gamma$ as reference configurations. ${}_0C_{ijkl}$ and ${}_tC_{ijkl}$ are the elasticity tensors referred to ${}^0\Gamma$ and ${}^t\Gamma$, respectively, and, ${}_te^P_{kl}$, ${}_0\varepsilon^P_{kl}$ and ${}_t\varepsilon^P_{kl}$ are the plastic components of the incremental strains. With the small strain assumption, the elasticity tensor can be considered to be independent of the configuration and both of them can be expressed as

$$ C_{ijkl} = 2\,G\,\delta_{ik}\,\delta_{jl} + \lambda_E\,\delta_{ij}\,\delta_{kl} \tag{2.39} $$

where

$$ G = \frac{E}{2\,(\,1 + \nu\,)} \tag{2.40} $$

$$ \lambda_E = \frac{\nu\,E}{(\,1 + \nu\,)(\,1 - 2\,\nu\,)} \tag{2.41} $$

with E and ν as the elastic modulus and Poisson ratio of the material. In the following derivation, the 2nd Piola-Kirchhoff stress and Green-Lagrange strain with respect to the original configuration are used. Similar equations can be obtained with the Cauchy stress and small strain.

The classical von-Mises yield function is employed here (Chen and Han, 1988) which is

$$ F\,(\,{}^t_0S_{ij}, \sigma_Y\,) = \overline{S} - \sigma_Y = 0 \tag{2.42} $$

where σ_Y is the yield stress and $\overline{S}$ is effective stress defined as

$$ \overline{S} = \sqrt{\frac{3}{2}\,{}^t_0s_{ij}\,{}^t_0s_{ij}} \tag{2.43} $$

with ${}^t_0s_{ij}$ as the deviator tensor of the 2nd Piola-Kirchhoff stress tensor, which is defined by following equation

$$ {}^t_0s_{ij} = {}^t_0S_{ij} - \frac{{}^t_0S_{kk}}{3}\,\delta_{ij} \tag{2.44} $$

The associated flow rule is used which assumes plastic strain increments to be normal to the yield surface (Chen and Han, 1988). Thus,

$$ {}_{\delta}\varepsilon_{ij}^{P} = d\lambda \frac{\partial F({}_{\delta}^{t}S_{ij}, \sigma_Y)}{\partial {}_{\delta}^{t}s_{ij}} \tag{2.45} $$

where $d\lambda$ is the plastic strain parameter which is a scalar proportionality factor. From the definition of the yield function in Eq. (2.42) and carrying out the partial differentiation, Eq. (2.45) becomes

$$ {}_{\delta}\varepsilon_{ij}^{P} = d\lambda \frac{3}{2} \frac{{}_{\delta}^{t}s_{ij}}{\bar{S}} \tag{2.46} $$

Prager's consistency condition, to insure that the stress point in stress space stays on the yield surface, is obtained by differentiation of Eq. (2.42) to yield

$$ dF = \frac{\partial F}{\partial {}_{\delta}^{t}s_{ij}} {}_{\delta}s_{ij} + \frac{\partial F}{\partial \sigma_Y} \frac{d\sigma_Y}{d\bar{\varepsilon}^P} \frac{d\bar{\varepsilon}^P}{d\lambda} d\lambda = 0 \tag{2.47} $$

where ${}_{\delta}s_{ij}$ is the incremental deviator stress tensor and $d\bar{\varepsilon}^P$ is the incremental effective plastic strain which is defined as

$$ d\bar{\varepsilon}^P = \sqrt{\frac{2}{3} {}_{\delta}\varepsilon_{ij}^{P} {}_{\delta}\varepsilon_{ij}^{P}} \tag{2.48} $$

Substituting Eq. (2.46) into Eq. (2.48), yields

$$ d\bar{\varepsilon}^P = \frac{d\lambda}{\bar{S}} \sqrt{\frac{3}{2} {}_{\delta}^{t}s_{ij} {}_{\delta}^{t}s_{ij}} = d\lambda \tag{2.49} $$

Substituting Eqs. (2.38a) and (2.45) into Eq. (2.47) and grouping the terms according to the plastic strain parameter $d\lambda$, yields

$$ \frac{\partial F}{\partial {}_{\delta}^{t}s_{ij}} C_{ijkl} {}_{\delta}\varepsilon_{ij} - \left(\frac{\partial F}{\partial {}_{\delta}^{t}s_{ij}} C_{ijkl} \frac{\partial F}{\partial {}_{\delta}^{t}s_{ij}} + \frac{d\sigma_Y}{d\bar{\varepsilon}^P} \frac{d\bar{\varepsilon}^P}{d\lambda} \right) d\lambda = 0 \tag{2.50} $$

Solving Eq. (2.50), $d\lambda$ can be obtained as

$$ d\lambda = \frac{\frac{\partial F}{\partial {}_{\delta}^{t}s_{ij}} C_{ijkl} {}_{\delta}\varepsilon_{kl}}{\frac{\partial F}{\partial {}_{\delta}^{t}s_{ij}} C_{ijkl} \frac{\partial F}{\partial {}_{\delta}^{t}s_{ij}} + \frac{d\sigma_y}{d\bar{\varepsilon}^P} \frac{d\bar{\varepsilon}^P}{d\lambda}} \tag{2.51} $$

Substituting Eq. (2.51) into Eq. (2.45), the incremental plastic strains are obtained as

$$ {}_0\varepsilon^P_{mn} = P_{mnkl}\, {}_0\varepsilon_{kl} \tag{2.52} $$

where

$$ P_{mnkl} = \frac{\dfrac{\partial F}{\partial {}_0^t s_{mn}} \dfrac{\partial F}{\partial {}_0^t s_{ij}} C_{ijkl}}{\dfrac{\partial F}{\partial {}_0^t s_{ij}} C_{ijrs} \dfrac{\partial F}{\partial {}_0^t s_{rs}} + \dfrac{d\sigma_Y}{d\bar{\varepsilon}^P} \dfrac{d\bar{\varepsilon}^P}{d\lambda}} \tag{2.53} $$

Substituting Eq. (2.52) into Eq. (2.38a), the incremental elastic-plastic relationship is obtained as

$$ {}_0S_{rs} = C^{EP}_{rskl}\, {}_0\varepsilon_{kl} \tag{2.54} $$

where C^{EP}_{rskl} is the elastic-plastic tensor of the material at the current configuration, and is defined as

$$ C^{EP}_{rskl} = C_{rsmn} (\delta_{km} \delta_{ln} - P_{mnkl}) \tag{2.55} $$

Eq. (2.54) defines the general form of the incremental elastic-plastic stress-strain relationship.

The expression of the elastic-plastic tensor C^{EP}_{rskl} can be further detailed and simplified with following derivation. Substituting Eq. (2.39) and the derivative of the yield function with respect to stress components into the numerator of Eq. (2.51), Eq. (2.51) becomes

$$ \frac{\partial F}{\partial {}_0^t s_{ij}} C_{ijkl}\, {}_0\varepsilon_{kl} = \frac{3}{2} \frac{{}_0^t s_{ij}}{\bar{S}} (2\, G\, \delta_{ik} \delta_{jl} + \lambda_E \delta_{ij} \delta_{kl})\, {}_0\varepsilon_{kl} = \frac{3\, G}{\bar{S}}\, {}_0^t s_{ij}\, {}_0\varepsilon_{kl} \tag{2.56} $$

Similarly, the first term of the denominator of Eq. (2.51) becomes

$$ \frac{\partial F}{\partial {}_0^t s_{ij}} C_{ijkl} \frac{\partial F}{\partial {}_0^t s_{ij}} = \frac{3\, G}{\bar{S}}\, {}_0^t s_{kl} \frac{3}{2} \frac{{}_0^t s_{kl}}{\bar{S}} = 3\, G \tag{2.57} $$

Eq. (2.49) results in the following equation

$$ \frac{d\bar{\varepsilon}^P}{d\lambda} = 1 \tag{2.58} $$

and the second term in the denominator of Eq. (2.51) can be derived, with reference to a uniaxial stress-strain test as shown in Fig. 2.4, as

$$\frac{d\sigma_y}{d\bar{\varepsilon}^P} = \frac{E\,E_T}{E - E_T} = H' \tag{2.59}$$

Substituting Eqs. (2.56) to (2.58) into Eq. (2.51), it becomes

$$d\lambda = \frac{{}^t_0 s_{ij}}{(1 + H'/(3G))\,\bar{S}}\,{}_0\varepsilon_{kl} \tag{2.60}$$

and Eq. (2.53) becomes

$$P_{mnkl} = \frac{3\,{}^t_0 s_{ij}\,{}^t_0 s_{ij}}{2\,(1 + H'/(3G))\,\bar{S}^2} \tag{2.61}$$

Finally, substituting Eqs. (2.39) and (2.61) into Eq. (2.55), yields

$${}^tC^{EPS}_{rskl} = (2G\delta_{rk}\,\delta_{sl} + \lambda_E\,\delta_{rs}\,\delta_{kl}) - \frac{3G}{(1 + H'/(3G))\,\bar{S}^2}\,{}^t_0 s_{kl}\,{}^t_0 s_{kl} \tag{2.62}$$

It should be pointed out that H' defined in Eq. (2.59) is infinitely large for an elastic stress state. Therefore, the elastic-plastic tensor of the material in Eq. (2.62) reverts back to the elasticity tensor. Hence, Eq. (2.62) defines a material tensor covering both elastic and elastic-plastic stress states.

From the general elastic-plastic constitutive relation defined in Eqs. (2.54) and (2.62), a specialized constitutive relation for shell structure can be established by introducing the assumption that the normal stress component in the thickness direction is zero. In the Cartesian shell-aligned coordinate system, let the subscripts 1, 2, and 3 correspond to $\bar{r}$, $\bar{s}$, and t direction, respectively. The constraint condition of zero stress in the t direction can be expressed in following equation

$${}_0S_{33} = {}^tC^{EPS}_{33kl}\,{}_0\varepsilon_{kl} = 0 \tag{2.63}$$

Solving Eq. (2.63) for the strain component in the t direction, the following equation is obtained

$$ {}_0\varepsilon_{33} = -\frac{{}^tC^{EPS}_{33kl}}{{}^tC^{EPS}_{3333}} {}_0\varepsilon_{kl} (1 - \delta_{3k}\delta_{3l}) \tag{2.64} $$

Substituting Eq. (2.64) into Eq. (2.54), the elastic-plastic constitutive relation for the shell structure can be worked out as

$$ {}_0S_{ij} = {}^tC^{EPS}_{ijkl} {}_0\varepsilon_{kl} \tag{2.65} $$

where ${}^tC^{EPS}_{ijkl}$ is the elastic-plastic tensor for shell structures and is defined as

$$ {}^tC^{EPS}_{ijkl} = (1 - \delta_{3i}\delta_{3j}) \left({}^tC^{EP}_{ijkl} - \frac{{}^tC^{EP}_{ij33}\, {}^tC^{EP}_{33kl}}{{}^tC^{EP}_{3333}} \right) \tag{2.66} $$

To obtain the elastic-plastic tensor in the global Cartesian coordinate system, the transformation defined in Eq. (2.17) for the linear formulation is also valid for the nonlinear formulation discussed in this section.

2.1.2.5 Equation of Virtual Work

Having defined the stress and strain tensors in Sect. 2.1.2.3 and constitutive relations in Sect. 2.1.2.4, equation of virtual work of the body can be developed. Two formulations, the total and updated Lagrangian formulations, are commonly adopted for nonlinear analysis of structures with the difference being the choice of the reference configuration. The total Lagrangian formulation has ${}^0\Gamma$ as the reference configuration, and therefore, all the quantities such as strains, stresses and constitutive relation are evaluated in ${}^0\Gamma$. In the updated Lagrangian formulation, ${}^t\Gamma$ is taken as reference configuration for the solution at time t+Δt. Both formulations can include all kinematic nonlinear effects and material nonlinear effects. In this section, virtual equations for both formulations will be presented.

The virtual equation of displacements for the total Lagrangian formulation is

$$ \int_{{}^0V} {}^{t+\Delta t}_0S_{ij}\, \delta^{t+\Delta t}{}_0\varepsilon_{ij}\, d^0V = \int_{{}^0V} F_i\, \delta^{t+\Delta t}u_i\, d^0V + \int_{{}^0S} T_i\, \delta^{t+\Delta t}u_i\, d^0S \tag{2.67} $$

where

$$ {}^{t+\Delta t}_{0}S_{ij} = {}^{t}_{0}S_{ij} + {}_{0}S_{ij} \tag{2.68} $$

$$ {}^{t+\Delta t}_{0}\varepsilon_{ij} = {}^{t}_{0}\varepsilon_{ij} + {}_{0}\varepsilon_{ij} \tag{2.69} $$

Decomposing the strain increment into linear and nonlinear components, Eq. (2.36) becomes

$$ {}_{0}\varepsilon_{ij} = {}_{0}e_{ij} + {}_{0}\eta_{ij} \tag{2.70} $$

where

$$ {}_{0}e_{ij} = \frac{1}{2}\left(\frac{\partial u_i}{\partial {}^{0}x_j} + \frac{\partial u_j}{\partial {}^{0}x_i} + \frac{\partial {}^{t}u_k}{\partial {}^{0}x_i}\frac{\partial u_k}{\partial {}^{0}x_j} + \frac{\partial u_k}{\partial {}^{0}x_i}\frac{\partial {}^{t}u_k}{\partial {}^{0}x_j} \right) \tag{2.71} $$

$$ {}_{0}\eta_{ij} = \frac{1}{2}\frac{\partial u_k}{\partial {}^{0}x_i}\frac{\partial u_k}{\partial {}^{0}x_j} \tag{2.72} $$

Substituting Eqs. (2.65) into (2.68) and the result into Eq. (2.67), and noting that $\delta^{t+\Delta t}{}_{0}\varepsilon_{ij} = \delta_{0}\varepsilon_{ij}$ and $\delta^{t+\Delta t}u_i = \delta u_i$, Eq. (2.67) becomes

$$ \int_{{}^{0}V} {}^{t}C^{EPS}_{ijrs}\, {}_{0}\varepsilon_{rs}\, \delta_{0}\varepsilon_{ij}\, d^{0}V + \int_{{}^{0}V} {}^{t}_{0}S_{ij}\, \delta_{0}\eta_{ij}\, d^{0}V = \int_{{}^{0}V} F_i\, \delta u_i\, d^{0}V + \int_{{}^{0}S} T_i\, \delta u_i\, d^{0}S - \int_{{}^{0}V} {}^{t}_{0}S_{ij}\, \delta_{0}e_{ij}\, d^{0}V \tag{2.73} $$

By introducing approximation that ${}_{0}\varepsilon_{rs} = {}_{0}e_{rs}$ and $\delta_{0}\varepsilon_{rs} = \delta_{0}e_{rs}$ into the first term of Eq. (2.73), the linearized virtual work equation for the total Lagrangian formulation is obtained as

$$ \int_{{}^{0}V} {}^{t}C^{EPS}_{ijrs}\, {}_{0}e_{rs}\, \delta_{0}e_{ij}\, d^{0}V + \int_{{}^{0}V} {}^{t}_{0}S_{ij}\, \delta_{0}\eta_{ij}\, d^{0}V = \int_{{}^{0}V} F_i\, \delta u_i\, d^{0}V + \int_{{}^{0}S} T_i\, \delta u_i\, d^{0}S - \int_{{}^{0}V} {}^{t}_{0}S_{ij}\, \delta_{0}e_{ij}\, d^{0}V \tag{2.74} $$

This equation is the basic equation for further finite element discretization which will be discussed in Sect. 2.1.3.

Similar equations can be developed for the updated Lagrangian formulation. The equations are presented in the following without derivation. The stresses and strains are decomposed as

$$ {}^{t+\Delta t}_{t}S_{ij} = {}^{t}\tau_{ij} + {}_{t}S_{ij} \tag{2.75} $$

$$ {}^{t+\Delta t}_{t}\varepsilon_{ij} = {}_{t}\varepsilon_{ij} \tag{2.76} $$

where the strain increment can be decomposed into linear and nonlinear components as

$$ {}_{t}\varepsilon_{ij} = {}_{t}e_{ij} + {}_{t}\eta_{ij} \tag{2.77} $$

The linear components of the strain increment are defined in Eq. (2.34) and the nonlinear component in following equation

$$ {}_{t}\eta_{ij} = \frac{1}{2}\frac{\partial u_k}{\partial {}^{t}x_i}\frac{\partial u_k}{\partial {}^{t}x_j} \tag{2.78} $$

The linearized equation of virtual displacements for the updated Lagrangian formulation is

$$ \int_{{}^{t}V} {}^{t}C^{EPS}_{ijrs}\, {}_{t}e_{rs}\, \delta_{t}e_{ij}\, d^{t}V + \int_{{}^{t}V} {}^{t}\tau_{ij}\, \delta_{t}\eta_{ij}\, d^{t}V = \int_{{}^{0}V} F_i\, \delta u_i\, d^{0}V + \int_{{}^{0}S} T_i\, \delta u_i\, d^{0}S - \int_{{}^{t}V} {}^{t}\tau_{ij}\, \delta_{t}e_{ij}\, d^{t}V \tag{2.79} $$

The integrations of the body forces and surface tractions on the right side of Eq. (2.79) are performed over ${}^{0}\Gamma$ because the body forces and surface tractions are assumed to be conservative, and these integrations are usually carried out only once at the beginning of the solution procedure. However, if the load such as pressure is treated as displacement dependent load, the integration of the load terms should be carried out over ${}^{t}\Gamma$ and updated properly as the solution proceeds.

2.1.3 Finite Element Discretization

In the previous sections, the continuum mechanics equations for linear and nonlinear analysis, which form the basis of general and displacement-based finite element analysis, are presented. Following the procedure of finite element discretization, the

governing finite element equations can be developed. In this section, only the discretization of the nonlinear equations is discussed. As linear analysis is a special case of nonlinear analysis, the governing finite element equations for this case can be established by a similar procedure.

The basic steps in the derivation of the governing finite equations are : (1) the selection of the interpolation functions; (2) the interpolation of the element coordinates and the displacements with the appropriate interpolation functions in the governing continuum mechanics equations; and, (3) by invoking the principle of virtual displacements for each of the nodal displacements in turn, the governing finite element equations are obtained. Since the governing equilibrium equations of an assemblage of elements can be constructed by the direct stiffness procedure from the contribution of each element, only a typical single element needs to be considered in the derivation.

Considering the element coordinate and displacement interpolations, it should be recognized that it is important to employ the isoparametric or the subparametric finite element approximations, which is to employ the same or lower order interpolation for the coordinates than for the displacements at any and all times during the motion of the element. Since the new element coordinates are obtained by adding the element displacements to the original coordinates, isoparametric finite element approximation assures that an assemblage of elements which are displacement-compatible across element boundaries in the original configuration will preserve this compatibility in all subsequent configurations.

In this section, matrix and vector notation will be used extensively. The correspondences between the tensor notations in previous sections and the matrix notations will be defined when they first occur, except for very obvious correspondences. As a convention, the matrices and vectors are denoted by bold characters, and their components by plain characters with right subscripts. The supscripts and left subscripts used in tensor notation are usually preserved in matrix notation.

2.1.3.1 Interpolation of Coordinates and Displacements

In this section, the interpolation of the coordinates and displacements for the "variable number of node" isoparametric shell element is discussed. A typical eight-node element in its original position and its configuration at time t is shown in Fig. 2.5. The coordinates of a generic point in the shell element which undergoes very large

displacements and rotations can be expressed in terms of the interpolation of nodal coordinates and normal direction as (Bathe, 1982)

$$ {}^{t}x_i = \sum_{k=1}^{N} h_k \, {}^{t}x_i^k + \frac{t}{2} \sum_{k=1}^{N} a_k \, h_k \, {}^{t}V_{3i}^k \tag{2.80} $$

A close resemblance between Eq. (2.80) and Eq. (2.20) is recognized by realizing that the summations in the first and second terms in Eq. (2.80) are the interpolations of coordinates on mid-surface of the element and the normal direction, respectively. N stands for the number of nodes in the element which can be varied with typical values of 4, 8, and 16 for linear, quadratic and cubic interpolation. The h_k are the interpolation functions which are defined in Figs. 2.6 and 2.7 corresponding to 8 and 16-node elements, respectively.

The summation in Eq. (2.80) is carried over all the nodes within the element. The subscript or supscript k is not a index in tensor notation, instead it is simply a indication of association with node k. This can be translated into a rule applying to equations in Sect. 2.1.3 that the summation indicated by the summation symbol does not follow the summation convention in tensor notation.

Applying the same interpolation for coordinates in Eq. (2.80) to displacements and its increment defined in Eqs. (2.21) and (2.22), they becomes

$$ {}^{t}u_i = \sum_{k=1}^{N} h_k \, {}^{t}u_i^k + \frac{t}{2} \sum_{k=1}^{N} a_k \, h_k \, ({}^{t}V_{3i}^k - {}^{0}V_{3i}^k) \tag{2.81} $$

$$ u_i = \sum_{k=1}^{N} h_k \, u_i^k + \frac{t}{2} \sum_{k=1}^{N} a_k \, h_k \, (-{}^{t}V_{2i}^k \, \alpha_k + {}^{t}V_{1i}^k \, \beta_k) \tag{2.82} $$

The finite element solution will yield the variables nodal point k, such as u_i^k, α_k and β_k, which can then be employed to evaluate accurately ${}^{t+\Delta t}V_3^k$ by the following integration

$$ {}^{t+\Delta t}V_3^k = {}^{t}V_3^k + \int_{\Delta t} (-{}^{\tau}V_2^k \, d\alpha_k(t) + {}^{\tau}V_1^k \, d\beta_k(t)) \tag{2.83} $$

${}^{t+\Delta t}V_3^k$ are needed to define the configuration and total displacement at time t+Δt in Eqs. (2.80) and (2.81). Carrying out the integration in only one interval of integration corresponds to the assumption which is demonstrated in Fig. 2.2 and used in Eqs. (2.7) and (2.82).

In matrix form, Eq. (2.82) becomes

$$\mathbf{u} = \mathbf{H}\,\hat{\mathbf{u}} \tag{2.84}$$

where

$$\mathbf{u}^T = [\ u_1\ \ u_2\ \ u_3\ ] \tag{2.85}$$

$$\hat{\mathbf{u}}^T = [\ u_1^1\ \ u_2^1\ \ u_3^1\ \ \alpha_1\ \ \beta_1\ \cdots\ u_1^N\ \ u_2^N\ \ u_3^N\ \ \alpha_N\ \ \beta_N\ ] \tag{2.86}$$

$$\mathbf{H} = \begin{bmatrix} & h_k & 0 & 0 & t\,h_k\,{}^tg_{11}^k & t\,h_k\,{}^tg_{21}^k & \\ \cdots & 0 & h_k & 0 & t\,h_k\,{}^tg_{12}^k & t\,h_k\,{}^tg_{22}^k & \cdots \\ & 0 & 0 & h_k & t\,h_k\,{}^tg_{13}^k & t\,h_k\,{}^tg_{23}^k & \end{bmatrix} \tag{2.87}$$

for nodal point k

with ${}^tg_{1i}^k$ and ${}^tg_{2i}^k$ defined as

$${}^tg_{1i}^k = -\frac{1}{2}\,a_k\,{}^tV_{2i}^k \tag{2.88a}$$

$${}^tg_{2i}^k = \frac{1}{2}\,a_k\,{}^tV_{1i}^k \tag{2.88b}$$

2.1.3.2 Strain-Displacement Matrices

Having the incremental displacement discretized in Eqs. (2.82) and (2.87), the strain-displacement matrices of the shell element can be worked out by evaluating the derivatives with which the strain-displacement relations are defined. As discussed in Sect. 2.1.2, the Green-Lagrange strains employed by the total and updated Lagrangian formulations have different expressions which will result in different expressions for strain-displacement matrices. To keep the volume of the thesis in reasonable size, only the updated Lagrangian formulation is discretized and the detailed equations and definitions of matrices are then presented.

Considering the incremental displacement s in Eq. (2.82), the derivatives with respect to the natural coordinates r, s, and t are obtained as

$$\begin{Bmatrix} u_{i,r} \\ u_{i,s} \\ u_{i,t} \end{Bmatrix} = \sum_{k=1}^{N} \begin{bmatrix} h_{k,r} & t\,{}^tg_{1i}^k\,h_{k,r} & t\,{}^tg_{2i}^k\,h_{k,r} \\ h_{k,s} & t\,{}^tg_{1i}^k\,h_{k,s} & t\,{}^tg_{2i}^k\,h_{k,s} \\ 0 & {}^tg_{1i}^k\,h_k & {}^tg_{2i}^k\,h_k \end{bmatrix} \begin{Bmatrix} u_i^k \\ \alpha_k \\ \beta_k \end{Bmatrix} \tag{2.89}$$

To evaluate the derivatives with respect to the global Cartesian coordinates at time t, ${}^t x_i$, the Jacobian transformation is defined in the following as it is in Eq. (2.12) for linear analysis. That is

$$\frac{\partial}{\partial {}^t\mathbf{x}} = {}^t\mathbf{J}^{-1} \frac{\partial}{\partial \mathbf{r}} \tag{2.90}$$

where the Jacobian matrix, ${}^t\mathbf{J}$, contains the derivatives of the current coordinates ${}^t x_i$ expressed by Eq. (2.80) with respect to the natural coordinates r, s, and t, as required by Eq. (2.10).

Substituting Eq. (2.89) into Eq. (2.90), the derivatives of incremental displacements with respect to the global Cartesian coordinates are obtained as

$$\begin{Bmatrix} \dfrac{\partial u_i}{\partial {}^t x_1} \\ \dfrac{\partial u_i}{\partial {}^t x_2} \\ \dfrac{\partial u_i}{\partial {}^t x_3} \end{Bmatrix} = \sum_{k=1}^{N} \begin{bmatrix} {}_t h_{k,1} & {}^t g^k_{1i}\, {}_t G^k_1 & {}^t g^k_{2i}\, {}_t G^k_1 \\ {}_t h_{k,2} & {}^t g^k_{1i}\, {}_t G^k_2 & {}^t g^k_{2i}\, {}_t G^k_2 \\ {}_t h_{k,3} & {}^t g^k_{1i}\, {}_t G^k_3 & {}^t g^k_{2i}\, {}_t G^k_3 \end{bmatrix} \begin{Bmatrix} u^k_i \\ \alpha_k \\ \beta_k \end{Bmatrix} \tag{2.91}$$

where

$${}_t h_{k,i} = {}^t J^{-1}_{i1}\, h_{k,r} + {}^t J^{-1}_{i2}\, h_{k,s} \tag{2.92a}$$

$${}_t G^k_i = t\,({}^t J^{-1}_{i1}\, h_{k,r} + {}^t J^{-1}_{i2}\, h_{k,s}) + {}^t J^{-1}_{i3}\, h_k \tag{2.92b}$$

and ${}^t J^{-1}_{ij}$ is the element (i,j) of the matrix ${}^t\mathbf{J}^{-1}$ in Eq. (2.90).

With the displacement derivative defined in Eq. (2.91), the strain-displacement matrices can be directly assembled. As in Eq. (2.70), the strain increment is decomposed into linear components and nonlinear components which are as following in matrix notation

$${}_t\boldsymbol{\varepsilon} = {}_t\mathbf{e} + {}_t\boldsymbol{\eta} \tag{2.93}$$

where

$${}_t\boldsymbol{\varepsilon}^T = [\, {}_t\varepsilon_{11}\ \ {}_t\varepsilon_{22}\ \ {}_t\varepsilon_{33}\ \ 2{}_t\varepsilon_{12}\ \ 2{}_t\varepsilon_{23}\ \ 2{}_t\varepsilon_{13}] \tag{2.94a}$$

$${}_t\mathbf{e}^T = [\, {}_t e_{11}\ \ {}_t e_{22}\ \ {}_t e_{33}\ \ 2{}_t e_{12}\ \ 2{}_t e_{23}\ \ 2{}_t e_{13}] \tag{2.94b}$$

$${}_t\boldsymbol{\eta}^T = [\, {}_t\eta_{11}\ \ {}_t\eta_{22}\ \ {}_t\eta_{33}\ \ 2{}_t\eta_{12}\ \ 2{}_t\eta_{23}\ \ 2{}_t\eta_{13}] \tag{2.94c}$$

Substituting the displacement derivatives in Eq. (2.91) into Eq. (2.34), the strain components are obtained as

$$ {}_t\mathbf{e} = {}_t^t\mathbf{B}_L \, \hat{\mathbf{u}} \tag{2.95} $$

where

$$ {}_t^t\mathbf{B}_L = \begin{bmatrix} \cdots & {}_th_{k,1} & 0 & 0 & {}^tg^k_{11}\,{}_tG^k_1 & {}^tg^k_{21}\,{}_tG^k_1 & \\ & 0 & {}_th_{k,2} & 0 & {}^tg^k_{12}\,{}_tG^k_2 & {}^tg^k_{22}\,{}_tG^k_2 & \\ & 0 & 0 & {}_th_{k,3} & {}^tg^k_{13}\,{}_tG^k_3 & {}^tg^k_{23}\,{}_tG^k_3 & \cdots \\ & {}_th_{k,2} & {}_th_{k,1} & 0 & ({}^tg^k_{11}\,{}_tG^k_2 + {}^tg^k_{12}\,{}_tG^k_1) & ({}^tg^k_{21}\,{}_tG^k_2 + {}^tg^k_{22}\,{}_tG^k_1) & \\ & 0 & {}_th_{k,3} & {}_th_{k,2} & ({}^tg^k_{12}\,{}_tG^k_3 + {}^tg^k_{13}\,{}_tG^k_2) & ({}^tg^k_{22}\,{}_tG^k_3 + {}^tg^k_{23}\,{}_tG^k_2) & \\ & {}_th_{k,3} & 0 & {}_th_{k,1} & ({}^tg^k_{11}\,{}_tG^k_3 + {}^tg^k_{13}\,{}_tG^k_1) & ({}^tg^k_{21}\,{}_tG^k_3 + {}^tg^k_{23}\,{}_tG^k_1) & \end{bmatrix} \tag{2.96} $$

for nodal point k

The nonlinear strain-displacement matrix will be written in a form integrated together with the stresses for the calculation of virtual work as in Eq. (2.79). The integrand of the second term on the left hand side of Eq. (2.79) can be expressed as

$$ {}^t\tau_{ij}\,\delta_t\eta_{ij} = \delta\hat{\mathbf{u}}^T\,{}_t^t\mathbf{B}_{NL}^T\,{}^t\tau\,{}_t^t\mathbf{B}_{NL}\,\hat{\mathbf{u}} \tag{2.97} $$

where

$$ {}_t^t\mathbf{B}_{NL} = \begin{bmatrix} \cdots & {}_th_{k,1} & 0 & 0 & {}^tg^k_{11}\,{}_tG^k_1 & {}^tg^k_{21}\,{}_tG^k_1 & \\ & 0 & {}_th_{k,1} & 0 & {}^tg^k_{12}\,{}_tG^k_1 & {}^tg^k_{22}\,{}_tG^k_1 & \\ & 0 & 0 & {}_th_{k,1} & {}^tg^k_{13}\,{}_tG^k_1 & {}^tg^k_{23}\,{}_tG^k_1 & \\ & {}_th_{k,2} & 0 & 0 & {}^tg^k_{11}\,{}_tG^k_2 & {}^tg^k_{21}\,{}_tG^k_2 & \\ & 0 & {}_th_{k,2} & 0 & {}^tg^k_{12}\,{}_tG^k_2 & {}^tg^k_{22}\,{}_tG^k_2 & \cdots \\ & 0 & 0 & {}_th_{k,2} & {}^tg^k_{13}\,{}_tG^k_2 & {}^tg^k_{23}\,{}_tG^k_2 & \\ & {}_th_{k,3} & 0 & 0 & {}^tg^k_{11}\,{}_tG^k_3 & {}^tg^k_{21}\,{}_tG^k_3 & \\ & 0 & {}_th_{k,3} & 0 & {}^tg^k_{12}\,{}_tG^k_3 & {}^tg^k_{22}\,{}_tG^k_3 & \\ & 0 & 0 & {}_th_{k,3} & {}^tg^k_{13}\,{}_tG^k_3 & {}^tg^k_{23}\,{}_tG^k_3 & \end{bmatrix} \tag{2.98} $$

for nodal point k

and

$$
{}^t\tau = \begin{bmatrix} {}^t\tau_{11}\,\mathbf{I}_3 & & \text{symm.} \\ {}^t\tau_{12}\,\mathbf{I}_3 & {}^t\tau_{22}\,\mathbf{I}_3 & \\ {}^t\tau_{13}\,\mathbf{I}_3 & {}^t\tau_{23}\,\mathbf{I}_3 & {}^t\tau_{33}\,\mathbf{I}_3 \end{bmatrix} \tag{2.99}
$$

with

$$
\mathbf{I}_3 = \begin{bmatrix} 1 & 0 & 0 \\ 0 & 1 & 0 \\ 0 & 0 & 1 \end{bmatrix} \tag{2.100}
$$

While the stress matrix is defined in Eq. (2.99), the stress vector is defined as

$$
{}^t\hat{\tau}^T = \left[{}^t\tau_{11}\ {}^t\tau_{22}\ {}^t\tau_{33}\ {}^t\tau_{12}\ {}^t\tau_{23}\ {}^t\tau_{13}\right] \tag{2.101}
$$

2.1.3.3 Finite Element Equation and Stiffness Matrices

With the interpolation functions and strain-displacement matrices defined in Sects. 2.1.3.1 and 2.1.3.2, the virtual work equation can be discretized. For the similar reason in previous section, only equations for updated Lagrangian formulation are presented.

Substituting Eqs. (2.84), (2.95) and (2.97) into the virtual work equation of Eq. (2.79), it becomes

$$
\begin{aligned}
&\sum \delta\hat{\mathbf{u}}^T \int_{{}^tV_e} {}^t\mathbf{B}_L^T\, {}^t\mathbf{C}^{EPS}\, {}^t\mathbf{B}_L\, d^tV\, \hat{\mathbf{u}} + \sum \delta\hat{\mathbf{u}}^T \int_{{}^tV_e} {}^t\mathbf{B}_{NL}^T\, {}^t\tau\, {}^t\mathbf{B}_{NL}\, d^tV\, \hat{\mathbf{u}} = \\
&\sum \delta\hat{\mathbf{u}}^T \int_{{}^0V_e} \mathbf{H}^T \mathbf{F}\, d^0V + \sum \delta\hat{\mathbf{u}}^T \int_{{}^0S_e} \mathbf{H}^T \mathbf{T}\, d^0S - \sum \delta\hat{\mathbf{u}}^T \int_{{}^tV_e} {}^t\mathbf{B}_L^T\, {}^t\hat{\tau}\, d^tV
\end{aligned} \tag{2.102}
$$

To simplify above equation, following definition of stiffness matrices and load vectors are introduced. The element elastic-plastic stiffness matrix and the geometric stiffness matrix are defined as

$$
\hat{\mathbf{K}}_{EP} = \int_{{}^tV_e} {}^t\mathbf{B}_L^T\, {}^t\mathbf{C}^{EPS}\, {}^t\mathbf{B}_L\, d^tV \tag{2.103}
$$

$$
\hat{\mathbf{K}}_G = \int_{{}^tV_e} {}^t\mathbf{B}_{NL}^T\, {}^t\tau\, {}^t\mathbf{B}_{NL}\, d^tV \tag{2.104}
$$

The applied load vector and internal load vector are defined as

$$\hat{\mathbf{P}} = \int_{{}^0V_e} \mathbf{H}^T \mathbf{F}\, d^0V + \int_{{}^0S_e} \mathbf{H}^T \mathbf{T}\, d^0S \tag{2.105}$$

$$\hat{\mathbf{Q}} = \int_{{}^tV_e} {}^t\mathbf{B}_L^T\, {}^t\hat{\tau}\, d^tV \tag{2.106}$$

With matrices and vectors defined above, Eq. (2.102) becomes

$$\sum \delta\hat{\mathbf{u}}^T \left(\left(\hat{\mathbf{K}}_{EP} + \hat{\mathbf{K}}_G \right) \hat{\mathbf{u}} - \hat{\mathbf{P}} + \hat{\mathbf{Q}} \right) = 0 \tag{2.107}$$

where the summation is over all elements in the analysis model. By the direct stiffness procedure, the equilibrium equation is obtained as

$$\left(\mathbf{K}_{EP} + \mathbf{K}_G \right) \mathbf{u} = \mathbf{P} - \mathbf{Q} \tag{2.108}$$

where $\mathbf{K}_{EP}$, $\mathbf{K}_G$, $\mathbf{P}$ and $\mathbf{Q}$ are global stiffness matrices and load vectors assembled from the corresponding element stiffness matrices and load vectors.

For total Lagrangian formulation, similar equations can be obtained. The main differences are that the original configuration is the reference configuration to which all the measurements should refer, and an extra term in strain expression has to be dealt with.

2.2 BEHAVIORAL CHARACTERISTICS

Shell structures have complex behavior which includes the effects of material yielding, loading conditions, large displacements, local and overall buckling and post-peak softening. Considering the special case of buried pipelines, the behavior is further complicated by the interaction between the pipeline and surrounding soil. It is believed to be beneficial to first have a overview on general shell behavior before fully exploring the behavior of buried pipelines as will be done in subsequent chapters. A general discussion on shell behavior also helps to define the required numerical solution techniques for shell analysis. Therefore, the following aspects of the general shell behavior are discussed in this section : elastic and inelastic response; buckling behavior; the effects of prebuckling deformation and large displacements; and, postbuckling and softening behavior. To limit the scope of the discussion, the emphasis is on unstiffened cylindrical shells subjected to

load combinations of axial force, bending moment and internal pressure, because these particular conditions are most representative for a pipeline. The general concepts of buckling will be presented followed by more specific discussion on the behavior of cylindrical shells under axial load and bending moment.

2.2.1 Concepts of Shell Buckling

The response of a shell structure depends on the material properties, geometric configuration, loading and boundary conditions. A shell structure fails when the maximum loading capacity as a beam or column is reached or when shell buckling occurs. Only relatively thick shells can behave as beams or columns whose failure is governed by the maximum loading capacity with undeformed cross-section. Then it can be treated as a normal beam or column. The behavior of shell structures is, however, dominated by shell buckling because of the thinness of shell wall. Shell buckling is a very complex phenomenon, and no effort is made to cover all aspects of buckling. In the following some physical explanations and definitions will be introduced to establish the basic concepts of shell buckling.

2.2.1.1 Nonlinear Collapse and Bifurcation Buckling

Shell buckling is the direct consequence of the thinness of the shell wall, as has been pointed out, for example, by Bushnell (1984). The membrane stiffness is in general several orders of magnitude greater than the bending stiffness. A thin shell can absorb a great deal of membrane strain energy without much deformation. It must deform much more in order to absorb an equivalent amount of bending strain energy. If the shell is loaded in such a way that most of its strain energy is in the form of membrane compression, and if there is a way that this stored membrane energy can be converted into bending energy, the shell may fail rather dramatically in a process called buckling as it exchanges its membrane energy for bending energy. Very large deflections are generally required to convert a given amount of membrane energy into bending energy.

The way in which buckling occurs depends on how the shell is loaded and on its geometric and material properties. The prebuckling deformation and stress may also affect the buckling process if significant non-uniformity and nonlinearity are introduced by the prebuckling process. There are two types of buckling, namely, *nonlinear collapse* and *bifurcation buckling*. If the stiffness of the structure, or the slope of the load-deflection curve has zero or negative slope and if the load is maintained as the structure deforms, such

as gravity loading, failure of the structure is usually dramatic and almost instantaneous. This type of instability failure is often called *snap-through*, because the structure will deform in a dynamic manner to an equilibrium configuration in the postbuckling regime for which the deformation may be very large. Nonlinear collapse, or snap-through buckling, can be predicted by means of nonlinear incremental analysis which follows the deformation history of the structure to locate the *limit point*.

Nonlinear collapse is a phenomenon that depends on both the loading system and the structure. A structure may initiate snap-through at different configurations for an active loading system and a reactive loading system. An *active loading system* applies specified loads directly on the structure and keeps them constant, such as gravity load. A *reactive loading system* applies loads by imposing deformations. As a result, the magnitudes of the loads depend on the stiffness of loading system. For an active loading system, snap-through initiates at the limit point on the load-deflection curve, where the energy delivered by the constant external load is larger than that the structure can absorb. This is shown in Fig. 2.12. For a reactive loading system, snap-through may initiate at a configuration in the post-peak region, where the loading system is softer than the structure. As a result, the reduction in load-carrying capacity of the structure is larger than the reduction in the external load, and the load system delivers more energy than that the structure can absorb. This is shown in Fig. 2.12. In practical application, however, the stiffness of the loading system is difficult to determine. The limit point can be conservatively taken as an approximation of the initiation of snap-through for reactive loading system. Consequently in the rest of this work the snap-through is, in general, considered to be initiated at the limit point.

Bifurcation buckling refers to another type of instability. At the buckling load, or the bifurcation point, two or more possible equilibrium paths cross each other, and the deformation begins to grow into a new pattern which is quite different from the prebuckling pattern. Whether the structure will fail immediately after bifurcation buckling depends on the postbuckling behavior of the structure. The onset of bifurcation buckling can be predicted by means of an eigenvalue analysis.

In the static analysis of perfect structures, both types of buckling are possible to occur as illustrated in Fig. 2.8. Taking the axially loaded cylindrical shell as an example, two situations may occurs as shown in Fig. 2.8(a) and 2.8(b). In the first situation, the cylinder deforms axisymmetrically along the equilibrium path OA until a maximum or *limit load* is reached at point A. The perfect shell will fail if the load is maintained, following

either the path ABC along which it continues to deform axisymmetrically, or the other path ABD along which it first deforms axisymmetrically from A to B and then non-symmetrically from B to D. Snap-through occurs at point A and bifurcation buckling at point B. The equilibrium path OABC, corresponding to the axisymmetric mode of deformation, is called the *primary* path. The path BD, corresponding to non-symmetrical mode of deformation, is called the *secondary* path. Since bifurcation buckling occurs after the snap-through, bifurcation buckling is less significant in this particular case with regard to the load carrying capacity of the structure.

A common situation is shown in Fig. 2.8(b). The bifurcation point B occurs before the limit load is reached. The primary path OAC and postbuckling path BD correspond to the axisymmetric and non-symmetrical deformation, respectively. The failure of the structure would generally be characterized by rapidly growing non-symmetrical deformations. In other words, deformation would generally follow the path OBD. In this case the limit load of the perfect structure is of less engineering significance than the bifurcation point.

2.2.1.2 Various Types of Bifurcation Buckling

For a perfect shell, various types of bifurcation buckling are shown in Fig. 2.9. A linearized model of elastic stability, that is a classical eigenvalue formulation of the buckling problem, would result in the response of neutral postbuckling shown in Fig. 2.9(a), where the amplitude of the bifurcation buckling mode is undetermined. In other words, the load P remains constant with increasing buckling mode displacement. Restricted to perfect alignment and the linear formulation, this type of response can, in general, only represent the initial postbuckling response immediately after the bifurcation point.

If nonlinear postbuckling effects are accounted for, equilibrium paths for most structures have the forms shown in Fig. 2.9(b,c,d). The asymmetric nature of the curves in Fig. 2.9(b) indicates that the structure continues to carry loads above the bifurcation load if it is forced to buckle one way. However, it collapses if it is allowed to buckle in the other way. An example of this type of behavior is for a structure with parts that come in contact and support each other for positive deflections but move away from each other, forming gaps, for similar negative deflections. The symmetric stable postbuckling behavior shown in Fig. 2.9(c) is typical of axially compressed isotropic flat plates and stiffened cylindrical shells. The symmetrical unstable postbuckling behavior shown in Fig. 2.9(d) is typical of

the early post-bifurcation regimes of axially compressed thin cylindrical shells and externally pressurized thin spherical shells.

The response of a shell structure is complicated by the fact that both snap-through and bifurcation buckling may occur. The possible equilibrium paths are summarized in Fig. 2.10 (Bushnell, 1985) based on the discussion in Sect. 2.2.1.1 and above paragraphs. The response predicted depends on the analytical approach applied to the prediction. Bifurcation buckling predicted by the classical eigenvalue formulation, in which all prebuckling deformations are neglected, is illustrated by point No. 1 in Fig. 2.10. The points corresponding to the extended eigenvalue formulation, which includes the effect of prebuckling, are Nos. 2 and 3 in Fig. 2.10. This illustrate the effects of prebuckling deformations with linear and nonlinear paths, respectively. The postbuckling behavior may follow path No. 3a in Fig. 2.10 with stable postbuckling behavior or No. 3b with unstable postbuckling behavior. In both cases, the postbuckling behavior can be symmetric or non-symmetric. In the course of the postbuckling path, secondary bifurcation points may occur as indicated by point No. 4 in Fig. 2.10. The structure may exhibit limit point buckling behavior as shown by point No. 5 in Fig. 2.10 with the possibility of bifurcation points occurring before or after the limit point.

Based on the discussion of the response of shell structures summarized in Fig. 2.10, it is recognized that any analytical approach for the complete treatment of the nonlinear and instability response of shell structures should at least contain the following two components : (1) a nonlinear incremental solution technique which can follow the entire equilibrium path; and, (2) a general bifurcation point detection-algorithm with the possibility of evaluation of the eigenvector to be used as a starting vector for the secondary equilibrium path.

2.2.1.3 Imperfection Sensitivity

In the case of real structures, unavoidable imperfections always exist. These imperfections may arise from many different sources, such as, the manufacture process, handling and transportation, material non-uniformity, imperfect alignment and geometric shape, etc. Because the imperfections usually contain, or resemble, components of both prebuckling and postbuckling deformation patterns, bifurcation buckling cannot occur in a imperfect structure. As an example, the response of a linear elastic imperfect thin cylinder subjected to axial compression will follow a primary path OEF shown by the dashed line in Fig. 2.8(b), with the failure corresponding to the snap-through limit point E at the collapse

load. The relationship between the response of the perfect and imperfect cylinder can be established by the following observations. The failure of the perfect cylinder is characterized by bifurcation buckling into a non-symmetric deformation pattern, while the failure of the imperfect cylinder beyond the limit point E involves rapid development of the non-symmetric postbuckling deformation pattern. The postbuckling deformation pattern and equilibrium paths of the perfect and imperfect cylinder in the deep postbuckling regime are very close.

For the various types of postbuckling behavior shown by the solid lines in Fig. 2.9 for perfect shells, response of linearly elastic imperfect shells are illustrated by the dashed lines in the corresponding figures. The correlation between the response of perfect and imperfect shells is demonstrated by the fact that the path of the perfect shell serves as an asymptotic path for the imperfect shell with the major difference around the bifurcation point. For shell structures with unstable postbuckling behavior, there is a difference between the bifurcation load of the perfect structure, P_c, and the limit load of the imperfect structure, P_s. The magnitude of the difference depends on the amplitude of the initial imperfection and the shape of the postbuckling path. The structure is called *imperfection sensitive* if its maximum load carrying capability is significantly reduced by imperfections.

Since imperfections may be responsible for significant reduction in load carrying capability of imperfection sensitive structures, great effort has been made to analyze and predict the magnitudes of reductions associated with imperfection sensitivity. There are mainly two types of approaches for imperfection sensitivity analysis. One is the nonlinear incremental analysis approach to trace the equilibrium path and the limit load of a structure with assumed initial imperfections, which may include prebuckling and postbuckling deformation patterns or only one of these components (Donnell and Wan, 1950; Hutchinson, 1965; Arbocz and Babcock, 1969; and, Pickney *et al*, 1983). The other is the application of Koiter's theory (Koiter, 1945, 1963a) to the initial postbuckling range (Koiter, 1963b; Tennyson and Muggeridge, 1969; Hutchinson and Amazigo, 1967; and, Amazigo and Budiansky, 1972).

The presence of imperfections converts the behavior of a perfect structure. which is usually dominated by bifurcation buckling, into that of an imperfect structure characterized by limit point collapse or snap-through. As a result, the analytical approach for an imperfect structure needs to have only the ability to trace the entire equilibrium path using a nonlinear incremental solution technique.

2.2.1.4 Effects of Prebuckling Deformation and Yielding

Significant influence on bifurcation behavior can arise from the effects of nontrivial prebuckling deformation and material yielding. There are two principal kinds of influence that the prebuckling state has on the bifurcation load and mode (Bushnell, 1985). First, the loaded shell has a different prebuckling shape from the unloaded shell, and for a given prebuckling membrane stress distribution this new shape may have different effects on the stability of the structure than for the original undeformed shape. Second, the prebuckling membrane stress distribution is an important factor to the stability. Given a prebuckling shape of the shell, different prebuckling membrane stress distributions may have drastic effects on the bifurcation load and mode shape.

Material yielding increases the non-uniformity and nonlinearity of the prebuckling response. Because yielding usually occurs in a localized area in a shell structure which introduces a relatively weakened area with regard to stiffness, the bifurcation behavior can be significantly altered. Elastic buckling is usually more sensitive to imperfections. Elastic-plastic buckling is more sensitive to prebuckling deformations, particularly to the non-uniform structural stiffness and stress distributions.

Boundary conditions also have important effects on the bifurcation load and the mode shape. The influences of boundary conditions on the stability are present through their influences on the prebuckling membrane stress distributions and deformations, and the structural stiffness at the boundary. As much as 20% difference in bifurcation load can be introduced by different boundary conditions (Hutchinson, 1965).

2.2.2 Cylindrical Shell under Axial Load

The axially compressed cylindrical shell has been a classical shell buckling problem for a long time and still attracts much attention at present. Numerous papers have been published to investigate the buckling behavior of compressed cylindrical shells, both analytically and experimentally. Instead of doing a comprehensive review on this subject, only some aspects of the buckling behavior will be discussed in this section. These include: the linear elastic buckling theory; buckling modes; nonlinear collapse; imperfection sensitivity; and, the influence of inelastic prebuckling deformations and boundary conditions.

2.2.2.1 Linear Elastic Buckling Theory

Within the framework of elastic small-displacement theory, the behavior of axially compressed cylindrical shells is governed by the following equation if the prebuckling deformation can be determined with sufficient accuracy by the linear membrane equations (Brush and Almroth, 1975).

$$D \nabla^8 w + \sigma t \nabla^4 \left(\frac{\partial^2 w}{\partial x^2}\right) + \frac{E t}{R^2} \frac{\partial^4 w}{\partial x^4} = 0 \tag{2.109a}$$

in which ∇^2 is the biharmonic operator

$$\nabla^2 = \frac{\partial^2}{\partial x^2} + \frac{\partial^2}{\partial y^2} \tag{2.109b}$$

and $D = \frac{E t^3}{12 (1-\nu^2)}$ is the bending stiffness, E and ν are Young's modulus and Poisson's ratio, R and t are the shell radius and thickness, σ is the axial stress, x is the coordinate in the axial direction, and w is displacement in the radial direction.

A critical equation can be derived from Eq. (2.109a) which is (Brush and Almroth, 1975)

$$\sigma = \frac{(\overline{m}^2+n^2)^2}{\overline{m}^2} \frac{E t^2}{12 (1-\nu^2) R^2} + \frac{\overline{m}^2}{(\overline{m}^2+n^2)^2} E \tag{2.110a}$$

where $$\overline{m} = \frac{m \pi R}{L} \tag{2.110b}$$

and m, n are the number of buckling waves in the longitudinal and circumferential directions, respectively. L in Eq. (2.110b) is the length of the cylinder. The buckling stress is the minimum solution of Eq. (2.110a) and it is determined for the cylinders of intermediate length and short length as in the following. Cylinders are classified into short and intermediate length according to the Batdorf parameter Z which is defined as (Brush and Almroth, 1975)

$$Z = \left(\frac{L}{R}\right)^2 \left(\frac{R}{t}\right) \sqrt{(1-\nu^2)} \tag{2.111}$$

Short cylinders are defined by $Z < 2.85$, and long cylinders are defined as those that buckle like Euler columns with undeformed cross section. The cylinders of intermediate length are cylinders with $Z > 2.85$ that have shell buckling characteristics.

For cylinders of intermediate length, the buckling stress determined for simply supported boundary conditions is obtained as

$$\sigma_{cr} = \frac{E}{\sqrt{3\,(1-\nu^2)}}\left(\frac{t}{R}\right) \tag{2.112a}$$

If ν is 0.3, Eq. (2.112a) becomes

$$\sigma_{cr} = 0.605\,E\left(\frac{t}{R}\right) \tag{2.112b}$$

For short cylinders, the buckling stress is obtained as

$$\sigma_{cr} = \frac{k\,\pi^2 E}{12\,(1-\nu^2)}\left(\frac{t}{L}\right)^2 \tag{2.113}$$

where $k = \dfrac{1 + 12\,Z^2}{\pi^4}$ for simply supported edges (2.114)

and $k = \dfrac{4 + 3\,Z^2}{\pi^4}$ for fully clamped edges (2.115)

2.2.2.2 Buckling Modes

Buckling modes of an axially compressed cylindrical shells depend on the type of buckling, the material and geometric properties. The elastic bifurcation buckling for perfect cylinders has two common modes (Chajes, 1985), namely, axisymmetric and non-axisymmetric buckling modes, as shown in Fig. 2.11. In general, cylinders with high diameter to thickness ratio, D/t, tend to buckle in the non-axisymmetric mode shown in Fig. 2.11(b), which is often called the "diamond mode". Cylinders with relative low D/t ratio tend to buckle in the axisymmetric mode shown in Fig. 2.11(a) which is also called the "bulging mode".

A cylinder buckled in the elastic-plastic range would usually have the axisymmetric mode. Instead of having bulges developed uniformly over the length, the deformation

would concentrate more in outward bulges near the ends where the buckling usually starts due to the radial restraint provided by the end conditions.

The mode shape for nonlinear collapse, or snap-through buckling, in the deep postbuckling range is a series of fully developed folds that contact each other to cover the entire length of the cylinder (Bushnell, 1985).

2.2.2.3 Imperfection Sensitivity

The problem of buckling of axially compressed cylindrical shells has received far more attention than most problems in structural mechanics because of the extraordinary discrepancy between the test and theory which remained unexplained for so many years. A summary and illustrations of this discrepancy can be found in many references such as the book by Brush and Almroth (1975). It has been found and confirmed by many researchers that this discrepancy arises from the extreme sensitivity of the buckling load to initial imperfections.

The axially compressed cylinder is very sensitive to small initial imperfections because the buckling load corresponds to a mode for which the axial and circumferential wavelengths are quite small compared to the radius, and the buckling is insensitive to wavelength. Thus, a great variety of small initial imperfections occuring anywhere on the entire shell surface would contain significant components of critical or almost critical bifurcation buckling mode shapes, which grow as the load increases, and eventually cause snap-through at a load far below that predicted for bifurcation buckling of the perfect shell.

The axially compressed cylinder buckling in the plastic range is not as sensitive to initial imperfection as is the elastic cylinder (Gellin, 1979, and Hutchinson, 1972). Bushnell (1985) concluded that the following facts have contributed to reduce the imperfection sensitivity of plastic buckling. First, the tangent modulus of most metals decreases by more than an order of magnitude within a stress range of 20% of the yield stress after the material yields. Second, high quality cylinders with the relatively low D/t required for plastic buckling are easier to fabricate than those with high D/t, and therefore the imperfections are relatively small. Third, predictable axisymmetric bulges due to radial end restraints grow as the load increases and are much more significant than any unknown imperfections due to fabrication and handling. The combination of these facts dramatically reduce the effect of random unknown imperfections and [illegible] reliable prediction of buckling load possible.

The nature of the imperfection sensitivity of axially compressed cylinders is determined by their postbuckling behavior. Both elastic and plastic buckling have unstable postbuckling behavior in the initial postbuckling range where a significant drop of load carrying capability occurs. The drop for elastic buckling is much more significant than that for plastic buckling which makes elastic buckling more sensitive to initial imperfections than plastic buckling.

2.2.2.4 Effects of Internal Pressure

The behavior of cylindrical shells under axial compression and internal pressure were studied by several researchers (Harris *et al*, 1957, 1961; and, Almroth, 1966). The internal pressure has been found to influence two principal aspects, the buckling mode and the buckling load.

For a cylinder which buckles elastically in a non-axisymmetric buckling mode, the buckles become smaller and more elongated in the circumferential direction as the internal pressure increases. Very high pressure can change the buckling of the cylinder from elastic buckling to elastic-plastic buckling and from the non-axisymmetric buckling mode to the axisymmetric mode. For a cylinder originally buckled in the axisymmetric mode, internal pressure reduces the dimension of the buckles in the longitudinal direction.

The elastic buckling load is relatively insensitive to the internal pressure. The plastic buckling load is usually reduced by internal pressure because of earlier yielding in the material. The cylinders with higher internal pressure are also found to be somewhat less sensitive to initial imperfections than those with lower internal pressure, because the prebuckling deformations introduced by internal pressure remove part of the initial imperfections, particularly the non-axisymmetric components.

2.2.3 Cylindrical Shell under Bending

Many aspects of the behavior of cylindrical shells under bending are similar to those of axially compressed cylinders, Nevertheless, cylinders under bending have some different behavioral characteristics because of the strain gradient over the cross-section and the ovalization introduced by bending deformation. In the following discussion, more attention is given to these differences than to the similarities. Nonlinear collapse and bifurcation buckling are covered in Sect. 2.2.3.1, and the effects of prebuckling and internal pressure in Sect. 2.2.3.2.

2.2.3.1 Nonlinear Collapse and Bifurcation Buckling

As for axially loaded cylinders, the failure of cylinders under bending has two forms. One is nonlinear collapse because the cross-section of the cylinder flattens as bending moment increases. As a consequence, its bending stiffness deteriorates, and the primary path in terms of moment-curvature curve exhibits a maximum. When this maximum moment is reached, the cylinders fails in a snap-through manner. The other is bifurcation buckling that is initiated and concentrated on the compressive side of the cylinder. Some available elastic solutions are reviewed in the following.

For an infinitely long cylinder, the nonlinear collapse moment was found by Brazier (1926) as

$$M = \frac{2\sqrt{2}}{9} \frac{E \pi R t^2}{\sqrt{1-\nu^2}} \tag{2.116}$$

If the maximum stress caused by this moment is computed with the use of the undistorted cross-section properties, it is found (with $\nu = 0.3$) to be

$$\sigma_{cr} = 0.33\, E \left(\frac{t}{R}\right) \tag{2.117}$$

The bifurcation buckling problem was solved by Seide and Weingarten (1961). Assuming that the prebuckling behavior can be defined with sufficient accuracy by a linear membrane solution, the critical buckling stress is found to be only 1.5 percent higher than the critical uniform compression stress for a shell with $D/t = 200$. For thinner shells the difference is even smaller. Thus for a practical purposes, the critical buckling stress for a uniformly compressed cylinder can be taken as the critical buckling stress for a cylinder under bending which is

$$\sigma_{cr} = 0.605\, E \left(\frac{t}{R}\right) \tag{2.118}$$

This value for bifurcation buckling is well above the critical stress for collapse in Eq. (2.117).

For a cylinder of finite length, boundary condition usually restrict deformations so that the cross-section remains circular. This restrains the cross-sectional flattening over the entire length. Finite length cylinders therefore collapse at load levels that are higher than the

one predicted by Brazier's equation in Eq. (2.117). For sufficiently short cylinders, the prebuckling behavior is approximated well by the linear membrane solution, and the collapse stress is close to the classical critical stress in Eq. (2.118) without considering initial imperfections.

For a cylinder of finite length, the displacement pattern associated with the secondary path is not orthogonal to the prebuckling displacement because of the effects of boundary conditions. Therefore, bifurcation buckling in its exact sense does not exist. However, the displacement pattern associated with the secondary path, as a component of the prebuckling displacement, is extremely small until a load level is reached at which it begins to grow rapidly. The structural behavior is therefore approximately the same as if a bifurcation point does exist.

2.2.3.2 Effects of Prebuckling Deformation and Internal Pressure

Prebuckling deformation has more significant influence on buckling behavior for a cylinder under bending than for an axially compressed cylinder, because of the interaction between the prebuckling deformation and the buckling load and mode. The flattening of the cross-section decreases the local radius of the cross-section and therefore increases the actual bending stress. Consequently, it reduces the load level at which the wrinkling pattern appears. Local yielding of material from prebuckling deformation reduces the structural stiffness and introduces non-uniformity and nonlinearity which also reduces the buckling load.

The strain gradient on the cross-section helps to restrain the buckling mode to a narrow strip on the compressive side, and makes the drop of the load carrying capability in the initial postbuckling range less significant. Therefore, the cylinder under bending is less sensitive to initial imperfections than the axially compressed cylinder.

If a cylinder with initial imperfections buckles in the plastic range, there is usually a principal buckle which is larger in terms of wavelength and amplitude than the others. The postbuckling deformation tends to concentrate in the principal buckle. The principal buckle for a cylinder without internal pressure is more likely to be an inward buckle, but the one for a cylinder with high internal pressure is an outward bulge type of buckle (Bouwkamp and Stephen, 1973). For a plastically buckled cylinder, internal pressure would in general increase the critical buckling strain but reduce the critical buckling moment.

2.2.4 Comments

In shell buckling problem, most of the attention has been given to the prediction of the critical buckling load either analytically or experimentally, because shell structures are implicitly assumed to be load carrying structures. But there are some shell structures, such as buried pipelines, for which the principal loads are deformation imposed loads rather than the externally applied loads. In these cases, the load carrying capability is less significant because the externally applied loads alone cannot fail the structure and deformation imposed loads are self-limiting in nature. The failures of this type of structure are more likely to be controlled by deformation, and therefore the prediction of postbuckling deformation including the deformation pattern and its amplitude is more important than the prediction of critical buckling load. Since postbuckling deformation, in general, is not sensitive to initial imperfections, as shown in Fig. 2.9, the analysis with respect to imperfections can be deemphasized for these structures.

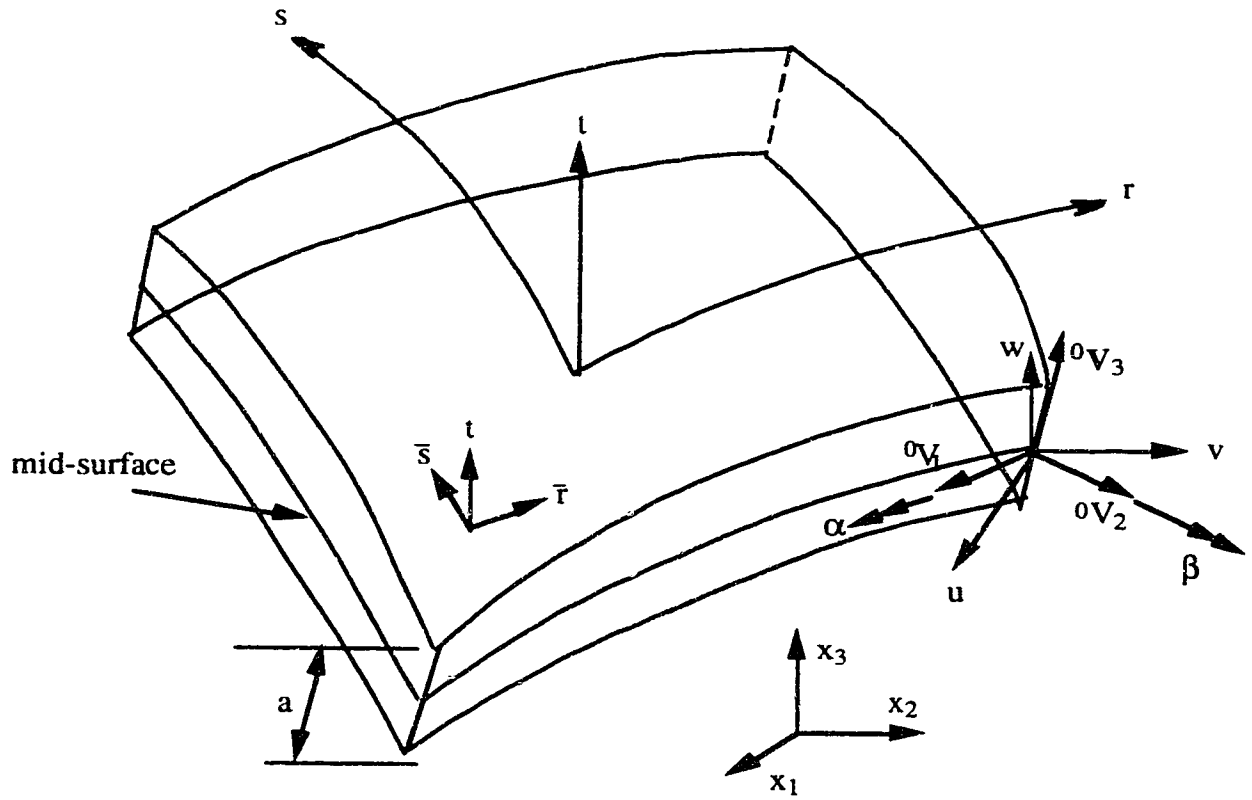

Fig. 2.1 Coordinate Systems for Shell Element

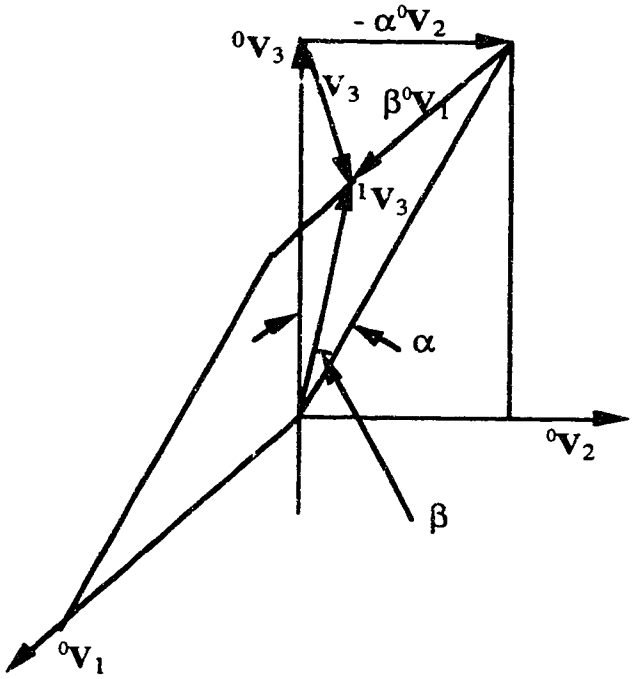

Fig. 2.2 Relation Between the Increment of Normal Direction and Its Rotations

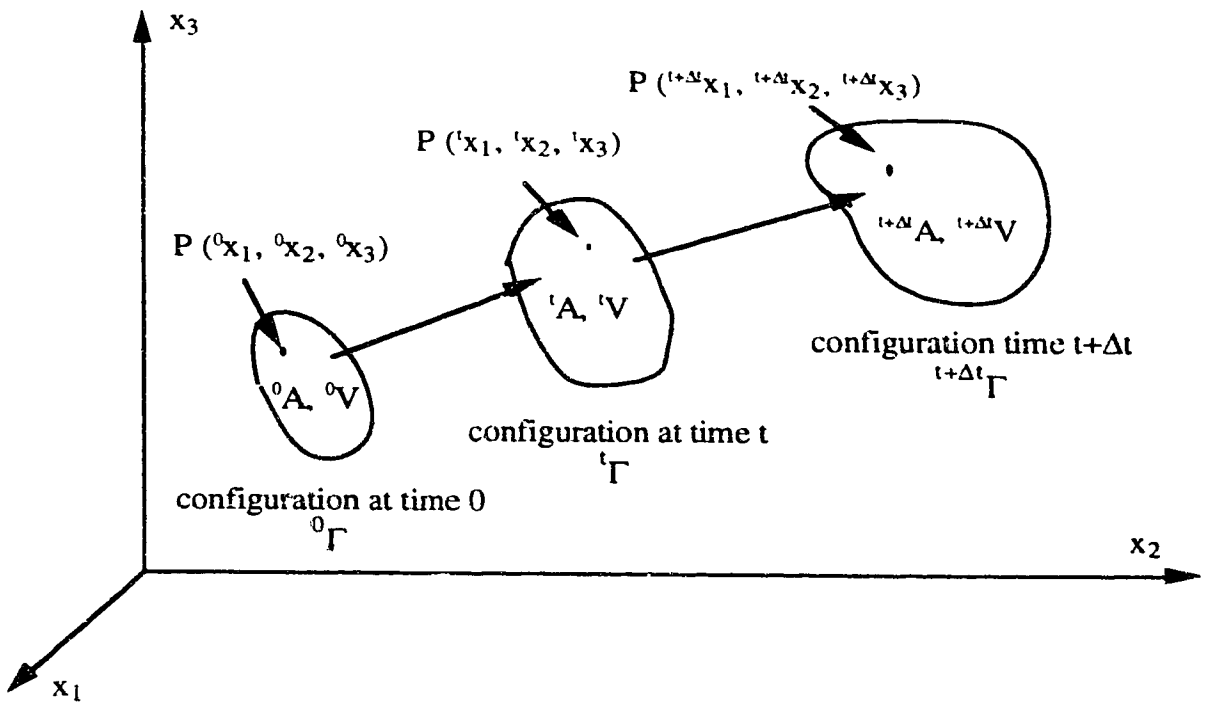

Fig. 2.3 Motion of Body in Stationary Cartesian Coordinate System

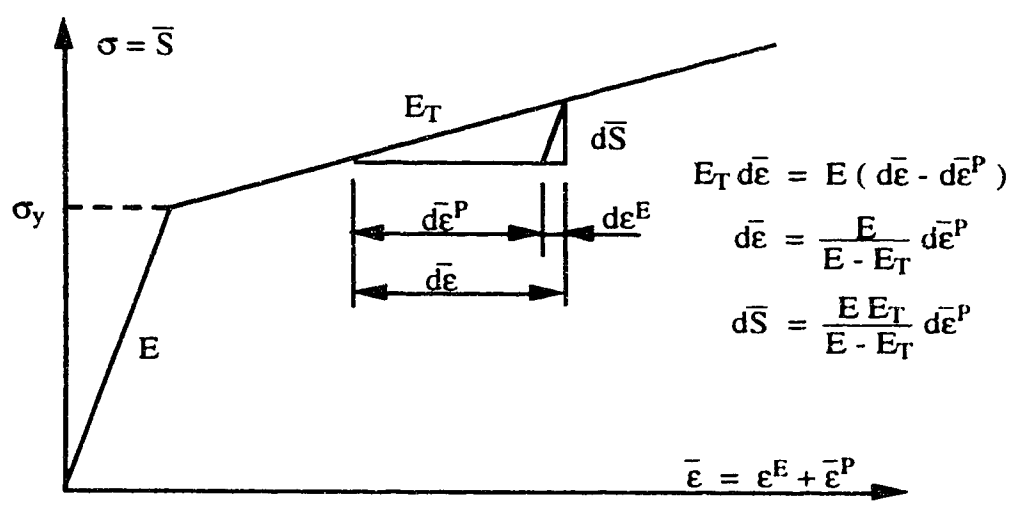

$$E_T\, d\bar{\varepsilon} = E\,(d\bar{\varepsilon} - d\bar{\varepsilon}^P)$$

$$d\bar{\varepsilon} = \frac{E}{E - E_T}\, d\bar{\varepsilon}^P$$

$$d\bar{S} = \frac{E\,E_T}{E - E_T}\, d\bar{\varepsilon}^P$$

Fig. 2.4 Equivalent Uniaxial Stress-Strain Curve

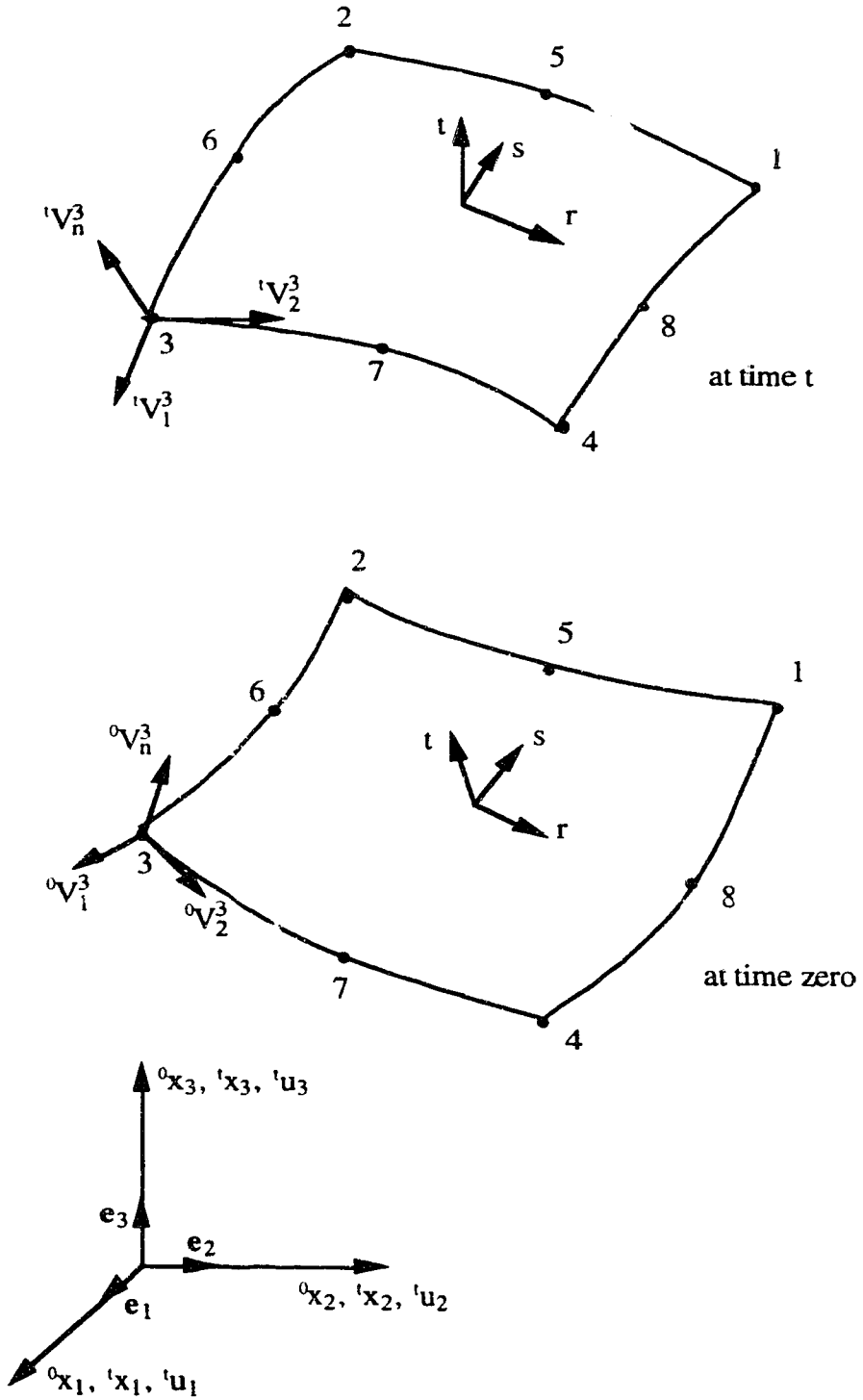

Fig. 2.5 Shell Element Undergoing Large Displacements and Rotations

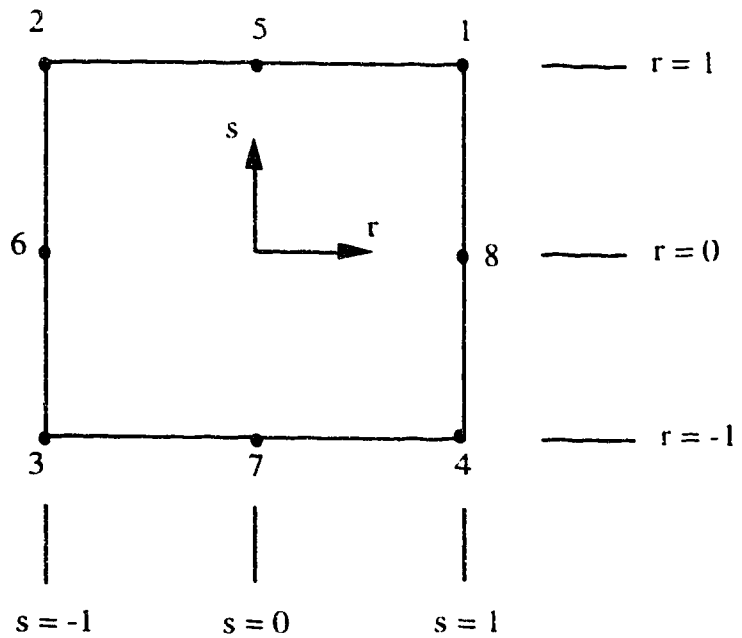

$$h_1 = \frac{1}{4} r s (1 + r) (1 + s)$$

$$h_2 = \frac{1}{4} r s (1 - r) (1 + s)$$

$$h_3 = \frac{1}{4} r s (1 - r) (1 - s)$$

$$h_4 = \frac{1}{4} r s (1 + r) (1 - s)$$

$$h_5 = \frac{1}{2} s (1 - r^2) (1 + s)$$

$$h_6 = -\frac{1}{2} r (1 - s^2) (1 - r)$$

$$h_7 = -\frac{1}{2} s (1 - r^2) (1 - s)$$

$$h_8 = \frac{1}{2} r (1 - s^2) (1 + r)$$

Fig. 2.6 Interpolation Functions for Eight-Node Shell Element

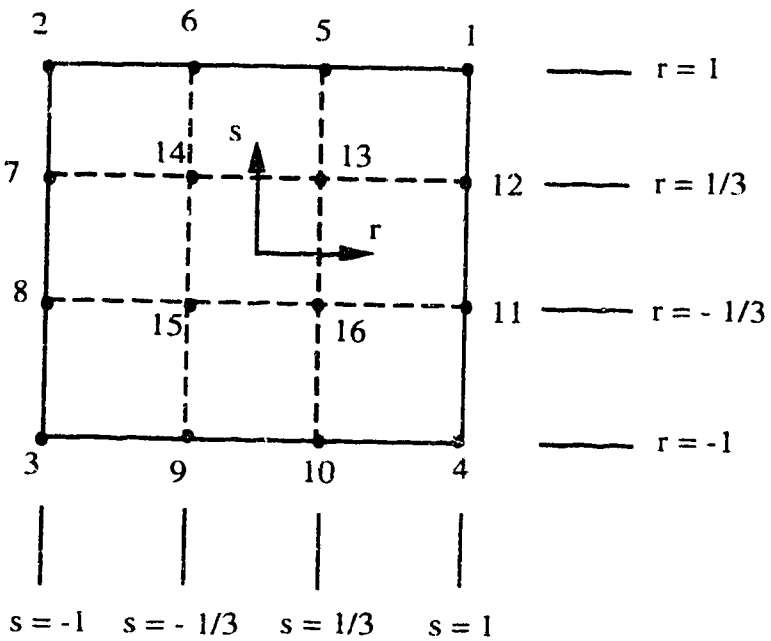

$$h_1 = \frac{81}{256}(r^2-\frac{1}{9})(s^2-\frac{1}{9})(1+r)(1+s)$$
$$h_2 = \frac{81}{256}(r^2-\frac{1}{9})(s^2-\frac{1}{9})(1-r)(1+s)$$
$$h_3 = \frac{81}{256}(r^2-\frac{1}{9})(s^2-\frac{1}{9})(1-r)(1-s)$$
$$h_4 = \frac{81}{256}(r^2-\frac{1}{9})(s^2-\frac{1}{9})(1+r)(1-s)$$
$$h_5 = \frac{243}{256}(r+\frac{1}{3})(s^2-\frac{1}{9})(1-r^2)(1+s)$$
$$h_6 = \frac{243}{256}(-r+\frac{1}{3})(s^2-\frac{1}{9})(1-r^2)(1+s)$$
$$h_7 = \frac{243}{256}(r^2-\frac{1}{9})(s+\frac{1}{3})(1-r)(1-s^2)$$
$$h_8 = \frac{243}{256}(r^2-\frac{1}{9})(-s+\frac{1}{3})(1-r)(1-s^2)$$
$$h_9 = \frac{243}{256}(-r+\frac{1}{3})(s^2-\frac{1}{9})(1-r^2)(1-s)$$
$$h_{10} = \frac{243}{256}(r+\frac{1}{3})(s^2-\frac{1}{9})(1-r^2)(1-s)$$
$$h_{11} = \frac{243}{256}(r^2-\frac{1}{9})(-s+\frac{1}{3})(1+r)(1-s^2)$$
$$h_{12} = \frac{243}{256}(r^2-\frac{1}{9})(s+\frac{1}{3})(1+r)(1-s^2)$$
$$h_{13} = \frac{729}{256}(r+\frac{1}{3})(s+\frac{1}{3})(1-r^2)(1-s^2)$$
$$h_{14} = \frac{729}{256}(-r+\frac{1}{3})(s+\frac{1}{3})(1-r^2)(1-s^2)$$
$$h_{15} = \frac{729}{256}(-r+\frac{1}{3})(-s+\frac{1}{3})(1-r^2)(1-s^2)$$
$$h_{16} = \frac{729}{256}(r+\frac{1}{3})(-s+\frac{1}{3})(1-r^2)(1-s^2)$$

Fig. 2.7 Interpolation Functions for Sixteen-Node Shell Element

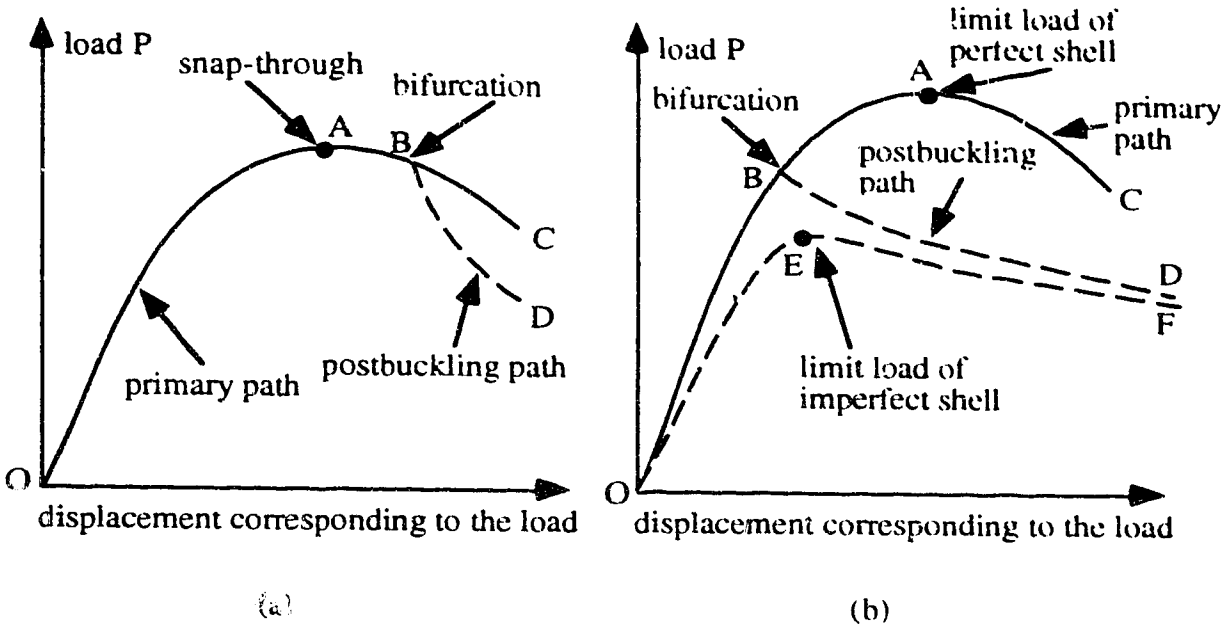

Fig. 2.8 Snap-Through and Bifurcation Buckling for Axially Compressed Cylinder

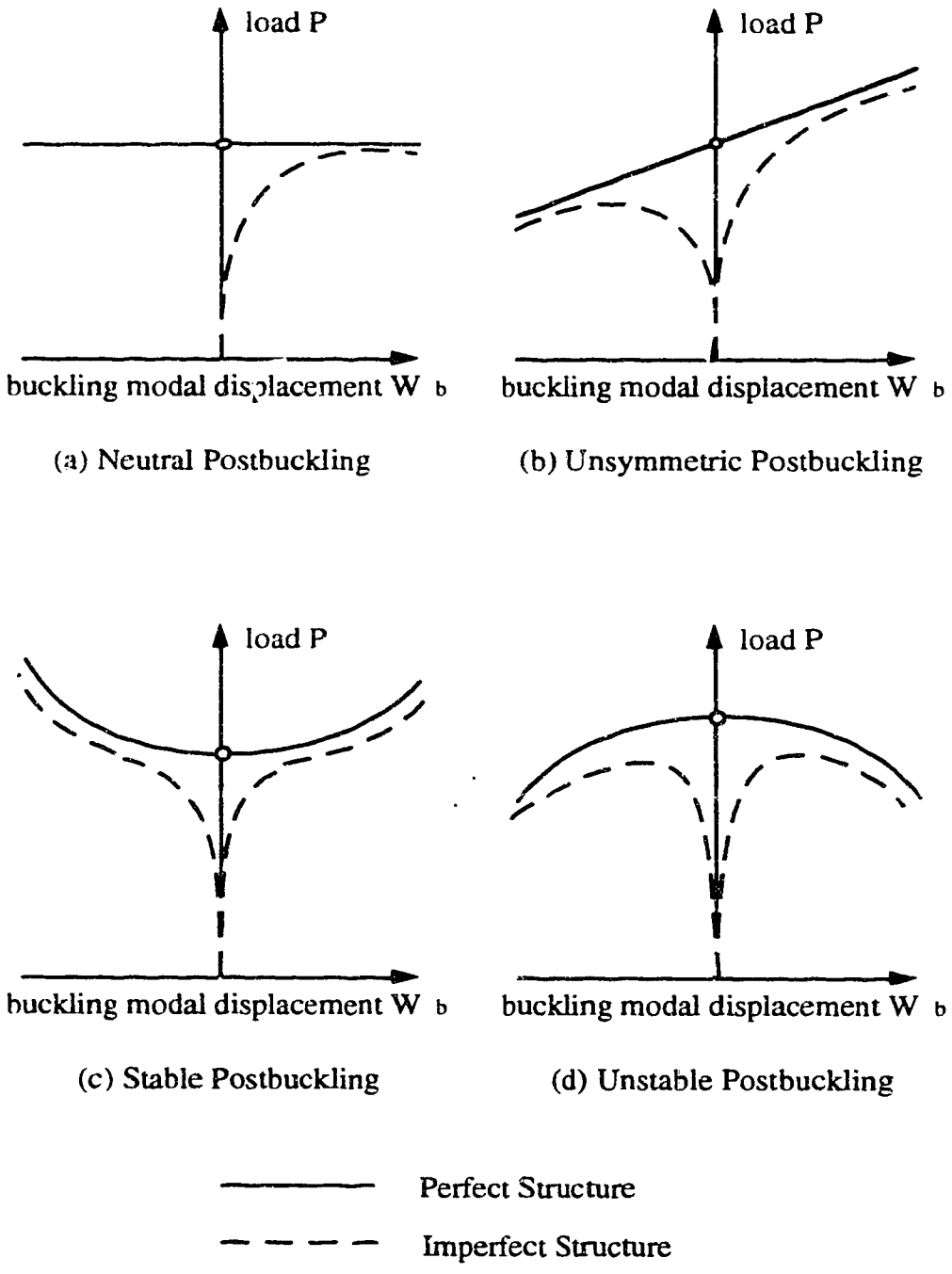

Fig. 2.9 Various Types of Load-Displacement Relations

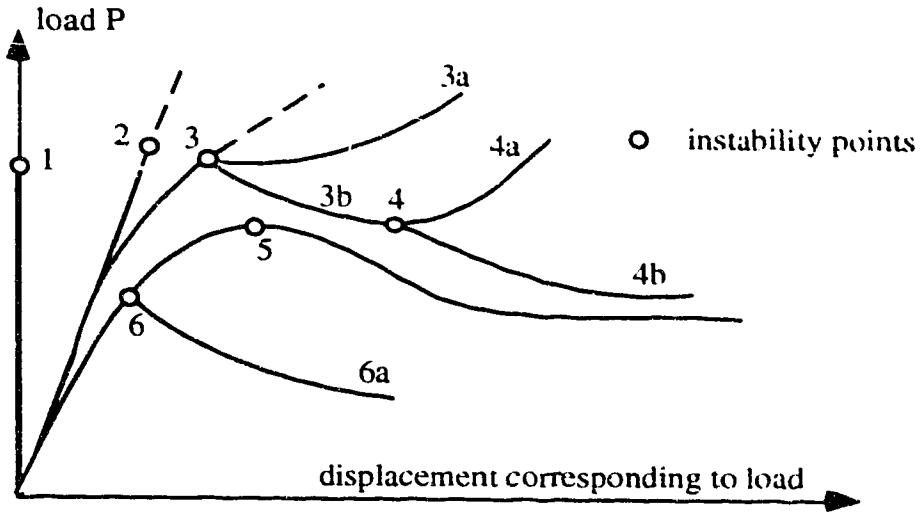

Fig. 2.10 Equilibrium Paths with Snap-Through and Bifurcation Buckling

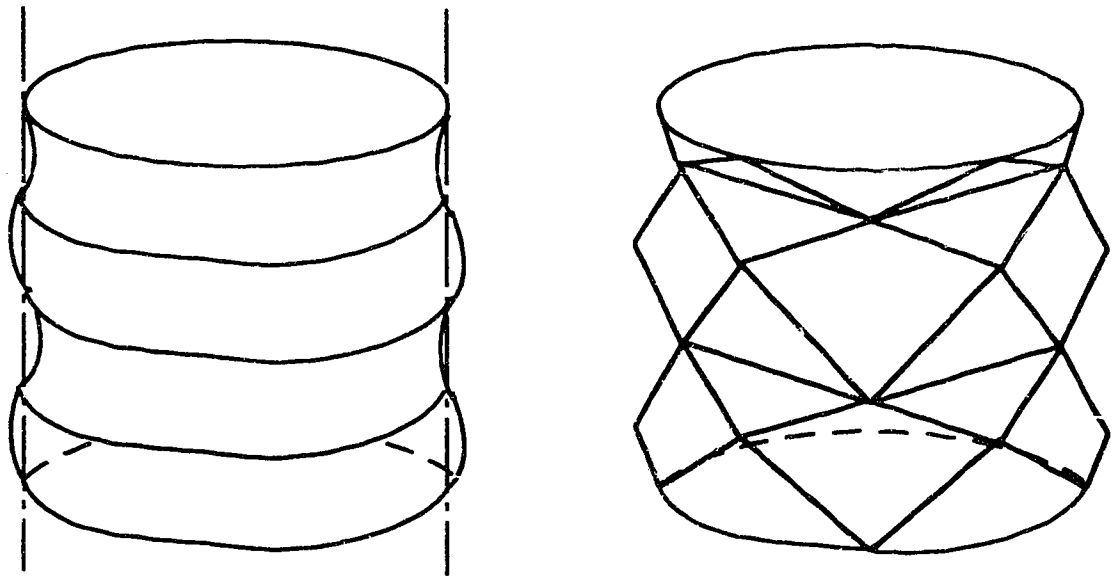

(a) axisymmetric mode (b) non-axisymmetric mode

Fig. 2.11 Bifurcation Buckling Modes for Perfect Elastic Cylinder

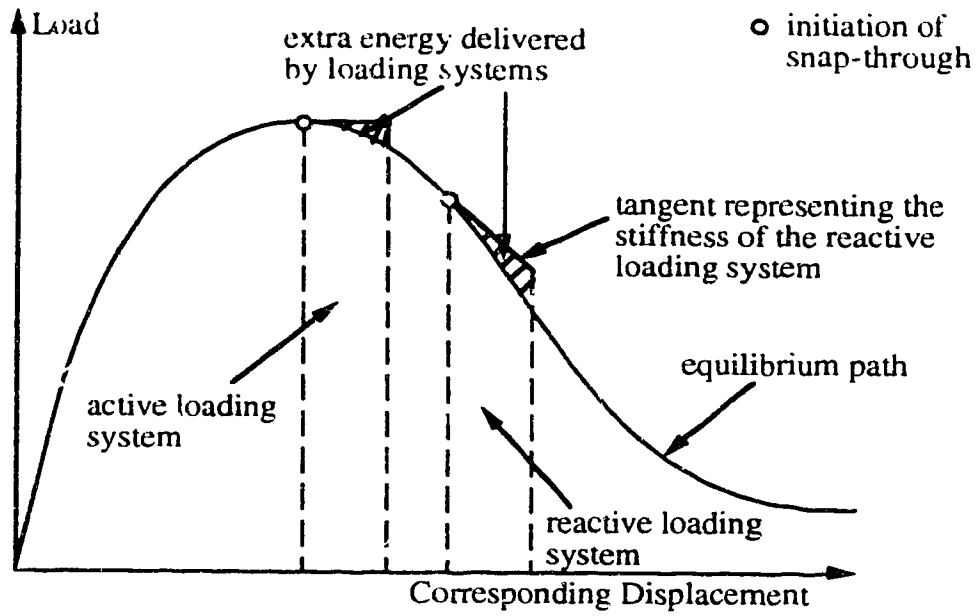

Fig. 2.12 Initiation of Snap-Through under Active and Reactive Loading Systems

CHAPTER 3 NUMERICAL SOLUTION TECHNIQUES

In this chapter, the solution technique for the set of nonlinear algebraic equations that arises after discretization of a nonlinear continuum is treated in some detail. The chapter starts with an overview of existing procedures that can be used to obtain a properly converged solution. The arc-length control technique is considered to be one of the most elegant procedures for nonlinear structural analysis at the present time. However, deficiencies are found when it is applied to three-dimensional shell analysis with softening characteristic. An improved iterative arc-length control is then proposed. Finally, a solution procedure designed for postbuckling analysis is developed based on a direct search technique which has been commonly used in optimization. As a basic tool for subsequent analysis, such a robust and efficient solution procedure is a very important component of this project.

3.1 OVERVIEW OF SOLUTION PROCEDURES

A difficulty in nonlinear analysis is the dependency of the stiffness and internal forces on the displacements, which has to be accounted for by the solution procedure. Various procedures have been developed with different ways to deal with this dependency. The most desirable features of solution procedures are stability and efficiency, but it is often difficult to accomplish both of them simultaneously, especially for problems with severe nonlinearity and local conditions of loading and unloading. If the fundamental phenomena required by the analysis can be captured by the solution procedure, approximation and simplification can be introduced to improve its efficiency, which is often sacrificed to insure stability. Consequently many alternatives have been explored and it is not the intention herein to review all solution procedures developed in the past. In this section, the incremental-iterative procedure for static analysis of nonlinear structures is first reviewed. This defines a basic formulation for solution procedures. The Newton-Raphson procedure, which is the classical procedure, is then discussed. Control techniques such as load, displacement, arc-length and indirect control are then presented. Finally, the reduction method and multi-dimensional search techniques are introduced. This serves as background for the solution procedure developed herein based on a search technique, as discussed in Sect. 3.3.

3.1.1 Incremental-Iterative Solution Procedure

Nonlinear finite element analysis will, in general, end up with the following set of

equations

$$\mathbf{K}\,\mathbf{u} = \mathbf{P} - \mathbf{Q} \tag{3.1}$$

where $\mathbf{K}$ is the stiffness matrix, $\mathbf{u}$ is the incremental nodal displacement vector, and $\mathbf{P}$ and $\mathbf{Q}$ are the external and the equilibrating force vectors respectively as shown in Fig. 3.1. For nonlinear analysis, $\mathbf{K}$ and $\mathbf{Q}$ depend on the displacements and stresses in the structure which is a direct consequence of the nonlinear structural behavior. When a structure is in equilibrium, the difference between the equilibrating forces and the external loads vanish.

In principle it would be possible to impose the entire external load in a single step, but this is not very sensible in practical applications because iterative procedures usually have a hard time to converge towards a proper solution for large load steps, and the path-dependent material behavior requires relatively small strain increments to insure the accuracy of the prediction. Consequently, it is recommended to apply the total external load in a number of small loading steps (or increments). Such a procedure is usually called an *incremental procedure* and is illustrated in Fig. 3.2. Starting from a known displacement vector $\mathbf{u}_n$, an incremental displacement may be calculated according to

$$\mathbf{K}\,\Delta\mathbf{u} = \Delta\mathbf{P} + \mathbf{P}_n - \mathbf{Q} \tag{3.2}$$

where the total external load is decomposed to a contribution $\mathbf{P}_n$ that is already present at the beginning of the load step and a load increment $\Delta\mathbf{P}$.

In the solution by incremental noniterative procedures, a significant drifting of the predicted path from the true equilibrium path may occur as shown in Fig. 3.2. There are two principal reasons for the drifting. One is the unbalanced loads at the end of each loading step because perfect convergence is seldom accomplished. These unbalanced loads will be carried along in all subsequent loading steps, which implies that the errors will be accumulated and cause a significant drift. The other is the fact that the tangential stiffness matrix may be derived through linearization of the nonlinear equations at the beginning of the loading step which is only valid, strictly speaking, at the beginning of the loading step. The tangent stiffness matrix is only an approximation for the loading step, and an error is therefore introduced and accumulated. This gradual departure of the numerical solution from the true solution can be prevented or at least substantially reduced, by adding equilibrium iterations within each loading step which defines an *incremental-iterative procedure*.

In an incremental-iterative solution procedure, a first estimate for the displacement increment is made through

$$\Delta \mathbf{u}_1 = \mathbf{K}^{-1} (\Delta \mathbf{P} + \mathbf{P}_n - \mathbf{Q}_0) \tag{3.3}$$

where the subscript 1 for $\Delta \mathbf{u}$ signifies the estimate in the first iteration for the incremental displacement vector. Likewise, the subscript 0 of the internal force vector Q relates to the fact that the vector is calculated using the stresses at the beginning of the loading step or the end of the previous loading step. From the incremental displacement vector $\Delta \mathbf{u}_1$, a first estimate of the $\Delta \varepsilon_1$ strain increment can be calculated, and then the stress increment $\Delta \sigma_1$ can be evaluated through the tangential stress-strain law. In a finite element formulation the equilibrating forces after the first iteration are given by (see Eq. (2.106))

$$\mathbf{Q}_1 = \int \mathbf{B}^T (\sigma_0 + \Delta \sigma_1) \, dV \tag{3.4}$$

where $\mathbf{B}$ is the strain-displacement operator, and σ_0 is stress at the previous converged configuration. In general, equilibrating forces $\mathbf{Q}_1$ are not in balance with the external load $\Delta \mathbf{P}+\mathbf{P}_n$. For this reason a correction to the displacement increment is necessary which is

$$\mathbf{du}_2 = \mathbf{K}^{-1} (\Delta \mathbf{P} + \mathbf{P}_n - \mathbf{Q}_1) \tag{3.5}$$

The accumulated displacement increment becomes (see Fig. 3.3)

$$\Delta \mathbf{u}_2 = \Delta \mathbf{u}_1 + \mathbf{du}_2 \tag{3.6}$$

Repetition of this process can be formulated mathematically as

$$\mathbf{du}_{j+1} = \mathbf{K}^{-1} (\Delta \mathbf{P} + \mathbf{P}_n - \mathbf{Q}_j) \tag{3.7}$$

$$\Delta \mathbf{u}_{j+1} = \Delta \mathbf{u}_j + \mathbf{du}_{j+1} \tag{3.8}$$

$$\Delta \varepsilon_{j+1} = \mathbf{B} \, \Delta \mathbf{u}_{j+1} \tag{3.9}$$

$$\Delta \sigma_{j+1} = f(\Delta \varepsilon_{j+1}) \tag{3.10}$$

$$\sigma_{j+1} = \sigma_0 + \Delta \sigma_{j+1} \tag{3.11}$$

This iterative process ultimately results in stresses that are in equilibrium with each other

and with the applied external load to within some user-prescribed convergence tolerance.

3.1.2 Newton-Raphson Iterative Procedures

Newton-Raphson (N-R) iteration is one of the classical iterative procedures. In the full Newton-Raphson iteration, the tangent stiffness matrix is updated and factorized in every iteration as shown in Fig. 3.4. The advantage of this scheme is quadratic convergence which becomes the characteristic of N-R iteration. The disadvantage is the high cost to evaluate and factorize the stiffness matrix in every iteration, which may not be necessary.

It is recognized that updating the stiffness matrix in every iteration, as in the full N-R iteration, is by no means necessary since it is quite irrelevant which stiffness matrix is being used to iterate towards equilibrium as long as the stresses are determined in a proper manner and the resulting equilibrating force vector is computed on the basis of these stresses. This has motivated several researchers to seek for methods which obviate the need to construct and decompose a tangent stiffness matrix in every iteration. There are, in general, two classes of such methods. In the first class, the stiffness is obtained by setting up a new tangent stiffness, either every few iterations or only once within a loading step. Basically, it is assumed that the stiffness matrix varies so slowly that the stiffness matrix set up in a particular iteration serves as a sufficiently accurate approximation of the tangent stiffness matrix for several subsequent iterations. The second class of methods consists of the so called Quasi-Newton or Secant-Newton methods. These methods apply updates on existing tangential matrices such that the stiffness in the subsequent iterations is computed using a multi-dimensional secant approximation.

One example of the alternatives on the full N-R scheme, that exists within the first class defined above, is *modified N-R iteration* as shown in Fig. 3.5. Here the stiffness matrix is set up and decomposed only at the beginning of every loading step. The modified N-R iteration loses the quadratic convergence characteristic of the full N-R iteration, but often the slowing down of the convergence rate is off-set by the gain in computer time within each iteration.

3.1.3 Load and Displacement Control

There are two methods to control the application of the load and the process of achieving convergence within each loading step. First, the external load can be directly applied in a number of steps and kept constant for that step. This is usually called *load*

control because a specific load level is specified for each of loading step. Second, the increments of one or more displacements can be prescribed which causes development of stress increments within the specimen and then results in incremental reactive nodal forces at the nodes where the displacement increments are prescribed. Summation of these generated incremental nodal forces gives the total reactive forces, which equal the external loads, for the prescribed displacements. This process is often called *displacement control.*

Often the physics of the problems dictates which type of application is the most obvious choice. However when there is no preference for either load or displacement control from a physical point of view, the latter method is nearly always to be preferred. One reason for this is that the tangent stiffness matrix is better conditioned for displacement control than for load control, and consequently faster convergence of the iterative procedure can be expected. Another reason is that under load control, the tangent stiffness matrix becomes singular at a limit point in the load-deflection diagram. The tangent stiffness matrix of the displacement controlled problem on the other hand does not become singular.

Decomposing the incremental displacement vector **du** into a vector that contains only degrees of freedom that are free, $\mathbf{du}_f$, and displacement increments that have prescribed nonzero values, $\mathbf{du}_p$, it can be written for the first and subsequent increments, respectively, as

$$\mathbf{du}^1 = \begin{Bmatrix} \mathbf{du}_f^1 \\ \mathbf{du}_p^1 \end{Bmatrix} \tag{3.12a}$$

$$\mathbf{du}^j = \begin{Bmatrix} \mathbf{du}_f^j \\ 0 \end{Bmatrix} \qquad j = 2,3,\cdots \tag{3.12b}$$

In a similar way the tangent stiffness matrix can be partitioned as follows

$$\mathbf{K} = \begin{bmatrix} \mathbf{K}_{ff} & \mathbf{K}_{fp} \\ \mathbf{K}_{pf} & \mathbf{K}_{pp} \end{bmatrix} \tag{3.13}$$

With Eqs. (3.12) and (3.13), Eq. (3.2) becomes

$$\begin{bmatrix} \mathbf{K}_{ff} & \mathbf{K}_{fp} \\ \mathbf{K}_{pf} & \mathbf{K}_{pp} \end{bmatrix} \begin{Bmatrix} \mathbf{du}_f^{j+1} \\ \mathbf{du}_p^{j+1} \end{Bmatrix} = - \begin{Bmatrix} \mathbf{Q}_f^j \\ 0 \end{Bmatrix} \tag{3.14}$$

where $\mathbf{Q}_f^j$ are the equilibrating forces corresponding to the free degrees of freedom,

respectively, at the end of the iteration j in the loading step n. It has been assumed in Eq. (3.14) that no other forces act on the structure apart from the prescribed displacements. The free displacement increment can be determined by solving the first equation in Eq. (3.14). For the first iteration it becomes

$$\mathbf{du}_f^1 = -\mathbf{K}_{ff}^{-1}(\mathbf{K}_{fp}\,\mathbf{du}_p^1 + \mathbf{Q}_{nf}^0) \tag{3.15}$$

and for subsequent iterations, it becomes

$$\mathbf{du}_f^{j+1} = -\mathbf{K}_{ff}^{-1}\,\mathbf{Q}_n^j \qquad j = 1,2,\cdots,n \tag{3.16}$$

Comparison of Eqs. (3.2) and (3.15) shows that for the first iteration the external load, $\Delta\mathbf{P}+\mathbf{P}_n$, must be replaced by the 'equivalent force vector', $\mathbf{K}_{fp}\,\mathbf{du}_p^1$, when switching from load to displacement control. In the subsequent iterations, this contribution vanishes for displacement control.

The most important mathematical difference between load control and displacement control lies in the fact that load control requires the inversion (or in practice the LDU-decomposion) of the stiffness matrix $\mathbf{K}$ while in the latter method only the reduced stiffness matrix $\mathbf{K}_{ff}$ needs to be inverted. Graphically, the solution for the load controlled process may be represented by the intersection between the horizontal line on the load-displacement diagram, which characterizes the load level imposed on the structure, and the load-displacement path as shown in Fig. 3.6. In a displacement controlled process an intersection between the vertical line, which characterizes the magnitude of the displacement, and the load-displacement path as shown in Fig. 3.7 represents the solution. As shown in Fig. 3.6 the load controlled iterative process diverges when the horizontal line does not intersect the load-displacement path. This condition manifests itself in an unbounded growth of unbalanced load. Consequently, load control is not applicable to problems which exhibit limit point and, thereafter, snap-through behavior.

Displacement control does not share this disadvantage, since the intersection between a vertical line and load-displacement path can always be found for this type of behavior. Nevertheless, some types of structural behavior are still not traceable with a displacement controlled procedure. An example is shown in Fig. 3.7 where snap-back behavior, which is often encountered in thin shells and cracking of concrete, is illustrated. A restriction on displacement control is that displacement control, in general, can be applied to only one degree of freedom. It can be applied to more degrees of freedom if the relative

ratios between these degrees of freedom are specified.

3.1.4 Arc-Length Control and Indirect Displacement Control

Due to the limitations of load and displacement controls, alternative are sought. One of the most elegant procedures that can be used to analyze nonlinear structural response is known as *arc-length control* (Wempner, 1971, Riks, 1972, 1979, and Ramm, 1980). This method can be explained starting from Eq. (3.7) as follows. Expressing the load increment $\Delta\mathbf{P}$ by $\Delta\lambda_{j+1}\widehat{\mathbf{P}}$, with λ as a scalar load factor and $\widehat{\mathbf{P}}$ as a reference load vector, gives

$$d\mathbf{u}_{j+1} = \mathbf{K}^{-1}\left(\Delta\lambda_{j+1}\widehat{\mathbf{P}} + \mathbf{P}_n - \mathbf{Q}_j\right) \tag{3.17}$$

for the correction to the displacement increment, where

$$\Delta\lambda_{j+1} = \Delta\lambda_j + d\lambda_{j+1} \tag{3.18}$$

The essence of the arc-length control is now that the correction to the displacement increment in iteration j+1, $d\mathbf{u}_{j+1}$, is conceived to be the sum of two separate contributions. The first part is purely due to the external load components that are being incremented within this load step and represented by the reference load $\widehat{\mathbf{P}}$

$$d\mathbf{u}^{I}_{j+1} = \mathbf{K}^{-1}\,\widehat{\mathbf{P}} \tag{3.19}$$

The second part is the response to the unbalanced forces, namely the difference between the sum of all external loads and the equilibrating forces after iteration j,

$$d\mathbf{u}^{II}_{j+1} = \mathbf{K}^{-1}\left(\Delta\lambda_j\widehat{\mathbf{P}} + \mathbf{P}_n - \mathbf{Q}_j\right) \tag{3.20}$$

Comparison of Eqs. (3.19) and (3.20) with Eq. (3.17) shows that

$$d\mathbf{u}_{j+1} = d\lambda_{j+1}\,d\mathbf{u}^{I}_{j+1} + d\mathbf{u}^{II}_{j+1} \tag{3.21}$$

The crucial difference from load control is that the increment of scalar load factor is no longer fixed and is considered as an additional variable, which is determined by an additional equation that is usually called the *constraint equation.* This constraint equation is established based on a constraint condition on the step size, such as, that the Euclidean norm of the accumulated incremental displacement vector,$\Delta\mathbf{u}_{j+1}$, and the accumulated increment of load factor, $\Delta\lambda_{j+1}$, in a load step remains constant during the loading step,

i.e.

$$\Delta \mathbf{u}_{j+1}^T \Delta \mathbf{u}_{j+1} + \Delta\lambda_{j+1}^2 = \Delta l^2 \tag{3.22}$$

where Δl is a prescribed reference length. By substituting Eqs. (3.8) and (3.21) into Eq. (3.22), an algebraic equation is obtained which can be used to determine $d\lambda_{j+1}$. A simplification can be introduced by linearization of Eq. (3.22).

Expansion of Eq. (3.22) is

$$\begin{aligned}(\Delta \mathbf{u}_j^T \Delta \mathbf{u}_j + \Delta\lambda_j^2 - \Delta l^2) + 2\,(\Delta \mathbf{u}_j^T d\mathbf{u}_{j+1} + \Delta\lambda_j\, d\lambda_{j+1}) \\ + (d\mathbf{u}_{j+1}^T d\mathbf{u}_{j+1} + d\lambda_{j+1}^2) = 0\end{aligned} \tag{3.23}$$

Since Eq. (3.22) is valid at iteration j, the first bracket in the above equation vanishes. Ignoring the second order terms in the third bracket, Eq. (3.23) becomes

$$\Delta \mathbf{u}_j^T d\mathbf{u}_{j+1} + \Delta\lambda_j\, d\lambda_{j+1} = 0 \tag{3.24a}$$

This equation requires that the increment in iteration j+1 in the load-displacement space, $(d\mathbf{u}_{j+1}, d\lambda_{j+1})$, is perpendicular to the accumulated increment up to iteration j, $(\Delta\mathbf{u}_j, \Delta\lambda_j)$. Substituting Eq. (3.21) into Eq. (3.23), $d\lambda_{j+1}$ can be solved as

$$d\lambda_{j+1} = -\frac{\Delta \mathbf{u}_j^T d\mathbf{u}_{j+1}^{II}}{\Delta \mathbf{u}_j^T d\mathbf{u}_{j+1}^{I} + \Delta\lambda_j} \tag{3.24b}$$

To further simplify the constraint equation, Eq. (3.24a) may be replaced by

$$\Delta \mathbf{u}_1^T d\mathbf{u}_{j+1} + \Delta\lambda_1\, d\lambda_{j+1} = 0 \tag{3.25a}$$

where the accumulated increments are replaced by the increments of the displacement and load factor in the first iteration (or predictor step). As a result, Eq. (3.24b) becomes

$$d\lambda_{j+1} = -\frac{\Delta \mathbf{u}_1^T d\mathbf{u}_{j+1}^{II}}{\Delta \mathbf{u}_1^T d\mathbf{u}_{j+1}^{I} + \Delta\lambda_1} \tag{3.25b}$$

The form of equation defined in Eq. (3.25a) with its solution in Eq. (3.25b) is usually called the *linear constraint equation* because of the linear relation between the incremental load factor and the displacement increments due to the unbalanced forces. The iterative

process is graphically shown in Fig. 3.8 where the modified N-R iteration procedure is assumed. The iteration is along a line perpendicular to the first increment defined by $\Delta \mathbf{u}_1$ and $\Delta\lambda_1$, and approaches the intersection of this line and the equilibrium path which defines the converged solution.

The constraint equation defined in Eq. (3.22) which results in a quadratic algebraic equation for the incremental load factor is usually called the *spherical constraint equation* because it defines the iteration on a sphere in the load-displacement space and converges to the intersection of the sphere and the equilibrium path. The iterative process based on the spherical constraint equation is, as shown in Fig. 3.10, along a circular curve. An intersection of this curve and the equilibrium path is ensured.

The spherical constraint equation can be generalized into a general quadratic equation as

$$\Delta \mathbf{u}_{j+1}^T \Delta \mathbf{u}_{j+1} + \zeta \Delta\lambda_{j+1}^2 = \Delta l^2 \tag{3.26}$$

where ζ is a constant which permits different weights to be assigned to the relative significance of the increments of displacement and load factor. When ζ equals to one, Eq. (3.26) defines the spherical constraint equation. When ζ equals to zero, the equation is often referred to as the *cylindrical constraint equation*. For other values the equation becomes, the so called, *ellipsoidal constraint equation*. A large value of the constant ζ essentially converts the arc-length control in Eq. (3.26) into a load control.

Bellini (1987) reviewed and compared these three forms of quadratic constraint control equations, namely, the spherical, cylindrical and ellipsoidal constraint equations. Based on numerical studies of six cases including several benchmark problems, the cylindrical constraint equation was recommended for snap-through behavior. For snap-back behavior and paths with very stiff loading and unloading where the load increments are obviously more important, an ellipsoidal constraint equation should be used. In this case, a proper way to determine the value of constant ζ should be used.

Arc-length methods may fail in cases which involve highly localized failure or bifurcation modes (de Borst, 1987), because the norm of the global displacement increment on which the arc-length method is based may not be sensitive enough to control highly localized displacement increments. As an alternative, the *indirect displacement control* technique was developed (de Borst, 1987,1988; and, Rots, 1988). To distinguish between

the methods, the method of displacement control applied on one or more degrees of freedom in Sect. 3.1.3 is called *direct displacement control.*

The basic idea of indirect displacement control is that the norm of the displacement increment in the arc-length control equation is replaced by the norm of a weighted displacement increment as

$$\Delta \mathbf{u}_{j+1}^{T} \mathbf{W} \Delta \mathbf{u}_{j+1} + \zeta \Delta \lambda_{j+1}^{2} = \Delta l^{2} \tag{3.27}$$

where **W** is a weighting matrix. The weights applied to the components of the displacement increment can be chosen in such a way that the norm of the weighted displacement increment will be sensitive to selected localized failure or bifurcation modes. Since the failure or bifurcation modes are problem dependent, selection of the weight matrix **W** depends on the individual problem and the experience of analyst. Therefore, the application of indirect displacement control is limited.

3.1.5 Reduction Methods

Researchers have been attempting to develop analytical models and robust solution techniques which can capture the essence of overall structural behavior in an efficient and cost-effective manner. Detailed solutions are not always necessary as long as the analysis can provide the designer with sufficient information. Among various alternatives to iteration on the full system obtained from discretization of the structure, *reduction methods* (Noor, 1980, 1981a, and 1981b) are one approach which shows some promise. Ideas similar to the reduction methods have been extensively used in dynamic analysis. In dynamic analysis of large structures, the response is described in terms of the superposition of a small number of displacement patterns associated with the natural modes of vibration of lowest frequencies. It is generally accepted that this technique is capable of capturing the essence of the structural response to global actions. It is believed that a similar technique can also be used to capture the essence of the nonlinear static response of many common types of structures in sufficient detail to provide the designer with the information which he requires to make judgements on the performance of structures.

The principal idea of reduction methods for nonlinear analysis is to limit the displacement increments of the discretized structure to some known displacement modes which form the reduced basis, and leads to a system with a considerably smaller number of degrees of freedom than the system on the natural basis defined directly by the

discretization. Selection of these displacement modes, or *base vectors*, is the most important step in reduction methods and determines the capability of the base vectors to model the incremental displacements on the natural basis and, consequently, the accuracy of the solution.

There are four general criteria for selection of base vectors, summarized (Noor, 1981b) in the following. First, the vectors must be linearly independent and span a solution space in the neighborhood of the solution point on the equilibrium path under current consideration. Second, the generation of these vectors should be both simple and computationally inexpensive and the number of vectors that can be generated should be variable. The vectors should be a subset of a complete basis in which the displacement increment can be fully represented. Third, the vectors should have good approximation properties in the sense that they provide satisfactory solution on a large interval of the equilibrium path. Finally, the application of reduction methods based on the selected vectors should simplify the tracing of post-buckling behavior.

Several options for base vectors have been proposed in the past. Nonlinear incremental displacements and their various orders of path derivatives were used (Noor, 1980; and, Noor and Peters, 1981a). Global shape functions derived according to a set of rules were selected by Almroth *et al* (1978). Wilson *et al* (1982) developed a procedure to obtain a set of Ritz vectors which were used in dynamic analysis and can potentially be used as base vectors in static analysis. Eigenmodes have been used as base vectors by Nagy and Konig (1979) and Napoleao *et al* (1990, 1991a, and 1991b). These are some of the best explored options at present time. In the following, discussion will focus on the reduction methods based on eigenmodes.

The incremental displacements for materially nonlinear structures, such as concrete beams, were found to be accurately approximated by a linear combination of a few eigenmodes corresponding to the lowest eigenvalues (Napoleao *et al*, 1991a). Mathematically the approximation can be expressed as

$$\Delta \mathbf{u} = \Phi \alpha \tag{3.28}$$

where Φ is a matrix composed of base vectors and α is the *reduced displacement increment vector* which is composed of a magnitude (ie. generalized coordinate) for each corresponding base vector. All the base vectors must be kinematically admissible, i.e. they should satisfy the prescribed displacement boundary conditions and strain compatibility,

and are assumed to be normalized. The number of base vectors, or the number of reduced degrees of freedom, is much smaller than the number of degrees of freedom on the natural basis, and a typical number of 3 has been used (Napoleao *et al*, 1991b) for concrete beam structures.

A general solution strategy based on eigenvectors for materially nonlinear structures has been developed (Napoleao *et al*, 1991b). With the approximation defined in Eq. (3.28), the system equations on the natural basis in Eq. (3.2) can be converted into the system of equations on the reduced basis as

$$\Lambda \alpha = \gamma \tag{3.29}$$

where Λ is the reduced stiffness and γ are the reduced generalized unbalanced forces. These quantities are defined as

$$\Lambda = \Phi^T \mathbf{K} \Phi \tag{3.30}$$

$$\gamma = \Phi^T (\Delta \mathbf{P} + \mathbf{P}_n - \mathbf{Q}) \tag{3.31}$$

Based on the reduced system in Eq. (3.29) and together with solution procedures and control technique discussed in Sect. 3.1.1 to 3.1.4, a solution approach can be formulated. The details can be found in Napoleao et al (1991b).

In this reduction method the iteration is carried out on the reduced basis and the base vectors change throughout the history of the structural response. But the displacements are accumulated in the natural basis and consequently will have acceptable accuracy if the displacements within each of the load steps are adequately represented. The detail of local behavior is retained because the evaluation of strains, stresses and unbalanced forces is always carried out at the local level on the natural basis. However, the influence of the loading at the local level is filtered through the eigenvectors and only affects the behavior of the overall structures insofar as it affects the lower energy eigenmodes.

This reduction technique does not have a cost advantage on the basis of iteration by iteration, because the tangent stiffness matrix on the natural basis still must be assembled and factorized, and additional cost is required for eigen-analysis. However, this technique appears to be very robust and the penalty for carrying out eigen-analysis appears to be overcome by the more rapid convergence characteristics. In the example of a deep concrete

beam, the overall efficiency was improved by a factor of 2. Therefore, this approach appears to be com[illegible]e with some of the more standard solution procedures.

3.1.6 Direct Search Techniques

Search techniques in static analysis of nonlinear structures are often associated with line searches. These are used as techniques in combination with an iterative procedure, to improve the convergence characteristics of the iterative procedure. The direct search technique discussed here is, however, much more sophisticated and serves as an independent solution procedure rather than a part of an equilibrium iteration procedure.

Many engineering problem, such as optimum design of structures and structural analysis, can be formulated mathematically in the following form

$$\text{Find solution } \mathbf{x}^* \text{ such that } f(\mathbf{x}^*) = \text{minimum } f(\mathbf{x}) \tag{3.32}$$

where $\mathbf{x}$ is the state variable vector, that defines the state of the system under consideration, and $f(\mathbf{x})$ is the objective function which defines the preference for the selection of the solution. For example, in the classical problem of optimum structural design, namely, minimum weight design problem, $f(\mathbf{x})$ is the weight of the concerned structure and $\mathbf{x}$ is a set of possible selections of the dimensions of structure components. The solution is searched in the feasible solution domain.

A nonlinear structural analysis problem can also be formulated in the form of a minimization problem, where the objective function $f(x)$ can be selected in a number of ways. It may be taken as the norm of unbalanced forces, or the magnitude of maximum components of unbalanced forces, or the energy corresponding to unbalanced forces. The state variables can be displacements, or some generalized displacements based on selected displacement modes, and the load factor representing the applied load. This can be mathematically expressed, for example, as

$$\text{Find solution } \Delta\mathbf{u}^* \text{ such that } \|\mathbf{U}(\mathbf{u}_n+\Delta\mathbf{u}^*)\| = \text{minimum } \|\mathbf{U}(\mathbf{u}_n+\Delta\mathbf{u})\| \tag{3.33}$$

where $\Delta\mathbf{u}$ is the displacement increment on the natural basis and $\|\mathbf{U}(\mathbf{u}_n+\Delta\mathbf{u})\|$ is the norm of the unbalanced forces which is related to displacements through stresses and strains. The possible minimum of the objective function in this case is zero.

If a solution $\Delta\mathbf{u}^*$ that results in a minimum value of zero for the norm of the unbalanced forces is found, and correct strain-displacement relations and stress-strain

relations are used, it can be concluded that a new equilibrium configuration is then established. Comparing with the equilibrium formulation commonly used in finite element structural analysis, differences are found within each of the solution steps. In the equilibrium formulation, the new equilibrium configuration is established by an iterative procedure on equilibrium equations, while in the minimization formulation, it is achieved by a direct search among possible displacement increments.

The solution in the minimization formulation does not have to satisfy a set of equations such as the equilibrium equations in an equilibrium formulation. Consequently, solution procedures based on equilibrium iteration are obviously not appropriate. *Direct search methods* as one of the effective solution procedures for minimization formulations are well developed (Fox, 1971, Aoki, 1971, Dixon, 1972 and Wolfe, 1978). There are many techniques that can be employed to solve the problem defined in Eq. (3.33). These can be grouped into two categories. The first category consists of gradient based methods which require the calculation of the first order derivatives to determine the best direction for search. The second category consists of direct search techniques in which finite differences are used to replace the derivatives. This type of technique is particularly suitable to the problem where the derivatives of the objective function with respect to the state variables are difficult to obtain. Nonlinear structural analysis is an example of this kind where the derivatives of the norm of the unbalanced forces with respect to displacement increments are next to impossible to obtain. Therefore, direct search techniques will be employed, herein, for nonlinear structural analysis. There are many methods in the category of direct search technique, among which the method proposed by Powell (1964, 1966) is one of the most efficient methods. The details of the method will be discussed in Sect. 3.3, where a solution procedure for nonlinear structural analysis is developed.

3.2 EQUILIBRIUM ITERATION WITH AN IMPROVED METHOD OF ARC-LENGTH CONTROL

Shell model analysis is carried out in this study using a general purpose program developed at the University of Stuttgart, Germany (Stegmuller, 1984), known as Nonlinear Inelastic Structural Analysis (NISA), which contains a carefully developed shell element and a solution technique with arc-length controlled equilibrium iteration. Unfortunately, difficulties and inefficiencies arise for postbuckling analysis of thin shell structures from the existing solution technique in NISA. Consequently, a more robust and efficient solution technique has been developed that is based on an *improved arc-length control*, combined with full and modified N-R iterative procedures, proper loading and convergence criteria.

This section begins with a brief description of the existing solution technique in NISA, followed by discussion of its deficiencies and details of the proposed improved technique.

3.2.1 Existing Solution Technique in Program NISA

The equilibrium iteration procedure is either full or modified N-R iteration combined with the linear constraint equation of the arc-length control technique. This is considered to be one of the procedures representing the state-of- art for nonlinear structural analysis. Newton-Raphson iteration and arc-length control have been discussed in Sects. 3.1.2 and 3.1.4, respectively. The convergence of the iteration is measured by the ratio between the norm of the displacement increment at iteration j and the norm of the accumulated displacement increment up to iteration j, i.e.

$$\frac{\|\mathbf{du_j}\|}{\|\Delta\mathbf{u_j}\|} \leq \xi_d \tag{3.34}$$

where ξ_d is a specified tolerance for the displacement increment. A typical value of ξ_d can be one percent in the elastic ascending region, but is relaxed somewhat in the region with significant nonlinearity and in the post-peak region.

The loading criterion refers to the way to impose applied loads on the structure. In the existing solution technique, loads are applied incrementally, and whether the structure is in the state of loading or unloading is determined by whether one or more negative pivots are found in the process of factorization of the global stiffness matrix. The loading criterion states that the structure is in a state of loading if the current stiffness matrix is found to be positive definite. Otherwise an unloading state is assumed. The stiffness matrix can be shown to be positive definite if no negative pivot is found. This is because the number of negative eigenvalues of a matrix is equal to the number of negative pivots of the matrix (Strang, 1988), and if all the eigenvalues are positive, the matrix must be positive definite.

3.2.2 Discussion of the Existing Solution Techniques of NISA

Based on numerical examples and experience with program NISA, several problems that result from deficiencies of the solution technique were found and are summarized below. Five aspects will be examined in the following. They are : iterative procedure; the arc-length constraint equation; the convergence criteria; the loading criterion; and, the reference arc-length.

Newton-Raphson iteration is the standard iterative procedure for nonlinear structural analysis. As discussed in Sect. 3.1.2, full N-R iteration is more stable and is preferable in solution steps involving highly local and nonlinear behavior. On the other hand, modified N-R iteration is more cost-effective and should be used as long as convergence can be achieved. A difficult decision faced by the analyst is to determine a proper iterative scheme for the coming load step. This is sometimes very difficult, especially in the postbuckling region where deformation is localized, and the nonlinear effects due to plastification of material and large displacements are significant. Since the analyst cannot afford to use full N-R iteration all the way if he wants to carry the analysis into the deep postbuckling region, a combination of full and modified N-R iteration is usually required, where modified N-R iteration is the default but full N-R iteration is activated automatically whenever it is necessary. This combination is deemed to achieve the best efficiency and stability of the solution procedure.

The linear constraint equation for arc-length control is defined in Eq. (3.25). The process of iteration with linear constraint equation is to find iteratively the intersection of a "plane" normal to the first increment in the load-displacement space and the equilibrium path, as shown in Fig. 3.8. If this intersection does not exist, as for the responses shown in Fig. 3.9, which are often encountered for thin shell structures with relatively high diameter-to-thickness ratios, the linearized arc-length control leads to divergence. At other times, the size of the load steps has to be kept extremely small in order to achieve convergence. Obviously a better arc-length equation is needed to prevent failures of the solution process associated with the linear constraint equation. The fundamental problem is that the constraint only restricts the direction of subsequent displacement increments and places no limit on the magnitude of the accumulated displacement increment in the load step. This problem can be prevented by a quadratic arc-length equation.

The convergence criterion defined in Eq. (3.34) is generally accepted for analysis of common structures. This is based on the fact that only if the unbalanced forces become very small does the displacement increment at iteration j, du_j, becomes very small. Consequently, Eq. (3.34) can be satisfied. However, in order to insure the unbalanced forces are small enough, the tolerance in Eq. (3.34), ξ_d, is normally required to be very small. For example tolerance 10^{-4} is often required but sometimes difficult to achieve, especially in the postbuckling region. As a result, convergence may be misjudged and a significant amount of time may be wasted to satisfy the extremely small tolerance. The

problem here is that the displacement convergence criterion in Eq. (3.34) is not a direct measurement of the accuracy of the equilibrium configuration. A convergence criterion based on the magnitude of unbalanced forces should be used together with displacement criterion to insure that both displacement and unbalanced forces converge to a reasonable accuracy.

The loading criterion used in NISA is based on the positive definiteness of the tangent stiffness matrix. If one or more negative pivot elements of the factorized tangent stiffness matrix is detected, a negative load increment is assumed for the predictor step of the iteration. This criterion works well on the ascending branch of the equilibrium path where the structure is generally in the loading state. Here loading and unloading correspond to a load increase and decrease, respectively. However, difficulty arises for the descending branch which is typical for postbuckling behavior of thin shell structures. On the descending branch, both loading and unloading states correspond to load decreases, with the difference in the nature of the displacement increment. In general, loading is accompanied by an increase in magnitude of the displacement and amplification of the displacement pattern. Unloading is associated with a decrease in the magnitude of the principal displacement pattern. Loading and unloading cannot be identified conclusively by the positive definiteness of the stiffness matrix either, because a stiffness matrix that is not positive definite can be associated with either loading or unloading. Consequently, a loading criterion based on an increment of applied load cannot effectively develop the solution into the deep postbuckling region. A loading criterion based on incremental imposed deformation can prevent confusion between the loading and unloading.

The reference arc-length, Δl, in the arc-length equation is found to have significant influence on the overall efficiency and stability of the solution process. A large reference arc-length will likely lead to difficulty on convergence because the convergence characteristics of the iteration procedure are only valid locally. On the other hand, a small one increases the number of the load steps and reduces the efficiency. In the existing solution technique in NISA, however, no effort is made to adjust the reference arc-length to achieve maximum efficiency. Consideration should be given to this aspect, especially for users with little experience with the solution technique and the type of problem to be analyzed.

In attempting to meet the requirements arising from the deficiencies of the existing solution technique as discussed above, a more robust and efficient technique has been developed. This is detailed in the following sections.

3.2.3 Modified Arc-Length Constraint Equation

As discussed in Sect. 3.2.2, a quadratic arc-length equation may be employed to prevent the deficiencies arising from the linear constraint equation. The general form of quadratic arc-length equation is defined in Eq. (3.26) with the displacement increment being expressed by Eq. (3.21). Substituting Eq. (3.21) into Eq. (3.26), it becomes a quadratic equation in terms of the load factor increment, $d\lambda_{j+1}$, i.e.

$$A\, d\lambda_{j+1}^2 + B\, d\lambda_{j+1} + C = 0 \tag{3.35}$$

where

$$A = \mathbf{du}_{j+1}^{I\,T}\, \mathbf{du}_{j+1}^{I} + \zeta \tag{3.36a}$$

$$B = 2\,(\, \mathbf{du}_{j+1}^{I\,T}\, \mathbf{du}_{j+1}^{II} + \Delta\mathbf{u}_j^T\, \mathbf{du}_{j+1}^{I} + \zeta\, \Delta\lambda_j\,) \tag{3.36b}$$

$$C = \mathbf{du}_{j+1}^{II\,T}\, \mathbf{du}_{j+1}^{II} + 2\,\Delta\mathbf{u}_j^T\, \mathbf{du}_{j+1}^{II} + \Delta\mathbf{u}_j^T\, \Delta\mathbf{u}_j + \zeta\, \Delta\lambda_j^2 - \Delta l^2 \tag{3.36c}$$

To have at least one real root from Eq. (3.35), which is necessary for the existence of a physically meaningful load factor increment, the following condition has to be satisfied, i.e.

$$B^2 - 4\,A\,C \geq 0 \tag{3.37}$$

This is not always true. Numerical examples indicate that the condition in Eq. (3.37) cannot be satisfied when the contribution of the displacement increment from unbalanced forces, $\mathbf{du}_{j+1}^{II}$, is significant compared to the contribution from reference load, $\mathbf{du}_{j+1}^{I}$. Consequently, the solution process based on the arc-length Eq. (3.35) fails.

To prevent failures in the solution process, a relaxation factor β is introduced into Eq. (3.21) as

$$\mathbf{du}_{j+1} = d\lambda_{j+1}\, \mathbf{du}_{j+1}^{I} + \beta\, \mathbf{du}_{j+1}^{II} \qquad 0 \leq \beta \leq 1 \tag{3.38}$$

where β is referred to as the relaxation factor. When β is set to be one, Eq. (3.38) reverts to Eq. (3.21). Mathematically, the relaxation factor β is introduced to satisfy the condition in Eq. (3.37). As will be shown later, Eq. (3.37) can always be satisfied as long as a proper value of factor β is used. A physical interpretation of the relaxation factor β is that only a fraction of the unbalanced forces are taken into account in some of the iterations

rather than the full amount of unbalanced force in every iteration, as is common in iterative procedures. Equivalently, the iterative procedure based on Eq. (3.38) can be viewed as one where the unbalanced forces are applied partly. Consequently the number of iterations may be increased, but the stability of iterative process can be improved and failure of the solution can be prevented. Substituting Eq. (3.38) into Eq. (3.26), Eq. (3.26) becomes the quadratic equation, Eq. (3.35), with B and C defined as

$$B = 2\,(\,\beta\, \mathbf{du}^{I}_{j+1}{}^{T}\, \mathbf{du}^{II}_{j+1} + \Delta\mathbf{u}_j^{T}\, \mathbf{du}^{I}_{j+1} + \zeta\, \Delta\lambda_j\,) \tag{3.39b}$$

$$C = \beta^2\, \mathbf{du}^{II}_{j+1}{}^{T}\, \mathbf{du}^{II}_{j+1} + 2\,\beta\, \Delta\mathbf{u}_j^{T}\, \mathbf{du}^{II}_{j+1} + \Delta\mathbf{u}_j^{T}\, \Delta\mathbf{u}_j + \zeta\, \Delta\lambda_j^2 - \Delta l^2 \tag{3.39c}$$

For a proper value of β, the real roots of Eq. (3.35) can be solved as

$$\alpha_{1,2} = \frac{-B \pm \sqrt{B^2 - 4\,A\,C}}{2\,A} \tag{3.40}$$

Normally two real roots exist but only one value can be chosen to be the load factor increment. The following criterion is used for this selection (Bellini and Chulya, 1987).

$$d\lambda_{j+1} = \alpha_1 \qquad \text{if } \Delta\mathbf{u}_j\,(\alpha_2\, \mathbf{du}^{I}_{j+1} + \beta\, \mathbf{du}^{II}_{j+1}) < \Delta\mathbf{u}_j\,(\alpha_1\, \mathbf{du}^{I}_{j+1} + \beta\, \mathbf{du}^{II}_{j+1}) \tag{3.41a}$$

$$d\lambda_{j+1} = \alpha_2 \qquad \text{if } \Delta\mathbf{u}_j\,(\alpha_1\, \mathbf{du}^{I}_{j+1} + \beta\, \mathbf{du}^{II}_{j+1}) < \Delta\mathbf{u}_j\,(\alpha_2\, \mathbf{du}^{I}_{j+1} + \beta\, \mathbf{du}^{II}_{j+1}) \tag{3.41b}$$

This criterion is based on experience and intuition to keep the direction of displacement increment as close as possible to that of accumulated displacement increment.

The possible range of factor β is determined in the following. The factor β is supposed to vary between zero to one, including one, and has to satisfy condition in Eq. (3.37). Substituting A, B and C defined in Eqs. (3.36a), (3.39b) and (3.39c) into Eq. (3.37), and setting it equal to zero, Eq. (3.37) becomes a quadratic equation in terms of the relaxation factor β, i.e.

$$D\,\beta^2 + E\,\beta + F = 0 \tag{3.42}$$

where

$$D = (\mathbf{du}^{I}_{j+1}{}^{T}\, \mathbf{du}^{I}_{j+1})^2 - (\mathbf{du}^{I}_{j+1}{}^{T}\, \mathbf{du}^{I}_{j+1})\,(\mathbf{du}^{II}_{j+1}{}^{T}\, \mathbf{du}^{II}_{j+1}) - \zeta\, \mathbf{du}^{II}_{j+1}{}^{T}\, \mathbf{du}^{II}_{j+1} \tag{3.43a}$$

$$E = 2\,(\Delta \mathbf{u}_j^T\, d\mathbf{u}_{j+1}^{I})\,(d\mathbf{u}_{j+1}^{I\,T}\, d\mathbf{u}_{j+1}^{II}) + 2\,\zeta\,\Delta\lambda_j\,(d\mathbf{u}_{j+1}^{I\,T}\, d\mathbf{u}_{j+1}^{II}) - 2\,(d\mathbf{u}_{j+1}^{I\,T}\, d\mathbf{u}_{j+1}^{I})\,(\Delta \mathbf{u}_j^T\, d\mathbf{u}_{j+1}^{II}) - 2\,\zeta\,\Delta \mathbf{u}_j^T\, d\mathbf{u}_{j+1}^{II} \tag{3.43b}$$

$$F = (\Delta \mathbf{u}_j^T\, d\mathbf{u}_{j+1}^{I} + \zeta\,\Delta\lambda_j)^2 - (d\mathbf{u}_{j+1}^{I\,T}\, d\mathbf{u}_{j+1}^{I} + \zeta)\,(\Delta \mathbf{u}_j^T \Delta \mathbf{u}_j + \zeta\,\Delta\lambda_j^2 - \Delta l^2) \tag{3.43c}$$

Real roots for equation (3.42) are guaranteed because the condition $E^2 - 4\,D\,F \geq 0$ can always be satisfied. This can be proved by the following facts. By using Eq. (3.26) for iteration j, the second term in Eq. (3.43c) vanishes and $F \geq 0$ is valid under all conditions. Noting that the first term in Eq. (3.43a) can be expressed as

$$(\, d\mathbf{u}_{j+1}^{I\,T}\, d\mathbf{u}_{j+1}^{II}\,)^2 = (\, d\mathbf{u}_{j+1}^{I\,T}\, d\mathbf{u}_{j+1}^{I}\,)\,(\, d\mathbf{u}_{j+1}^{II\,T}\, d\mathbf{u}_{j+1}^{II}\,)\cos^2\theta \tag{3.44}$$

in which θ is the angle between vectors $d\mathbf{u}_{j+1}^{I}$ and $d\mathbf{u}_{j+1}^{II}$, and ζ is positive number, D is obviously a non-positive number. As a result, the condition $E^2 - 4\,D\,F \geq 0$ is satisfied under all conditions. The roots are

$$\beta_{1,2} = \frac{-E \pm \sqrt{E^2 - 4\,D\,F}}{2\,E} \tag{3.45}$$

where $\beta_1 \leq 0$ and $\beta_2 \geq 0$. Eq. (3.37) is satisfied when the value of β is between these two roots. The acceptable range for factor β can be determined as

$$0 < \beta \leq \beta_{max} \tag{3.46}$$

where $$\beta_{max} = \min(\,1,\, \beta_2) \tag{3.47}$$

Obviously, the magnitude of β_{max} has an influence on the efficiency of the solution process, and smaller values are likely to reduce the efficiency. To prevent extreme conditions with nearly zero values of β_{max}, the default modified N-R iteration is replaced by full N-R iteration when β_{max} is less then 0.01. This combination can, in general, insure the stability of the solution procedure and achieve the best efficiency possible.

The reference arc-length should be adjusted as iteration proceeds to achieve maximum efficiency. Since the optimum value largely depends on the structural behavior and the current state of the structure, it is very difficult to develop a universal method to choose a generally applicable value. Therefore, an automatic adjustment was implemented

in NISA (Stegmuller, 1984) as

$$\Delta l_{new} = \sqrt{\frac{N_{opt}}{N_{old}}}\ \Delta l_{old} \tag{3.48}$$

where N_{opt} is the prescribed optimal number of iterations, and N_{old} is the number of iterations for the previous load step. By Eq. (3.48) the reference arc-length is decreased when the convergence becomes slow, and increased when convergence becomes rapid. Based on experience accumulated in this project, Eq. (3.48) is too sensitive for cylindrical shell analysis. A revision is used as

$$\Delta l_{new} = \sqrt[4]{\frac{N_{opt}}{N_{old}}}\ \Delta l_{old} \tag{3.49}$$

Eqs. (3.48) and (3.49) are based on the assumption that the current load step has similar convergence characteristics to the previous one, which is sometimes not true. In addition, a good initial estimation of reference arc-length is difficult to obtain for a new problem to be analyzed. Consequently, the reference arc-length may be excessive even with the adjustment defined in Eq. (3.49). Then the iterative procedure either converges very slowly, or does not converge within the specified maximum number of iterations. For these cases, the reference arc-length is reduced by a factor of 0.3 to 0.5, and the iterative procedure is restarted from the previous equilibrium configuration.

3.2.4 Loading and Convergence Criteria

As discussed in Sect. 3.2.2, a loading criterion based on incrementally imposed deformation can effectively follow the solution deep into the postbuckling region. For a structural system, there is always a principal loading system and a corresponding principal deformation pattern. Examples are an axial load and axial shortening for an axially compressed cylinder, and, end moment and end rotations for a bent cylinder. The principal deformation pattern monotonically increases in all regions for structures without snap-back behavior.

The loading criterion can be established based on the fact that the principal loading system, which is represented by the reference loads, always does positive work on the increments of the principal deformation pattern under a state of loading except for snap-back behavior. Snap-back can be distinguished from elastic unloading by checking the positive definiteness of the tangent stiffness matrix. The tangent stiffness matrix is, in

general, positive definite for elastic unloading, and is not positive definite for snap-back. The loading criterion is established in such a way that the structure is kept in a state of loading along the entire load-deformation curve.

For the predictive step (j = 0) in the loading step, $d\mathbf{u}^{II}_{j+1}$, $\Delta\mathbf{u}_j$ and $\Delta\lambda_j$ are zero and Eq. (3.40) gives

$$\alpha_{1,2} = \pm \frac{\Delta l}{\sqrt{d\mathbf{u}_1^{I\,T}\, d\mathbf{u}_1^{I} + \zeta}} \tag{3.50}$$

To determine which root should be used, the criterion in Eq. (3.41) is not applicable because the accumulated displacement increment in this load step is zero before the first iteration. The displacement increment for predictive step can be expressed as

$$\Delta\mathbf{u}_1 = \Delta\lambda_1\, d\mathbf{u}_1^{I} \tag{3.51}$$

where the direction of the displacement increment is determined by following loading criterion

$$\Delta\lambda_1 = \alpha_1 \qquad \text{if } \hat{\mathbf{P}}^T d\mathbf{u}_1^{I} > 0 \text{ and NPE} = 0 \tag{3.52a}$$

$$\Delta\lambda_1 = \alpha_2 \qquad \text{if } \hat{\mathbf{P}}^T d\mathbf{u}_1^{I} > 0 \text{ and NPE} > 0 \tag{3.52b}$$

$$\Delta\lambda_1 = \alpha_2 \qquad \text{if } \hat{\mathbf{P}}^T d\mathbf{u}_1^{I} < 0 \tag{3.52c}$$

where $\hat{\mathbf{P}}$ is the reference load and NPE is the *number of negative pivot elements* in the diagonalized tangent stiffness matrix. The number of negative pivot elements is equal to the number of negative eigenvalues of the tangent stiffness matrix (Strang, 1988). Therefore, the tangent stiffness matrix is positive definite if NPE is zero, and is not if NPE is larger than zero.

This loading criterion can be explained in the following. Load-deformation curves, in general, can be divided into an ascending branch and a descending branch. On the ascending branch, the tangent stiffness matrix is positive definite and consequently NPE is zero. The tangent stiffness matrix is, however, no longer positive definite in the descending branch and NPE is larger than zero. As a result, the condition of NPE in Eqs. (3.52a) and (3.52b) can, in general, distinguish the ascending and descending branches of the load-deformation curve. On the descending branch for thin shell structures, snap-through and

snap-back behavior are expected which are characterized by the increases and decreases in the magnitude of the principal displacement pattern. These two behaviors can be distinguished by the slope of the load-deformation curve. The slope is negative for snap-through behavior and positive for snap-back behavior. This can be, in turn, represented by the sign of the work done by the reference load on the displacement increment corresponding to the reference load, $\widehat{\mathbf{P}}^T d\mathbf{u}_1^I$. Consequently, checking on the sign of the work, $\widehat{\mathbf{P}}^T d\mathbf{u}_1^I$, would indicate the direction of the first displacement increment in the load step. In summary, the conditions stated in Eq. (3.52a) define the loading state. The conditions in Eq. (3.52b) define the loading state with snap-back behavior, and that in Eq. (3.52c) defines the loading state with snap-through behavior on the descending branch. For the subsequent iterations, the state of loading can be, in general, insured by the selection criterion in Eq. (3.41).

The convergence criteria needs to be modified to include unbalanced forces, as discussed in Sect. 3.2.2. In addition to the displacement convergence criterion defined in Eq. (3.34), a force convergence criterion added is

$$\frac{\|\Delta \mathbf{U}\|}{\|\widehat{\mathbf{P}}\|} \leq \xi_f \tag{3.53}$$

where ξ_f is a small positive number used as specified tolerance for unbalanced force. The recommended value for ξ_f is one percent. This can be relaxed in regions of difficult in convergence. With the force convergence criterion, the tolerance for displacement convergence criterion ξ_d can be relaxed to 10 percent or even larger in the postbuckling region without great loss in accuracy due to the accumulated error, because the size of load step is generally small. The fundamental principle for choosing numbers for tolerances is to insure that the unbalanced forces are bounded and that the solution can be continued with acceptable accuracy in the next load step.

3.2.5 Flow Chart

The flow chart of the solution procedure based on equilibrium iteration with the modified arc-length method is shown in Fig. 3.11. Emphasis in the flow chart is on the new features discussed in Sects. 3.2.3 and 3.2.4.

3.3 SOLUTION PROCEDURE BASED ON DIRECT SEARCH TECHNIQUE

In this section, discussion about a direct search solution procedure, which is a completely different approach from the one described in Sect. 3.2, will be presented. As demonstrated in Sect. 3.1.6, a problem of nonlinear structural analysis can be formulated as a minimization problem, for which a direct search technique may be employed to obtain the solution. This solution procedure is intended to be an alternative to the arc-length technique for use in the postbuckling region where it is expected to be more stable and efficient than solution procedures based on equilibrium iterations. The formulation is first presented, and the selected direct search technique is then described. Finally, the solution procedure, and its characteristics and application, are discussed.

3.3.1 Formulation

The concept for the minimization formulation of nonlinear structural analysis on the natural basis has been expressed in Eq. (3.33). If the number of degrees of freedom is NDOF, the number of search directions which have to be searched to get the solution is NDOF+1, which are each of the degrees of freedom and the load factor. A *search direction* is a direction in a multi-dimensional space along which a one-dimensional search is carried out. Noting that the time required to get a solution depends on the number of search directions, this formulation is obviously not appropriate for large structural systems. One of the alternatives is to formulate the problem based on a reduced basis as discussed in Sect. 3.1.5 for reduction methods. The displacement increment in the load step, defined in Eq. (3.28), is

$$\Delta \mathbf{u} = \Phi \alpha \tag{3.28}$$

where Φ is a matrix composed of base vectors which do not change during the load step, and α is the reduced set of generalized displacement coordinate increments for the displacement increment which is referred to as the *generalized displacement increment.* The number of degrees of freedom of the generalized displacement increment is significantly smaller than that for the displacement increment on the natural basis. The rational for Eq. (3.28) is explained (Napoleao *et al*, 1991a, 1991b) for materially nonlinear problems where the base vectors are taken to be eigenvectors of the current tangent stiffness matrix. It is assumed that the same arguments can be extended to shell analysis with both geometrical and material nonlinearities.

The solution to be solved is now for the generalized displacement increments, α. Consequently the formulation of minimization problem becomes

Find the solution α^* such that $\|\mathbf{U}(\mathbf{u}_{pre}+\Phi\,\alpha^*)\| = \text{minimum}\|\mathbf{U}(\mathbf{u}_{pre}+\Phi\,\alpha)\|$ (3.54)

where $\mathbf{u}_{pre}$ is the total displacement at previously converged configuration. Each of the base vectors defines a search direction in this formulation. Assuming the number of base vectors is NBV, Eq. (3.28) converts a problem with NDOF+1 search directions into one with NBV+1 search directions. Eigenvectors are used as base vectors, as in the reduction method (Napoleao *et al*, 1991b). The accuracy and efficiency depend on the direct search method employed and the representativeness of the sub-space spanned by the base vectors. These are discussed in following sections.

3.3.2 Powell's Search Method

Powell's direct search method is considered to be one of the most efficient methods and it is intended for multi-dimensional search problems. Before discussing its details, a one-dimensional search technique, or line search technique, which is fundamental to all direct search methods, is introduced.

3.3.2.1 A One-Dimensional Search Technique

One-dimensional search means searching along one direction which degenerates any multi-variable function into a single-variable function, or, geometrically, from a multi-dimensional surface to a one-dimensional curve. Similarly, some of the techniques utilize the function values and derivatives, while others use the function values only. To be consistent with direct search techniques, only those that do not use derivatives can be employed. The parabolic interpolation method is the most efficient one of its kind for relatively smooth curves and consequently was chosen to be employed in this project.

The objective function is denoted as $f(x)$ with x_0 as the initial point. A one-dimensional search is carried out to find the minimum of the objective function in the neighborhood of x_0. This process includes following steps.

Step 1 : Find a region $[x_1, x_2]$ which includes the initial point x_0 and the solution x^*. This is true if $f(x_0) < f(x_1)$ and $f(x_0) < f(x_2)$ for $x_1 < x_0 < x_2$.

Step 2 : Interpolate parabolically through points x_1, x_0 and x_2 to approximate the

objective function, as

$$\varphi(x) = \frac{(x-x_1)(x-x_2)}{(x_0-x_1)(x_0-x_2)} f(x_0) + \frac{(x-x_0)(x-x_2)}{(x_1-x_0)(x_1-x_2)} f(x_1) + \frac{(x-x_0)(x-x_1)}{(x_2-x_0)(x_2-x_1)} f(x_2) \quad (3.55)$$

Step 3 : Obtain the minimum point of the parabolic curve $\bar{x}$ as an estimation of the solution x^*, where

$$\bar{x} = \frac{(x_1^2-x_2^2) f(x_0) + (x_2^2-x_0^2) f(x_1) + (x_0^2-x_1^2) f(x_2)}{2\,(\,(x_1-x_2) f(x_0) + (x_2-x_0) f(x_1) + (x_0-x_1) f(x_2)\,)} \quad (3.56)$$

Step 4 : Check the accuracy of the estimation. Since both the solution x^* and its estimation $\bar{x}$ are in the region $[x_1, x_2]$, the error between x^* and $\bar{x}$ is certainly less than the difference between x_1 and x_2. Therefore, the accuracy can be insured if

$$|x_2 - x_1| < \xi \quad (3.57)$$

where ξ is a small positive number used as a prescribed tolerance. If condition (3.57) is satisfied, the solution is obtained as

$$x^* = \frac{1}{2}(\,x_1 + x_2\,) \quad (3.58)$$

with acceptable accuracy. If not, one of the boundary point is set to $\bar{x}$ to get the new reduced region and step 2 to 4 are repeated until the solution is obtained. This process is shown in the flow chart in Fig. 3.12.

3.3.2.2 A Multi-Dimensional Search Technique

With the one-dimensional search technique described in previous section, a *multi-dimensional search* technique developed by Powell (1964, 1966) can be presented. In the multi-dimensional search problem, the efficiency is largely dependent on the selection of the search direction provided that the same one-dimensional search technique is used. The search process begins from an initial point and searches along one given search direction to find the local minimum point on the line by the one-dimensional search technique. Next, the line search is followed from the previous local minimum point along the next search direction. This process is repeated until a solution is obtained. The natural choice for search directions are the directions defined by the reduced basis vectors. But this may not be the most efficient choice. Powell's method generates a set of search directions in the search process, with little extra work, which significantly improves the efficiency of the search

process.

The procedure is outlined in flow chart in Fig. 3.13. In the flow chart, ϕ_i represents a base vector, $\mathbf{P}_i$ represents a search direction, and α_k^i is the estimated solution point after search along the ith direction in the kth search cycle. A *search cycle* includes line searches along all search directions that are linearly independent. The process is terminated by two criteria. The first is a converged solution. This is defined by the difference between the solution estimates at the beginning and end of a search cycle, i.e.

$$\frac{\left\| \alpha_k^{NBV+1} - \alpha_k^0 \right\|}{\left\| \alpha_k^{NBV+1} \right\|} \leq \xi_1 \tag{3.59}$$

where NBV is the number of base vectors. The second criterion is based on the magnitude of the unbalanced forces and the difference between them for the solution estimates at the beginning and end of a search cycle, i.e.

$$\frac{\left\| \mathbf{U}(\alpha_k^{NBV+1}) \right\|}{\left\| \hat{\mathbf{P}} \right\|} \leq \xi_2 \tag{3.60}$$

and

$$\frac{\left| \left\| \mathbf{U}(\alpha_k^{NBV+1}) \right\| - \left\| \mathbf{U}(\alpha_k^0) \right\| \right|}{\left\| \hat{\mathbf{P}} \right\|} \leq \xi_3 \tag{3.61}$$

In Eqs. (3.60) and (3.61) $\left\| \hat{\mathbf{P}} \right\|$ is the norm of reference load.

If Eqs. (3.59) and (3.61) are satisfied, a converged solution, which is acceptable in terms of the accuracy of the equilibrium state, has been obtained as

$$\alpha^* = \alpha_k^{NBV+1} \tag{3.62}$$

If Eq. (3.59) is satisfied and Eq. (3.60) is not, the solution is converged but is not accurate enough. If Eq. (3.61) is satisfied, the search process is converging very slowly. The above two conditions mean that the base vectors are no longer able to represent the displacement increment with sufficient accuracy. Updating or increasing the number of base vectors is necessary. More detail about this is contained in the next section where the solution technique based on the direct search method is presented.

3.3.3 Solution Procedure

A solution technique based on the direct search method requires several other

components in addition to the search method described previously. They are : the generation and updating of base vectors; the starting point for the search process; and, the convergence criteria.

Since no special effort is made to develop a procedure for efficient generation of high quality base vectors, eigenvectors are used as base vectors following the work done by Napoleao *et al* (1991a, 1991b, 1990). To get the eigenvectors corresponding to the lowest eigenvalues, a shift technique in eigen-analysis is often required because the lowest eigenvalues become negative in the postbuckling region. The number of base vectors can be managed by specifying three parameters based primarily on experience. These are the reference number, the incremental number, and the maximum number of base vectors, denoted as NBVR, NBVI and NBVM, respectively. The reference number is the number that would normally be used. When more base vectors are needed to improve the representation, an additional NBVI base vectors are added as long as the total number of base vectors do not exceed the maximum number NBVM. The maximum number is imposed to prevent excessive computation. Typical numbers are, for example, 3 for NBVR and NBVI, and 9 for NBVM. These have been used in the analysis of an axially compressed cylinder to be discussed later in this section.

To determine the starting point, a predictor step is required to get the initial displacement increment α_0^0. The magnitude of initial displacement increment is restricted by the step size Δl which is similar to the reference arc-length used in the solution procedure with equilibrium iterations. The direction of α_0^0 is determined by the ratio between its components. The following equations are proposed for α_0^0

$$\alpha_0^0 = \Delta l \theta \tag{3.63}$$

where

$$\theta_i = \frac{\phi_i^T \Delta \mathbf{u}_{pre}}{\|\Delta \mathbf{u}_{pre}\|} \tag{3.64}$$

with $\Delta \mathbf{u}_{pre}$ as the accumulated displacement increment in the previously converged load step. Noting that base vectors ϕ_i are unit vectors, it is obvious that θ is also a unit vector and the norm of α_0^0 is equal to Δl. Eq. (3.63) is based on the assumption that the displacement increment in the current load step is similar to that in previous load step. This assumption is more satisfactory in the postbuckling region where the solution procedure is intended to apply, because the buckling mode is well developed and deformation is mainly

in the form of amplification of the principal deformation pattern. Consequently, it is reasonable to expect displacement increments similar to each other. On the other hand, the quality of the starting point is more likely to increase the number of search cycles and less important to the stability of the search process.

The convergence criteria have been discussed in Sect. 3.3.2.2 and are used as the terminating condition of the search process.

The solution technique is outlined in the flow chart in Fig. 3.13 where it has been combined with the flow chart for Powell's multi-dimensional search method.

3.3.4 Application and Comments

The solution procedure described in Sect. 3.3.3 can be applied independently in any region of solution path with little modification. However, best efficiency can be achieved from the combination of solution procedures based on equilibrium iteration and the direct search procedure. The equilibrium iterative procedure is used in the prebuckling and initial postbuckling regions, while the direct search procedure is used for the deep postbuckling region. The convergence characteristics of the equilibrium iteration are more sensitive to the state of the structure and the condition of its stiffness matrix than those of the direct search procedure. In the prebuckling region, a well conditioned stiffness matrix requires relatively few iterations and few updates of the stiffness matrix. Consequently, the equilibrium iterative procedure is expected to be more efficient than the direct search procedure, for which two search cycles are usually the minimum requirement. In the initial postbuckling region, the dominant buckling modes are not well developed, and frequent updates of base vectors and more base vectors are probably needed to represent the displacement increment accurately if the direct search procedure is applied in this region. This is highly demanding and reduces the efficiency. However, in the deep postbuckling region, the deteriorated stiffness matrix results in significantly more iterations and updates of the stiffness matrix. The stability of the iterative procedure may even be lost. On the other hand, for the search method detrimental effects of the stiffness matrix depend only on the quality of base vectors. These may not be very sensitive, because dominant buckling modes are well developed. Consequently, the direct search procedure is expected to be more robust and efficient in this region.

The stability of the direct search procedure is almost guaranteed by the fact that the search process proceeds by comparing the norms of unbalanced forces and therefore a

better estimation of solution is obtained after search along each of search directions in every search cycle. The efficiency, or in other words, how fast the search process converges and how accurate the converged solution is, is mainly dependent on the representativeness and the number of base vectors. The penalty to carry out eigen-analysis when it is needed is expected to be compensated for by savings in the following three aspects. The first is the fact that assembling and factorization of the stiffness matrix is no longer needed. The second is the expected higher convergence rate, if a search cycle is counted as being equivalent to an iteration. Finally, convergence can be achieved in significantly larger step sizes compared to the equilibrium iterative procedure. As a result, a very significant saving in computational effort can be achieved.

3.4 NUMERICAL EXAMPLE

To illustrate the performance of the solution procedures, for both the equilibrium iterative procedure and the direct search procedure, a numerical example is presented in this section.

An axially compressed cylinder is analyzed as an axisymmetric model. The cylinder is 12.75 inches (324 mm) in diameter, 0.25 inches (6.35 mm) in wall thickness and 48 inches (1219 mm) in length. The axisymmetric model consists of twelve 5-node axisymmetric elements and 49 nodes as described in Fig. 3.14. The rotations at both ends are restricted, but the radial displacements are free at both ends. The axial displacement is fixed at one end and the compressive force is applied at the other end. A bilinear stress-strain curve is used as the material property representation, with an elastic modulus of 29600 ksi (204092 MPa), yield strength of 52 ksi (358.5 MPa) and strain hardening modulus of 94.44 ksi (651.2 MPa).

The analysis is carried out by the equilibrium iterative procedure from the beginning to end, as shown in Fig. 3.15, in terms of the dimensionless average stress-strain curve. The solution in the deep postbuckling region is repeated by the direct search procedure also shown in Fig. 3.15. The difference between the solutions from the two solution procedures is negligible and very good agreement has been achieved. This conclusion can be further demonstrated by the good agreement between the deformed configurations of the cylinder in the final solution steps from both solution procedures, as shown in Fig. 3.16. It can be seen that two buckles along the longitudinal direction are well developed and the deformed configurations obtained from the two solution procedures agree with each other in terms of the location of the buckles, and both the magnitudes and wavelengths of the buckles.

Some comparisons on performance of solution procedures are summarized in the following. The equilibrium iterative procedure used 87 solution steps and 2541 seconds to cover the region, while the direct search procedure used 7 solution steps and 883 seconds to cover the same region. The typical number of iterations for the equilibrium iterative procedure is 4 with a range from 2 to 8. For all 7 solution steps in the direct search procedure, only 2 search cycles are needed. The time needed for one search cycle is certainly much more than that for one equilibrium iteration. However the rapid convergence characteristics and the stability for solution steps of much larger size make the total time needed for the direct search procedure be about one third of that for the equilibrium iterative procedure. The technique employed for eigen-analysis is the sub-space iteration technique (Bathe, 1982) which is contained in the program NISA.

It is not the intention to conclude that the direct search procedure is more stable and efficient than the equilibrium procedure by this one example. However, this example shows sufficient potential of the direct search procedure in order for it to be employed as an alternative to the equilibrium iterative procedure for postbuckling analysis. It is possible to achieve comparable accuracy of the solutions with much less computer time consumed.

Despite the promise of the direct search procedure shown by this example, the postbuckling analyses to be discussed in Ch. 4 are carried out by the equilibrium iterative procedure. This is because the time available has not permitted the direct search procedure to be tested on three-dimensional shell analysis.

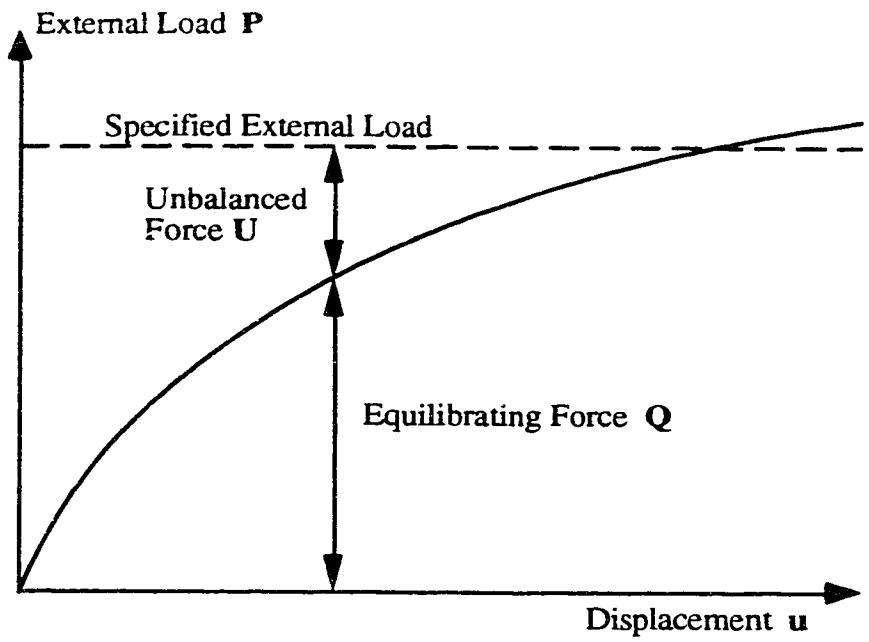

Fig. 3.1 Graphical Il ration of External, Internal and Unbalanced Forces

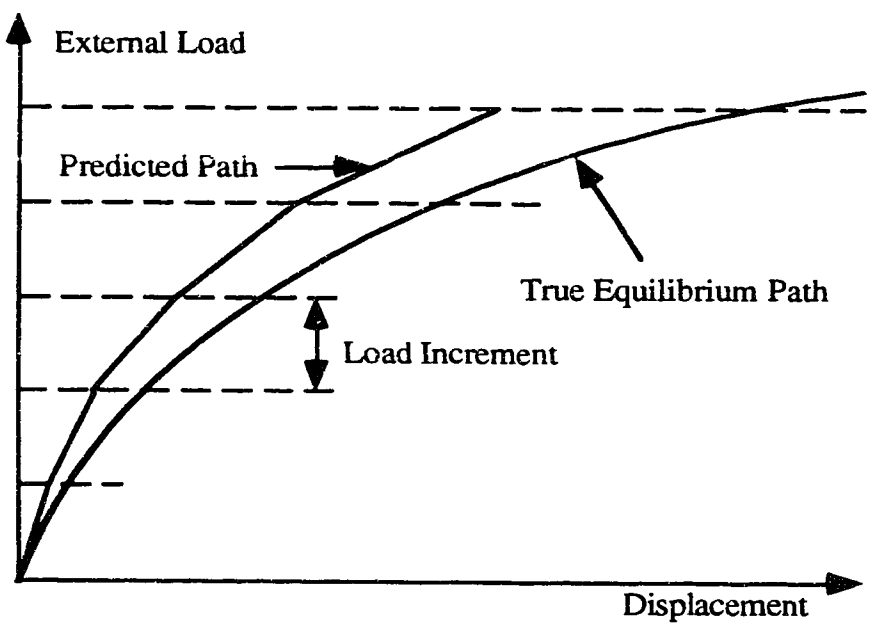

Fig. 3.2 Purely Incremental Solution Procedure and Drifting Tendency

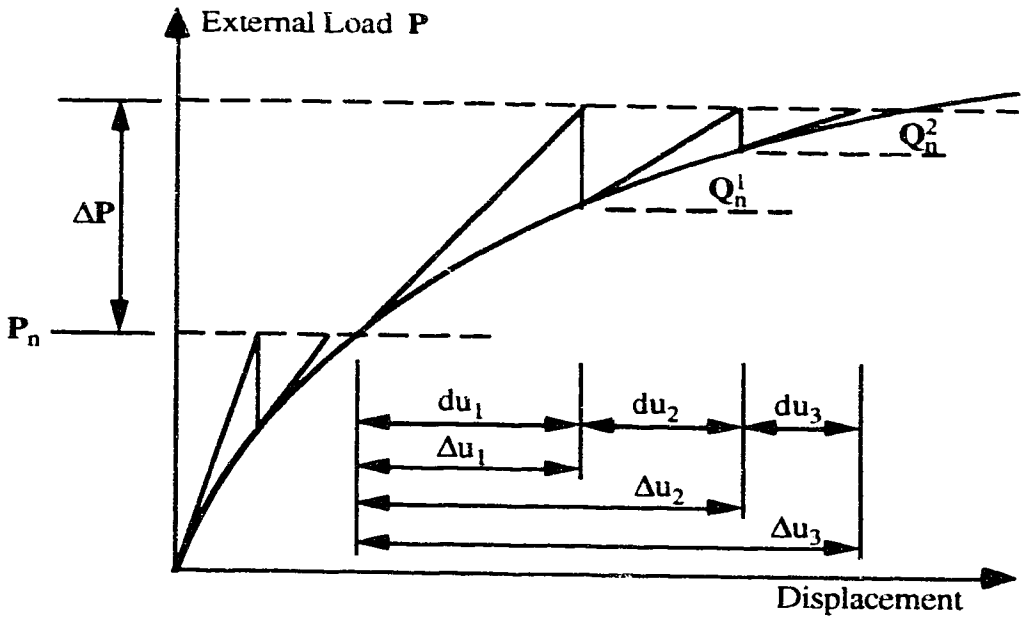

Fig. 3.3 Incremental-Iterative Solution Procedure

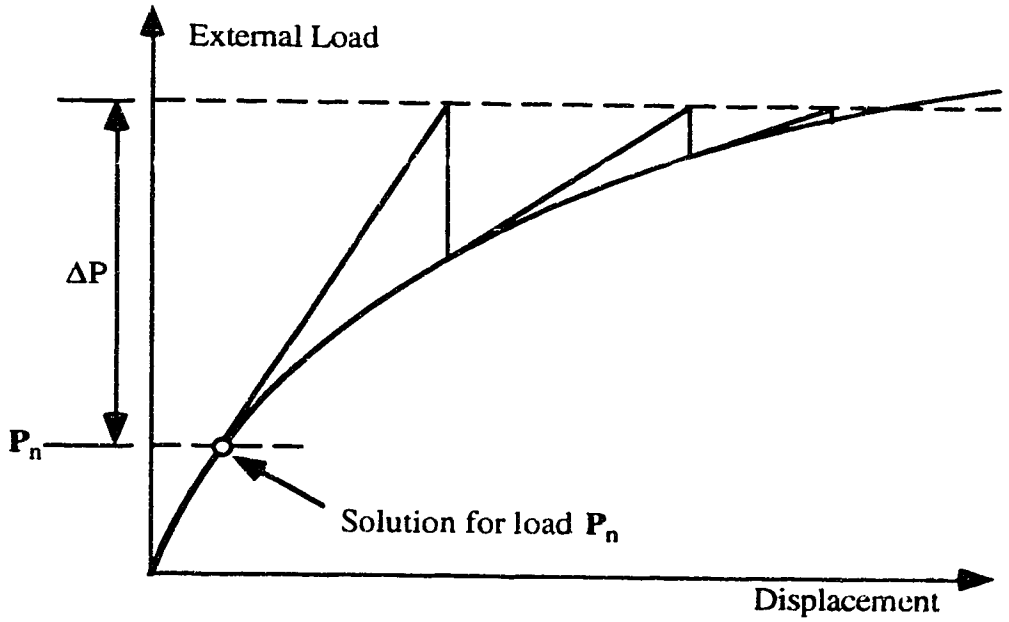

Fig. 3.4 Full Newton-Raphson Iteration Scheme

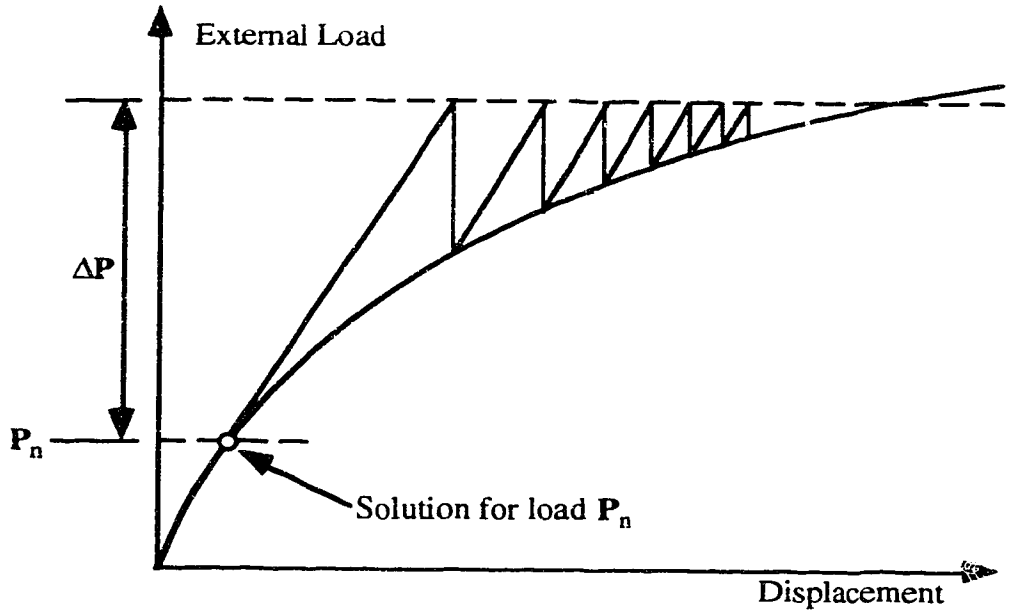

Fig. 3.5 Modified Newton-Raphson Iteration Scheme

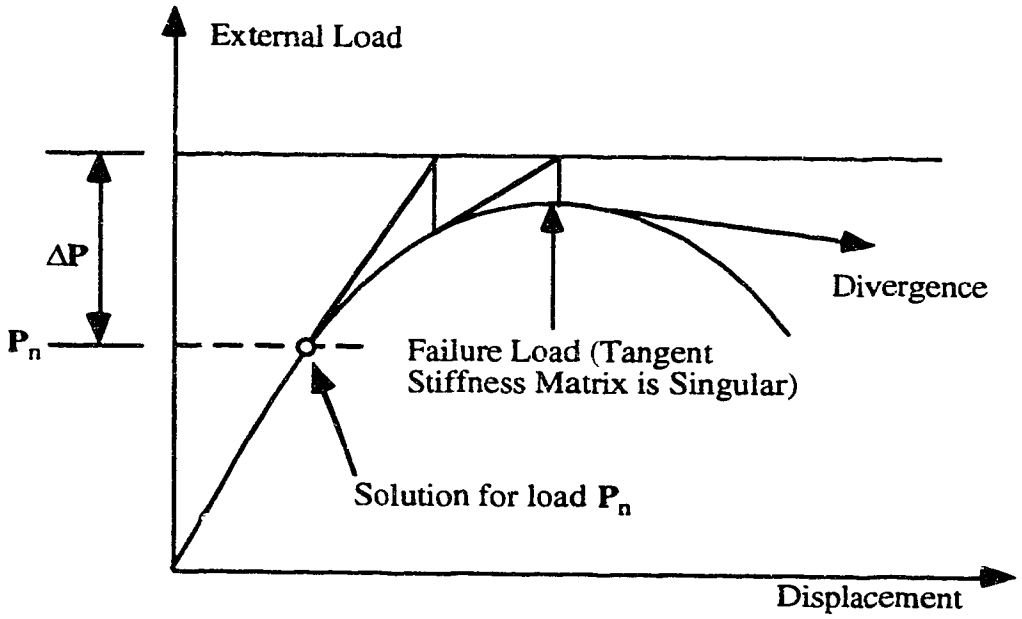

Fig. 3.6 Divergence of Load Controlled Iterative Procedure

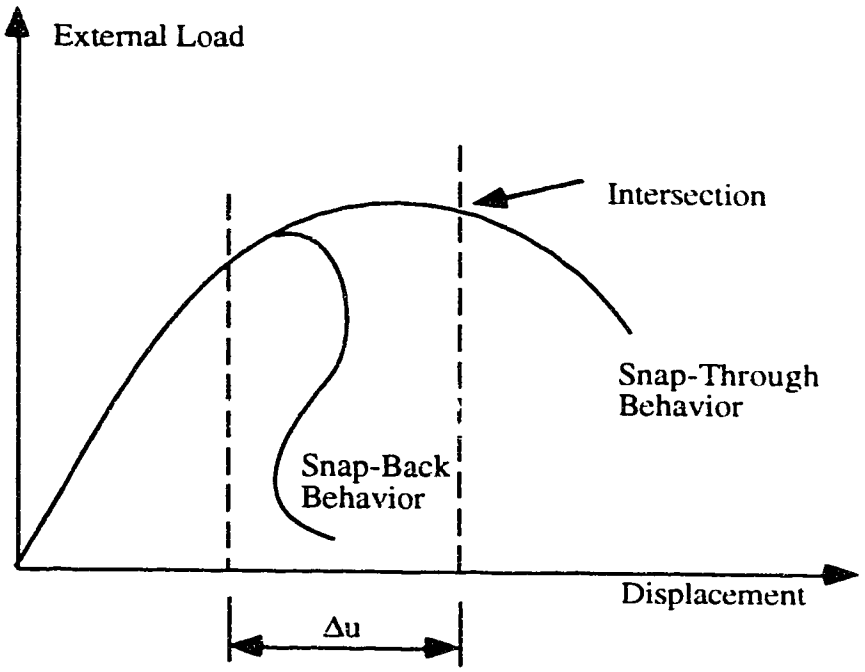

Fig. 3.7 Displacement Control and Snap-Through and Snap-Back Behavior

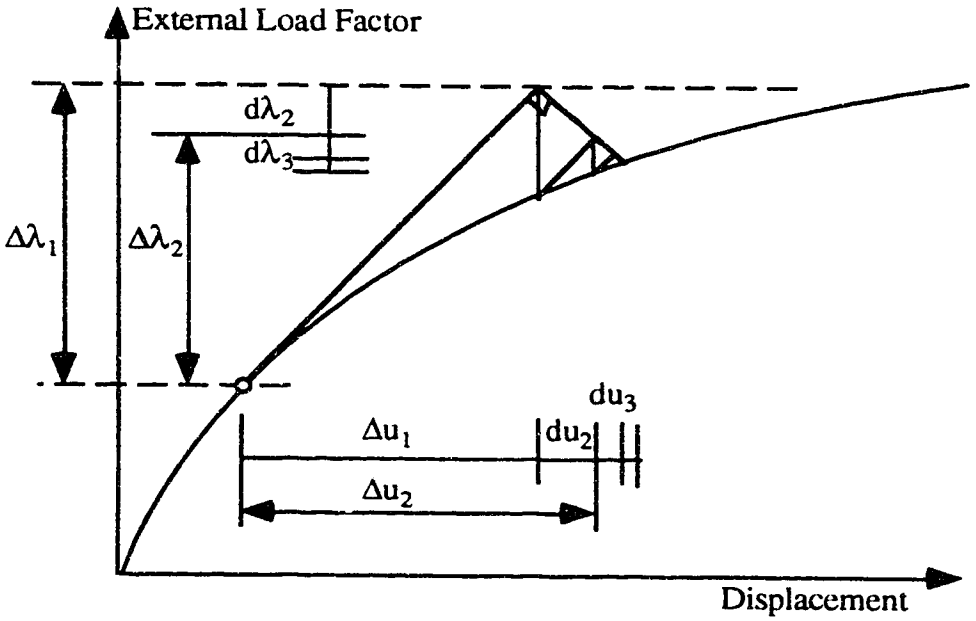

Fig. 3.8 Iterative Procedure with Linear Arc-Length Equation

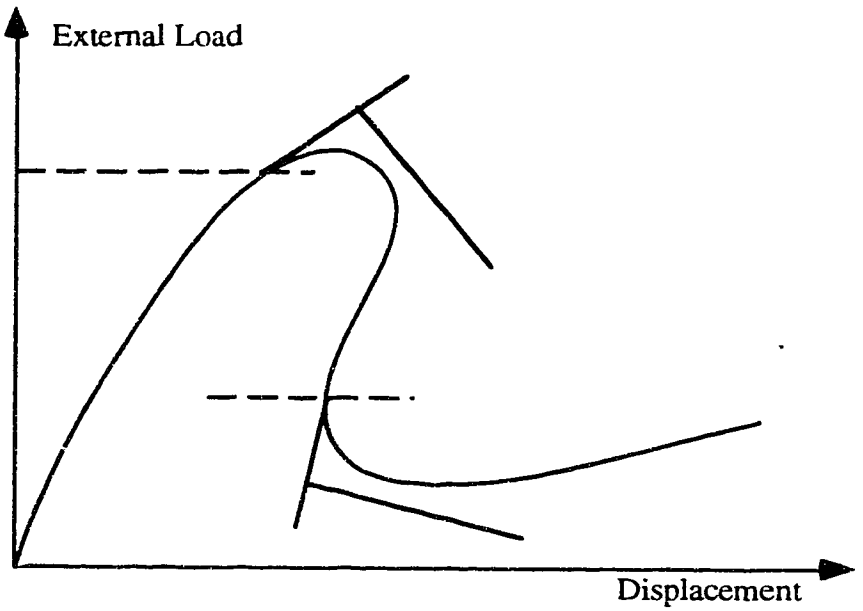

Fig. 3.9 Failure Examples of Linear Arc-Length Control

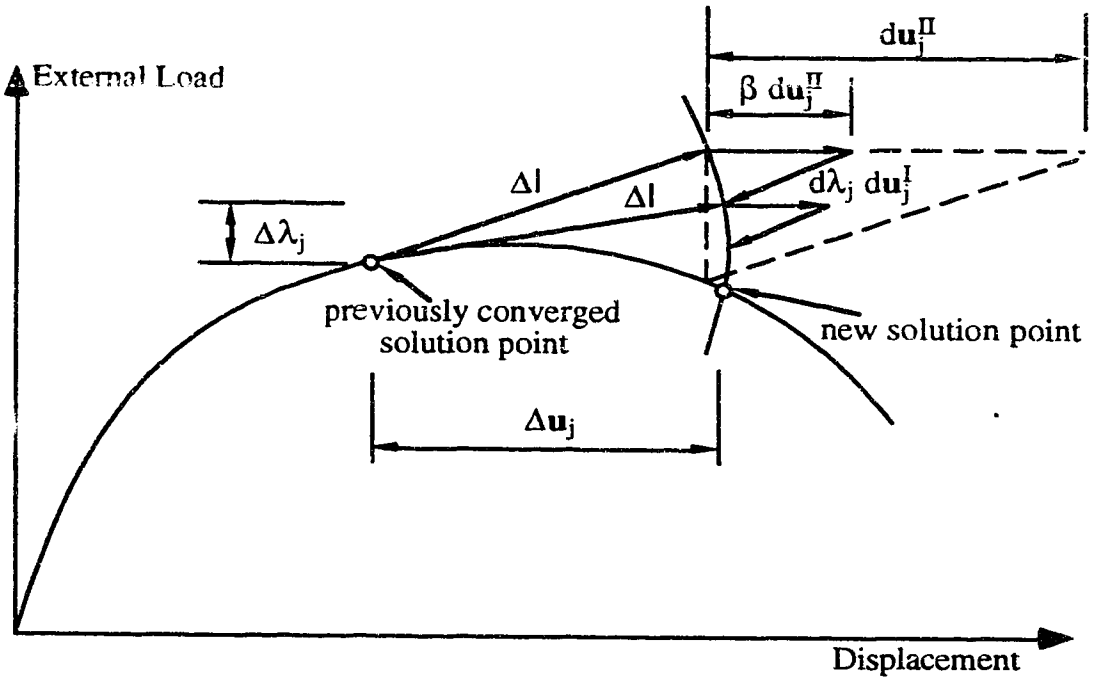

Fig. 3.10 Iterative Process for Quadratic Constraint Equation of Arc-Length Control

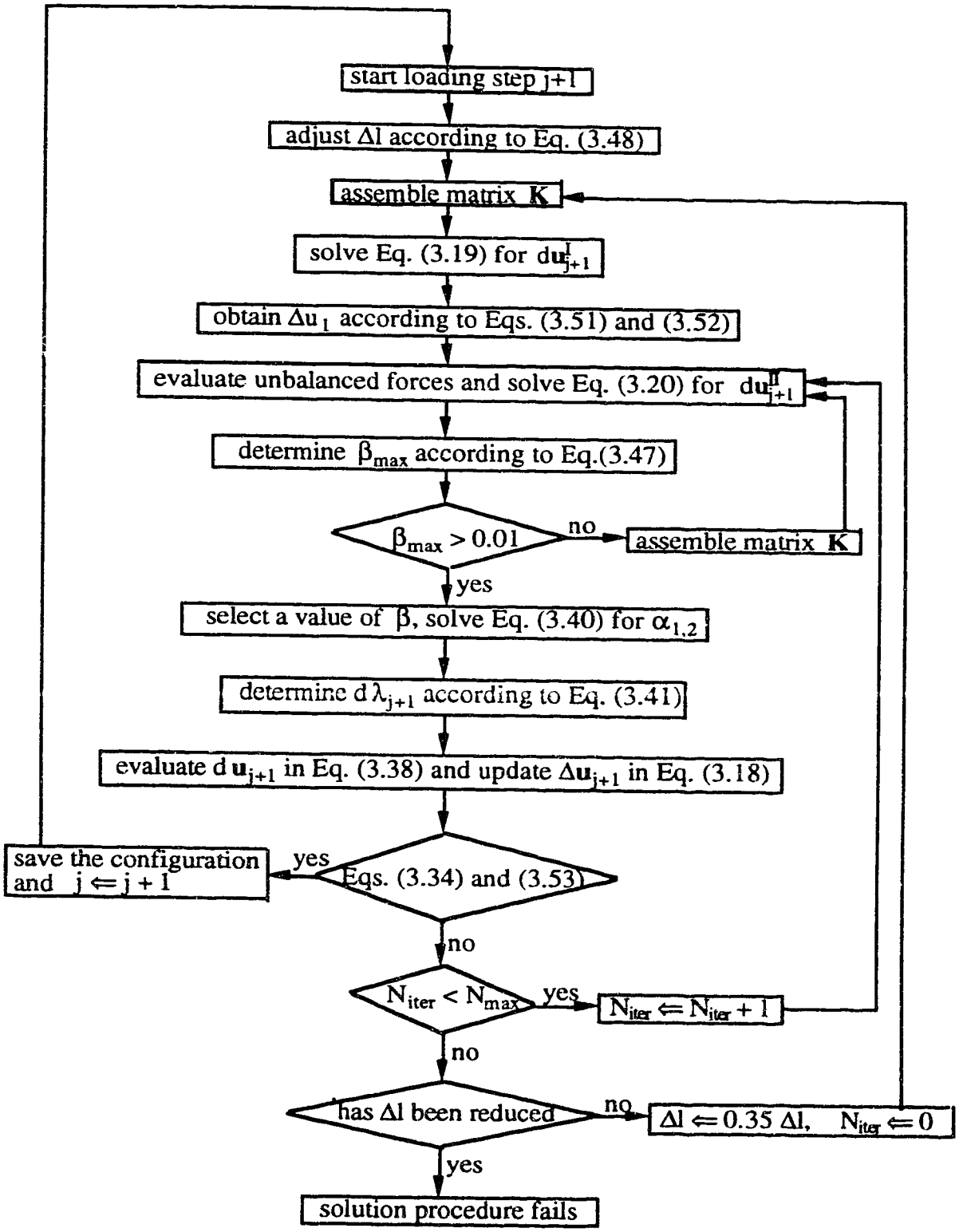

Fig.3.11 Flow Chart of Equilibrium Iteration with Modified Arc-Length Control

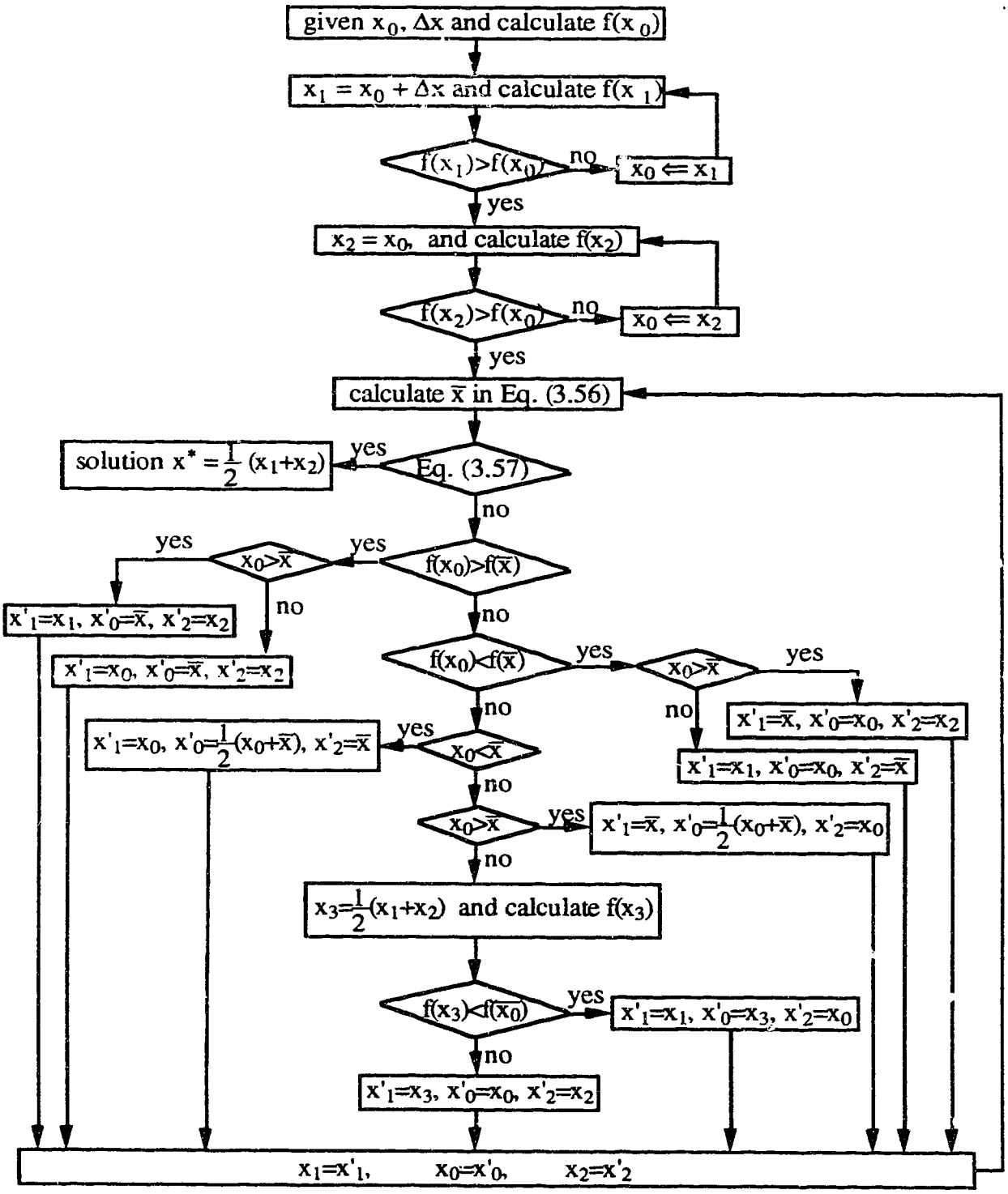

Fig.3.12 Flow Chart of Parabolic Interpolation One-Dimensional Search Method

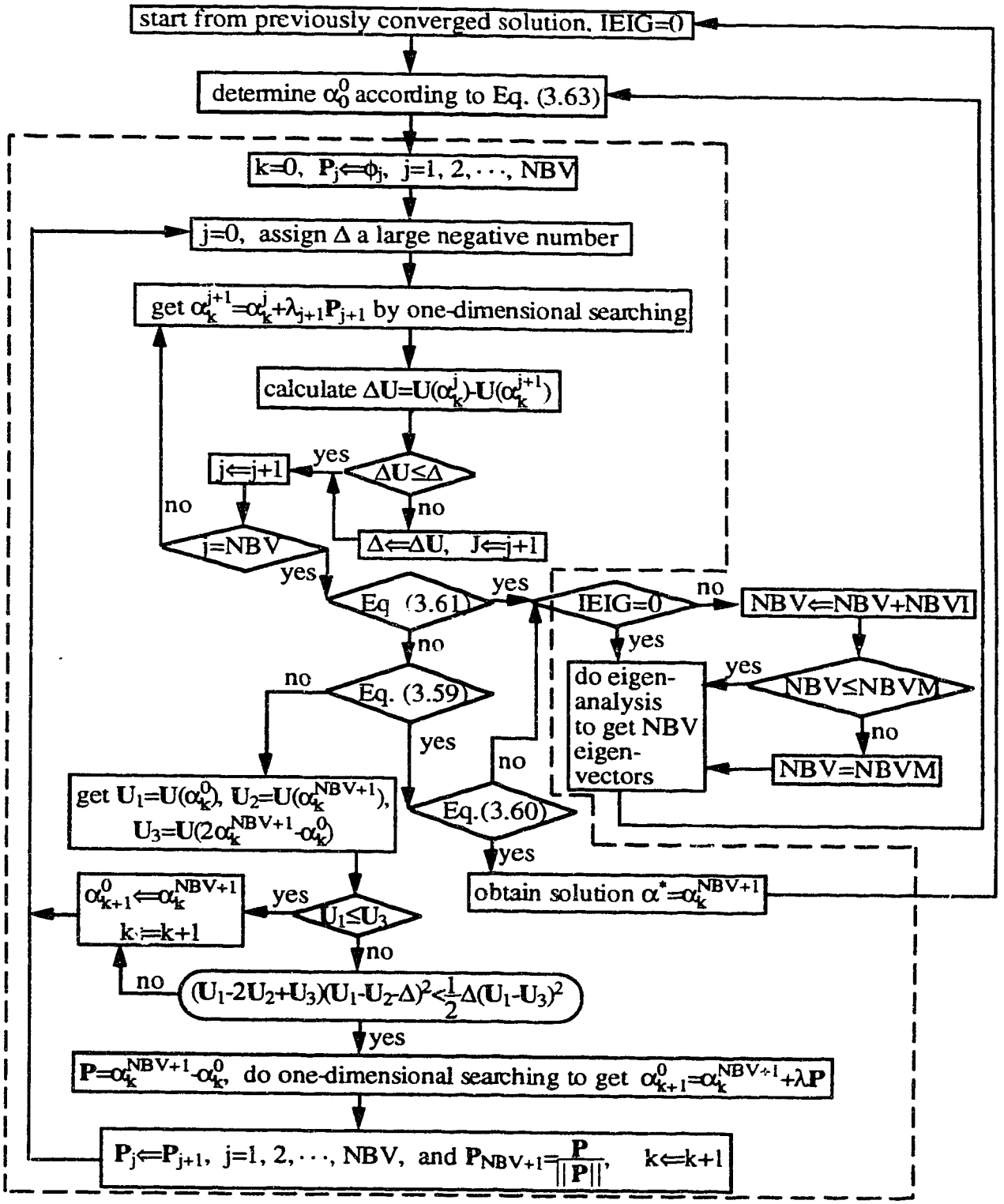

Fig. 3.13 Flow Chart of Solution Technique Based on Direct Search Method

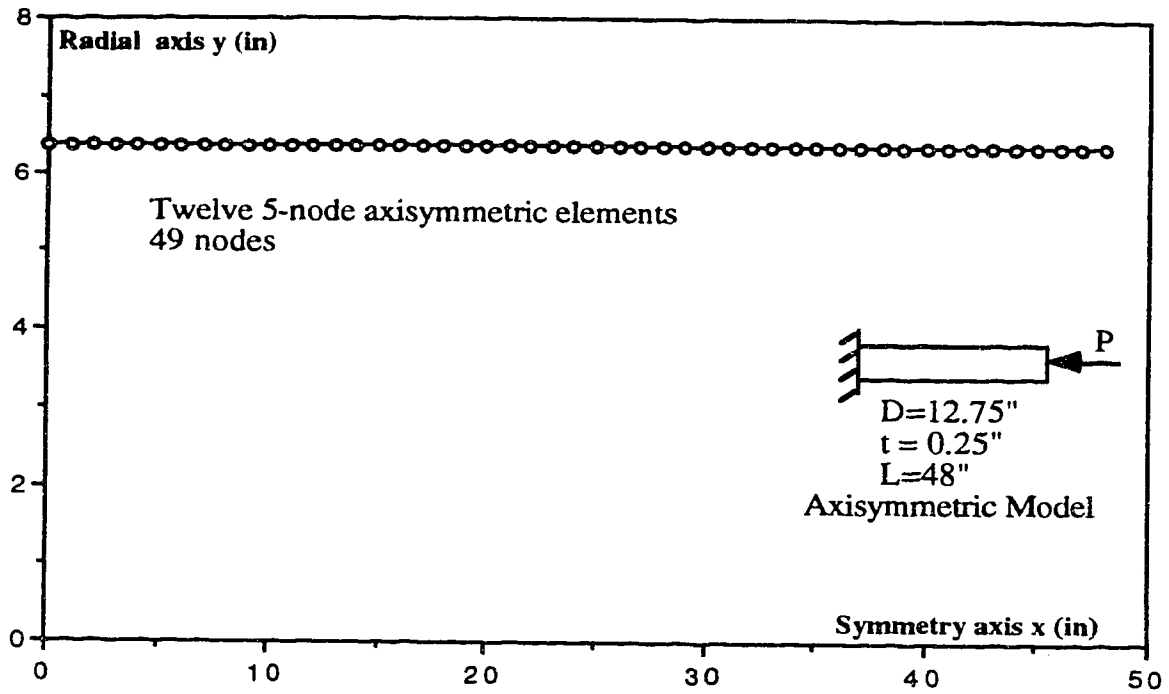

Fig. 3.14 Initial Configuration of the Axisymmetric Finite Element Model for the Axially Compressed Cylinder

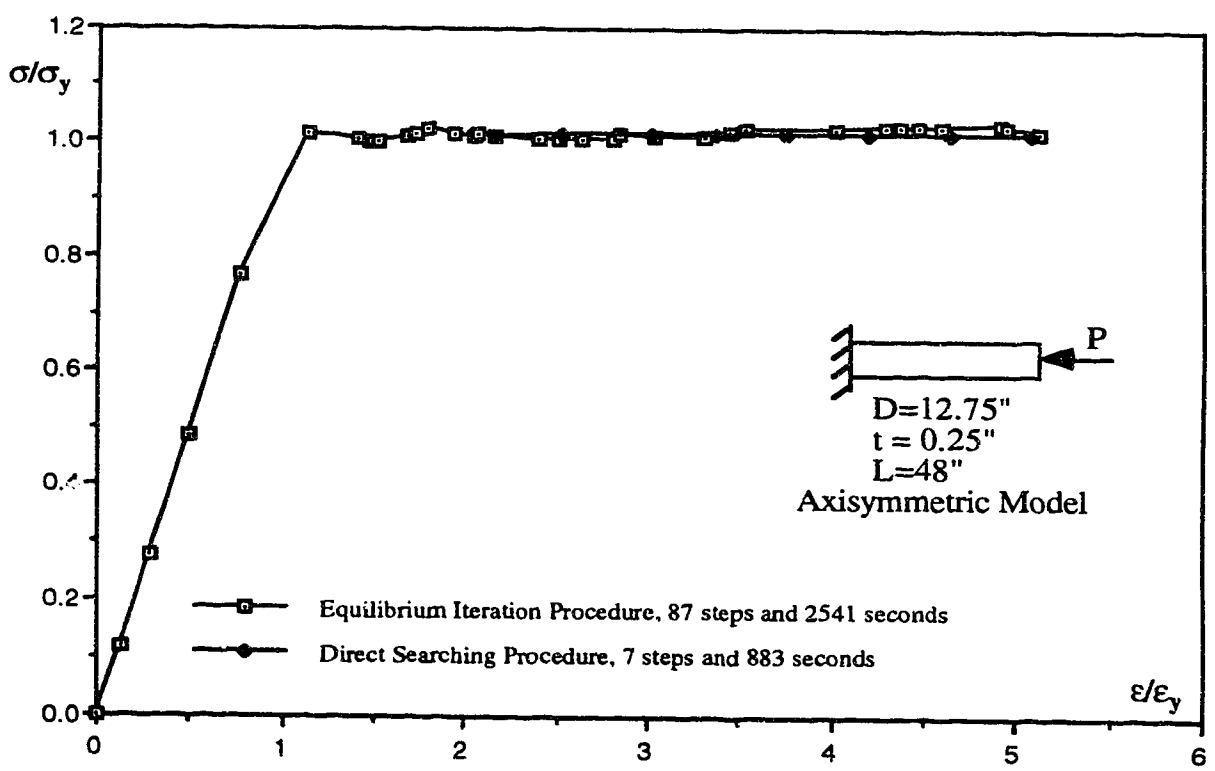

Fig. 3.15 Dimensionless Average Stress-Strain Curves for Solution Procedure Comparison

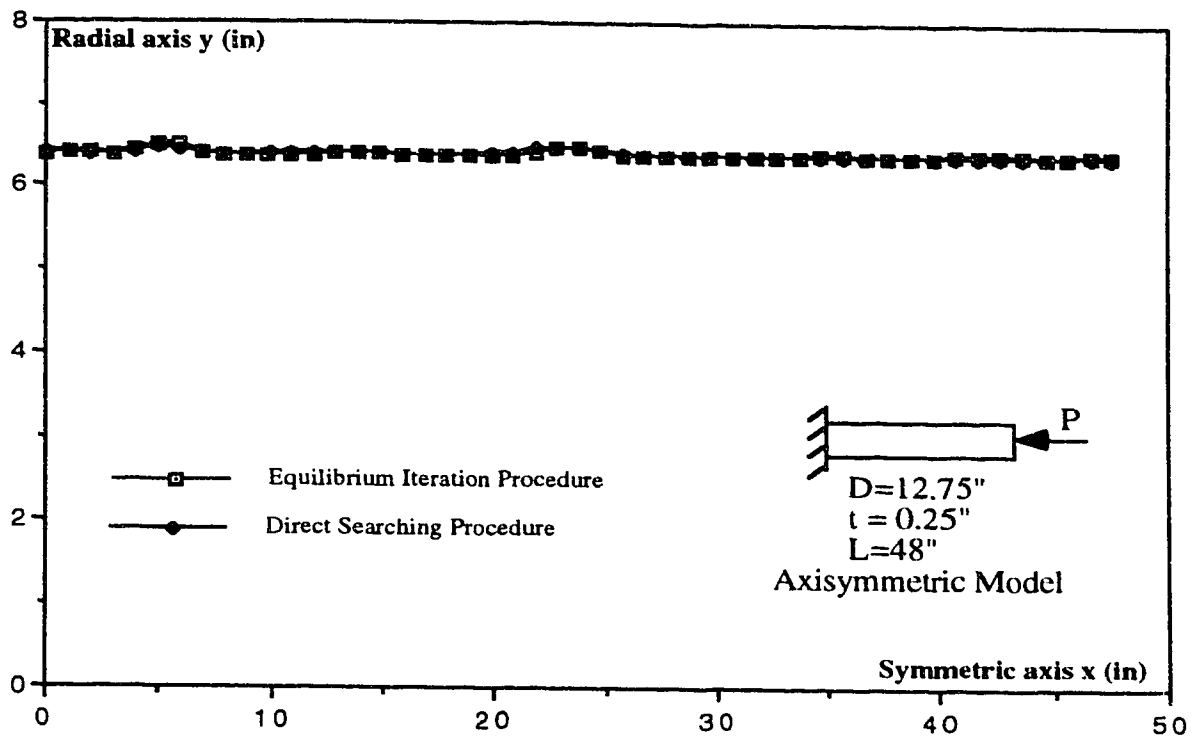

Fig. 3.16 Comparison of Deformed Configurations

CHAPTER 4 POSTBUCKLING ANALYSIS OF PIPE SEGMENTS

Overall, a pipeline behaves as a beam structure. However, a segment of pipeline can be sensitive to the local deformation due to the instability of the pipe wall when it is subjected to applied loads and imposed deformations. The local and the overall behaviors interact with each other and the result of the interaction determines the response of the pipeline. The conceptual approach to the analysis of pipeline response has been discussed in Sect. 1.3. In general, there are two steps : in the first, a three-dimensional shell model is used to analyze the local behavior. In the second step, the effects of the local behavior are integrated into the overall behavior by using a beam model based on the pipeline-beam element developed herein. The development of the pipeline-beam element, and the analysis of the overall behavior of pipeline, will be discussed in Chapters 6 and 7. The current chapter and Ch. 5 are devoted to the analysis of local shell buckling behavior of pipe segments.

The formulation for, and general discussion of, shell buckling have been presented in Chapter 2 which is the theoretical foundation of shell buckling and postbuckling analysis. A robust solution technique has been developed in Chapter 3 which is the basic numerical tool to carry out the shell analysis. The local behavior of pipelines with large D/t is dominated by local shell buckling. Two important aspects are the onset of buckling and the postbuckling response. Postbuckling analysis is the topic of the current chapter and the identification of the onset of buckling will be discussed in next chapter. The discussions about postbuckling analysis include its significance and scope, the finite element model used, and the summary of the characteristics of postbuckling behavior.

4.1 SIGNIFICANCE AND SCOPE OF POSTBUCKLING ANALYSIS

Postbuckling analysis is advantageous for pipeline analysis and design because a better understanding of postbuckling behavior will lead to more economic and safe design and operation of pipelines. There is a real potential to allow the local deformation of pipelines to extend into the postbuckling region in order to optimize pipeline operation, because the initiation of buckling alone should not impair the normal operation of the line. The postbuckling analysis will be carried out on a pipe segment by using a three-dimensional shell model. Because the shell model analysis has a large number of degrees of freedom, elastic-plastic material behavior and large displacements, this is a very demanding task. Due to limited computer and human resources, the scope of postbuckling analysis has

had to be limited to a reasonable number of cases. In this section, the significance of postbuckling analysis is discussed to rationalize the great efforts that have been made in carrying out the postbuckling analyses, and the scope of these analyses is defined.

4.1.1 Significance of Postbuckling Analysis

Postbuckling analysis is a means to explore postbuckling behavior, and therefore the significance of the postbuckling analysis is determined by the significance of the postbuckling behavior. At present the significance of the postbuckling behavior of load carrying structures is better understood than that of structures subjected to imposed deformations. For load carrying structures, it is important to know whether the postbuckling behavior is hardening or softening because in the former case buckling only means a change in the load carrying mechanism, while in the later case it predicts catastrophic failure. For structures subjected to imposed deformation, the load carrying capacity does not cause failure because the structure is not required to carry significant loads. However, the hardening and softening characteristics of the postbuckling load-carrying capacity lead to very different characteristics of the localization of the deformation and strain, and this, in turn, determines the limit states for this type of structure.

A buried pipeline in an Arctic or sub-Arctic region is typical of structures subject to imposed deformation in addition to applied loads. The applied loads are the internal pressure, which is constant during operation, and the overburden loads due to the soil cover above the pipelines. These applied loads alone are sustainable by the pipeline well into the deep postbuckling region. In addition to these applied loads, pipelines are subject to deformation imposed loads such as axial load due to temperature differential and lateral loads due to differential settlements, frost heave and fault movements. The reactions of pipelines to these deformation imposed loads largely depends on the stiffness of the pipeline and the restraint of the soil on the line. When the stiffness of a pipeline deteriorates, the reactions are eventually reduced to a negligible level. Consequently, the load-carrying capacity of pipelines, with respect to these deformation imposed loads, is not a major concern.

The limit states of the pipeline may be considered to be leaking and excessive deformation of cross-section. Leaking is obviously an ultimate limit state which is due to the initiation and propagation of cracks under applied loads and deformation. Prediction of a leakage limit state requires the utilization of fracture mechanics and is beyond the scope of this study. Excessive deformation of the cross-section is considered to be a service limit

state. The industry has not yet defined limits on deformations of the cross-section in a rational way. For the purpose of this study the limit may be defined as a state where the passage of on-line inspection equipment, so called pigging devices, is blocked. Prediction of such deformation states is one of the objectives of this study.

For structures such as buried pipelines, postbuckling behavior has special importance, because the service limit state of pipelines is determined by the postbuckling deformation. The prebuckling deformation is in general very small and can certainly be tolerated. Knowing only the hardening or softening characteristics of the postbuckling behavior is no longer sufficient, as it is for the load carrying structures, because it is the development of deformation in the postbuckling region which is important. As a result, the postbuckling analysis has to be carried out into the deep postbuckling region. This is very different from the postbuckling analysis in the initial postbuckling region because it places heavy demands on the required solution technique and computer resources.

In summary, postbuckling behavior is the basis on which to develop rational limit states design criteria for pipelines subjected to imposed deformation.

4.1.2 Scope of the Postbuckling Analysis

The postbuckling behavior of pipelines is affected by many factors such as the pipe geometry, the pipe material properties and load conditions. The pipe geometry is characterized by the diameter D, the wall thickness t, and the D/t ratio. In the modern pipeline industry, typical pipelines can be as small as 12.75 inches (324 mm) in diameter with D/t ratio of 52 (Workman, 1981), and as large as 48 inches (1219 mm) in diameter with D/t ratio of 104 (Bouwkamp and Stephen, 1973). The postbuckling behavior of these pipelines is expected to differ significantly. The pipe material properties are also expected to influence postbuckling behavior because of the differences in yield strength, the shape of the stress-strain curve, and the tangential modulus.

The loading condition is obviously an important factor because the deformation response for a given pipeline is largely determined by the load conditions and loading history. The operating load condition of pipelines varies from one pipeline to another and from one location to another. Typical loads for a buried pipeline segment are internal pressure, axial load due to temperature differential, and imposed curvature due to differential settlements. The transverse load due to soil cover above the pipeline is usually small and can be neglected for simplification. The internal pressure and axial load can be

assumed constant although they have different values at different locations. The bending moment arising from the imposed deformation is assumed to be uniform over the length of the pipe segment and changing in its magnitude to simulate the increasing differential settlements.

The analyses were carried out by program NISA (Stegmuller, 1984) on a SUN SPARK 1+ station and later on a SUN ELC station. As the postbuckling analysis is required to be continued deep into the postbuckling region, a successful analysis of a specimen includes hundreds of load steps and takes a few weeks of elapsed time. Consequently, the number of specimens which can be analyzed in a limited period is highly restricted. Based on this fact, it was decided that the postbuckling analysis would be confined to one particular pipe geometry with one particular material property. This would be sufficient to investigate the physical phenomena and techniques of analysis.

The effects of the operating load conditions are systematically investigated. Three levels of internal pressure have been chosen to cover the possible range. The pressures produce hoop stresses of 0, 35, and 72 percent of the yield strength. The latter percentage was the highest ratio allowed in the previous design code for oil pipelines (Canadian Standard Association, 1990). Four levels of axial load have been chosen for the low and middle levels of internal pressure. They are 0, 10, 20 and 40 percent of the axial yield load in compression. Five levels of axial load at the high level of internal pressure are chosen. They are at the ratios of 0, 20, and 40 percent for both compression and tension. The highest ratio of the axial yield load is considered to be the maximum level produced by temperature differential in the Norman Wells pipeline, and was recommended by Interprovincial Pipe Line Company Ltd. The combination of the above different levels of pressure and axial load gives thirteen specimen loading conditions which are listed in Table 4.1. In addition to constant pressure and axial load, bending moment is applied for all the specimens as the active load.

A name is assigned to each of the simulated specimens. It is composed of three letters followed by a two-digit number. The first letter is P which identifies this series of analysis as a postbuckling analysis series. The second letter is one of L, M and H which represent low, middle and high levels of internal pressure, respectively. The third letter is either C or T which represents compressive or tensile axial load. The two-digit number is the percentage of axial load with respect to the axial yield load.

4.2 FINITE ELEMENT MODEL

The finite element model for postbuckling analysis of a pipe segment is discussed in this section. This includes the finite element mesh, boundary and loading conditions, and material properties. The finite element model is for simulation of the behavior of a typical pipe segment under operating conditions. Consequently, the model is required to have the capability to capture the characteristic behavior of the pipe segment. This requires that the mesh is of a proper size to model the deformation. This deformation is often localized at one or two locations. The boundary conditions are properly defined to simulate a pipe segment as a part of a pipeline. In addition, the material properties should be representative since different material characteristics would certainly result in different postbuckling behavior.

4.2.1 Finite Element Mesh

Consistent with the defined scope in Sect. 4.1.2, only one particular geometry is used for postbuckling analysis. The pipe is 48 inches (1219 mm) in outside diameter and 0.462 inches (11.7 mm) in wall- thickness. This particular size is that used for the Trans-Alaska Pipeline (Bouwkamp and Stephen, 1974) which is probably the largest size used for a major oil pipeline. The diameter-thickness ratio (D/t) is about 104 which also represents an up-bound for oil pipelines. Since pipes with high D/t ratio are expected to be more sensitive to effects of buckling, this particular geometry is chosen to highlight the postbuckling behavior. In addition, the test series carried out at Berkeley (Bouwkamp and Stephen, 1974) is considered to contain the best experimental results available for a full-sized pipe. Consequently, some comparisons between the test results and this analysis are possible. The length of pipe segment is selected as 276 inches (7010 mm) which is about five and a half times the diameter. This length is considered to be moderate and allows the pipe segment to have shell buckling characteristics. The buckle localizes at a small portion of this length. This is the response observed in pipelines under test and therefore is the behavior to be simulated.

Two symmetry conditions are utilized to reduce the size of the model. These are the symmetry conditions in the bending plane and on the mid-span cross-section, which are in the x-z plane and y-z plane, respectively, of Fig. 4.1. The bending plane is defined by the global coordinate system x, z and the symmetry condition on the bending plane is supported, in general, by the observations from tests (Bouwkamp and Stephen, 1974; Jirsa

et al, 1972; Reddy, 1979; and, Sherman, 1976). A test program currently in progress at the University of Alberta also confirms this symmetry condition. The symmetry condition about the mid-span cross-section is more of an assumption than a fact. Elastic stability theory predicts that buckling waves in an axially compressed cylinder repeat themselves over the length. The symmetry condition about the mid-span cross-section is valid as long as the mid-span section occurs at the peak or bottom of a buckling wave. However, pipe segments usually buckle in the elastic-plastic range and the buckles are often localized at unpredictable locations due to the plasticity and initial imperfections. Consequently, the symmetry condition is only valid at the middle of the buckle. The mid-span cross-section is not the symmetry plane unless the buckle locates at the middle of pipe segment which is not always true. Nevertheless, because the main objective of postbuckling analysis is to investigate the behavior of a typical buckle, instead of the pipe segment as a whole, it is satisfactory to employ the symmetry condition about the mid-span cross-section provided that the complete buckle can be simulated. With the dominant buckle completely simulated somewhere in half of the pipe segment, the loading and deformation characteristics of the buckle can be studied.

With the symmetry conditions about the bending plane and the mid-span cross-section, only a quarter of the pipe segment needs to be discretized. The quarter pipe segment is divided into the main segment and boundary ring as shown in Fig. 4.2, with 132 inches (3353 mm) and 6 inches (152.4 mm) of length, respectively. The boundary ring is introduced for simulation of boundary and loading conditions which will be discussed in detail in the next section. The main segment is discretized by fourty-eight 16-node shell elements (Stegmuller, 1984), and the boundary ring by eighteen 4-node shell elements (Stegmuller, 1984). There are a total of 494 nodes and the mesh is uniform in both the main segment and the boundary ring. A side view and a three-dimensional view of the mesh are shown in Fig. 4.3. The mesh is uniform in longitudinal direction because the dominant buckle can be anywhere along the longitudinal direction. Although buckling usually initiates on the compressive side of the pipe segment, under combination of internal pressure, axial load and bending moment, it will develop and expand in the circumferential direction and sometimes covers the entire circumference. Consequently, the uniform mesh is used in circumferential direction.

The 16-node and 4-node shell elements shown in Fig. 4.4 have cubic and linear interpolations, in both the r and s directions, respectively. The elements can model large displacements and elastic-plastic response. The cubic interpolation gives the 16-node

element strong capability to model deformation with relatively lower nodal density and better convergence characteristics. The 4-node element is simple and appropriate to be used in the boundary ring where the major concern is to distribute applied load and fulfill the end boundary conditions (see Sect. 4.2.2).

4.2.2 Boundary and Loading Conditions

Boundary conditions are needed at the mid-span cross-section, end cross-section, and the top and bottom edges as shown in Fig. 4.2. The boundary conditions on the mid-span cross-section, and the top and bottom edges are obviously the symmetry conditions. On the top and bottom edges, the symmetry conditions are that the displacements in global y-direction, and the rotation about the global x and z axes are restricted. The symmetry conditions on the mid-span cross-section are more complicated. The local shell coordinate system is first defined in Fig. 4.4 as r, s and t where t is the normal direction of the shell, r is the perpendicular to t-direction in the t-x plane and s is the one in t-y plane. The symmetry conditions are that the displacements in global x-direction, and rotations about the t and s axes are zero. As shown in Fig. 4.1 the pipe segment is allowed to shorten or extend as it deforms, and the end cross-section has to be allowed to move if the mid-span cross-section is fixed in the $\tilde{x}$-direction. As an alternative, the mid-span cross-section can be allowed to move in order to fix the end cross-section and the rigid body displacements superimposed here will not affect the strain and stress states. Therefore the boundary condition of displacement on the mid-span cross-section can be modified to that where all the nodes on the mid-span cross-section have the same displacement in the x-direction. The boundary conditions of rotation remain the same and can be enforced by directly specifying the boundary codes because the rotational degrees of freedom are defined in the local shell coordinate system. The boundary condition on the top and bottom edges can be enforced in a similar way.

On the end cross-section, the boundary conditions are that the y-direction displacement at the geometric center of the cross-section is restricted to simulate the simple support at the end section, and the plane of end section remains plane to simulate the restraint provided by the rest of the pipeline connected to the pipe segment. Rotation of the end section about the geometric centroid and deformation of the section in the plane are permitted. Because of the decision to allow the mid-span cross-section to move, the x-direction displacement at the centroid of the end cross-section is restricted to zero. The plane end section condition is mainly due to the fact that the pipe segment is a part taken from the adjacent pipeline which does not buckle. This adjacent pipeline has strong axial

stiffness and provides restraint to prevent the out-of-plane deformation.

A boundary ring is used to enforce these boundary conditions as shown in Fig. 4.2. The boundary ring is assumed to be elastic and has the same wall thickness as the main segment. The support at the centroid is modelled as support on the horizontal diameter as shown in Fig. 4.1(b), and this approximation is acceptable as long as the deformation of the end cross-section is symmetric about its horizontal diameter. The plane end section condition is enforced by coupling the magnitude of the x-direction displacements of the corresponding nodal points on the compression and tension sides as shown in Fig. 4.5. There are 19 nodes on the end section which are uniformly distributed on the half circumference and symmetric about nodal point 485. Coupling the magnitude of the x-direction displacements of the corresponding nodal points combines the stiffness from compression and tension sides and has been proven to be able to prevent the out-of-plane deformation at the end section. However, this coupling can only be applied if symmetry about the horizontal diameter can be maintained on the deformed end cross-section. The elastic boundary ring helps to maintain this symmetry.

Internal pressure is applied on the element as an element load which is transformed into nodal load to satisfy equilibrium by the program NISA (Stegmuller, 1984). The external axial loads are applied at the end cross-section and the mid-span cross-section with equal magnitudes and opposite directions. The axial load on the end section is uniformly distributed. The forces on the mid-span cross-section can be distributed in any manner because the axial displacements are coupled. The bending moment is applied as a set of nodal forces on the end section which are converted from linearly distributed load as shown in Fig. 4.5. The elastic boundary ring helps to distribute the nodal loads and reduces the stress concentration which might cause initiation of premature buckling.

4.2.3 Material Property Representation

Pipe steel may exhibit different type stress-strain curves depending on the grade and composition. However, in this study it is limited to one particular stress-strain curve. A bilinear material model based on Grade XL 65 steel is used for simplicity. This model has elastic modulus of 29800 ksi (205500 MPa), Poisson ratio of 0.3, yield strength of 63.5 ksi (438 MPa) and strain hardening modulus of 124 ksi (855 MPa). The yield plateau is not modelled because the plateau is eliminated in the manufactory process. The strain softening portion is not included because the real strain in the pipe segment, in general, is not large enough to reach it.

4.3 CHARACTERISTICS OF POSTBUCKLING BEHAVIOR

Based on the solutions of the 13 specimens listed in Tab.4.1, the postbuckling behavior of pipe segments with respect to loading condition can be summarized in terms of the softening characteristics of the moment-curvature relations, the localization of deformation, the buckling modes, and the cross-sectional distortion. Postbuckling analysis produces an enormous volume of data which must be reduced to a proper form to characterize the postbuckling behavior. Some representative quantities must be defined to represent the solution and to present various aspects of the postbuckling behavior. These can be divided into two groups. One is based on longitudinal deformation and the other on cross-sectional deformation. In the following sub-sections, the representative quantities will be first defined, and the postbuckling behavior is then discussed.

4.3.1 Description of Deformation

The deformation is described in terms of the longitudinal deformation and cross-sectional deformation. To describe the longitudinal deformation, two cross-sections have to be first identified that define the *buckling segment* as shown in Fig. 4.6 (a). The buckling segment is a small segment which contains only the most significant buckle. The sections defining the buckling segment are assumed to be plane sections which is a valid assumption for most specimens because of the unloading state in the adjacent regions without buckling. Out-of-plane deformation may extend to adjacent regions which do not buckle and consequently the above assumption is not valid in all specimens. In these cases, a best fit plane should be used to replace the original cross-sectional plane and state variables on this best fit plane should be found by interpolation.

Having the buckling segment defined, and the half pipe segment defined by the mid-span and end cross-sections, which are plane sections due to the imposed boundary conditions, two sets of quantities can be defined. One is defined as the average curvature and strains on the buckling segment which is referred to as *local*, and the other is the average curvature and strains on the half pipe segment which is referred to as *overall*. The average curvatures are the relative rotations of the buckling segment and pipe segment divided by the corresponding lengths.

Three types of average strain are defined. These are the *compressive strain* of the extreme fiber on the compressive side, the *tensile strain* of the extreme fiber on the tension side and the *axial strain* at the centroidal axis of the cross-section. The local and overall

compressive and axial strains are defined as the relative shortening of the buckling segment and the pipe segments, respectively, at their specified positions divided by the corresponding original lengths. The local and overall tensile strains are defined as the relative extension of the buckling segment and the pipe segment, respectively, at the extreme fiber on tension side divided by the corresponding lengths. By these definitions, the compressive and axial strains are positive in compression, and tensile strain is positive in tension.

The cross-sectional deformation is defined on a cross-section to measure the most significant deformation, which is usually in the middle of the buckling segment. Two typical deformed cross-sections are shown in Fig. 4.6. The in-plane and out-of-plane diameters, D_{in} and D_{out}, define the representative dimensions of the cross-section in the global z and y directions, respectively. The in-plane and out-of-plane diameters, in general, represent the maximum and minimum diameters, D_{max} and D_{min}, with the correspondence shown in Fig. 4.6. The top and bottom radii are defined as the distances from the centroid of the cross-section to the top and bottom fibers. With these dimensions of the cross-section defined, the following four quantities can be defined to represent the cross-sectional deformation.

First, the *out-of-roundness* is defined as (Price and Anderson, 1991)

$$\text{out-of-roundness} = \frac{D_{max} - D_{min}}{D} \times 100\% \tag{4.1}$$

where D is the nominal diameter. Out-of-roundness is always a positive number which indicates the difference of the in-plane and out-of-plane dimensions of the cross-section. However, it does not distinguish between the deformation patterns shown in Fig. 4.6 (b) and (c).

This work proposes three other quantities to describe the cross-sectional distortion of pipes. The first two measures are

$$\text{diametric differential} = \frac{D_{out} - D_{in}}{D} \times 100\% \tag{4.2}$$

$$\text{diametric expansion} = \left(\frac{D_{out} + D_{in}}{D} - 1\right) \times 100\% \tag{4.3}$$

Diametric differential is intended for the deformation pattern in Fig. 4.6 (b). A positive diametric differential indicates the decrease in in-plane diameter and increase in out-of-plane diameter. When the deformation of this pattern reaches a limiting value, the passage of

inspection devices may be blocked. It should be noted that the out-of-roundness is the absolute value of the diametric differential. While the former is commonly used in oil and gas industry, the latter is the more informative because it differentiates between the two basic buckling modes. *Diametric expansion* is intended for the deformation pattern shown in Fig. 4.6 (c) where a positive number indicates an average increase in the dimension of the cross-section. When the deformation of this pattern reaches a limiting value, material failure may occur locally at the crease of the wrinkle. This is because large strain is introduced locally at the crease of the wrinkle.

The last quantity proposed as measure is the radius differential defined as

$$\text{radius differential} = \frac{R_{bot} - R_{top}}{R} \times 100\% \tag{4.4}$$

where R is the nominal radius. *Radius differential* represents the cross-sectional distortion due to reasons other than ovalization. Ovalization is the main component of cross-sectional distortion in the prebuckling state and is symmetric about y-axis. Therefore, there is no radius differential corresponding to ovalization.

4.3.2 Softening of Moment-Curvature Relations

The moment-local curvature curves are shown in Figs. 4.7 to 4.9 for specimens with low, middle and high levels of pressure, respectively. These figures indicate the sensitivity of the flexural behavior to axial loads. The local curvatures, instead of overall curvatures, are used because they are more representative of the buckling segment. In these figures, the moments and curvatures are nondimensionalized by the yield moment and yield curvature. The yield moment is the moment which, by itself, produces initial yielding in the extreme fibers on both the compression and tension sides of the pipe for a bilinear elastic-plastic model. This is calculated to be 52000 kip-in (5900 KN-m). The yield curvature is the curvature corresponding to initial yield in the extreme fibers, which is the curvature corresponding to the yield moment. It is calculated as 0.8965×10^{-4} (1/in). The yield strain used to nondimensionalize the strains is 0.002131 (in/in). In these figures and subsequent figures, moment, curvature, compressive strain at the extreme fiber, and axial strain at the centroid of the cross-section are denoted by M, ϕ, ε^c and ε^o, respectively. For the curvature and strains, the average measurements over the buckling segment and the pipe segment are indicated by one of the subscripts L and o, for local and overall, respectively.

The load carrying characteristics can be equally well represented by moment-local

compressive strain curves which are grouped in a similar way to the moment-curvature curves in Figs. 4.10 to 4.12. The local compressive strain includes both the average flexural deformation and the average axial deformation and probably is a better characterization of deformation at the extreme fiber than the local curvature. The moment-local curvature curves, of Figs. 4.7 to 4.9, are grouped according to the compressive axial load at levels of 0, 20 and 40 percent and are shown in Figs. 4.13 to 4.15. These figures indicate the sensitivity of the flexural behavior to internal pressure.

Softening is observed in moment-curvature curves of all 13 specimens. Softening in moment-curvature curves refers to behavior exhibiting decreasing moment carrying capacity with respect to increasing curvature. In general, the pipe segment experiences a linear elastic region up to the initiation of yielding, a gradual yielding region, and then a softening region. The elastic region exists in every specimen except Specimen PHC40 (see Figs. 4.9, 4.12 and 4.15) where the constant internal pressure and axial load initiate the yielding before any moment is applied. The gradual yielding region produces a yield plateau which usually contains the limit point with the maximum moment as for Specimens PLC00, PLC10, PHT20 and PHT40. The length of this yield plateau decreases as the levels of pressure and compressive axial load increase and virtually disappears for many specimens. The softening region exists in every moment-curvature curve. These usually contain a strong softening portion with a steep drop in moment carrying capacity followed by a softening portion where the moment carrying capacity drops relatively gradually with respect to the increase of curvature. The combination of strong and gradual softening portions repeats in the softening region for some specimens such as PHT20 and PHC00 (see Fig. 4.9), PMC20 (Fig. 4.8) and PLC20 (Fig. 4.10).

The maximum moments carried by specimens are greatly affected by the pressure and axial load. It varies from a maximum of 1.23 times the yield moment for Specimen PLC00, where no pressure and axial load are applied, to 0.11 time the yield moment for Specimen PHC40, where the maximum pressure and compressive axial load are applied. The capacity in the postbuckling region is affected by pressure and axial load in a similar way as for the maximum capacity. The effects of pressure on the moment carrying capacity are illustrated in Figs. 4.13 to 4.15. For the group with no axial load, the moment-curvature curves have the similar average slope in the postbuckling region and the internal pressure contributes mainly to the reductions in moment carrying capacity. For the group with 20 percent compressive axial load, the similar characteristics apply only to the specimens with low and middle levels of pressure. The specimen with the high level of

pressure has significantly reduced slope in the postbuckling region. For the group with 40 percent compressive axial load, the specimens with the middle and high levels of pressure have the significantly reduced slope in the postbuckling region.

The fundamental reason to have different slopes in the postbuckling region is the difference in the buckling modes. These may be dominated either by flexural deformation or axial deformation. For the flexural deformation dominated buckling mode, the buckle concentrates on the compressive side of the pipe segment. Examples are the buckling modes for Specimens PLC00 and PHC00 shown in Figs. 4.29 and 4.33. The axial deformation dominated buckling mode has the bulging developed over all or most of the circumference of the pipe segment, as shown in Fig. 4.32 for Specimen PMC40. The buckled section of the axial deformation dominated buckling mode, when it is fully developed, can only take a very small amount of moment. Consequently, the moment-curvature curves are flat with a small moment carrying capacity in the postbuckling region (see, for example, PHC40 on Fig. 4.15). On the other hand, the buckled configuration of the flexural deformation dominated buckling mode changes from a relatively strong moment configuration to weak as the buckling initiates and develops on the compressive side. As a result, the moment carried by the buckling section reduces continuously. Because the buckling is confined to the compressive side while the tensile side of the pipe segment remains strong, a significant negative moment may be developed which is required to stabilize the pipe segment under imposed curvature. This maintains the equilibrium state. A good illustration of this is the case of Specimen PLC40 as seen in Fig. 4.15.

4.3.3 Localization of Deformation

In the postbuckling region, the deformation localizes in the buckling segment for all the specimens. However, the degree of localization depends on the loading conditions. The localization of deformation is illustrated in this section by comparing the deformation of the buckling segment with that of the pipe segment. Since the boundary cross-sections of the buckling segment and the pipe segment are considered to be plane sections, the deformation can be described by local curvature and local axial strain for the buckling segment, and by overall curvature and overall axial strain for the pipe segment. These measures of deformation have been defined in Sect. 4.3.1. For these comparisons, the axial strain is defined as positive in compressive.

The comparison is first carried out for deformation paths of the buckling segment and pipe segment. The deformation path is the axial strain-curvature curve which indicates

the relative contributions of the axial and flexural components to the total deformation. Figs. 4.16 to 4.20 show the comparisons of deformation paths for Specimens PLC00, PLC40, PHC00, PHC40 and PHT40 as the typical examples. In each of these figures, the local and overall axial strain-curvature curves represents the deformation paths for buckling and pipe segments, respectively. The localization of deformation is clearly demonstrated in all these figures where the local curvature and axial strain are significantly larger than the overall curvature and axial strain. Different behaviors are also represented in these figures. These curves, both the local and overall paths, are approximately piecewise linear which means that the axial strains and curvatures are proportional to each other with different ratios for each of the sub-divisions. For specimens such as PLC00, PHC00 and PHT40 with flexural deformation dominated buckling modes, the localization is contributed more by flexural deformation which is indicated by the relative small slope of their deformation paths. For specimens such as PLC40 and PHC40 with axial deformation dominated buckling mode, the contribution of axial deformation is equally important as that of flexural deformation.

The importance of the axial deformation increases as the pressure and compressive axial load increase. This trend is illustrated by Fig. 4.21 and 4.22 where the deformation paths of the buckling segment are shown for Specimens PLC00 and PHC00, and, Specimens PHT40, PHC00 and PHC40, respectively. Figure 4.21 shows the effects of the pressure, while Fig. 4.22 shows the effects of the axial load. When the axial deformation increases its significance with respect to the flexural deformation, the buckling mode changes from flexural deformation dominated to axial deformation dominated.

The developments of deformation localization are shown in Figs. 4.23 to 4.28 in terms of the ratios of local and overall curvatures and the ratios of local and overall axial strains. These ratios are plotted with respect to overall curvature which represents the total relative rotation of the pipe segment. While unit ratio indicates the uniform deformation, deformation localization is observed in all the specimens. Higher pressure produces more significant localization which is demonstrated in Figs. 4.23 to 4.25 for specimens with the same axial loads. The localization is also initiated at smaller overall curvature for specimens with higher pressure. The effects of axial load are shown in Figs. 4.26 to 4.28 in terms of the localization of axial strains. The localization initiates at smaller overall curvature and develops faster for larger compressive axial load. These observations are consistent with the general conclusion that the internal pressure and compressive axial load increase the localization of deformation.

4.3.4 Buckling Modes

There are in general two types of buckling modes, the diamond mode and bulging mode. The inward-and-outward diamond buckling mode is shown in Figs. 4.29 and 4.30 where a side view, a three-dimensional view, and a rendered view of the deformed configurations for Specimens PLC00 and PLC40 are shown. Specimen PLC00 is subjected only to bending moment which produces the buckle in the mid-span of the pipe segment. Specimen PLC40 is subjected to the maximum compressive axial load applied in this series in addition to the bending moment, and the buckle formed in the region about a quarter span from the end. The bulging buckling mode is shown in Figs. 4.31 to 4.35 for the deformed configurations of Specimens PMC10, PMC40, PHC00, PHC40 and PHT40. The buckles may locate at the mid-span, as for Specimen PMC10, or off the mid-span, as for the other specimens shown in these figures.

It is clear that the buckling mode is primarily dependent on the internal pressure. Specimens without pressure will buckle in the diamond mode no matter what axial load is applied. However, for specimens with middle and high levels of pressure, the bulging mode is the buckling mode for all of them. Consequently, for geometry and material properties specified in this series, internal pressure at a relatively low level, certainly not higher than 35 percent, can prevent the pipe segment from buckling in the diamond buckling mode and force it to buckle in the bulging buckling mode. This conclusion may not be directly extendable to pipe segments with different geometry. However, according to the general shell behavior discussed in Sect. 2.2.2, shells with higher D/t ratios tend to buckle in diamond mode. Consequently, the conclusion obtained here is likely to be verified for pipe segments with D/t ratios lower than 104. Considering the fact that the pipes currently used in the oil and gas industry normally have smaller diameters and lower D/t ratios, it appears to be acceptable to generalize the conclusion about buckling modes, i.e. the pipe segment will buckle in the bulging buckling mode if there is internal pressure at a level which need not be higher than 35%.

In addition to the differences between the diamond and bulging buckling modes, differences are obvious between the buckling modes of Specimens PLC00 and PLC40 for the diamond buckling mode, and between those of Specimens PMC10 and PMC40 for the bulging buckling mode. The principal difference is in the dimensions of the buckles in the circumferential direction. The buckles of Specimens PLC00 and PMC10 are confined to the compressive side of the pipe segment. The buckles of Specimens PLC40 and PMC40,

however, cover most of, or the entire, circumference. The reason for the difference is the different combinations of the axial deformation and flexural deformation. When the flexural deformation dominates, the compressive region on the cross-section is confined to the compressive side, and so is the buckle. When significant compressive axial load is applied, as for Specimens PLC40, PMC40 and PHC40, the compressive region extends over most of the cross-section and buckles develop gradually to cover most of the circumference. Tensile axial load helps to confine the buckle to the compressive side of the cross-section. To distinguish between these two different characteristics, the names of *flexural deformation dominated* and *axial deformation dominated* buckling modes are used to refer to buckling modes confined to the compressive side and extended over most of circumference, respectively. Both diamond and bulging buckling modes can be dominated by flexural or axial deformation where examples are Specimens PLC00 and PLC40 in Figs. 4.29 and 4.30 for the diamond buckling mode and Specimens PHT40 and PMC40 in Figs. 4.35 and 4.31 for the bulging buckling mode. The axial load and internal pressure are both important factors to decide whether the axial deformation or the flexural deformation dominates the buckling mode. Increase in internal pressure and axial load would emphasize the importance of the axial deformation and lead to axial deformation dominated buckling modes.

The length that a buckle covers in the longitudinal direction can be called its *wavelength*. The wavelength of the most significant buckle is called the *principal wavelength*. The principal wavelength is actually the length of the buckling segment on which the local curvature and local strains are defined, and is used to show the dimension of buckles in the longitudinal direction and the effects of loading conditions. The principal wavelengths for all 13 specimens in this postbuckling analysis series are listed in Tab. 4.2. Two trends, in general can be observed. First the principal wavelengths of the specimens with diamond buckling mode tend to be larger than those with bulging buckling mode. This is seen in Table 4.2 by the fact that the principal wavelengths of specimens without pressure are in general larger than those with pressure. Secondly, the principal wavelengths of the specimens with flexural deformation dominated buckling mode are in general larger than those with axial deformation dominated buckling mode. The evidence can also be found in Tab. 4.2 where the specimens with higher level of pressure or axial load normally have relatively smaller principal wavelength.

4.3.5 Cross-Sectional Distortion

The cross-sectional distortion becomes important because limit states of excessive

deformation can be defined from the pattern and magnitude of the cross-sectional distortion. Depending on the buckling mode, different patterns of cross-sectional distortion are observed. Typical examples are shown by the solid lines in Figs. 4.36 to 4.39, for Specimens PLC00, PMC40 and PHC00. Deformed cross-sections are shown at four different stages of deformation for each of the selected specimens which are identified by the values of local curvatures. In general, the first one, (a), is corresponding to the state representing the buckling onset. The second stage, (b), is the point on the moment-curvature curve where the first significant softening starts. The limit point where the maximum moment is achieved may be close to the first stage if the limit point is reached right after the initiation of buckling, or to the second stage if the softening follows the limit point immediately. If the softening closely follows the initiation of buckling, only one deformed cross-section is shown. The fourth stage, (d), is the last point on the moment-curvature curve. For each of the deformed cross-sections, there is a reference section shown by dashed line which has the geometric center at the same location as the deformed section and is undeformed.

Specimen PLC00 is a typical example of a flexural deformation dominated diamond buckling mode and the development of cross-sectional distortion is shown in Fig. 4.36. For this type of buckling mode, the diameter in the bending plane, called the in-plane diameter, is significantly reduced while the diameter perpendicular to the bending plane, called the out-of-plane diameter, is increased. An appropriate measurement of the magnitude of cross-sectional distortion for this type of buckling mode is the diametric differential defined in Sect. 4.3.1 which is the normalized differential between the out-of-plane and in-plane diameters. The cross-sectional distortion develops from a minimum at the onset of buckling to very significant distortion in the deep postbuckling region. The scale of deformation is one to one for all the deformed cross-sections and the figures show the real proportions of the deformation.

Examples for the bulging buckling mode are shown in Figs. 4.37 and 4.38, for Specimens PMC40 and PHC00, where the former is an axial deformation dominated bulging buckling mode and the later is a flexural deformation dominated mode. For this type of bulging buckling mode, both in-plane and out-of-plane diameters increase as the curvature increases. When the buckling is dominated by axial deformation, the diameter increase is more uniform along the circumference, as in Fig. 4.37 (c) and (d) which is typical of axially symmetric buckling modes. When the flexural deformation dominates the buckling mode, the increase of in-plane diameter is larger than that of the out-of-plane

diameter as shown in Fig. 4.39. One of the best measurement for the magnitude of cross-sectional distortion for the bulging buckling mode is the diametric expansion defined in Sect. 4.3.1 which is the normalized average increase of in-plane and out-of-plane diameters.

The diametric differential is plotted with respect to the local curvature of the buckling segment in Figs. 4.39 to 4.41 for specimens with low, middle and high levels of pressure, respectively. It is positive for specimens with diamond buckling mode as shown in Fig. 4.39 and negative for specimens with bulging buckling mode dominated by flexural deformation such as Specimens PMC00, PMC10, PMC20, and PHC00. It becomes negligible for specimens with bulging buckling mode dominated by axial deformation such as Specimens PMC40, PHC20 and PHC40. Since the diametric differential is a measurement intended for diamond buckling mode, it is significant only if it is a large positive number. Consequently, it becomes less significant as the compressive axial load and internal pressure increase.

The diametric expansion is shown in Figs. 4.42 to 4.44 in a similar way as for diametric differential. It is less significant for specimens with diamond buckling modes where it is usually negative or very small. The diametric expansion becomes positive for all pressurized specimens. For the group of specimens with the middle level of pressure, the diametric expansions are very close for different levels of axial load until the buckles are developed on the entire circumference and the cross-sectional distortion starts to increase very rapidly with respect to the curvature. The group of specimens with the high level pressure shows more effects from axial load. In general, large compressive axial load increases the diametric expansion and large tensile axial load decreases it.

Specimen Identification	Constant Axial Load (kip)	Internal Pressure (ksi)
PLC40	-40% F_y	0
PLC20	-20% F_y	
PLC10	-10% F_y	
PLC00	0	
PMC40	-40% F_y	35% P_y
PMC20	-20% F_y	
PMC10	-10% F_y	
PMC00	0	
PHC40	-40% F_y	72% P_y
PHC20	-20% F_y	
PHC00	0	
PHT20	20% F_y	
PHT40	40% F_y	

NOTES : 48"x0.462" DSAW X65 pipe (1219mmx11.7mm)

$F_y = A\sigma_y = 4423.92$ (kip)

$$P_y = \frac{2\,t\,\sigma_y}{(D - 2\,t)} = 1.2464 \text{ (kis)}$$

Specimen Identification : PXYnn

P : P = Postbuckling analysis

X : L = Low internal pressurewith p/p_y of 0%
M= Medium internal pressure with p/p_y of 35%
H = High internal pressure with p/p_y of 72%

Ynn : Cnn = Compression with F/F_y of nn%
Tnn = Tension with F/F_y of nn%

Table 4.1 Specimens and Loading Conditions for Postbuckling Analysis

Specimen Identification	Principal Wavelenth		Buckling Mode
	(in)	(mm)	
PLC40	2x38.5	2x978	diamond
PLC20	2x33	2x838	diamond
PLC10	55	1397	diamond
PLC00	55	1397	diamond
PMC40	44	1118	bulging
PMC20	2x22	2x559	bulging
PMC10	44	1118	bulging
PMC00	27.5	699	bulging
PHC40	44	1118	bulging
PHC20	2x22	2x559	bulging
PHC00	27.5	699	bulging
PHT20	39	991	bulging
PHT40	44	1118	bulging

NOTES : The specimens with the principal wavelengths shown in the form of 2x(a number) are those with buckles in the mid-span of the pipe segment, and the principal wavelengths are doubled because of the symmetry conditions at the mid-span cross-section.

Table 4.2 The Principal Wavelengths of Specimens for Postbuckling Analysis

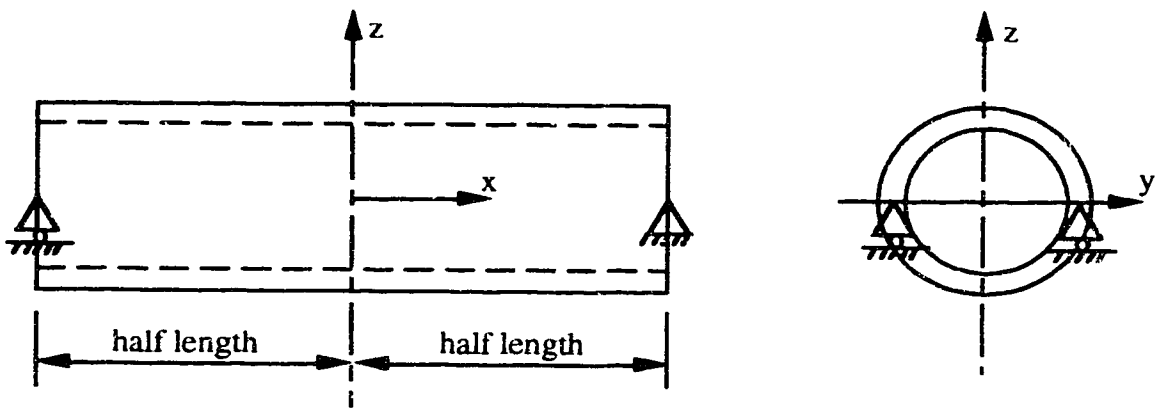

(a) mid-span cross-section (b) bending plane

Fig. 4.1 Symmetric Planes of Pipe Segments

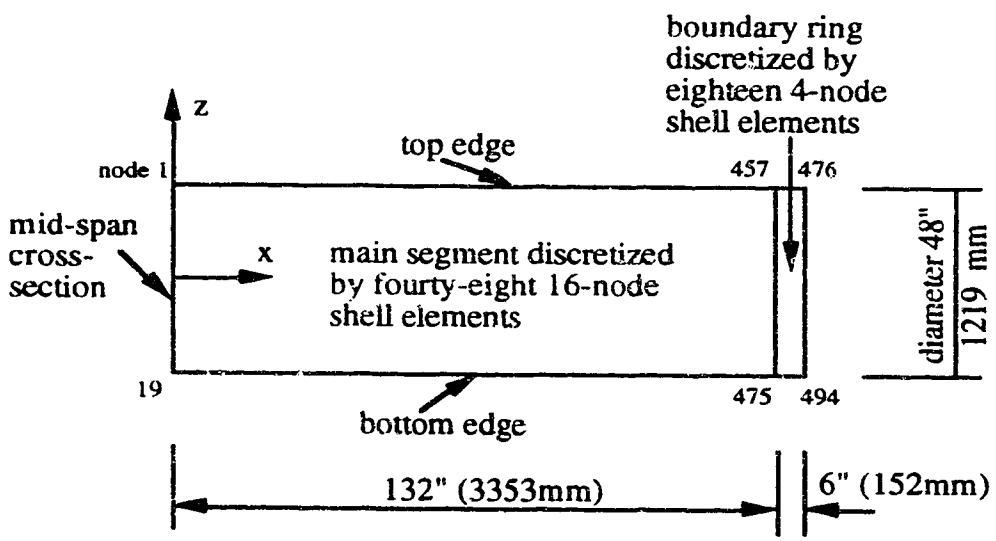

Fig. 4.2 Global Coordinate System and Dimension of the Quarter Pipe Segment

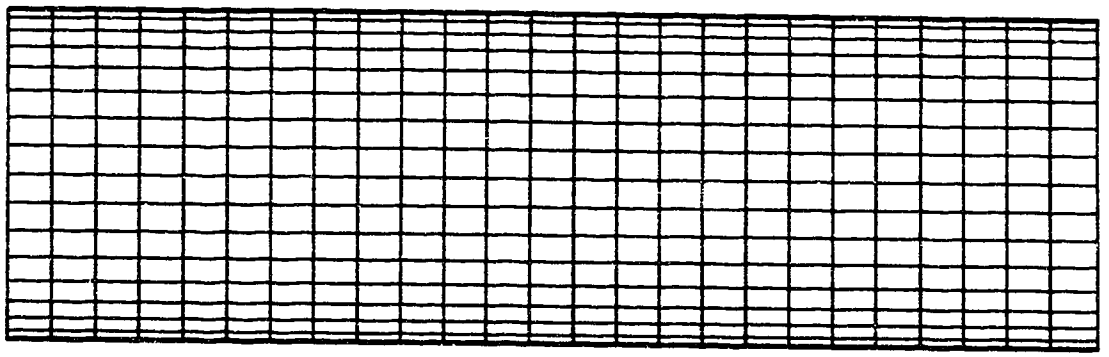

(a) Side View

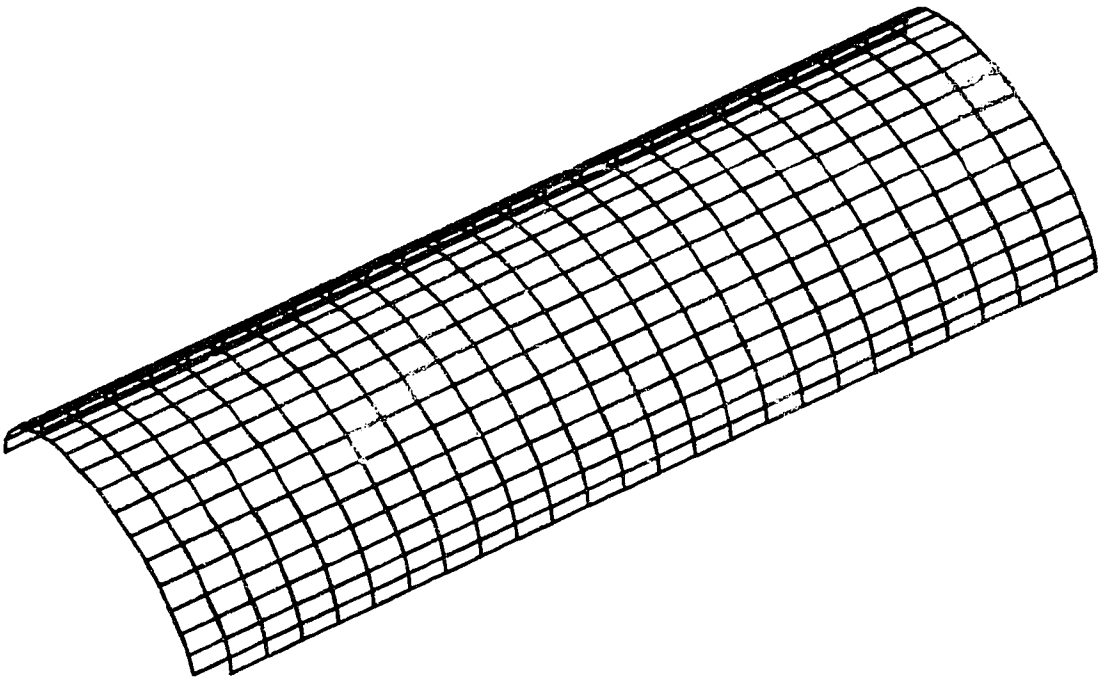

(b) Three Dimensional View

Fig. 4.3 Finite Element Mesh for Three Dimensional Shell Model of Pipe Segment

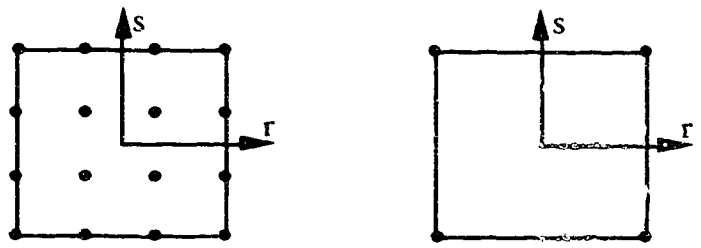

(a) 16-node element (b) 4-node element

Fig. 4.4 Nodal Layout of Shell Elements

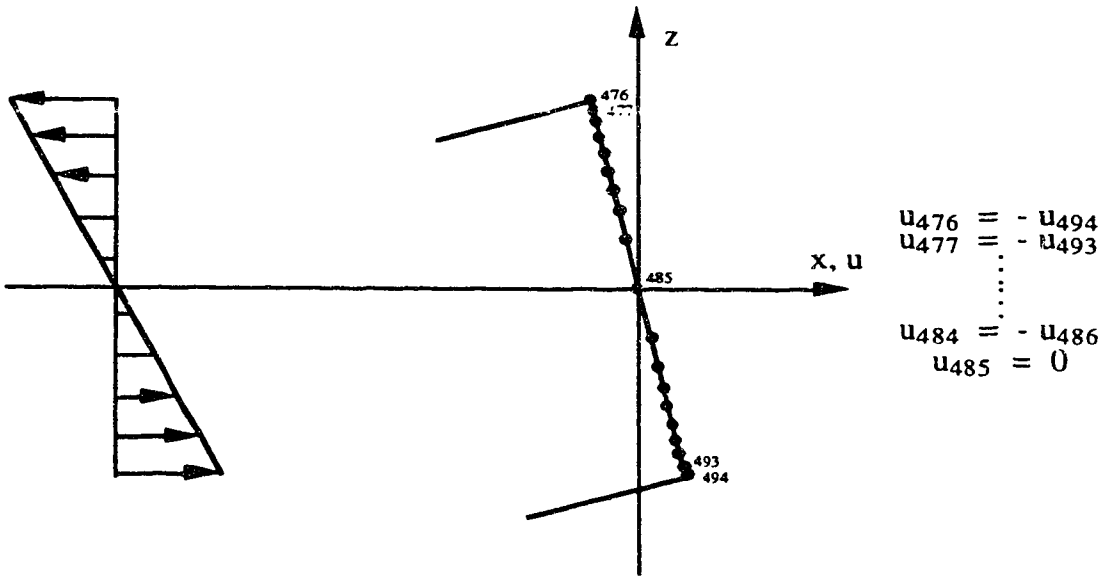

(a) applied bending moment (b) coupled displacements for the plane section condition

Fig. 4.5 Plane Section Condition and Applied Moment on the End Cross-Section

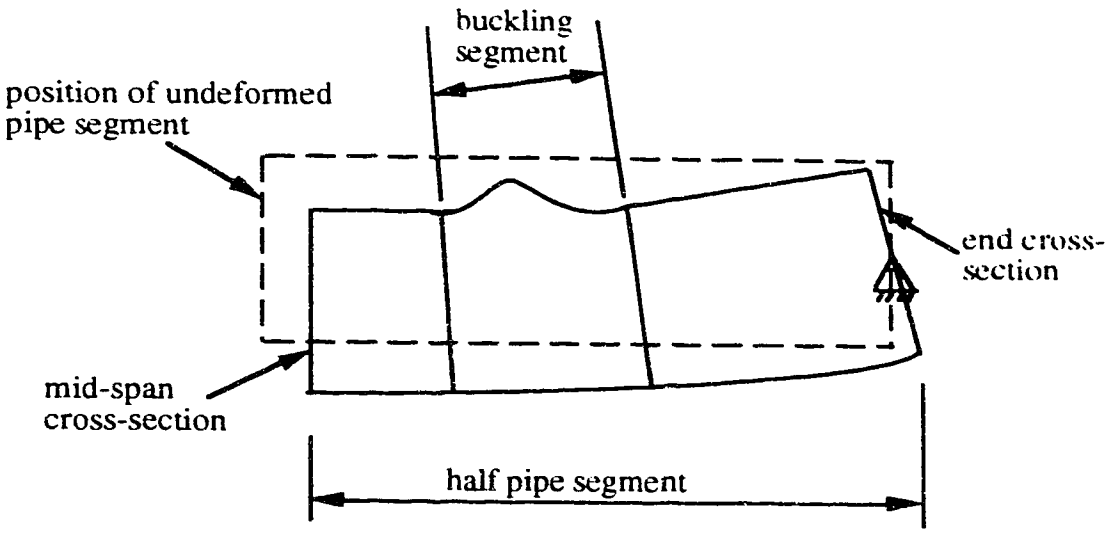

Local Curvature
Local Compressive Strain
Local Tensile Strain
Local Axial Strain

Overall Curvature
Overall Compressive Strain
Overall Tensile Strain
Overall Axial Strain

(a) representative quantities of postbuckling behavior in longitudinal direction

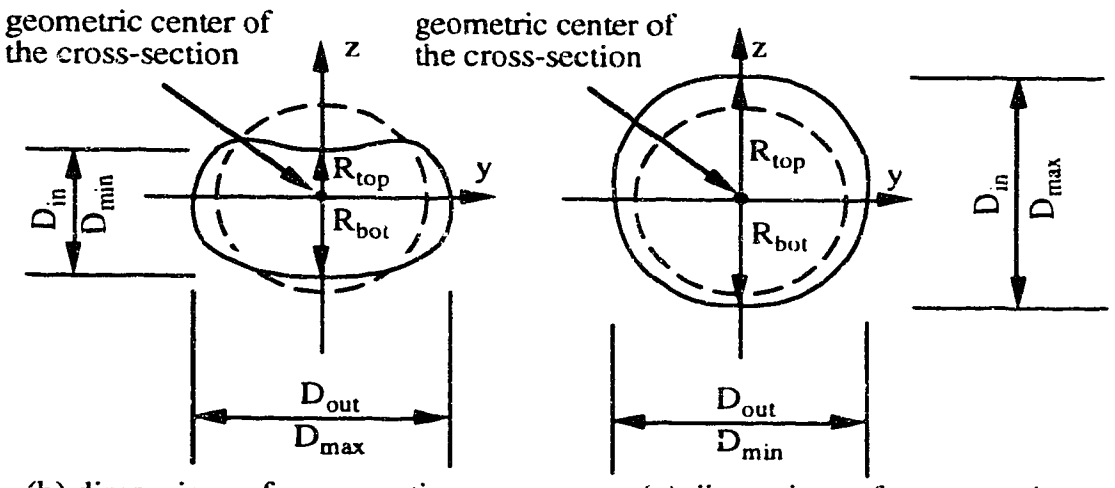

(b) dimensions of cross-section for diamond buckling mode

(c) dimensions of cross-section for bulging buckling mode

Fig. 4.6 Illustration of Representative Quantities for Postbuckling Behavior

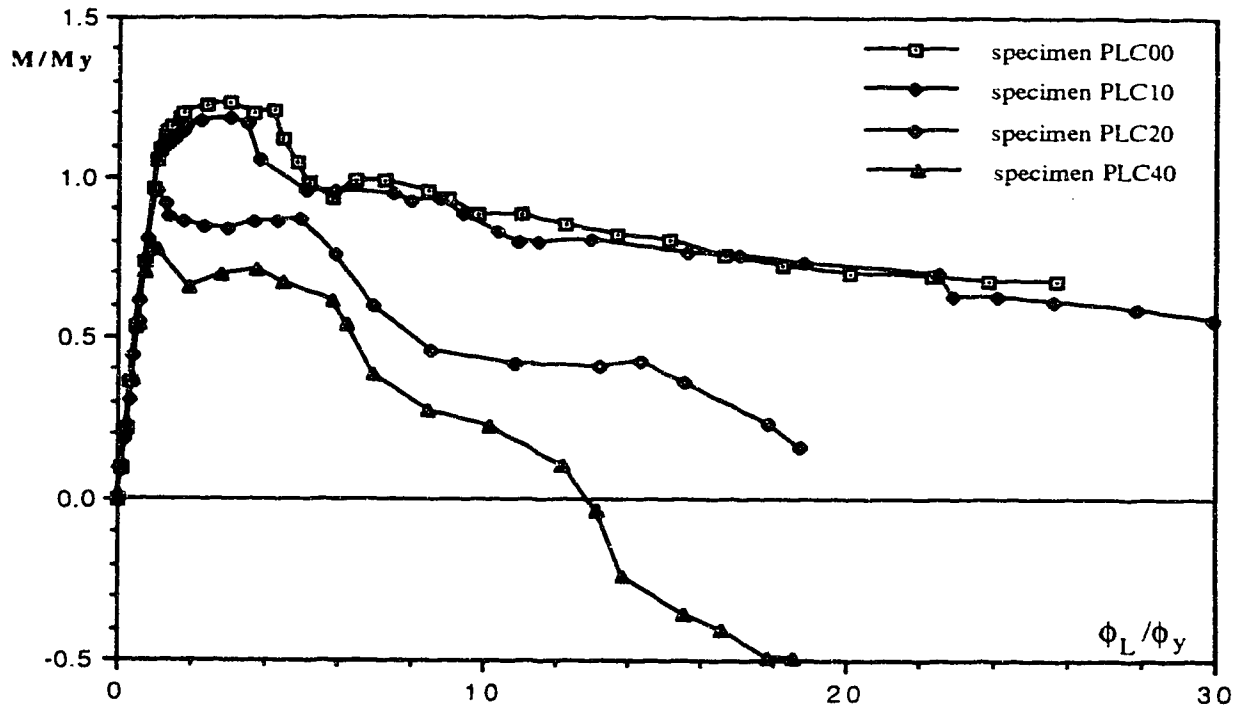

Fig. 4.7 Moment-Local Curvature Curves for Specimens with Low Level Pressure

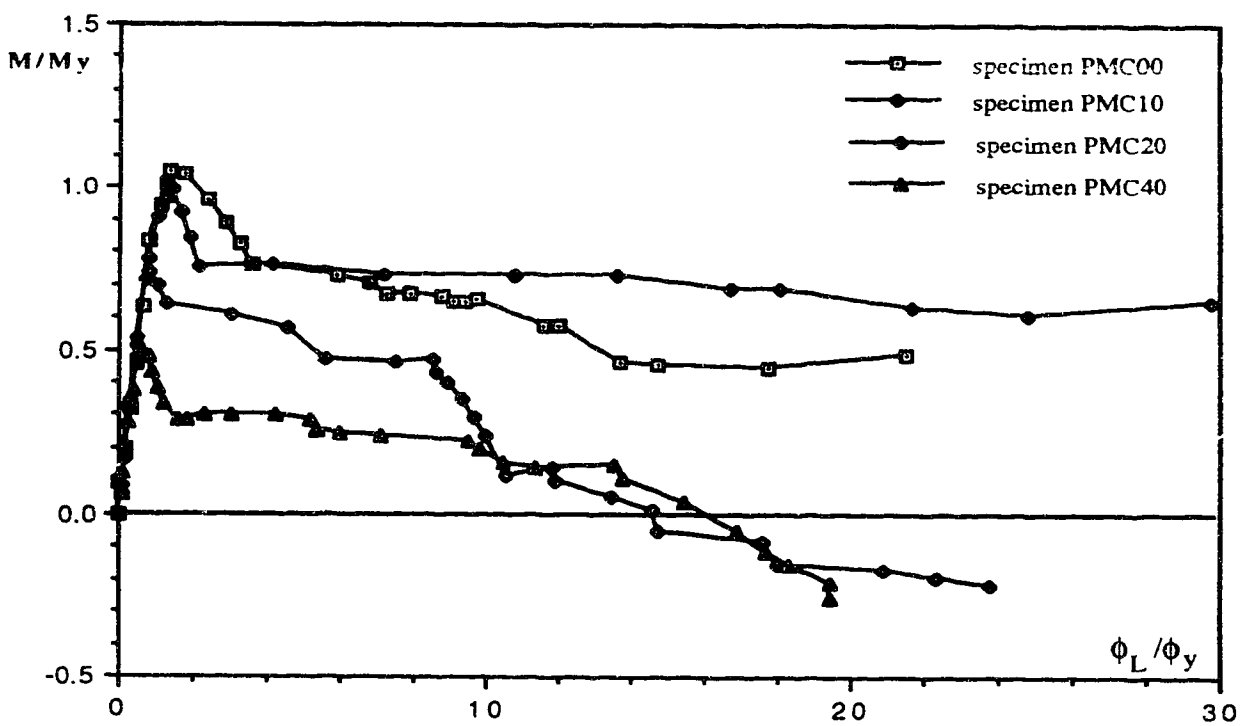

Fig. 4.8 Moment-Local Curvature Curves for Specimens with Middle Level Pressure

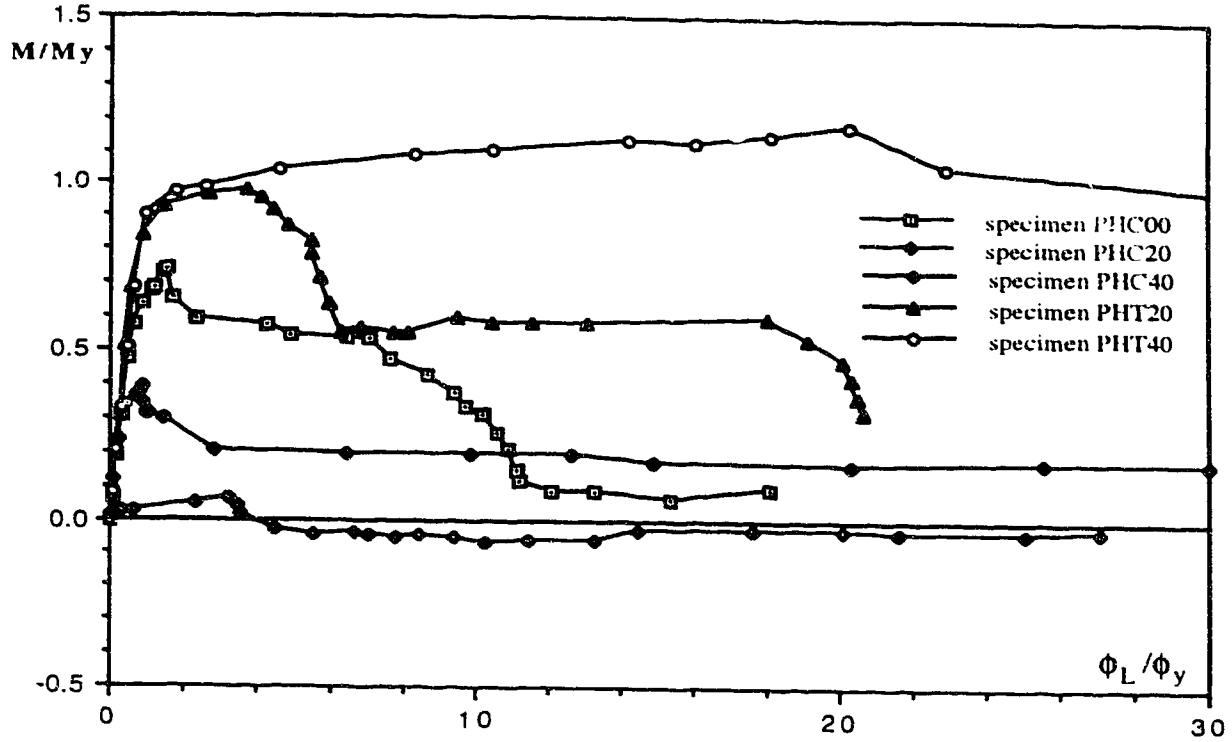

Fig. 4.9 Moment-Local Curvature Curves for Specimens with High Level Pressure

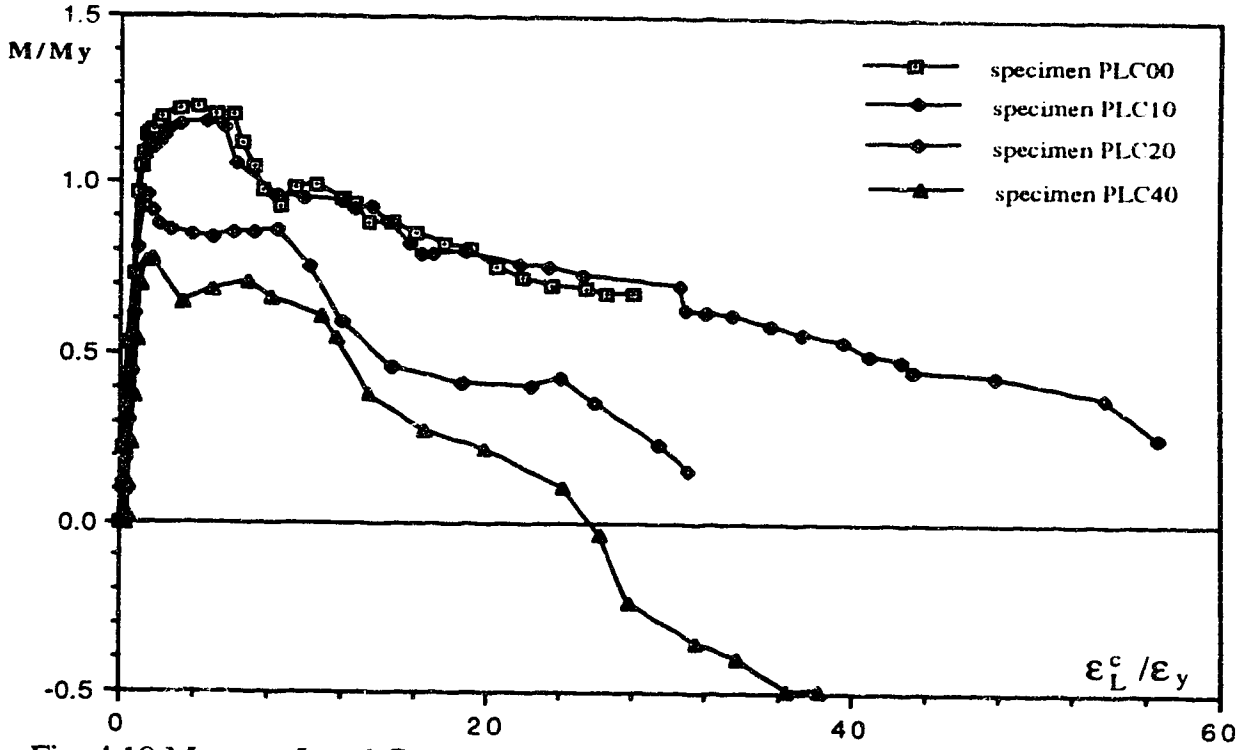

Fig. 4.10 Moment-Local Compressive Strain Curves for Specimens with Low Level Pressure

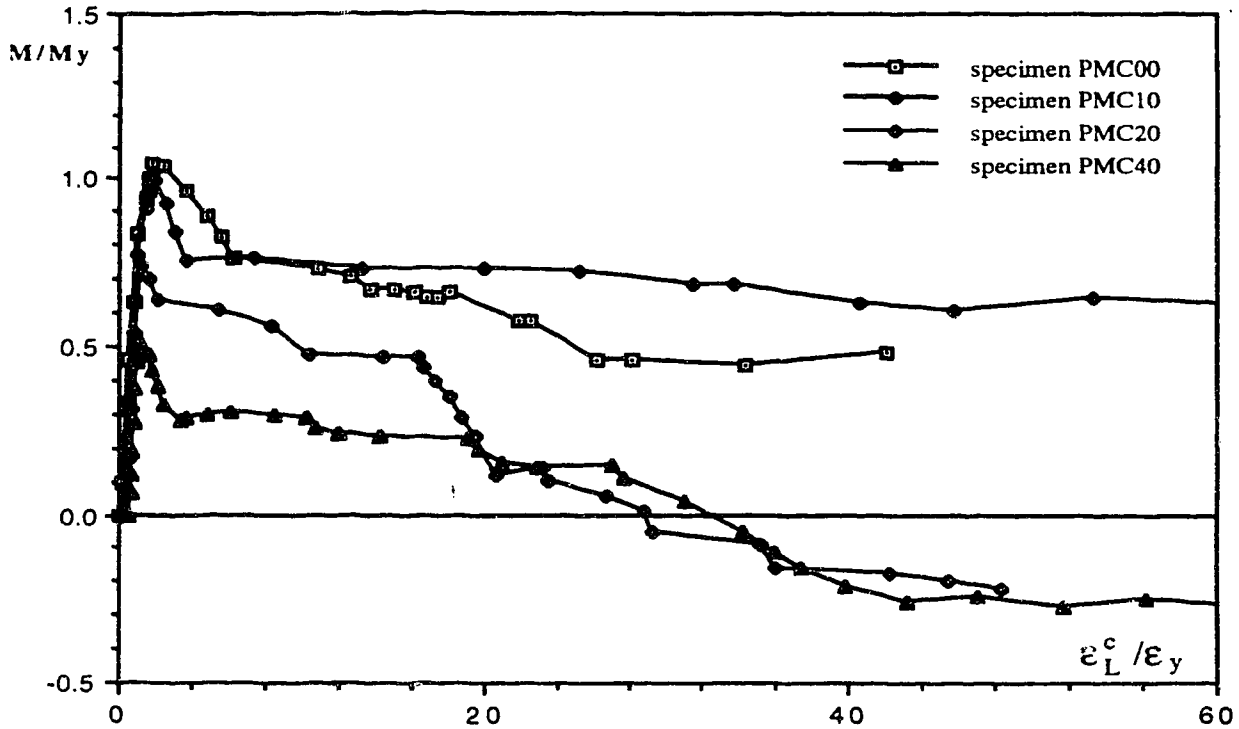

Fig. 4.11 Moment-Local Compressive Strain Curves for Specimens with Middle Level Pressure

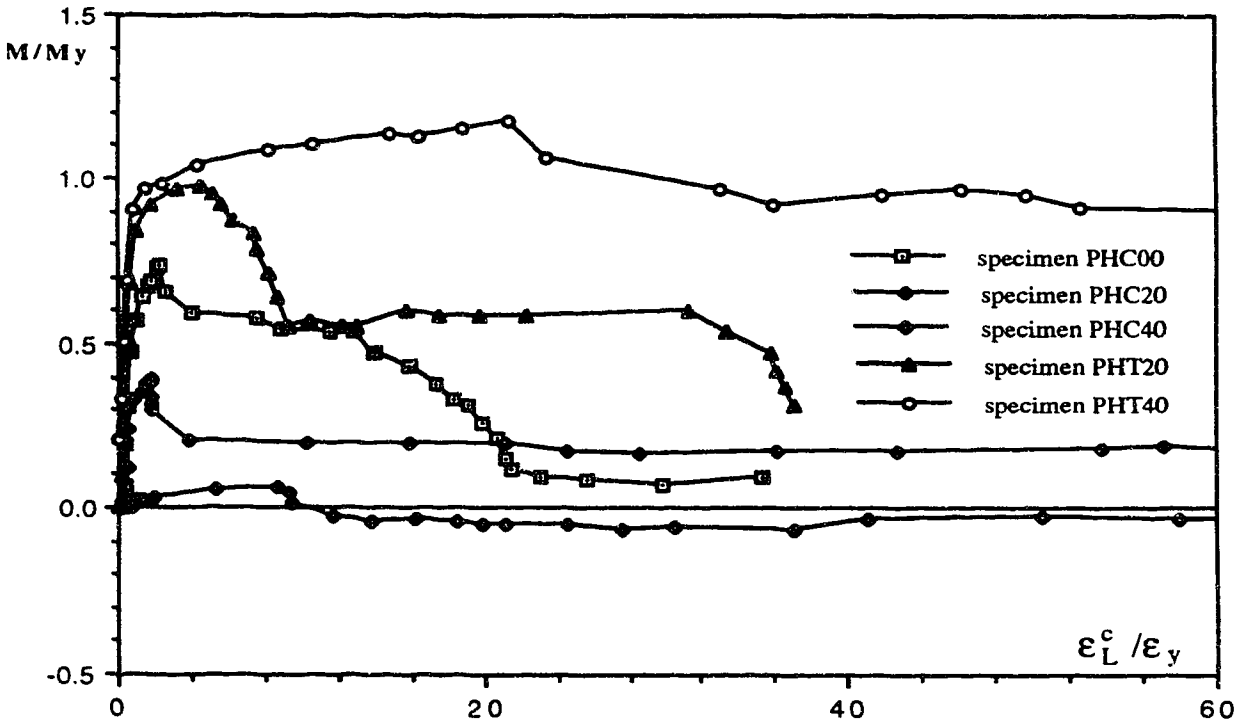

Fig. 4.12 Moment-Local Compressive Strain Curves for Specimens with High Level Pressure

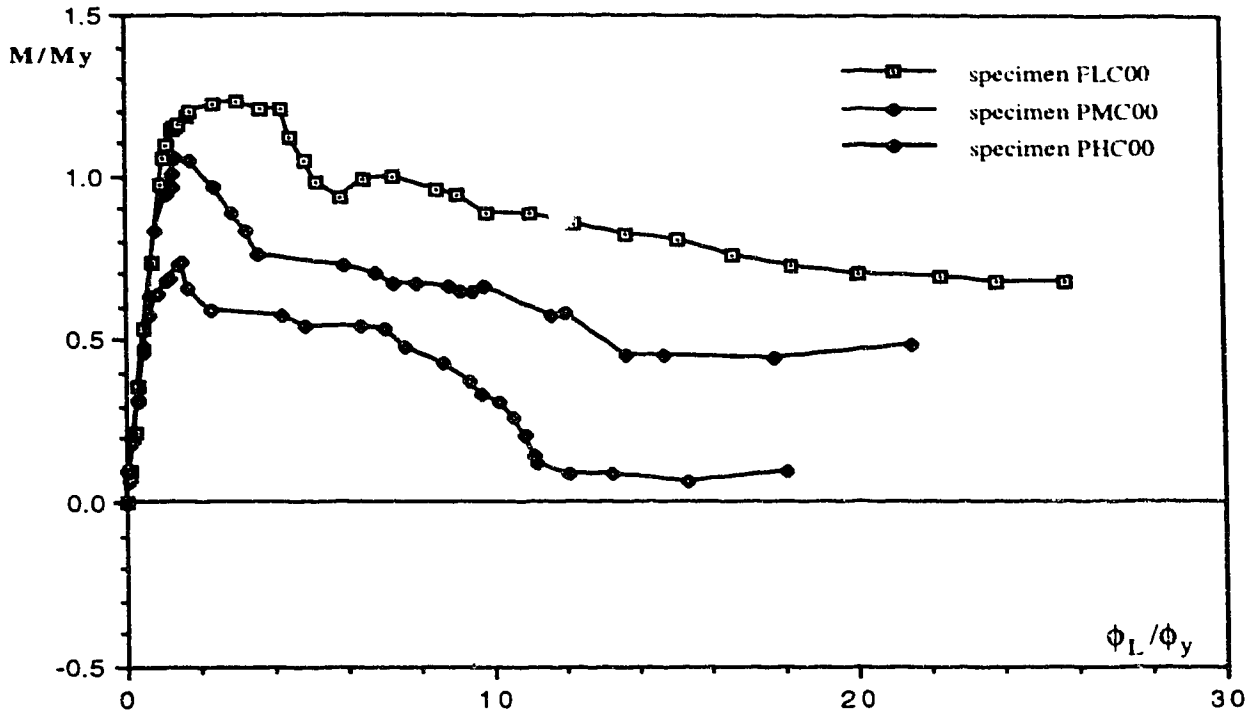

Fig. 4.13 Moment-Local Curvature Curves for Specimens without Axial Load

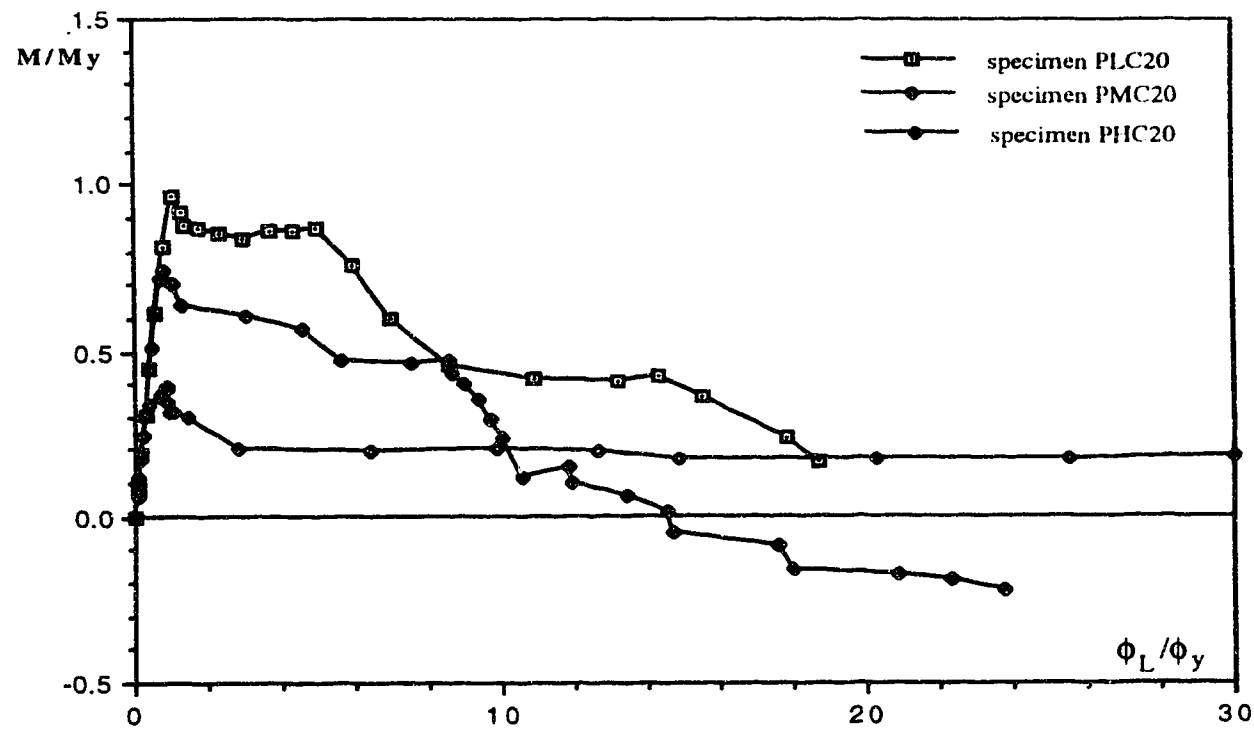

Fig. 4.14 Moment-Local Curvature Curves for Specimens with Axial Compressive Load at Level of 20%

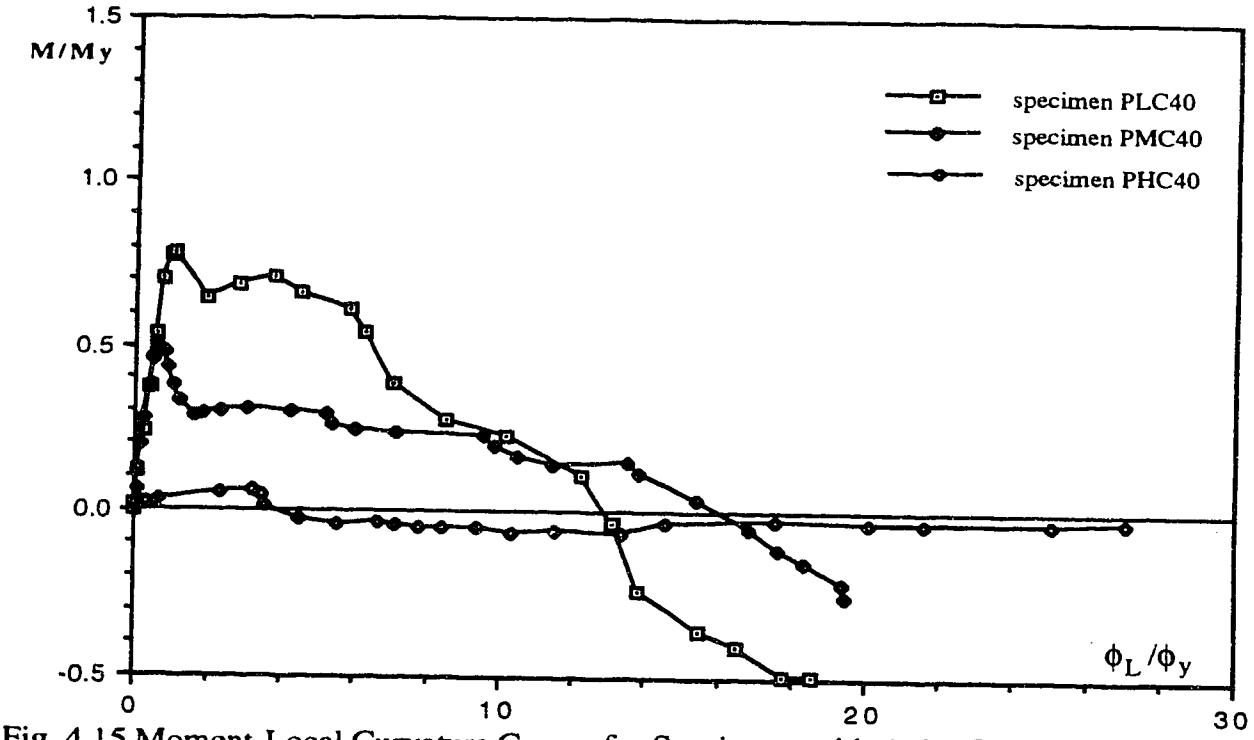

Fig. 4.15 Moment-Local Curvature Curves for Specimens with Axial Compressive Load at Level of 40%

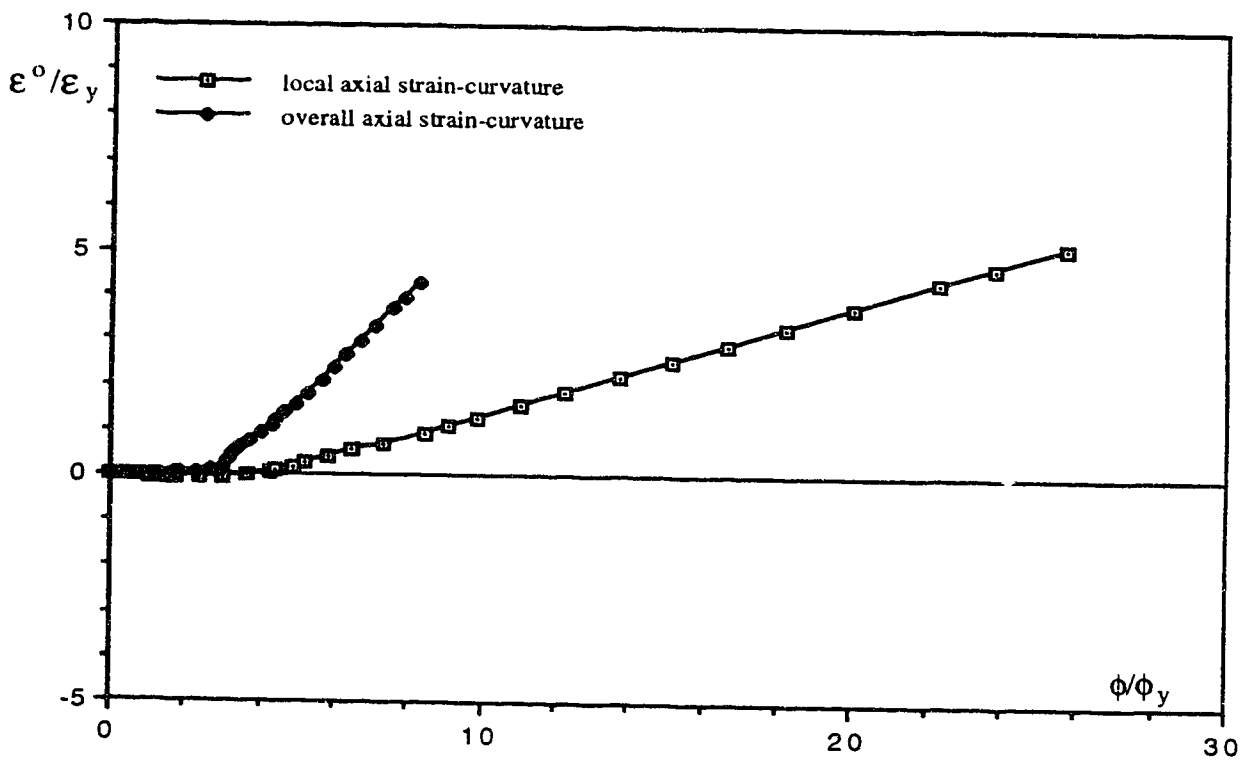

Fig. 4.16 Deformation Path of Specimen PLC00

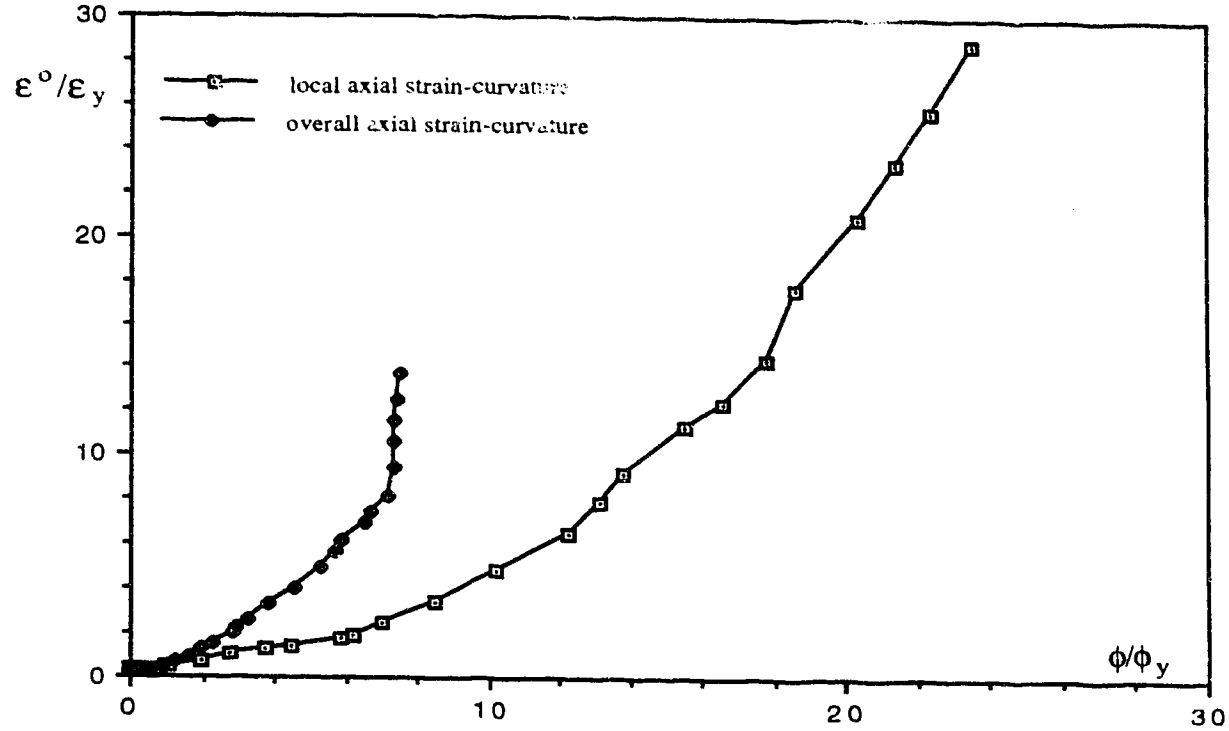

Fig. 4.17 Deformation Path of Specimen PLC40

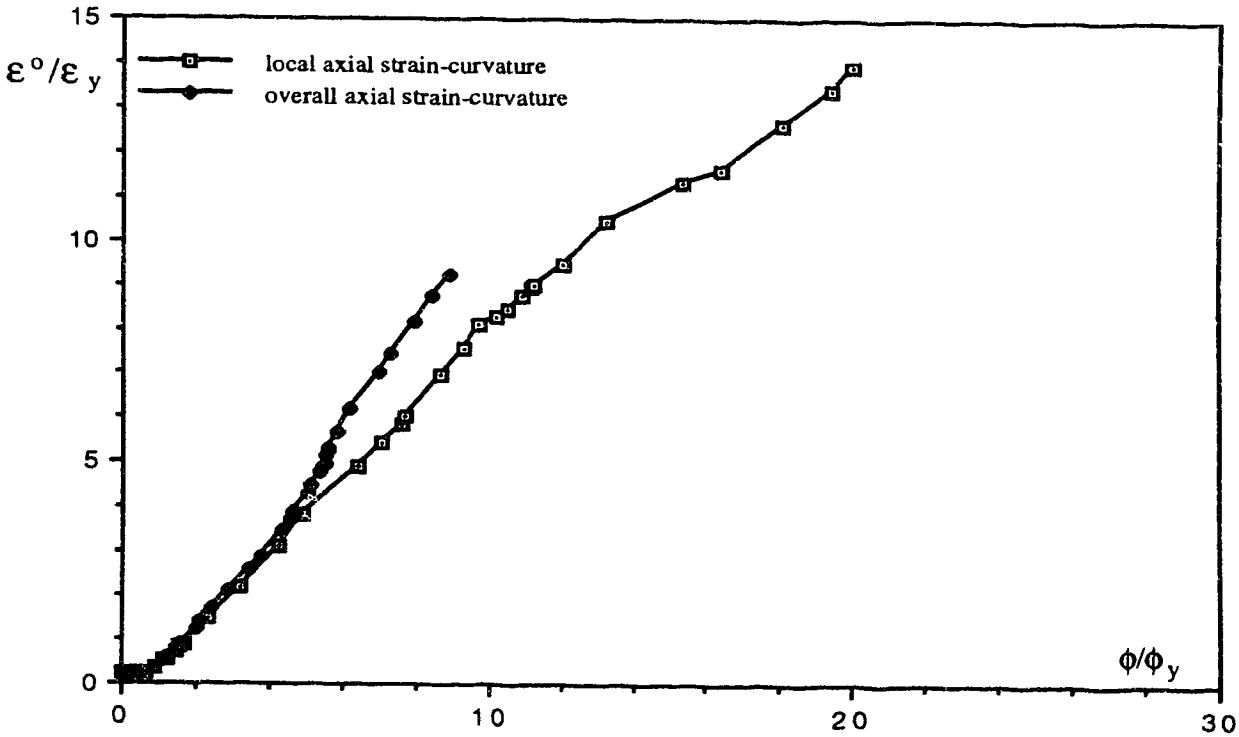

Fig. 4.18 Deformation Path of Specimen PHC00

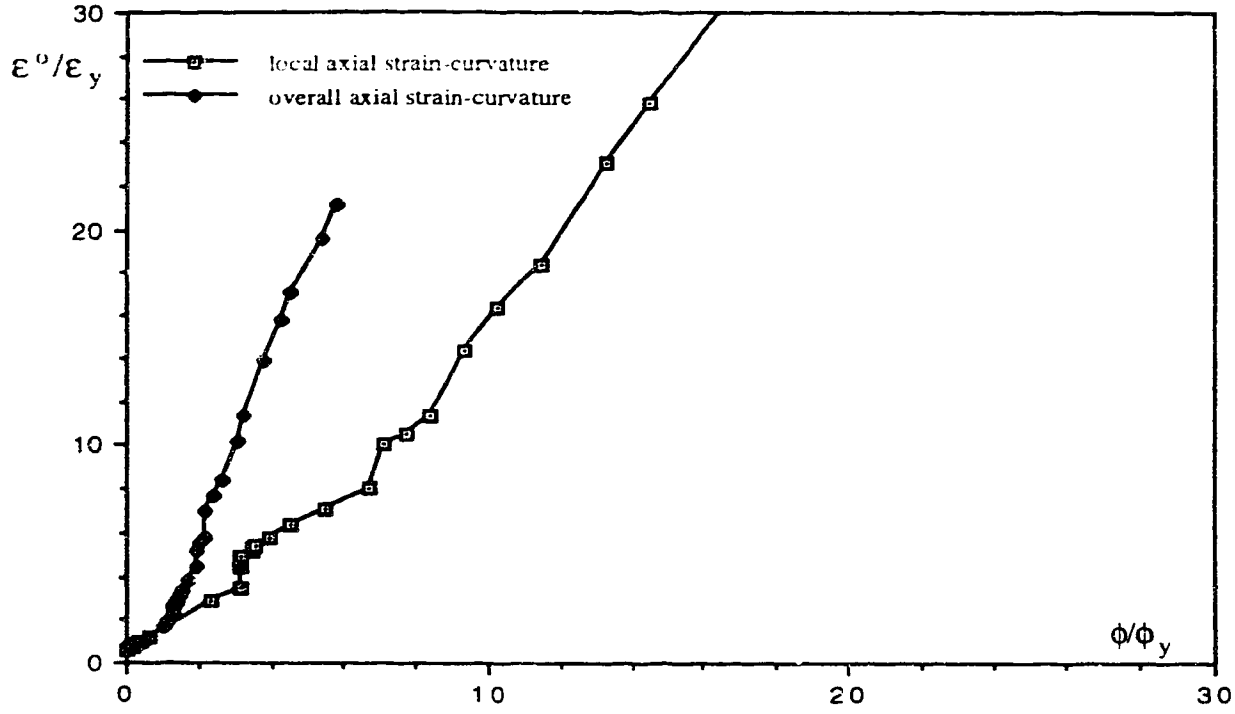

Fig. 4.19 Deformation Path of Specimen PHC40

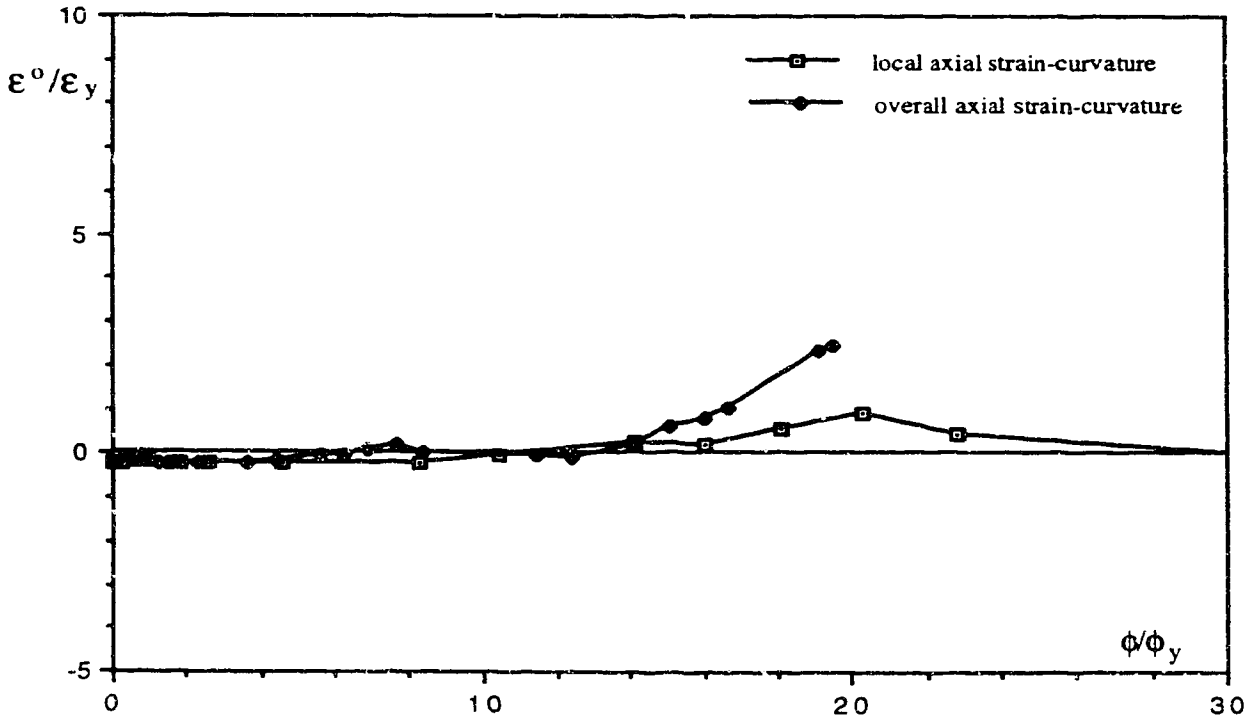

Fig. 4.20 Deformation Path of Specimen PHT40

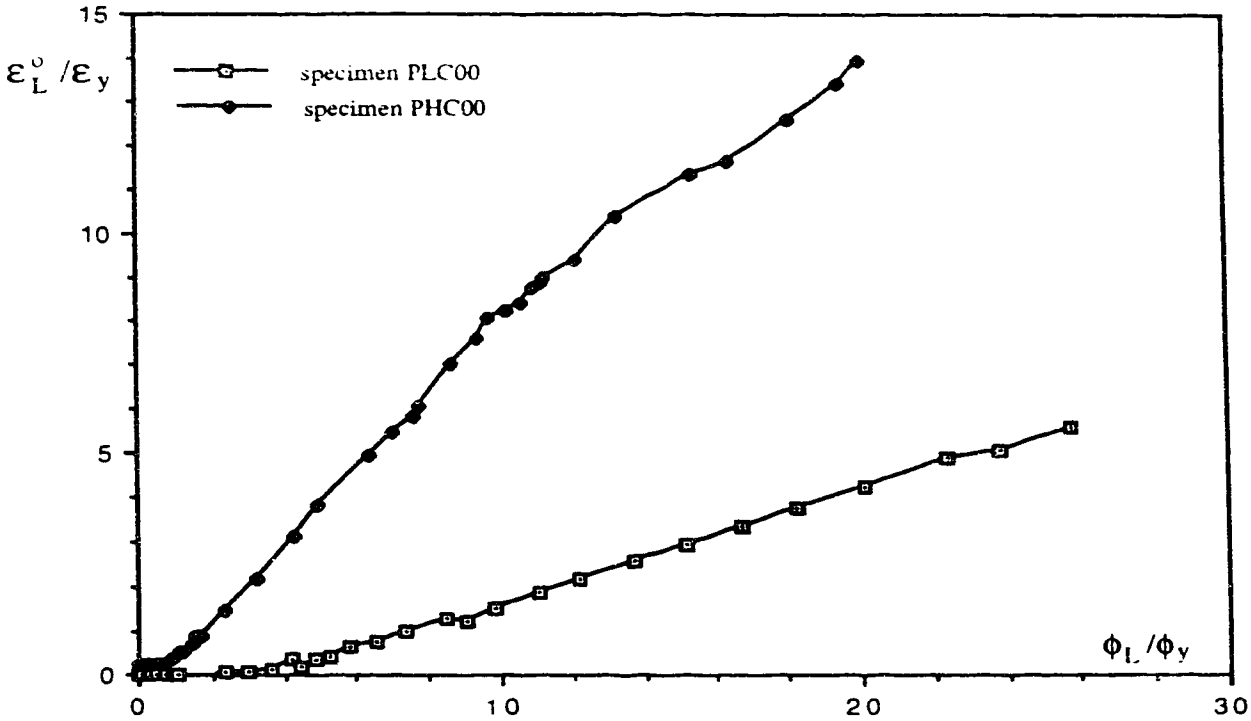

Fig. 4.21 Comparison of Local Deformation Paths for Specimens PLC00 and PHC00

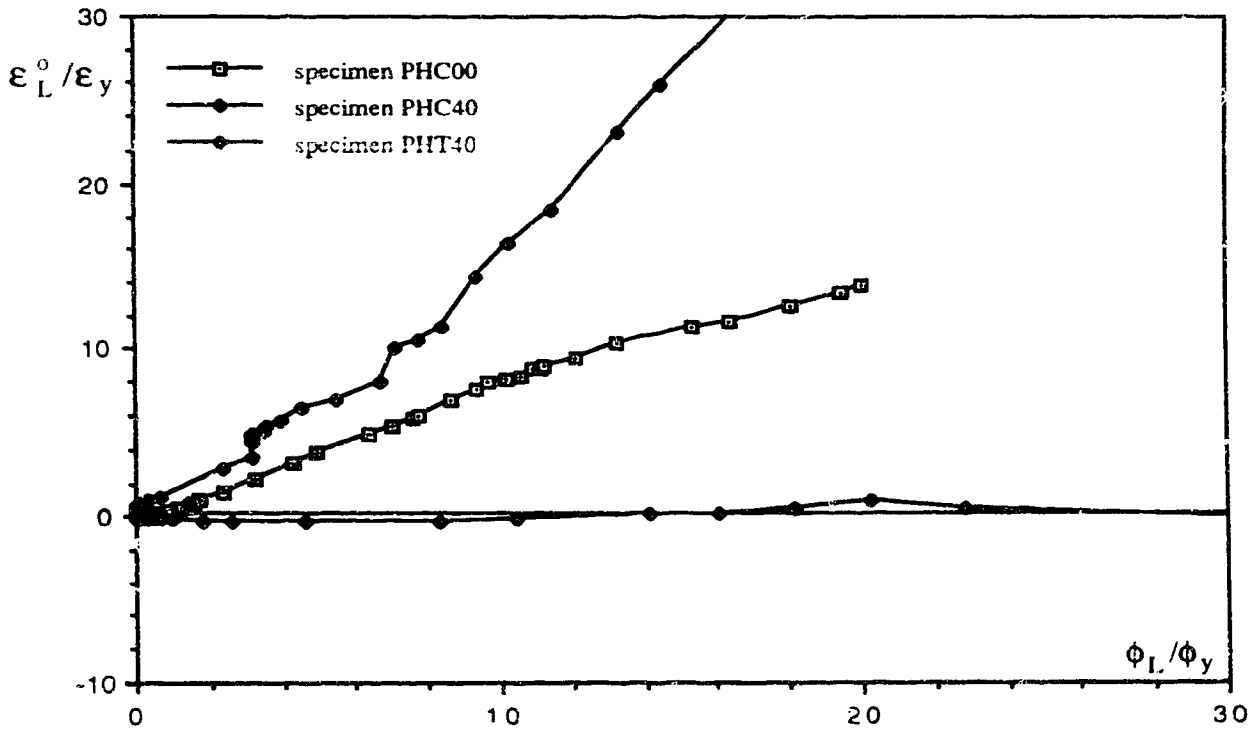

Fig. 4.22 Comparison of Local Deformation Paths for Specimens PHC00, PHC40 and PHT40

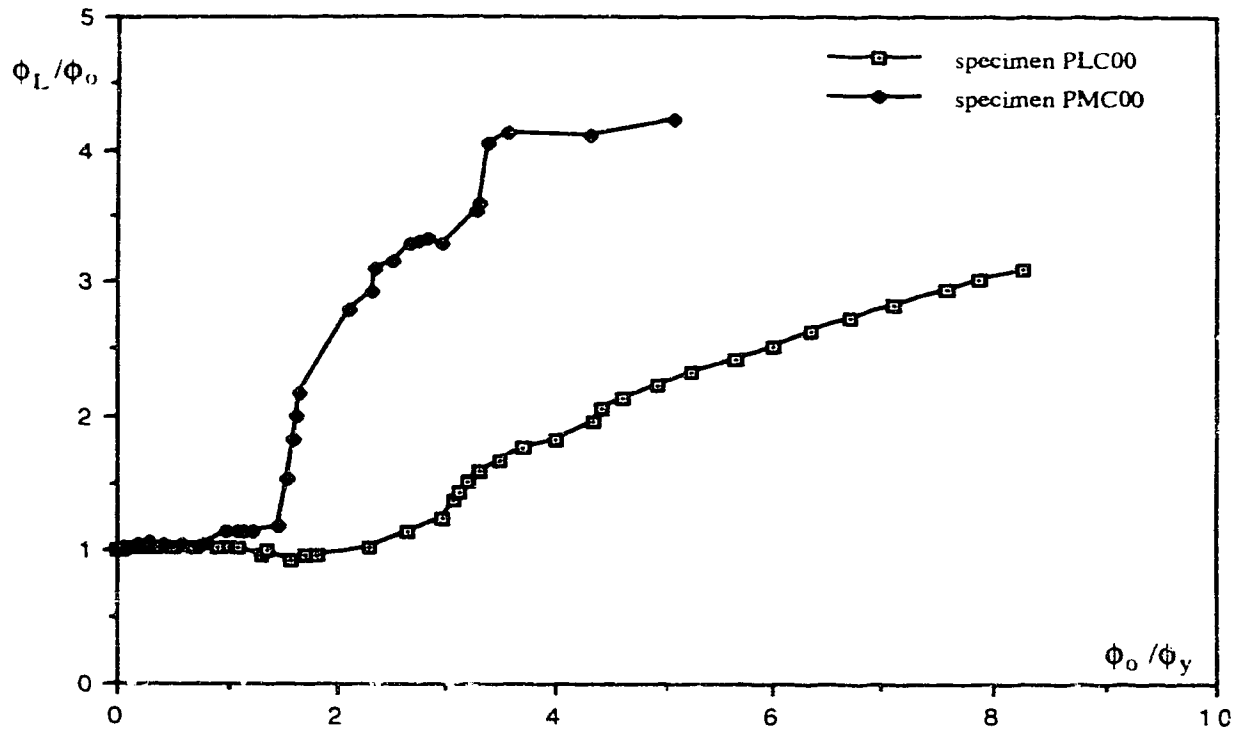

Fig. 4.23 Comparison of Curvature Localization for Specimens PLC00 and PMC00

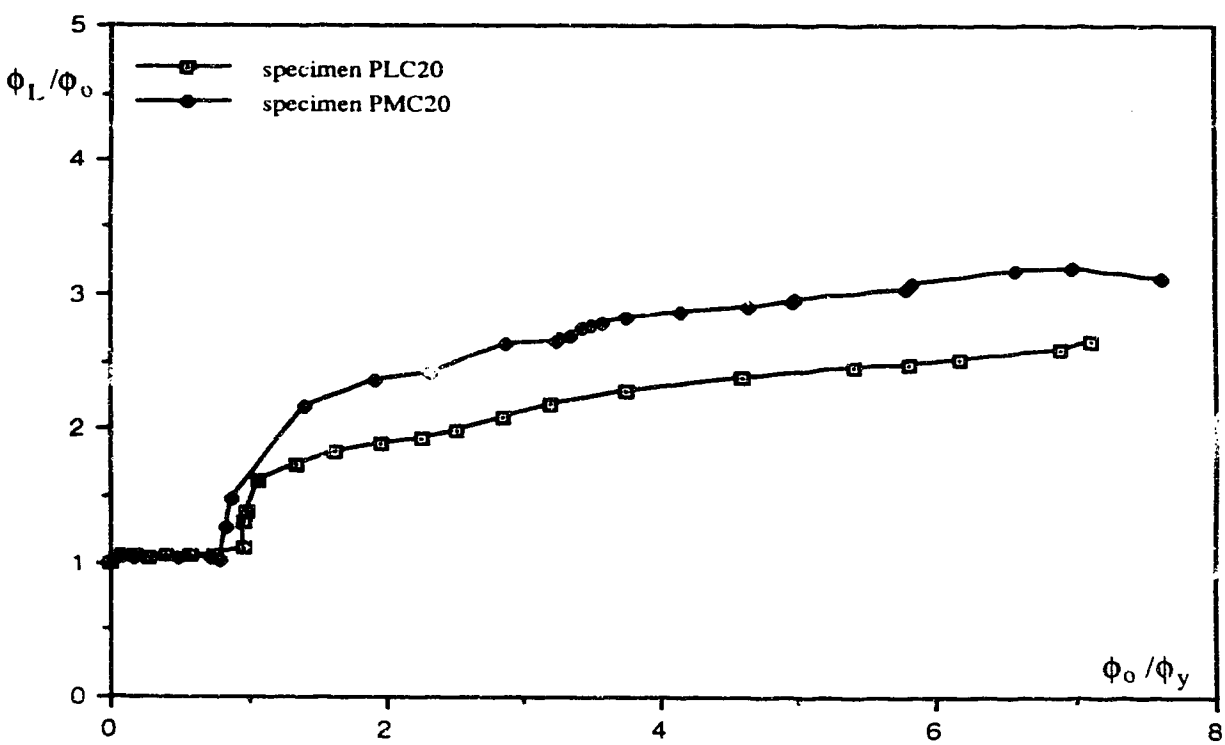

Fig. 4.24 Comparison of Curvature Localization for Specimens PLC20 and PMC20

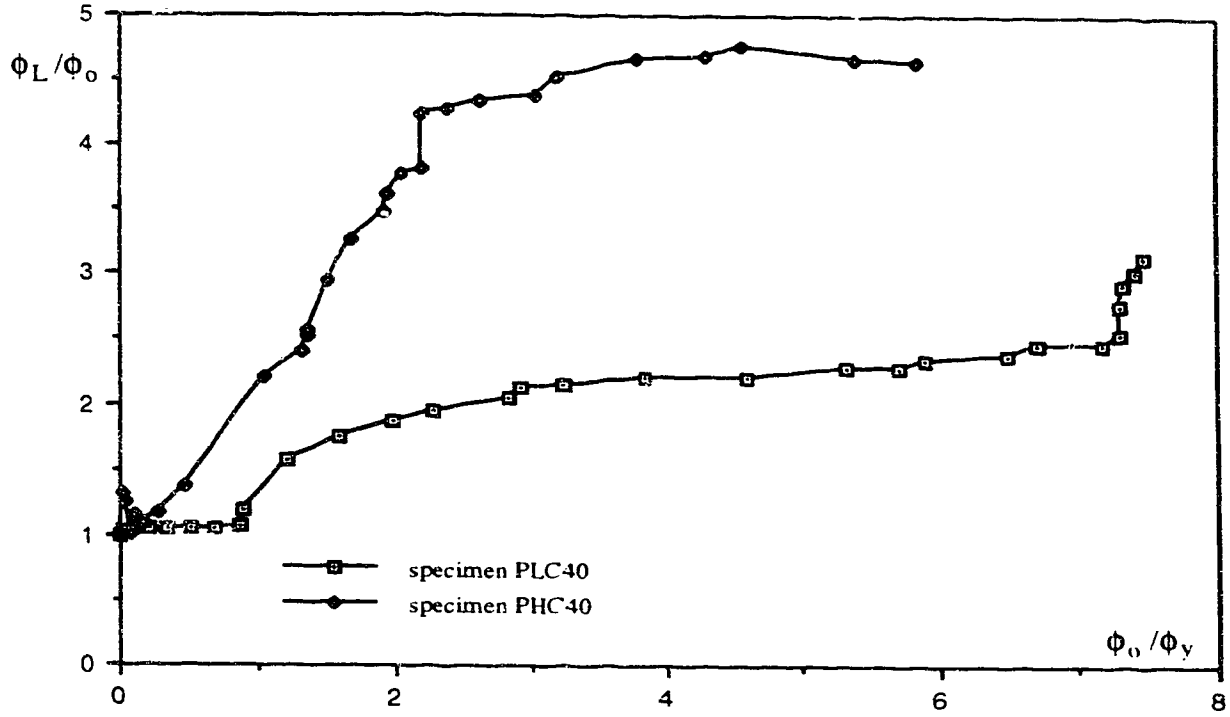

Fig. 4.25 Comparison of Curvature Localization for Specimens PLC40 and PHC40

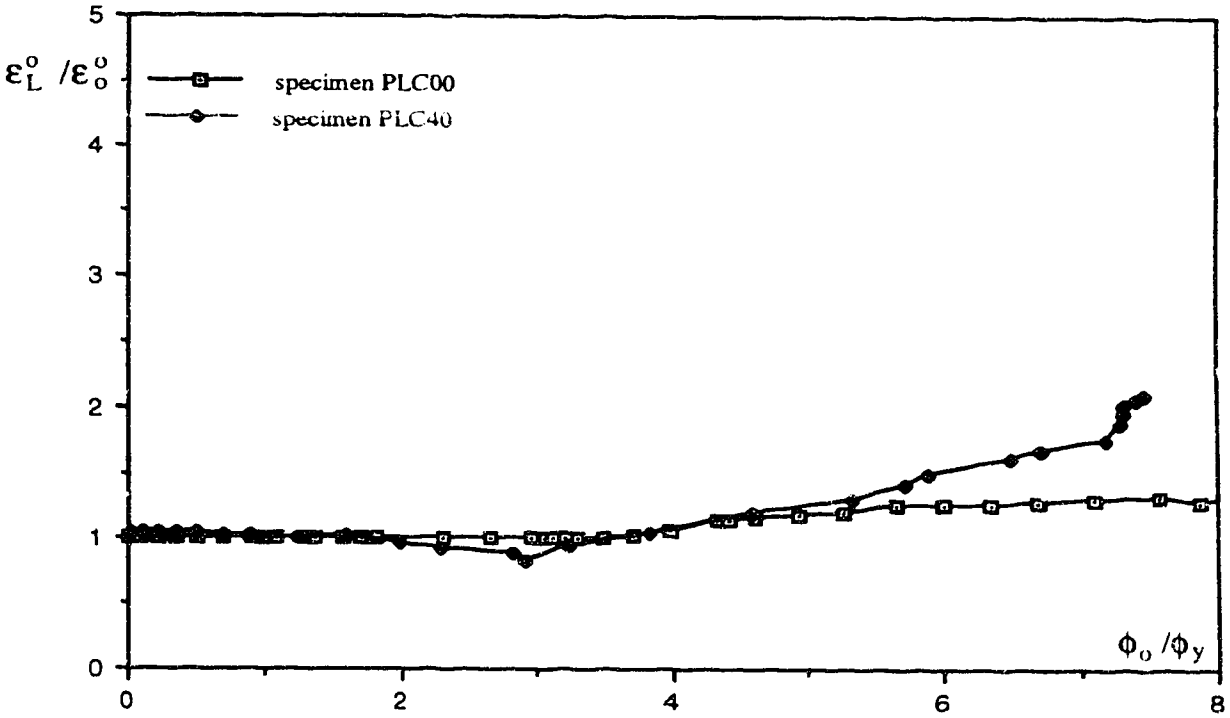

Fig. 4.26 Comparison of Axial Strain Localization for Specimens PLC00 and PLC40

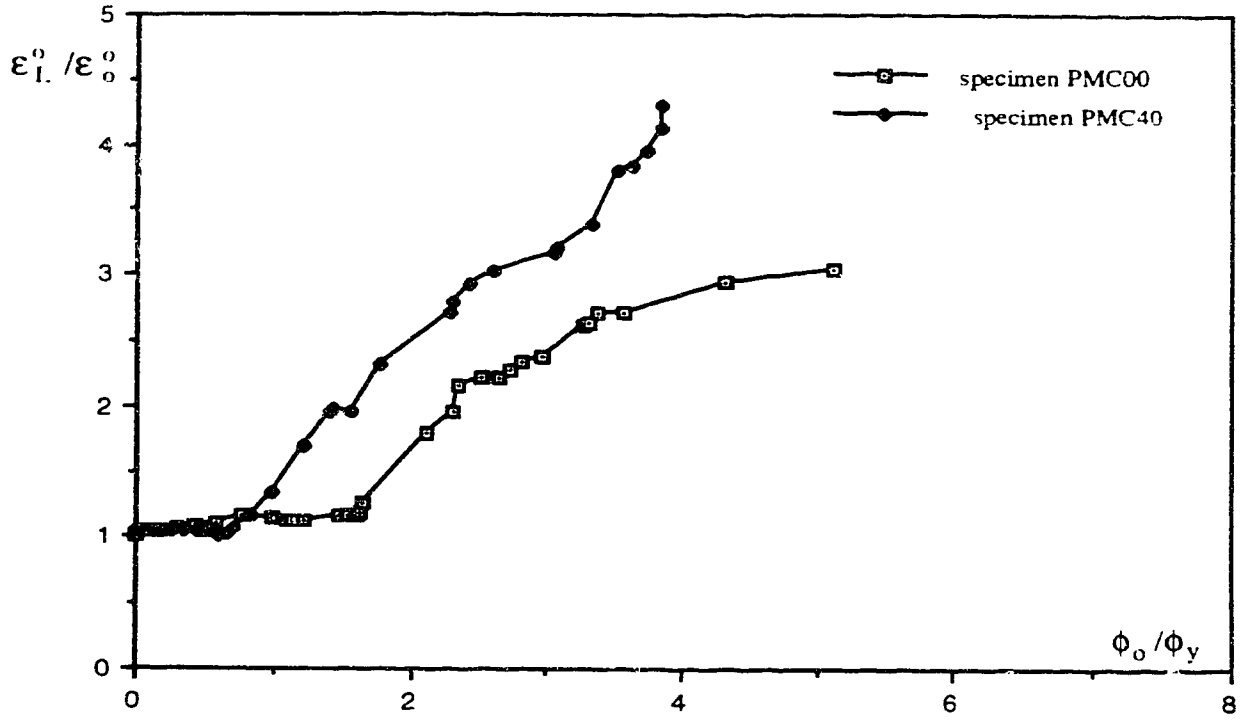

Fig. 4.27 Comparison of Axial Strain Localization for Specimens PMC00 and PMC40

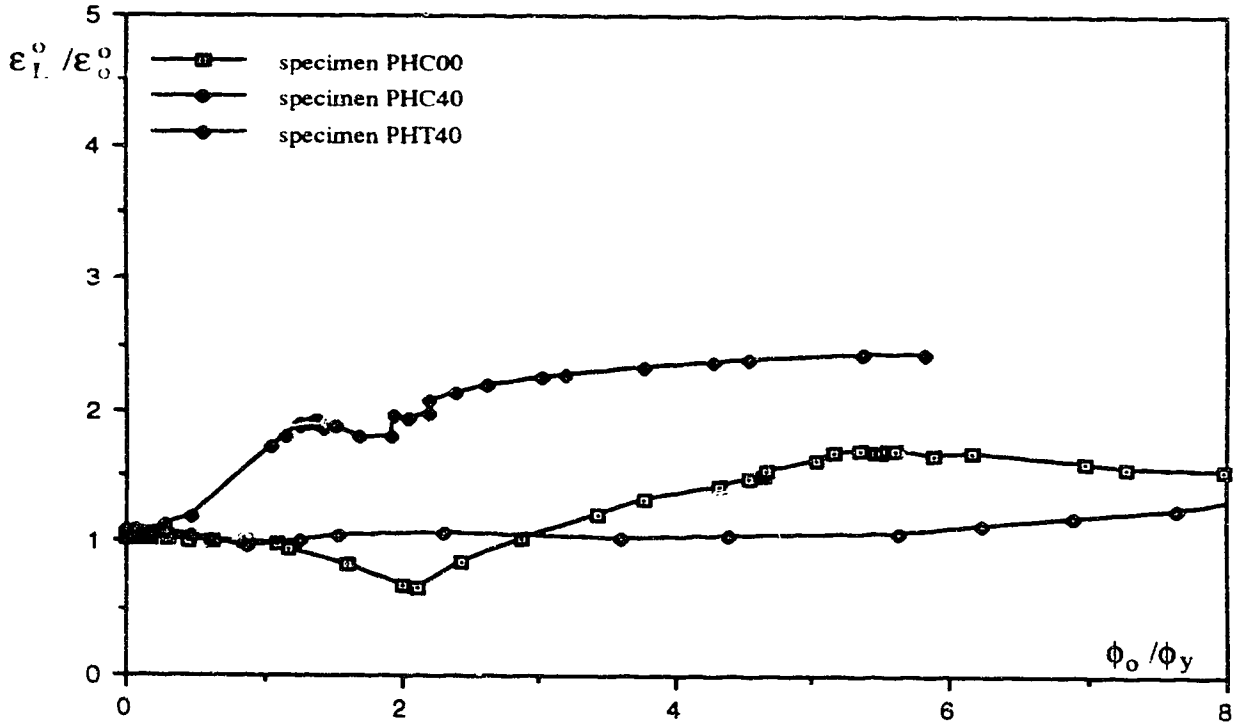

Fig. 4.28 Comparison of Axial Strain Localization for Specimens PHC00, PHC40 and PHT40

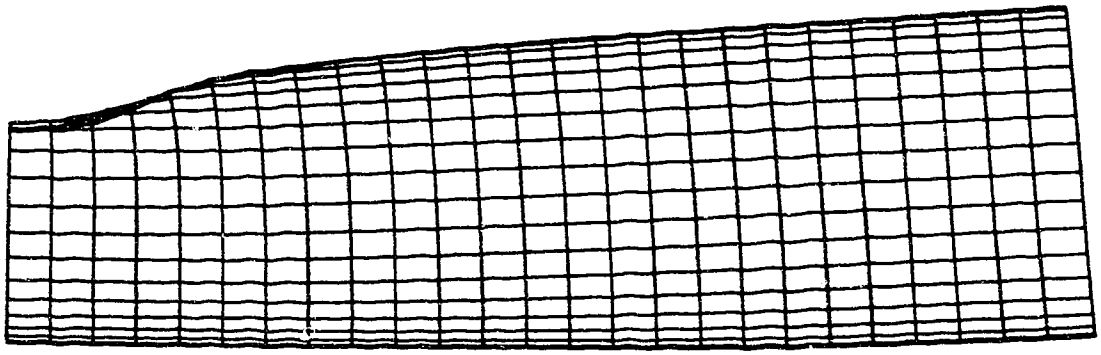

(a) Side View

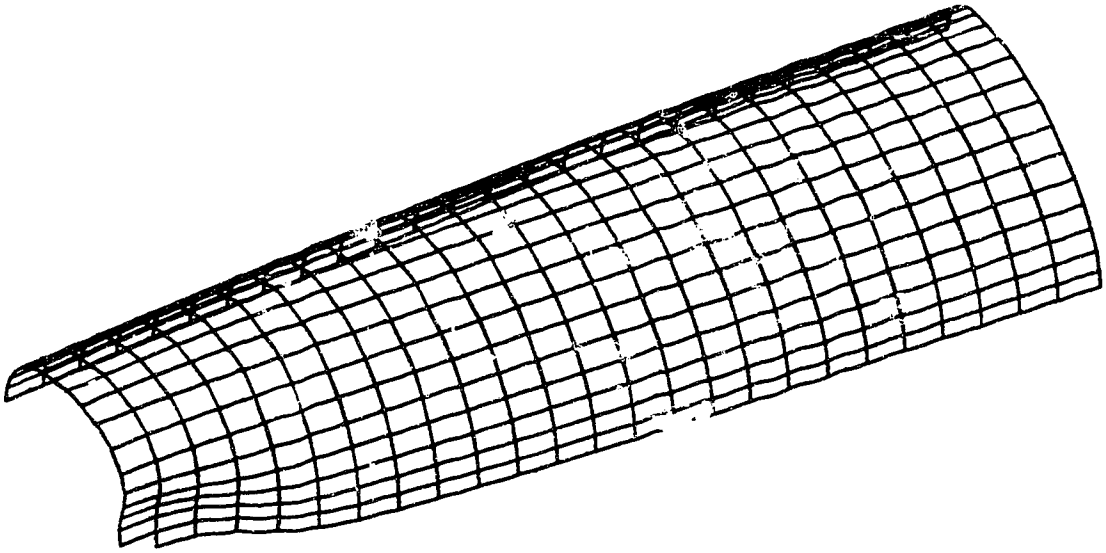

(b) Three Dimensional View

Fig. 4.29 Deformed Configuration of Specimen PLC00

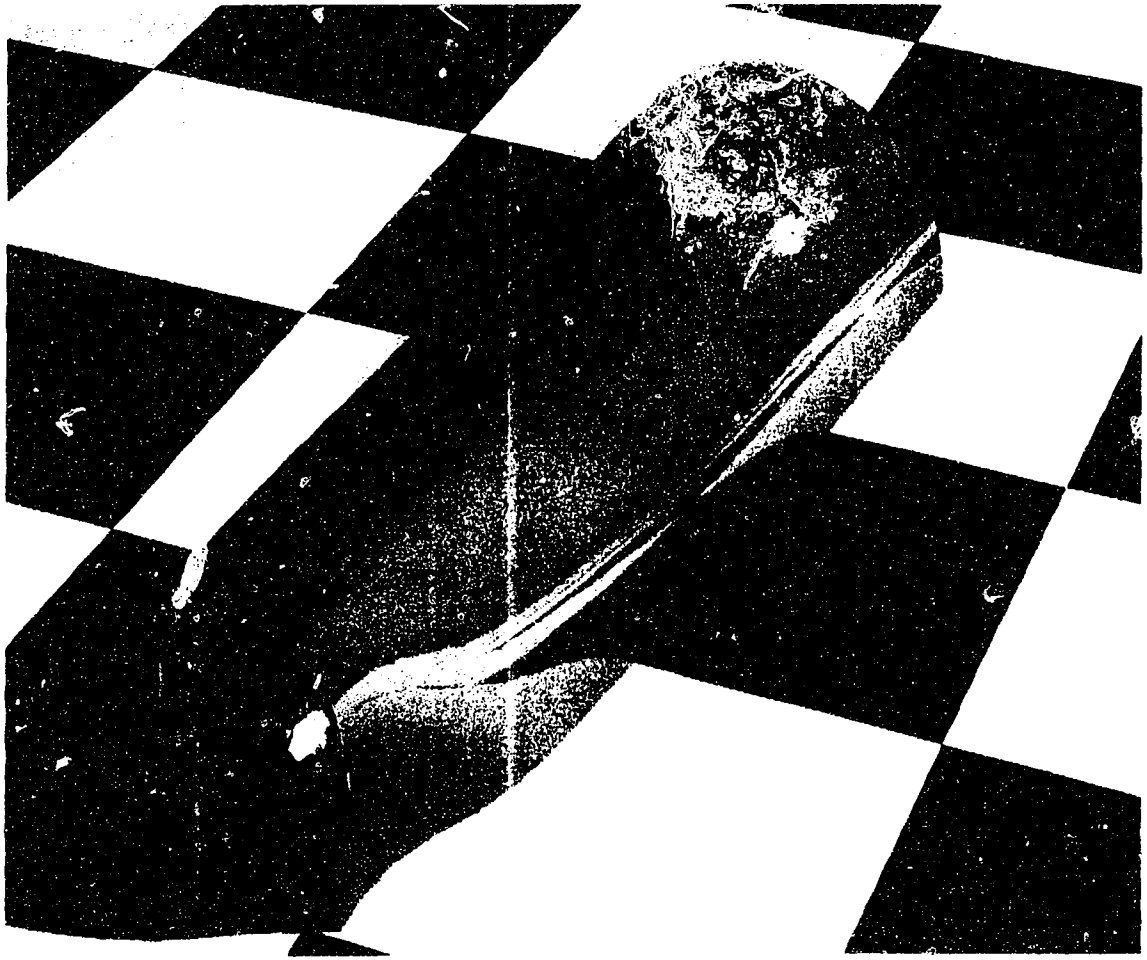

Fig. 4.29(c) Deformed Configuration of Specimen PLC00

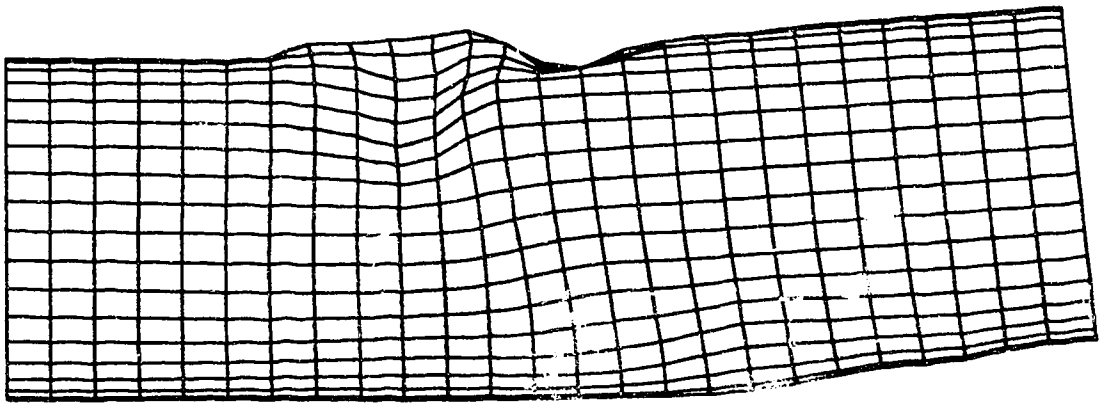

(a) Side View

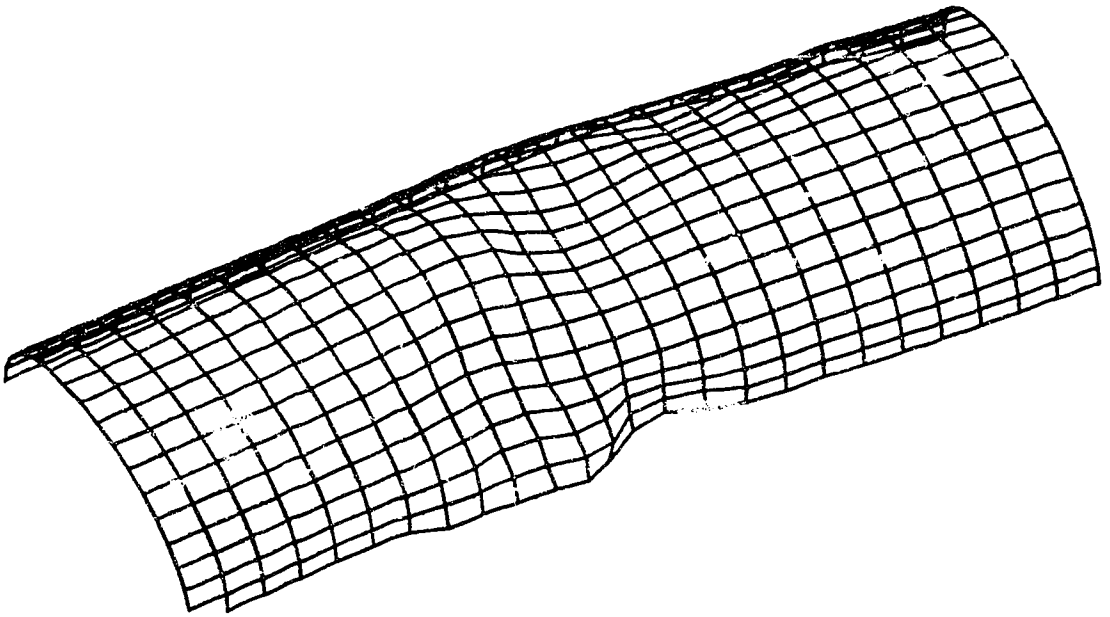

(b) Three Dimensional View

Fig. 4.30 Deformed Configuration of Specimen PLC40

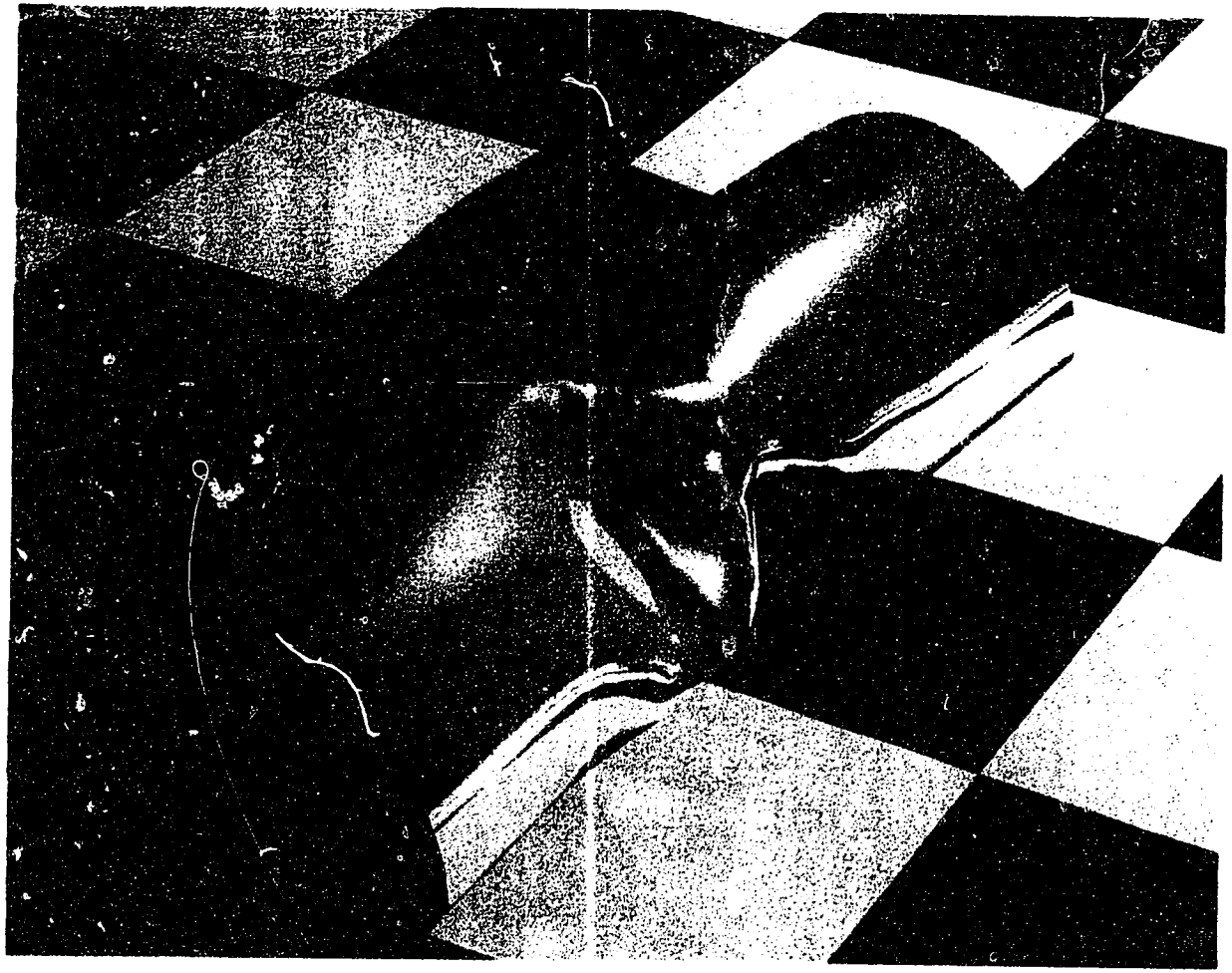

Fig. 4.30(c) Deformed Configuration of Specimen PLC40

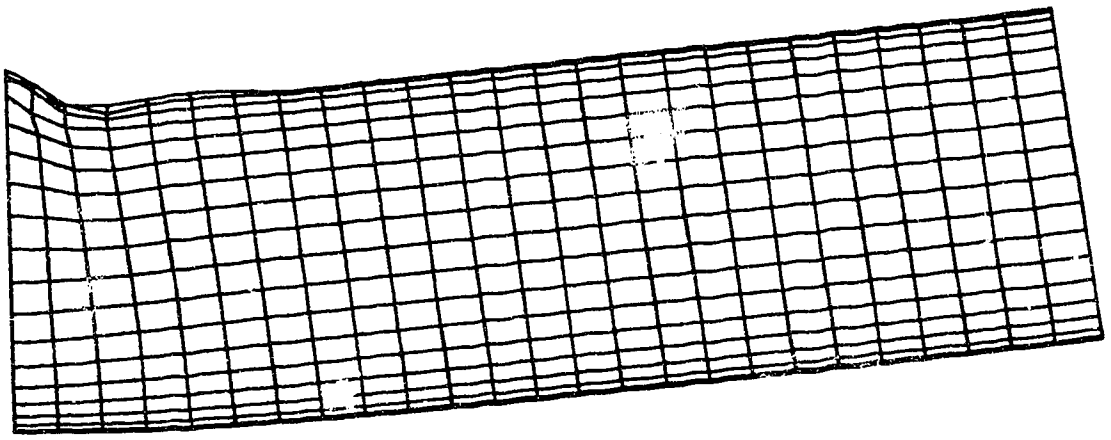

(a) Side View

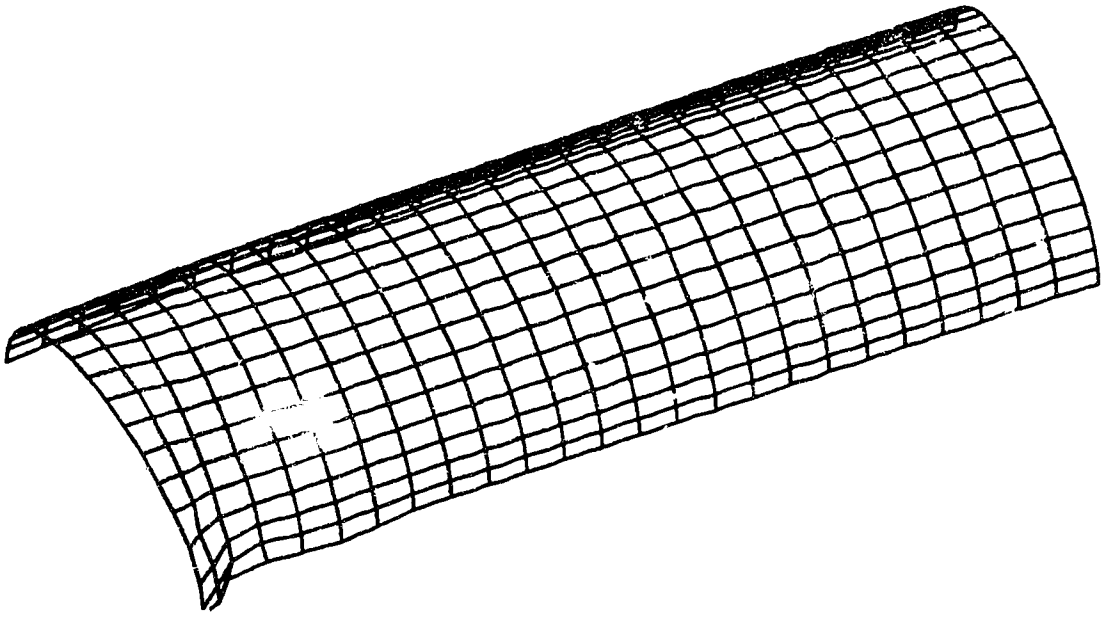

(b) Three Dimensional View

Fig. 4.31 Deformed Configuration of Specimen PMC10

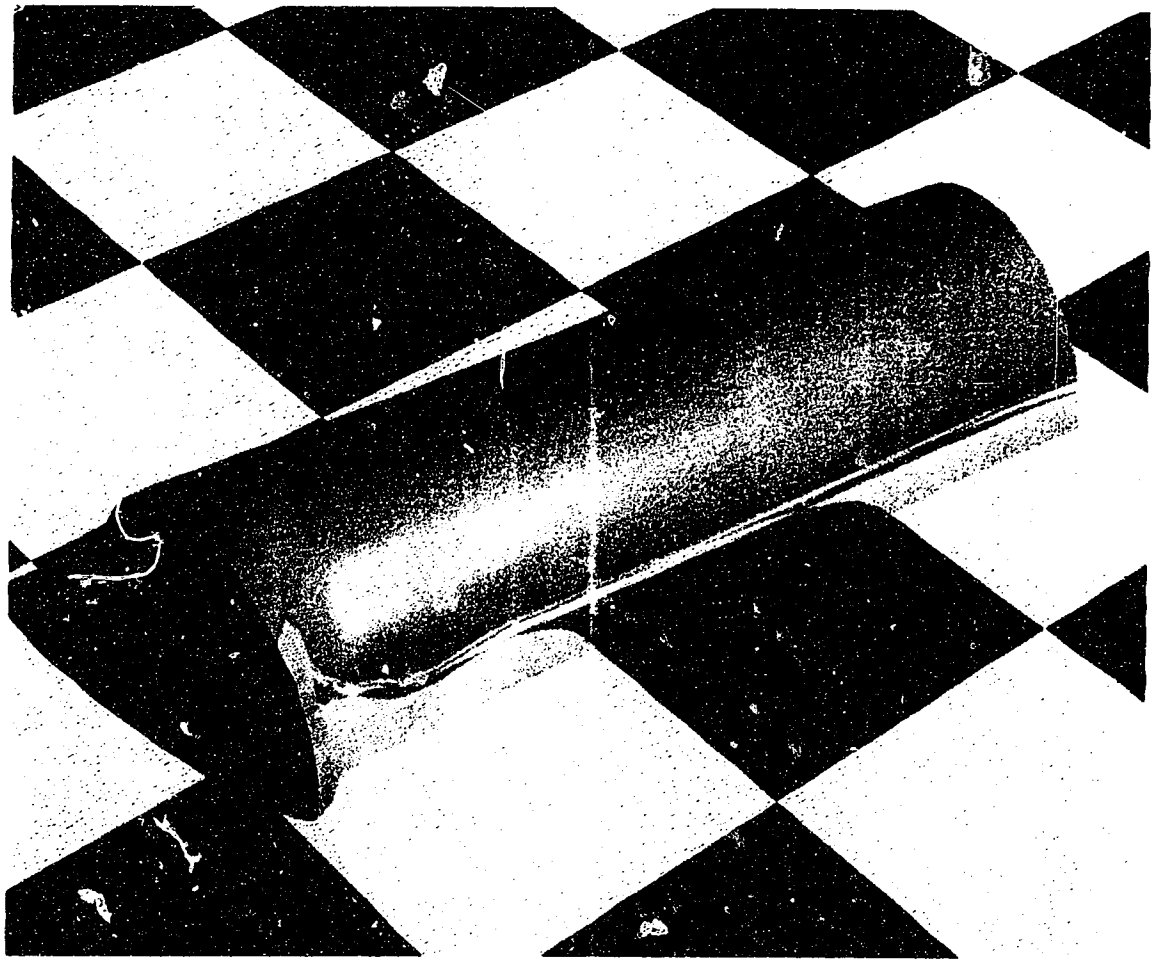

Fig. 4.31(c) Deformed Configuration of Specimen PMC10

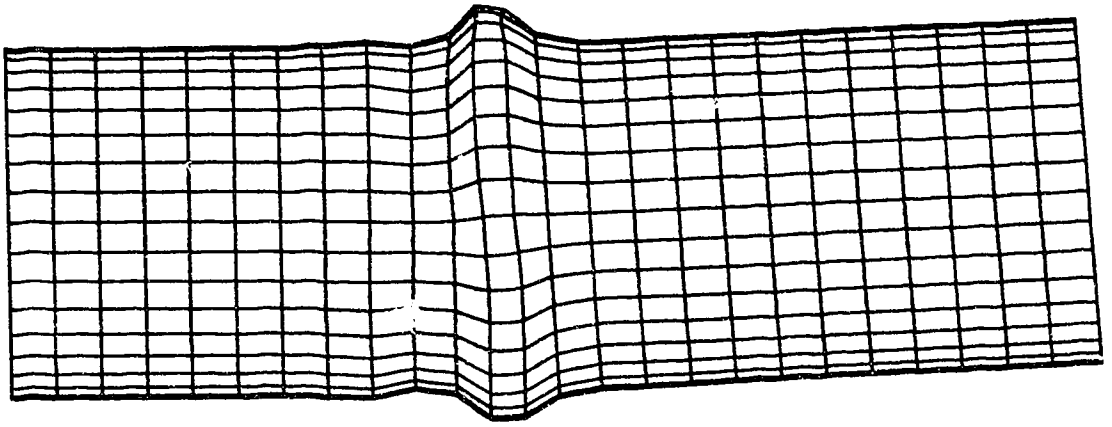

(a) Side View

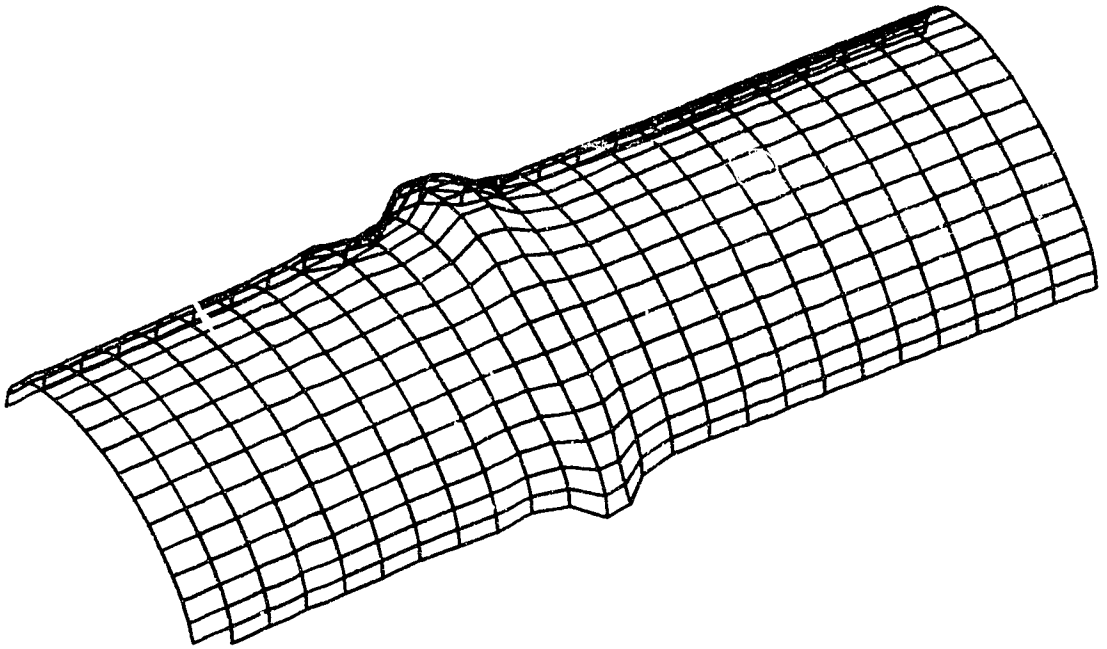

(b) Three Dimensional View

Fig. 4.32 Deformed Configuration of Specimen PMC40

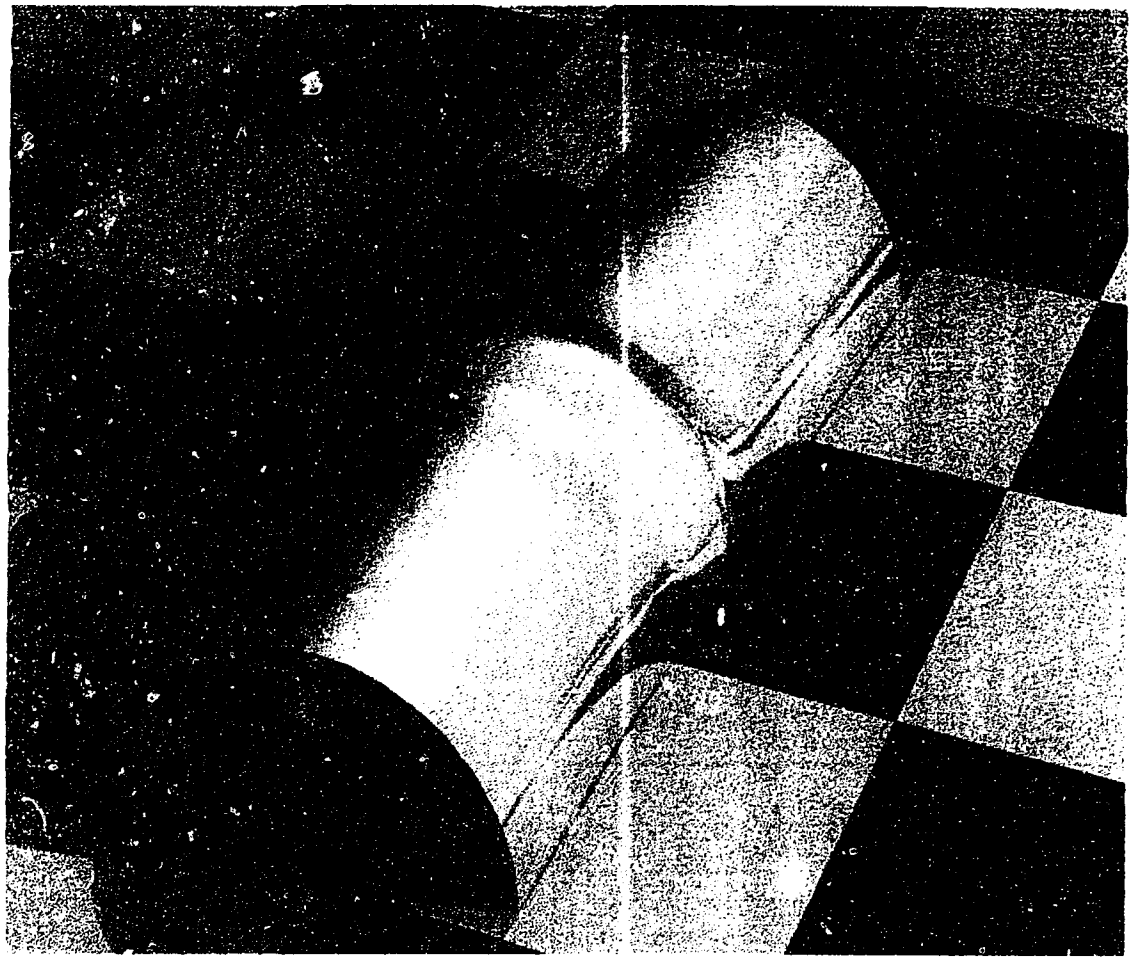

Fig. 4.32(c) Deformed Configuration of Specimen PMC40

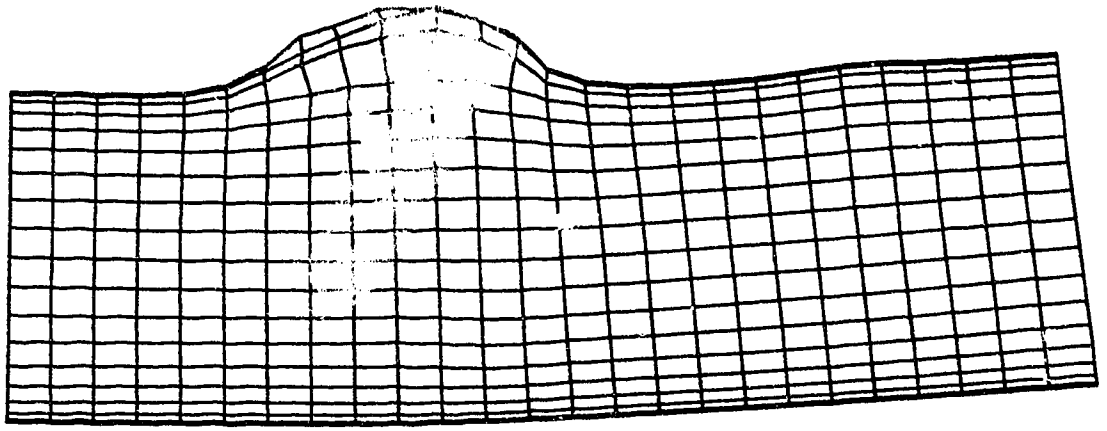

(a) Side View

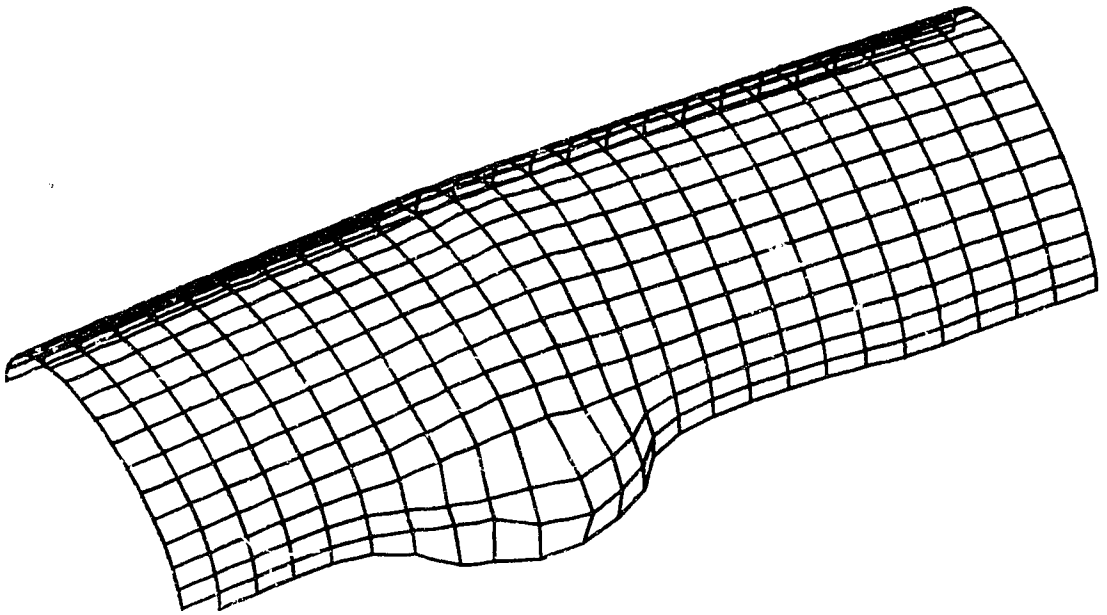

(b) Three Dimensional View

Fig. 4.33 Deformed Configuration of Specimen PHC00

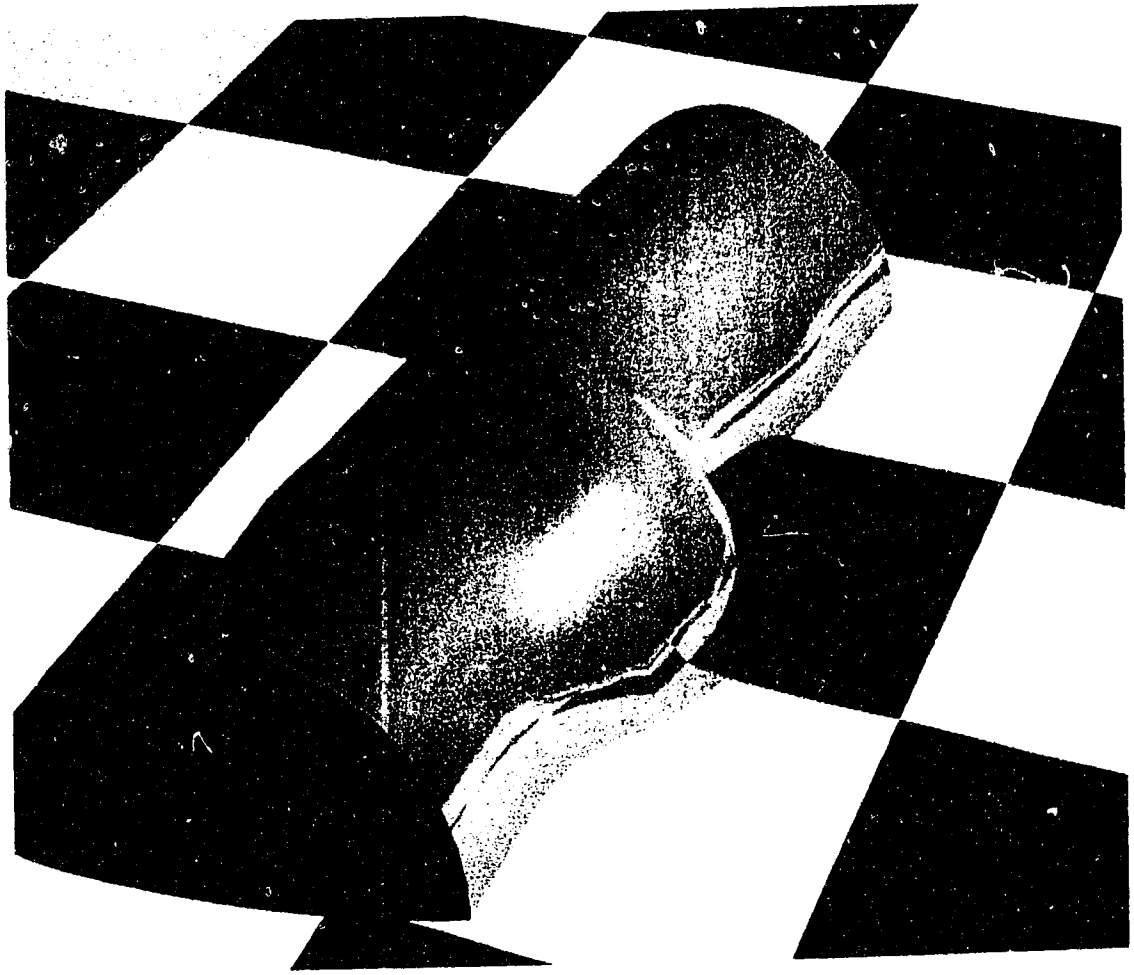

Fig. 4.33(c) Deformed Configuration of Specimen PHC00

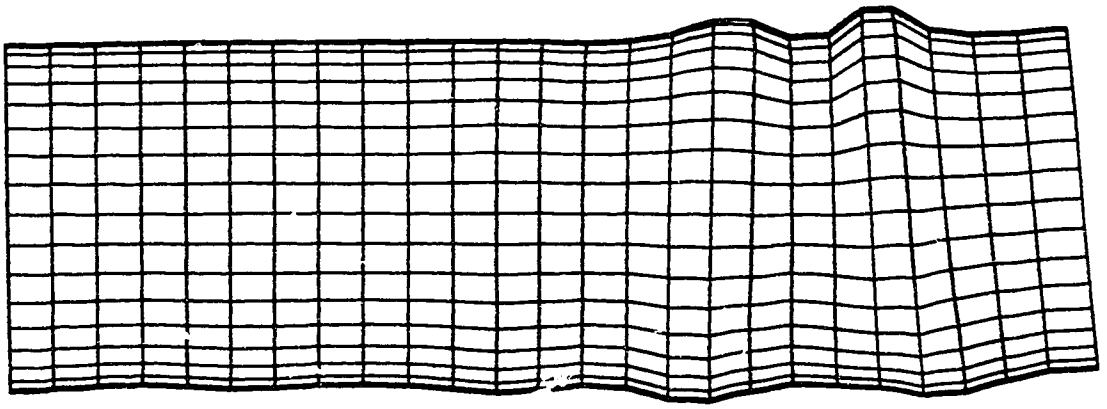

(a) Side View

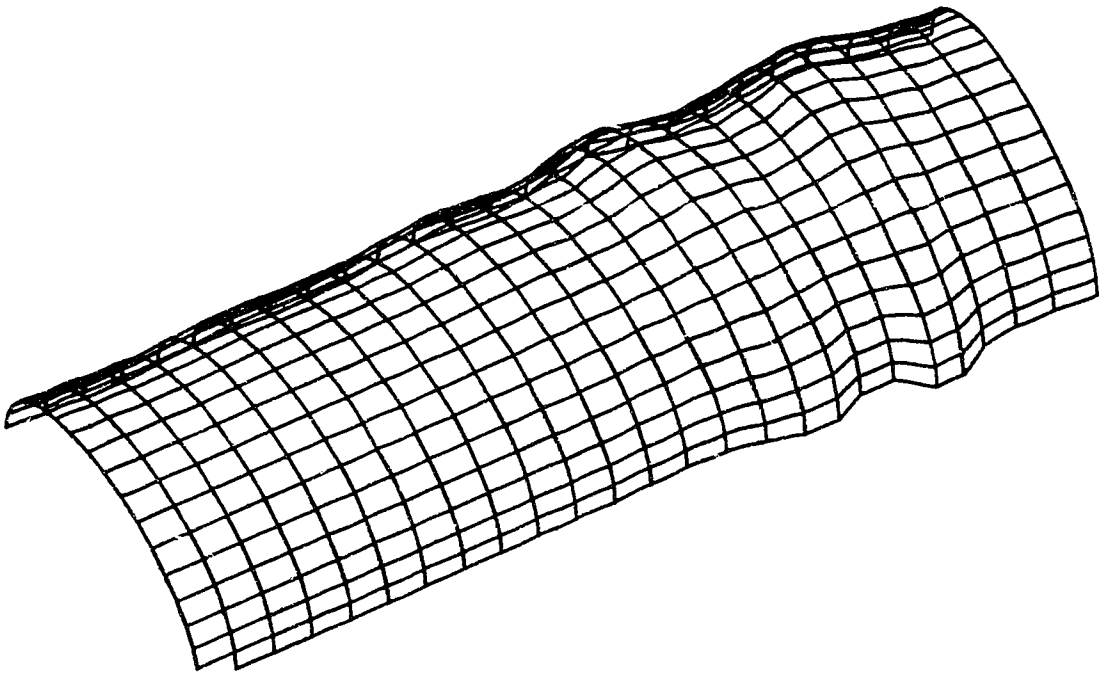

(b) Three Dimensional View

Fig. 4.34 Deformed Configuration of Specimen PHC40

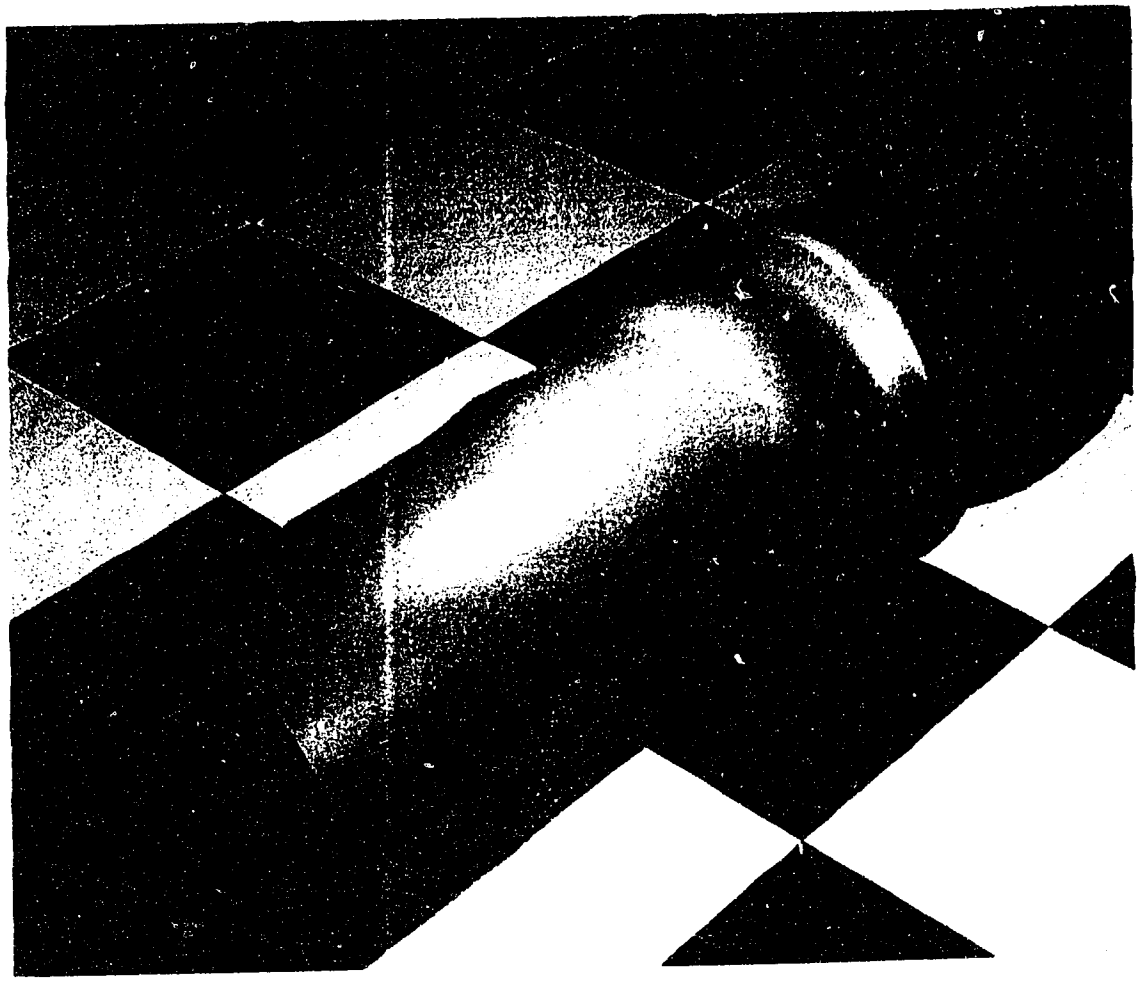

Fig. 4.34(c) Deformed Configuration of Specimen PHC40

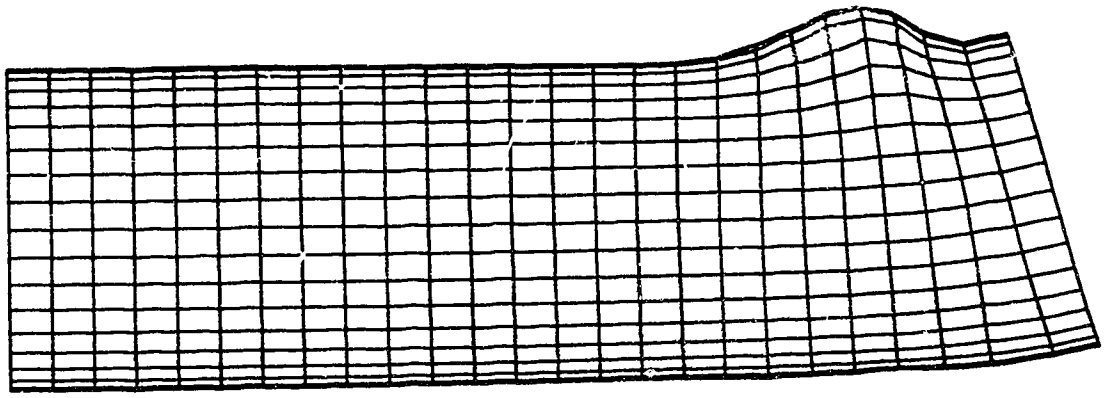

(a) Side View

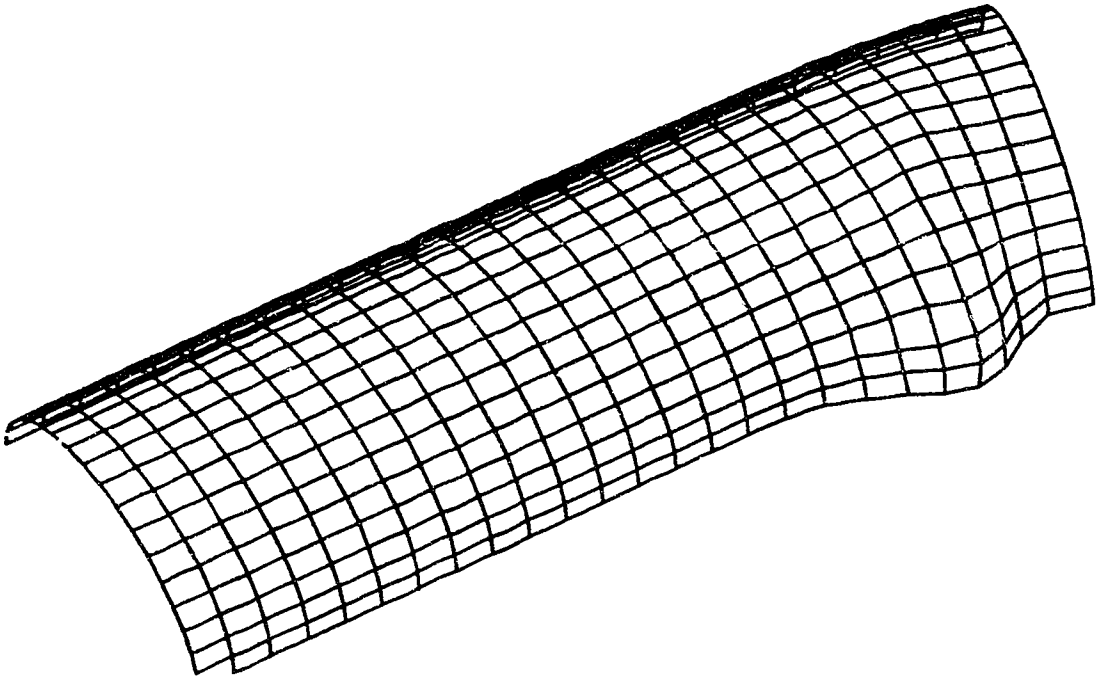

(b) Three Dimensional View

Fig. 4.35 Deformed Configuration of Specimen PHT40

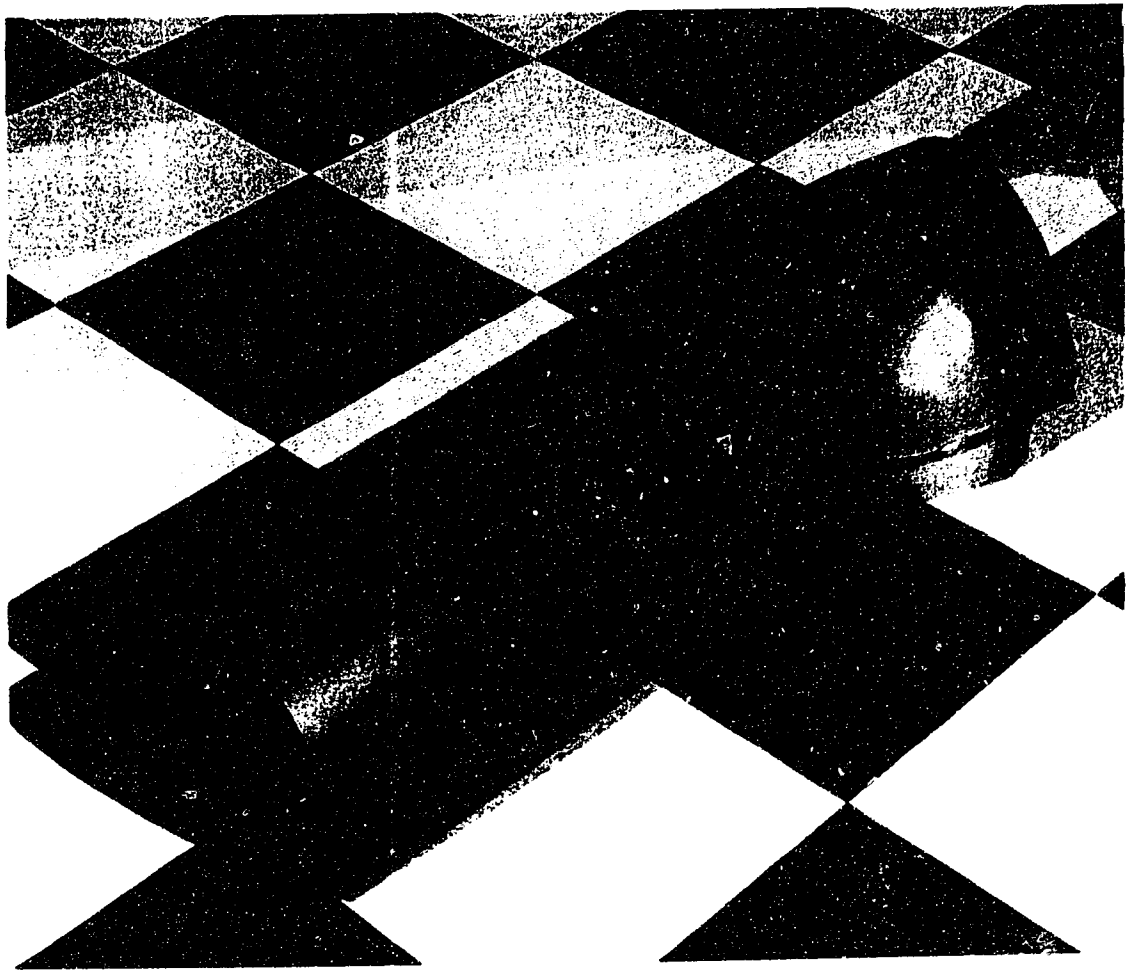

Fig. 4.35(c) Deformed Configuration of Specimen PHT40

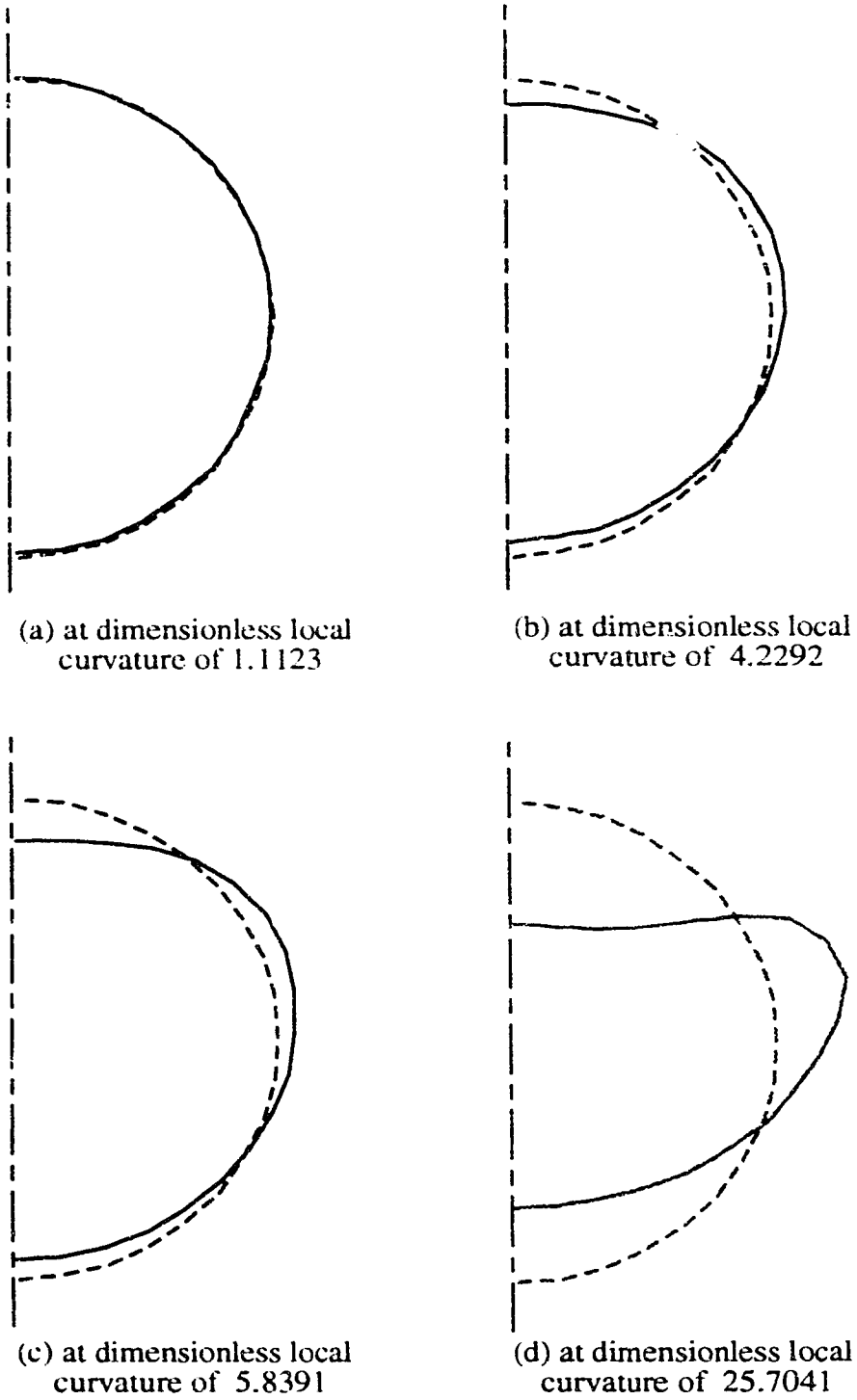

Fig. 4.36 Development of Cross-Sectional Distortion for Specimen PLC00 (Displacement Scale Equals to One)

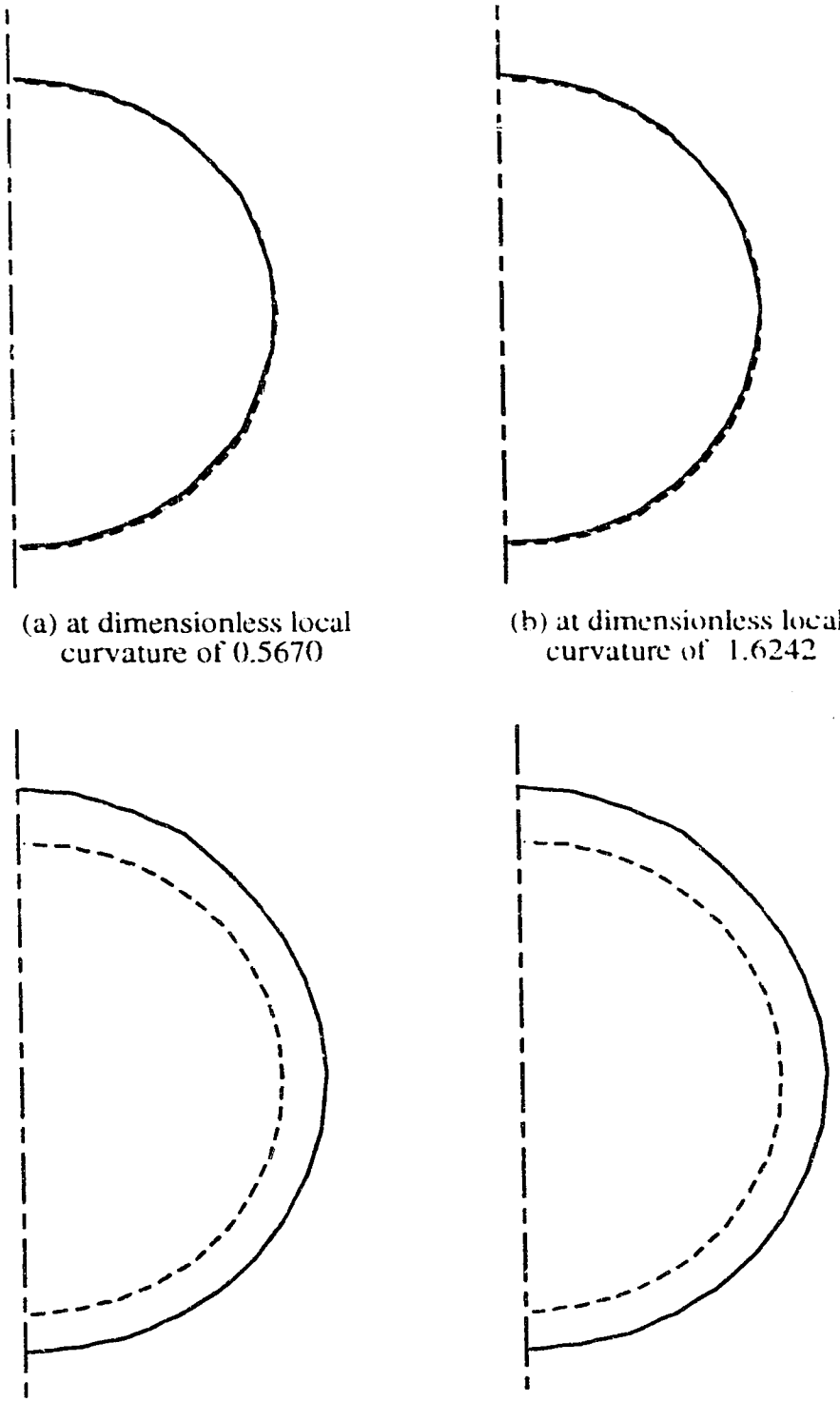

(a) at dimensionless local curvature of 0.5670

(b) at dimensionless local curvature of 1.6242

(c) at dimensionless local curvature of 13.4843

(d) at dimensionless local curvature of 18.4573

Fig. 4.37 Development of Cross-Sectional Distortion for Specimen PMC40 (Displacement Scale Equals to One)

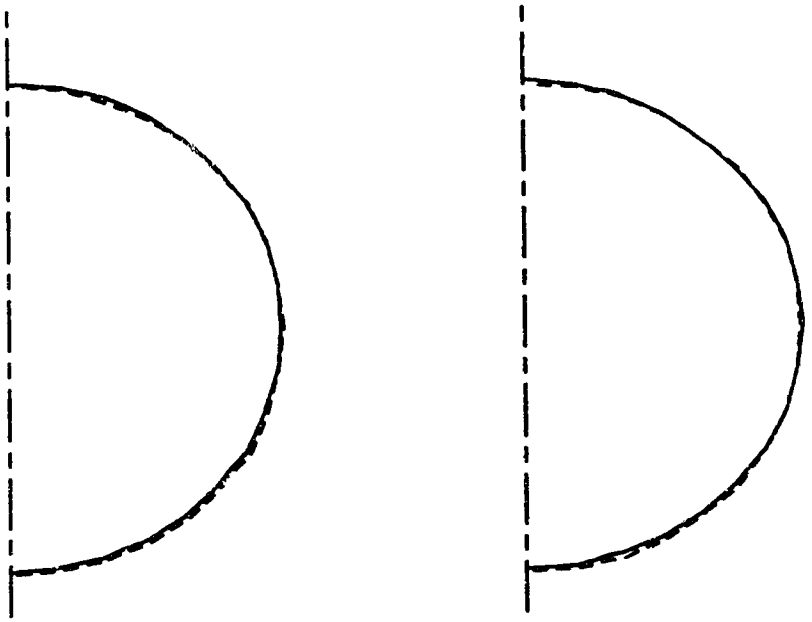

(a) at dimensionless local curvature of 1.4394

(b) at dimensionless local curvature of 7.0350

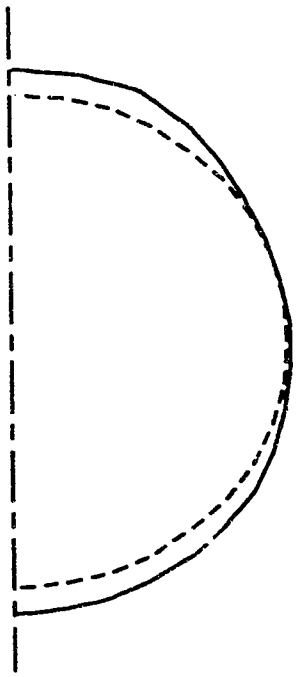

(c) at dimensionless local curvature of 12.0618

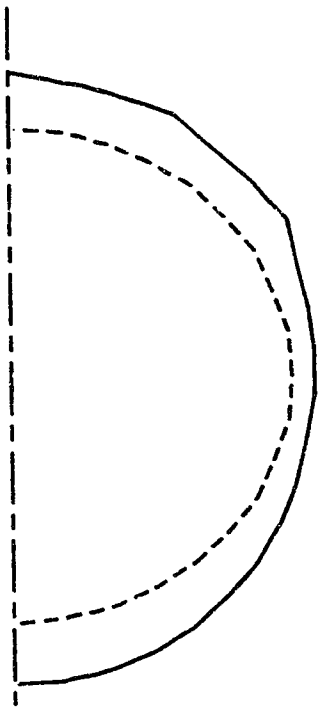

(d) at dimensionless local curvature of 19.9735

Fig. 4.38 Development of Cross-Sectional Distortion for Specimen PHC00 (Displacement Scale Equals to One)

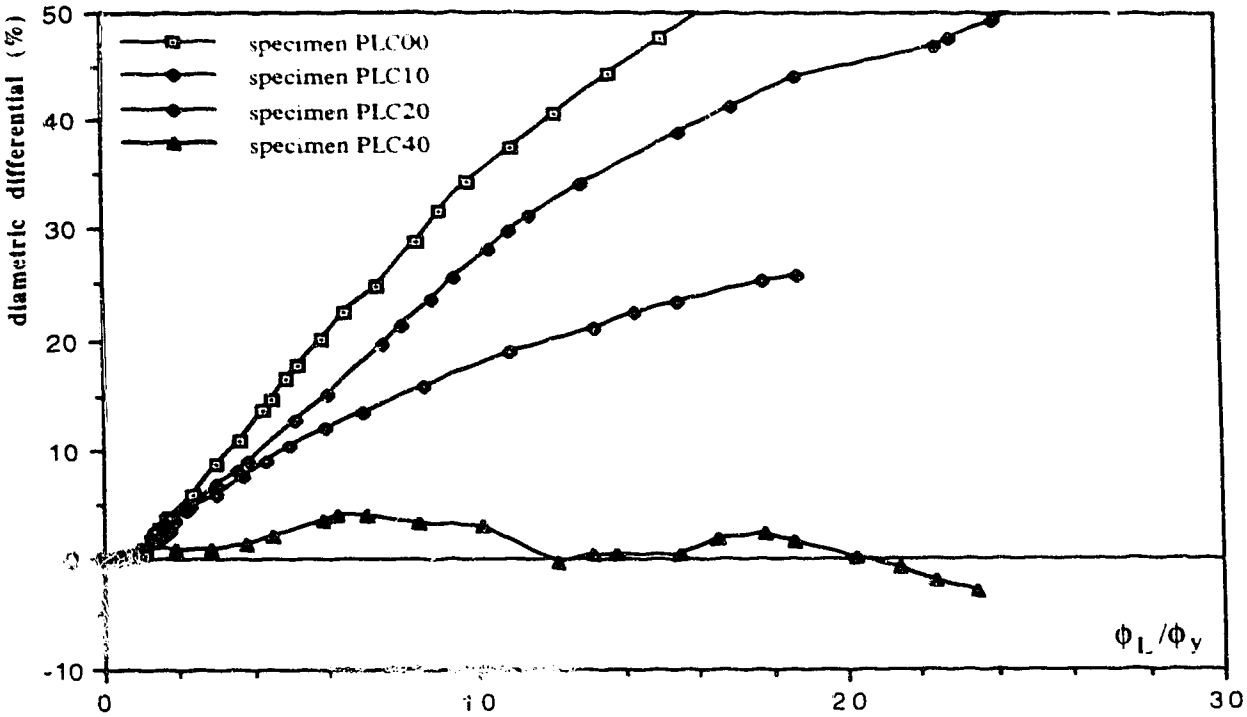

Fig. 4.39 Diametric Differential for Specimens with Low Level Pressure

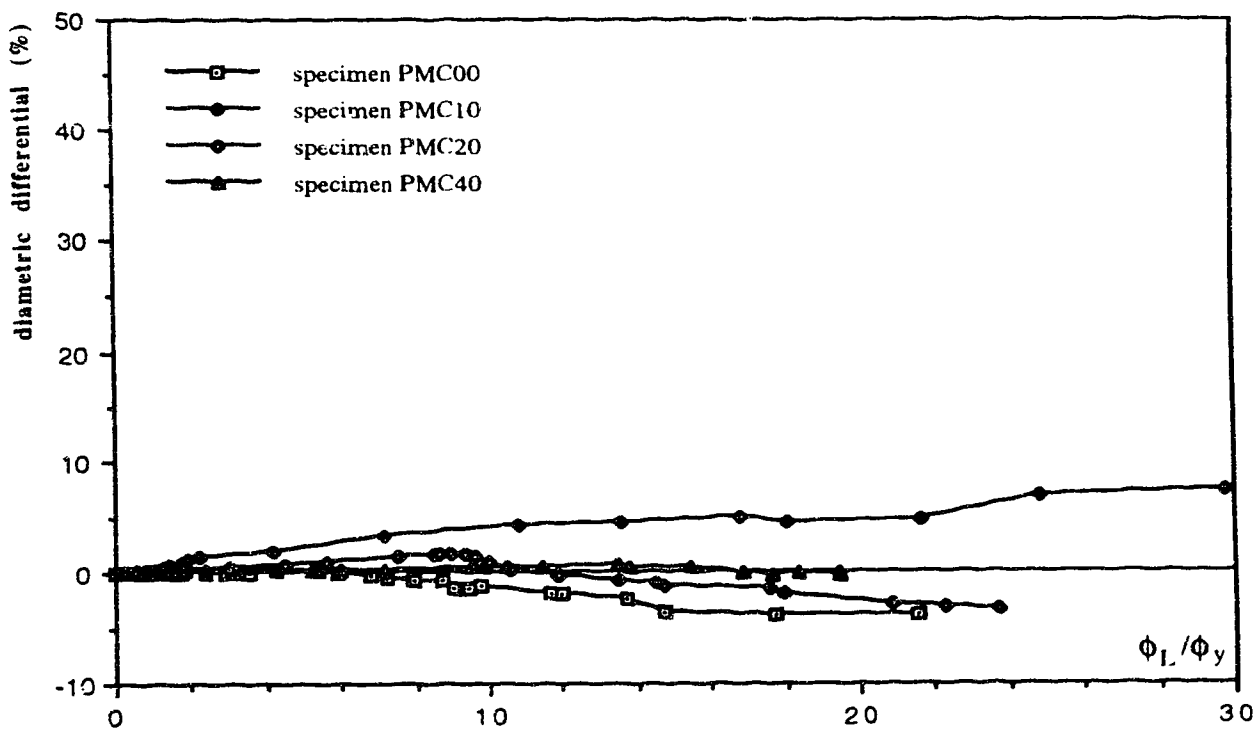

Fig. 4.40 Diametric Differential for Specimens with Middle Level Pressure

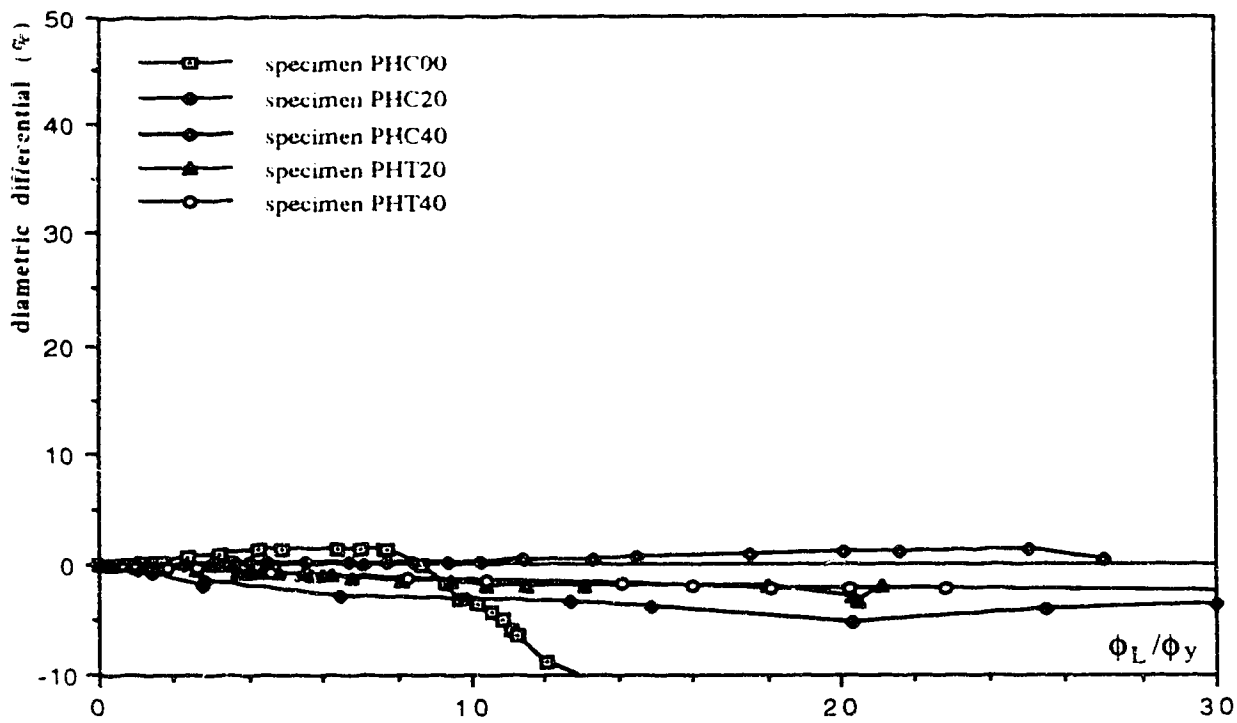

Fig. 4.41 Diametric Differential for Specimens with High Level Pressure

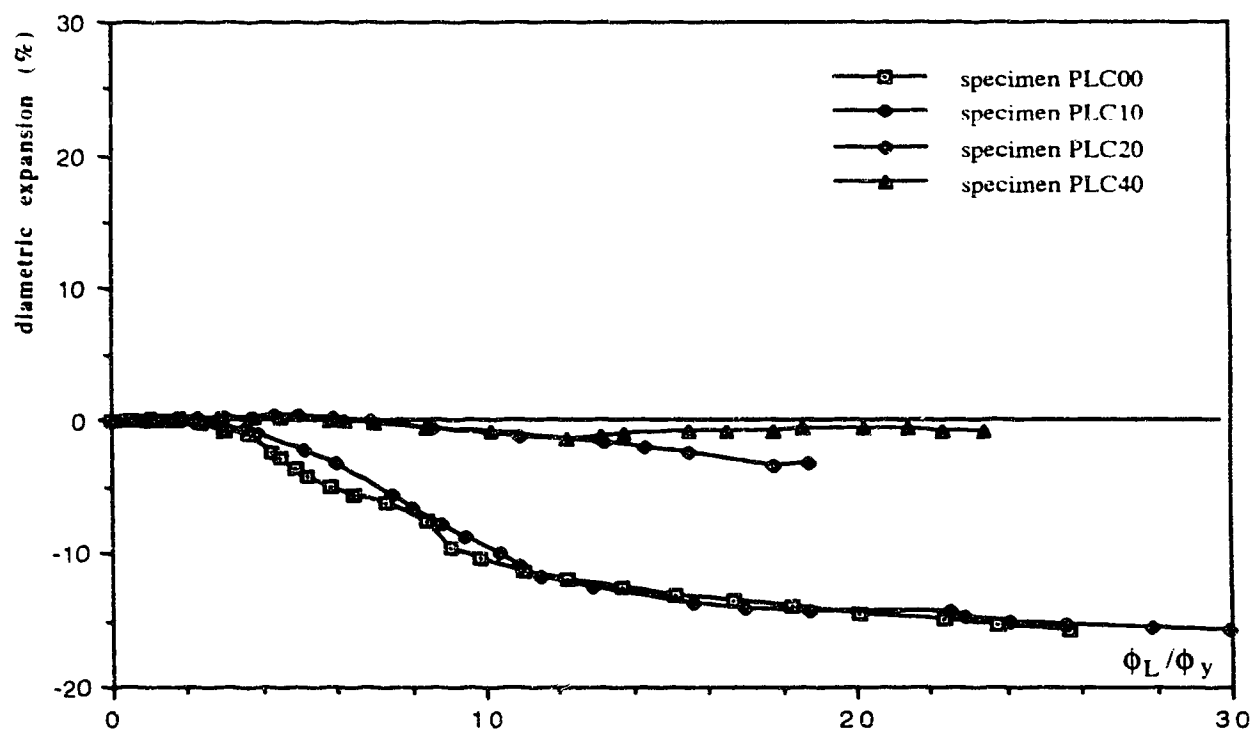

Fig. 4.42 Diametric Expansion for Specimens with Low Level Pressure

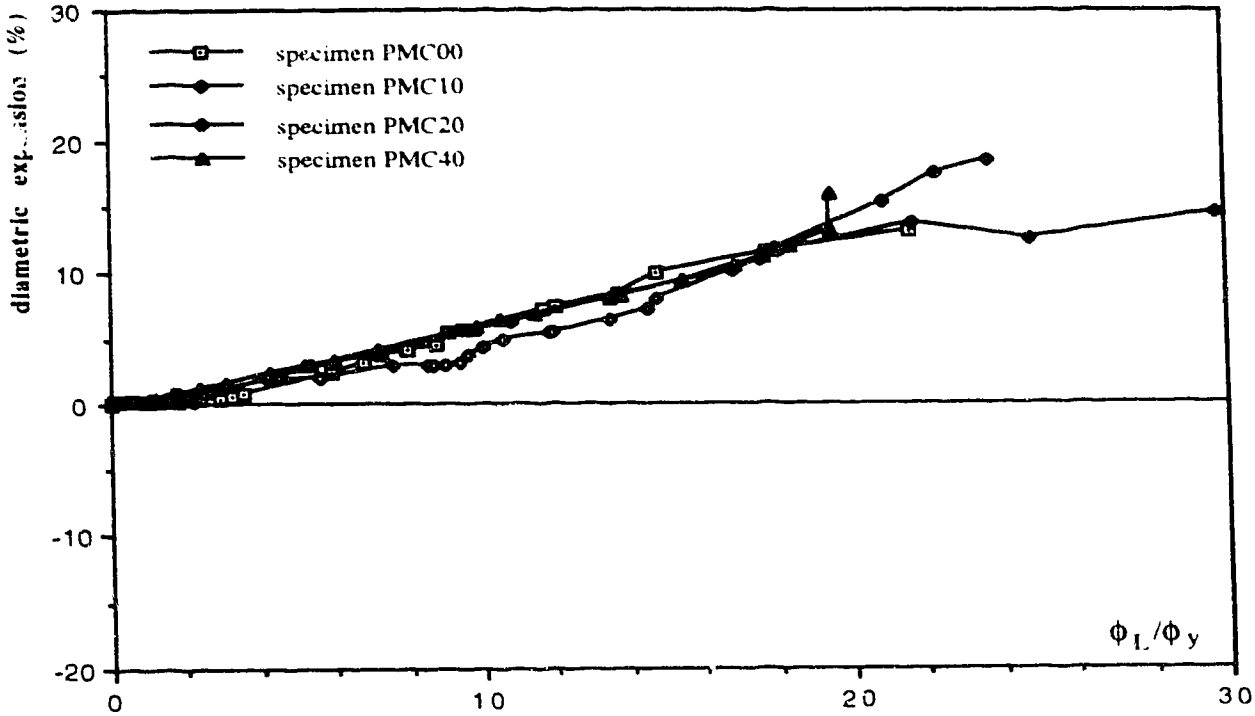

Fig. 4.43 Diametric Expansion for Specimens with Middle Level Pressure

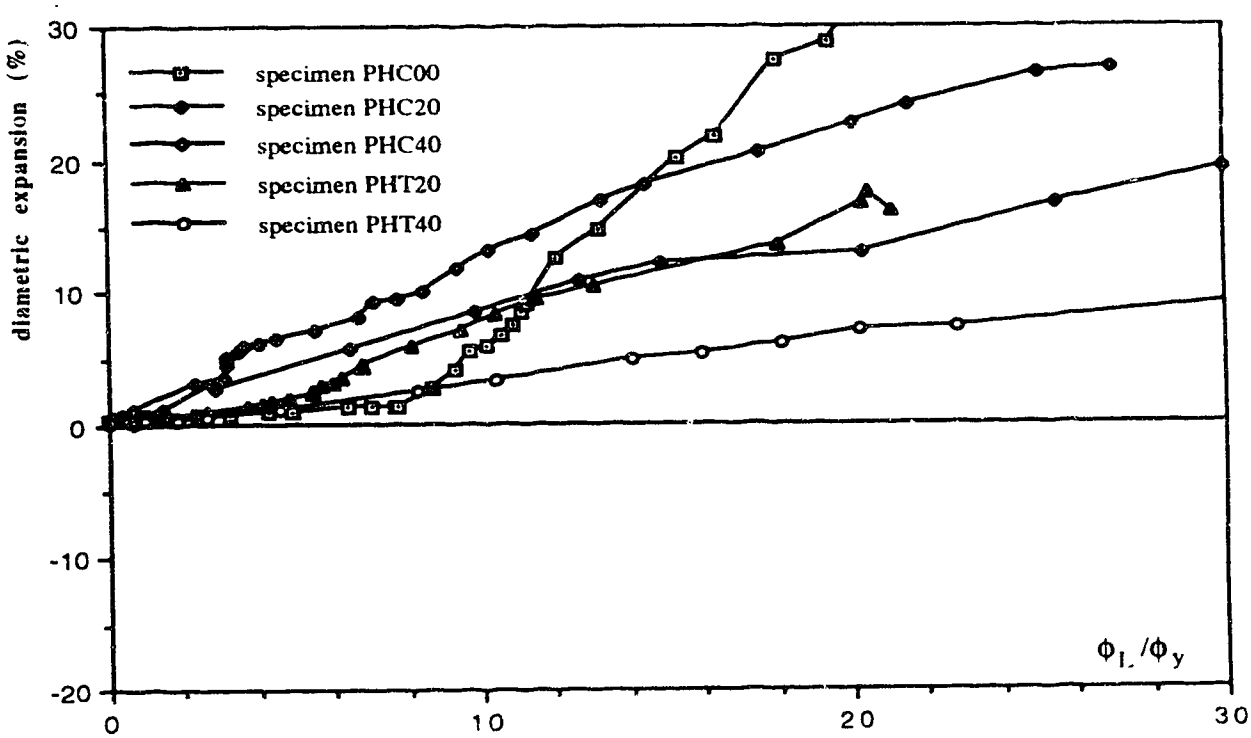

Fig. 4.44 Diametric Expansion for Specimens with High Level Pressure

CHAPTER 5 IDENTIFICATION OF WRINKLING INITIATION FOR PIPE SEGMENTS

The onset of buckling of pipelines has special significance because it is often used by the pipeline industry as the 'failure' condition. The result is that significant efforts have been made to predict the onset of buckling and determine a representative measurement of this state, such as, the maximum compressive strain at which buckling is incipient. This is usually referred to as the buckling strain. While the design condition based on the buckling strain can't be fully rationalized, its relationship to current practice makes the buckling strain an important aspect to be investigated. In this Chapter, the buckling strain will be defined and the predictive approaches will be reviewed. Following a discussion about the deficiency of using buckling strain as a design condition, concepts of initiation of wrinkling and wrinkling strain are introduced as alternatives. A procedure to identify the onset of wrinkling is then developed which includes some examples of verification. This procedure is applied to the specimens in the series of postbuckling analyses, which has been discussed in Ch. 4, and the wrinkling strains are determined. These illustrate the wrinkling behavior of pipe segments.

5.1 BUCKLING AND WRINKLING STRAINS

Buckling strain is the maximum compressive strain existing at the onset of buckling and may be used as the critical strain for pipelines subjected to deformation imposed loads. According to the shell buckling behavior discussed in Sect. 2.2.1.1, there are two types of buckling, namely, bifurcation buckling and snap-through. *Initiation of buckling* is calculated at either the bifurcation point or the initiation of snap-through, whichever occurs first. *Buckling strain* is then defined as the maximum compressive strain at the initiation of buckling. As discussed in Sect. 2.2.1.1, the initiation of snap-through depends on the loading system in addition to the behavior of structure. However, for present purposes it can be located at the limit point of the load-deflection curve. The *limit point* is the point where the maximum load carrying capacity is achieved. Some predictive approaches to the onset of buckling are briefly reviewed in the following. The deficiencies of these approaches for pipe segment are discussed. This leads to a new concept of wrinkling initiation.

5.1.1 Predictive Approaches for Buckling Strain

The two types of buckling phenomena require two different types of predictive

approach. In general, snap-through buckling needs a nonlinear incremental solution approach to predict the limit point. Physically, the limit point is the state where the maximum load carrying capacity is achieved and unloading is incipient. In order to clearly define the limit point on load-deflection curves, the solution technique should have the capability to carry the solution into the postbuckling region. Because the postbuckling behavior of pipe segments is characterized by softening (or unloading) in moment-curvature curves, as demonstrated in Sect.4.3.2, the solution technique should be able to handle sensitive unstable equilibrium paths. For pipe geometries commonly used in today's pipeline industry, it is essential that the effects of elastic-plastic behavior and large displacements are included in the solution. This is because, for these types of pipe segments, buckling usually initiates in the elastic-plastic region of material behavior and the pipe generally experiences large displacements prior to unloading. A suitable solution technique, that was developed for this project, has been described in Chapter 3.

Bifurcation buckling is normally predicted by eigen-analysis. Physically *bifurcation buckling* initiates at a *bifurcation point* which is the intersection of two or more possible equilibrium paths (Croll and Walker, 1972). For pipe segments, at least one of the equilibrium paths is unstable. Depending on the degree of complexity adopted, several alternate formulations of eigen-analysis can be used for prediction of bifurcation points. The simplest of these is *linear-elastic eigen-analysis*, which can be symbolically expressed as

$$([\mathbf{K}_E] - \lambda [\mathbf{K}_G]) \{\Delta \mathbf{u}\} = \{0\} \tag{5.1}$$

where $[\mathbf{K}_E]$ and $[\mathbf{K}_G]$ are the linear-elastic stiffness matrix and the geometric stiffness matrix, respectively. The quantities λ and $\{\Delta \mathbf{u}\}$ are the *eigen-value* and *eigen-vector*, respectively. This formulation is based on assumed linear-elastic behavior. A refined formulation is *elastic-plastic eigen-analysis* which can be established by including the elastic-plastic behavior and prebuckling deformation. It can be expressed as

$$([\mathbf{K}_{EP}] - \lambda [\mathbf{K}_G]) \{\Delta \mathbf{u}\} = \{0\} \tag{5.2}$$

where $[\mathbf{K}_{EP}]$ and $[\mathbf{K}_G]$ are the elastic-plastic stiffness matrix and the geometric stiffness matrix which are evaluated at an equilibrium configuration prior to, but close to, the bifurcation point. A nonlinear incremental solution procedure is needed to establish this equilibrium configuration. The effects of elastic-plastic behavior are reflected in $[\mathbf{K}_{EP}]$, the effects of the distribution of internal forces are represented by $[\mathbf{K}_G]$, and the effects of

prebuckling deformation are included in both $[\mathbf{K}_{EP}]$ and $[\mathbf{K}_G]$. The accuracy of the prediction based on the elastic-plastic eigen-analysis is largely dependent on the distance between the equilibrium configuration on which the equation of elastic-plastic eigen-analysis is established and the equilibrium configuration where the buckling is predicted to be initiated.

The most complicated and reliable procedure at present is the so called '*accompanying buckling analysis*' (Rammerstorfer, 1989). Accompanying buckling analysis is the combination of nonlinear incremental solution and elastic-plastic eigen-analysis and is used to predict the onset of bifurcation buckling of nonlinear structural systems (de Borst, 1988; Brendel and Ramm, 1979 and Rammerstorfer, 1982, 1989). This procedure includes generation of two curves. First, a load-deflection curve is obtained by carrying out the nonlinear incremental solution. Second, carrying out the elastic-plastic eigen-analysis, defined in Eq. (5.2), along the nonlinear equilibrium path at proper intervals, an eigenvalue-deflection curve is determined. These two curves are shown in Fig. 5.1. The intersection of these two curves is identified as the bifurcation point. The accompanying buckling analysis includes the effects of elastic-plastic behavior, prebuckling deformation and the distribution of internal forces in a similar manner to the elastic-plastic eigen-analysis. In addition, the accuracy of the prediction does not depend on where the elastic-plastic eigen-analyses are carried out as long as the intervals used are appropriate. Considering the fact that significant yielding may take place prior to initiation of buckling, linear-elastic eigen-analysis can't be used, and the elastic-plastic eigen-analysis may not be accurate because it is difficult to determine where the eigen-analysis should be carried out. Only the accompanying buckling analysis is a reliable approach to predict the bifurcation point for pipe segments.

5.1.2 Deficiencies of the Buckling Strain as a Failure Indicator

Deficiency of the buckling strain arises from the fact that the onset of buckling is difficult to identify and it is not a representative quantity characterizing the deformation of pipe segments, especially the local deformation. Discussions in the following are with respect to the buckling strain defined by bifurcation buckling and snap-through buckling.

Bifurcation buckling is a phenomenon associated with perfect structures. Perfect structures are characterized by perfect geometry and perfect loading and boundary conditions which result in uniform stress states and deformation which does not contain any component associated with the postbuckling equilibrium path.

If a structure is not perfect, bifurcation buckling is not possible. This is because components of nonuniform stress states and deformations associated with postbuckling paths exist from the very beginning of the loading history. These components increase as load increases and become more and more significant with respect to load carrying capacity and the characteristics of deformation. Eventually, the maximum load is achieved and unloading begins. Consequently, imperfections convert bifurcation buckling into snap-through buckling.

The real pipeline is always imperfect because of the unavoidable imperfections in material properties and geometry. In addition, the loading and boundary conditions also introduce imperfections. Therefore bifurcation buckling is not possible in real pipelines. The finite element model for pipe segments established in Sect. 4.2 is also not perfect because of the loading and boundary conditions. The axial load produces eccentricity which is larger in the middle of the pipe segment and increases as the flexural deformation increases. The use of the elastic ring at the ends of pipe segments introduces nonuniformity in ovalization along the length of pipe segments. Consequently, buckling strain based on bifurcation buckling is not reliable for pipe segments.

The predictive approaches based on snap-through buckling are applicable in principle because for pipe segments there is always a limit point and the initiation of snap-through can be approximately located at the limit point (see Sect. 2.2.1.1). The deficiency arises from the behavior of pipe segments. Typical moment-curvature curves are conceptually shown in Fig. 5.2 for pipe segments with high and low D/t ratios. Typically, these pipe segments are subject to combined constant axial load, constant internal pressure and monotonically increasing curvature. The pipe segments with a high D/t ratio tend to have significant unloading following the limit point. By contrast, those with a low D/t ratio tend to have a long yielding plateau before significant unloading begins. While the limit point can be, in general, identified, the difference in the moment-carrying capacity as yield deformation proceeds along the plateau is small and negligible. While the buckling moment is well defined for both types of behavior, the buckling strain may not be. For pipe segments with a long yield plateau, the strain can be amplified by a factor of 2 or 3 in the yield plateau while the difference in moment is minimal. Under these circumstances, the limit point where the maximum load is achieved losses its special significance with respect to the determination of the buckling strain. The buckling strain defined at the limit point becomes deficient.

In addition, buckling strain defined at the limit point does not nave any special significance as a measurement for characterizing the behavior of pipe segments. Since deformation state of a buried pipeline is more important than its load-carrying capacity relative to the imposed deformation, associating the critical strain with the maximum load-carrying capacity is neither necessary nor rational. At most, buckling implies that the deformation will localize and load carrying capacity will drop afterward. However, how the deformation will localize depends on the geometry, material properties, loading and boundary conditions. Consequently, the buckling strain defined at the limit point is not a representation of the deformation behavior of pipe segments characterized by localization. Instead, it is associated with maximum load-carrying capacity.

5.1.3 Initiation of Wrinkling

Since buckling strain cannot effectively represent the critical state of pipe segments subjected to imposed deformation, an alternative is needed. The concepts of initiation of wrinkling and wrinkling strain are introduced based on the fact that the critical state of such pipe segments can be characterized by the initiation of localization of deformation. Initiation of wrinkling and wrinkling strain are defined based on the growth of the nonuniform deformation component. *Initiation of wrinkling* is the point where nonuniform deformation begins to localize, and *wrinkling strain* is the maximum compressive strain at this initiation of wrinkling.

The initiation of wrinkling emphasizes the importance of the deformation and localized distortion. The moment-carrying capacity of pipe segments is largely considered as irrelevant. The concept of the initiation of wrinkling can accommodate the fact that the nonuniform deformation component exists at the very beginning of the loading history because of the imperfections in load and boundary conditions. It is more representative of the critical state of pipe segments because it is directly associated with the localization of deformation. Therefore it is expected to be a better alternative than initiation of buckling for use in pipeline design. However, similar to initiation of buckling, initiation of wrinkling is not a 'failure' condition and therefore can't be used as a limit states design condition.

Depending on the behavior of pipe segments, initiation of wrinkling may or may not be close to the limit point. Deformation localization is, in general, associated with significant unloading. Two typical behaviors shown in Fig. 5.2, for pipe segments with high D/t ratios the initiation of wrinkling is expected to be close to the limit point and

significant softening follows the limit point immediately. It may be different for pipe segments with low D/t ratios because of the long yield plateau. The wrinkling strain is , in general, expected to be close to or larger than the buckling strain because localization of deformation is the result of local buckling. Therefore, it begins only after local buckling is initiated, provided that the effects of imperfec. ns are limited.

5.2 WRINKLING ANALYSIS

Buckling analysis usually refers to the procedure to identify the initiation of buckling. By analogy, *wrinkling analysis* refers to the procedure to identify the initiation of wrinkling. To identify the initiation of wrinkling, the localization of deformation has to be first numerically described. The beginning of localization of deformation can then be determined. A procedure for that is discussed in following sub-sections. This proposed procedure is verified by comparing the predictions from this procedure with available test results.

5.2.1 Procedure of Wrinkling Analysis

The localization of deformation may be described in terms of localization of strain, curvature, and cross-sectional distortion, as defined in Sect. 4.3.1. Before the initiation of wrinkling, the strain and curvature distribute uniformly except for the secondary effects of the axial load, and the cross-sectional deformation is mainly in the form of ovalization. Recognizing the fact that non-uniform distribution of strain and curvature exist from the beginning because of initial imperfections, the onset for the first rapid increase of the nonuniform component, or the attainment of a limit tolerance on its magnitude, can be used as indication of initiation of wrinkling. The postbuckling behavior of pipe segments discussed in Sect. 4.3 shows the deformation is mainly localized in the vicinity of one location, the extent of which is called the *buckling segment*. The magnitude of the nonuniformity in strain and curvature can be represented by differences between the local strain and curvature defined on the buckling segment and the overall strain and curvature defined on the entire pipe segment. Typical examples are shown in Figs. 5.4 and 5.5. The local and overall strains .efer particularly to the average compressive strain at the extreme fiber. Consequently, comparing local strain and curvature with overall strain and curvature is one way to identify the onset of wrinkling.

The cross-sectional deformation is associated with the localization of deformation, in one way or another depending on factors such as geometry of the pipe segment, material

properties, and loading and boundary conditions. In spite of the differences, the cross-sectional deformation can be divided into two components. One is *ovalization* which is introduced by flexural deformation. The other can be called the *wrinkling component* because it is mainly introduced by deformation associated with local wrinkling.

Ovalization depends mainly on the curvature and stiffness distribution on the cross-section, and is essentially symmetric about the horizontal diameter. However, an asymmetric component of ovalization may be introduced by an asymmetric distribution of stiffness due to the applied axial load and internal pressure. The axial load combined with bending moment produces an asymmetric stress distribution over the cross-section, and the internal pressure makes the material yield at different longitudinal stresses in tension and compression.

The wrinkling component of the cross-sectional distortion is asymmetric in nature about the horizontal diameter, because the wrinkling is always initiated from the compression side of the pipe segment which is subject to the load combination such as axial load, pressure and imposed curvature. Although it is possible that the wrinkling component becomes approximately symmetric in the deep postbuckling region when the wrinkle is fully developed on the entire circumference, as shown in Figs. 4.32 and 4.37 for specimen PMC40, the asymmetric nature of the wrinkling component is still very evident in the initial postbuckling region. Consequently, the point of origin of the wrinkling component can be used as an additional indication for initiation of wrinkling.

The four measures defined in Sect. 4.3.1 to describe the cross-sectional deformation are : out-of-roundness; diametric differential, D_{diff}; diametric expansion, D_{exp}; and, radius differential, R_{diff}. Except for the last one, all of them describe the total cross-sectional deformation. The radius differential is a measurement of the asymmetric component of the cross-sectional deformation in terms of the difference between the radius on the compression side and the one on the tension side in the bending plane. The expression of R_{diff} has been given in Eq. (4.4). R_{diff} is negligibly small before the onset of wrinkling, and starts to grow at this onset, as shown in Fig. 5.3. Considering the fact that R_{diff} is not exactly zero, the initiation of wrinkling can be set at the point where the first rapid increase of R_{diff} is incipient or a value equal to a limiting tolerance of it is reached.

In summary, the initiation of wrinkling can be identified by examining the growth and magnitude of R_{diff}, and comparisons of the local strain and curvature with overall strain and curvature. Procedures to identify initiation of wrinkling can be established based on

these criteria. There are three major steps. The first step is to carry out the nonlinear incremental solution for the given pipe segment. This solution is similar to the one for postbuckling analysis except the solution does not need to be carried into the deep postbuckling region. The second step is reducing the data from the solution obtained. The radius differential is defined based on the cross-sectional deformation and the strain and curvature are defined based on the buckling segment and the pipe segment. These measurements are then presented in the form of a radius differential-local curvature curve, an overall curvature-local curvature curve and an overall strain-local strain curve. The last step is to determine the initiation of wrinkling from these curves according to the criteria discussed previously in this section. Generally, all three of these techniques are used in conjunction in order to evaluate the initiation of wrinkling.

5.2.2 Illustrations

The procedure for wrinkling analysis is demonstrated in the following by numerical examples. The geometry and material properties are taken from Specimens 20a, 16a and 10a reported by Jirsa et. al. (1972). The specimens are designated herein as DTR20, DTR16 and DTR10, respectively, where DTR represents the series of wrinkling analyses illustrating the effects of the D/t ratio on wrinkling strain. The two digit-number following represents the diameter of the specimens. The specimens have diameters of 20, 16 and 10.75 inches (508, 406.4 and 273 mm), and D/t ratios of 78.4, 61.5 and 46.1, respectively. The stress-strain curves in piecewise linear form are retrieved from the curves reported (Jirsa, 1972) and are listed in Table 5.1. All three specimens are only subject to bending moment.

In the figures shown in this chapter, radius differential is denoted by R_{diff}. Curvature and strain are denoted by ϕ and ε with subscripts L, o, and y which indicate local, overall and yield, respectively. Wrinkling strain is denoted by ε_w. Internal pressure and its yield value are denoted by p and p_y. Axial load, which is positive in tension, and its yield value, are denoted by F and F_y.

The results for the nonlinear solution for Specimen DTR20 are shown in Figs. 5.3 to 5.5. Figure 5.3 shows the radius differential-local curvature curve. Comparisons of overall with respect to local curvatures and strains are shown in Figs. 5.4 and 5.5, respectively. Similar to the presentation of the the results of postbuckling analysis, the curvatures and strains in these figures are normalized by the yield curvature and the yield strain. The onset of wrinkling can be clearly identified from these figures using the criteria

advanced in Sect. 5.2.1. It is indicated by a small arrow in each of the figures. The indication from the radius differential is the most obvious. The differences between the overall and local curvatures as well as between the overall and local strains start to grow at the onset of wrinkling identified from the growth of the radius differential. All plots indicate the initiation of wrinkling in a consistent manner. Therefore the onset of wrinkling is confirmed at a normalized curvature of 1.923 and a normalized strain at 1.950. The associated curvature and compressive strain are calculated as 3.58×10^{-4} in^{-1} (1.409×10^{-5} mm^{-1}) and 0.363%.

The nonlinear solutions for Specimens DTR16 and DTR10 are shown in Figs. 5.6 to 5.8 and in Figs. 5.9 to 5.11, respectively. As for Specimen DTR20, the onsets of wrinkling are clearly identified for both of these specimens. The indications from the radius differential, curvatures and strains are consistent with each other and a unique point has been identified as the onset of wrinkling for each of the specimens. The onset for Specimen DTR16 is identified at a curvature of 9.41×10^{-4} in^{-1} (3.705×10^{-5} mm^{-1}) and a strain of 0.804%. The one for Specimen DTR10 is identified at a curvature of 23.39×10^{-4} in^{-1} (9.209×10^{-5} mm^{-1}) and a strain of 1.300% .

Comparison between computed wrinkling strains of Specimens DTR20, DTR16 and DTR10 and the measured buckling strains are shown in Fig. 5.12. Good agreement is achieved. This is because the moment-curvature curves, as reported by Jirsa et. al. (1972), have significant unloading following the limit point at which the buckling strains are defined. Associated with the unloading, deformation localizes and local wrinkling grows. As a result, the onsets of wrinkling are identified to be very close to the limit points.

5.3 EFFECTS OF PIPE GEOMETRY ON WRINKLING STRAIN

The pipe geometry varies extensively dependent on the function of the pipeline, the cost effectiveness of the design and the technology available. The diameter of pipelines used in past decades for major pipelines in the oil industry ranges from as small as 12.75 inches (324 mm) to as large as 48 inches (1219 mm), and the D/t ratio ranges from 50 to 100. Some older pipelines have even smaller D/t ratios, such as 30. Due to the wide range of pipe geometry used in the pipeline industry, it is important to understand the effects of the pipe geometry on the wrinkling strain.

The geometry of a perfect pipe segment can be represented by the diameter and D/t ratio. Consequently, the effects of pipe geometry can be examined by studying the

dependence of wrinkling strain on these two geometric characteristics. This is done in the following sub-sections.

5.3.1 Effects of D/t Ratio

The D/t ratio of pipe segments has been proven to be one of the most important factors affecting wrinkling strains by both experimental and analytical studies. Examples are test programs (Bouwkamp and Stephen, 1974; and, Jirsa et. al., 1972), and the formula for classical elastic buckling strain (Eq. (1.1)) and for elastic-plastic buckling strain (Eq. (1.2)). The wrinkling strain is found to decrease as the D/t ratio increases. The buckling process shifts from buckling in elastic-plastic range at low D/t ratios to buckling elastically at high D/t ratios. Pipe segments are a type of cylindrical shell for which the common range of D/t ratios is from 30 to 100 and they usually buckle in the elastic-plastical range. The difference is, however, that pipe segments with low D/t ratios tend to have extensive plastic deformation before the initiation of wrinkling while those with high D/t ratio may have a relatively small component of plastic deformation.

The effects of D/t ratio are illustrated by the results of the DTR series of wrinkling analyses which have been presented in Sect. 5.2.2. The predictions of initiation of wrinkling are supported by test results as shown in Fig. 5.12. Figure 5.13 shows the computed wrinkling strains with respect to the D/t ratios for Specimens DTR20, DTR16 and DTR10. Although some differences in material properties exist as shown in Table 5.1 and the diameters are different, the effect of D/t ratio is dominant. The curve in Fig. 5.13 illustrates the effect of D/t ratio and confirms the conclusion that increasing D/t ratio corresponds to decreasing wrinkling strain. As the D/t ratio changes from 78 for Specimen DTR20 to 46 for Specimen DTR10, the wrinkling strain increases from 0.363 percent to 1.3 percent, which gives a factor of 3.6. This shows the great difference in wrinkling strain that may be associated with different geometries commonly used in the pipeline industry.

5.3.2 Effects of Diameter

Pipe diameter is believed to have insignificant effects on wrinkling strain. This conclusion is supported by the elastic buckling theory where the buckling strain is predicted in Eq. (1.1) to be independent of diameter. However, documented study of this in terms of both experiment and analysis appears to be inadequate. To illustrate the effects of diameter, a series of wrinkling analysis is carried out herein. The three specimens in this series are designated as DIA48, DIA24 and DIA12, respectively. The letters DIA indicate that the

series is devoted to the effects of the pipe diameter. The two-digit number represents the outer diameter of the pipes in inches. The specimens have diameters of 48, 24 and 12.75 inches (1219, 610 and 324 mm), respectively, and the D/t ratio is 103.9 for all three of them. The geometry and material property of these specimens are listed in Table 5.3. It should be pointed out that the Specimen DIA48 is exactly the same as the Specimen PLC00 in the series of postbuckling analysis.

The initiation of wrinkling is identified by the method described in Sect. 5.2 at 0.256%, 0.298% and 0.351% for Specimens DIA48, DIA24 and DIA12, respectively. The wrinkling strains are plotted with respect to the diameters in Fig. 5.14. The wrinkling strain is found to decrease as the diameter increases. With diameter changes from 12.75 inches to 48 inches, a reduction of 27% in wrinkling strain is introduced. Comparing this with the difference introduced by the D/t ratio, wrinkling strain is less sensitive to diameter.

5.4 EFFECTS OF LOADING CONDITION ON WRINKLING STRAINS

Pipelines in operation may experience various types of loading conditions depending on the operational and environmental conditions. In Arctic regions, a pipeline may be subject to the following typical loading conditions and their combinations :

(a) internal pressure due to oil transmitted in the pipeline
(b) axial compression due to temperature differential
(c) bending moment due to imposed deformation, and
(d) axial tension introduced by the catenary effect associated with the flexural deformation, where the longitudinal movement of the pipeline is restricted by surrounding soil.

The internal pressure may vary from zero to the value of the permissible hoop stress of 80 percent of SMYS. This value is 72 percent for pipelines built several years ago. The axial compression may vary from zero to a level at which an axial compressive force of 40 percent of the axial yield force is produced. This level represents a differential temperature of about 65 °C between the tie-in temperature and the operational temperature. The imposed deformation caused by soil settlements may be large enough to cause the moment to vary from zero to its yield moment and then push the pipe into the softening region after buckling is initiated. The tensile axial force may vary from zero to about 40 percent of the axial yield force under a differential settlement of 40 inches.

The combined loading condition is expected to have significant influence on the

wrinkling strain. The internal pressure has been proven to do so by both experimental and analytical studies (Bouwkamp and Stephen, 1974; and, Lara, 1987). The effects of axial load, however, have not been adequately studied. This is specially true for tensile axial force. In the following subsections, the effects of the loading condition are illustrated through numerical analyses of selected load combinations.

To demonstrate the effects of loading condition, thirteen specimens are selected for wrinkling analysis. The analyses are carried out as discussed in Sect. 5.2. The names and loading conditions for these specimens are listed in Table 5.2. These specimens are the same as those for postbuckling analysis in Ch. 4 with additional Specimens PLT40 and PMT40 which are added to illustrate the effect of pressure combined with tensile axial force. The strains and curvatures at the onset of wrinkling are listed in Table 5.2.

5.4.1 Effects of Internal Pressure

The wrinkling strains for the specimens in the series of postbuckling analysis are listed in Table 5.2 along with the loading conditions. If these specimens are divided into groups according to the applied axial load, the dependence of wrinkling strain on the internal pressure at different levels of axial load can be examined. Figure 5.15 shows the wrinkling strain-pressure curves without an axial load and with axial loads of $0.4F_y$ both in compression and tension, where F_y is the axial yield load. Each of these curves has three data points that correspond to the levels of internal pressure at 0, 35 percent and 72 percent. The Specimens PLC00, PMC00 and PHC00; PLC40, PMC40 and PHC40; and, PLT40, PMT40 and PHT40 are associated with the wrinkling strain-pressure curves without an axial load, and with compressive and tensile axial loads of $0.4F_y$, respectively.

Two opposite trends can be observed for the dependency of wrinkling strain on the internal pressure from Fig. 5.15. The wrinkling strain is found to increase as the internal pressure increases when the pipe segment is subject to no axial load and tensile axial load of $0.4F_y$. It is found to decrease as the internal pressure increases when compressive axial load of $0.4F_y$ is applied. The first trend agrees with the conclusion from test programs carried out by Bouwkamp and Stephen (1974) and the one at University of Alberta (Mohareb et. al., 1992). However, a comparable set of test results for the second trend has not been found.

It should be pointed out that all solutions for specimens in the series of postbuckling analysis are based on a simplified bilinear stress-strain curve, as defined in

Sect. 4.2.3. The stress-strain curve may have important influence on the wrinkling strain because the initiation of wrinkling is expected to be affected by the stiffness of pipe wall, which is determined by the tangent stiffness for elastic-plastic buckling. However, a systematic study of the effects of stress-strain curves has not been included in this work because of the variety of stress-strain curves and the difficulty to systematically describe them.

5.4.2 Effects of Axial Load

The effects of axial load can be examined in a similar manner as for internal pressure, if the specimens in the series of postbuckling analysis are grouped according to the levels of applied internal pressure. The wrinkling strains are plotted against the level of applied axial load for each of the groups, and the curves are shown in Fig. 5.16. The axial load is positive in tension. The specimens associated with the low level of pressure are PLC40, PLC20, PLC00 and PLT40. The specimens associated with the middle level of pressure are PMC40, PMC20, PMC00 and PMT40; and those with the high level of pressure are PHC40, PHC20, PHC00 and PHT40.

Figure 5.16 shows that the dependency of wrinkling strain on the axial load is affected by the level of applied internal pressure. For empty pipe segments, which correspond to the low level of pressure, the wrinkling strain decreases monotonically as the axial load changes from compression to tension. For pressurized pipe segments, which correspond to the middle and high levels of pressure, the wrinkling strain increases as the compressive axial load decreases and it decreases as the tensile axial load increases. In other words, both compressive and tensile axial loads reduce the wrinkling strain and the maximum wrinkling strain occurs for specimens without axial load for pressurized pipe segments.

Some supporting evidences for the findings here can be obtained from test results. In the test series carried out by Bouwkamp and Stephen (1974), Specimens No. 1 and No. 4 were subject to internal pressure of 942 psi (6.5 MPa) and 950 psi (6.6 MPa); and net axial load of 940 kips (4181 KN) and 266 kips (1183 KN) in compression, respectively. Converting the pressure and axial load into nondimensional pressure and axial load, they are 75.6 and 76.2 percent of yield pressure; and 21.3 and and 6 percent of axial yield load, respectively. While the levels of internal pressure were almost the same, the difference in the levels of axial load from 6 to 21.3 percent is obvious and is the major difference between these two specimens. The buckling strains were reported as 0.5735 percent and

0.8196 percent for the Specimen No. 1 and No. 4, respectively. This represented a 30 percent reduction in buckling strain as the compressive axial load increased from 6 percent to 21.3 percent. As a result, the trend observed in Fig. 5.16 with respect to the pressurized pipe segments is confirmed when they are subject to compressive axial load. Unfortunately, the t[illegible]ssociated with the empty pipe as well as pressurized pipe subjected to tensile axial load can't be confirmed because comparable test results are not available.

5.4.3 Rationale for Effects of Loading Condition

The dependency of wrinkling strain on internal pressure, axial load and their combination has been discussed in the previous sub-sections. It is more complicated than anticipated. The relations between wrinkling strain and pressure have different characteristics at different levels of axial load, and similarly for the relations between wrinkling strain and axial load with respect to different levels of internal pressure. These behaviors can be better understood by considering how loading conditions affect the wrinkling strain. The loading condition influences the wrinkling strain by its effects on the following four factors.

The first factor is the buckling mode. As discussed in Sect. 4.3.4, there are two basic types of buckling mode. One is a diamond buckling mode, which exhibits inward and outward displacements, and the other is an outward bulging buckling mode. The buckling mode that a particular specimen develops appears to be determined primarily by the presence or absence of pressure. Empty pipes, in general, buckle in the diamond buckling mode; pressurized pipes, however, buckle in the bulging mode.

The second factor is the longitudinal strain at which the initial yielding of the extreme compressive fiber occurs. The biaxial stress condition in the pipe wall results in an initial yield strain that is dependent on the applied internal pressure. It may be evaluated as $-\varepsilon_y$, $-0.885\varepsilon_y$ and $-0.636\varepsilon_y$ for the low, middle and high levels of pressure, respectively, where ε_y is the yield strain of the material. For the pipe segments discussed in this section, the numerical values are -0.2131%, -0.1886% and -0.1355%, respectively.

Figure 5.17 shows a side view of a pipe segment where the pipe segment is divided into two strips based on the fact that the buckling initiates on the compressive side. The strip where buckling occurs is called the *buckling strip*, and the other, the *supporting strip*. The stiffness of the latter is relatively large. The buckling strip is subject to a force intensity

in the longitudinal direction of N_b, where N_b represents the average magnitude per unit arc-length. The third and fourth factors influencing the wrinkling strain are the magnitude of the force intensity N_b and the restraint provided by the supporting strip. The magnitude of the force intensity N_b depends only on the internal pressure which controls the position of the stress point on the yield surface. The restraint provided by the supporting strip depends on the stiffness distribution around the cross-section, which is effected by both pressure and axial load.

Wrinkling strain can benefit from increasing pressure because the pressure changes the buckling mode from the diamond buckling mode to the bulging mode and the magnitude of the force intensity N_b is smaller for higher pressure. The detrimental effect of increasing pressure is that the pipe material in compression yields at a smaller longitudinal strain. Earlier yielding in general leads to earlier initiation of wrinkling, provided other conditions remain unchanged. The wrinkling strain is found to increase as pressure increases when the pipe segments are subject to no axial load, or tensile axial load of $0.4F_y$, as shown by lines C00 and T40 in Fig. 5.15. This is mainly due to the benefits obtained from increasing pressure.

Axial loads both in compression and tension have a detrimental effect on the wrinkling strain of a pressurized pipe segment (see lines M and H in Fig. 5.16). The reason for this is demonstrated by the stress distributions over the cross-section in Fig. 5.18, where the conditions for initial yielding of the extreme compressive fiber are shown for pipe segments with high pressure levels. The division between the buckling strip and the supporting strip depends on the stiffness distribution which is, in turn determined by the stress distribution. Since wrinkling initiates after initial yielding of the extreme compressive fiber, the yielding zone must penetrate toward the tension side of the pipe segment. The penetration of the yielding zone is limited for the Specimens PHC00 and PHT40 while it may be much more significant for Specimen PHC40 because of its almost uniform distribution of stress. As a result, the restraint provided by the supporting strip with regard to Specimen PHC40 is greatly reduced, which explains the trend observed in Fig. 5.16 that wrinkling strain for pressurized pipe segments decreases as the compressive axial load increases. When tensile axial load is applied, the supporting strip is weakened by the fact that substantial material on the tension side may be yielding as shown for Specimen PHT40 in Fig. 5.18. Effects on wrinkling strain similar to those for compressive axial load are, therefore, introduced by tensile axial load.

The wrinkling strain of empty pipe segments, however, is found to increase as the

compressive axial load increases (see line L in Fig. 5.16). As shown in Fig. 5.19, the supporting strip is not affected appreciably by the applied compressive axial load. Consequently, the detrimental effect of compressive axial load is minimized for empty pipe segments. On the other hand, the moment required to produce the initial yielding is significantly reduced by the applied axial load. As a result, the ovalization and the force to cause it are reduced, which is believed to be the factor responsible for the gain in wrinkling strain.

As discussed here, internal pressure, axial load and bending moment interact and their integrated effects determine initiation of wrinkling. Since the discussion and conclusions are based on solutions for pipe segments with a particular geometry and material property, direct extension to other pipe segments has not been attempted. However, the approach to evaluate wrinkling strain, and some typical characteristics have been demonstrated by studies in this section, and a mechanism providing a heuristic explanation for the behavioral trends due to the variation in loading conditions has been explored and discussed.

5.5 WRINKLING STRAIN FOR AXISYMMETRICALLY BUCKLED SPECIMENS

Pipe segments subjected to axially symmetric loads buckle in an axisymmetric buckling mode for the geometries commonly used in the pipeline industry. While the fact that pipelines experience combined loading conditions in the field is recognized, the buckling strain for specimens buckled in axisymmetric mode has played an important role for the designers and operators of pipelines. This is because the axisymmetric buckling strain of a pipe segment has been used as an approximation for the buckling strain of the same pipe segment subjected to combined loading. The assumption for this is that the axisymmetric buckling strain is not larger than the buckling strain under combined loading condition. This assumption has been used by Workman (1981), Popov (1973) and Row et. al. (1983a).

In the following, wrinkling analyses are carried out for several specimens subjected to axisymmetric load. The wrinkling strains obtained from these analyses are then compared with those of similar specimens subjected to bending moment.

5.5.1 Wrinkling Strains under Axisymmetrically Loading

For the purpose of comparison with specimens subjected to bending moment, a

series of axisymmetric specimens are selected. There are six specimens in this series and their designations consist of two characters and followed by a three-digit number as shown in Table 5.3. The first character is A which represents the series for axisymmetrically loaded pipe segments. The second character is one of L, M and H to indicate the levels of applied pressure. The three-digit number represents the D/t ratio of pipe segment. The geometry, material property and loading conditions are given in Table 5.3. Specimens AL078, AL061 and AL046 are intended to compare directly with Specimens DTR20, DTR16 and DTR10, respectively, and have precisely the same physical attributes. The group covers a range of D/t ratios from 46 to 78. Specimens AL104, AM104 and AH104 compare directly with Specimens PLC00, PMC00 and PHC00, respectively. This group covers the three levels of applied internal pressure. Similar to the first series, everything except the loading conditions are the same for each pairs of specimens.

The wrinkling strains for these six specimens are listed in Table 5.3. Comparison of wrinkling strain is shown in Figs. 5.20 and 5.21. The wrinkling strains for the pipe segments subjected to axisymmetric load, and for those subjected to pure bending moment, are plotted against the D/t ratio of pipe segments in Fig. 5.20 and against the levels of applied pressure in Fig. 5.21.

5.5.2 Comparisons

Two conclusions can be obtained from the comparisons in Figs. 5.20 and 5.21. For unpressurized pipe segments, the wrinkling strain for axisymmetric buckling is larger than wrinkling strain of the same pipe segment buckled under flexural deformation. This statement appears valid for the full range of D/t ratio (from 45 to 104) shown in Fig. 5.20. For pressurized pipe segments, the conclusion is opposite, i.e. the wrinkling strain of axisymmetric buckling is smaller than that of the same pipe segment buckled under pure flexural deformation (Fig. 5.21) except for low pressures. This statement appears valid for pressures that force the pipe segment to buckle in the bulging buckling mode. The wrinkling strain under bending moment can be 2 to 3 times as large as the one under axisymmetric load.

Two different reasons are believed to be responsible for the opposite conclusions obtained. For the empty pipe segments, the reason is the difference in buckling mode. Pipe segments loaded axisymmetrically buckle in the axisymmetric mode and this is true for all D/t ratios in the concerned range. However, the same pipe segments buckle in the diamond mode if they are subject to bending moment. The buckling in the diamond buckling mode

initiates earlier because of the ovalization and its driving force introduced by flexural deformation. The pressurized pipe segments buckle in a bulging buckling mode which will not be unfavorably affected by the ovalization. The restraint provided by the supporting strip helps to delay the initiation of wrinkling. As a result, wrinkling strain under flexural deformation is larger than the one in axisymmetric deformation.

The results of this study indicate that the design assumption, namely, that the buckling strain for general loading may be approximated by that for axisymmetric loading, discussed in the beginning of Sect. 5.5, is inaccurate. The assumption is not conservative for empty pipe segments, and can be overly conservative for pressurized pipe segments. Consequently, analyses based on this assumption may be misleading.

Specimen DTR20		Specimen DTR16		Specimen DTR10	
Stress (ksi)	Strain (%)	Stress (ksi)	Strain (%)	Stress (ksi)	Strain (%)
0.0	0.0	0.0	0.0	0.0	0.0
55.5	0.186	49.0	0.164	55.5	0.186
57.4	0.800	50.58	1.00	57.29	0.477
59.38	1.00	-	-	62.39	1.00

Table 5.1 Stress-Strain Curves for Specimens DTR20, DTR16 and DTR10 (Jirsa *et al*, 1972)

Specimen Identification	Internal Pressure	Axial Load	Wrinkling Strain	Wrinkling Curvature	Dimensionless Strain	Dimensionless Curvature
	p/p_y	F/F_y	(%in/in)	(10^{-4} /in)		
PLC40	0	-40%	0.3158	0.8470	1.4820	0.9448
PLC20	0	-20%	0.2927	0.9483	1.3737	1.0578
PLC00	0	0	0.2558	0.9972	1.2002	1.1123
PLT40	0	40%	0.1091	0.9447	0.5119	1.0538
PMC40	35%	-40%	0.2360	0.5083	1.1075	0.5670
PMC20	35%	-20%	0.2435	0.7173	1.1427	0.8001
PMC00	35%	0	0.3553	1.1758	1.6672	1.3115
PMT40	35%	40%	0.1331	0.7144	0.6245	0.7971
PHC40	72%	-40%	0.2055	0.1589	0.9643	0.1773
PHC20	72%	-20%	0.3032	0.6624	1.4227	0.7389
PHC00	72%	0	0.3686	1.0522	1.7298	1.1737
PHT20	72%	20%	0.2138	0.7999	1.0035	0.8922
PHT40	72%	40%	0.1552	0.8458	0.7284	0.9434

NOTES : $C_y = 0.8965 \times 10^{-4}$ (1/in) $\varepsilon_y = 0.002131$ (in/in) $F_y = 4423.98$ (kips) $p_y = 1.2464$ (ksi)

Table 5.2 Wrinkling Strains and Curvatures for Specimens in the Series of Postbuckling Analysis

Specimen Identification	Geometry		Material Property			Loading Condition			Wrinkling Initiation	
	Diameter D	D/t	Yield Strength	Yield Strain	Yield Curvature	Pressure Level	Axial Load	Bending Moment	Strain	Curvature
	(in)		(ksi)	(%)	(10^{-4}/in)	(%)			(%in/in)	(10^{-4}/in)
DTR20	20	78.4	55.5	0.186	1.86	0	-	active	0.363	3.58
DTR16	16	61.5	49.0	0.164	2.05	0	-	active	0.804	9.41
DTR10	10.75	46.1	55.5	0.186	3.46	0	-	active	1.300	23.39
DIA48	48	103.9	63.5	0.2131	0.8965	0	-	active	0.2558	0.9972
DIA24	24	103.9	63.5	0.2131	1.7750	0	-	active	0.2982	2.3370
DIA12	12.75	103.9	63.5	0.2131	3.3430	0	-	active	0.3511	5.4380
AL078	20	78.4	55.5	0.186	1.86	0	active	-	0.6089	-
AL061	16	61.5	49.0	0.164	2.05	0	active	-	1.0561	-
AL046	10.75	46.1	55.5	0.186	3.46	0	active	-	1.9082	-
AL104	48	103.9	63.5	0.2131	0.8965	0	active	-	0.4347	-
AM104	48	103.9	63.5	0.2131	0.8965	35	active	-	0.1713	-
AH104	48	103.9	63.5	0.2131	0.8965	72	active	-	0.1105	-

Table 5.3 Initiation of Wrinkling for Specimens in the Series of Wrinkling Analysis

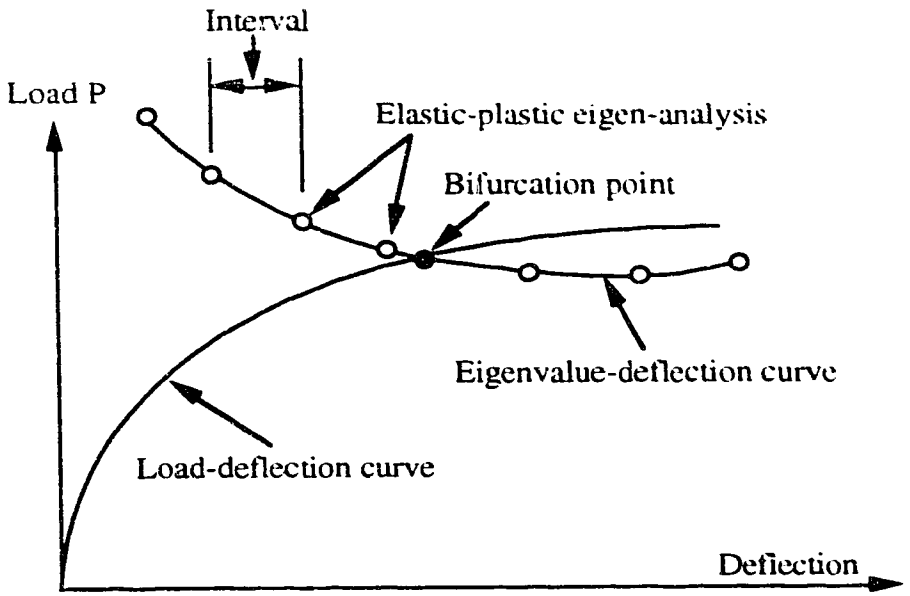

Fig. 5.1 Illustration of the Procedure of Accompanying Buckling Analysis

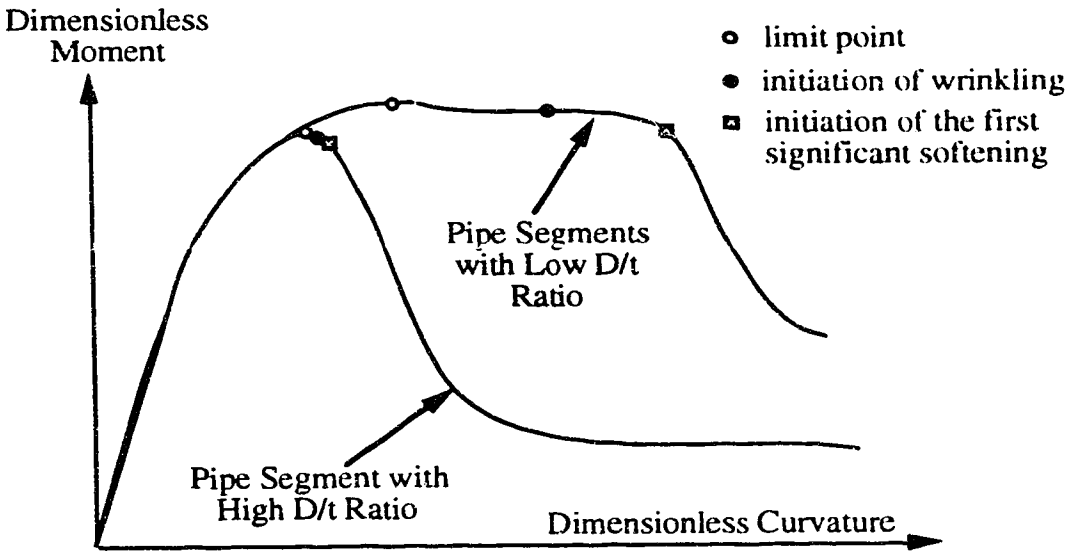

Fig. 5.2 Conceptual Moment-Curvature Curves for Pipe Segments

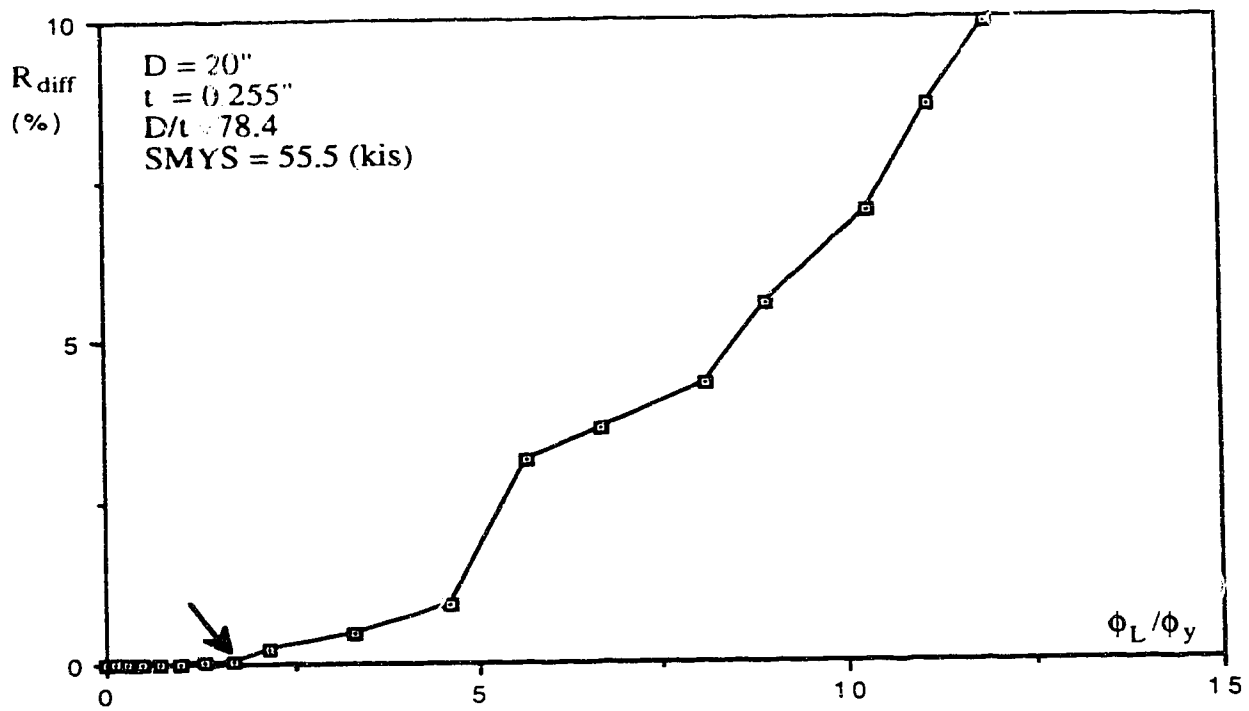

Fig. 5.3 Radius Differential-Local Curvature Curve for Specimen DTR20

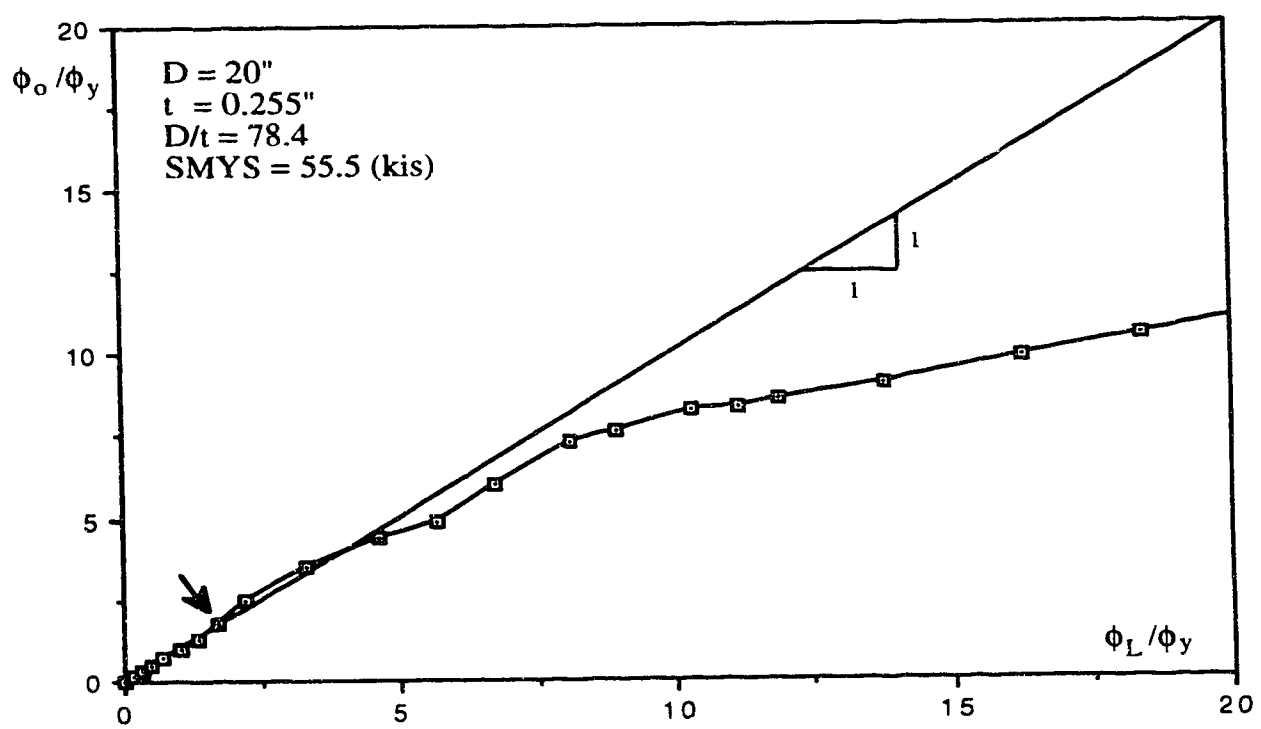

Fig. 5.4 Comparison of the Overall and Local Curvatures for Specimen DTR20

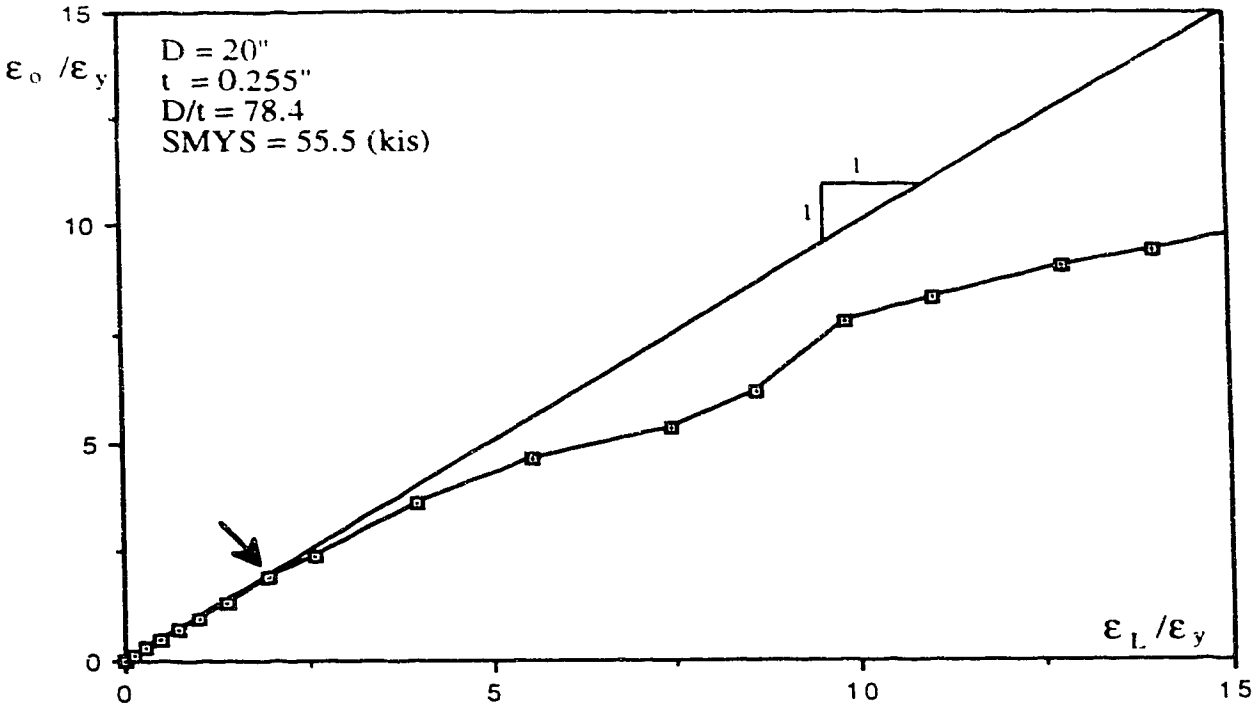

Fig. 5.5 Comparison of the Overall and Local Strains for Specimen DTR20

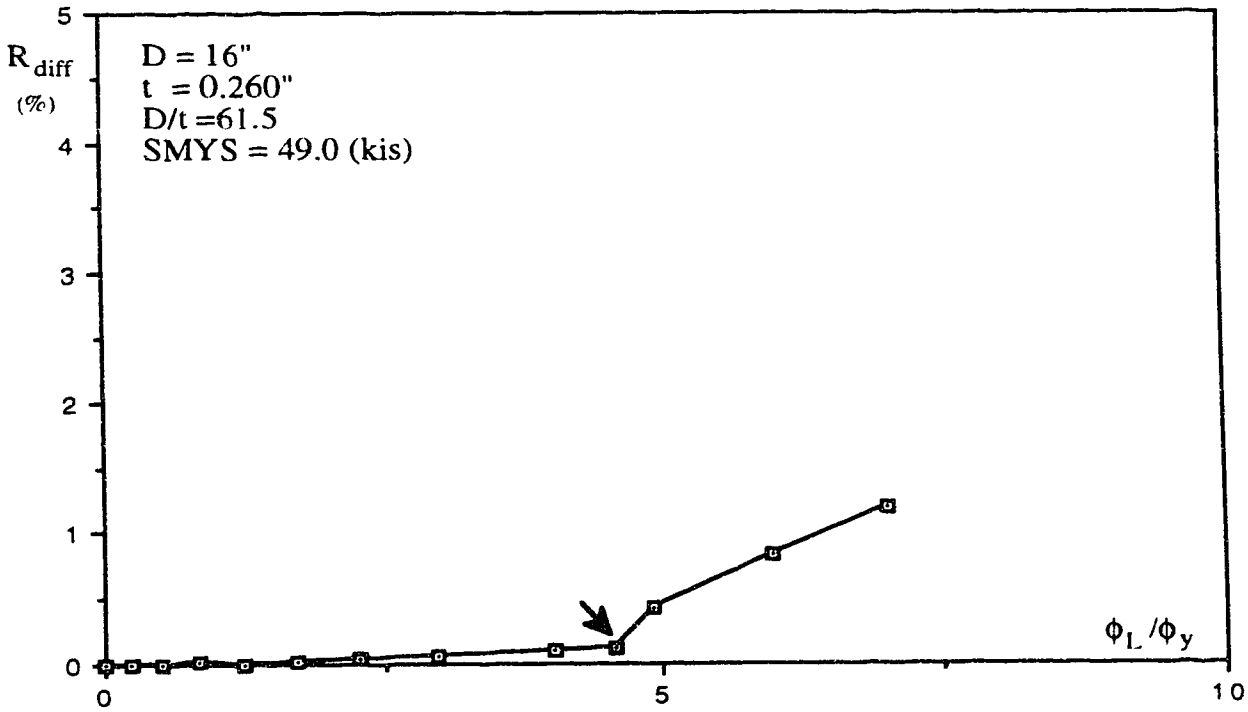

Fig. 5.6 Radius Differential-Local Curvature Curve for Specimen DTR16

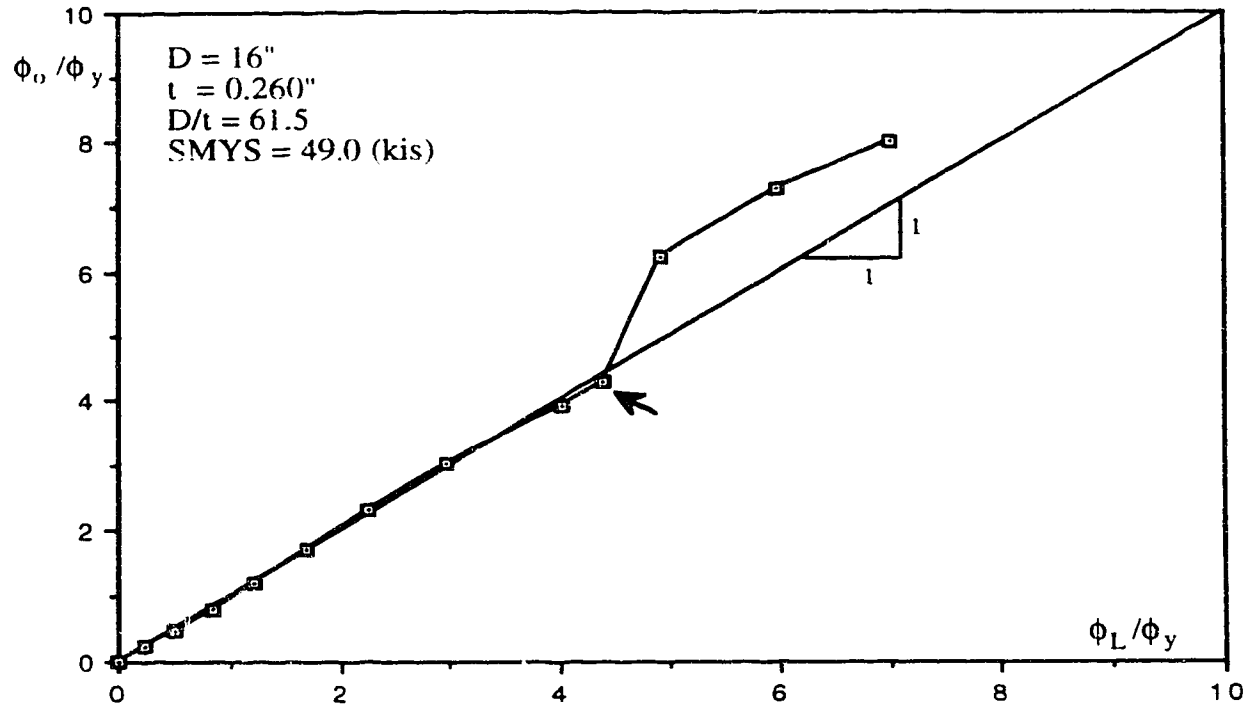

Fig. 5.7 Comparison of the Overall and Local Curvatures for Specimen DTR16

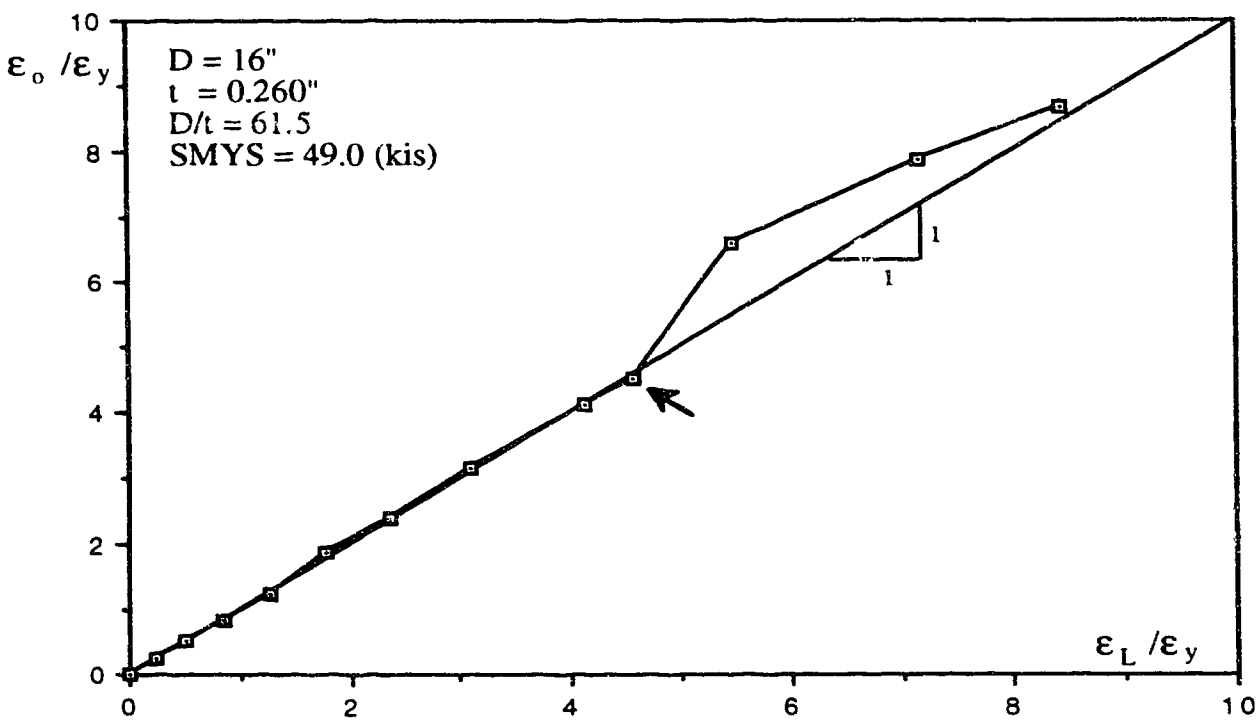

Fig. 5.8 Comparison of the Overall and Local Strains for Specimen DTR16

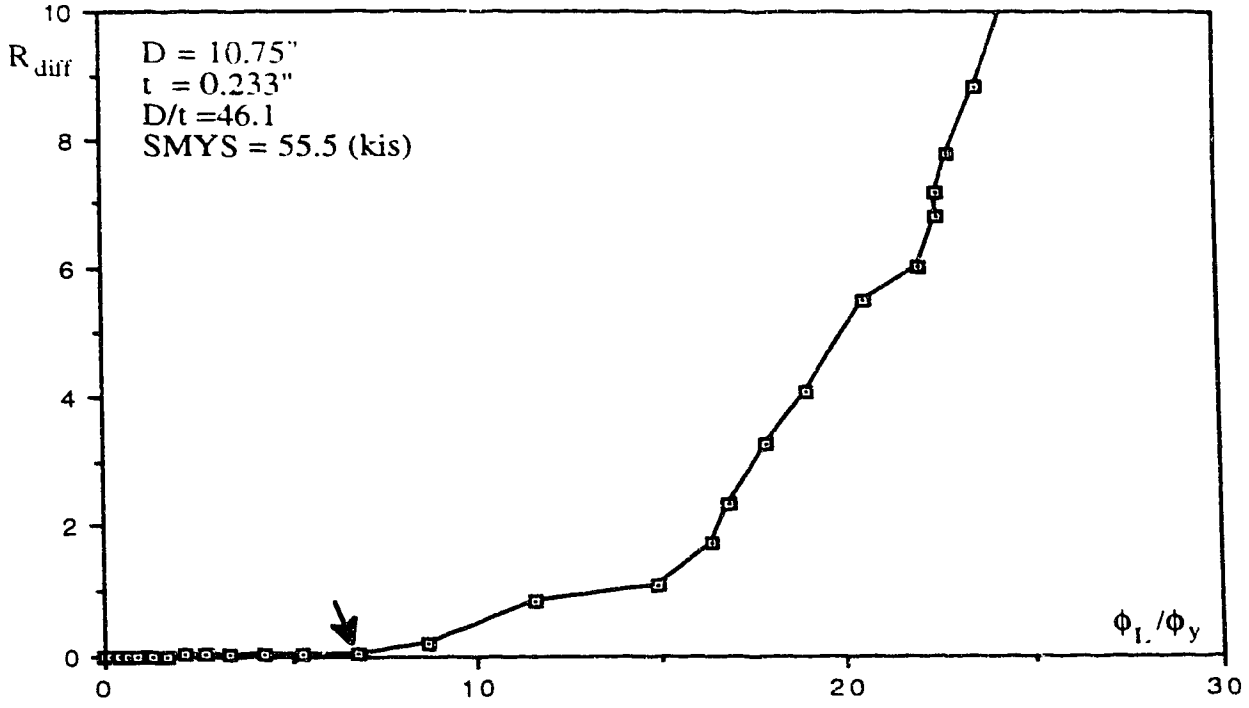

Fig. 5.9 Radius Differential-Local Curvature Curve for Specimen DTR10

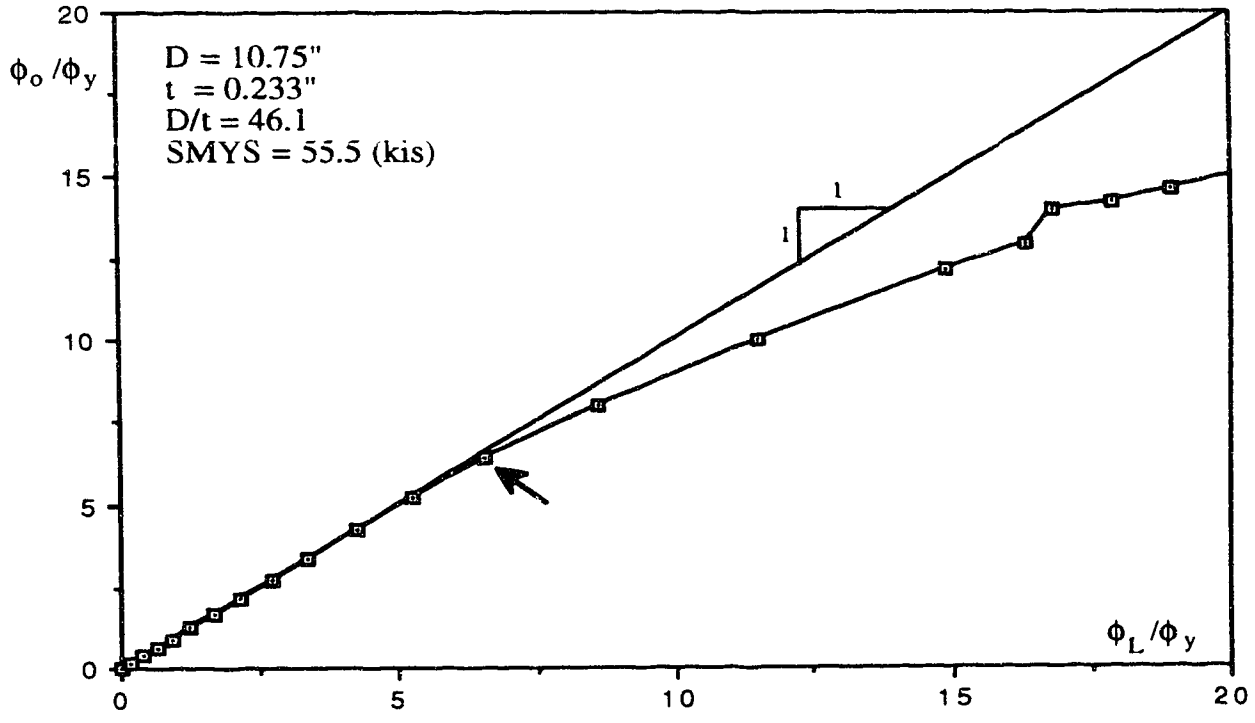

Fig. 5.10 Comparison of the Overall and Local Curvatures for Specimen DTR10

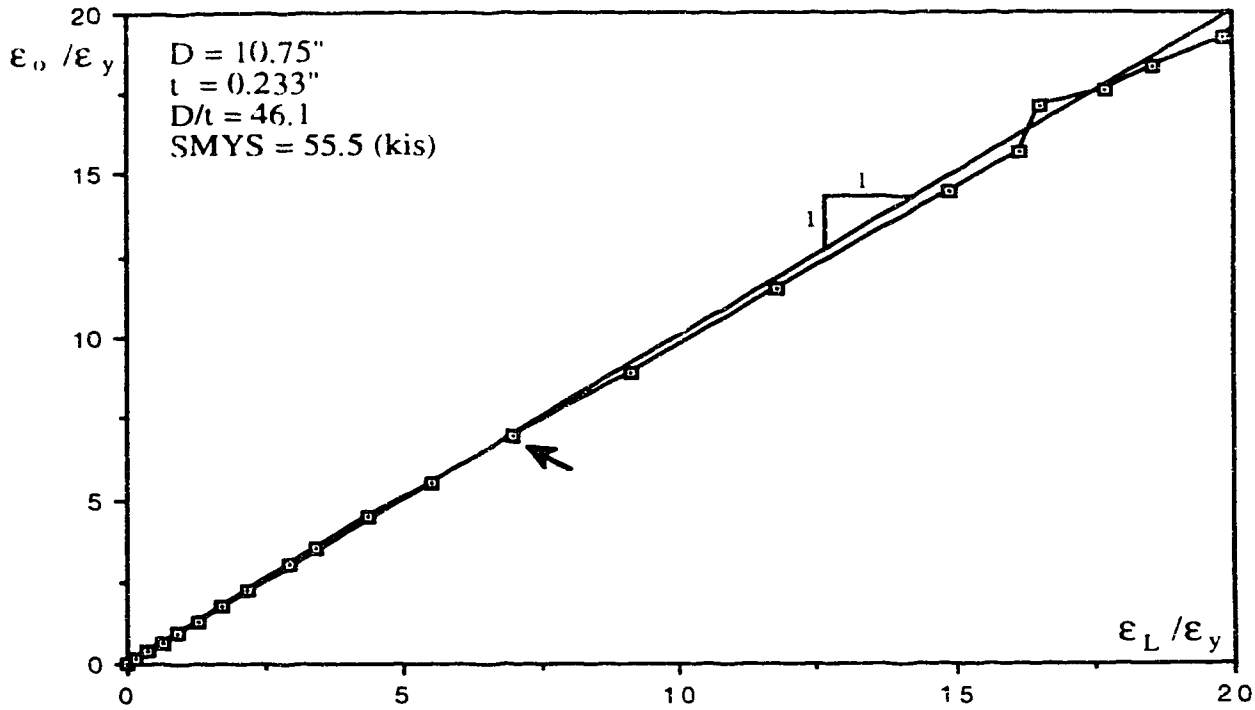

Fig. 5.11 Comparison of the Overall and Local Strains for Specimen DTR10

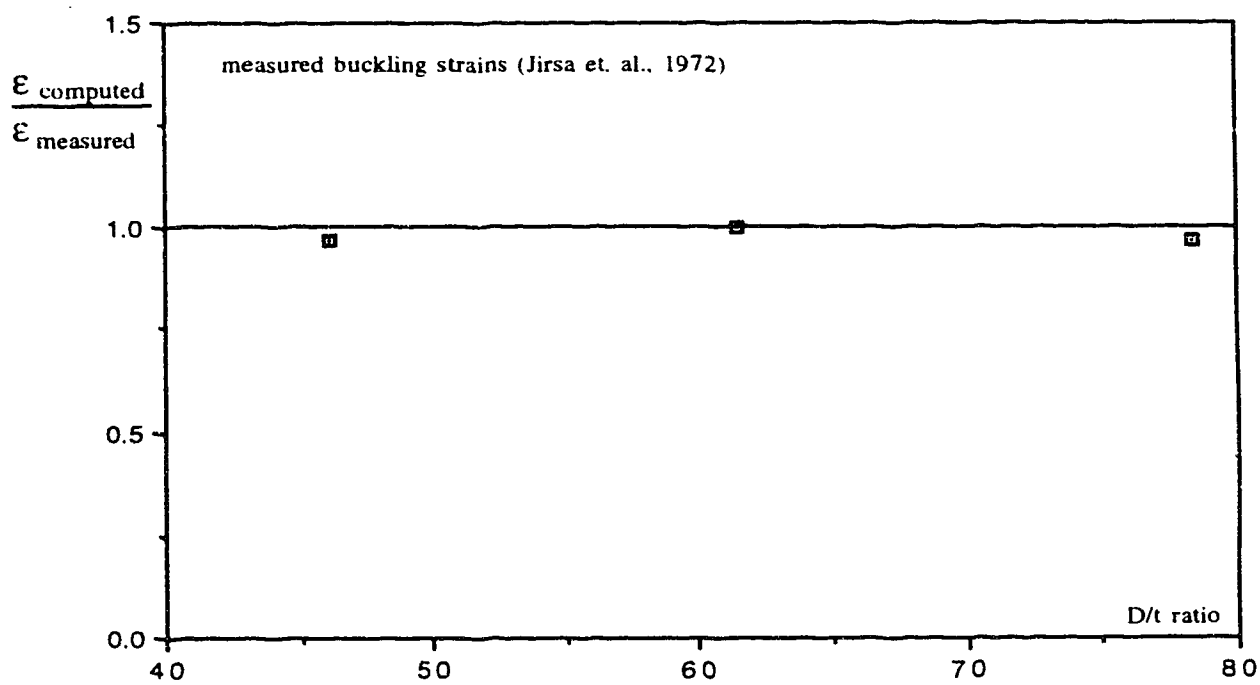

Fig. 5.12 Comparison of Predicted Wrinkling Strains with Measured Buckling Strains

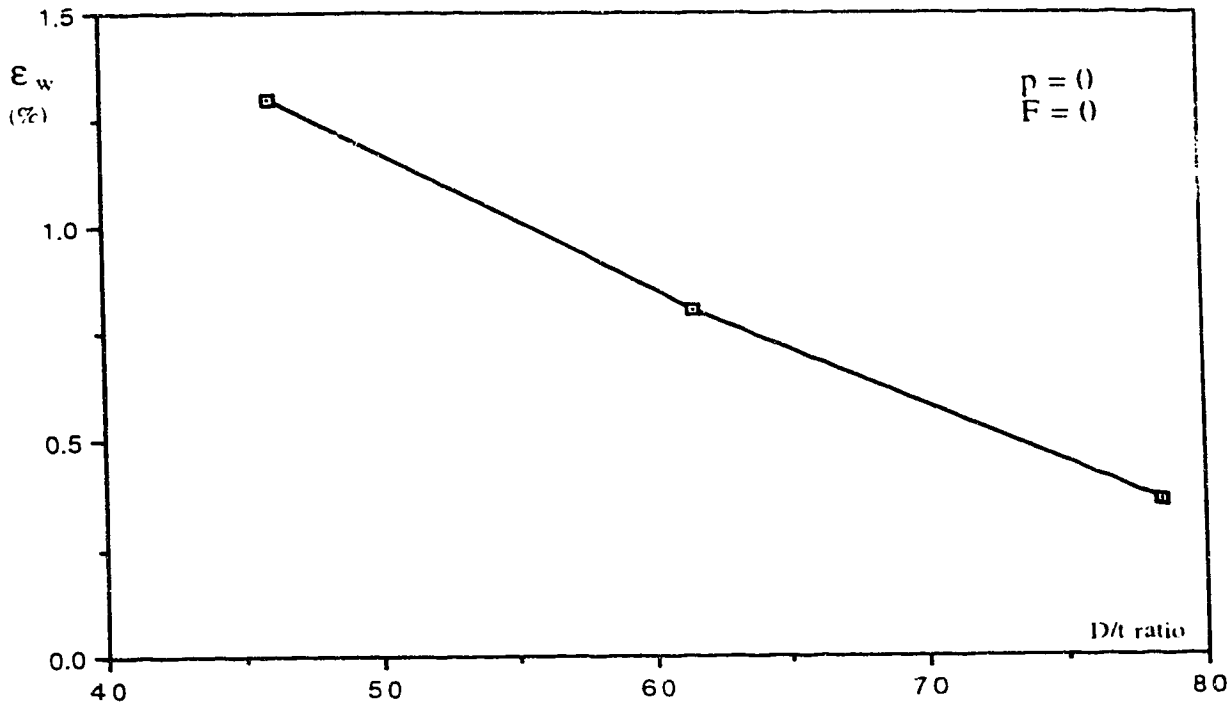

Fig. 5.13 Effects of the D/t Ratio on Wrinkling Strains

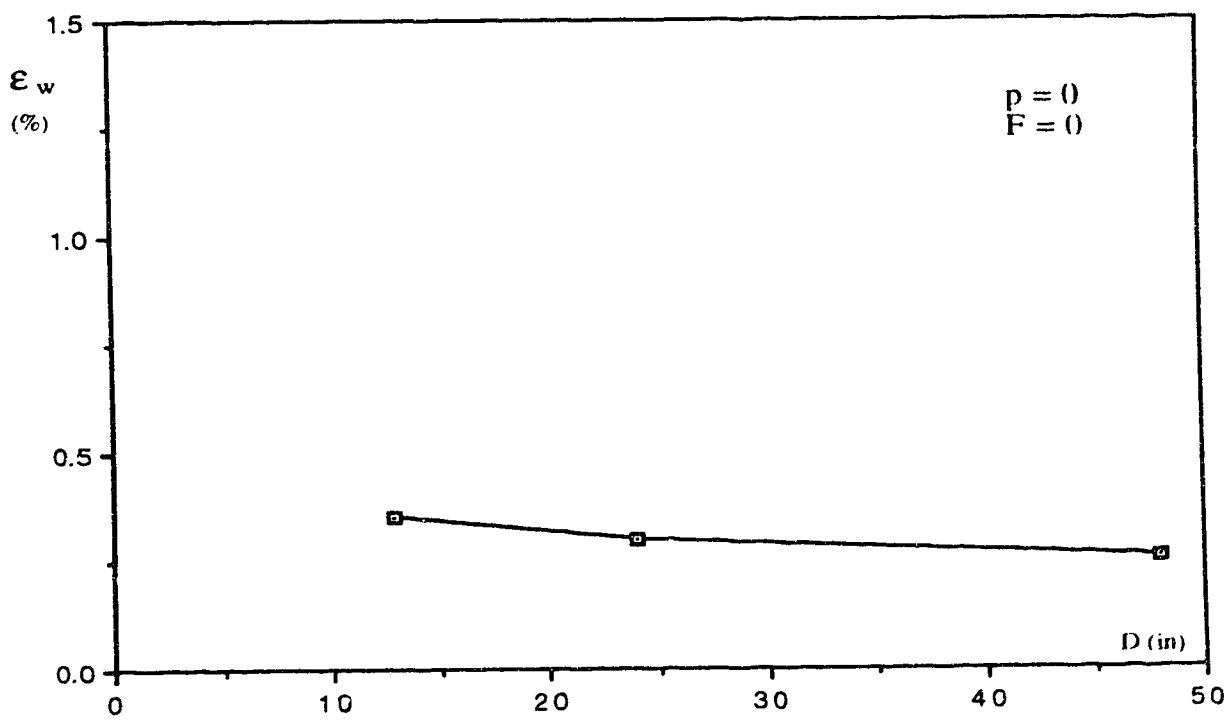

Fig. 5.14 Effects of the Diameter on Wrinkling Strains

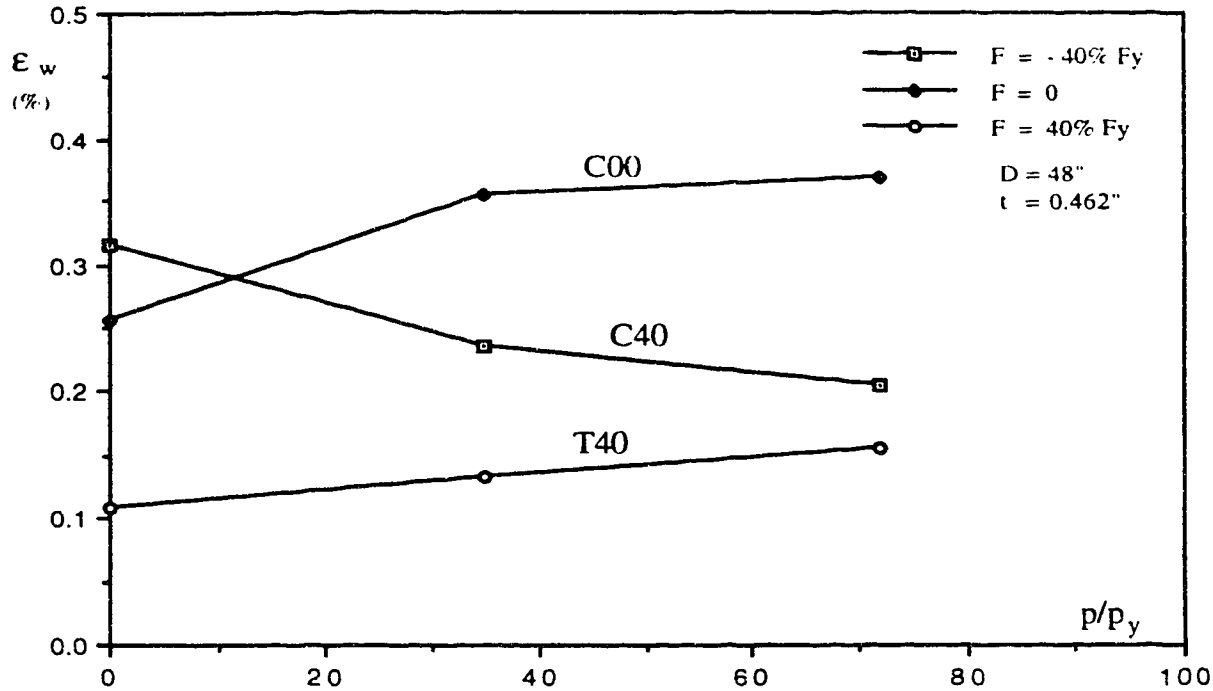

Fig. 5.15 Effects of Internal Pressure on Wrinkling Strain

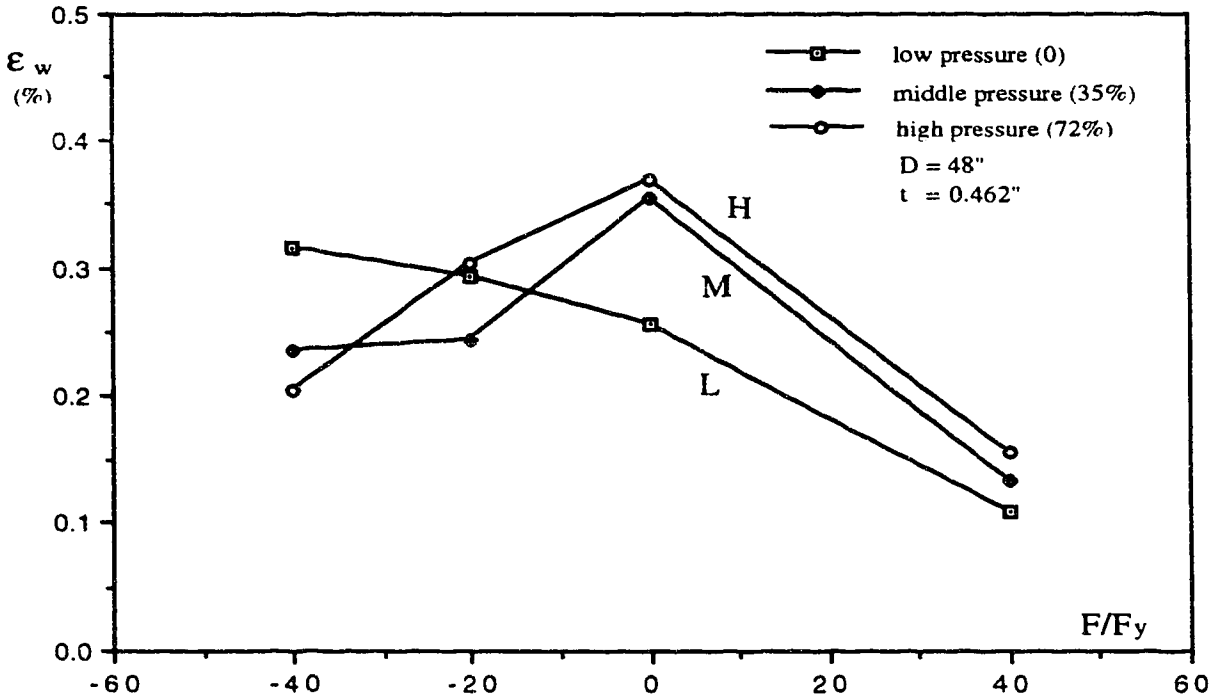

Fig. 5.16 Effects of Axial Load on Wrinkling Strain

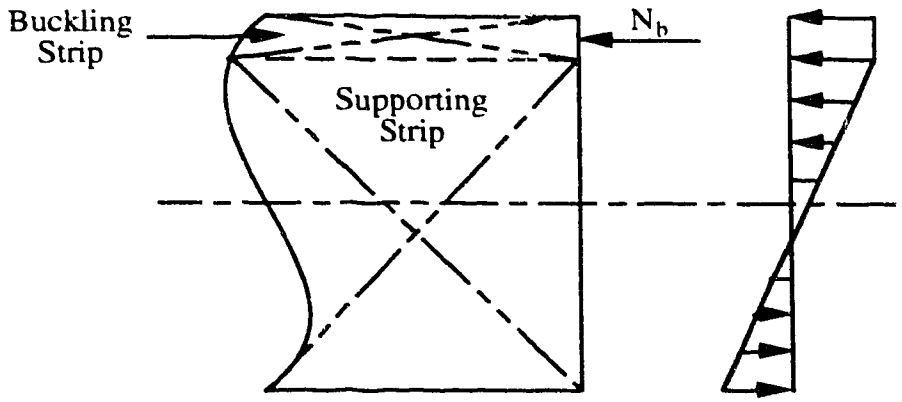

Fig. 5.17 Buckling Strip and Supporting Strip on the Cross-Section

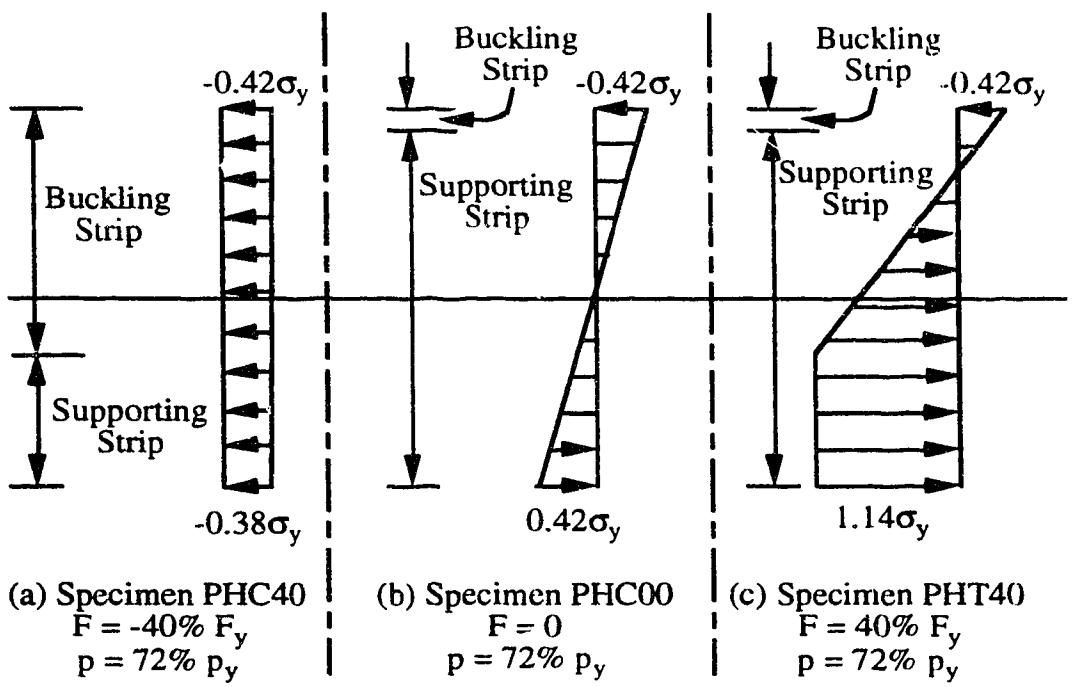

Fig. 5.18 Stress Distributions at the Initial Yielding for Pressurized Pipe Segments

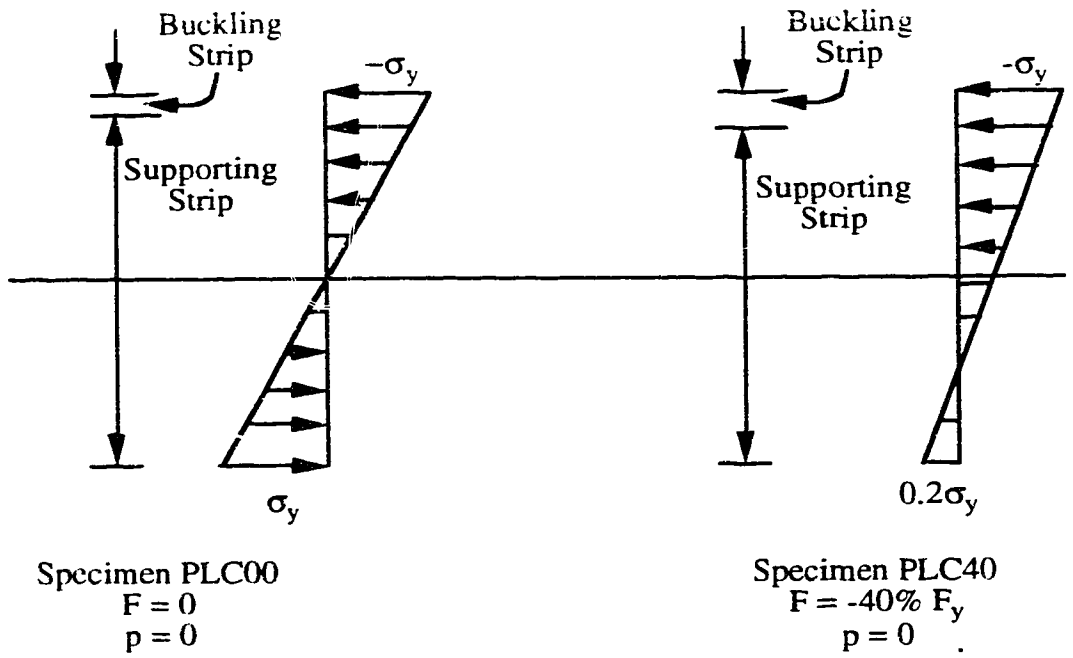

Fig. 5.19 Stress Distributions at the Initial Yielding for Empty Pipe Segments

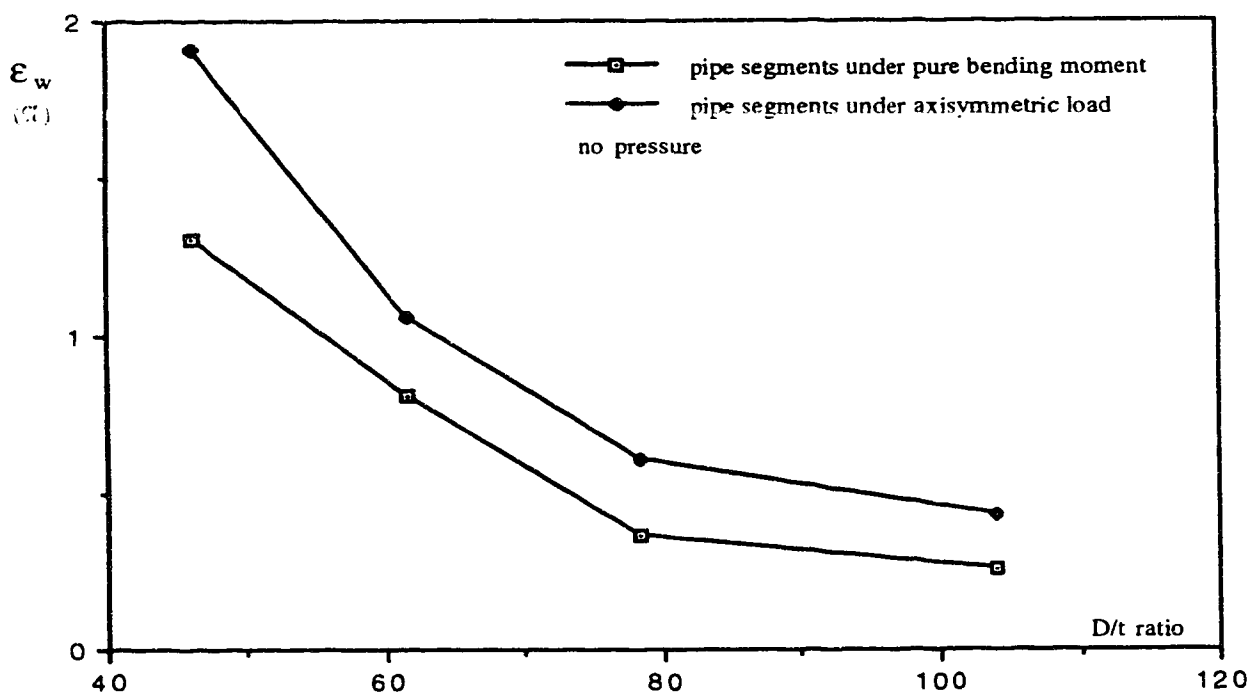

Fig. 5.20 Wrinkling Strains vs. D/t Ratio for Unpressurized Axisymmetric and Pure Bending Loadings

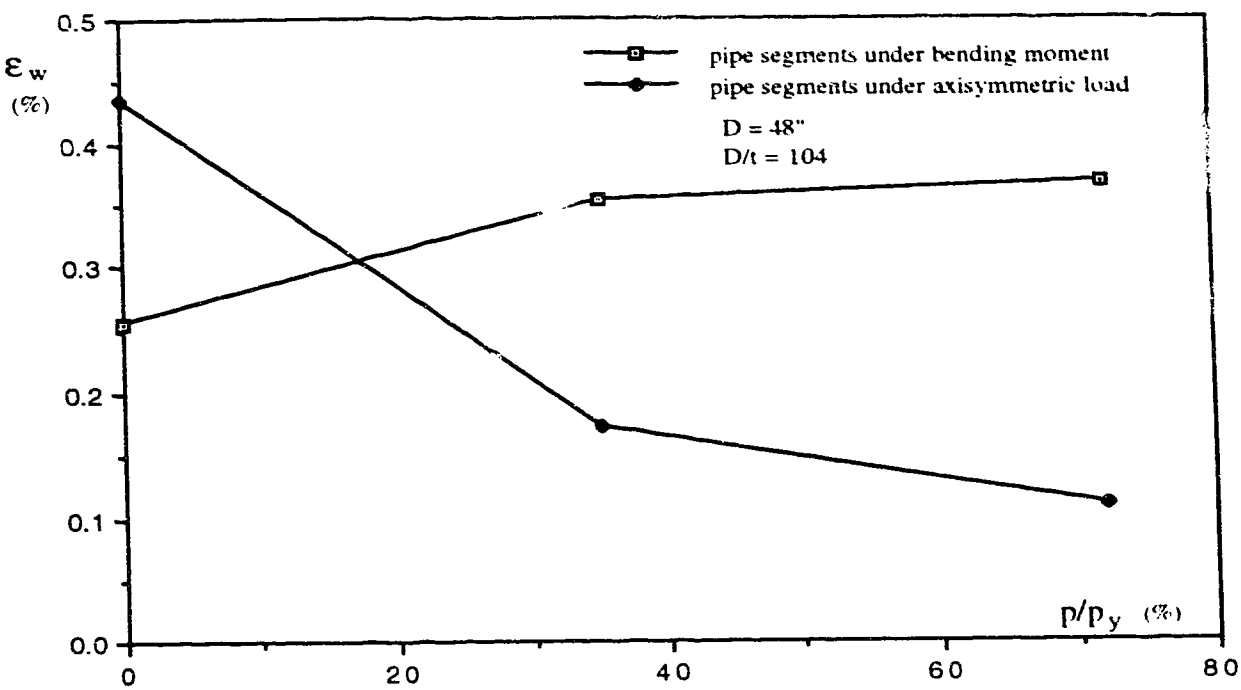

Fig. 5.21 Wrinkling Strains vs. Levels of Internal Pressure for Axisymmetric and Pure Bending Loadings

CHAPTER 6 FORMULATION OF PIPELINE-BEAM ELEMENT

Deformation analysis of pipelines subjected to imposed deformation is based on two types of model, the shell model and the beam model, as discussed in Sect. 1.3. The shell model and relevant solution techniques have been presented in Chapters 2 and 3. The results of analysis based on the shell model with respect to buckling and postbuckling behavior are summarized in Chapters 4 and 5, where the shell model analysis is essentially completed. Having done that, beam model analysis, which is another important aspect of the approach for deformation analysis, becomes the topic in the current and subsequent chapters. The beam model is designed to predict the overall behavior of pipelines subjected to imposed deformation. The important factors to be considered are pipeline-soil interaction, and the distribution and redistribution of deformation and internal forces. The beam model is established based on the pipeline-beam element developed in this chapter, which is intended to account for the deformation and loading characteristics of pipelines. The formulation of the pipeline-beam element is presented. This includes : the fundamental assumptions; the strain-displacement relations; the constitutive relations for both RMDI and ISPDR techniques (refer to Sect. 1.3.2); pipeline-soil interaction; the virtual work equation and its discretization; and, discussion on the generation procedure for determining SPD relations and their size dependency. The development of the program Analysis of Buried Pipelines (ABP) and the verification of the ISPDR technique are also described.

6.1 FUNDAMENTAL ASSUMPTIONS

In order to analyze pipeline response with or without the effect of local shell buckling, two solution techniques have been employed with the pipeline-beam element. These are the *Reduced Modulus Direct Integration* (RMDI) and *Integration of Stiffness-Property-Deformation Relations* (ISPDR) techniques as discussed in Sect. 1.3.2. Each of these solution techniques is based on its own assumptions which are summarized in the following.

For the RMDI technique, the following assumptions are made to develop the mathematical model. (1) Plane sections of the pipe remain plane and the pipe cross sections remain perfectly circular. (2) Shear stresses and radial stress are insignificant, and therefore can be ignored. Longitudinal and hoop stresses are accounted for. (3) The pipe yields according to the von Mises criterion. Following yield, plastic flow takes place according to the normality rule in plasticity theory. (4) Strain hardening is represented by a mixed strain

hardening rule with an appropriate choice of ratio between isotropic hardening and kinematic hardening. (5) Soil support can be modelled by discrete inelastic soil springs. (6) All the active deformations and stress distributions are symmetric about the vertical plane. These assumptions are based on the following interpretation of pipeline behavior.

The RMDI technique is intended for analysis excluding the effects of local buckling, and therefore, the first assumption is, at least, approximately justified, because the cross sectional distortion and warping result mainly from local buckling. A pipeline is a flexible line structure where axial and flexural deformations are dominant. Consequently, shear stresses have only minor influence on pipeline response. Since the pipe wall thickness is significantly smaller than pipe diameter and length, the radial stress is negligible compared to the longitudinal and hoop stresses. The second assumption is based on these facts. The third and fourth assumptions define the plasticity theory employed for analysis. Although many other theories are available, this theory is the one most commonly used for metal materials such as pipe steel. The soil support assumption basically assumes the ground can be divided into slices and the reaction of each slice of soil can be represented by soil springs such that interaction between slices can be ignored.This is the classical Winkler foundation type of assumption. It is not accurate in the sense that the interactions between slices of soil may sometimes be important. Nevertheless, considering the low accuracy of the available soil properties and the fact that the pipeline behavior is the focus of this project, this assumption should be acceptable.

For the ISPDR technique, *stiffness properties* of the cross-sections are defined by direct input of *Stiffness-Property-Deformation* (SPD) relations which are established from the shell model analysis of pipeline segments. The internal forces are directly related to the axial strains and curvatures by *stiffness coefficients* of the cross-sections which are determined by the stiffness properties. Consequently, the stress and strain distributions over the cross-section are no longer needed and neither are the assumptions (1) to (4) of the RMDI technique. However, some assumptions with respect to the generation and application of SPD relations are necessary to establish the constitutive relation for ISPDR technique. These assumptions will be discussed in the appropriate sections after the SPD relations are described. The definition of stiffness properties and stiffness coefficients are presented in Sect. 6.4.

6.2 STRAIN-DISPLACEMENT RELATIONS

The global and local coordinate systems for the pipe model are defined in Fig. 6.1,

where the x-axis of the local coordinate system passes through the centroidal axis of the cross-section, and the x-y plane defines the plane of bending deformation. The displacements u and v are in the directions of the x-axis and y-axis in the local coordinate system, respectively. The global coordinate system is denoted by $\tilde{x}$ and $\tilde{y}$, and all quantities defined in the global coordinate system are denoted similarly, with a tilde overscript.

Let ${}_t u_0$ and ${}_t v_0$ be the displacement increments at the centroidal axis of the cross-section relative to the reference configuration ${}^t\Gamma$ (see Fig.2.3), the displacement components of any point on the cross-section can be expressed as in the following equation by using the first assumption in Sect. 6.1

$$ {}_t u = {}_t u_0 - \frac{d_t v_0}{d^t x} y \tag{6.1a} $$

$$ {}_t v = {}_t v_0 \tag{6.1b} $$

The total displacements accumulated in the global coordinate system are then

$$ {}^{t+\Delta t}\tilde{u} = {}^t\tilde{u} + {}_t\tilde{u} \tag{6.2a} $$

$$ {}^{t+\Delta t}\tilde{v} = {}^t\tilde{v} + {}_t\tilde{v} \tag{6.2b} $$

and on the centroidal axis, particularly, they become

$$ {}^{t+\Delta t}\tilde{u}_0 = {}^t\tilde{u}_0 + {}_t\tilde{u}_0 \tag{6.3a} $$

$$ {}^{t+\Delta t}\tilde{v}_0 = {}^t\tilde{v}_0 + {}_t\tilde{v}_0 \tag{6.3b} $$

wh .he quantities with left superscript are the total values at the time indicated by the superscript, and the quantities without super-script are the increments. This notation, defined by Bathe (1982), will be generally applied in the following sections unless stated otherwise. The increments ${}_t\tilde{u}_0$ and ${}_t\tilde{v}_0$ are available from the solution of equilibrium equations, and the increments in the local coordinate system ${}_t u_0$ and ${}_t v_0$ are obtained by

$$ {}_t u_0 = \cos {}^t\alpha \, {}_t\tilde{u}_0 + \sin {}^t\alpha \, {}_t\tilde{v}_0 \tag{6.4a} $$

$$ {}_t v_0 = - \sin {}^t\alpha \, {}_t\tilde{u}_0 + \cos {}^t\alpha \, {}_t\tilde{v}_0 \tag{6.4b} $$

where

$$^{t}\alpha = \arctan\left(\frac{d^{t}\tilde{y}_0}{d^{t}\tilde{x}_0}\right) \tag{6.5}$$

is the angle between the global $\tilde{x}$-axis and local x-axis.

The only independent non-zero component of the strain is axial strain in the x-direction. The incremental form of the expression for this strain component can be derived from the general expression for three-dimensional strain tensor (Bathe, 1982) as

$$^{t+\Delta t}_{t}\varepsilon_x = {}^{t}\varepsilon_x + {}_{t}\varepsilon_x \tag{6.6}$$

$$_{t}\varepsilon_x = \frac{d\,_{t}u}{d^{t}x} + \frac{1}{2}\left(\left(\frac{d\,_{t}u}{d^{t}x}\right)^2 + \left(\frac{d\,_{t}v}{d^{t}x}\right)^2\right) \tag{6.7}$$

where the left subscripts indicate that the configuration $^{t}\Gamma$ is taken as the reference configuration. Substituting Eqs. (6.1) and (6.2) into Eq. (6.7), the strain component can be expressed in term of displacement components of the centroidal axis as

$$_{t}\varepsilon_x = \frac{d\,_{t}u_0}{d^{t}x} - y\frac{d^2\,_{t}v_0}{d^{t}x^2} + \frac{1}{2}\left(\left(\frac{d\,_{t}u_0}{d^{t}x} - y\frac{d^2\,_{t}v_0}{d^{t}x^2}\right)^2 + \left(\frac{d\,_{t}v_0}{d^{t}x}\right)^2\right) \tag{6.8}$$

Let us define the incremental linear axial strain at the centroidal axis and the incremental linear curvature as

$$_{t}\varepsilon_0^{L} = \frac{d\,_{t}u_0}{d^{t}x} \tag{6.9}$$

$$_{t}\phi^{L} = \frac{d^2\,_{t}v_0}{d^{t}x^2} \tag{6.10}$$

and the incremental rotation of the cross-section as

$$_{t}\theta = \frac{d\,_{t}v_0}{d^{t}x} \tag{6.11}$$

Substituting the definitions (6.9), (6.10) and (6.11) into Eq. (6.8) and ignoring the second order term of incremental linear curvature, the strain component becomes

$$_{t}\varepsilon_x = {}_{t}\varepsilon_x^{L} + {}_{t}\varepsilon_x^{NL} \tag{6.12}$$

where

$$ {}_t\varepsilon_x^L = {}_t\varepsilon_0^L - y\,{}_t\phi^L \tag{6.13} $$

$$ {}_t\varepsilon_x^{NL} = \frac{1}{2}\left(({}_t\varepsilon_0^L)^2 - 2\,y\,{}_t\varepsilon_0^L\,{}_t\phi^L + {}_t\theta^2 \right) \tag{6.14} $$

which can also be written as

$$ {}_t\varepsilon_x^{NL} = {}_t\varepsilon_0^{NL} - y\,{}_t\phi^{NL} \tag{6.15} $$

by using the definitions

$$ {}_t\varepsilon_0^{NL} = \frac{1}{2}\left(({}_t\varepsilon_0^L)^2 + {}_t\theta^2 \right) \tag{6.16} $$

$$ {}_t\phi^{NL} = {}_t\varepsilon_0^L\,{}_t\phi^L \tag{6.17} $$

Substituting Eqs. (6.13) and (6.15) into Eq. (6.12), yields

$$ {}_t\varepsilon_x = {}_t\varepsilon_0 - y\,{}_t\phi \tag{6.18} $$

where

$$ {}_t\varepsilon_0 = {}_t\varepsilon_0^L + {}_t\varepsilon_0^{NL} \tag{6.19} $$

$$ {}_t\phi = {}_t\phi^L + {}_t\phi^{NL} \tag{6.20} $$

are the total increments of axial strain and curvature.

6.3 CONSTITUTIVE RELATIONS FOR RMDI TECHNIQUE

The fundamental difference between the RMDI technique and the ISPDR technique in the beam model analysis of pipelines is the constitutive relation. In the RMDI technique, it is essentially correct to assume plane sections remain plane and circular because the effects of local buckling are not accounted for. Consequently, the internal forces of the pipeline-beam element are only dependent on the distribution of the longitudinal stresses. The internal forces can be defined as

$$ {}^tF = \int_A {}^tS_x\,dA \tag{6.21} $$

$$ {}^tM = -\int_A {}^tS_x\,y\,dA \tag{6.22} $$

where ${}^tF$ and ${}^tM$ are axial force and bending moment, respectively, and y is the coordinate in the bending plane. The constitutive relation can be specified on the stress-strain level where the stresses can be precisely evaluated incrementally from the strain increment.

In the ISPDR technique, the effects of local buckling are one of the major concerns to be considered. Because of the cross-sectional distortion introduced by local buckling, the internal forces depend on the current configuration of the deformed cross-section of the pipe in addition to the stress distribution over the cross-section. Since the beam-type model is not able to model cross-sectional distortion, the constitutive relation on the stress-strain level is not sufficient to define increments of internal forces. As an alternative, a direct relation between internal forces and deformations is employed. That is, because the distribution of stress and strain over the cross-section can no longer be evaluated from the beam model, the deformation of the cross-section can be represented by the axial strain increment at the centroidal axis, ${}_t\varepsilon_0$, and the curvature increment, ${}_t\phi$. The constitutive relation for the internal force-reference axis deformation can be expressed in differential form as

$$d^tF = \frac{\partial^tF}{\partial^t\varepsilon_0} d^t\varepsilon_0 + \frac{\partial^tF}{\partial^t\phi} d^t\phi \tag{6.23}$$

$$d^tM = \frac{\partial^tM}{\partial^t\varepsilon_0} d^t\varepsilon_0 + \frac{\partial^tM}{\partial^t\phi} d^t\phi \tag{6.24}$$

where $\frac{\partial^tF}{\partial^t\varepsilon_0}$, $\frac{\partial^tF}{\partial^t\phi}$, $\frac{\partial^tM}{\partial^t\varepsilon_0}$ and $\frac{\partial^tM}{\partial^t\phi}$ are the cross-sectional stiffness coefficients.

In the remainder of Sect. 6.3, discussions are focused on the constitutive relation for the RMDI technique, which is the stress-strain relation. The derivation of a specialized stress-strain relation for pipe, which has special stress and strain states, is first presented. The procedure for the evaluation of stress increments is then outlined. The generalized stress-generalized strain constitutive relation for the ISPDR technique is discussed in detail in Sect. 6.4.

6.3.1 Stress-Strain Relation

The stress-strain relationship for a pipeline-beam element is a uniaxial stress-strain relationship in the local coordinate system. Because the internal pressure, which is usually

constant, is an essential loading condition of pipeline. the constant circumferential stress introduced by the internal pressure must be fully accounted for in the stress-strain relationship. The use of plasticity theory based on von Mises yield criteria and the normality rule implies that the incremental plastic strain components should exist in three directions, while the incremental stress is in the x-direction only. Among the incremental plastic strain components, the component in the x-direction is independent and the other two can be related to it by the constraint conditions that the incremental stresses in these directions are zero. Therefore, the relationship between the independent stress increment and the independent strain increment can still be considered as a special type of uniaxial stress-strain relationship.

The general elastic-plastic stress-strain relation has been defined in Eqs. (2.59) and (2.62). If shear stresses and corresponding shear strains are neglected from these equations as assumed in Sect. 6.1 and the incremental stress-strain relation is expressed in matrix form, it becomes

$$\begin{Bmatrix} {}_tS_\theta \\ {}_tS_r \\ {}_tS_x \end{Bmatrix} = \begin{bmatrix} \lambda' & \lambda & \lambda \\ \lambda & \lambda' & \lambda \\ \lambda & \lambda & \lambda' \end{bmatrix} \begin{Bmatrix} {}_t\varepsilon_\theta \\ {}_t\varepsilon_r \\ {}_t\varepsilon_x \end{Bmatrix} - \begin{bmatrix} {}^tP_{\theta\theta} & {}^tP_{\theta r} & {}^tP_{\theta x} \\ {}^tP_{r\theta} & {}^tP_{rr} & {}^tP_{rx} \\ {}^tP_{x\theta} & {}^tP_{xr} & {}^tP_{xx} \end{bmatrix} \begin{Bmatrix} {}_t\varepsilon_\theta \\ {}_t\varepsilon_r \\ {}_t\varepsilon_x \end{Bmatrix} \tag{6.25}$$

where

$$\lambda' = \frac{E\,(1-\nu)}{(1+\nu)\,(1-2\nu)} \tag{6.26a}$$

$$\lambda = \frac{E\,\nu}{(1+\nu)\,(1-2\nu)} \tag{6.26b}$$

$${}^tP_{mn} = \frac{3\,G}{(1+H'/(3\,G))\;{}^t\overline{S}^2}\,{}^ts_{mm}\,{}^ts_{nn} \quad \text{with } m, n = \theta, r, x \tag{6.26c}$$

no summation for repeated indices

and the subscripts θ and r represent the hoop and radial directions. The deviator stress tensor is defined as

$${}^ts_{ij} = {}^tS_{ij} - \frac{1}{3}\,{}^tS_{kk}\,\delta_{ij} \tag{6.27}$$

By the assumption of zero radial stress, the normal components of deviator stress tensor becomes

$${}^ts_\theta = \frac{1}{3}\,(\,2\,{}^tS_\theta - {}^tS_x\,) \tag{6.28a}$$

$$ {}^{t}S_{r} = \frac{1}{3}\left({}^{t}S_{\theta} + {}^{t}S_{x} \right) \tag{6.28b} $$

$$ {}^{t}S_{x} = \frac{1}{3}\left(2\,{}^{t}S_{x} - {}^{t}S_{\theta} \right) \tag{6.28c} $$

where single subscript is used because only normal components are considered. The hoop stress ${}^{t}S_{\theta}$ can be calculated as

$$ {}^{t}S_{\theta} = \frac{D - 2t}{2t}\, p \tag{6.29} $$

with D and t as the outside diameter and wall thickness of the pipeline, and p as the internal pressure.

The stress increments in the radial and hoop directions are zero because the radial stress is assumed to be zero at all times and the hoop stress is constant due to the constant internal operating pressure of the pipeline. Applying these conditions to the first two equations in Eq. (6.25), they become

$$ \begin{Bmatrix} 0 \\ 0 \end{Bmatrix} = \left(\begin{bmatrix} \lambda' & \lambda \\ \lambda & \lambda' \end{bmatrix} - \begin{bmatrix} {}^{t}P_{\theta\theta} & {}^{t}P_{\theta r} \\ {}^{t}P_{r\theta} & {}^{t}P_{rr} \end{bmatrix} \right) \begin{Bmatrix} {}_{t}\varepsilon_{\theta} \\ {}_{t}\varepsilon_{r} \end{Bmatrix} + \left(\begin{Bmatrix} \lambda \\ \lambda \end{Bmatrix} - \begin{Bmatrix} {}^{t}P_{\theta x} \\ {}^{t}P_{rx} \end{Bmatrix} \right) {}_{t}\varepsilon_{x} \tag{6.30} $$

Solving Eq. (30), gives

$$ \begin{Bmatrix} {}_{t}\varepsilon_{\theta} \\ {}_{t}\varepsilon_{r} \end{Bmatrix} = \begin{Bmatrix} {}^{t}C_{\theta x} \\ {}^{t}C_{rx} \end{Bmatrix} {}_{t}\varepsilon_{x} \tag{6.31} $$

where

$$ \begin{Bmatrix} {}^{t}C_{\theta x} \\ {}^{t}C_{rx} \end{Bmatrix} = - \begin{bmatrix} \lambda' - {}^{t}P_{\theta\theta} & \lambda - {}^{t}P_{\theta r} \\ \lambda - {}^{t}P_{r\theta} & \lambda' - {}^{t}P_{rr} \end{bmatrix}^{-1} \begin{Bmatrix} \lambda - {}^{t}P_{\theta x} \\ \lambda - {}^{t}P_{rx} \end{Bmatrix} \tag{6.32} $$

The third equation of Eq. (6.25) gives the stress-strain relation between the independent stress and strain increments which can be expressed as

$$ {}_{t}S_{x} = {}^{t}C^{EP}\, {}_{t}\varepsilon_{x} \tag{6.33} $$

where ${}^{t}C^{EP}$ is the elastic-plastic modulus defined as

$$ {}^{t}C^{EP} = {}^{t}C_{\theta x}\,(\lambda - {}^{t}P_{x\theta}) + {}^{t}C_{rx}\,(\lambda - {}^{t}P_{xr}) + \lambda' - {}^{t}P_{xx} \tag{6.34} $$

It can be shown that Eq. (6.33) specializes to the elastic stress-strain relation for elastic

behavior as

$$ {}_tS_x = E\,{}_t\varepsilon_x \tag{6.35} $$

It should be pointed out that all the stress and strain components and stress-strain relations are defined in the local coordinate system.

The effective stress and incremental effective plastic strain can be expressed by the following, which can be derived from the general expressions in Eqs. (2.43) and (2.48).

$$ {}^t\bar{S} = \sqrt{\frac{1}{2}\left({}^tS_\theta^2 + {}^tS_x^2 + ({}^tS_x^2 - {}^tS_\theta^2)^2 \right)} \tag{6.36} $$

$$ {}_t\bar{\varepsilon}^P = \sqrt{\frac{2}{3}\left(({}_t\varepsilon_\theta^P)^2 + ({}_t\varepsilon_r^P)^2 + ({}_t\varepsilon_x^P)^2 \right)} \tag{6.37} $$

where the incremental plastic strain components are

$$ \begin{Bmatrix} {}_t\varepsilon_\theta^P \\ {}_t\varepsilon_r^P \\ {}_t\varepsilon_x^P \end{Bmatrix} = \frac{1}{E}\begin{bmatrix} 1 & -\nu & -\nu \\ -\nu & 1 & -\nu \\ -\nu & -\nu & 1 \end{bmatrix} \begin{bmatrix} {}^tP_{\theta\theta} & {}^tP_{\theta r} & {}^tP_{\theta x} \\ {}^tP_{r\theta} & {}^tP_{rr} & {}^tP_{rx} \\ {}^tP_{x\theta} & {}^tP_{xr} & {}^tP_{xx} \end{bmatrix} \begin{Bmatrix} {}^tC_{\theta x} \\ {}^tC_{rx} \\ 1 \end{Bmatrix} {}_t\varepsilon_x \tag{6.38} $$

The accumulated effective plastic strain is used to evaluate the current yield stress and tangent modulus from the effective stress-effective strain curve.

6.3.2 Solution Procedure to Evaluate the Stress Increment

In this section the solution procedure to evaluate the incremental stress for a given incremental strain is discussed. Assuming the solution at time t is known, i.e. the stresses ${}^tS_x$, strains ${}^t\varepsilon_x$, ${}^t\bar{\varepsilon}^P$ and displacements ${}^tu$, ${}^tv$ are known. The increments of displacements, and consequently the increments of strains are also known. The increments in stress and effective plastic strain are to be determined.

It should be pointed out that the incremental strain should always be evaluated with respect to the last equilibrium configuration in order to exclude the effects of false path which might be introduced by the equilibrium iteration process.

The solution procedure is based on a sub-increment technique (Chen and Han, 1988) which divides the strain increment into NSUB sub-increments. The number NSUB should be large enough to obtain the required precision. If the acceptable size for sub-

increments of strain is set to be 10 microstrain, the number NSUB can be estimated as

$$\text{NSUB} = \frac{{}_t\varepsilon_x}{0.00001} \tag{6.39}$$

For each sub-increment of strain $d_t\varepsilon_x^i$, the following steps are carried out to evaluate the incremental stress.

(1) Predict the sub-increment of stress based on elastic behavior in Eq. (6.35) and the total stress as

$${}^tS_x^T = {}^tS_x^{i-1} + E\, d_t\varepsilon_x^i$$

where the superscript T indicates a trial value.

(2) Evaluate the effective stress ${}^t\overline{S}^T$ by Eq. (6.36).

(3) Check the yield condition against the current yield strength, ${}^tS_Y$.

(i) If $f({}^t\overline{S}^T, {}^tS_Y) \leq 0$, then update the stress ${}^tS_x^i = {}^tS_x^T$ and go to step (1) for next sub-increment of strain.

(ii) If $f({}^t\overline{S}^T, {}^tS_Y) > 0$, then go to step (4)

(4) Determine the value of Q which defines the elastic fraction of this sub-increment of strain as $(1\text{-}Q)\, d\varepsilon_x$ and elastic-plastic fraction as $Q\, d\varepsilon_x$. the factor Q is equal to 1 for complete elastic-plastic sub-increment and 0 for complete elastic sub-increment of strain. Update the stress for elastic fraction according to Eq. (6.35) and go to next step for elastic-plastic fraction.

(5) Calculate the stress increment by Eq. (6.33) based on the current tangent modulus and stress state, and update the total stress to obtain ${}^tS_x^i$ as

$${}^tS_x^i = {}^tS_x^{i-1} + (1\text{-}Q)\, E\, d_t\varepsilon_x^i + Q\, {}^tC^{EP}\, d_t\varepsilon_x^i \tag{6.40}$$

Go to next step.

(6) Calculate the effective plastic strain increment by Eq. (6.37) and update the total effective plastic strain to obtain ${}^t\overline{\varepsilon}^{Pi}$. The calculation for the ith sub-increment of strain is finished here. Go to step (1) for the next sub-increment of strain.

The internal forces, ${}^tF$ and ${}^tM$, on the cross-section are integrated from the stress state which is evaluated by the above procedure. The number of the integration points for the integration process over the cross-section can be specified by the user of the program ABP. A number of 20 for a half of the cross-section is recommended. The element vector of internal force is integrated along the length of the element, and it is further assembled into the global equilibrating force vector. From the load vector and the equilibrating force vector, the unbalanced force vector can be determined and used to evaluate the next increment of the displacements and strains.

6.4 CONSTITUTIVE RELATION FOR ISPDR TECHNIQUE

The basis for the generalized constitutive relations for the ISPDR technique has been defined in terms of the relation between internal forces and strains in Eqs. (6.23) and (6.24). These are rewritten here as

$$d^tF = {}^tK_1\, d^t\varepsilon_0 + {}^tK_3\, d^t\phi \tag{6.41a}$$

$$d^tM = {}^tK_3\, d^t\varepsilon_0 + {}^tK_2\, d^t\phi \tag{6.41b}$$

where

$${}^tK_1 = \frac{\partial^tF}{\partial^t\varepsilon_0} \tag{6.42}$$

$${}^tK_2 = \frac{\partial^tM}{\partial^t\phi} \tag{6.43}$$

$${}^tK_3 = \frac{\partial^tF}{\partial^t\phi} = \frac{\partial^tM}{\partial^t\varepsilon_0} = {}^te\,{}^tK_1 \tag{6.44}$$

In Eq. (6.44), ${}^te$ is the distance from the elastic stiffness centroid to the tangential stiffness centroid of the cross-section of the current configuration. ${}^tK_1$, ${}^tK_2$ and ${}^tK_3$ are the *stiffness coefficients* of the cross-section. The relations defined in Eq. (6.44) will be proved in Sect. 6.4.5 under the condition of plane cross-sections remaining plane.

To fully define the generalized constitutive relation represented by Eq. (6.41), the evaluation of cross-sectional stiffness coefficients ${}^tK_1$, ${}^tK_2$ and ${}^tK_3$ needs to be detailed. The procedure for this evaluation has two major steps. One is to develop a generation procedure for stiffness-property-deformation (SPD) relations from the shell analysis

because the shell model analysis can't directly provide the above cross-sectional stiffness coefficients. The second step is to input SPD relations into the beam model and determine the cross-sectional stiffness coefficients of Eqs (6.41).

This section includes discussions on definition, application and generation of SPD relations in Sects. 6.4.1, 6.4.2, and 6.4.3, respectively. It also deals with relevant problems, such as, size dependence of SPD relations Sect. 6.4.4. As a supplement, the derivation of Eq. (6.44) is also demonstrated in Sect. 6.4.5.

6.4.1 Definition of SPD Relations

The SPD relations are a set of relations established from shell model analysis which can be used to define the cross-sectional stiffness coefficients ${}^tK_1$, ${}^tK_2$ and ${}^tK_3$ in Eqs. (6.42) to (6.44). One of the requirements on SPD relations, of course, is that cross-sectional stiffness coefficients can be expressed in terms of the quantities defined as SPD relations. However, a more important feature is that they must be able to be conveniently derivable from a simple shell model analysis because a very significant portion of the computational effort will be consumed by the generation of SPD relations. Considering the nature of the approximations associated with this solution procedure, it is acceptable to evaluate ${}^tK_1$, ${}^tK_2$ and ${}^tK_3$ approximately. On the other hand, it is almost impossible to evaluate them precisely.

In order to limit each of the SPD relations to a simple one dimensional form, one primary independent variable must be selected. The state of the pipeline in terms of its internal forces and strains depends on its geometric properties, such as diameter and thickness, and its material properties. In addition, it also depends on the loading conditions, where a typical load combination is bending moment, axial force and internal pressure, and on loading history. Since geometric and material properties are specified for a given design of pipeline, the loading condition and history are the variables. Among the loads, internal pressure is usually kept constant during operation. Axial load and corresponding axial strain mainly come from temperature effects and vary in a relatively narrow range. Only bending moment and its corresponding curvature vary extensively, depending on the externally applied loads and imposed deformations. Consequently, considering their relative importance, moment and curvature are taken as the *primary variables* while axial force and axial strain may be considered as *secondary variables*.

In the pair of primary variables, and in the pair of secondary variables, only one

variable is independent and the other is dependent because of the constitutive relations defined in Eq. (6.41). For each pair, either of them can be taken as the independent variable, and the state of the pipeline in terms of the internal forces and strains is completely defined if independent variable associated with each pair is defined. Considering the nature of deformation analysis and the fact that flexural deformation is the principal deformation pattern, curvature is taken as the primary independent variable. The SPD relations are then defined in the form of relations between each of required quantities and the curvature. In order to span the two-dimensional domain in terms of primary and secondary independent variables, several sets of one-dimensional relations need to be developed with different constant values of the secondary independent variable. The axial force is taken as the secondary independent variable because it is easier to keep constant than the axial strain in the simple shell analysis.

The *stiffness properties* required to define cross-sectional stiffness coefficients are the following five, which are defined in this way because they are derivable from the shell model analyses of a shell segment subjected to constant internal pressure and axial , and to variable moment. These analyses have been presented in Ch. 4.

(1) Property 1 - Flexural stiffness, ${}^tK_b$: The flexural stiffness is defined as

$$ {}^tK_b = \frac{\partial {}^tM}{\partial {}^t\phi} \qquad \text{with } {}^tF = \text{constant} \tag{6.45} $$

(2) Property 2 - Axial stiffness, ${}^tK_a$: The axial stiffness is defined as

$$ {}^tK_a = \frac{\partial {}^tF}{\partial {}^t\varepsilon_0} \qquad \text{with } d{}^tM = {}^tC\ {}^t\bar{v}_c\ d{}^tF \tag{6.46} $$

(3) Property 3 - Location of the elastic stiffness centroid of the cross-section, ${}^t\bar{v}_c$: The location of the elastic stiffness centroid for a deformable cross-section at any cross-section along the pipe, relative to its initial position, may be defined as

$$ {}^t\bar{v}_c = \frac{\int_A {}^tv\, dA}{\int_A dA} \tag{6.47} $$

(4) Property 4 - Location of the tangent stiffness centroid of the cross-section, ${}^t\bar{y}_s$: The

tangent stiffness centroid of the cross-section is defined as the centroid of the transformed area (Beer and Johnston, 1985) of the cross-section. The transformed area consist of the geometric area for which the wall thickness is adjusted in proportion to the incremental tangent modulus in the wall. This quantity is defined for the deformed cross-section as

$$ {}^t\bar{y}_s = \frac{\int_A {}^t y \, {}^t E \, dA}{\int_A {}^t E \, dA} \tag{6.48} $$

with ${}^tE$ as the current tangent modulus.

(5) Property 5 - Amplification factor, ${}^tC$: This factor relates the relative magnitude of the increment in secondary moment introduced by incremental deflection $d^t\bar{v}_c$ to that arising from the incremental axial force d^tF. The secondary moment, which has two components, can be expressed as

$$ (d^tM)_{secondary} = {}^tF \, d^t\bar{v}_c + {}^t\bar{v}_c \, d^tF = {}^tC \, {}^t\bar{v}_c \, d^tF \tag{6.49a} $$

where the amplification factor, ${}^tC$, is defined as

$$ {}^tC = 1 + \frac{{}^tF \, d^t\bar{v}_c}{{}^t\bar{v}_c \, d^tF} \tag{6.49b} $$

It should be noted that this factor is associated with the definition of property 2.

(6) Definition : The *SPD relations* consist of relations between the five stiffness properties identified above and the curvature. These properties are evaluated for each value of a set of constant axial forces which covers the possible range of the axial force for the problem under consideration.

6.4.2 Application of SPD Relations

The SPD relations defined in the previous section are specially designed to be used as constitutive relations for the ISPDR technique where the effects of local buckling can be approximately accounted for in the beam model of pipelines. In this section, the expressions for the cross-sectional stiffness coefficients defined in Eqs. (6.42) to (6.44), in terms of the cross-sectional stiffness properties defined in Eqs. (6.45) to (6.49), are presented.

From the definitions, the distance between elastic and tangent stiffness centroids, ${}^t e$, can be expressed as

$$ {}^t e = {}^t\bar{y}_s - {}^t\bar{v}_c \tag{6.50} $$

Applying the constraint of constant axial force in Eq. (6.45), to Eq. (6.41a), and considering Eq.(6.44), Eq. (6.41a) becomes

$$ 0 = {}^t K_1 \, d^t\varepsilon_0 + {}^t e \, {}^t K_1 \, d^t\phi \tag{6.51a} $$

From Eq. (6.51a), the increment of axial strain can be expressed as

$$ d^t\varepsilon_0 = - {}^t e \, \omega \, \varphi \tag{6.51b} $$

Substituting Eq. (6.51b) into Eq. (6.41b), this latter equation becomes

$$ d^t M = (- {}^t e^2 \, {}^t K_1 + {}^t K_2) \, d^t\phi \tag{6.52} $$

Comparing Eq. (6.52) with the definition in Eq. (6.45), the following relation is obtained

$$ {}^t K_b = - {}^t e^2 \, {}^t K_1 + {}^t K_2 \tag{6.53} $$

Applying the constraint in Eq. (6.46), to Eq. (6.41b), and considering Eq. (6.44), Eq. (6.41b) becomes

$$ {}^t C \, {}^t\bar{v}_c \, d^t F = {}^t e \, {}^t K_1 \, d^t\varepsilon_0 + {}^t K_2 \, d^t\phi \tag{6.54a} $$

Solving Eq. (6.54a) for $d^t\phi$ results in

$$ d^t\phi = \frac{{}^t C \, {}^t\bar{v}_c \, d^t F - {}^t e \, {}^t K_1 \, d^t\varepsilon_0}{{}^t K_2} \tag{6.54b} $$

Substituting Eq. (6.54b) into Eq. (6.41a) and making some algebraic rearrangements, Eq. (6.41a) may be written as

$$ \frac{d^t F}{d^t\varepsilon_0} = \frac{{}^t K_1 \, {}^t K_2 - {}^t e^2 \, {}^t K_1^2}{{}^t K_2 - {}^t e \, {}^t C \, {}^t\bar{v}_c \, {}^t K_1} \tag{6.55} $$

Comparing Eq. (6.55) with the definition in Eq. (6.46), yields

$$ {}^{t}K_a = \frac{{}^{t}K_1\,{}^{t}K_2 - {}^{t}e^2\,{}^{t}K_1^2}{{}^{t}K_2 - {}^{t}e\,{}^{t}C\,{}^{t}\bar{v}_c\,{}^{t}K_1} \tag{6.56} $$

Solving Eqs. (6.53) and (6.56) for ${}^{t}K_1$ and ${}^{t}K_2$ results in

$$ {}^{t}K_1 = \frac{{}^{t}K_a\,{}^{t}K_b}{{}^{t}K_b - {}^{t}e^2\,{}^{t}K_a + {}^{t}e\,{}^{t}C\,{}^{t}\bar{v}_c\,{}^{t}K_a} \tag{6.57a} $$

$$ {}^{t}K_2 = \frac{{}^{t}K_b^2 + {}^{t}e\,{}^{t}C\,{}^{t}\bar{v}_c\,{}^{t}K_a\,{}^{t}K_b}{{}^{t}K_b - {}^{t}e^2\,{}^{t}K_a + {}^{t}e\,{}^{t}C\,{}^{t}\bar{v}_c\,{}^{t}K_a} \tag{6.57b} $$

By Eqs. (6.57) and (6.44), the cross-sectional stiffness coefficients are fully defined in terms of the cross-sectional stiffness properties. Using the incremental notation of Sect. 6.2 for displacement increments, Eq. (6.41) can now be written as

$$ {}_{t}F = {}^{t}K_1\,{}_{t}\varepsilon_0 + {}^{t}K_3\,{}_{t}\phi \tag{6.58a} $$

$$ {}_{t}M = {}^{t}K_3\,{}_{t}\varepsilon_0 + {}^{t}K_2\,{}_{t}\phi \tag{6.58b} $$

which is the incremental constitutive relation for the ISPDR technique.

6.4.3 Generation of SPD Relations

The generation of SPD relations is carried out by a procedure of running the shell model analysis and abstracting the information necessary to construct the SPD relations. For each value of constant axial force, there are five relations that need to be constructed, and the values of the constant axial force should be selected to be able to cover the range of axial force which may possibly occur in the operating line. The following discussions will describe the generation procedure for a set of SPD relations corresponding to a given value of constant axial force.

A three-dimensional shell model of a pipeline segment is used in the analysis, as discussed in Sect. 4.2 and defined in Figs. 4.1 and 4.6. The model is used to simulate a pipeline segment simply supported at both ends and subjected to constant axial load, constant internal pressure, and incremental moment, as shown in Fig. 6.2. A particular segment which contains the most severe local buckling is chosen and the average response of this segment is used to construct the SPD relations. In principle this selected segment could be located anywhere on the pipeline segment, as indicated in Fig. 4.6a, although it is

more likely to be located in the central part than at the ends. The geometric and material properties for the shell model are the same as those of the pipeline to be analyzed in the beam model.

Two types of run of the shell model analysis, which can be called the *primary run* and the *secondary run*, respectively, are necessary to define the five SPD relations. The primary run starts from the initial state, and proceeds with an incremental solution at proper step-sizes subjected to constant axial load, constant internal pressure and incremental bending moment. The primary run is stopped when the deformation of the pipeline becomes large enough so that the pipeline is obviously no longer operational. The secondary runs start from any equilibrium state on the path of the primary run, and proceed with one step incremental solutions of relatively small step-size consistent with constant applied moment, constant internal pressure and incremental axial load. The secondary runs are stopped after one step.

The primary run provides the information to construct three SPD relations at the specified axial force. These are: the moment-curvature relation which defines the flexural stiffness, ${}^tK_b$ of Eq. (6.45); the ${}^t\bar{v}_c$-curvature relation defining the location of the elastic stiffness centroid by Eq. (6.47); and the ${}^t\bar{y}_s$-curvature relation defining the location of the tangent stiffness centroid, as given by Eq. (6.48). A series of secondary runs along the path of the primary run at proper intervals provides the information to construct two SPD relations at the specified axial force. These are the axial stiffness ${}^tK_a$-curvature relation defining the axial stiffness of Eq. (6.46), and the ${}^tC$-curvature relation defining the amplification factor of Eq. (6.49). Plots of these relationships will be given subsequently, but typical of these plots are the moment-curvature curves in Figs. 4.7 to 4.9. Nevertheless, the reader may wish to refer at this time to the sets of properties in Figs. 6.22 to 6.26, which illustrate all five of the properties.

The moment-curvature relation comes naturally out of the primary run except that moment and curvature are defined as the average moment and average curvature on the buckling segment. The flexural stiffness, ${}^tK_b$, is the slope of moment-curvature curve according to definition in Eq. (6.45), since the axial force is constant. The location of the elastic stiffness centroid, ${}^t\bar{v}_c$, and the location of the tangent stiffness centroid, ${}^t\bar{y}_s$, are obtained by integration over the cross-section according to the definition in Eqs. (6.47) and (6.48). The integration should be carried out over several cross-sections and their average is used to define SPD relations for the buckling segment.

The secondary runs start at a given curvature and axial load, with an axial load increment. This increment is, in general, tensile due to the fact that the axial force in the pipeline increases as the imposed differential settlement increases. The axial stiffness K_a can be obtained according to the definition in Eq. (6.46) assuming that the condition in Eq. (6.46) is satisfied which is verified in the following.

In the shell model of the pipeline shown in Fig. 6.2, the differential moment at any section has three components, and may be expressed as

$$d^tM = (d^tM)_a + {}^tF\, d^t\bar{v}_c + {}^t\bar{v}_c\, d^tF \tag{6.59}$$

where $(d^tM)_a$ is increment of the applied moment, ${}^tF$ and d^tF are the compressive axial load and its increment respectively. In the secondary run, applied moment is kept constant, so Eq. (6.59) becomes

$$d^tM = {}^tC\, {}^t\bar{v}_c\, d^tF \tag{6.60}$$

where ${}^tC$ is defined in Eq. (6.49). Eq. (6.60) is obviously consistent with the condition in Eq. (6.46). The amplification factor ${}^tC$ can be obtained from the secondary run, because the increments of ${}^t\bar{v}_c$ and ${}^tF$ are available from this secondary run.

6.4.4 Size Dependence of SPD Relations

From the generation procedure of SPD relations, it is obvious that SPD relations are dependent on the length of the buckling segment which contains the principal buckle. In the following this will be referred as the *principal wavelength*. The size dependence is implicit in the use of average curvature, average moment, average axial stiffness and average locations of the elastic and tangent stiffness centroids. More significant localization is expected if a smaller principal wavelength is used. On the other hand, the effects of local buckling are not properly represented by SPD relations if a larger principal wavelength is used.

To properly account for size dependence, the SPD relations must be applied properly. The main idea is to apply SPD relations in a manner similar to that in which they are generated. First of all, there are two regions in the SPD relations to be identified. These are the prebuckling region and the postbuckling region. In the prebuckling region, the effects of local buckling are not present and therefore the curvature and moment are uniform except for the secondary effects from axial load eccentricity which is not

significant. Consequently, the effect of size dependence is negligible.

In the postbuckling region, significant non-uniformity is introduced by local buckling, and strong size dependence is therefore expected. The size dependence of the curvature is illustrated by Figs. 4.23 to 4.25. To account for the size effect of SPD relations in their application procedure, the size of the pipeline-beam elements is set to equal the principal wavelength in the regions where buckling is expected to occur. The average deformation quantities defined over the buckling segment are identified as *local* quantities. Larger sized elements may be used in the region where buckling is not expected to occur. This reduces the number of elements without impairment of accuracy because the size effects are negligible in these regions. In addition, the average curvature of the pipeline-beam element is used to evaluate the flexural and axial stiffness, locations of elastic and tangent stiffness centroids, and amplification factor through SPD relations.

The average curvature in an element can be defined by integration along the length as

$$ {}^{t}\bar{\phi} = \frac{\int_{{}^{t}L} {}^{t}\phi \, d^{t}x}{\int_{{}^{t}L} d^{t}x} \tag{6.61} $$

As a result, the SPD relations to be used as constitutive relations relate average increments of internal forces and strains over the length of an element where length is chosen as the principle wavelength.

6.4.5 Derivation of Equation (6.44)

Equation (6.44), which expresses coupling between stiffness coefficients in terms of the axial stiffness coefficient ${}^{t}K_{1}$ and the distance between the elastic and tangent stiffness centroid, ${}^{t}e$, was introduced without derivation . The derivation for this equation is presented in this section.

Two systems of deformation coordinate and their corresponding forces are shown in Fig. 6.3. System I has the elastic stiffness centroidal axis as the reference axis. System II has the instantaneous tangent stiffness centroidal axis as the reference axis. The incremental axial strains are measured, and the incremental axial forces and moments are

assumed to act, at the reference axes. In System II, the instantaneous tangent stiffness centroidal axis becomes the uncoupled reference axis provided that the distribution of current modulus over the cross section is unchanged when $d\phi = 0$, $d\varepsilon_s \neq 0$, and $d\phi \neq 0$, $d\varepsilon_s = 0$. Assuming this condition is valid, Eq. (6.44) can be proved as following.

First of all, it should be realized that the axial stiffness in System I and System II are equal to each other, i.e.

$$\frac{\partial^t F}{\partial^t \varepsilon_0} = \frac{\partial^t F}{\partial^t \varepsilon_s} = {}^tK_1 \tag{6.62}$$

because both of them are the axial stiffness under the same incremental strain condition which is a uniform axial strain increment over entire cross-section.

If the curvature increment is assumed to be zero, by Bernouli's assumption there is a uniform axial strain increment over entire cross section. Therefore

$$d^t\varepsilon_s = d^t\varepsilon_0 \tag{6.63}$$

$$d^tF = {}^tK_1\, d^t\varepsilon_0 \tag{6.64}$$

In the uncoupled system, incremental forces can be expressed as

$$d^tF = {}^tK_1\, d^t\varepsilon_s \tag{6.65}$$

$$d^tM_s = 0 \tag{6.66}$$

Replacing the incremental axial force in Eq. (6.65) by a statically equivalent system with the force moved to c from axis s and using Eq. (6.63), the incremental moment in System I can be expressed as

$$d^tM = d^tM_s - (-\,d^tF)\,{}^te = {}^te\,{}^tK_1\, d^t\varepsilon_0 \tag{6.67}$$

From Eq. (6.67) and the condition of zero incremental curvature, the following equation can be obtained directly

$$\frac{\partial^t M}{\partial^t \varepsilon_0} = {}^te\,{}^tK_1 \tag{6.68}$$

which is one of the equations in Eq. (6.44).

If the incremental strain at the elastic stiffness centroid is assumed to be zero and curvature increment is nonzero, the incremental axial strain and force in System II can be expressed as

$$d^t\varepsilon_s = {}^te\, d^t\phi \tag{6.69}$$

$$d^tF = {}^tK_1\, d^t\varepsilon_s = {}^te\, {}^tK_1\, d^t\phi \tag{6.70}$$

From Eq. (6.70) and the condition of $d^t\varepsilon_0 = 0$, following equation can be directly obtained

$$\frac{\partial^t F}{\partial^t \phi} = {}^te\, {}^tK_1 \tag{6.71}$$

which is the other one of the equations in Eq. (6.44).

6.5 PIPELINE-SOIL INTERACTION

Pipeline-soil interaction is expected to play an important role in the response of buried pipelines, especially for pipelines in arctic environments where many external loads are imposed through pipeline-soil interaction. The fundamental assumption for pipeline-soil interaction models is that the effects of soil on the pipeline can be modelled by a series of *soil springs* as assumed in Sect. 6.1. To establish the interaction model, the ground profile must be described at all stages of deformation. The deformations of the soil springs can then be determined according to the relative positions of the pipeline and the ground profile. By using the constitutive relations of the soil springs, which describe the relation between the spring forces and spring deformations, the reactive forces of the soil springs can be defined. The three basic aspects of this process are discussed in following subsections.

6.5.1 Ground Profile

Ground profile here refers to the configuration of supporting soil beneath the pipeline. This configuration depends on many factors such as differential thaw settlement, frost heave and fault movement. In this project, focus will be concentrated on the effects of differential thaw settlement, although the approach employed here can be extended to other applications. Before defining the ground profile, the differential thaw settlement configurations are examined in the following.

Two possible differential thaw settlement configuration are shown in Figs. 6.4 and

6.5 (Nyman, 1983). These represent two different mechanisms. The first is caused by a non-uniform thaw front which may be introduced by non-uniform heat transfer. The second is due to non-uniform thaw settlement soil properties because the presence of thaw stable permafrost or rock. In spite of different mechanisms, the resulting ground profiles and their effects on pipeline response are similar, and consequently, they can be treated in the same way in analysis. The configuration of the ground profile can be divided into the *settlement zone*, *transition zone* and *stable zone* along the pipeline. For long settlement zones, the maximum pipe stresses and strains are located in the vicinity of the transition zone. As the length of settlement zone decreases, the pipe stiffness plays a more active role in transmitting overburden load to the transition zone, and relocates maximum pipe stresses and strains toward the center of the settlement zone.

With respect to the ground profile, the following assumptions are introduced. The length of settlement zone is assumed to be large enough so that the maximum stresses and strains are located in the vicinity of the transition zone and each of the transition zones can be analyzed independently. As a result, the analytical model includes only a transition zone and parts of the settlement and stable zones. Soil is assumed to settle uniformly in the settlement zone and not to settle at all in the stable zone. The length of the transition may be relatively short. As a result, the pipeline may separate from the supporting soil in the transition zone, and adjacent parts of the settlement and stable zones, because of the stiffness of the pipeline. Based on these assumptions the ground profile can be described, in principle, by straight horizontal lines in the stable and settlement zones and a curve in the transition zone which connects the two straight lines. Three representations to define the ground profile are introduced in the following.

The first representation is a simplification of the real ground profile and consists of three straight lines as shown in Fig. 6.6. It can be called a *stepwise ground profile* and arises naturally if the length of the transition zone of ground profile is reduced to zero. It appears to be unrealistic. However, considering that the pipeline separates from supporting soil in the transition zone and a part of the adjacent settlement zone, the simplification is acceptable. The benefit of a stepwise ground profile is that only one parameter, the differential settlement $^t\delta$, is needed to fully describe it.

The second representation is called the *smooth ground profile* where the ground transition zone is filled by a smooth curve as shown in Fig. 6.7. The shape of this curve assumed here consists of two parts which are symmetric about a center origin, located at the middle of the transition zone and at half the differential settlement. It is constructed for

the conditions that the ground profile is continuous up to the second order derivative at both ends and at the center of the transition zone. It is described, in terms of the coordinate system of Fig. 6.6, by the following expressions

$$ {}^{t}\tilde{y}_G = 0 \qquad \tilde{x} < -L_{TR} \qquad (6.72a) $$

$$ {}^{t}\tilde{y}_G = -\frac{{}^{t}\delta}{2L_{TR}^3}\left(2(L_{TR}+\tilde{x})^3 - \frac{(L_{TR}+\tilde{x})^4}{L_{TR}}\right) \qquad -L_{TR} \le \tilde{x} \le 0 \qquad (6.72b) $$

$$ {}^{t}\tilde{y}_G = -{}^{t}\delta + \frac{{}^{t}\delta}{2L_{TR}^3}\left(2(L_{TR}-\tilde{x})^3 - \frac{(L_{TR}-\tilde{x})^4}{L_{TR}}\right) \qquad 0 \le \tilde{x} \le L_{TR} \qquad (6.72c) $$

$$ {}^{t}\tilde{y}_G = -{}^{t}\delta \qquad \tilde{x} > L_{TR} \qquad (6.72d) $$

where ${}^{t}\delta$ and L_{TR} are the differential settlement and the half length of the transition zone. This smooth ground profile allows the effect of the shape of the transition zone to be considered in an approximate but simple way. It can be used to study the effect of the length of transition zone in a systematic manner because the length of transition zone is the only parameter apart from the differential settlement.

The last representation is a *piecewise linear ground profile*, where the transition is composed of piecewise straight lines connecting the positions of points at certain locations. When the differential settlement is increased, settlements at those points are proportionally increased. This scheme allows any configuration to be defined and the real ground profile to be represented as closely as possible.

6.5.2 Deformation of Soil Springs

There are three types of reaction from soil surrounding the pipeline considered by the model. These are : support from the soil beneath the pipeline; reaction from the soil above the pipeline; and, friction along the pipeline. They are modelled by bearing springs, uplifting springs and longitudinal springs, respectively. The deformations of these springs are determined according to the relative position of the pipeline and the soil. The constitutive relations for these springs will be discussed in next section.

Both the bearing and uplifting springs are bearing type springs which can take only compressive force. Consequently, for a pair of bearing and uplifting springs acting on the same cross-section of a pipeline, only one of them is active at anytime. To identify the

active and inactive springs, the concept of gap width is introduced and denoted as ${}^t d$, as shown in Fig. 6.7. The *gap width* for a cross-section is defined as the separation distance between the pipeline and ground profile in the direction normal to the current pipeline configuration at the cross-section. It can be evaluated for each type of ground profile as in the following.

For the stepwise ground profile of Fig. 6.6, and any given cross-section on the pipeline (${}^t\tilde{x}_0$, ${}^t\tilde{y}_0$), the corresponding point on the ground profile with the same $\tilde{x}$-coordinate is (${}^t\tilde{x}_0$, $-{}^t\delta$) in the settlement zone or (${}^t\tilde{x}_0$, 0) in the stable zone. The vertical distance is then

$$ {}^t d_y = {}^t\tilde{y}_0 + {}^t\delta \qquad \text{if } {}^t\tilde{x}_0 > 0 \tag{6.73a} $$

$$ {}^t d_y = {}^t\tilde{y}_0 \qquad \text{if } {}^t\tilde{x}_0 \le 0 \tag{6.73b} $$

With the help of Fig. 6.6, the gap width can be expressed as

$$ {}^t d = \frac{{}^t d_y}{\cos\beta} \qquad \text{if } {}^t d_y > 0, \text{ and, } {}^t d_y \tan\beta \le {}^t\tilde{x}_0 \text{ or } {}^t\tilde{x}_0 < 0 \tag{6.74a} $$

$$ {}^t d = \frac{{}^t\tilde{x}_0}{\sin\beta} \qquad \text{if } {}^t d_y > 0, \text{ and, } 0 \le {}^t\tilde{x}_0 \le {}^t d_y \tan\beta \tag{6.74b} $$

$$ {}^t d = 0 \qquad \text{if } {}^t d_y \le 0 \tag{6.74c} $$

where β is the angle between the normal direction of pipeline and $\tilde{y}$-axis.

For the smooth ground profile of Fig. 6.7, Eq. (6.73) becomes

$$ {}^t d_y = {}^t\tilde{y}_0 - {}^t\tilde{y}_G \tag{6.75} $$

where ${}^t\tilde{y}_G$ is the undeformed ground configuration evaluated through Eq. (6.72) by substituting ${}^t\tilde{x}_0$. The gap width can be expressed as

$$ {}^t d = \frac{{}^t d_y \sin\gamma}{\sin\beta\ \cos\gamma + \sin\gamma\ \cos\beta} \qquad \text{if } {}^t d_y > 0 \tag{6.76a} $$

$$ {}^t d = 0 \qquad \text{if } {}^t d_y < 0 \tag{6.76b} $$

where angles β and γ are defined in Fig. 6.7.

The angle β can be easily evaluated as long as the current position of the pipeline is given. In order to evaluate angle γ, the intersection of the normal line of the pipeline at the given cross-section and ground profile, point S in Fig. 6.7, has to be determined. This can be solved numerically when the normal direction of pipeline and ground profile curve in Eq. (6.72) are available. Eq. (6.76) is also applicable to piecewise ground profile as long as the angles are properly evaluated.

With the gap width defined and evaluated, the active spring can be easily identified between bearing spring and uplift spring. The bearing spring is active when gap width is equal to zero and the uplift spring is active when gap width is greater than zero.

The incremental deformation of the springs are evaluated in the local coordinate system as

$$ {}_t\Delta_{BS} = -{}_tv_0 \qquad \text{if } {}^td = 0 \tag{6.77a} $$

$$ {}_t\Delta_{BS} = 0 \qquad \text{if } {}^td > 0 \tag{6.77b} $$

$$ {}_t\Delta_{US} = 0 \qquad \text{if } {}^td = 0 \tag{6.78a} $$

$$ {}_t\Delta_{US} = -{}_tv_0 \qquad \text{if } {}^td > 0 \tag{6.78b} $$

$$ {}_t\Delta_{LS} = -{}_tu_0 \tag{6.79} $$

where ${}_t\Delta_{BS}$, ${}_t\Delta_{US}$ and ${}_t\Delta_{LS}$ are deformation increments for bearing, uplifting and longitudinal springs, respectively, and ${}^td$ is defined in Eqs. (6.74) or (6.76) where it is applicable.

6.5.3 Constitutive Relations for Soil Springs

The constitutive relations for soil springs are defined in terms of relations between the force and deformation of the springs, which are assumed to be elastic-plastic. The relations for bearing and uplifting springs are one-sided functions with nonzero stiffness on the compressive deformation side only due to the fact that the tensile strength of soil is negligible. The relation for longitudinal spring is a symmetric function with respect to compressive and tensile deformation. Typical relations are shown in Fig. 6.8.

The incremental spring forces, which are defined in the local coordinate system on

the current deformed configuration and denoted by ${}_tF_{BS}$, ${}_tF_{US}$ and ${}_tF_{LS}$, are

$$ {}_tF_{BS} = {}^tK_{BS}\, {}_t\Delta_{BS} \tag{6.80a} $$

$$ {}_tF_{US} = {}^tK_{US}\, {}_t\Delta_{US} \tag{6.80b} $$

$$ {}_tF_{LS} = {}^tK_{LS}\, {}_t\Delta_{LS} \tag{6.80c} $$

where ${}^tK_{BS}$, ${}^tK_{US}$ and ${}^tK_{LS}$ are the current tangential stiffness of bearing, uplifting and longitudinal springs. The sign of spring forces is usually defined as positive for tensile deformation and negative for compressive deformation. However, the sign convention used here is based on the reactive forces exerted by the springs on pipeline. The spring forces are positive if their reaction on the pipeline is positive in the local coordinate system.

6.6 INCREMENTAL VIRTUAL WORK EQUATION

The virtual work equation has been discussed in Sect. 2.12.5 where a general equation is given for total Lagrangian formulation in Eq. (2.67) and equations of shell structure are given for both total and updated Lagrangian formulations in Eqs. (2.74) and (2.79), respectively. For the pipeline-beam element, the special stress-strain states and pipeline-soil interaction results a special form of virtual work equation. Since different constitutive relations are used for RMDI and ISPDR techniques as discussed in Sects. 6.3 and 6.4, the incremental virtual work equation will be established separately for these two techniques. Nevertheless, the equations obtained are the same except for some details as demonstrated in following sub-sections.

6.6.1 Incremental Virtual Work Equation for RMDI Technique

For the RMDI technique, the virtual work equation can be derived from the general virtual work equation, in Eq. (2.67), based on stress and strain components of the pipeline-beam element. It can be expressed as

$$ \int_{{}^tV} {}^{t+\Delta t}_{\ \ t}S_x\, \delta^{t+\Delta t}_{\ \ t}\varepsilon_x\, d^tV + \int_{{}^tV} {}^{t+\Delta t}_{\ \ t}S_\theta\, \delta^{t+\Delta t}_{\ \ t}\varepsilon_\theta\, d^tV + \int_{{}^tL} ({}^{t+\Delta t}_{\ \ t}F_{BS} + {}^{t+\Delta t}_{\ \ t}F_{BS})\, \delta^{t+\Delta t}v_0\, d^tx + \int_{{}^tL} {}^{t+\Delta t}_{\ \ t}F_{LS}\, \delta^{t+\Delta t}u_0\, d^tx = \delta^{t+\Delta t}W_{ext} \tag{6.81} $$

where the first two terms are virtual work of stress of pipeline and the second two terms

come from soil springs. The right-hand side of the equation is the external virtual work due to applied load. Considering following relationships

$$ {}^{t+\Delta t}_{t}S_x = {}^{t}S_x + {}_{t}S_x \tag{6.82} $$

$$ {}^{t+\Delta t}_{t}S_\theta = {}^{t}S_\theta = \text{constant} \tag{6.83} $$

$$ \delta^{t+\Delta t}_{t}\varepsilon_x = \delta_t\varepsilon_x = \delta_t\varepsilon_x^{L} + \delta_t\varepsilon_x^{NL} \tag{6.84} $$

$$ \delta^{t+\Delta t}_{t}\varepsilon_\theta = \delta_t\varepsilon_\theta = {}^{t}C_{\theta x}\,\delta_t\varepsilon_x \tag{6.85} $$

where Eqs. (6.31), (6.12) and (6.32) are used to obtain Eqs. (6.83), (6.84) and (6.85), respectively, the first two terms in Eq. (6.81) becomes

$$ \begin{aligned} \mathrm{I} + \mathrm{II} = & \int_{{}^tV} {}_tS_x\,\delta_t\varepsilon_x^{L}\,d^tV + \int_{{}^tV} ({}^tS_x\,\delta_t\varepsilon_x^{NL} + {}^tC_{\theta x}\,{}^tS_\theta\,\delta_t\varepsilon_x^{NL})\,d^tV \\ & + \int_{{}^tV} ({}^tS_x\,\delta_t\varepsilon_\theta^{L} + {}^tC_{\theta x}\,{}^tS_\theta\,\delta_t\varepsilon_x^{L})\,d^tV + \int_{{}^tV} {}_tS_x\,\delta_t\varepsilon_x^{NL}\,d^tV \end{aligned} $$

where the roman number I and II represent the first two terms. Substituting Eqs. (6.17), (6.18) and (6.33) into above equation and carrying out the integration over the cross-section, it becomes

$$ \begin{aligned} \mathrm{I} + \mathrm{II} = & \int_{{}^tL} (({}^tK_1\,{}_t\varepsilon_\delta^{L} + {}^tK_3\,{}_t\phi^{L})\,\delta_t\varepsilon_\delta^{L} + ({}^tK_3\,{}_t\varepsilon_\delta^{L} + {}^tK_2\,{}_t\phi^{L})\,\delta_t\phi^{L})\,d^tx \\ & + \int_{{}^tL} ({}^tF_{eq}\,\delta_t\varepsilon_\delta^{NL} + {}^tM_{eq}\,\delta_t\phi^{NL})\,d^tx + \int_{{}^tL} ({}^tF_{eq}\,\delta_t\varepsilon_\delta^{L} + {}^tM_{eq}\,\delta_t\phi^{L})\,d^tx \end{aligned} \tag{6.86} $$

where the higher order terms are ignored, and

$$ {}^tK_1 = \int_{{}^tA} {}^tC^{EP}\,d^tA \tag{6.87a} $$

$$ {}^tK_2 = \int_{{}^tA} {}^tC^{EP}\,y^2\,d^tA \tag{6.87b} $$

$$ {}^tK_3 = -\int_{{}^tA} {}^tC^{EP}\,y\,d^tA \tag{6.87c} $$

are the cross-sectional stiffness coefficients, which are the same as those defined in Eqs. (6.42) to (6.44) under the assumption of plane section remaining plane, and the current tangent modulus ${}^tC^{EP}$ is defined in Eq. (6.34). The total equivalent internal forces at time t in the above equation are defined as

$$ {}^tF_{eq} = \int_{{}^tA} ({}^tS_x + {}^tC_{\theta x}\, {}^tS_\theta)\, d^tA \tag{6.88a} $$

$$ {}^tM_{eq} = -\int_{{}^tA} ({}^tS_x + {}^tC_{\theta x}\, {}^tS_\theta)\, y\, d^tA \tag{6.88b} $$

The equivalent total internal forces consists of the contribution of the axial stress and the hoop stress and are defined based on equivalent virtual work.

Considering Eq. (6.80), the second two terms in Eq. (6.81) becomes

$$ \begin{aligned} \mathrm{III} + \mathrm{IV} = & \int_{{}^tL} ({}^tK_{BS}\, {}_t\Delta_{BS} + {}^tK_{US}\, {}_t\Delta_{US})\, \delta_t v_0\, d^tx + \int_{{}^tL} {}^tK_{LS}\, {}_t\Delta_{LS}\, \delta_t u_0\, d^tx \\ & + \int_{{}^tL} ({}^tF_{BS} + {}^tF_{US})\, \delta_t v_0\, d^tx + \int_{{}^tL} {}^tF_{LS}\, \delta_t u_0\, d^tx \end{aligned} \tag{6.89} $$

where III and IV represent the third and fourth terms in Eq. (6.81).

Substituting Eqs. (6.86) and (6.89) into (6.81), it becomes

$$ \begin{aligned} & \int_{{}^tL} (({}^tK_1\, {}_t\varepsilon^L + {}^tK_3\, {}_t\phi^L)\, \delta_t\varepsilon^L + ({}^tK_3\, {}_t\varepsilon^L + {}^tK_2\, {}_t\phi^L)\, \delta_t\phi^L)\, d^tx + \\ & \int_{{}^tL} ({}^tF_{eq}\, \delta_t\varepsilon^{NL} + {}^tM_{eq}\, \delta_t\phi^{NL})\, d^tx + \int_{{}^tL} (({}^tK_{BS}\, {}_t\Delta_{BS} + {}^tK_{US}\, {}_t\Delta_{US})\, \delta_t v_0 + {}^tK_{LS}\, {}_t\Delta_{LS}\, \delta_t u_0)\, d^tx \\ & = \delta^{t+\Delta t}W_{ext} - \int_{{}^tL} ({}^tF_{eq}\, \delta_t\varepsilon^L + {}^tM_{eq}\, \delta_t\phi^L)\, d^tx - \int_{{}^tL} (({}^tF_{BS} + {}^tF_{US})\, \delta_t v_0 + {}^tF_{LS}\, \delta_t u_0)\, d^tx \end{aligned} \tag{6.90} $$

This is the incremental virtual work equation for the pipeline-beam element based on the RMDI technique.

6.6.2 Incremental Virtual Work Equation for ISPDR Technique

The virtual work equation for the pipeline-beam element based on the ISPDR technique is established in a similar procedure to that in the previous section. However, it is based on internal forces and strain components because the constitutive relations employed in the ISPDR technique are defined based on these quantities. With the internal forces and the generalized strains Eq. (2.79) becomes

$$\int_{{}^tL} ({}^{t+\Delta t}F\ \delta^{t+\Delta t}{}_t\varepsilon_0 + {}^{t+\Delta t}M\ \delta^{t+\Delta t}{}_t\phi)\ d^tx + \int_{{}^tL} ({}^{t+\Delta t}_tF_{BS} + {}^{t+\Delta t}_tF_{US})\ \delta_t v_0\ d^tx + \int_{{}^tL} ({}^{t+\Delta t}_tF_{LS}\ \delta_t u_0\ d^tx = \delta^{t+\Delta t}W_{ext} \tag{6.91}$$

Considering Eqs. (6.18) to (6.24) and (6.41) and ignoring the higher order terms, the first term in Eq. (6.91) becomes

$$I = \int_{{}^tL} (({}^tK_1\ {}_t\varepsilon_0^L + {}^tK_3\ {}_t\phi^L)\ \delta_t\varepsilon_0^L + ({}^tK_3\ {}_t\varepsilon_0^L + {}^tK_2\ {}_t\phi^L)\ \delta_t\phi^L)\ d^tx + \int_{{}^tL} ({}^tF\ \delta_t\varepsilon_0^{NL} + {}^tM\ \delta_t\phi^{NL})\ d^tx + \int_{{}^tL} ({}^tF\ \delta_t\varepsilon_0^L + {}^tM\ \delta_t\phi^L)\ d^tx \tag{6.92}$$

where ${}^tF$ and ${}^tM$ are defined in Eqs. (6.22) and (6.23). Substituting Eqs. (6.92) and (6.89) into Eq. (6.91), it becomes identical with Eq. (6.90) except that the cross-sectional stiffness coefficients and total internal forces are defined in Eqs. (6.42) to (6.44), (6.22) and (6.23) for the ISPDR technique, while they are defined in Eq. (6.87) and (6.88) for the RMDI technique.

6.7 FINITE ELEMENT DISCRETIZATION

Having the incremental virtual work equation established in Eq. (6.90), which is applicable to both the RMDI and ISPDR techniques with properly defined cross-sectional stiffness coefficients and internal forces, the finite element discretization can be carried out. The discretization procedure includes : interpolation of the displacements; matrix expressions of strain-displacement and constitutive relations; matrix expressions of spring deformation-displacement and spring force-deformation relations; and, finally, the finite element equilibrium equations with the stiffness matrices and load vectors properly defined.

Each of these aspects will be discussed in the following sub-sections.

6.7.1 Interpolation of Displacements

A pipeline-beam element is shown in Fig. 6.9 where three nodes are used and three degrees of freedom ${}^t u$, ${}^t v$ and ${}^t\theta$ are assigned to each node. The dimensionless local coordinate ${}^t r$ is introduced for convenience which is defined as

$$ {}^t r = \frac{2\,{}^t x}{{}^t L} \tag{6.93} $$

where ${}^t L$ is the current length of the element. The displacement increments in local coordinate system can be expressed as

$$ \begin{Bmatrix} {}_t u_0 \\ {}_t v_0 \end{Bmatrix} = \left[{}^t \mathbf{H} \right] \{ {}_t \mathbf{u}_e \} \tag{6.94a} $$

where

$$ \left[{}^t \mathbf{H} \right] = \begin{bmatrix} {}^t H_1 & 0 & 0 & {}^t H_4 & 0 & 0 & {}^t H_7 & 0 & 0 \\ 0 & {}^t H_2 & {}^t H_3 & 0 & {}^t H_5 & {}^t H_6 & 0 & {}^t H_8 & {}^t H_9 \end{bmatrix} \tag{6.94b} $$

$$ \langle {}_t \mathbf{u}_e \rangle = \langle\, {}_t u_1 \quad {}_t v_1 \quad {}_t \theta_1 \quad {}_t u_2 \quad {}_t v_2 \quad {}_t \theta_2 \quad {}_t u_3 \quad {}_t v_3 \quad {}_t \theta_3 \,\rangle \tag{6.95} $$

In matrix expressions, bold characters represent matrices and vectors, and plain characters represent their components. In addition, { } represents a column vector, < > represent a row vector, and [ ] is used for matrices.

The interpolation functions in Eq. (6.94b) are defined as

$$ {}^t H_1 = -\frac{1}{2}\,{}^t r\,(1 - {}^t r) \tag{6.96a} $$

$$ {}^t H_2 = \frac{3}{4}\,{}^t r^2\,(1 - {}^t r)^2\,(\,{}^t r + \frac{3}{4}\,) \tag{6.96b} $$

$$ {}^t H_3 = \frac{{}^t L}{8}\,{}^t r^2\,(1 - {}^t r)^2\,(1 + {}^t r) \tag{6.96c} $$

$$ {}^t H_4 = (1 - {}^t r^2) \tag{6.96d} $$

$$ {}^t H_5 = (1 - {}^t r^2)^2 \tag{6.96e} $$

$$ {}^{t}H_6 = \frac{{}^{t}L}{2}\,{}^{t}r\,(1 - {}^{t}r^2)^2 \tag{6.96f} $$

$$ {}^{t}H_7 = \frac{1}{2}\,{}^{t}r\,(1 + {}^{t}r) \tag{6.96g} $$

$$ {}^{t}H_8 = -\frac{3}{4}\,{}^{t}r^2\,(1 + {}^{t}r)^2\,({}^{t}r - \frac{3}{4}) \tag{6.96h} $$

$$ {}^{t}H_9 = -\frac{{}^{t}L}{8}\,{}^{t}r^2\,(1 + {}^{t}r)^2\,(1 - {}^{t}r) \tag{6.96i} $$

Since there are six displacement components associated with transverse displacement and three associated with longitudinal displacement, the interpolations are quadratic for longitudinal displacement and fifth order for transverse displacement. This is done for two reasons. One is that linearly varied axial strain is necessary to model the axial force distribution within the element. The other is that the minimum length of the element is limited by the principal wavelength because of the size dependence of SPD relations as discussed in Sect. 4.4.4. Consequently, relatively higher order interpolation is beneficial to the convergence and accuracy of the element.

The nodal displacement increments in the local coordinate system can be obtained by the following transformation

$$ \{{}_t\mathbf{u}_e\} = \begin{bmatrix} [{}^t\mathbf{T}] & 0 & 0 \\ 0 & [{}^t\mathbf{T}] & 0 \\ 0 & 0 & [{}^t\mathbf{T}] \end{bmatrix} \{{}_t\tilde{\mathbf{u}}_e\} \tag{6.97} $$

where $\{{}_t\tilde{\mathbf{u}}_e\}$ is the nodal displacement increment vector in the global coordinate system, and

$$ [{}^t\mathbf{T}] = \begin{bmatrix} \cos{}^t\alpha & \sin{}^t\alpha & 0 \\ -\sin{}^t\alpha & \cos{}^t\alpha & 0 \\ 0 & 0 & 1 \end{bmatrix} \tag{6.98a} $$

with

$$ {}^t\alpha = \arcsin\left(\frac{{}^ty_3 - {}^ty_1}{{}^tL}\right) \tag{6.98b} $$

This is the incremental form of the element orientation. The differential form is defined in Eq. (6.5).

6.7.2 Strain-Displacement Matrices

The strains have been defined in Sect. 6.2 with linear components being defined in Eqs. (6.9) and (6.10) and nonlinear components in Eqs. (6.15) and (6.16). Substituting the discretized displacement increment in Eq. (6.94) into Eqs. (6.9) and (6.10), the linear strain components becomes

$$\begin{Bmatrix} {}_t\varepsilon_0^L \\ {}_t\phi^L \end{Bmatrix} = \left[{}^t\mathbf{B}^L\right]\{{}_t\mathbf{u}_e\} \tag{6.99}$$

where

$$\left[{}^t\mathbf{B}^L\right] = \begin{bmatrix} {}^tH_1' & 0 & 0 & {}^tH_4' & 0 & 0 & {}^tH_7' & 0 & 0 \\ 0 & {}^tH_2'' & {}^tH_3'' & 0 & {}^tH_5'' & {}^tH_6'' & 0 & {}^tH_8'' & {}^tH_9'' \end{bmatrix} \tag{6.100}$$

The single prime ' and double prime " in Eq. (6.100) represent the first and second order derivatives with respect to the local element coordinate ${}^tx$. Similarly, the nonlinear axial strain component can be expressed as

$${}_t\varepsilon_0^{NL} = \frac{1}{2}\langle{}_t\mathbf{u}_e\rangle\left[{}^t\mathbf{B}_1^{NL}\right]^T\left[{}^t\mathbf{B}_1^{NL}\right]\{{}_t\mathbf{u}_e\} \tag{6.101}$$

where

$$\left[{}^t\mathbf{B}_1^{NL}\right] = \begin{bmatrix} {}^tH_1' & 0 & 0 & {}^tH_4' & 0 & 0 & {}^tH_7' & 0 & 0 \\ 0 & {}^tH_2' & {}^tH_3' & 0 & {}^tH_5' & {}^tH_6' & 0 & {}^tH_8' & {}^tH_9' \end{bmatrix} \tag{6.102}$$

Applying variation on Eq. (6.101), the variation of nonlinear strain increments becomes

$$\delta_t\varepsilon_0^{NL} = \langle\delta_t\mathbf{u}_e\rangle\left[{}^t\mathbf{B}_1^{NL}\right]^T\left[{}^t\mathbf{B}_1^{NL}\right]\{{}_t\mathbf{u}_e\} \tag{6.103}$$

The variation of the nonlinear curvature increment can be expressed as

$$\delta_t\phi^{NL} = \langle\delta_t\mathbf{u}_e\rangle\left[{}^t\mathbf{B}^L\right]^T\left[{}^t\mathbf{B}_2^{NL}\right]\{{}_t\mathbf{u}_e\} \tag{6.104}$$

where

$$\left[{}^t\mathbf{B}_2^{NL}\right] = \begin{bmatrix} 0 & {}^tH_2'' & {}^tH_3'' & 0 & {}^tH_5'' & {}^tH_6'' & 0 & {}^tH_8'' & {}^tH_9'' \\ {}^tH_1' & 0 & 0 & {}^tH_4' & 0 & 0 & {}^tH_7' & 0 & 0 \end{bmatrix} \tag{6.105}$$

The deformation of soil springs are defined in Eqs. (6.77) to (6.79) which can be expressed in terms of nodal displacement increments as

$$\begin{Bmatrix} {}_t\Delta_{LS} \\ {}_t\Delta_{BS} \\ {}_t\Delta_{US} \end{Bmatrix} = \left[{}^t\mathbf{B}^S\right]\{{}_t\mathbf{u}_e\} \tag{6.106a}$$

where

$$\left[{}^t\mathbf{B}^S\right] = \begin{bmatrix} -{}^tH_1 & 0 & 0 & & -{}^tH_7 & 0 & 0 \\ 0 & -{}^tH_2(1-\xi) & -{}^tH_3(1-\xi) & \cdots\cdots & 0 & -{}^tH_8(1-\xi) & -{}^tH_9(1-\xi) \\ 0 & -{}^tH_2\xi & -{}^tH_3\xi & & 0 & -{}^tH_8\xi & -{}^tH_9\xi \end{bmatrix} \tag{6.106b}$$

The parameter ξ in above equation is defined as

$$\xi = 0 \qquad \text{if } {}^td(r) = 0 \tag{6.107a}$$

$$\xi = 1 \qquad \text{if } {}^td(r) > 0 \tag{6.107b}$$

6.7.3 Finite Element Equilibrium Equations

Having displacements, pipe strains and spring deformations discretized in the previous two sections, the incremental virtual work equation established in Sect. 6.6 can be discretized to obtain the finite element equilibrium equations. Substituting Eqs. (6.94), (6.99), (6.103), (6.104) and (6.106) into Eq. (6.90), yields

$$\begin{aligned} &\sum \int_{{}^tL_e} <\delta_t\mathbf{u}_e>\left[{}^t\mathbf{B}^L\right]^T\left[{}^t\mathbf{D}^P\right]\left[{}^t\mathbf{B}^L\right]\{{}_t\mathbf{u}_e\}\,d^tx + \sum \int_{{}^tL_e} <\delta_t\mathbf{u}_e> \left(\left[{}^t\mathbf{B}_1^{NL}\right]^T\left[{}^t\mathbf{F}\right]\left[{}^t\mathbf{B}_1^{NL}\right]\right. \\ &\left. + \left[{}^t\mathbf{B}^L\right]^T\left[{}^t\mathbf{M}\right]\left[{}^t\mathbf{B}_2^{NL}\right]\right)\{{}_t\mathbf{u}_e\}\,d^tx + \sum \int_{{}^tL_e} <\delta_t\mathbf{u}_e>\left[{}^t\mathbf{H}\right]^T\left[{}^t\mathbf{D}^S\right]\left[{}^t\mathbf{B}^S\right]\{{}_t\mathbf{u}_e\}\,d^tx = \\ &\sum \left(<\delta_t\mathbf{u}_e>\left\{{}^t\mathbf{P}^e_{ext}\right\} - \int_{{}^tL_e} <\delta_t\mathbf{u}_e>\left[{}^t\mathbf{B}^L\right]^T\begin{Bmatrix} {}^tF \\ {}^tM \end{Bmatrix} d^tx - \int_{{}^tL_e} <\delta_t\mathbf{u}_e>\left[{}^t\mathbf{H}\right]^T\begin{Bmatrix} {}^tF_{LS} \\ {}^tF_{BS}+{}^tF_{US} \end{Bmatrix} d^tx \right) \end{aligned} \tag{6.108}$$

In this equation, the cross-sectional stiffness matrix for pipe and soil springs are defined as

$$\left[{}^{t}\mathbf{D}^{P}\right] = \begin{bmatrix} {}^{t}K_1 & {}^{t}K_3 \\ {}^{t}K_3 & {}^{t}K_2 \end{bmatrix} \tag{6.109}$$

$$\left[{}^{t}\mathbf{D}^{S}\right] = \begin{bmatrix} {}^{t}K_{LS} & 0 & 0 \\ 0 & {}^{t}K_{BS} & {}^{t}K_{LS} \end{bmatrix} \tag{6.110}$$

where ${}^{t}K_1$, ${}^{t}K_2$ and ${}^{t}K_3$ are defined by integrations in Eq. (6.87) for RMDI technique and by Eqs. (6.57) and (6.44) for ISPDR technique. The internal force matrices are defined as

$$\left[{}^{t}\mathbf{F}\right] = \begin{bmatrix} {}^{t}F & 0 \\ 0 & {}^{t}F \end{bmatrix} \tag{6.111a}$$

$$\left[{}^{t}\mathbf{M}\right] = \begin{bmatrix} {}^{t}M & 0 \\ 0 & {}^{t}M \end{bmatrix} \tag{6.111b}$$

where ${}^{t}F$ and ${}^{t}M$ are the equivalent total internal forces defined in Eq. (6.88) for the RMDI technique, and are the total internal forces defined in Eqs. (6.21) and (6.22) for the ISPDR technique.

The elastic-plastic stiffness matrix, geometric stiffness matrix, and soil spring stiffness matrix at the element level are defined, respectively, as

$$\left[{}^{t}\mathbf{K}^{e}_{EP}\right] = \int_{{}^{t}L_e} \left[{}^{t}\mathbf{B}^{L}\right]^{T}\left[{}^{t}\mathbf{D}^{P}\right]\left[{}^{t}\mathbf{B}^{L}\right] d^{t}x \tag{6.112a}$$

$$\left[{}^{t}\mathbf{K}^{e}_{G}\right] = \int_{{}^{t}L_e} \left(\left[{}^{t}\mathbf{B}_1^{NL}\right]^{T}\left[{}^{t}\mathbf{F}\right]\left[{}^{t}\mathbf{B}_1^{NL}\right] + \left[{}^{t}\mathbf{B}^{L}\right]^{T}\left[{}^{t}\mathbf{M}\right]\left[{}^{t}\mathbf{B}_2^{NL}\right]\right) d^{t}x \tag{6.112b}$$

$$\left[{}^{t}\mathbf{K}^{e}_{S}\right] = \int_{{}^{t}L_e} \left[{}^{t}\mathbf{H}\right]^{T}\left[{}^{t}\mathbf{D}^{S}\right]\left[{}^{t}\mathbf{B}^{S}\right] d^{t}x \tag{6.112c}$$

The element vectors of internal load for pipe and soil springs are defined as

$$\left\{{}^{t}\mathbf{Q}^{e}_{P}\right\} = \int_{{}^{t}L_e} \left[{}^{t}\mathbf{B}^{L}\right]^{T} \begin{Bmatrix} {}^{t}F \\ {}^{t}M \end{Bmatrix} d^{t}x \tag{6.113a}$$

$$\left\{{}^{t}\mathbf{Q}_{S}^{e}\right\} = \int_{{}^{t}L_e} \left[{}^{t}\mathbf{H}\right]^{T} \begin{Bmatrix} {}^{t}F_{LS} \\ {}^{t}F_{BS}+{}^{t}F_{US} \end{Bmatrix} d^{t}x \tag{6.113b}$$

Substituting Eqs. (6.112) and (6.113) into Eq. (6.108), yields

$$\begin{aligned} \sum <\delta_{t}\mathbf{u}_{e}> \left(\left[{}^{t}\mathbf{K}_{EP}^{e}\right] + \left[{}^{t}\mathbf{K}_{G}^{e}\right] + \left[{}^{t}\mathbf{K}_{S}^{e}\right] \right) \left\{{}_{t}\mathbf{u}_{e}\right\} &= \\ \sum <\delta_{t}\mathbf{u}_{e}> \left(\left\{{}^{t}\mathbf{P}_{ext}^{e}\right\} - \left\{{}^{t}\mathbf{Q}_{P}^{e}\right\} - \left\{{}^{t}\mathbf{Q}_{S}^{e}\right\} \right) & \end{aligned} \tag{6.114}$$

The transformations for element stiffness matrices and load vectors from the local element coordinate system to the global coordinate system are carried out, for example, as

$$\left[{}^{t}\widetilde{\mathbf{K}}_{EP}\right] = \begin{bmatrix} \left[{}^{t}\mathbf{T}\right] & 0 & 0 \\ 0 & \left[{}^{t}\mathbf{T}\right] & 0 \\ 0 & 0 & \left[{}^{t}\mathbf{T}\right] \end{bmatrix}^{T} \left[{}^{t}\mathbf{K}_{EP}^{e}\right] \begin{bmatrix} \left[{}^{t}\mathbf{T}\right] & 0 & 0 \\ 0 & \left[{}^{t}\mathbf{T}\right] & 0 \\ 0 & 0 & \left[{}^{t}\mathbf{T}\right] \end{bmatrix} \tag{6.115a}$$

and

$$\left\{{}^{t}\widetilde{\mathbf{Q}}_{P}\right\} = \begin{bmatrix} \left[{}^{t}\mathbf{T}\right] & 0 & 0 \\ 0 & \left[{}^{t}\mathbf{T}\right] & 0 \\ 0 & 0 & \left[{}^{t}\mathbf{T}\right] \end{bmatrix} \left\{{}^{t}\mathbf{Q}_{P}^{e}\right\} \tag{6.115b}$$

where $\left[{}^{t}\mathbf{T}\right]$ is defined in Eq. (6.98).

By the direct stiffness assembly procedure in the global coordinate system and applying variational principle, the incremental finite element equilibrium equations are obtained as

$$\left(\left[{}^{t}\widetilde{\mathbf{K}}_{EP}\right] + \left[{}^{t}\widetilde{\mathbf{K}}_{G}\right] + \left[{}^{t}\widetilde{\mathbf{K}}_{S}\right] \right) \left\{{}_{t}\widetilde{\mathbf{u}}\right\} = \left\{{}^{t}\widetilde{\mathbf{P}}_{ext}\right\} - \left\{{}^{t}\widetilde{\mathbf{Q}}_{P}\right\} - \left\{{}^{t}\widetilde{\mathbf{Q}}_{S}\right\} \tag{6.116}$$

6.8 DEVELOPMENT OF PROGRAM ABP AND VERIFICATION OF ISPDR TECHNIQUE

The finite element formulation of the pipeline-beam element has been presented in Sect. 6.7. Based on this formulation, a program for Analysis of Buried Pipelines (ABP) has been developed which can be used for settlement analysis in addition to analysis for normal operating load conditions. In this section, two problems will be addressed. One is

discussions on some aspects of the formulation which have not been covered in the previous sections, including the treatment of internal pressure and the solution technique. The other is the verification of the ISPDR technique. As has been proposed in Sect. 1.3.2.3, the verification can be carried out in two steps. The first step is to establish confidence in the RMDI technique implemented in program ABP by comparing the results of typical examples from the RMDI technique to those obtained from the program PIPLIN (Structural Software Development, Inc., 1989). Secondly, the ISPDR technique can be verified by comparing the results from the ISPDR technique with those from the RMDI technique. Direct comparison between the ISPDR technique and program PIPLIN cannot be obtained because program PIPLIN cannot provide sufficient information to construct SPD relations. Detailed discussions of these topics are presented in following sub-sections.

6.8.1 Internal Pressure

Internal pressure obviously causes hoop stress. This has been dealt with in the stress-strain relation for the pipeline-beam element in Sect. 6.3. If the pipeline is restrained the internal pressure also produces axial tensile force because of the Poisson's ratio effect. In addition, internal pressure would introduce transverse forces if the pipeline is not perfectly straight. For a perfectly straight pipeline, the axial forces due to internal pressure are absorbed in the region near the ends by the longitudinal restraint. However, if the pipeline is curved, transverse forces are introduced because of the direction change of the axial forces due to the internal pressure, and the magnitude of these transverse forces depends on the curvature. Because the axial forces due to internal pressure are always in the direction of the centroidal axis of pipeline, the effects of axial forces due to internal pressure are deformation dependent and should be treated as follower-type of loads.

In program ABP, the axial forces due to internal pressure are calculated based on the current deformed configuration. This means that updates are necessary in every solution step and every iteration for pressure induced axial forces. For a curved pipeline the associated transverse loads are evaluated and updated in this process.

6.8.2 Solution Technique

A special solution technique is employed for settlement analysis of buried pipelines because the deformation in the pipeline is activated by imposed differential settlement through the pipeline-soil interaction mechanisms. Arc-length control techniques, discussed in Sect. 3.2, cannot be directly and conveniently applied because there is no well defined

reference load in the settlement analysis. In settlement analysis, external loads are applied in the form of incremental differential settlement, i.e. the base of transverse soil springs, including bearing and uplifting springs, moves in the settlement zone from a equilibrium configuration. As a result, unbalanced forces are introduced which deform the pipeline to a new equilibrium configuration. Unfortunately, these unbalanced forces depend on the current states of the pipeline and soil springs and on the incremental settlement. Consequently, they can not be used as the reference load.

Newton-Raphson (N-R) iteration (see Sect. 3.1.2) cannot be directly applied either, because when the base of the transverse springs move, the pipeline in the settlement zone loses transverse support if the increment of differential settlement is larger than the accumulated deformation in the bearing springs. The deformations of bearing springs in most of the settlement zone are very small because they are introduced by overburden loads above the pipeline, and the efficiency would be unacceptably low if the increment of differential settlement is limited to be smaller than the deformation in the bearing springs. The displacement increment of an iteration can be very large if the pipeline loses transverse support in the settlement zone. This would certainly lead the iterative procedure to diverge. Therefore, N-R iterations, both full and modified N-R iteration, are not directly applicable to settlement analysis.

The solution technique used in program ABP is a full N-R iterative technique combined with an upper limit on the displacement increment acceptable for each iteration. This upper limit is introduced to prevent very large displacement increments due to loss of support in the settlement zone and to insure the convergence of the iterative procedure. The full N-R iterative technique is necessary because the stiffness of the pipeline-soil spring system varies all the time. When an increment of differential settlement is imposed, the pipeline is separated from bearing springs in the settlement zone which becomes inactive and unbalanced forces are introduced. The unbalanced forces deform the pipeline gradually and the pipeline starts to contact the bearing springs from the far end toward the transition zone as the deformation increases. In this process, the bearing springs gradually change from inactive to active and so does their stiffness. The modified N-R iterative technique is not able to take this change into account.

A proper value of the upper limit on the displacement increment for each iteration can be found by numerical experimentations. As an alternative, a rule based on experience is summarized here. For a given increment of differential settlement, find a solution step with any value of an upper limit as long as it converges. Then calculate the norm of the total

displacement increment for this solution step. One-third to half of this norm is usually a good value for the upper limit on incremental displacement for each iteration.

6.8.3 Comparison between Program ABP and PIPLIN

This section presents comparisons between the RMDI technique (See Sects. 1.3.2.1 and 6.3) in program ABP and program PIPLIN. This is the first step for the verification of the ISPDR technique (see Sects. 1.3.2.2, 1.3.2.3 and 6.4). PIPLIN is a program which has been commonly used in the pipeline industry for many years and is said to be the best commercial program available for pipeline analysis and design. Good agreement between the solutions from the RMDI technique in program ABP and from program PIPLIN would verify that program ABP, independently developed in this project, is reliable. The RMDI technique is similar to the solution technique in program PIPLIN because both of them have stress-strain constitutive relations, and plasticity theory based on the von Mises yield condition and the normality flow rule.

Two examples are used for comparison between programs ABP and PIPLIN. In the first example, a pipeline of 650 feet (198 m) in length subjected to differential settlement is analyzed. In the second example, a similar pipeline is analyzed when subjected to incremental temperature and internal pressure in addition to differential settlement. The pipeline has a diameter of 12.75 inches (324 mm) and wall thickness of 0.247 inches (6.27 mm). A stepwise transition zone is assumed in both examples with 275 feet (84 m) in the stable zone and 375 feet (114 m) in the settlement zone. The material properties of the pipeline and the soil properties are the same as those for some sections of the pipeline from Norman Wells to Zama (Canuck Engineering Ltd., 1983). The material property of the pipeline is nonlinear with elastic-plastic hardening. The finite element model is shown in Fig. 6.10 for both examples. Supplemental information needed for the second example is the increment of temperature 65 °F (36.1 °C), the expansion coefficient of 6.5×10^{-6}/°F (11.7×10^{-6}/°C) and the internal pressure of 1.44 ksi (9.93 MPa).

The examples in this section are grouped together with the examples in the following Sect. 6.8.4 as a series for verification, designated as the V-series. Therefore, the examples in this section are denoted as V1 and V2 for convenience, in which V2 includes the temperature and pressure effects and V1 does not.

The results of the RMDI technique in Program ABP are compared with those of program PIPLIN in terms of the deformed configurations, distributions of moment and

curvature and the development of critical moment and curvature with the increasing differential settlement. The *critical moment and curvature* is the moment and curvature at the corss-section with the maximum curvature along the pipeline which is located at about 30 inches (762 mm) from the step discontinuity, in the stable zone, for both examples. Comparisons are shown in Figs. 6.11 to 6.15 for example V1 and in Figs. 6.16 to 6.20 for example V2. The deformed configurations and distributions of moment and curvature are taken at a differential settlement of 40 inches (1016 mm) which is the representative upper-bound on differential settlement. Excellent agreement has been found between the two sets of solution for both examples. This establishes the creditability of, and confidence in, the RMDI technique implemented in program ABP.

6.8.4 Comparison between ISPDR and RMDI Techniques

Comparison between the ISPDR technique (see Sects. 1.3.2.1 and 6.3) and the RMDI technique (see Sects. 1.3.2.2 and 6.4) is the second step to verify the ISPDR technique to be applicable to settlement analysis of pipelines. The question about the applicability of the ISPDR technique arises from the fact that the stiffness of the pipe is calculated from two separate integration processes in the ISPDR technique. These are : the integration over the cross-section in the generation procedure of the SPD relations; and, the integration over the length in the solution procedure. Different deformation paths in the generation procedure, from those in the solution procedure, lead to the concerns on the applicability of the ISPDR technique. Good comparison would demonstrate that the effects of the differences in deformation paths are small and verify the applicability of the ISPDR technique in settlement analysis of pipelines.

Comparison is carried out between the results of RMDI and ISPDR techniques for two typical examples. The examples are for a pipeline subjected to differential settlement with two different sets of material properties. The first example has the normal pipe material properties specified as an elastic-plastic hardening (EPH) stress-strain relationship, and the second one has a set of assumed material properties with an elastic-plastic softening (EPS) stress-strain relationship. This latter example is used to simulate softening similar to postbuckling behavior of thin shells. These two examples are denoted as V3 and V4, respectively. Neither of these examples includes temperature or pressure effects. The difference between them is confined to the type of material properties.

The solutions of the RMDI technique are straightforward to obtain, while those of the ISPDR technique involve the separation of the two procedures, namely, the generation

procedure and the solution procedure. In normal application of the ISPDR technique, a three-dimensional shell model has to be used to generate the SPD relations. However, for validation purposes, the RMDI technique of the beam model can be used with a softening material. This eliminates all the differences between the solution from the ISPDR technique and that from the RMDI technique except the difference of deformation paths between the generation and solution procedures.

The beam model for generation of SPD relations is shown in Fig. 6.21 where a pipe segment of 60 inches (1524 mm) is loaded as a simply supported beam. The pipe has a diameter of 12.75 inches (324 mm) and wall thickness of 0.247 inches (6.27 mm). A 20 inch (508 mm) segment in the center has been used to construct the SPD relations where a length of 20 inches (508 mm) is picked as the principal wavelength. The principal wavelength is less significant in this particular case because no local buckling will be present in the beam model. The loading condition is bending moment combined with constant axial force at four and five different levels, for examples V3 and V4, respectively. At each of these levels, there are five SPD relations to be constructed as discussed in Sect. 6.4.3. This produces twenty and twenty five SPD relations for the EPH and EPS materials, respectively. The generated SPD relations are shown in Figs. 6.22 to 6.26 for the EPH material and in Figs. 6.27 to 6.31 for the EPS material. These figures are graphical representations of properties 1 to 5 defined in Eqs. (6.45) to (6.49) in Sect. 6.4.1. They are in piecewise linear form and are appropriate idealizations created to be used as input for the solution procedure of the ISPDR technique.

The finite element model for the settlement analysis in examples V3 and V4 is the same as the model used for examples V1 and V2 (Fig. 6.10) except that the properties of the uplift springs are changed to be the same as those of the bearing springs. The length of elements in the regions adjacent to the transition zone is 20 inches (508 mm) which corresponds to the principal wavelength used to construct the SPD relations. Comparisons of the results from the RMDI and ISPDR techniques are presented in terms of the deformed configurations, distributions of moment and curvature, and the development of critical moment and curvature with the increasing differential settlement. Figs. 6.32 to 6.36 show the comparisons for example V3 and Figs. 6.37 to 6.41 for example V4. The deformed configuration and distributions of moment and curvature are taken at differential settlements of 34 inches (864 mm) and 44 inches (1118 mm) for examples V3 and V4, respectively. Excellent agreement, in general, has been found between these two sets of solution.

Based on the two-step verification in the previous and current sections, it can be

concluded that the ISPDR technique in program ABP is applicable to settlement analysis of buried pipelines and the accuracy is good enough for engineering prediction of the behavior of pipelines even though some approximaticns are adopted. In addition, the program ABP developed in this project has been shown to provide correct results..

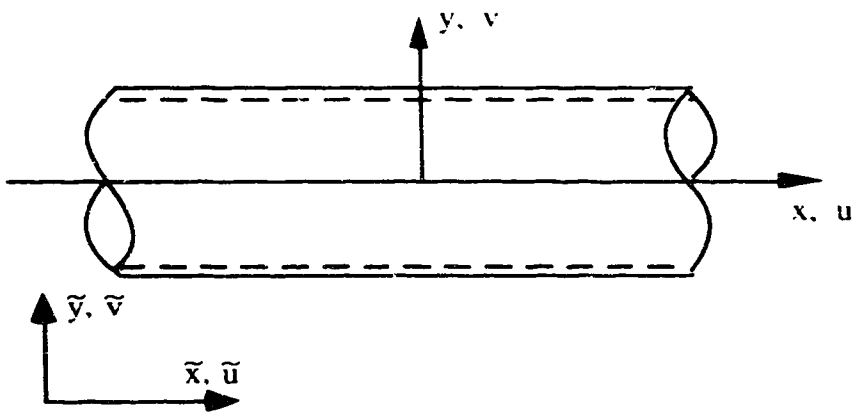

Fig. 6.1 Coordinate Systems and Displacements

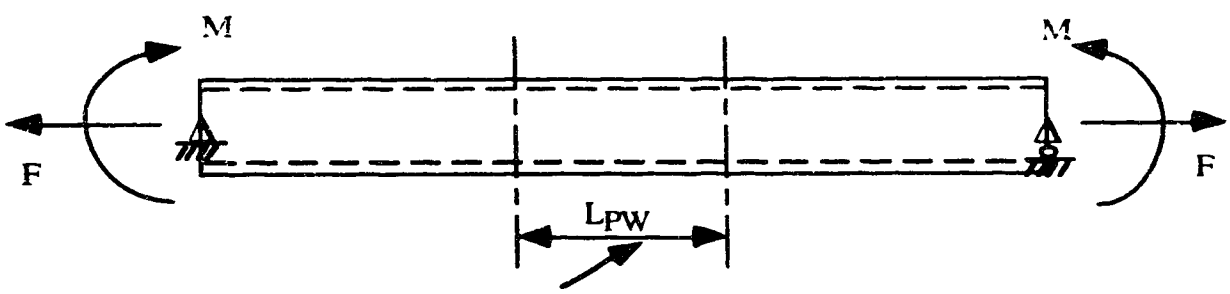

The segment includs the principal buckle and on its average response the SPD relations are constructed

note: L_{PW} is the principal wavelength
F is the constant axial force
M is the increasing moment
The pipe segment is discretized by shell elements

Fig. 6.2 Loading and Boundary Conditions of the Shell Model for Generation of SPD Relations

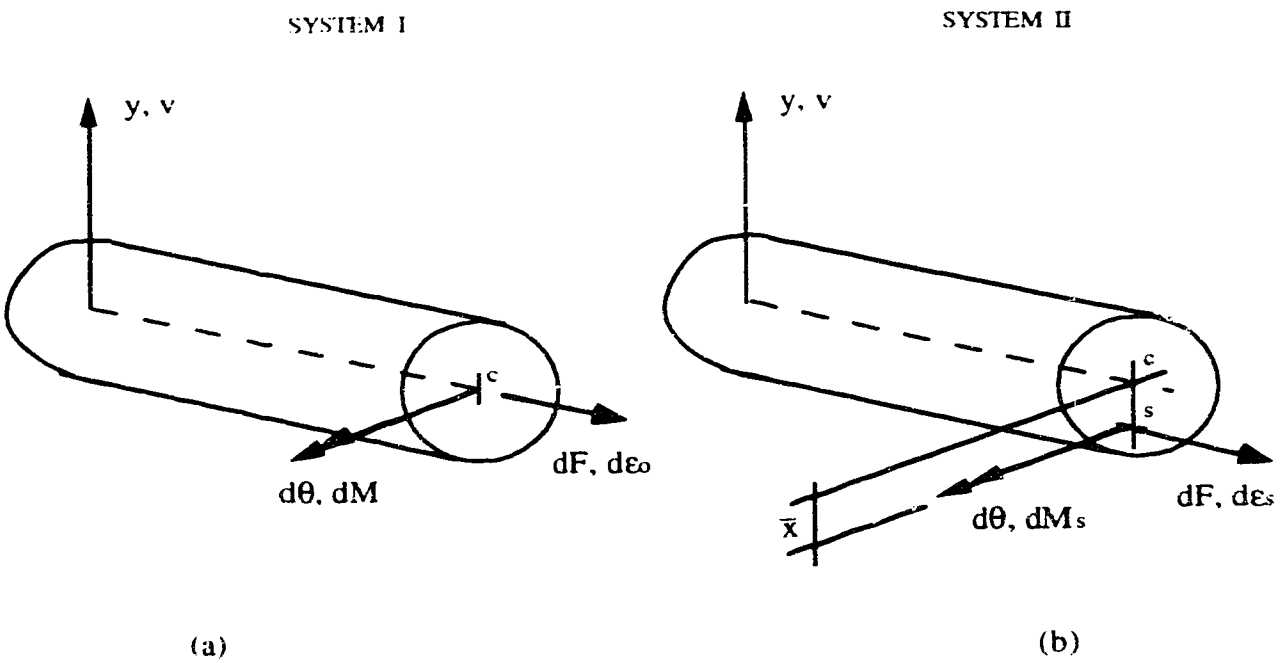

Fig. 6.3 Two Reference Systems on Pipe Cross-Sections

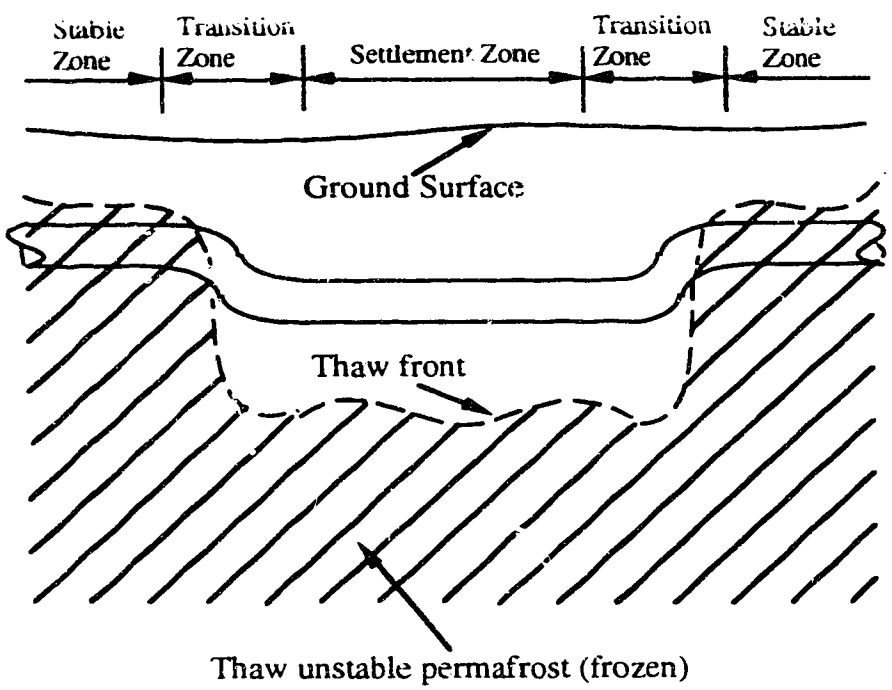

Fig. 6.4 Differential Thaw Settlement Due to Non-Uniform Thaw Front

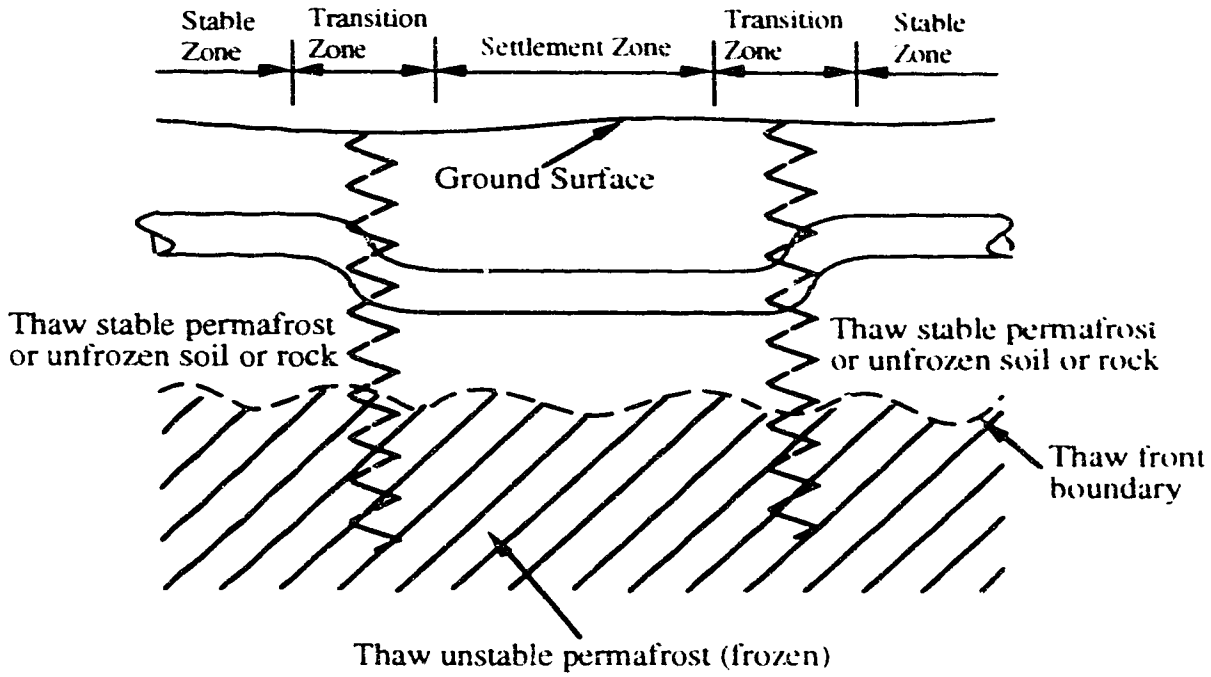

Fig. 6.5 Differential Thaw Settlement Due to Non-Uniform Thaw Settlement Soil Properties

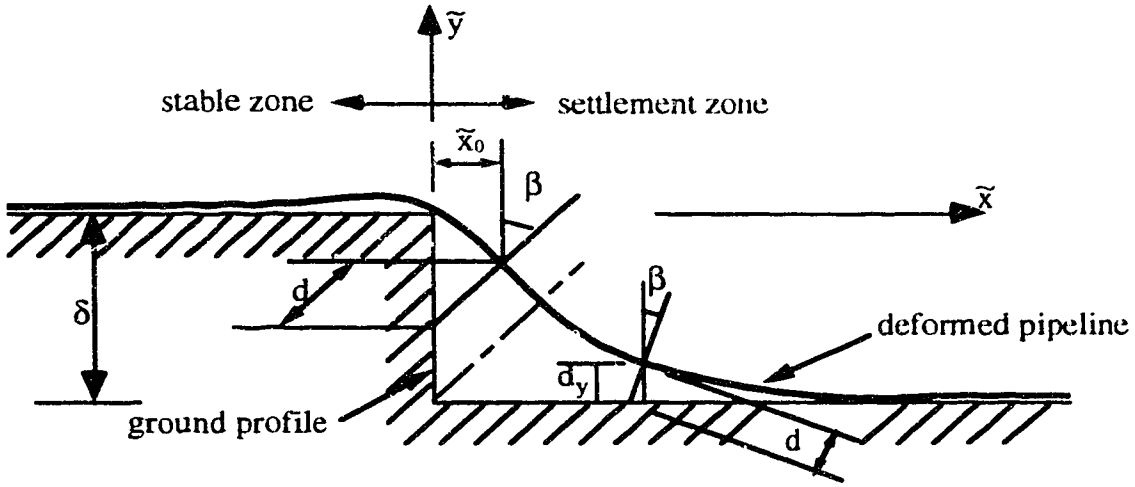

Fig. 6.6 The Step-Wise Ground Profile and Definition of the Gap Width

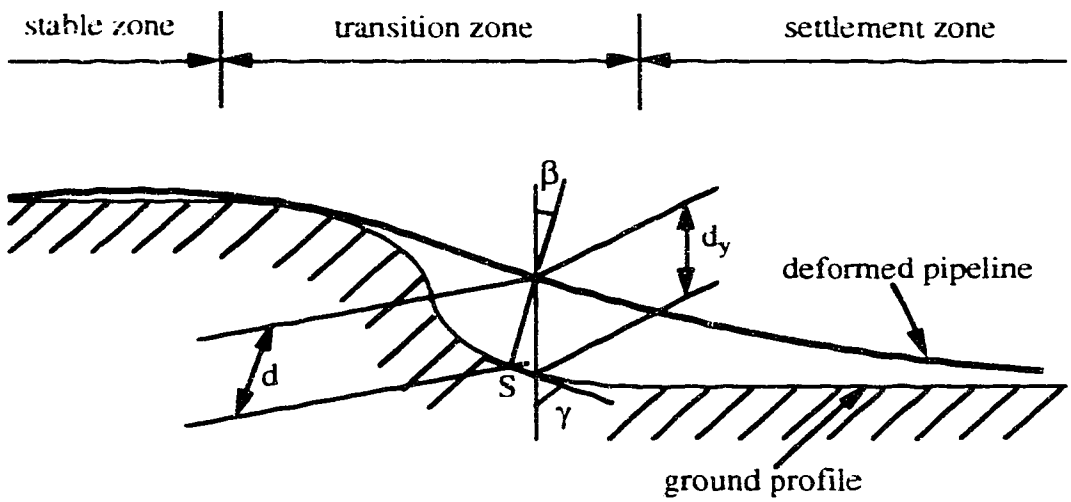

Fig. 6.7 The Smooth Ground Profile and Definition of the Gap Width

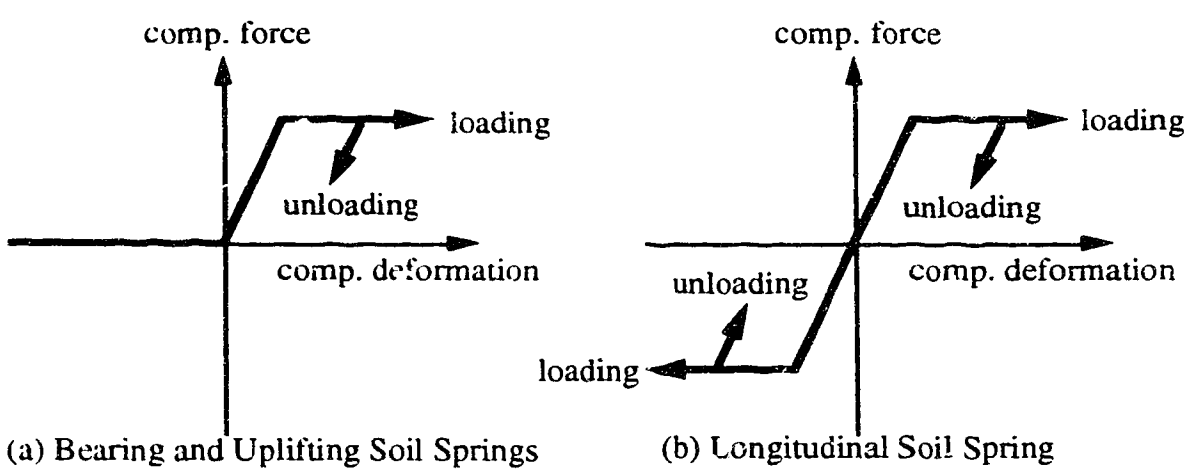

(a) Bearing and Uplifting Soil Springs (b) Longitudinal Soil Spring

Fig. 6.8 Typical Constitutive Relations for Soil Springs

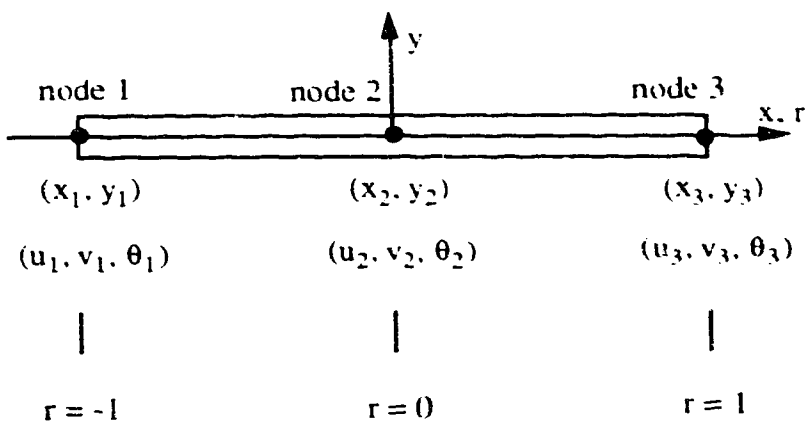

Fig. 6.9 Nodal Configuration of the Pipeline-Beam Element

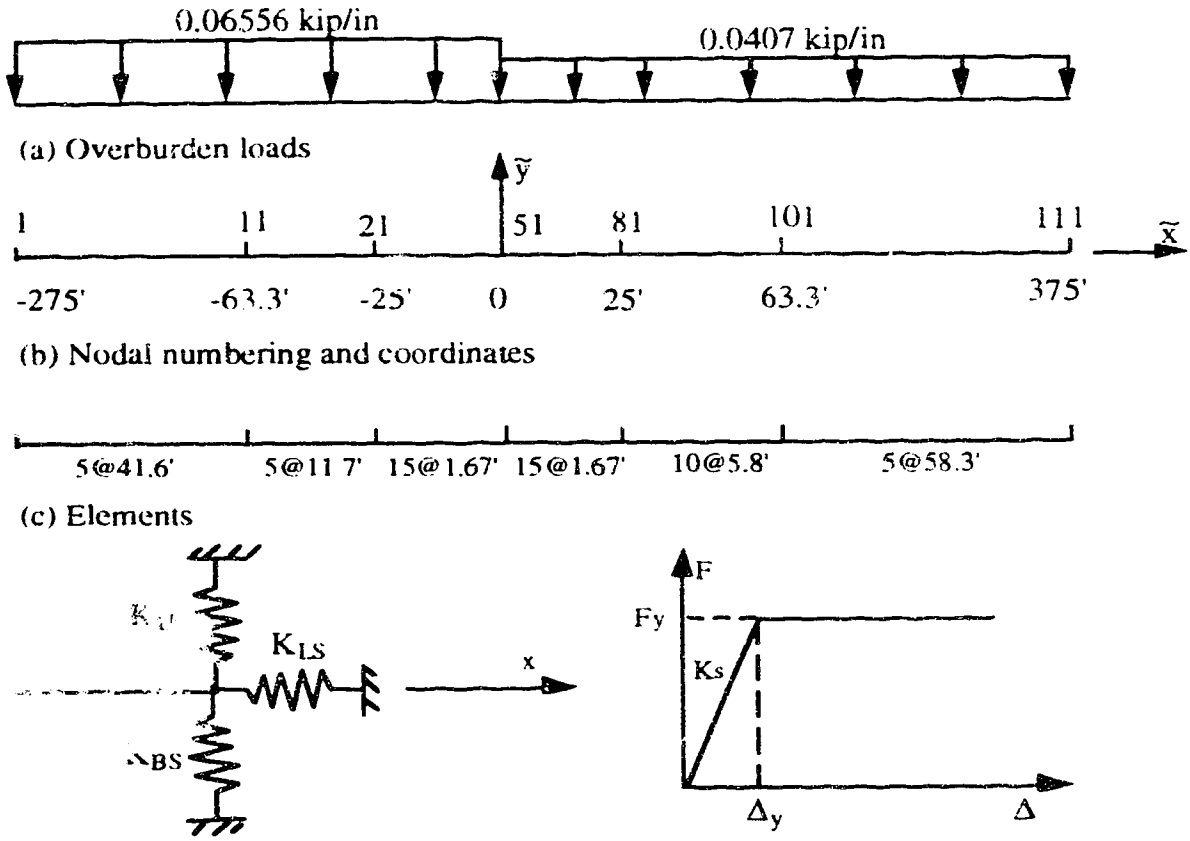

(d) Soil springs distributed over the length (e) Soil spring characteristics

Bearing Spring	Uplifting Spring	Longitudinal Spring
$K_{BS} = 0.83$ kis $\Delta_{By} = 1.2$ in $F_{By} = 1.0$ kip/in	For $\tilde{x} \le 0$ $K_{US} = 0.42$ kis $\Delta_{Uy} = 1.2$ in $F_{Uy} = 0.5$ kip/in	For $\tilde{x} \le -25'$ and $\tilde{x} \ge 25'$ $K_{LS} = 1.0$ kis $\Delta_{Ly} = 0.25$ in $F_{Ly} = 0.25$ kip/in
	For $\tilde{x} > 0$ $K_{US} = 0.0083$ kis $\Delta_{Uy} =$ [illegible] in $F_{Uy} = 0.001$ kip/in	For $-25' < \tilde{x} < 25'$ $K_{LS} = 0.2$ kis $\Delta_{Ly} = 0.25$ in $F_{Ly} = 0.05$ kip/in

(f) Soil spring properies

stress (kis)	40.0	48.0	52.0	70.0
strain (%)	0.137	0.210	0.500	5.09

(g) Stress-strain relation for pipe

Fig. 6.10 Finite Element Model for Settlement Analysis of the Pipelines

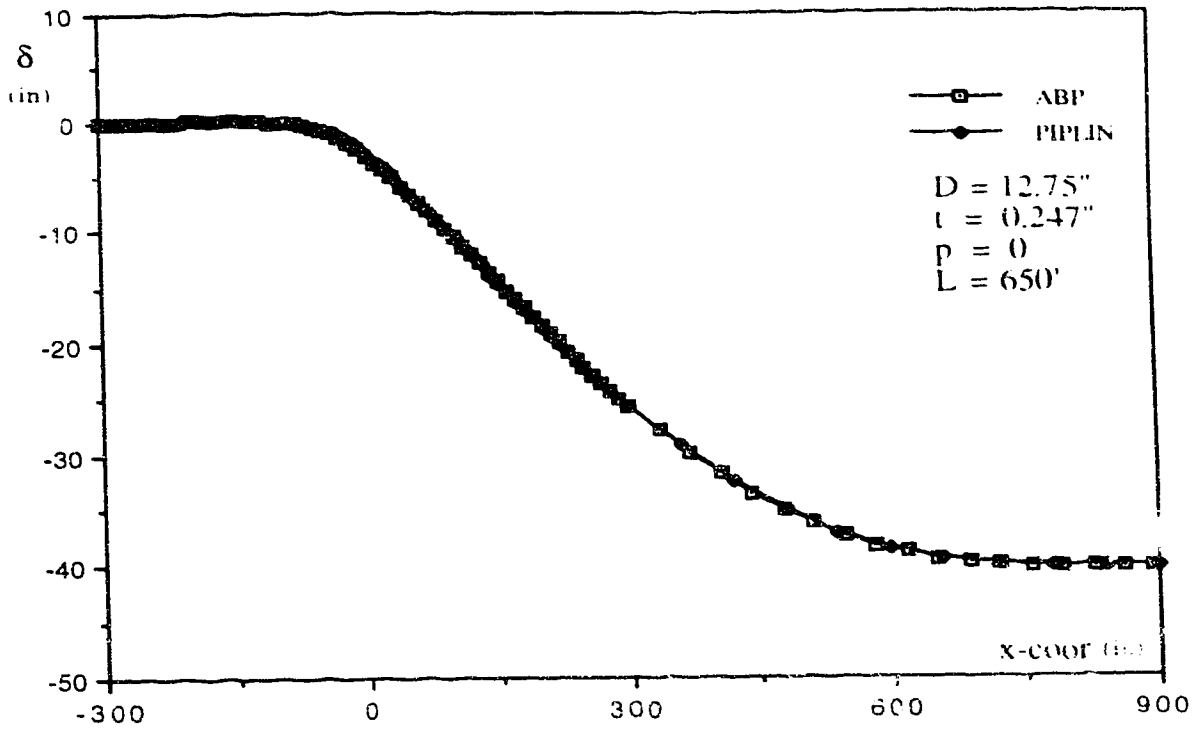

Fig. 6.11 Comparison of Deformed Configuration of Example V1

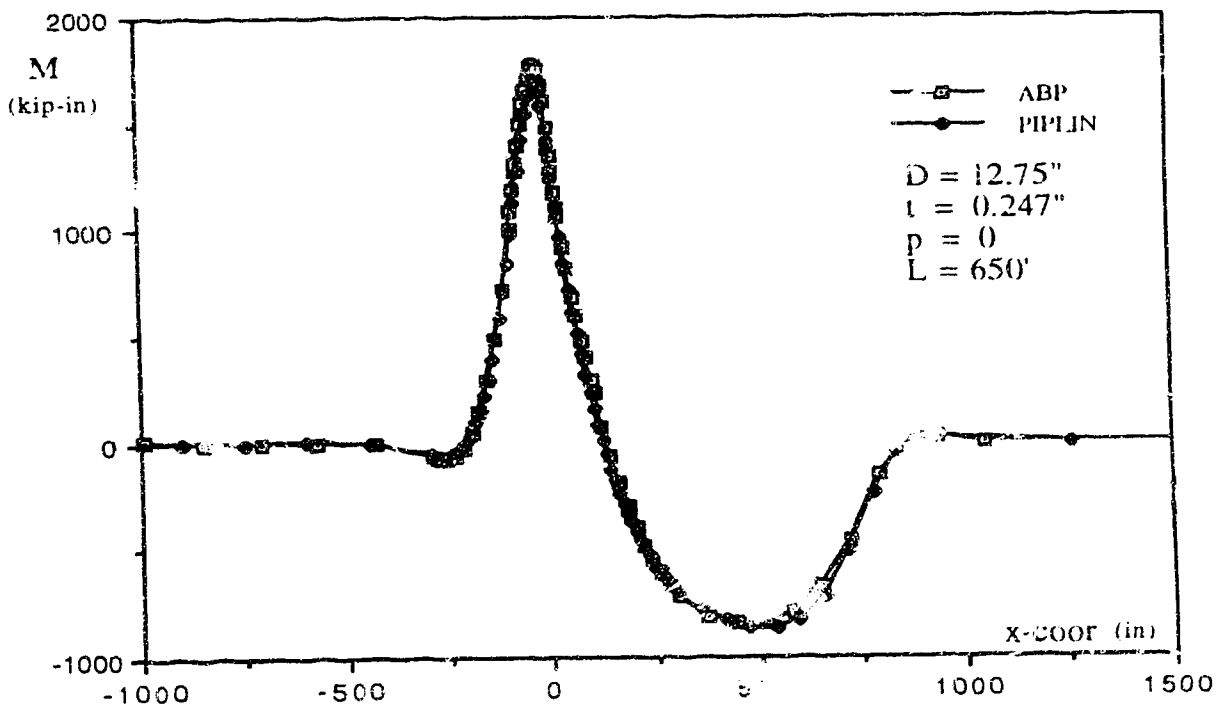

Fig. 6.12 Comparison of Moment Distributions of Example V1

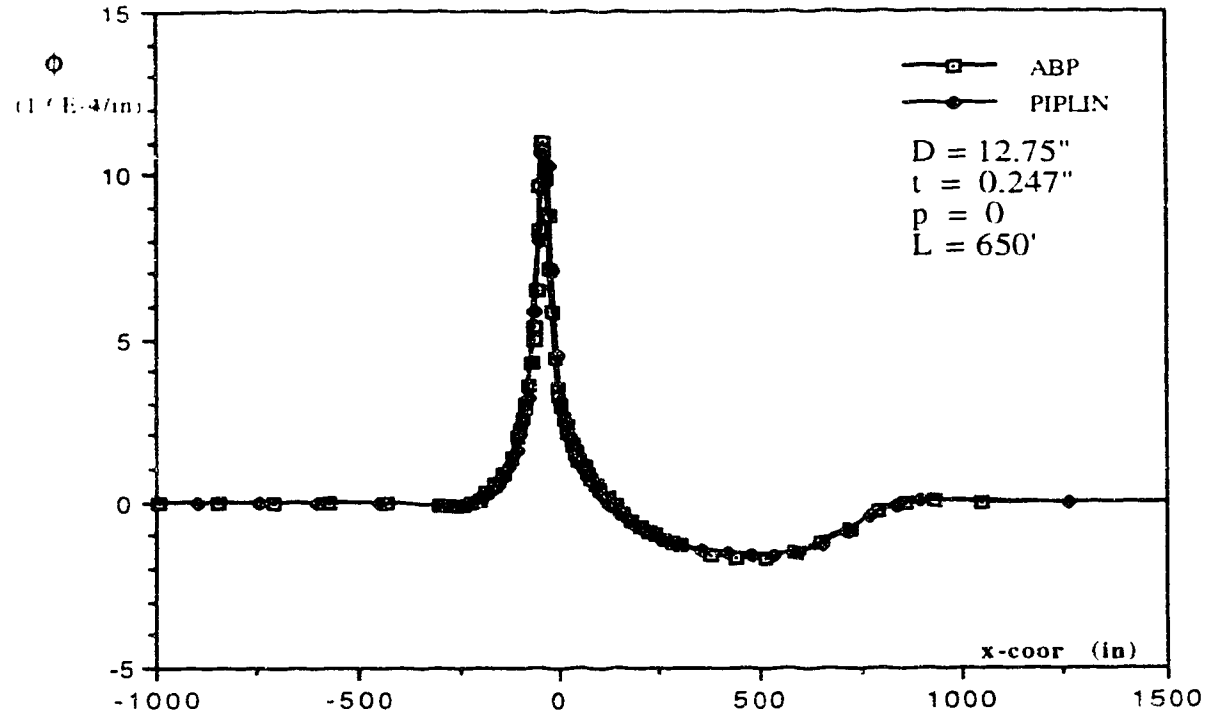

Fig. 6.13 Comparison of Curvature Distributions of Example V1

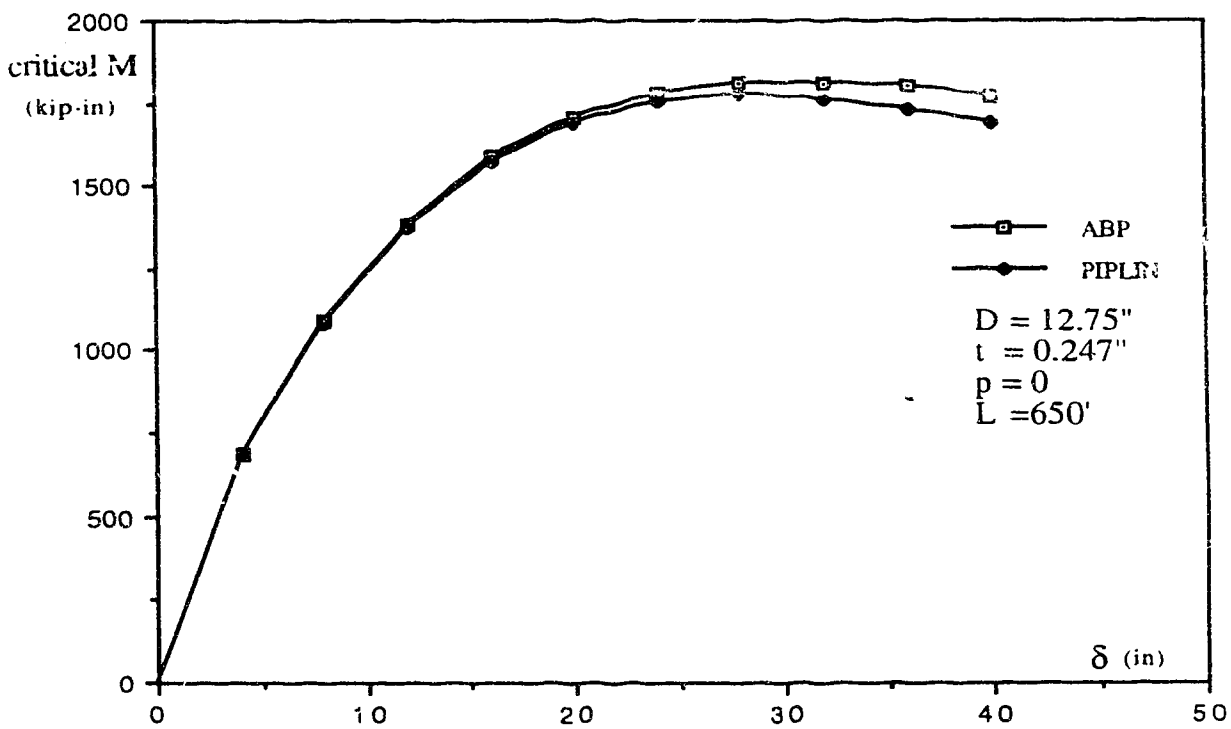

Fig. 6.14 Comparison of Critical Moment-Settlement Curves of Example V1

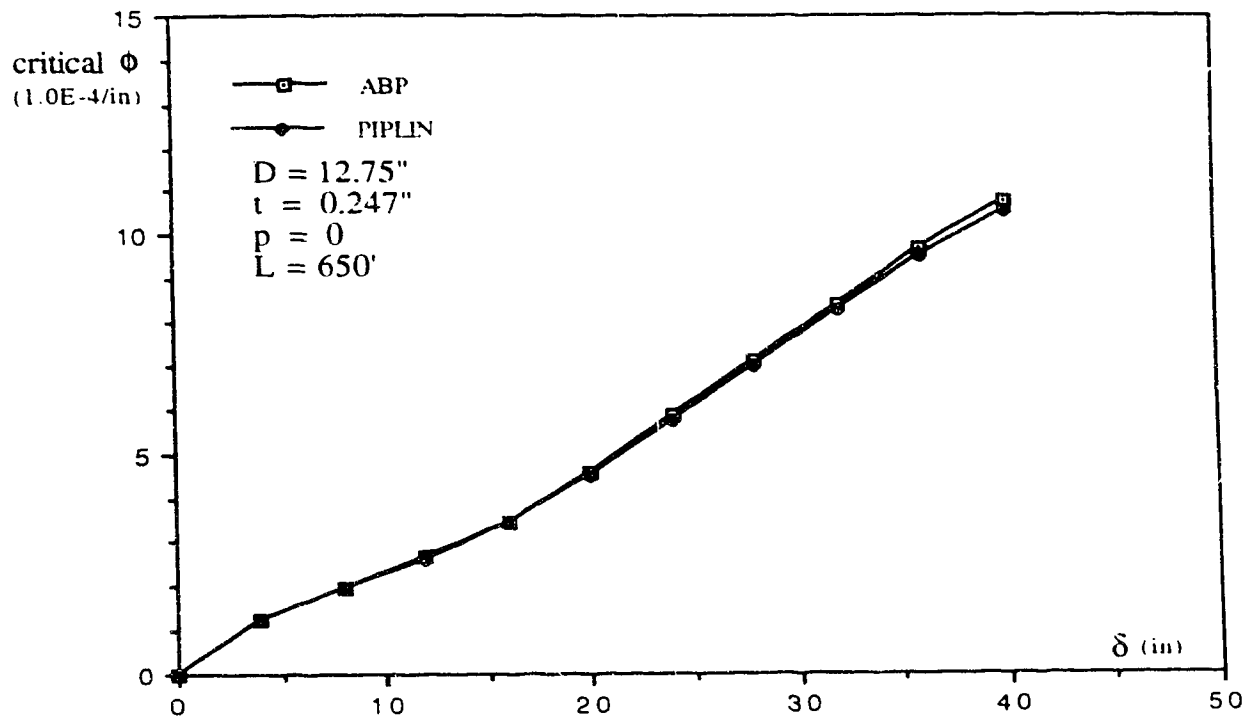

Fig. 6.15 Comparison of Critical Curvature-Settlement Curves of Example V1

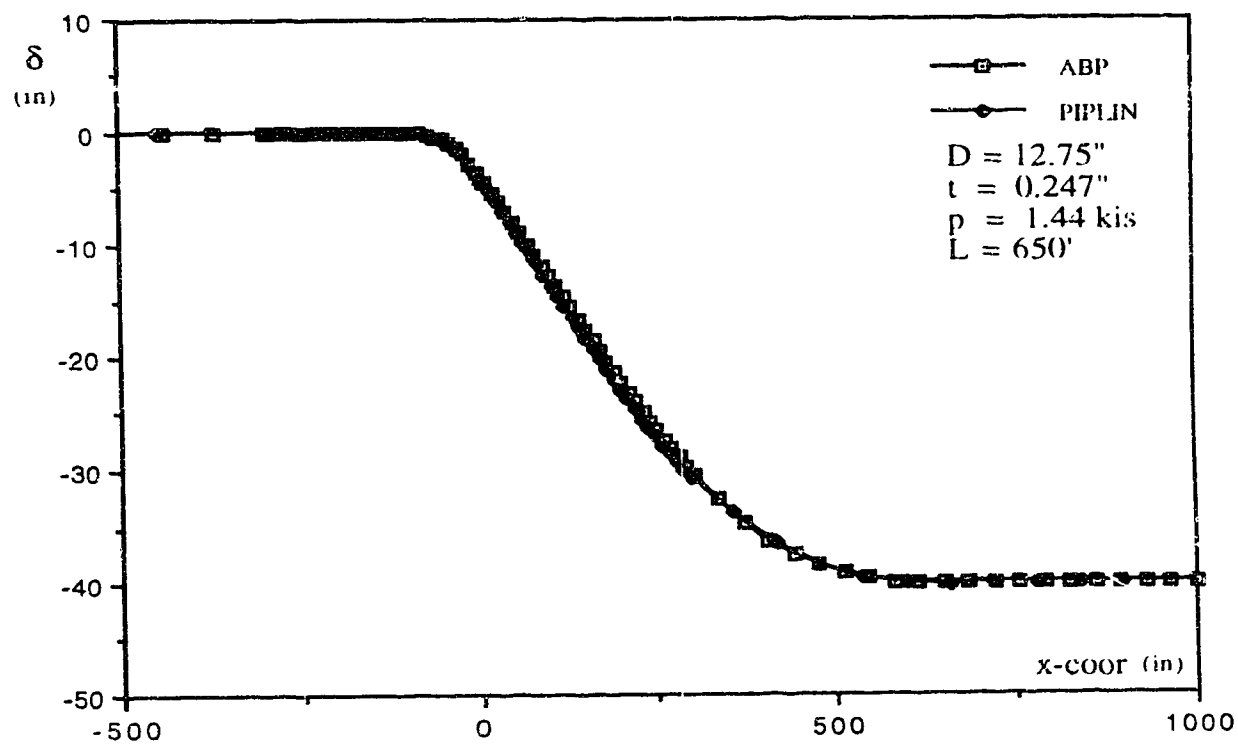

Fig. 6.16 Comparison of Deformed Configurations of Example V2

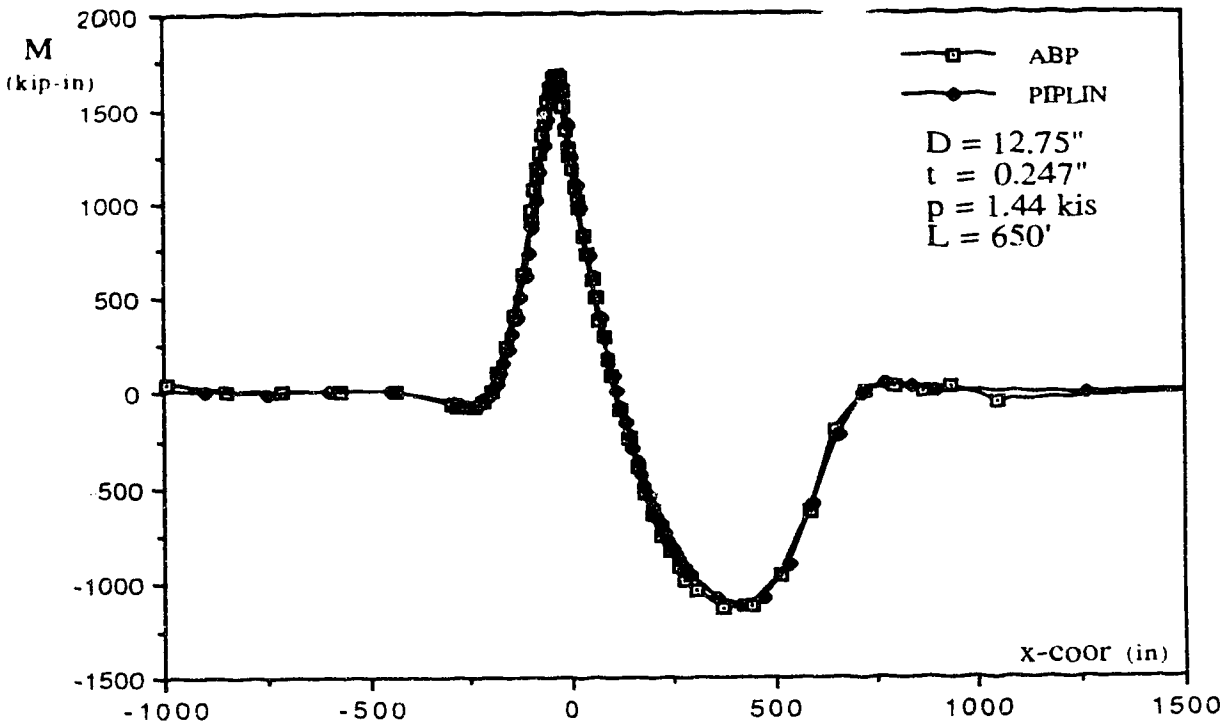

Fig. 6.17 Comparison of Moment Distributions of Example V2

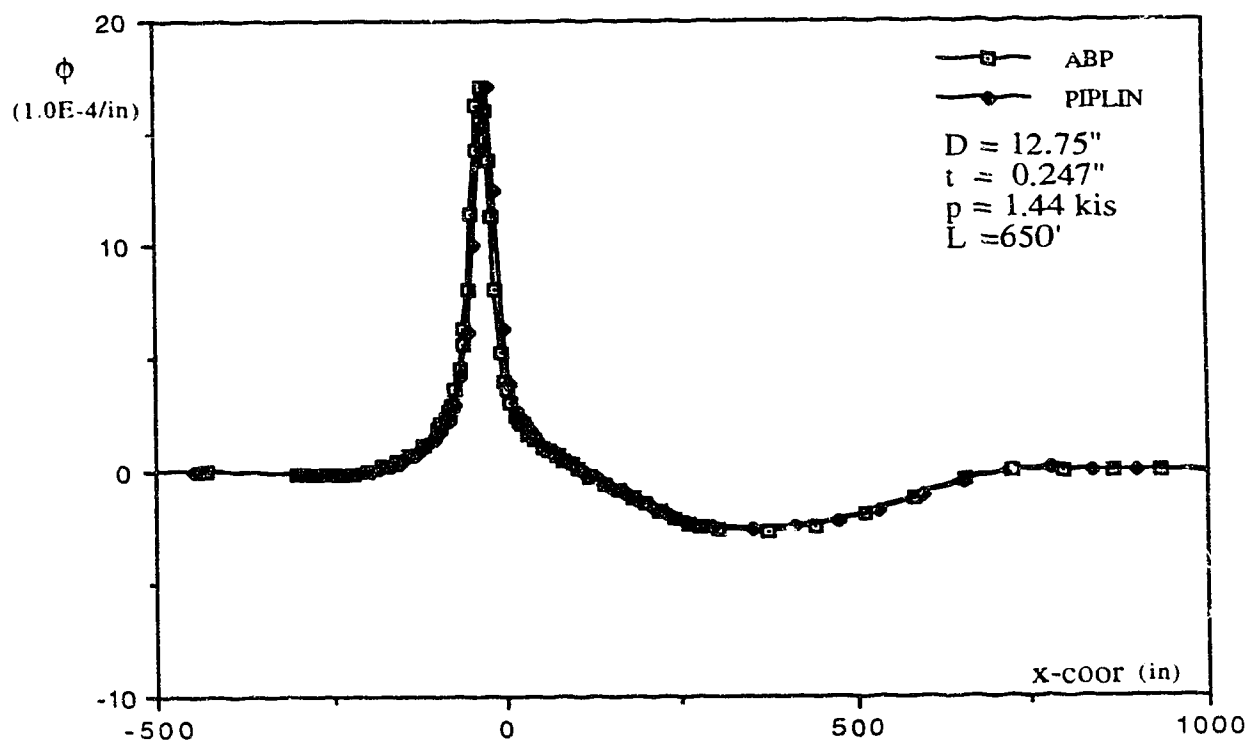

Fig. 6.18 Comparison of Curvature Distributions of Example V2

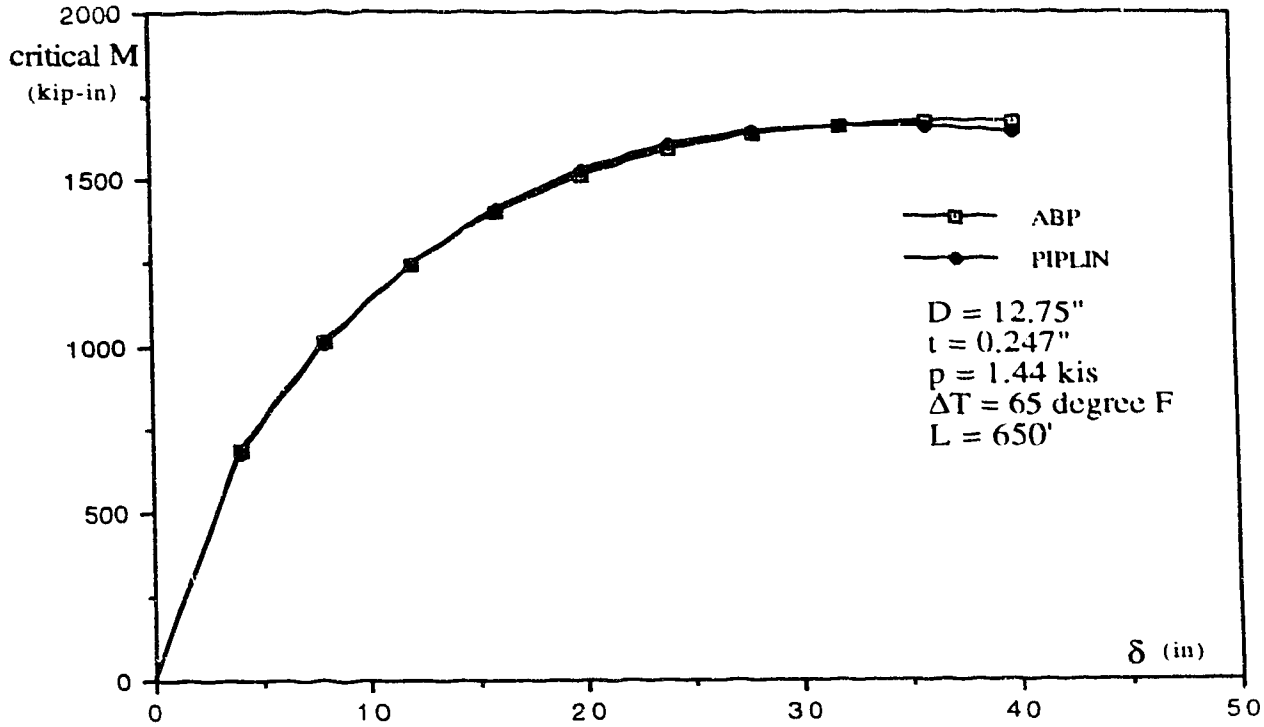

Fig. 6.19 Comparison of Critical Moment-Settlement Curves of Example V2

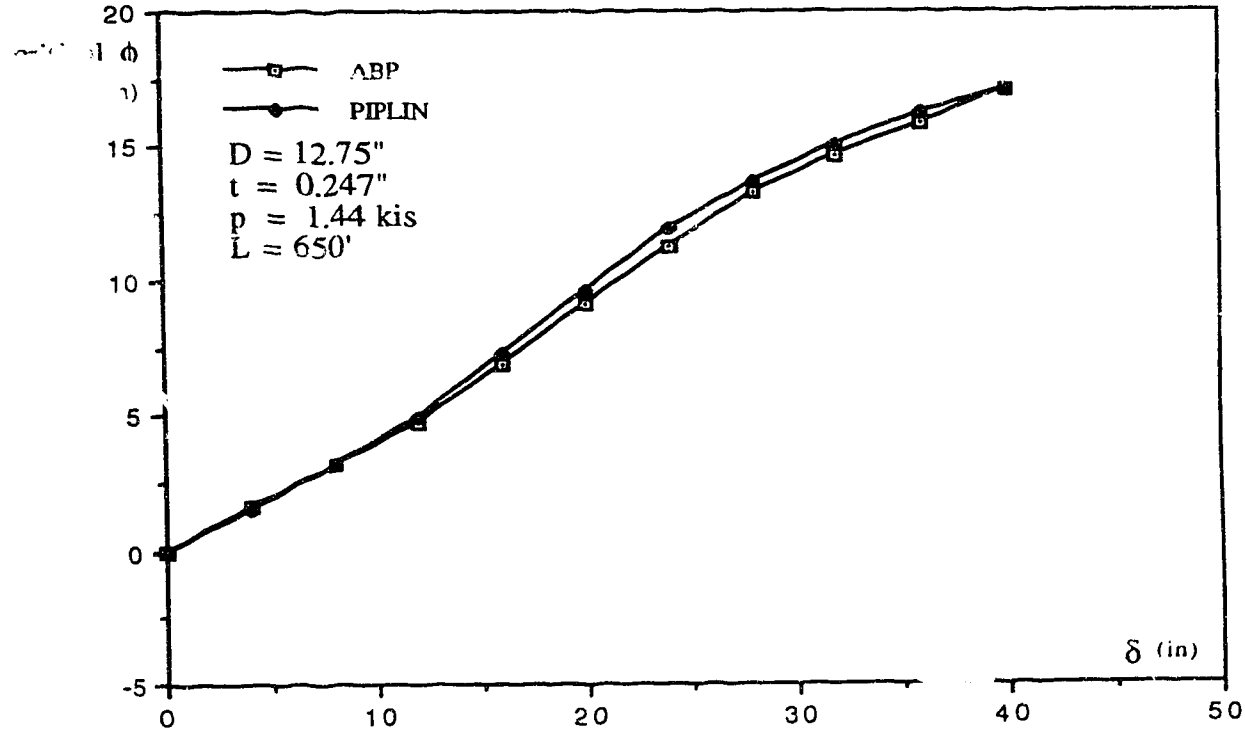

Fig. 6.20 Comparison of Critical Curvature-Settlement Curves of Example V2

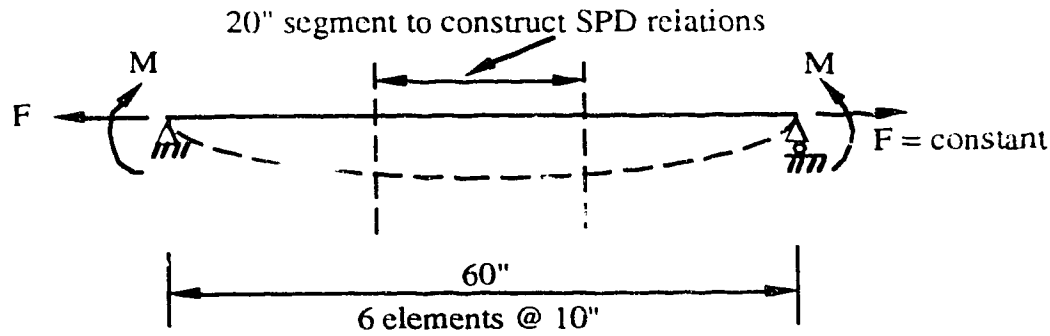

(a) Dimensions, loading and boundary conditions

EPH	stress (kis)	0	40.0	48.0	52.0	70.0	
	strain (%)	0	0.137	0.210	0.500	5.09	
EPS	stress (kis)	0	40.0	48.0	50.0	40.0	22.0
	strain (%)	0	0.137	0.210	0.355	0.500	5.09

(b) Stress-strain relations for EPH and EPS materials

Level	F/F_y	F (kip)
1	-40%	-158.30
2	-20%	-79.15
3	0%	0
4	20%	79.15
5	40%	158.30

note : F_y = 395.75 (kip) is the axial yielding force

(c) Load levels of constant axial load

Fig. 6.21 Beam Model for Generation of SPD Relations

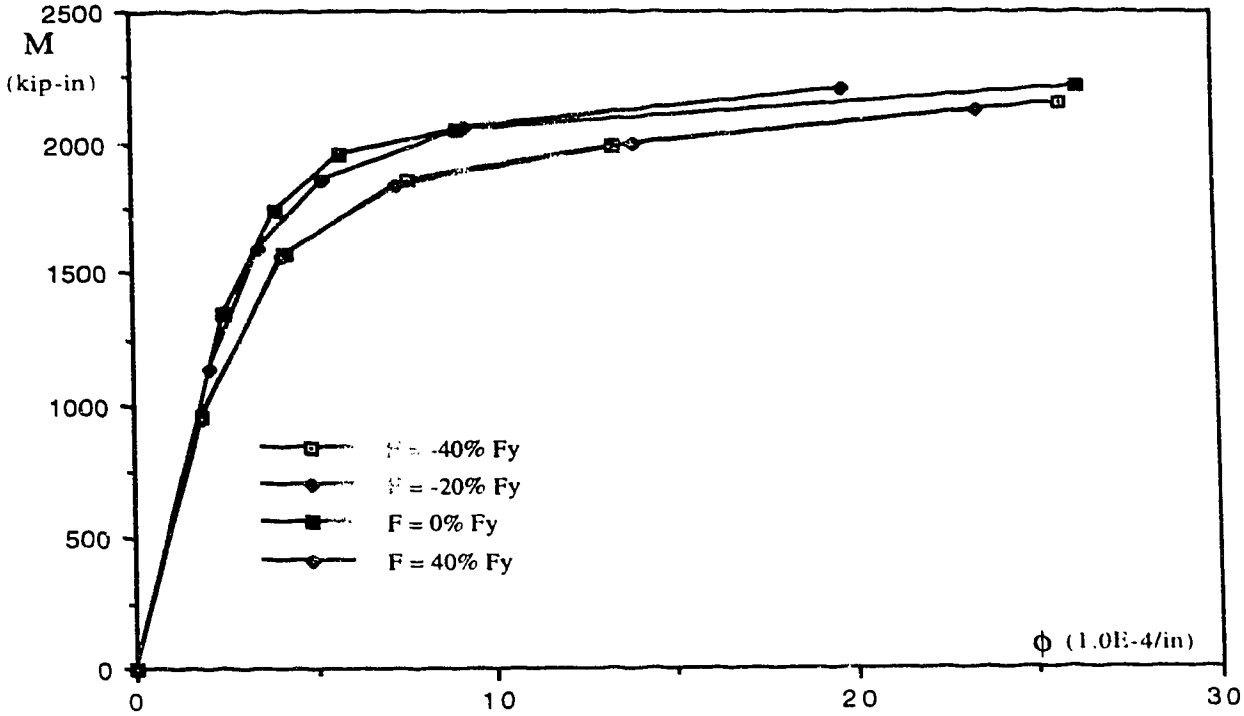

Fig. 6.22 Generated Moment-Curvature Curves for the EPH Material

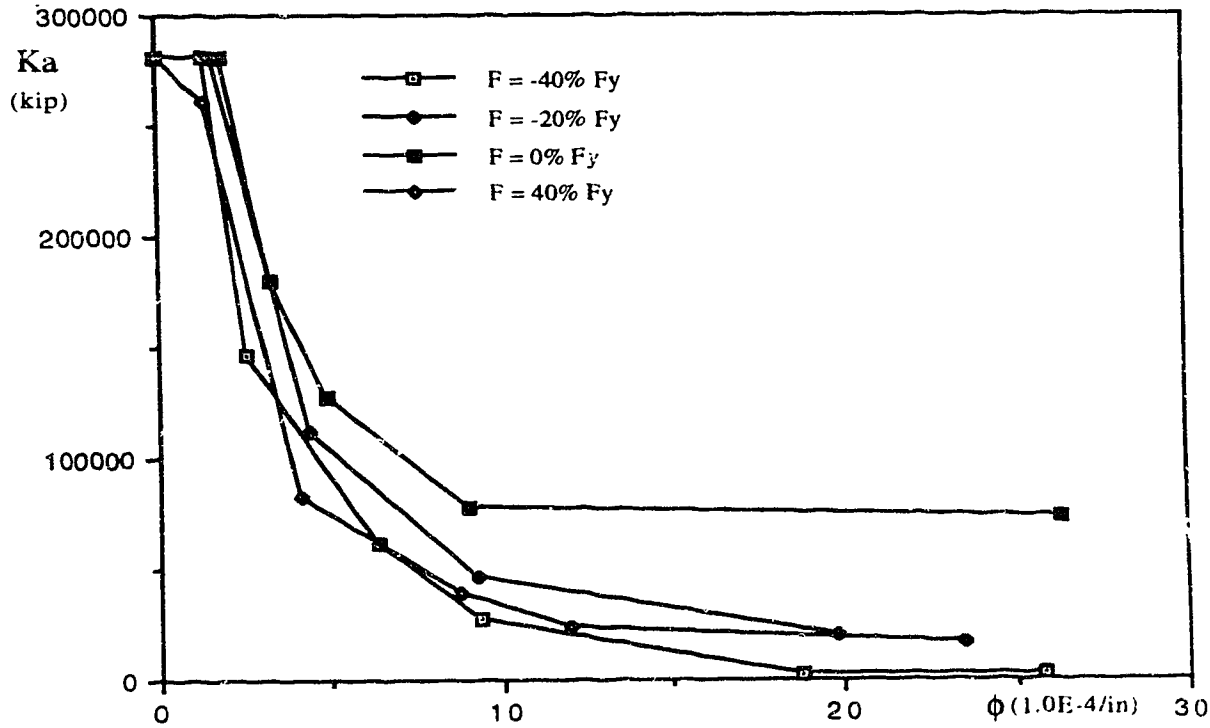

Fig. 6.23 Generated Axial Stiffness-Curvature Curves for the EPH Material

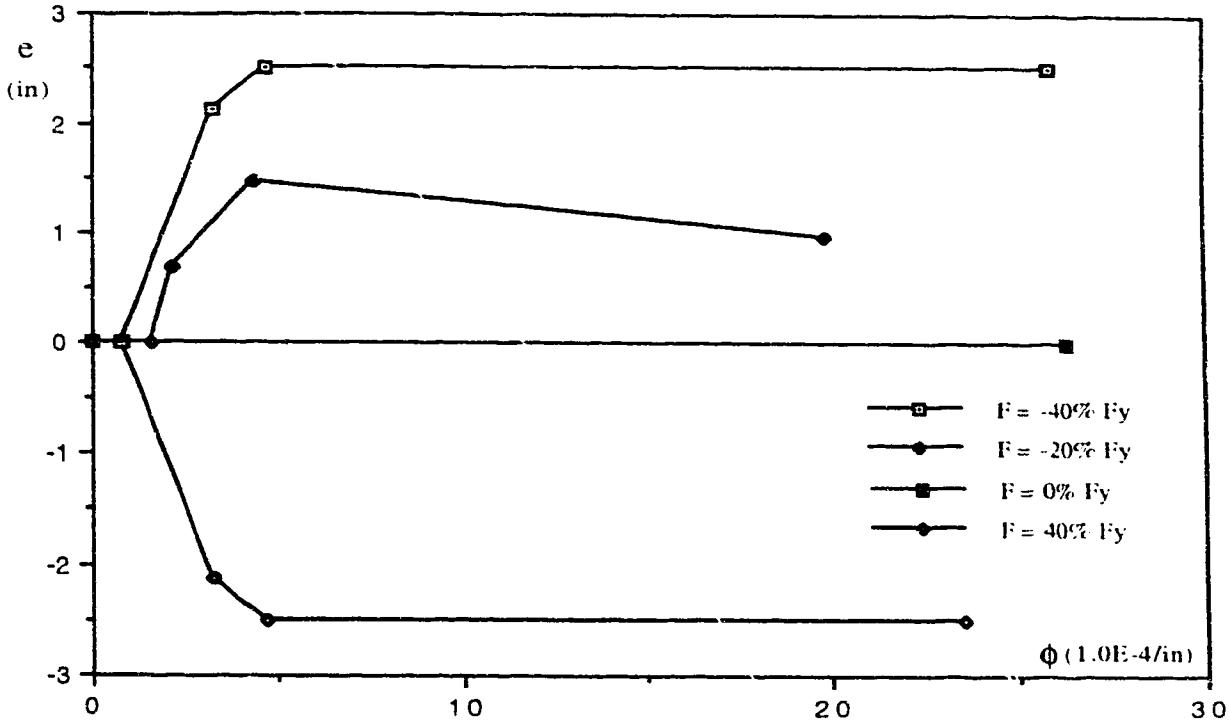

Fig. 6.24 Generated Shift Distance-Curvature Curves for the EPH Material

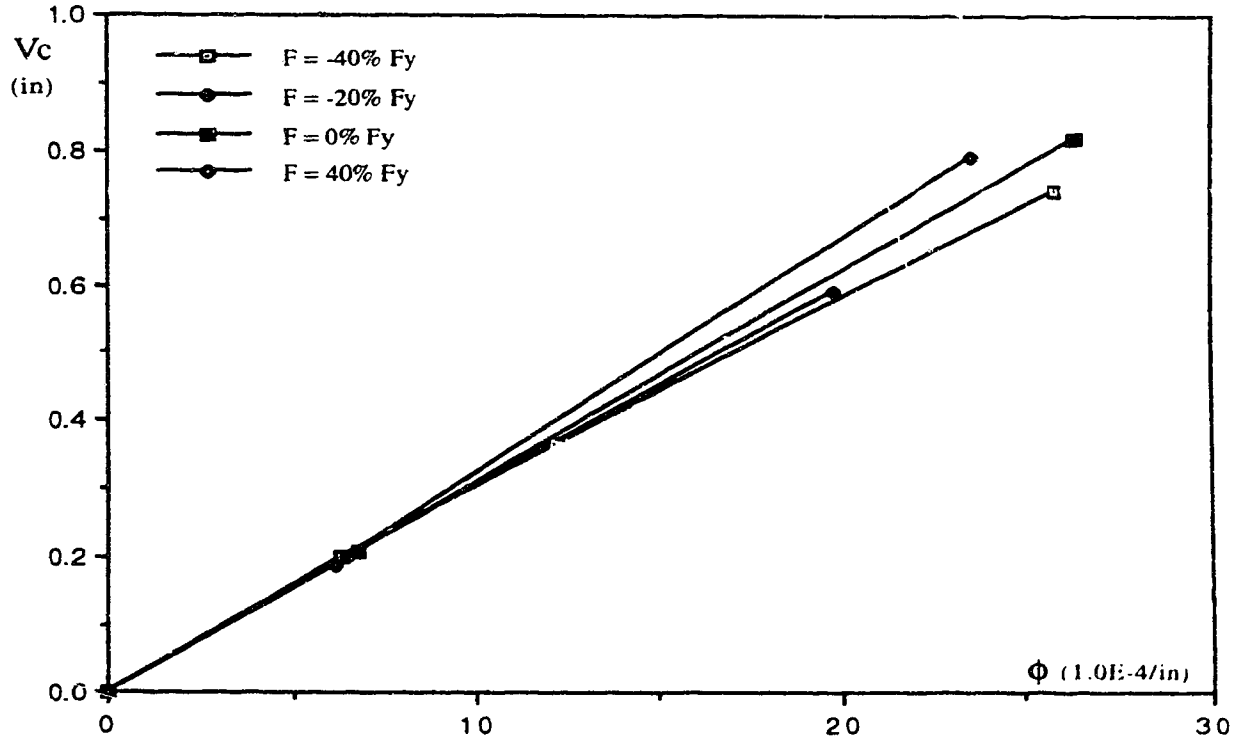

Fig. 6.25 Generated Deflection of Geometric Center-Curvature Curves for the EPH

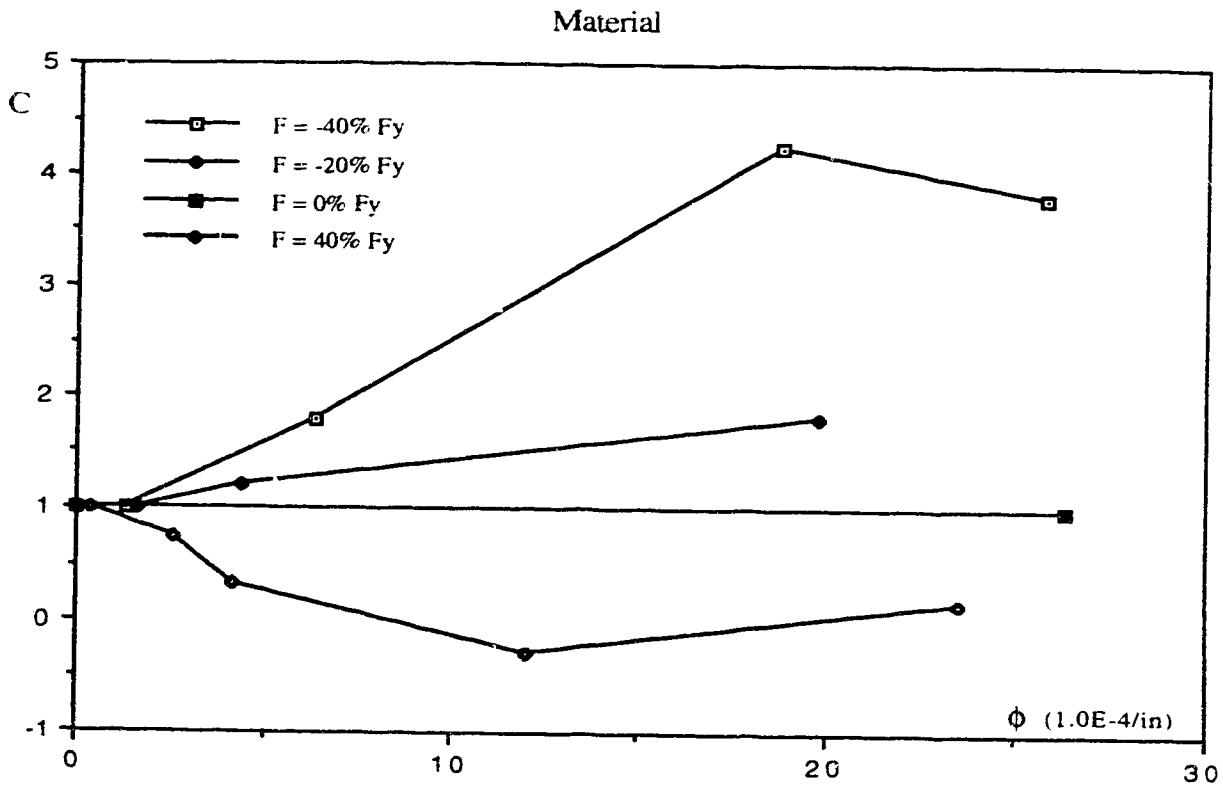

Fig. 6.26 Generated Amplification Factor-Curvature Curves for the EPH Material

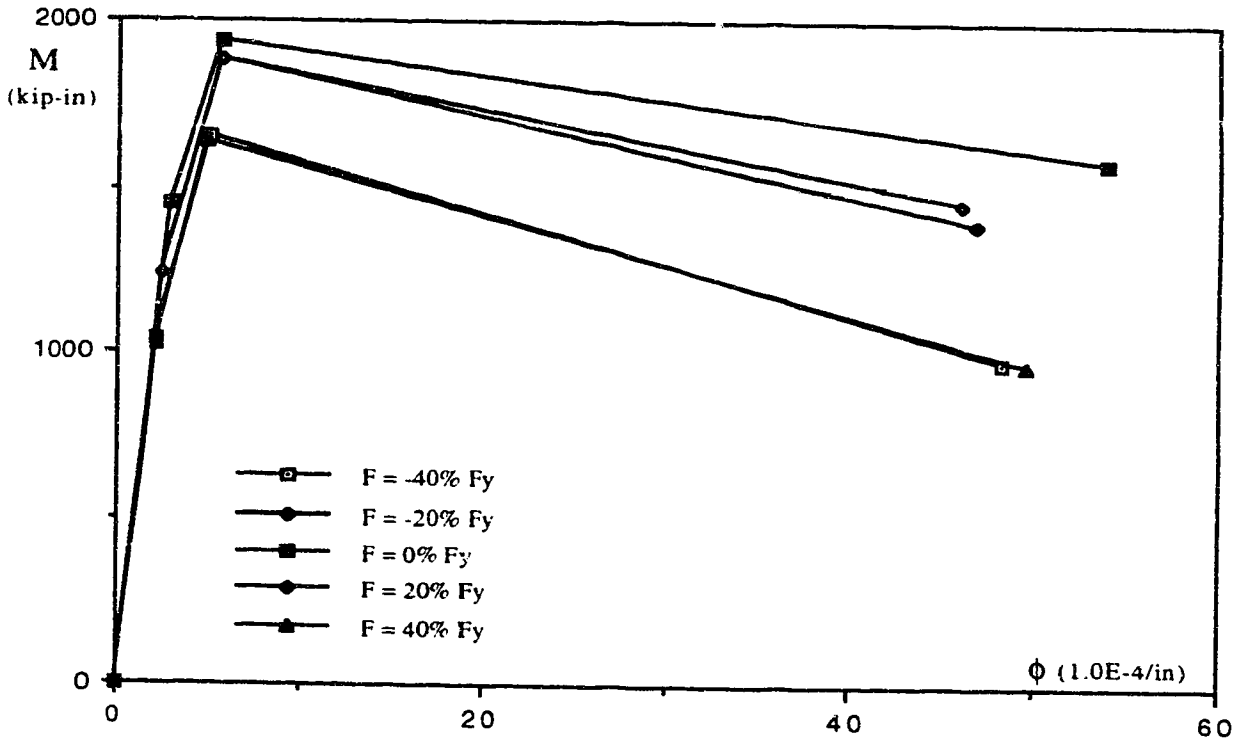

Fig. 6.27 Generated Moment-Curvature Curves for the EPS Material

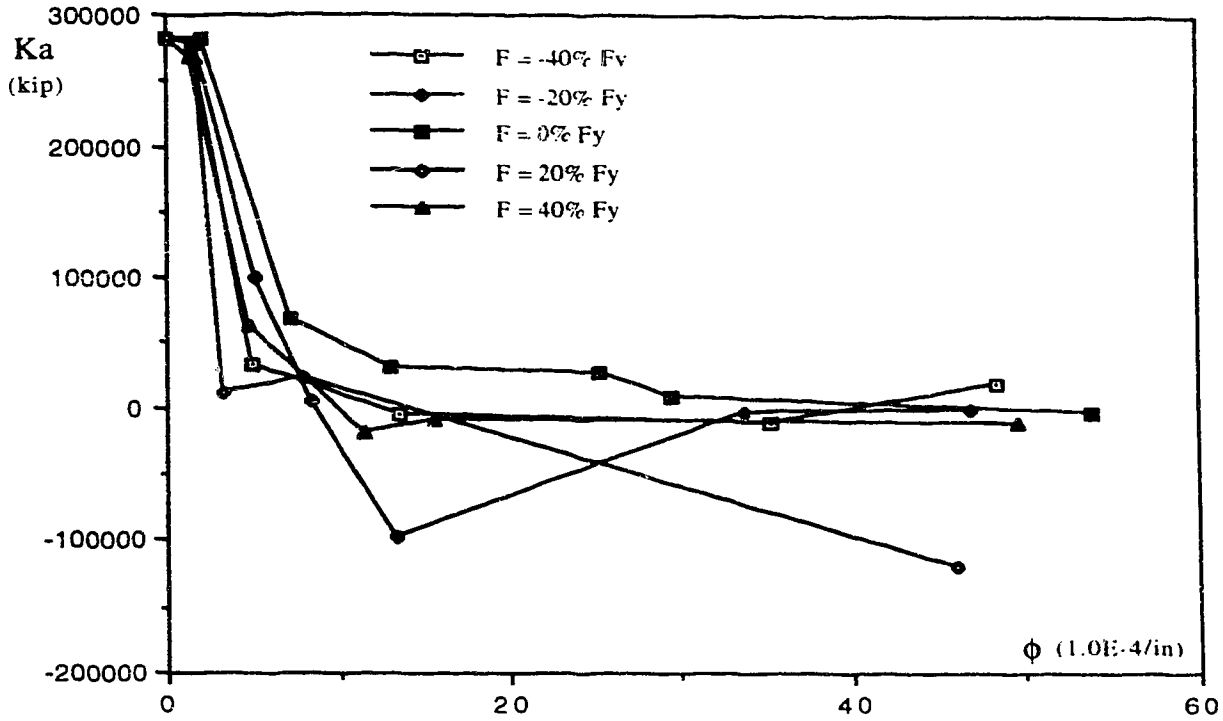

Fig. 6.28 Generated Axial Stiffness-Curvature Curves for the EPS Material

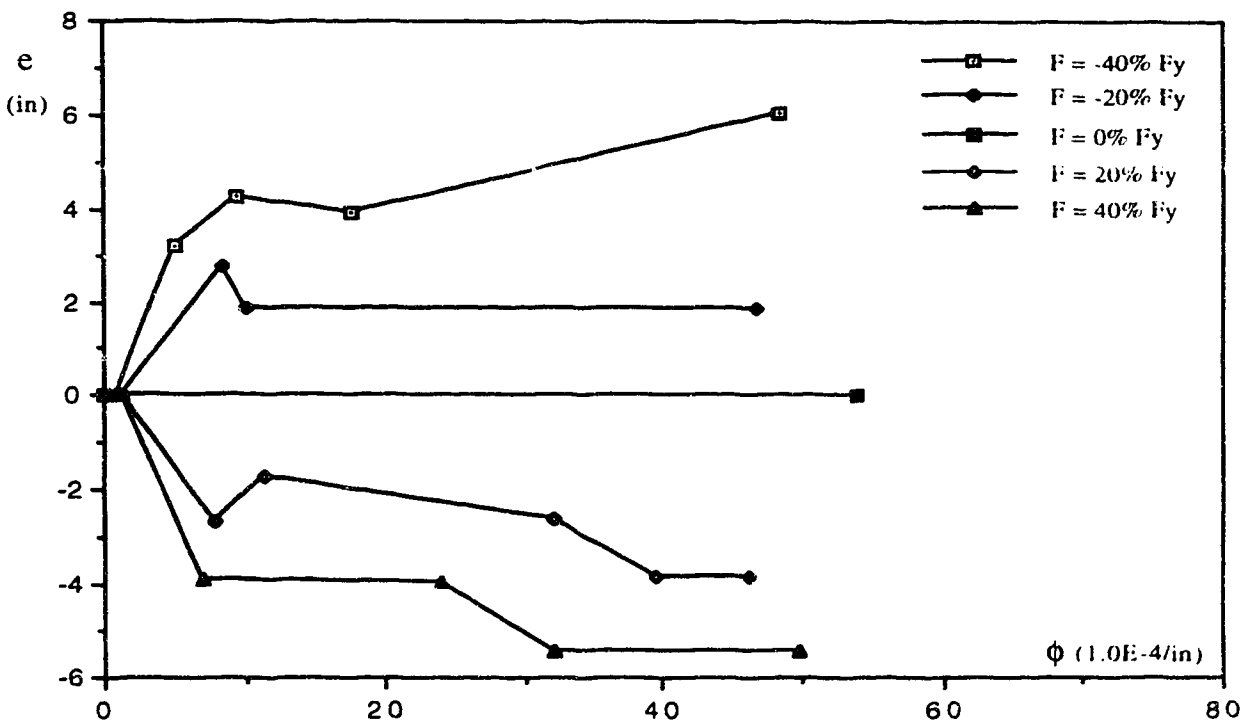

Fig. 6.29 Generated Shift Distance-Curvature Curves for the EPS Material

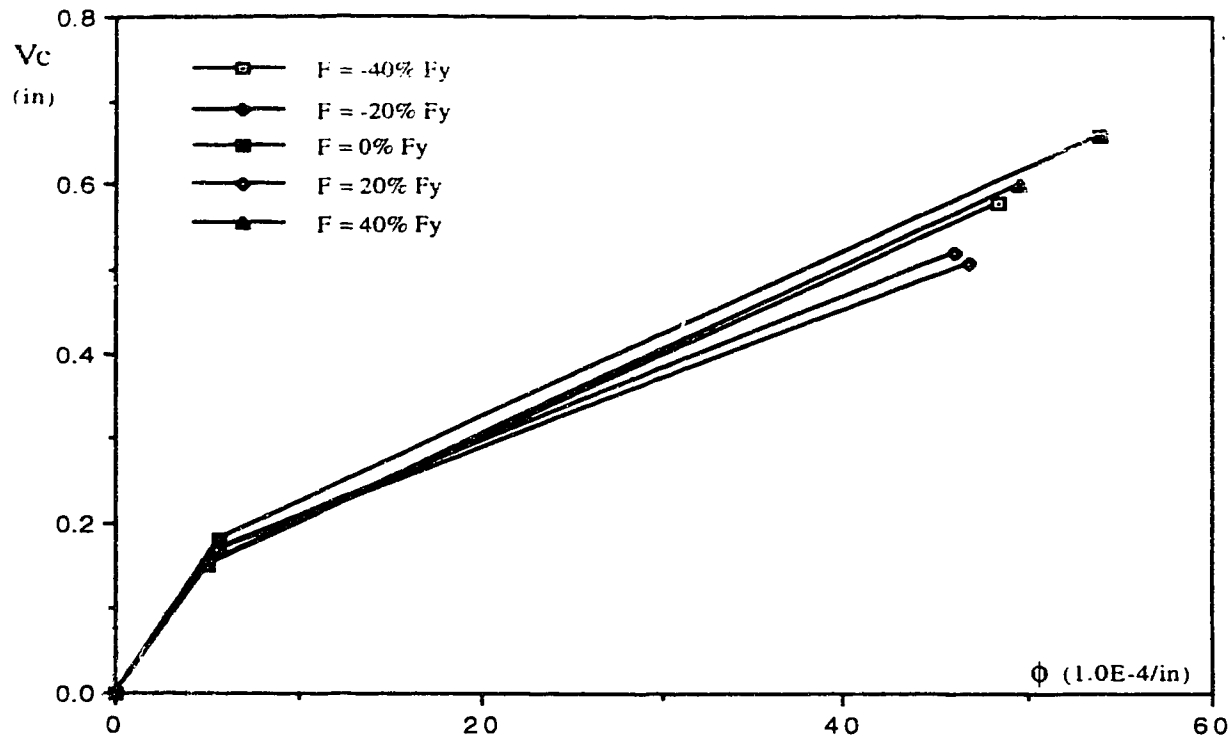

Fig. 6.30 Generated Deflection of Geometric Center-Curvature Curves for the EPS Material

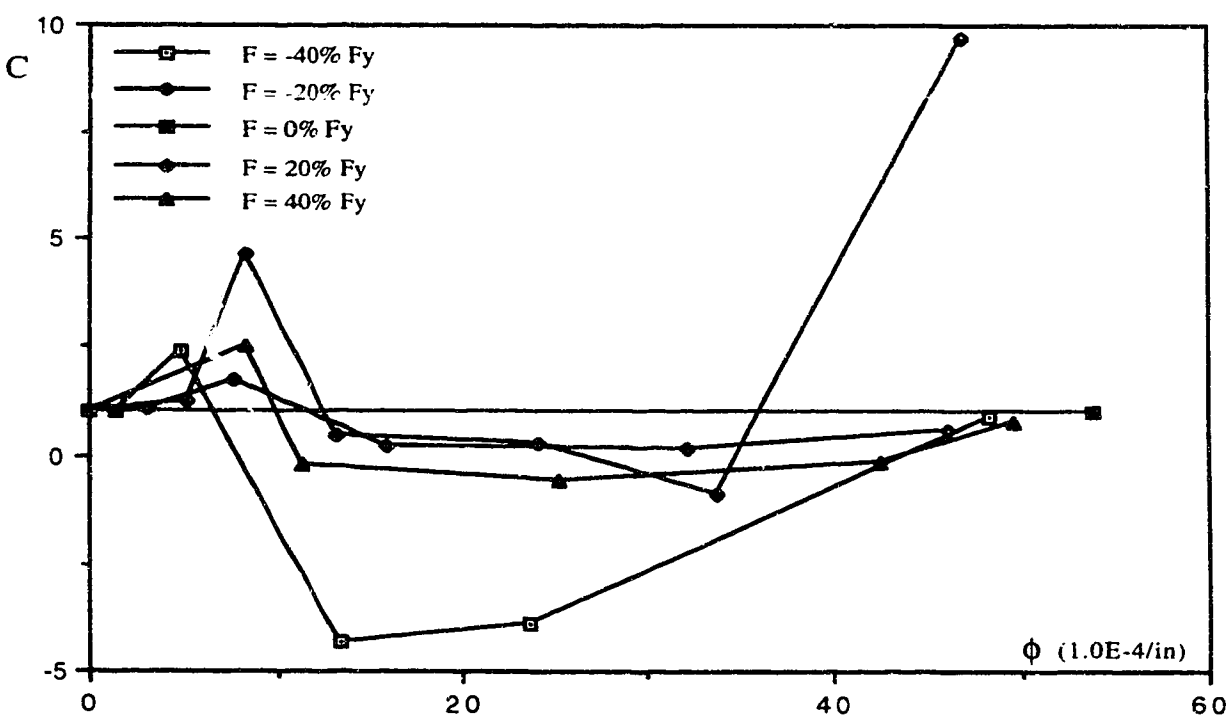

Fig. 6.31 Generated Amplification Factor-Curvature Curves for the EPS Material

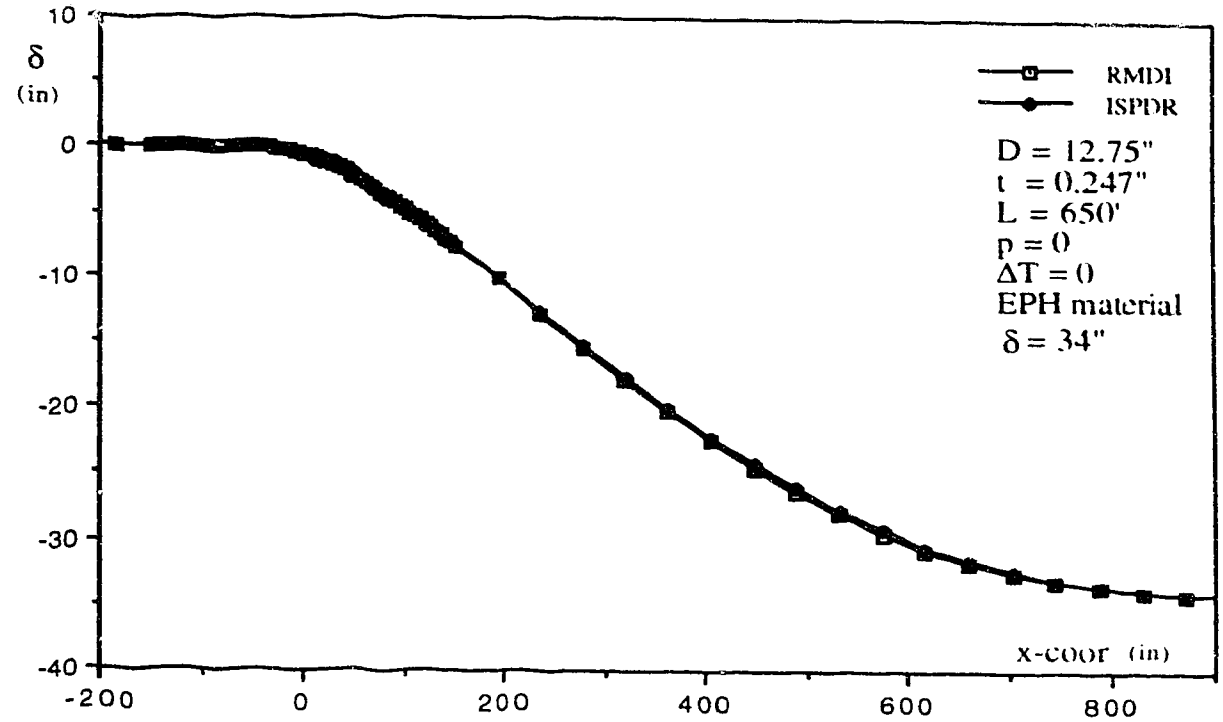

Fig. 6.32 Comparison of Deformed Configurations for Example V3

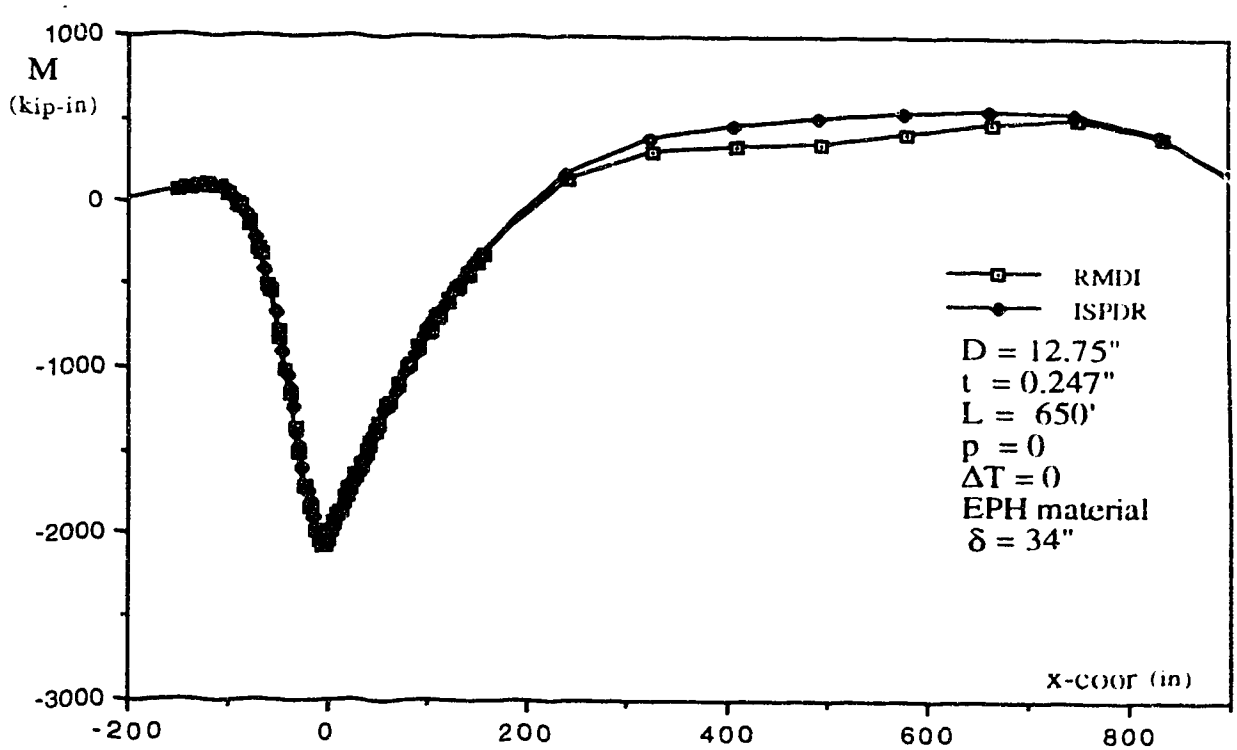

Fig. 6.33 Comparison of Moment Distributions for Example V3

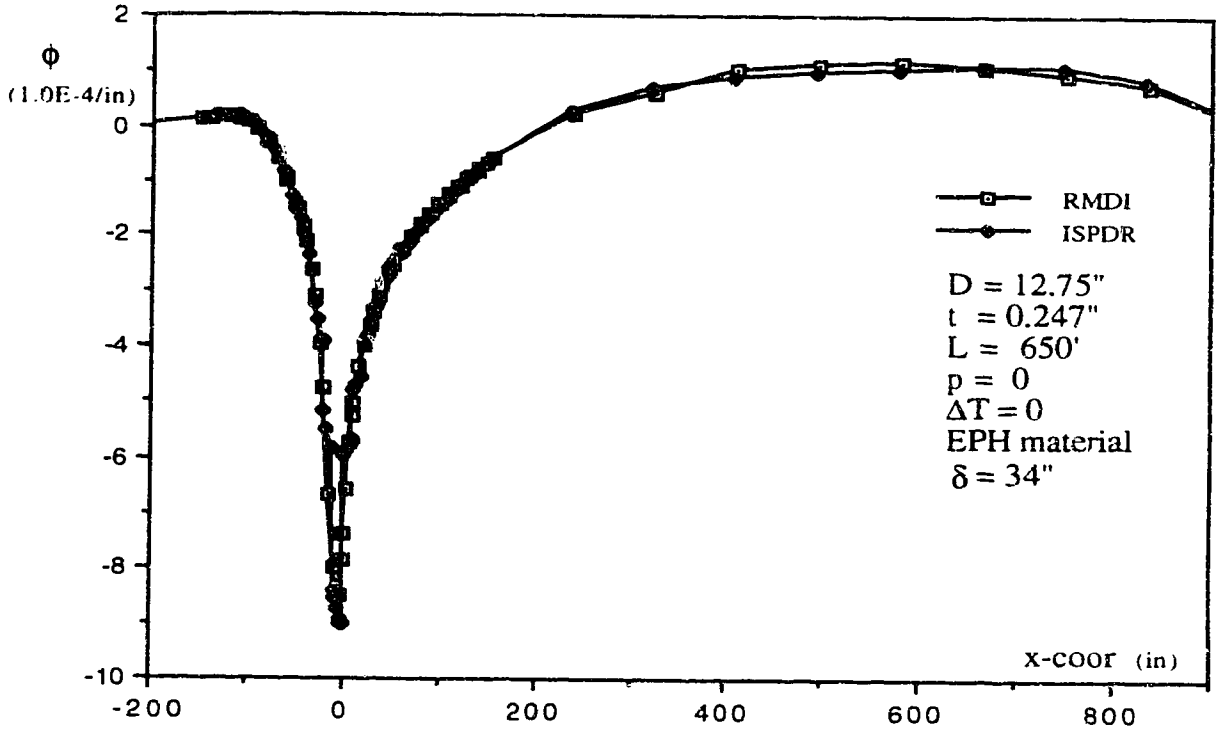

Fig. 6.34 Comparison of Curvature Distributions for Example V3

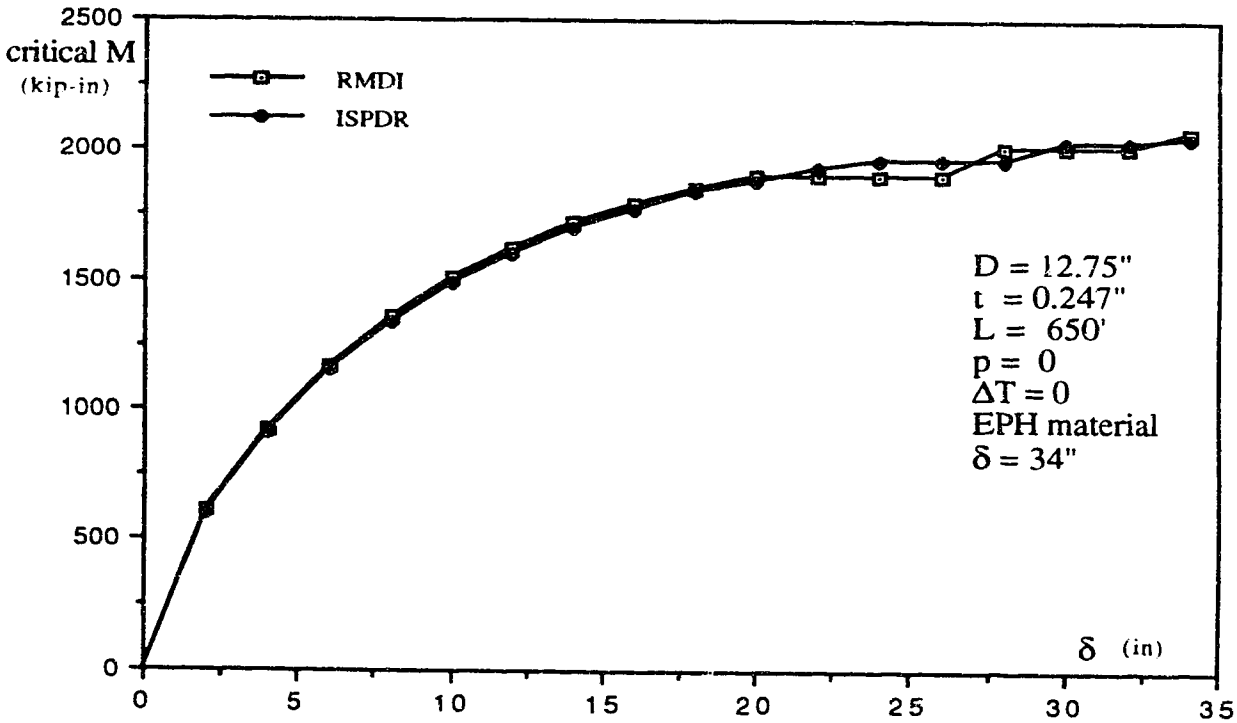

Fig. 6.35 Comparison of Critical Moment-Settlement Curves for Example V3

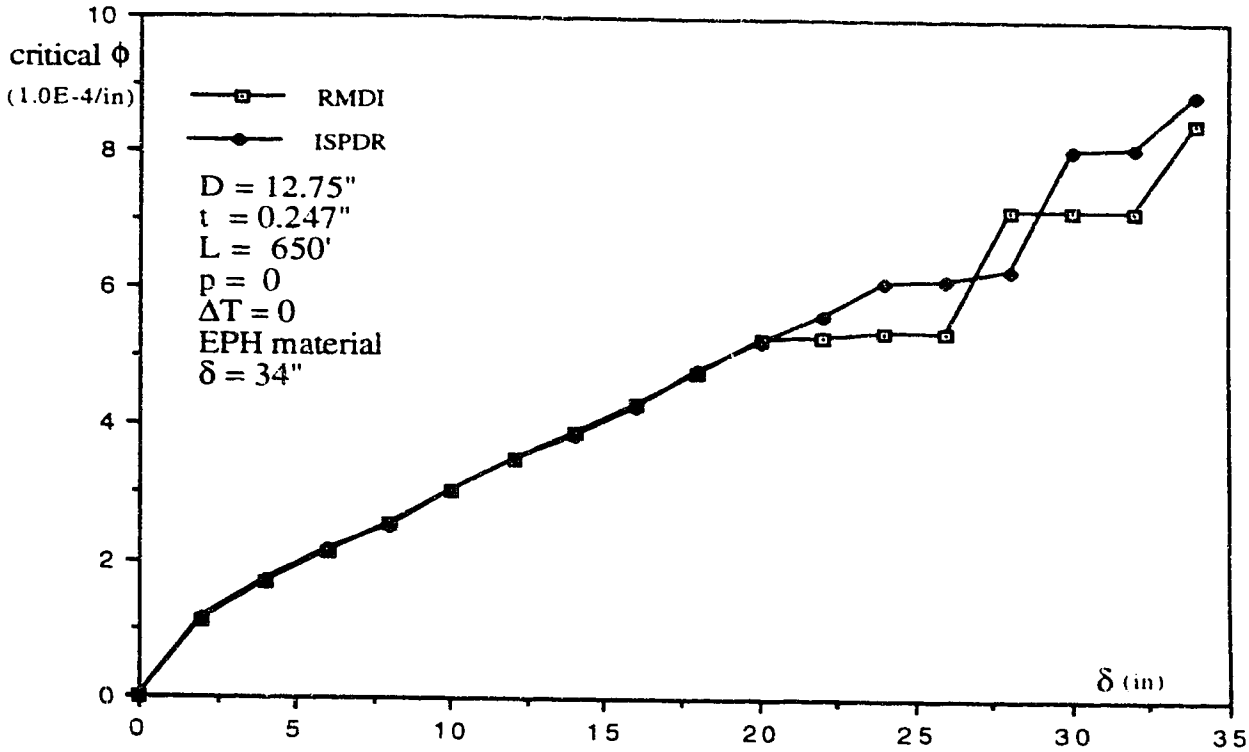

Fig. 6.36 Comparison of Critical Curvature-Settlement Curves for Example V3

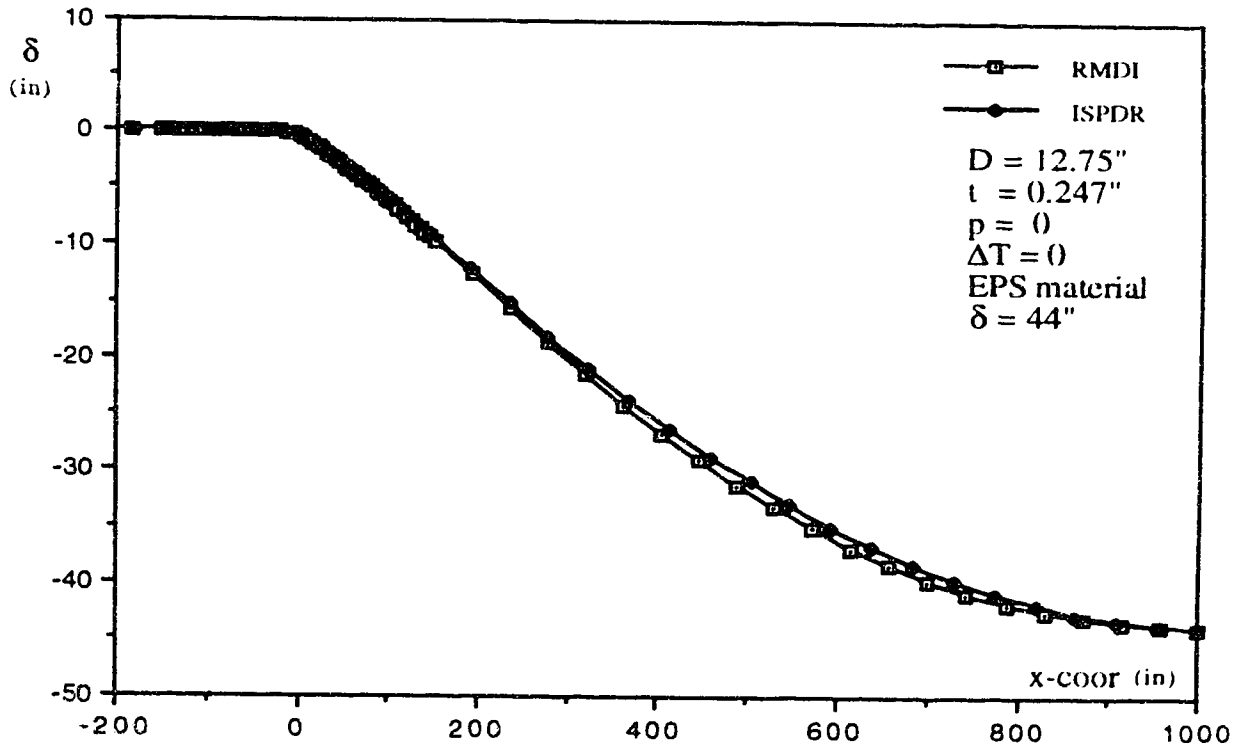

Fig. 6.37 Comparison of Deformed Configurations for Example V4

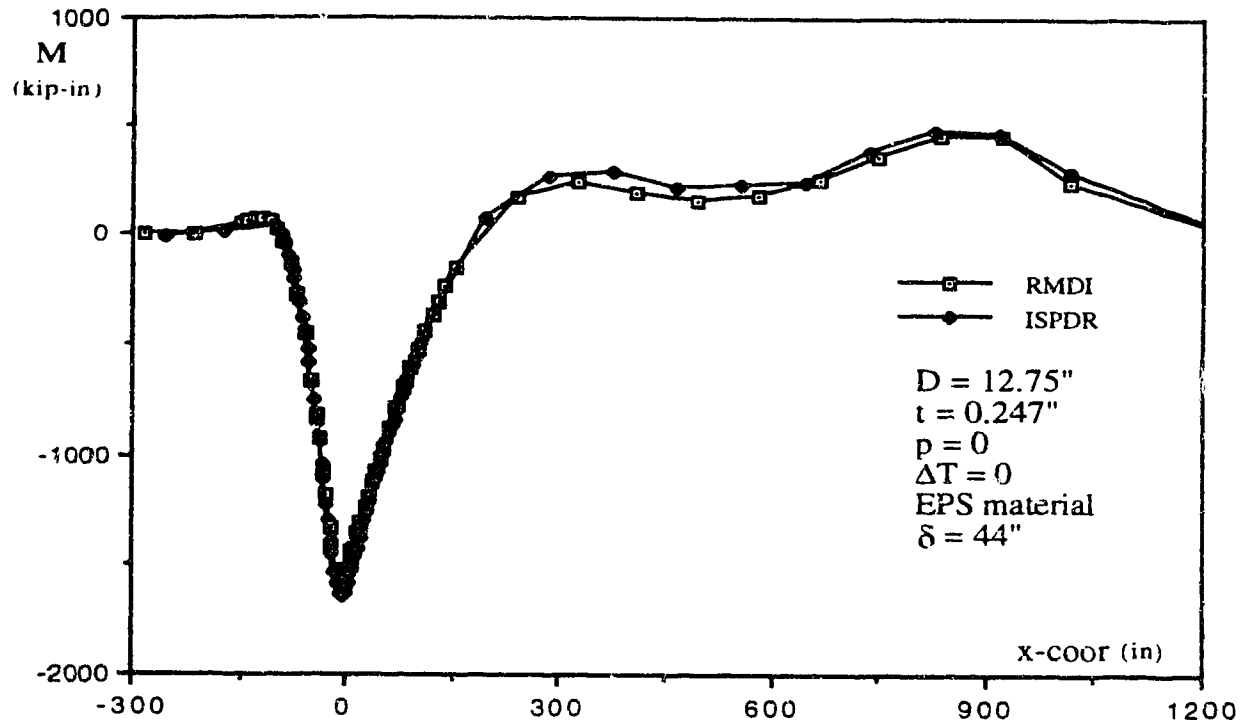

Fig. 6.38 Comparison of Moment Distributions for Example V4

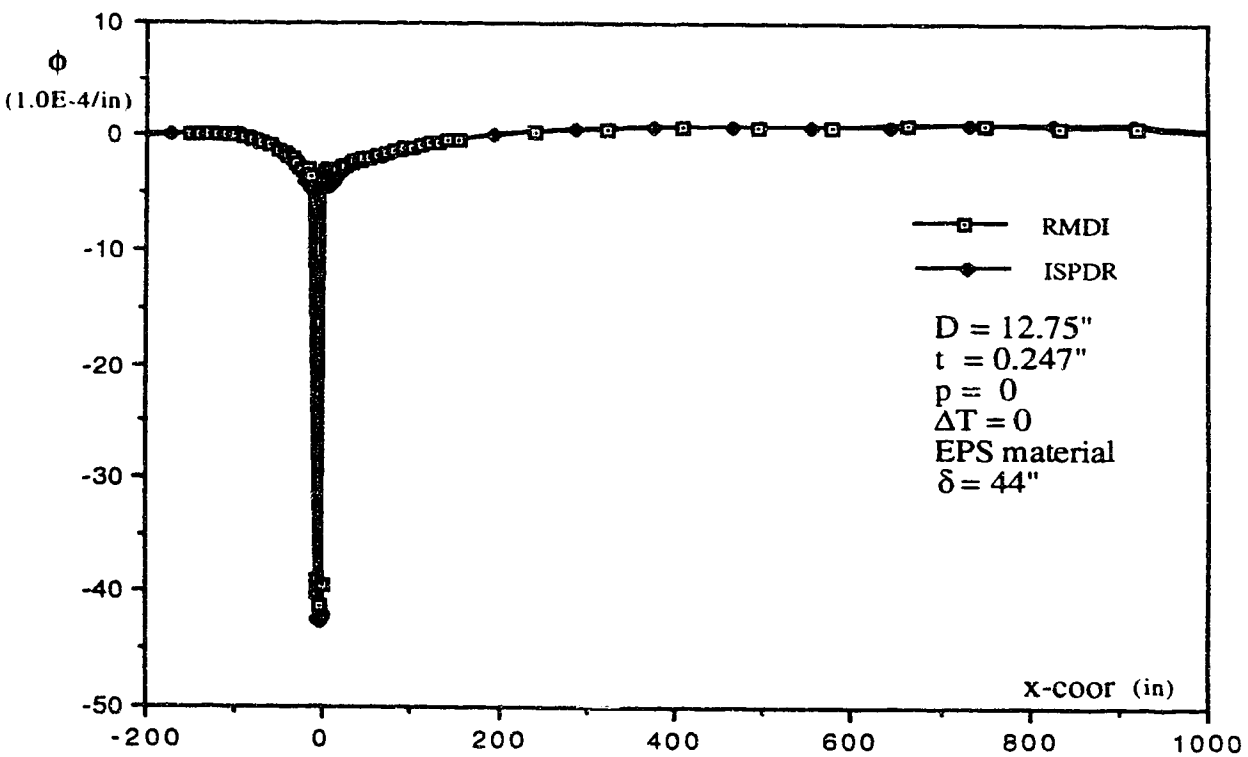

Fig. 6.39 Comparison of Curvature Distributions for Example V4

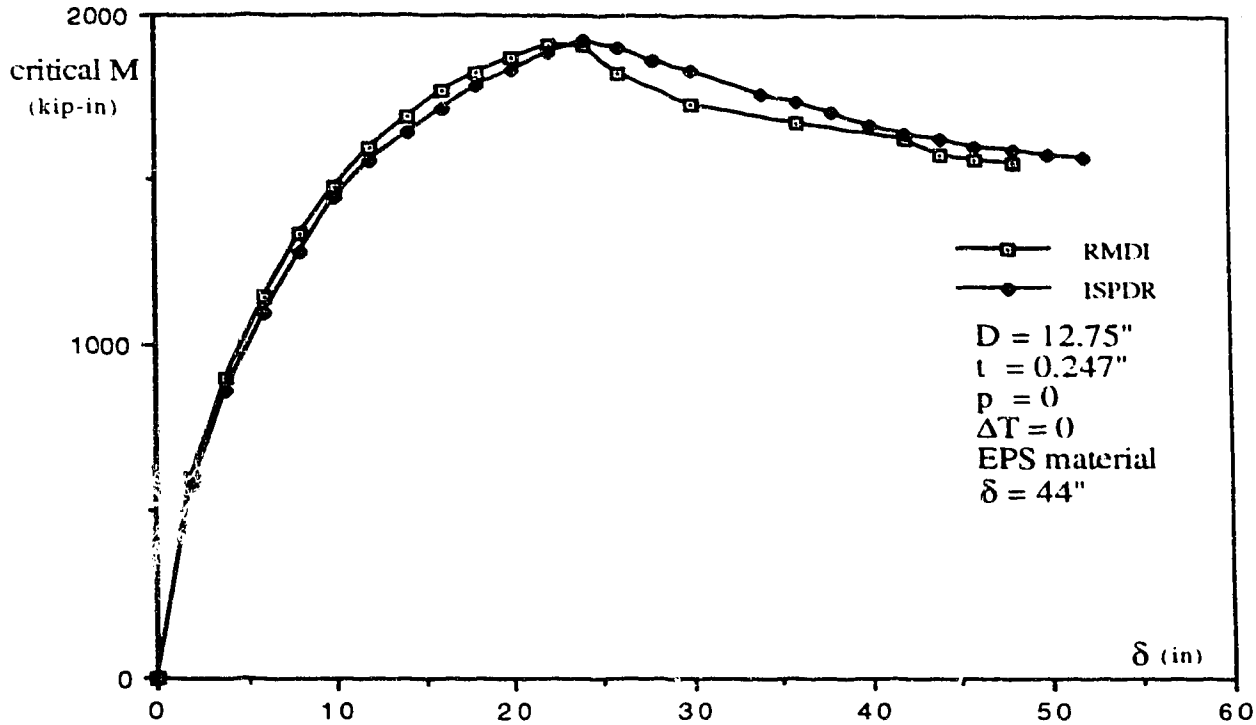

Fig. 6.40 Comparison of Critical Moment-Settlement Curves for Example V4

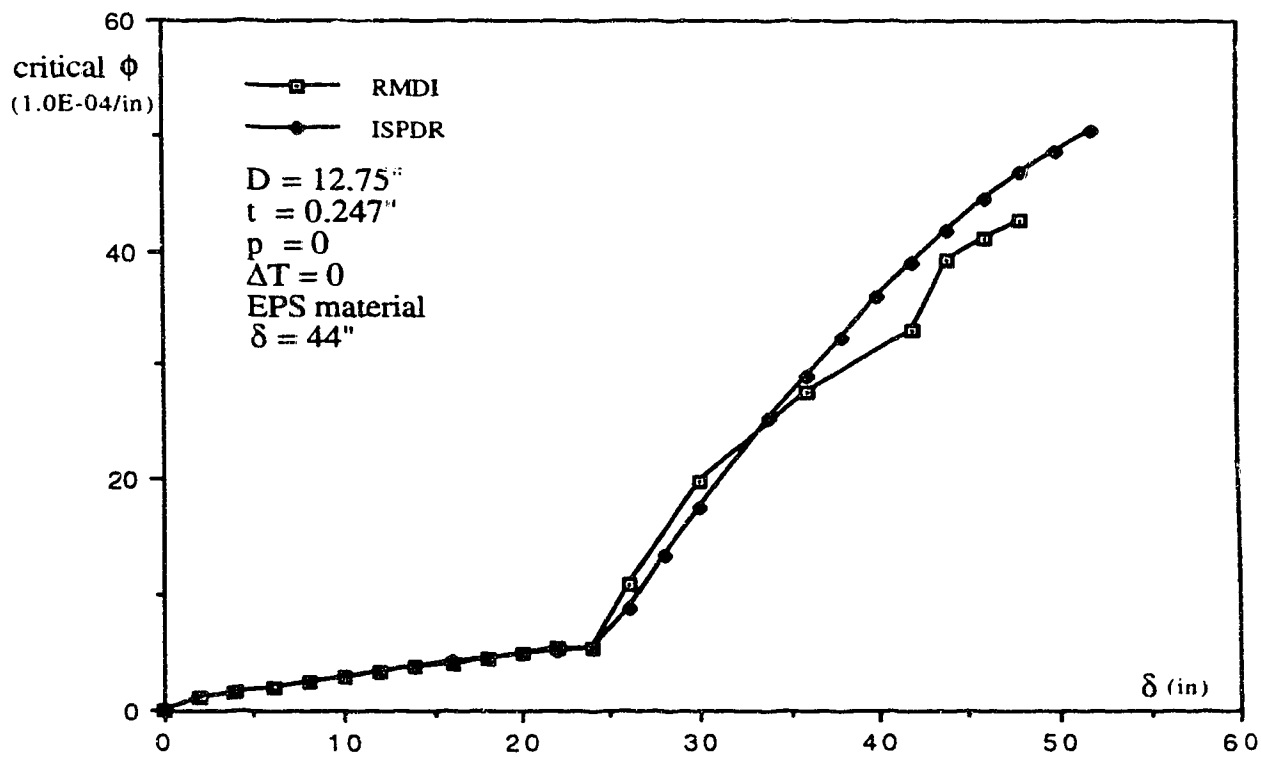

Fig. 6.41 Comparison of Critical Curvature-Settlement Curves for Example V4

CHAPTER 7 ANALYSIS OF PIPELINES SUBJECTED TO DIFFERENTIAL SETTLEMENT

Differential settlement is one of the critical loading conditions imposed on buried pipelines. As a result, response prediction of pipelines under imposed differential settlement becomes an essential part for both design of new pipelines and evaluation of existing pipelines. A pipeline subjected to differential settlement behaves, overall, as a beam supported by soil. The response depends on the stiffness of the pipeline, the loads, and the support, as well as the restraint provided by the surrounding soil. The models developed for settlement analysis (Nyman, 1983 and Row *et al*, 1983b) are basically confined to behavior in which beam-type behavior is simulated. However, local buckling of the pipe wall changes the stiffness properties of the pipeline and introduces localization of deformation which interacts with the overall behavior. Then the integration of the overall and local behaviors determines the response of pipelines. Simulation of the local behavior of pipelines is not included in Nyman's model (1983) and is inadequate in Row's model (1983b). This implies that these models are not applicable to the analysis of pipelines for which deformation beyond the initiation of local buckling occurs.

The approach for settlement analysis of pipelines developed in this project was conceptually outlined in Sect. 1.3. It consists of two phases. In the first phase, the local behavior of the pipeline is analyzed by utilizing a three-dimensional shell model of a pipeline segment. This model includes the effects of large displacements and nonlinear material response. The local behavior obtained from this type of analysis is then represented by the stiffness property-deformation (SPD) relations which are extracted from the analysis. In the second phase, pipelines are modelled by pipeline-beam elements and the SPD relations generated from the first phase are used to define the stiffness properties of the pipeline-beam elements. This is an effort to reflect the interaction between overall and local behavior. The pipeline-beam element is fully described in Ch. 6 which includes definitions of the SPD relations and the rationale for them. The solution technique used to carry out the analysis which simulates the interaction between the overall and local behavior is the integration of stiffness property-deformation relations (ISPDR). It has been discussed in detail in Ch. 6.

In this chapter, behavior of pipelines subjected to differential settlement is predicted. The chapter starts in Sect. 7.1 with the description of the model based on the pipeline-beam element. This includes discretization of the pipeline, properties of soil

springs and generated SPD relations. Analysis is carried out for a number of specimens, where the specimens are specified in such a way that the influences of each of (a) soil springs, (b) local buckling and (c) the temperature differential, can be investigated. The solutions including the effects of local buckling are carried out by the ISPDR technique and those excluding the effects of local buckling are carried out by the RMDI technique. More information on both ISPDR and RMDI techniques is available in Sect. 1.3.2 and Ch. 6. Based on the solutions obtained, a sensitivity study investigating the behavior in general, and effects of local buckling and temperature differential, are summarized in Sect. 7.2; and, the influences of geotechnical parameters on the behavior are discussed in Sect. 7.3.

7.1 ANALYTICAL MODEL BASED ON THE PIPELINE-BEAM ELEMENT

The model for analysis of pipelines subjected to differential settlement consists of a series of pipeline-beam elements and soil springs along the pipeline. The discretization is discussed in Sect. 7.1.1. It is followed by a description of the properties of the soil springs in Sect. 7.1.2. The stiffness properties of the pipeline are defined by SPD relations generated from shell analysis of a segment of the same pipeline. This is presented in Sect. 7.1.3. The last sub-section, Sect. 7.1.4, provides the detailed definition of specimens that are analyzed in this chapter for the sensitivity study.

7.1.1 Discretization

The pipeline considered here is of 48 inch (1219 mm) diameter and 0.462 inch (11.7 mm) wall thickness. Analysis in this chapter is confined to pipelines of this particular size because SPD relations are available only for this size. Generation of full sets of SPD relations is very time-consuming since it is based on many runs of nonlinear analysis of a large shell structure. However, the approach used for the analysis is applicable to all pipe sizes. The length of the pipeline is not important to the response of the pipeline provided that it is long enough to allow surrounding soil to completely damp out the longitudinal movement at both ends of the pipeline. The length of the pipeline is chosen as 12000 inches (305 m) with 4000 inches (102 m) in the stable zone and 8000 inches (203 m) in the settlement zone.

The size of the pipeline-beam element in the active areas is determined by the principal wavelength of the specimens whose responses have been used to define the SPD relations. This is because the SPD relations are size dependent as discussed in Sect. 6.4.4. The principal wavelength has been defined in Sect. 4.3.4 and Table 4.2 lists the principal

wavelengths for all the specimens in the series of postbuckling analyses. The average of principal wavelengths for last five specimens in Table 4.2, which have the high level of internal pressure, is about 40 inches (1016 mm). Consequently, the element size in the regions where local buckling is expected is set to 40 inches (1016 mm). In the other regions, the size of element can be gradually increased to reduce the scale of the model. The schematic discretization of the pipeline is shown in Fig. 7.1. There are total 131 nodes and 65 elements.

For the same reason as that which limits the analysis in this chapter to a specific size of pipeline, the analysis is also limited to a specific level of internal pressure. This is 72 percent of the yield pressure. This is necessary because analysis at each different level of pressure would require a completely different set of SPD relations and it is not possible to obtain such sets in the limited period of time available.

The soil surrounding the pipeline is modelled by bearing, uplift and longitudinal soil springs. Each element has nine springs of each type uniformly distributed over the length of element. The properties of these springs are defined in the next sub-section.

The overburden load is specified as a uniformly distributed load of 0.25 kip/in (43.8 KN/m). It is used to simulate the self weight of the soil above the pipeline and the pipeline itself. Because the influence of the overburden load is believed to be small and the magnitude of overburden load varies in a relatively narrow range, the overburden load is not taken as a parameter to be studied in this chapter.

7.1.2 Properties of Soil Springs

Several models to determine the properties of soil springs have been proposed (Nyman, 1983; Selig, 1988; and, Wagner *et al*, 1989) where the properties of soil springs in terms of stiffness and strength are related to parameters such as : coefficient of earth pressure, effective angle of internal friction, the state of soil (frozen or unfrozen), pipe diameter, and cover depth. If a particular pipeline is to be analyzed, it is necessary to evaluate the properties of soil springs from a particular set of soil parameters in a relatively rational way, such as, from the models mentioned above. However, the objective of the analysis in this chapter is to explore the general behavior of pipelines when they are subject to differential settlement and to investigate the sensitivity of the behavior of pipelines to variations in the properties of soil springs. Therefore, a single set of soil spring properties can be used as long as it is representative.

Typical soil conditions in northern Alberta have been measured (Canuck Engineering Ltd., 1983) for the construction of the pipeline from Norman Wells to Zama. A set of properties of soil springs was extracted from the measurements of these soil conditions. Taking advantage of these available data, the representative properties of soil springs can be obtained by converting the existing data for the pipeline with diameter of 12.75 inches (324 mm) into data for a pipeline with diameter of 48 inches (1219 mm). The conversion is carried out under the assumption that the stiffness and strength of the soil springs are proportional to the diameter of the pipeline. This implies that the yield displacement is independent of the diameter. This assumption may not be accurate in the sense that the relationship between stiffness and strength of the soil springs and the diameter of the pipeline may not be exactly linear. But the linear portion is certainly the principal portion and the assumption is supported by Nyman's model (1983). The properties of soil springs for both pipelines are listed in Table 7.1.

The longitudinal springs are given two sets of properties. One is stronger than the other. The relatively weak springs are applied in a region 1000 inches (25.4 m) long. This region starts from the transition, at x-coordinate of zero, and extends into the settlement zone. The stronger springs are applied over the rest of the pipeline.

7.1.3 Generated SPD Relations

A set of SPD relations has been generated by the shell model analyses in Ch. 4 for a pipeline with diameter of 48 inches (1219 mm) and thickness of 0.462 inches (11.7 mm) and subject to internal pressure of 72 percent of the yield pressure. The analyses required are those of Specimens PHC40, PHC20, PHC00, PHT20 and PHT40, which are part of the series of postbuckling analysis discussed in Ch. 4. The procedure to generate SPD relations has been discussed in detail in Sect. 6.4.3.

The SPD relations are defined at five levels of constant axial load, i.e. 40 percent, 20 percent and zero in both compression and tension. At each level of constant axial load, five quantities are defined in terms of their relations with respect to the curvature, ϕ. They are moment, M; axial stiffness, K_a; distance between the centroids of elastic and tangent stiffness of the cross-section, e; deflection of the centroid of elastic stiffness, v_c; and, the amplification factor, C, to represent the secondary effect of axial load. As a result, the set of SPD relations includes 25 relationships and are shown in Figs. 7.2 to 7.6. All the quantities are based on the average response of the buckling segment which is about 40

inches (1016 mm) long and contains the principal buckle. The SPD relations have been idealized into a set of peicewise linear curves to facilitate their description.

For the analyses which exclude the effects of local buckling, the material relationship is directly defined by the stress-strain relation. The stress-strain relation used for the line of pipe analysis in this chapter is the same as the one used for shell analysis in Ch. 4 which is specified in Sect. 4.2.3.

7.1.4 Specification of Specimens

The analyses carried out in this chapter are for the purpose of studying the behavior of buried pipelines subjected to differential settlement and its sensitivity to the influences of various geotechnical parameters. This is reflected in the selection of specimens. Before the specification of specimens is discussed, the factors and parameters which are expected to have significant effects on the response of pipelines are outlined in the following.

The first factor is local buckling. As discussed in the beginning of this chapter, local buckling is one of the factors which have not been dealt with adequately in established models. The behavior characterized by local buckling is expected to interact with overall behavior and, therefore, to influence the response of pipelines. This influence is characterized by the fact that the postbuckling response of pipeline segments is unstable. The local buckling effect can be investigated by comparing solutions including and excluding local buckling effects while other conditions remain identical to each other, i.e. by comparing solutions obtained by the ISPDR and RMDI techniques, respectively.

The geotechnical input includes stiffness and strength of soil springs of each type. The effect of each geotechnical parameter can be studied by comparing the solutions for different values of the parameters being investigated while the other conditions remain the same. Each of the springs has three parameter. They are stiffness, strength and yield displacement. Two of them are independent because of the material model assumed for soil springs in Sect. 6.5.3. To further reduce the independent parameters, it is assumed that the yield displacement is constant while the stiffness and strength vary, because the yield displacement is believed to be less influential on the response of pipelines. As a result, the strength of springs is proportional to the stiffness of springs, and only one of them is independent.

For bearing and uplift soil springs, the influences can be studied by varying the stiffness and strength of the springs over entire length of the pipeline. The type of variation

can occur in different locations along the route of the pipeline. For the longitudinal soil springs, two aspects should be looked at. One is the stiffness and strength of longitudinal springs in all zones. The other is the length of the region where relatively weak springs are applied. As discussed in Sect. 7.1.2, two different sets of properties of longitudinal springs are applied to different regions of the pipeline. Relatively weak springs are applied in the region which starts from the transition and extends to the settlement zone. The length of this region was believed to be influential on the response of the pipeline because it affects the way that tensile axial force is built up and distributed. Consequently, this length was taken as a parameter to be investigated.

Apart from the stiffness and strength of the soil springs, the ground profile in the transition zone was also expected to have significant influence on the response of pipelines. By assuming that the ground profile is the smooth ground profile defined in Sect. 6.5.1, the effect of the ground profile can be studied by varying the length of the transition zone.

Temperature differential introduces initial axial force into pipelines and therefore changes their response. Significant effect can be expected from temperature differential since the difference between the moment-curvature curves with different levels of axial load is obvious in Figs. 4.7 to 4.9, and in Fig. 7.2. Figure 7.2 is an approximation of Fig. 4.9 with each curve simplified into a smaller number of piecewise linear segments. The effects of temperature differential can be studied by comparing solutions with different magnitudes of temperature differential.

Specimens selected to study all of the above parameters are listed in Table 7.2. They are divided into groups according their role. Explanations about the name of each series and that of each specimen are shown in Table 7.3. First is the reference Specimen NOM whose condition is taken as the reference for other specimens. The properties of soil springs for Specimen NOM are those defined in Table 7.1. The length of transition zone is zero which implies the ground profile in the transition zone is a step-wise ground profile as defined in Sect. 6.5.1. The length of the region where relatively weak longitudinal springs are applied is 1000 inches (25.4 m). The temperature differential for Specimen NOM is zero. The next specimen is TENOM where the only difference from the Specimen NOM is a 75 °F (41.7 °C) temperature differential. This temperature differential would produce an axial compressive force of 22 percent of the axial yield force. All other specimens belong to one of following groups. They are referred to as the USA, BSA, LSS, LSL, TPL and BE groups. The USA group is used to study the effects of strength variation of uplift springs in all zones. The BSA group is intended for the effects of strength variation of bearing

springs in all zones. The LSS and LSL groups are for longitudinal soil springs. The first looks at the effects of strength variation of longitudinal springs in all zones, and the second examines the effects of length variation of the region with weak longitudinal springs. The TPL group is designated for the effects of ground profile in the transition zone which is represented by the length of transition zone. Finally, the BE group excludes local buckling in order to isolate its effects. Every group has two specimens. Except for the BE and TPL groups, one of the specimens has a smaller value of the parameter under consideration than Specimen NOM, and the other has a larger value of the parameter under consideration than Specimen NOM. In general, the smaller value is set at one-fifth of the reference value and the larger value at five times the reference value. The numbers listed in Table 7.2 define the condition for each specimen and represent the ratios between the values of the parameter for the specified specimen and the reference specimen. The column for length of transition zone is an exception where the numbers indicate the real length of the transition zone in feet.

7.2 BEHAVIOR OF PIPELINES SUBJECTED TO DIFFERENTIAL SETTLEMENT

Behavior of pipelines subjected to differential settlement is discussed in this section. The discussion is focused on the development of curvature and moment as the settlement increases and their distributions at a given settlement. The effects of local buckling on the behavior is investigated for different soil conditions. The importance of the interaction of the local buckling with the overall behavior of the pipeline is demonstrated by exhibiting the significant influences of local buckling. Finally, the effects of temperature differential are discussed.

7.2.1 Behavior

The solution of Specimen NOM is shown in Figs. 7.7 to 7.13 as a representative example. For these figures and subsequent figures in this chapter, moment, curvature, axial force and differential settlement are denoted by M, ϕ, F and δ, respectively. The solution of Specimen BENOM is also shown in these figures for comparison and will be discussed in the next sub-section. After a differential settlement of 31 inches (787 mm) is imposed on the pipeline, the deformed configuration is shown in Fig. 7.7. The dashed line in the same figure represents the final ground profile, with differential settlement of 31 inches (787 mm), where the changes in the ground profile introduced by interaction between the pipeline and surrounding soil is not included. It can be seen that flexural deformations are

localized in two critical segments. One is in the stable zone (negative x-coordinates) and the other is in the settlement zone (with positive x-coordinates). The localization of flexural deformation is more clearly demonstrated by the distribution of curvature shown in Fig. 7.8. The curvature is highly localized in critical segments, both in the stable and settlement zones. While the curvature is negligible in most regions, the curvature in the critical segments is as high as 0.0018/in (7.087×10^{-5}/mm) which is about 20 times the yield curvature under pure bending condition. The critical curvature in the stable zone and in the settlement zone closely resemble each other for this particular specimen, but this is not always true. Depending on the properties of the soil springs, one of these can be significantly larger than the other. Under such circumstances, more deformation will localize in one of the critical segments. Corresponding to the distribution of curvature, the distribution of moment is shown in Fig. 7.9. The maximum moments occur in the critical segments as expected, and the moment tapers off more gradually in comparison to the curvature. This is because of the characteristics of the moment-curvature relationship where a nearly flat plateau is introduced by yielding of pipe material. It is also due to the fact that softening of the pipeline in the critical segments, which is associated with postbuckling behavior, results in elastic unloading in the pipeline everywhere except in the critical segments.

The developments of curvature and moment are shown in Figs. 7.10 to 7.13 for the critical segments in the stable zone and the settlement zone, respectively. The critical curvature and moment are negative in the stable zone and positive in the settlement zone in the coordinate system defined in the formulation in Ch. 6. The curvature increases monotonically as the settlement increases as shown in Figs. 7.10 and 7.12. In general, there are three stages in the development of curvature. In the first stage, the curvature-settlement relation is essentially linear. This corresponds to settlement from 0 to 8 inches (0 to 203 mm) for Specimen NOM. In the second stage, yielding of the pipeline initiates in the critical segments and the curvature grows at higher rate with respect to differential settlement. The curvature-settlement relation is nonlinear. This corresponds to settlement from 8 to 16 inches (203 to 406 mm). In the third stage, the moment-curvature relation of the pipeline starts to soften and deformation localizes in the critical segments. This results in rapid growth of curvature with respect to differential settlement. This latter stage is from settlements of 16 inches (406 mm) and up for Specimen NOM. For the critical curvature in the settlement zone, the average slopes in each of three stages are calculated as 0.1114×10^{-4} /in, 0.3083×10^{-4}/in and 0.9431×10^{-4}/in per inch of differential settlement, respectively. The differences among these slopes are obvious and significant.

The moment-settlement curves shown in Figs. 7.11 and 7.13 indicate the same division into three stages. Each of them has its characteristic. The curves are essentially linear in the first stage and nonlinear and monotonically increasing in the second stage. These indicate elastic behavior and elastic-plastic behavior, respectively. The third stage is, in general, associated with softening behavior which is characteristic of postbuckling behavior. As indicated by the average slopes calculated above, both plastification of pipe material and postbuckling softening contribute to the localization of deformation. The influence of postbuckling softening may be as large as three times of that of plastification.

It should be pointed out as a convention that the curvatures and moments presented in the solutions with the effects of local buckling are the average curvatures and moments in the elements. This is because in these solutions, which are solved by the ISPDR technique, the average curvature and moment are the representative measurements due to the application of the SPD relations. SPD relations are defined based on the average response of a pipeline segment of length equal to the principal wavelength from three-dimensional shell analysis (Table 4.2). They are applied to elements in the line of pipe analysis as a base on which the average property of the elements is determined. The solutions without the effects of local buckling, which are solved by the RMDI technique and will be discussed in the Sect. 7.2.2, are represented by curvature and moments at each integration point. Each of the critical segments for solutions with local buckling effects consists of only one element. This is because of the softening behavior of pipeline segments and the convention to use average curvature and moment to represent the solutions. However, the critical segments for solutions without local buckling effects may consist of several integration points due to the hardening elastic-plastic behavior.

7.2.2 Effects of Local Buckling

7.2.2.1 Comparisons of the Solutions for NOM and BENOM

The effects of local buckling are first demonstrated by the comparisons of the solutions for Specimens NOM and BENOM which are shown in Fig. 7.7 to 7.13. Specimen BENOM has the identical conditions on soil springs with Specimen NOM; and, the only difference is in the stiffness properties of the pipeline. The effects of local buckling are included for Specimen NOM in the SPD relations and the ISPDR solution technique. The effects of local buckling, however, are not included for Specimen BENOM which was determined from direct input of stress-strain relations and the RMDI solution technique.

Consequently, the differences between the solutions may be considered to be the effects of local buckling under the given soil conditions and temperature differential.

Figure 7.8 shows that the differences between the deformations are significant in the two critical segments and insignificant over the rest of the pipeline. The differences that can be observed from these figures are the length of the critical segments in which the deformation is localized, and the magnitude of the maximum curvatures. The solution with buckling effects has a relatively shorter length of critical segment and a significantly larger maximum curvature. This indicates that more deformation is localized in shorter segments due to the effects of local buckling. The solution with buckling has smaller moment, as shown in Fig. 7.9. This is due to the softening behavior in the postbuckling region.

The development of the critical curvatures and moments with respect to the differential settlement are shown in Figs. 7.10 to 7.13. There are three stages on the curvature-settlement curves and moment-settlement curves for Specimen NOM. Each stage has different characteristic. The curves for Specimen BENOM, however, only have first two stages, i.e. the stage with linear response and the one with elastic-plastic response. Since pipeline segments do not soften if the effects of local buckling are not included, the third stage with softening response cannot be seen in the solution of Specimen BENOM. The curves in Figs. 7.10 and 7.13 show that the differences between the solutions are negligible in the first stage and small in the second stage. The differences increases rapidly in the third stage which occurs for settlement greater than 16 inches. This is because, in the third stage, softening introduces significant localization of deformation into the critical segments, and elastic unloading in the rest of the pipeline. For non-softening the other solution continues with the hardening response and the entire pipeline continues to be loaded, either elastically or elastic-plastically.

7.2.2.2 Comparisons of the Solutions for TENOM and BETMP

To show the effects of local buckling under temperature differential, solutions for Specimens TENOM and BETMP are presented. The solution of Specimen TENOM includes buckling effects and that for Specimen BETMP does not. As shown in Table 7.2, the only difference between Specimen TENOM and NOM is that Specimen TENOM has temperature differential of 75 °F (41.7 °C) which results in a small initial axial force in compression. Both solutions are shown in Figs. 7.14 to 7.17. The effects of local buckling shown by this pair of solutions are obviously greater than those for solutions of Specimens NOM and BENOM. This is because of the interaction between the effects of local buckling

and temperature differential. This interaction can be explained through the change of the axial force in the pipeline. The axial force in pipelines increases as the imposed differential settlement increases because the slope length of the pipe is greater than the horizontal length. The effects of temperature differential is to change the initial axial force. A pipeline would have about 22 percent of the axial yield force in tension if the pipeline is subject to no temperature differential and is pressurized to produce hoop stress up to 72 percent of the yield strength. On the other hand, the same pipeline would have negligible initial axial force if it is subject to a temperature differential of 75 °F (41.7 °C) in addition to the pressure.

Different characteristics can be observed from the moment-curvature curves with no axial force and 20 percent of the axial yield force in tension as shown in Fig. 7.2. The moment-curvature curve without axial force has virtually no plastic plateau and negligible postbuckling strength. The other, however, has a visible plastic plateau and considerable remaining strength in the postbuckling region. With these differences in mind, local buckling behavior is expected to have a more significant influence on localization of deformation when there is a positive temperature differential.

7.2.2.3 Comparisons of the Solution for BSA02 and BEB02

The next pair of solutions is for Specimens BSA02 and BEB02. Similarly the solution of Specimen BSA02 includes local buckling effects and the other does not. Comparing to Specimen NOM, the only difference for these two specimens is the stiffness and strength of the bearing springs which have been reduced to one-fifth of the reference values in all zones. The solutions are shown in Figs. 7.18 to 7.21. The distributions of curvatures and moments at settlement of 31 inches are shown in Figs. 7.18 and 7.19 where the effects of local buckling are almost invisible. The effects of local buckling are more influential when the settlement is further increased as demonstrated by the critical curvature-settlement curves and critical moment-settlement curves in Figs. 7.20 and 7.21. In overall, the effects of local buckling under the condition of soft bearing spring are apparently less significant that those under the normal condition. This indicates the interaction between the local buckling effects and soil condition.

In summary, the effects of local buckling on the response of pipelines, particularly the localization of deformation, are significant. They start to grow rapidly and become obvious when the critical segments starts to soften. The effects of local buckling depend on the temperature differential (see Sect. 7.2.2.2) and soil conditions imposed on the pipeline (see Sect. 7.2.2.3). Strong interaction between local buckling effects and temperature

differential and soil conditions have been demonstrated in this Sect. 7.2.2.

7.2.3 Effects of Temperature Differential

Temperature differential is expected to have an important influence on the response of pipelines subjected to differential settlement. The influence can be demonstrated by comparison between solutions for Specimens NOM and TENOM. The solutions for both specimens have been discussed with respect to the effects of local buckling in Sects. 7.2.2.1 and 7.2.2.2. Both solutions for Specimens NOM and TENOM include effects of local buckling and are solved by ISPDR technique. A temperature differential of 75 °F (41.7 °C) is the only difference in the condition of Specimens NOM and TENOM. The comparison of these solutions is shown in Figs. 7.22 to 7.26.

Because of the temperature differential, Specimen TENOM has more deformation localization than Specimen NOM. This is more obvious at the critical segment in the stable zone as shown in Figs. 7.22 and 7.23. The location of this critical segment is one element closer to the transition of the ground profile than the one for Specimen NOM. The moments are smaller for Specimen TENOM in both critical segments at the settlement of 22 inches which is clearly shown in Fig. 7.24. The development of the critical curvature and moment with respect to differential settlement are shown in Figs. 7.25 and 7.26. The critical curvature of Specimen TENOM starts to increase rapidly at smaller settlement than for Specimen NOM. From Fig. 7.25, this starting point can be identified at settlement of about 8 inches (203 mm) for Specimen TENOM and 16 inches (406 mm) for Specimen NOM. This is the principal reason for the fact that deformation localization at the critical segment is apparently more significant for Specimen TENOM. The critical curvatures for both specimen grow at more or less the same rate with respect to the settlement once they start to grow rapidly. The moment-settlement curves in Fig. 7.26 show similar characteristics. Both of them have a linear elastic region, a nonlinear elastic-plastic region and a softening region. In the softening region, both of them have a significant drop in moment capacity followed by a relatively stabilized response. The differences are, however, obvious in two aspects. First, the maximum moment capacity of Specimen TENOM is lower and is reached earlier. Second, the drop of moment capacity is larger for Specimen TENOM and consequently the remaining capacity is significantly lower.

The differences discussed above are a direct consequence of the imposed temperature differential. As discussed in Sect. 7.2.2.2 the temperature differential of 75 °F changes the initial axial force in the pipeline from about 22 percent of the axial yield force in

tension to a negligible level. As a result, the response of the critical segments have different characteristics which are represented by moment-curvature curves without axial force and with 20 percent of the axial yield force in Fig. 7.2. The moment-curvature curves without axial force, which is more representative of Specimen TENOM, has lower maximum moment capacity and starts to soften at smaller curvature. These characteristics are responsible for the differences in the solutions for Specimens TENOM and NOM and have been reflected in the solutions as discussed along with the comparison of the solutions.

7.3 EFFECTS OF GEOTECHNICAL PARAMETERS

Geotechnical parameters considered here include the stiffness and strength of bearing, uplift and longitudinal soil springs and the length of transition zone of the ground profile. The effects of each of these parameters will be investigated in one of the following sub-sections. To study one parameter, two specimens are analyzed to compare with the reference Specimen NOM. One specimen has the value of the parameter under consideration at one-fifth of the reference value and the other at five times the reference value. These values serve as estimates of the lower and upper bounds of the parameter. The effects of each parameter can be demonstrated by comparison of the solutions for these three specimens.

7.3.1 Effects of the Bearing Soil Springs

The specimens used to study the effects of bearing springs are BSA02 and BSA50. The parameter under consideration is either the strength or the stiffness of bearing springs, because only one of them is independent (see Sect. 7.1.4). Specimens BSA02 and BSA50 have the smaller and larger stiffness and strength of bearing springs, respectively, than for Specimen NOM. The solutions are shown in Figs. 7.27 to 7.30 along with the solution of Specimen NOM. The deformed configurations in Fig. 7.27 show the great influence of the stiffness and strength of the bearing springs. From the deformed configurations, the critical segments in both the stable zone and settlement zone can be identified. They can be verified by the curvature distributions.

As a general rule, the critical segment in the settlement zone is located at the element just before the pipeline starts to be supported by bearing springs. The pipeline between the transition and the critical segment in the settlement zone lifts off the ground and consequently is not supported by the bearing springs. The critical segment in the stable zone is located at the element just before the start of the region of yielding in the bearing

springs. The bearing springs between the critical segment and the transition have yielded and reached their full strength. Due to the the perfectly plastic behavior assumed for soil springs, bearing springs in this region do not provide any resistance to additional displacements. For specimens discussed here, the critical segments are indicated in Fig. 7.27. The interesting fact is that the critical segments in the stable zone are located far apart while those in the settlement zone are located very close to each other.

To rationally explain this fact, more details need to be examined. The pipeline is subject to overburden load, which is constant over the length of the pipeline, and the transverse forces generated by uplift and bearing springs. Only one of the uplift and bearing springs is active at any location for any configuration as defined and discussed in Sect. 6.5.3. A conceptual free body diagram of the pipeline at the transition is shown in Fig. 7.49 where the axial forces are neglected to simplify the diagram. As shown in Fig. 4.49, the uplift springs are only active in the region between the transition and the critical location in the settlement zone where the pipeline lifts off the ground. The bearing springs yield in the region between the transition and the critical location in the stable zone. Because of the slope of the pipeline around the transition zone and the significant axial load in tension, the bearing springs in the stable zone tend to pick up most of the load generated by the uplift springs. From Fig. 7.49, it is clear that the distance between the transition and the critical location in the settlement zone depends primarily on the magnitude of the load generated by the uplift springs and the capacity of the pipeline to resist the transverse load; and, the distance between the transition and the critical location in the stable zone depends primarily on the load to be supported by the bearing springs and the strength of the bearing springs.

With respect to Specimens BSA02, BSA50 and NOM, the solutions in Fig. 7.27 show that the critical locations in the settlement zone are close to each other. As a result, about the same amount of load is generated by the uplift springs because the strengths of the uplift springs are the same for all three specimens and the lengths of the region which lifts off are approximately equal. However, the strengths of bearing springs are much different for these three specimens. Consequently, the length of the region with yielded bearing springs is largest for Specimen BSA02 and smallest for Specimen BSA50. The localization of deformation is shown in the distributions of curvature in Fig. 7.28. At a settlement of 31 inches (0.79 m), localization of deformation at the critical segments is significant for Specimen BSA50 and NOM. The critical curvature of Specimen BSA50 is obviously larger than that of Specimen NOM. The localization of deformation for Specimen

BSA02 can barely be seen in the settlement zone and has yet to be developed up to settlement of 31 inches (0.79 m) in the stable zone.

The differences with respect to the localization of deformation are also shown in the critical curvature-settlement curves in Fig. 7.29 and critical moment-settlement curves in Fig. 7.30. The curves for Specimen BSA02 remain essentially in the region of linear response up to settlement of 32 inches (0.81 m) and starts to yield afterward. On the other hand, the curves for Specimen BSA50 have linear response only up to a settlement of 4 inches (0.1 m) and softening response from 8 inches (0.2 m) and beyond. Comparing these latter values with 8 and 16 inches (0.2 and 0.4 m) for Specimen NOM, Specimen BSA50 yields and softens at significantly smaller settlement. This is because of the higher strength and stiffness of the bearing springs which make the moment in the critical segments increase more rapidly.

In summary, the effects of the stiffness and strength of bearing springs has great influence on the response of the pipeline, particularly on the localization of deformation in the critical segments. As a result, the settlement corresponding to a given curvature may vary from just a few inches to 40 inches as the strength and stiffness of the bearing springs change from the lower bound to upper bound. The principal reason is that bearing springs of low strengths yield over longer lengths in the stable zone. This allows the deformation to occur on a longer segment of the pipeline and in a more gradual manner.

7.3.2 Effects of the Uplift Soil Springs

The effects of uplift soil springs can be studied by examining the solutions of Specimens USA02, USA50 and NOM. These specimens are identical except for the stiffness and strength of the uplift springs. The stiffness of the soil springs is assumed to be proportional to their strength, and therefore, only one of them is independent. The strength of the uplift springs is one-fifth of the reference value for Specimen USA02 and five times for Specimen USA50. The reference value of the strength of uplift springs is the one applied to Specimen NOM. The solutions for this group of specimens are shown in Figs. 7.31 to Fig.7.34.

First, the deformed configurations of the pipeline at a settlement of 24 inches (0.61 m), as shown in Fig. 7.31, are examined. A clear observation is that the critical segments in the stable zone are located close to each other and those in the settlement zone are located further apart. This behavior is opposite to the behavior observed in the solutions of

Specimens BSA02, BSA50 and NOM, which were discussed in Sect. 7.3.1. The behavior can also be explained conceptually based on the free body diagram of the pipeline in the transition region which, as in the previous sub-section, is shown in Fig. 7.49.

For this group of specimens, the properties of bearing springs are identical. However, the strength of uplift springs is different for each of the specimens. The length of the lifted segment of the pipeline, or the distance between the transition and the critical location in the settlement zone, is determined primarily by the transverse load generated by the uplift springs and the moment capacity of the pipeline to resist transverse loads. The moment capacity of the pipeline is approximately the same for Specimens USA02, USA50 and NOM, with a limited difference introduced by axial force which varies within a narrow range for this group of specimens. This can be verified by the moment-settlement curves in Fig. 7.34 where the moment capacities for all three specimens are clearly defined. As a result, the load generated by the uplift springs becomes the primary factor to determine the length of the lifted segment. As shown in Fig. 7.49, the intensity of the transverse load generated by the uplift spring is limited by the strength of uplift springs. Consequently, a lower strength of the uplift springs results in a longer lifted segment. This is clearly demonstrated by Fig. 7.31.

The effects of the strength of the uplift springs on localization of deformation is great and is shown by the distribution of curvatures in Fig. 7.32. The localization of deformation is most significant for Specimen USA50 with the upper bound strength of the uplift springs and least significant for Specimen USA02 with lower bound strength. At a settlement of 24 inches (0.61 m), the critical curvature of Specimen USA50 is about 5 times that of the critical curvature of Specimen USA02 in the stable zone, and is about 14 times that in the settlement zone. These number show that the effects of the uplift springs can change the response of pipelines from virtually no localization of deformation to very significant localization.

The curvature-settlement curves in Fig. 7.33 and the moment-settlement curves in Fig. 7.34 further illustrate the influence of the uplift springs. As discussed in Sect. 7.2.1, the history of critical curvature and moment with respect to the settlement can be divided into three stages of different characteristics which are linear, nonlinear and softening response. For Specimen NOM, the linear response ends at a settlement of 8 inches (0.2 m) and the softening response starts at a settlement of 16 inches (0.41 m). These numbers become 6 inches (0.15 m) and 12 inches (0.30 m) for Specimen USA50; and, 14 inches (0.36 m) and 24 inches (0.61 m) for Specimen USA02, respectively. These numbers

indicate a trend that the differential settlements covered by both the linear and nonlinear response stages increase as the strength of the uplift springs decrease. As a result of this trend, a much larger differential settlement can be tolerated by the pipeline if the strength of the uplift springs is reduced.

7.3.3 Effects of the Longitudinal Soil Springs

The effects of the longitudinal springs may be studied by examining two group of solutions. The first group consists of Specimens LSS02, LSS50 and NOM which focuses on the effects of the strength and stiffness of the longitudinal springs. The second group consists of Specimens LSL02, LSL50 and NOM which demonstrates the effects of the length of the region where relatively weak longitudinal springs are applied.

Specimens LSS02 and LSS50 are the same as Specimen NOM except for the properties of the longitudinal springs. The strength and stiffness of the longitudinal springs are one-fifth of the reference value of Specimen NOM for Specimen LSS02 and five times for Specimen LSS50. The length of the region with relatively weak longitudinal springs is 1000 inches (25.4 m) and is the same for all three specimens in this group. The solutions are shown in Figs. 7.35 to 7.40. The deformed configurations at a settlement of 28 inches (0.71 m) in Fig. 7.35 essentially overlap each other with some differences at the critical segment in the settlement zone. The distribution of curvature in Fig. 7.36 show that the critical segments of all three specimens lie at exactly the same locations both in the stable and settlement zones. The differences in the critical curvatures in both stable and settlement zones are not nearly as great as those due to the effects of the bearing or uplift springs discussed in Sects. 7.3.1 and 7.3.2. The critical curvature-settlement curves in the settlement zone in Fig. 7.37 indicate the critical curvature for Specimen LSS02 with the lower bound strength of longitudinal springs is larger than those for other two specimens. This is mainly because the region of softening response starts earlier for Specimen LSS02 as shown in Fig. 7.38.

To explain the mechanism of how the longitudinal springs influence the response, the distributions of axial force at a settlement of 28 inches (0.71 m), and the critical axial force-settlement curves, are shown in Figs. 7.39 and 7.40, respectively. Due to different strengths of the longitudinal springs two types of distribution of axial force are produced in the pipeline, which are represented by the curves for Specimens LSS02 and LSS50 in Fig. 7.39, respectively. The distribution of axial force for Specimen LSS02 is nearly uniform because of the low strength of longitudinal springs. The distribution for Specimen LSS50

is, however, non-uniform with the maximum axial force close to the transition. The axial force decreases rapidly away from the transition in the stable zone because of the high strength of the longitudinal springs. In the settlement zone, the axial force decreases slowly in the first 1000 inches (25.4 m), where the relatively weak longitudinal springs are applied and decreases rapidly afterward. This indicates that the axial deformation is restricted to a shorter length close to the transition by stronger longitudinal springs, and a larger axial force is built up. Figure 7.40 illustrates more clearly that the critical axial force increases as the strength of longitudinal springs increases. As a result, the localization of deformation is less significant for Specimen LSS50, and is more significant for Specimen LSS02 than for Specimen NOM. This is because larger tensile axial force corresponds to relatively longer plastic plateau and relatively less unstable postbuckling behavior as shown clearly in Fig. 7.2.

The second group of specimens is designated to the effects of the length of the region where relatively weak longitudinal springs are applied. This length is 200 inches (5 m), 1000 inches (25.4 m) and 5000 inches (127 m) for Specimens LSL02, NOM and LSL50, respectively. Since the strength of the relatively weak longitudinal springs is only about one-fifth of the normal value for longitudinal springs in stable zone and remote settlement zone, application of these relatively weak springs over different length results in significant difference in the axial restriction provided by longitudinal springs. In addition, the region with the relatively weak longitudinal springs, which extends from the transition into settlement zone, is the most important region for the building up of axial force in tension at the critical segments. By the same mechanism discussed previously in this subsection, substantial differences in the response of pipelines are introduced. They are illustrated by solutions in Figs. 7.41 to 7.44. The deformed configurations at a settlement of 29 inches (0.74 m), as shown in Fig. 7.41, show noticeable differences at the critical segments both in the stable and the settlement zones. These differences are reflected in Fig. 7.42 where the curvature distributions are displayed. The critical curvature for Specimen LSL02, where the length is shorter and axial restriction is stronger, is significantly less than the critical curvatures of the other two. The critical segments lie at the same locations both in the stable and settlement zones. Fig. 7.43 shows that the critical curvatures agrees well with each other up to 16 inches (0.41 m) and difference develops rapidly afterward because the axial force built up by strong axial restraint stabilizes the softening response in the case of Specimen LSL02.

7.3.4 Effects of Ground Profile in Transition Zone

In all the solutions discussed in the previous sub-sections, the ground profile in the transition zone is assumed to be a step-wise ground profile as defined in Sect. 6.5.1 and shown in Fig. 6.6. This implies that the settlement occurs over a negligible length. In reality, however, settlements may occur over wide ranges of length. To study the effects of the ground profile in the transition zone, two specimens, TPL05 and TPL20, are analyzed. The lengths of transition zone are 5 and 20 feet for Specimens TPL05 and TPL20, respectively. The smooth ground profile defined in Eq. (6.72), and shown in Fig. 6.7, is assumed. This ground profile may not be that which occurs in the field but it simplifies the description of ground profile to one parameter which is the length of the transition zone. This length is believed to be the most important parameter representing the ground profile.

The solutions for Specimens TPL05, TPL20 and NOM are shown in Figs. 7.45 to 7.48. Some differences in deformed configurations can be observed in Fig. 7.45, particularly at the critical segments. The curvature distributions at a settlement of 31 inches (0.79 m) in Fig. 7.46 illustrate that the localization of deformation is reduced as the length of transition zone increases. This is more apparent at the critical location in the settlement zone. The critical curvature reduced by 37 percent as the length of transition zone increases from zero to 20 feet. This reduction is large enough to make the ground profile one of the factors to be studied. The critical curvature-settlement curves are shown in Fig. 7.47. The slope of the curve for Specimen TPL20 in the softening region is obviously smaller than those of other two curves, and this is a result of less localization of deformation occuring in Specimen TPL20.

Soil Spring		pipeline with diameter of 12.75 inches			pipeline with diameter of 48 inches		
		Ultimate Resistance	Ultimate Displacement	Stiffness	Ultimate Resistance	Ultimate Displacement	Stiffness
		(kip/in)	(in)	(kip/in^2)	(kip/in)	(in)	(kip/in^2)
Uplift Spring		1.0	1.2	0.8333	3.7647	1.2	3.1371
Bearing Spring		1.0	1.2	0.8333	3.7647	1.2	3.1371
Longi-tudinal Spring	transition and adjacent sett-lement zones	0.05	0.25	0.2	0.1882	0.25	0.7529
	other zones	0.25	0.25	1.0	0.9412	0.25	3.7647

Table 7.1 Conversion of Properties of Soil Springs

Series	Specimen	Uplift Spring	Bearing Spring	Longitudinal Spring		Length of Transition Zone	Temperature Differential (°F)	Effect of Buckling
				Strength	Length			
	NOM	1.0	1.0	1.0	1.0	0.0	0.0	yes
	TENOM	1.0	1.0	1.0	1.0	0.0	75	yes
USA	USA02	0.2	1.0	1.0	1.0	0.0	0.0	yes
	USA50	5.0	1.0	1.0	1.0	0.0	0.0	yes
BSA	BSA02	1.0	0.2	1.0	1.0	0.0	0.0	yes
	BSA50	1.0	5.0	1.0	1.0	0.0	0.0	yes
LSS	LSS02	1.0	1.0	0.2	1.0	0.0	0.0	yes
	LSS50	1.0	1.0	5.0	1.0	0.0	0.0	yes
LSL	LSL02	1.0	1.0	1.0	0.2	0.0	0.0	yes
	LSS50	1.0	1.0	1.0	5.0	0.0	0.0	yes
TPL	TPL05	1.0	1.0	1.0	1.0	5.0	0.0	yes
	TPL20	1.0	1.0	1.0	1.0	20.0	0.0	yes
BE	BENOM	1.0	1.0	1.0	1.0	0.0	0.0	no
	BETMP	1.0	1.0	1.0	1.0	0.0	75	no
	BEB02	1.0	0.2	1.0	1.0	0.0	0.0	no

Table 7.2 Specification of Specimens for Settlement Analysis

a) Acronym Abbreviations

NOM = **NOM**inal specimen with σ_θ=0.72 σ_Y and parameters in Table 7.1
BE = **NOM** with **B**uckling **E**xcluded
BSA = **NOM** with variation in **B**earing **S**prings in **A**ll zones
USA = **NOM** with variation in **U**plift **S**prings in **A**ll zones
LSS = **NOM** with variation in **L**ongitudinal **S**pring **S**trength in all zones
LSL = **NOM** with variation in **L**ength of region of weak **L**ongitudinal **S**prings
TPL = **NOM** with variation in **T**ransition **P**rofile **L**ength
BENOM=NOM with **B**uckling **E**xcluded
TENOM=NOM with **TE**mperature differential
BETMP =NOM with **B**uckling **E**xcluded and **TeMP**erature differential

b)Numerical Values of Parameters

Behind an acronym, 02 = parameter reduced to 20% of value for **NOM**, and
.50 = parameter increased to 500% of value for **NOM**
Except for acronym **TPL** where 05 = a transition zone of 5 feet (1525 mm)
and 20 = a transition zone of 20 feet (6100 mm)

Table 7.3 Definition of Series and Specimens for Settlement Analysis

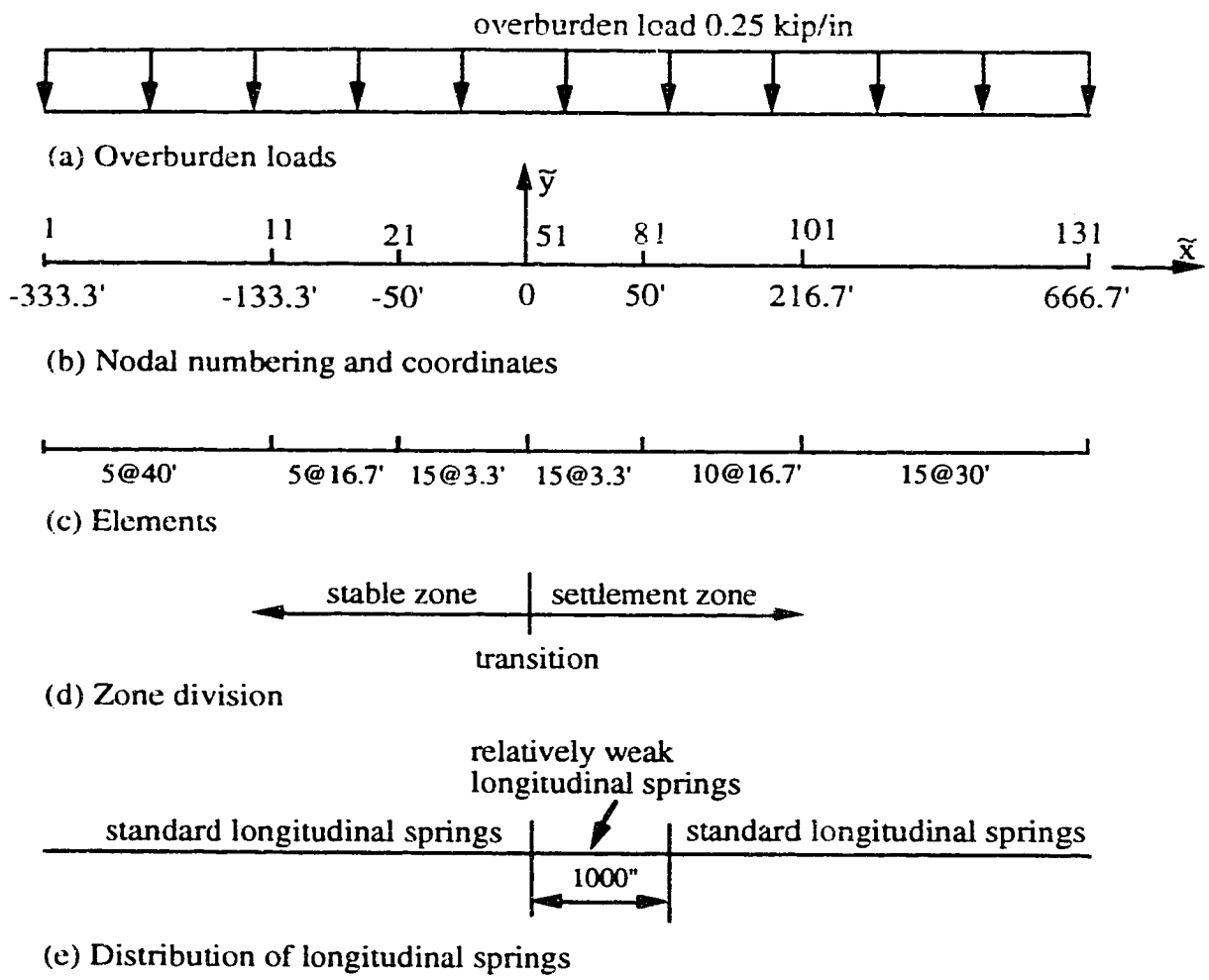

Fig. 7.1 Discretization of Pipelines

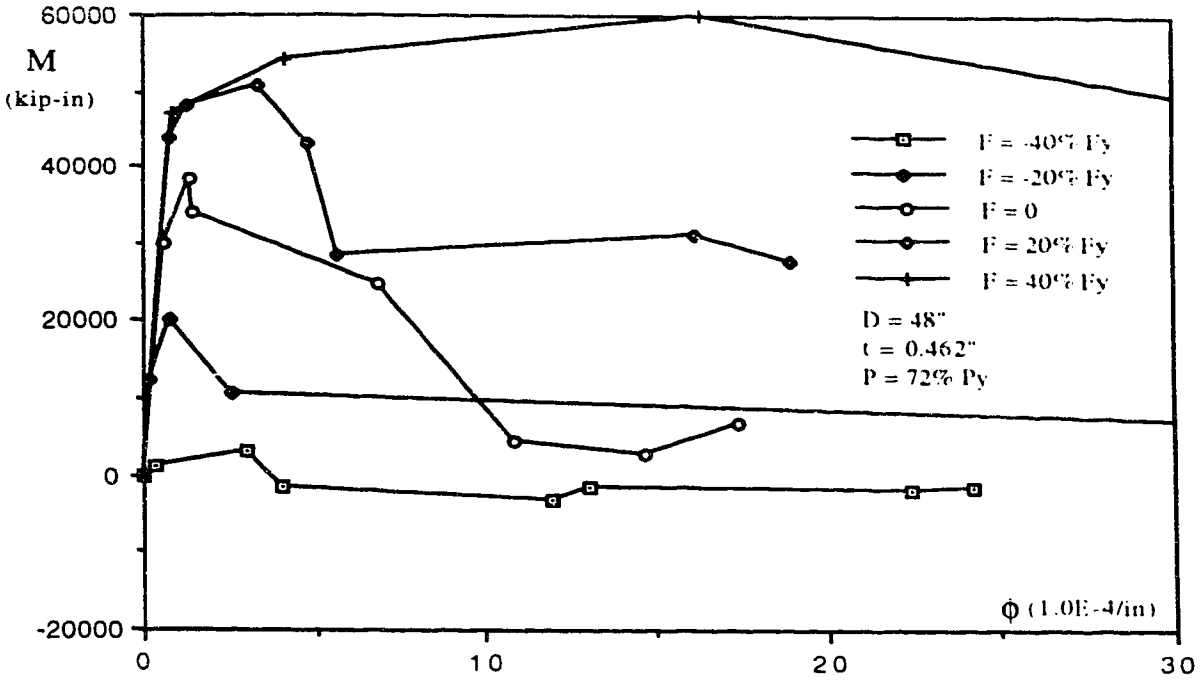

Fig. 7.2 SPD Relations for Moment vs. Curvature

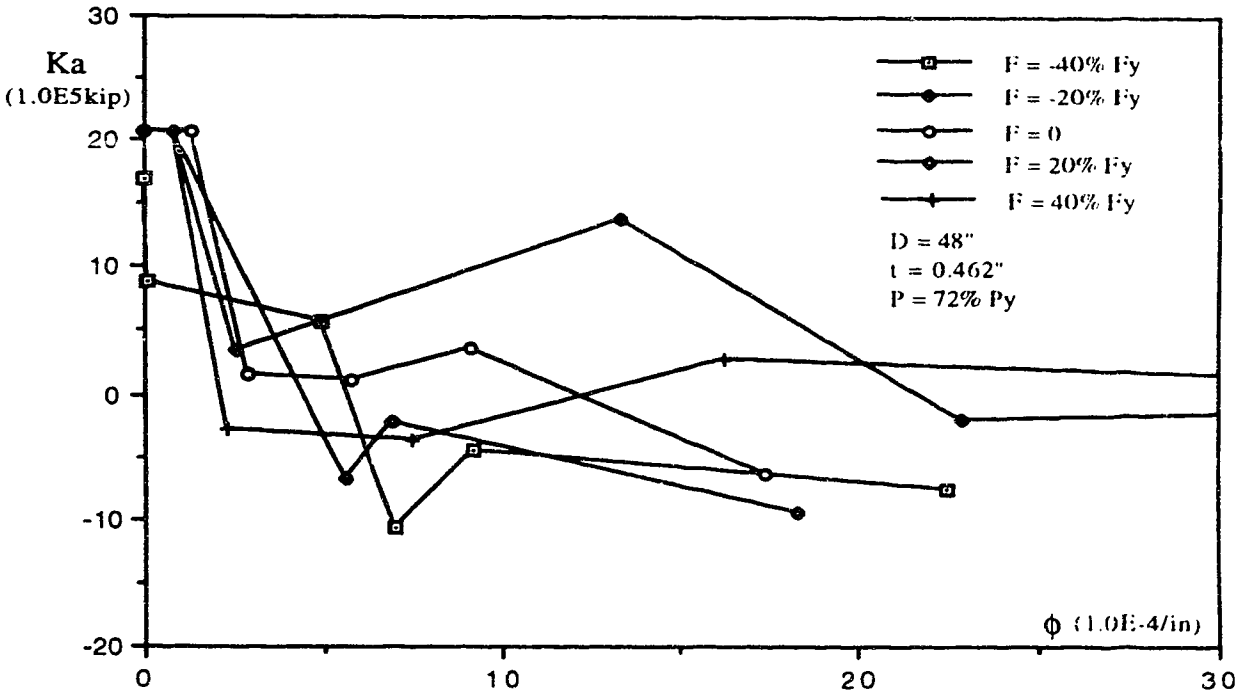

Fig. 7.3 SPD Relations for Axial Stiffness vs. Curvature

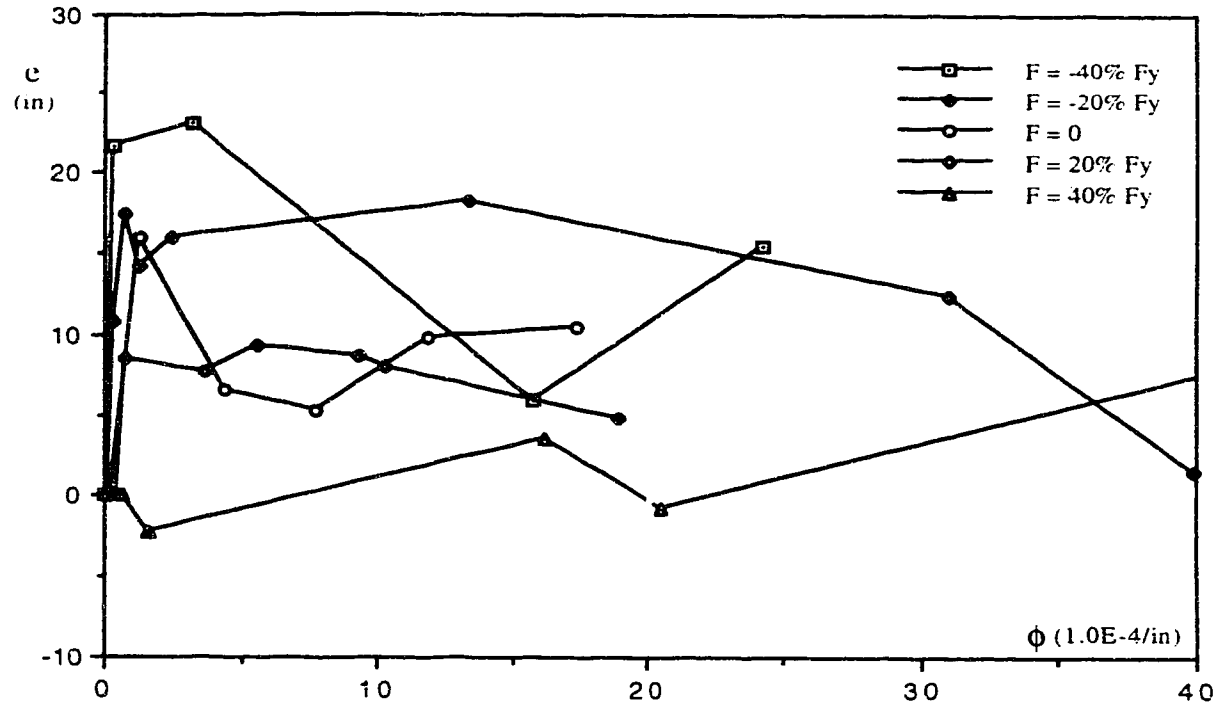

Fig. 7.4 SPD Relations for Distance Between the Centroids of Elastic and Tangent Stiffness vs. Curvature

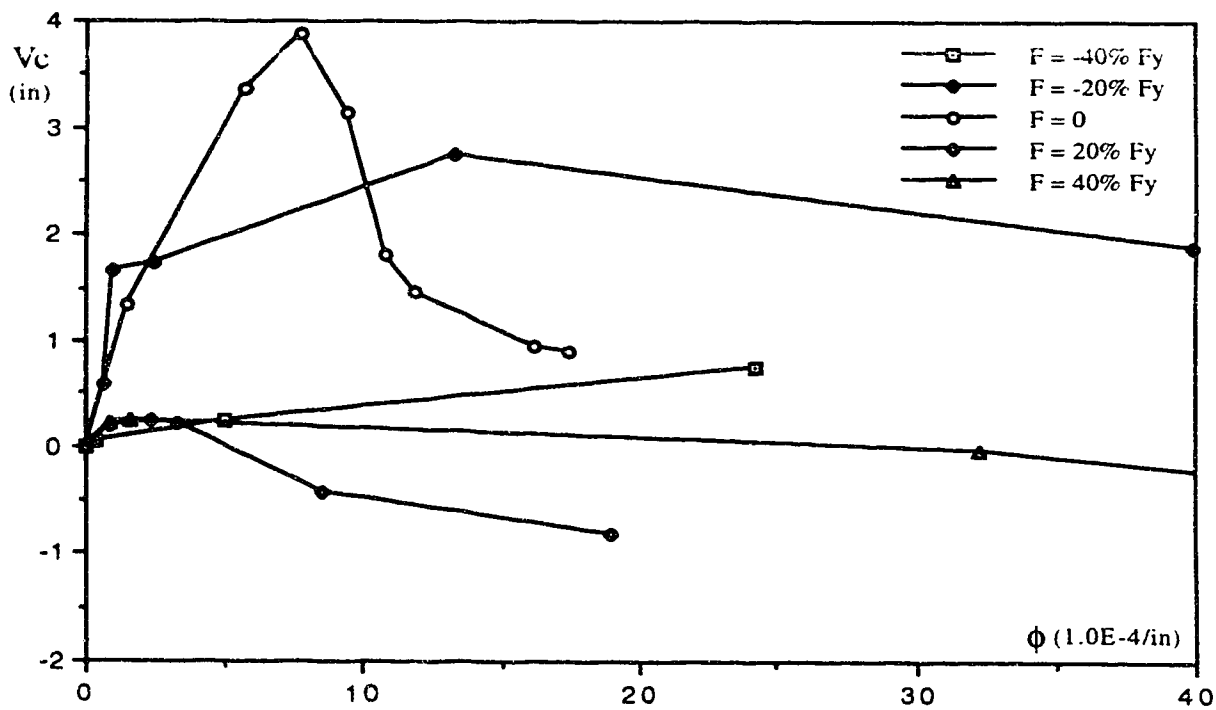

Fig. 7.5 SPD Relations for Deflection of the Centroid of Elastic Stiffness vs.Curvature

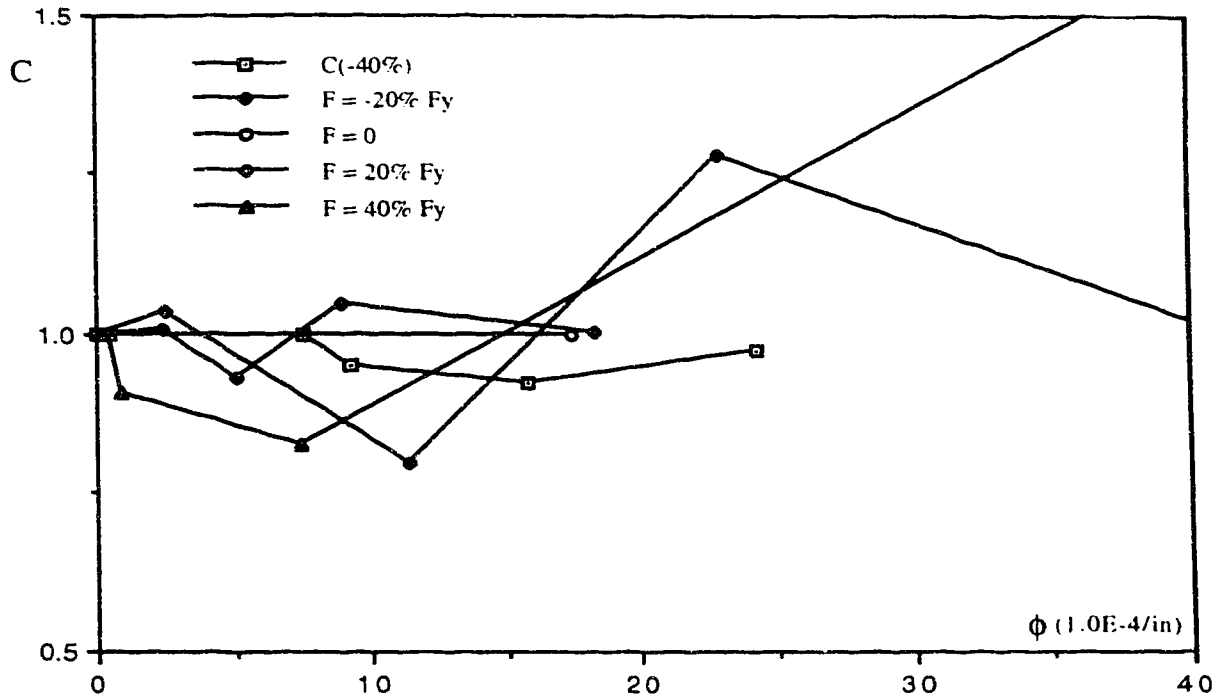

Fig. 7.6 SPD Relations for Amplification Factor vs. Curvature

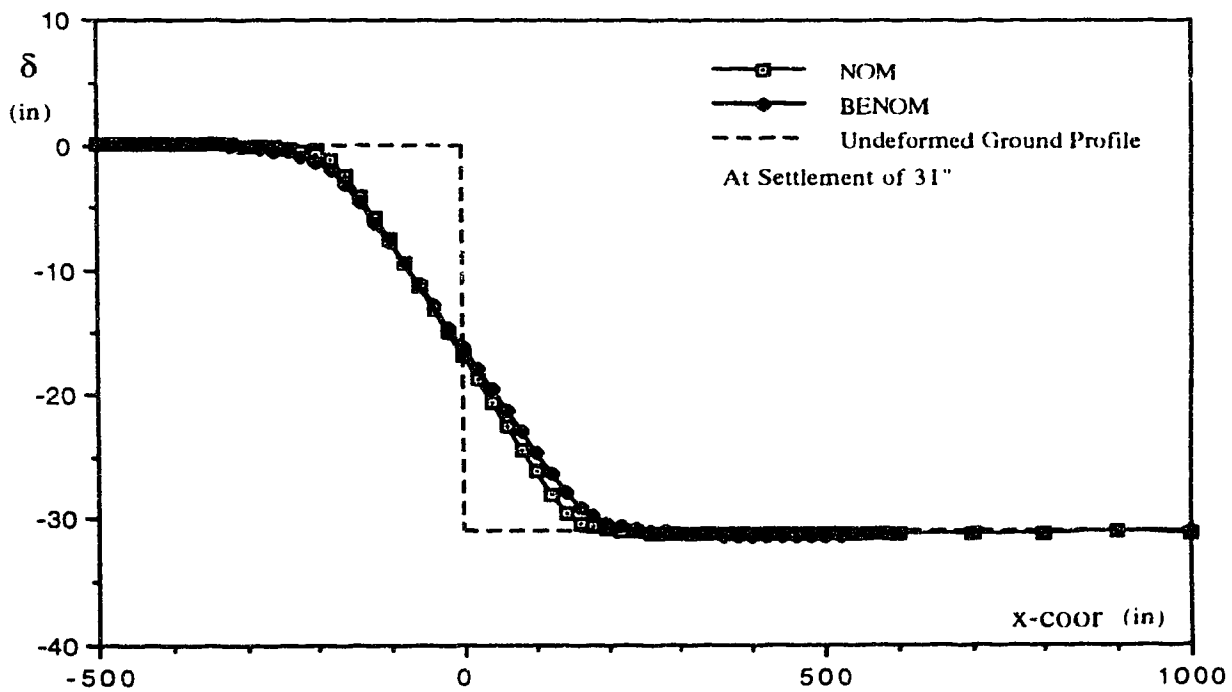

Fig. 7.7 Deformed Configurations for Specimens NOM and BENOM

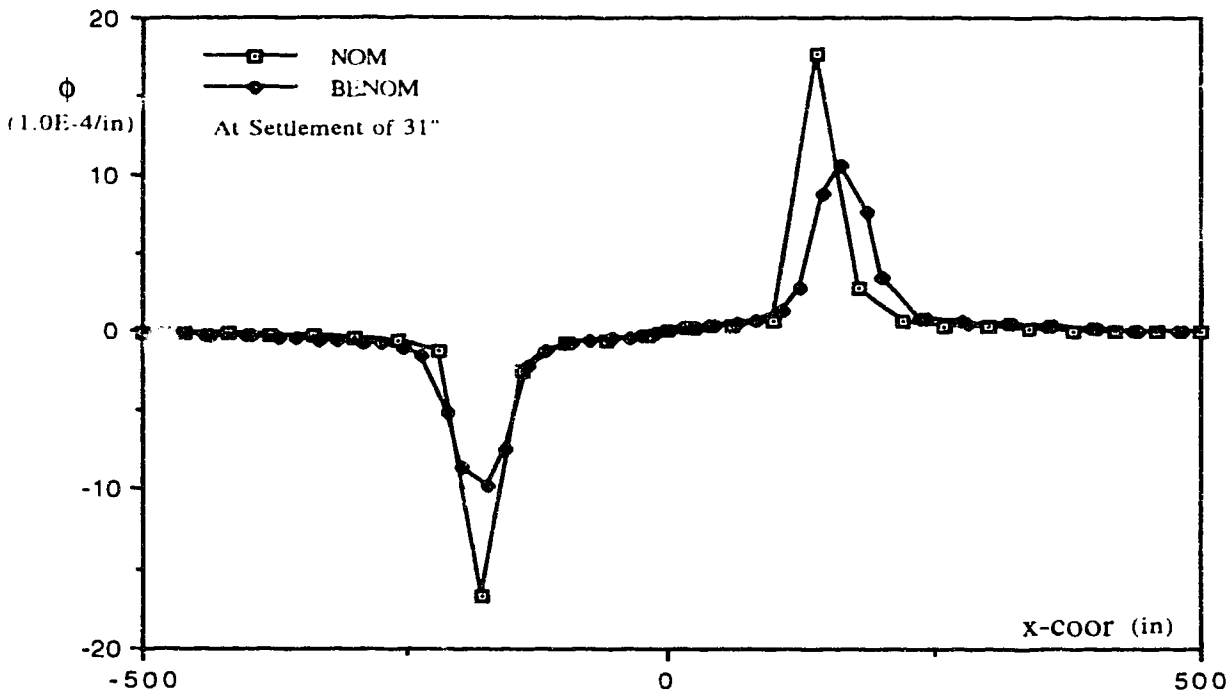

Fig. 7.8 Distributions of Curvature for Specimens NOM and BENOM

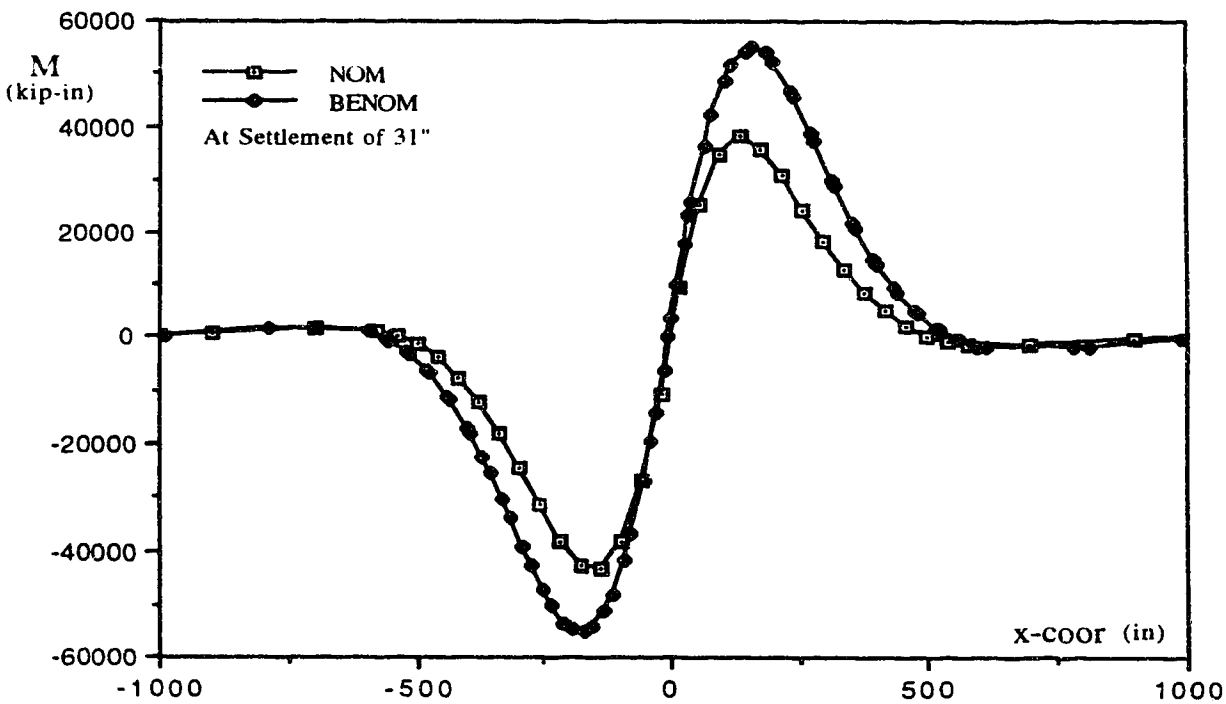

Fig. 7.9 Distributions of Moment for Specimens NOM and BENOM

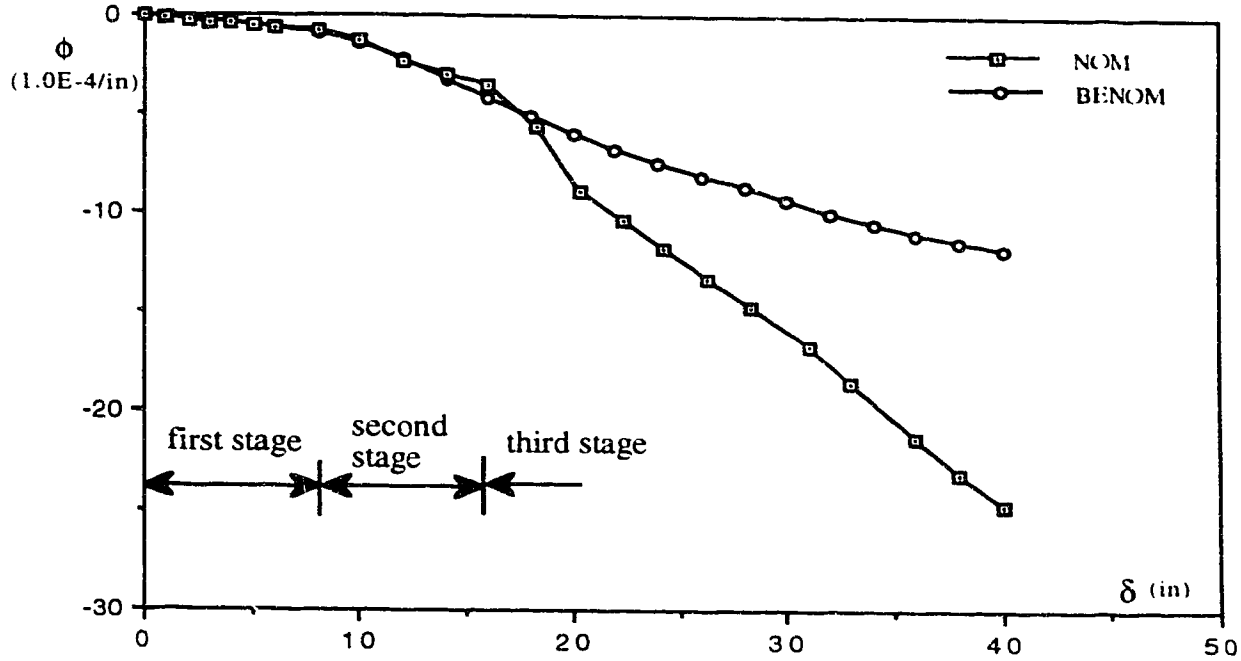

Fig. 7.10 Critical Curvature-Settlement Curves in the Stable Zone for Specimens NOM and BENOM

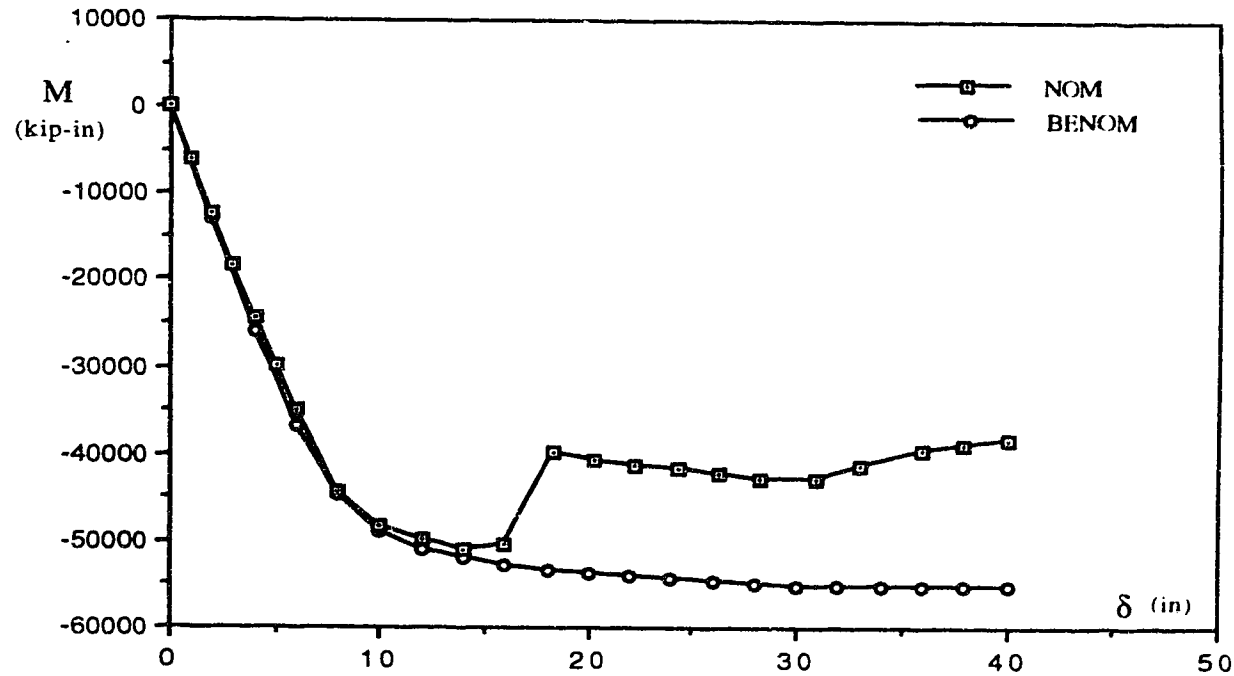

Fig. 7.11 Critical Moment-Settlement Curves in the Stable Zone for Specimens NOM and BENOM

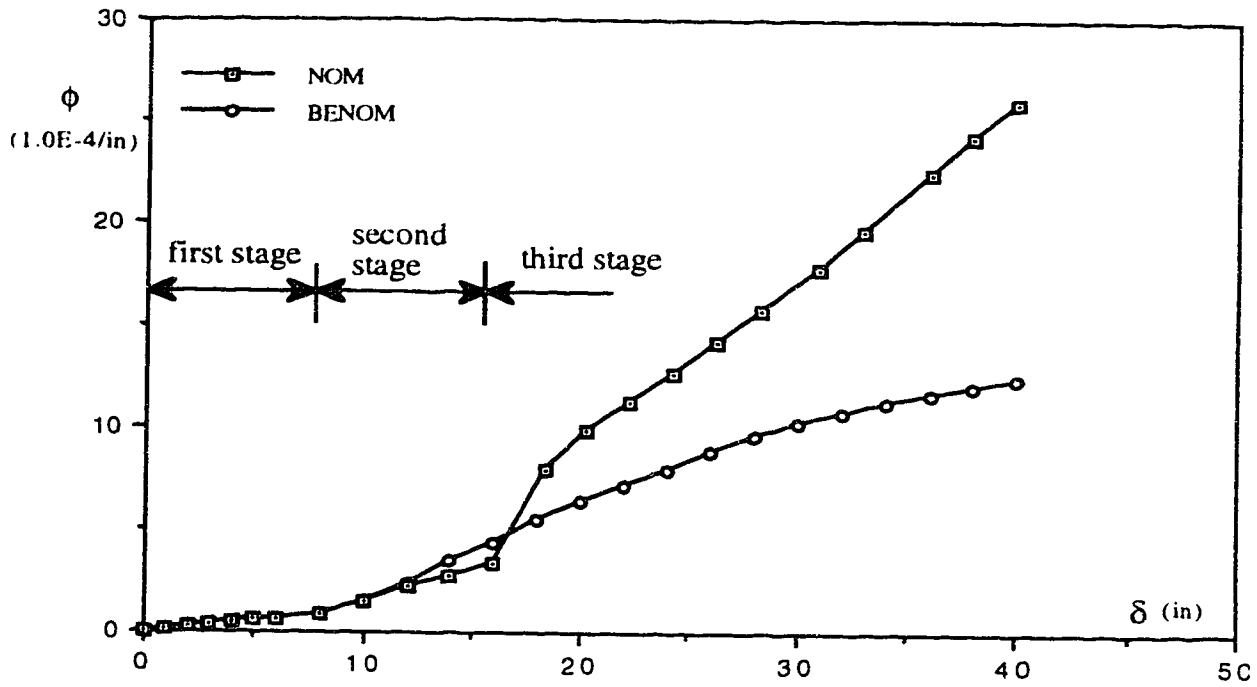

Fig. 7.12 Critical Curvature-Settlement Curves in the Settlement Zone for Specimens NOM and BENOM

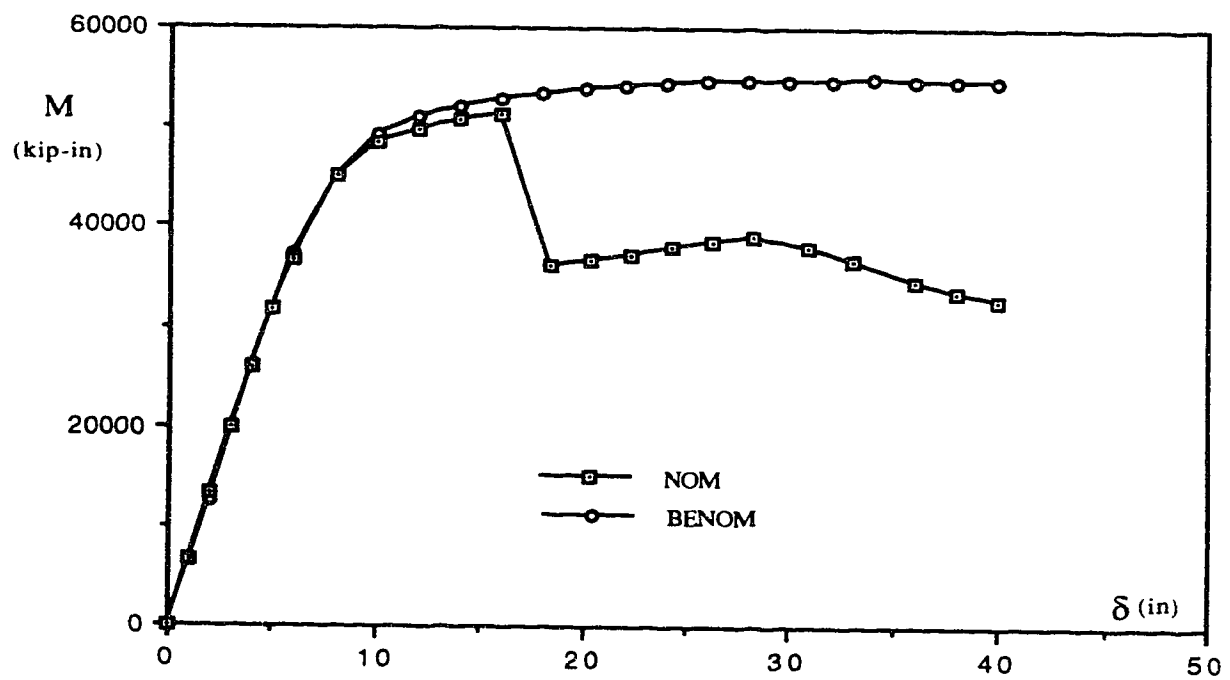

Fig. 7.13 Critical Moment-Settlement Curves in the Settlement Zone for Specimens NOM and BENOM

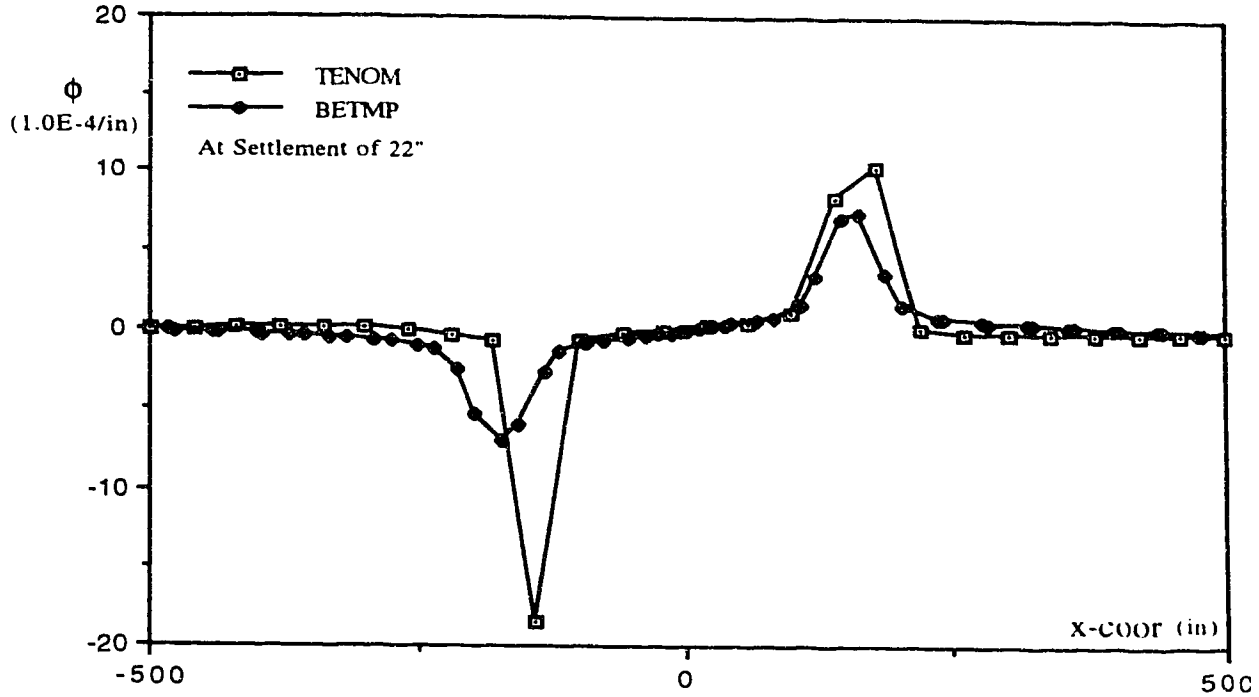

Fig. 7.14 Distributions of Curvature for Specimens TENOM and BETMP

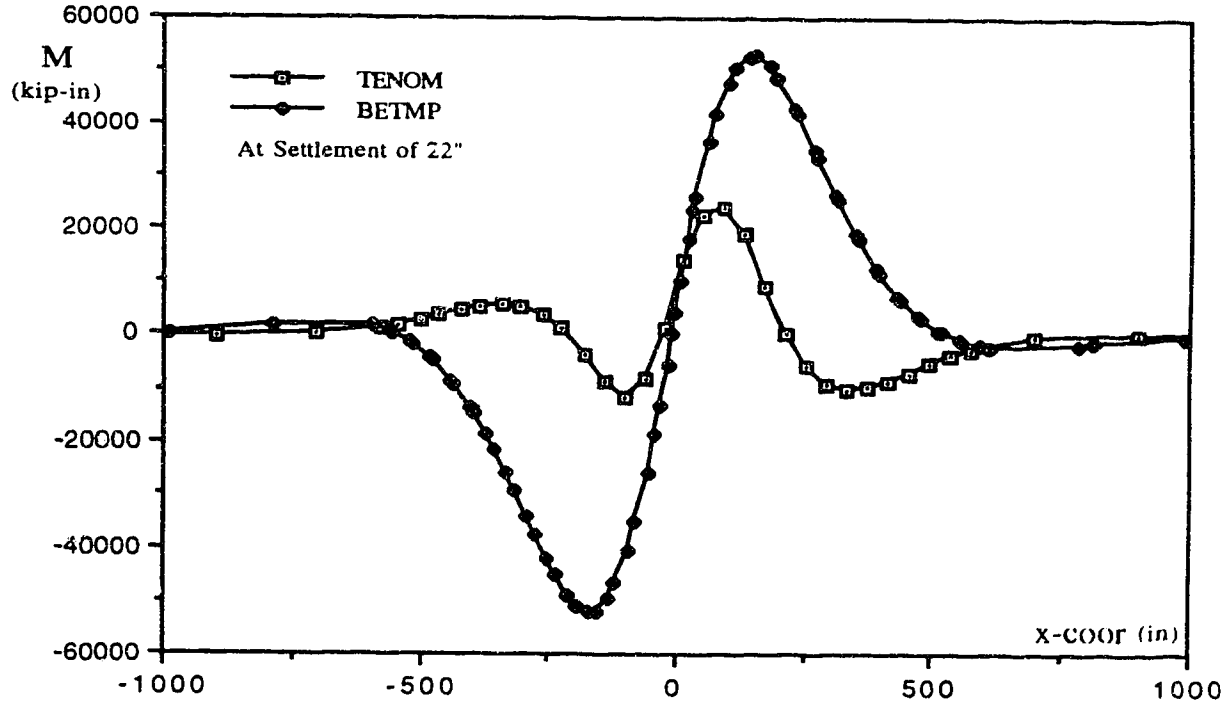

Fig. 7.15 Distributions of Moment for Specimens TENOM and BETMP

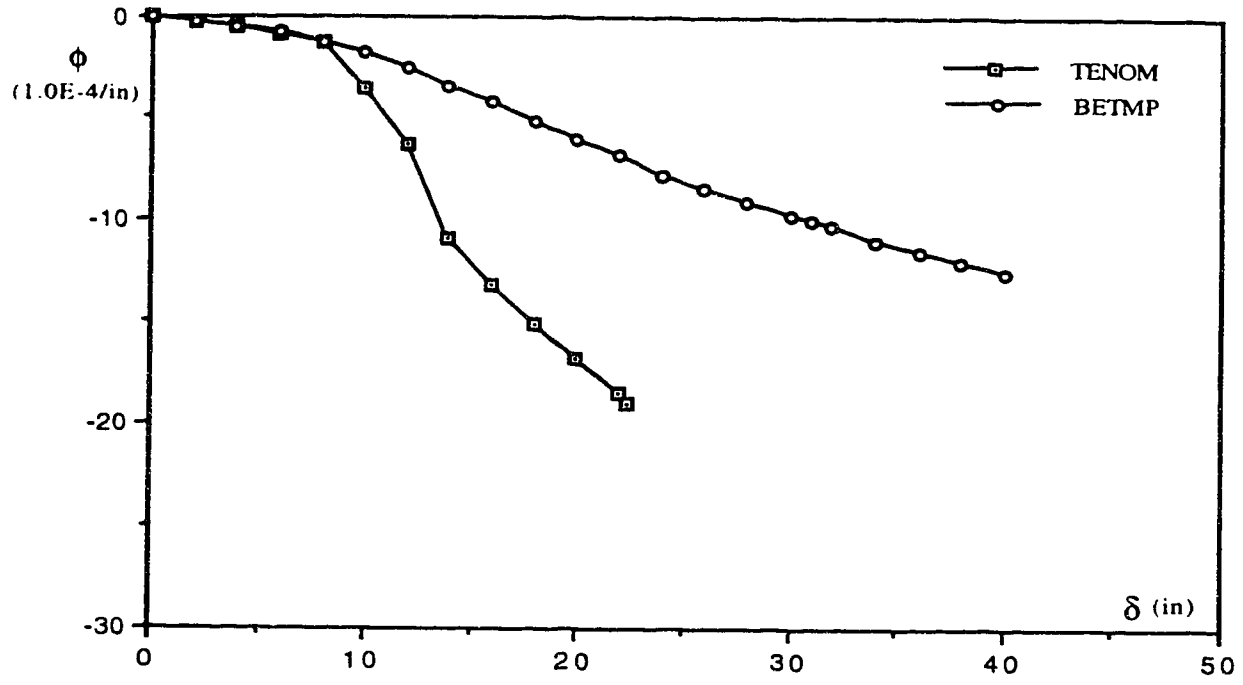

Fig. 7.16 Critical Curvature-Settlement Curves in the Stable Zone for Specimens TENOM and BETMP

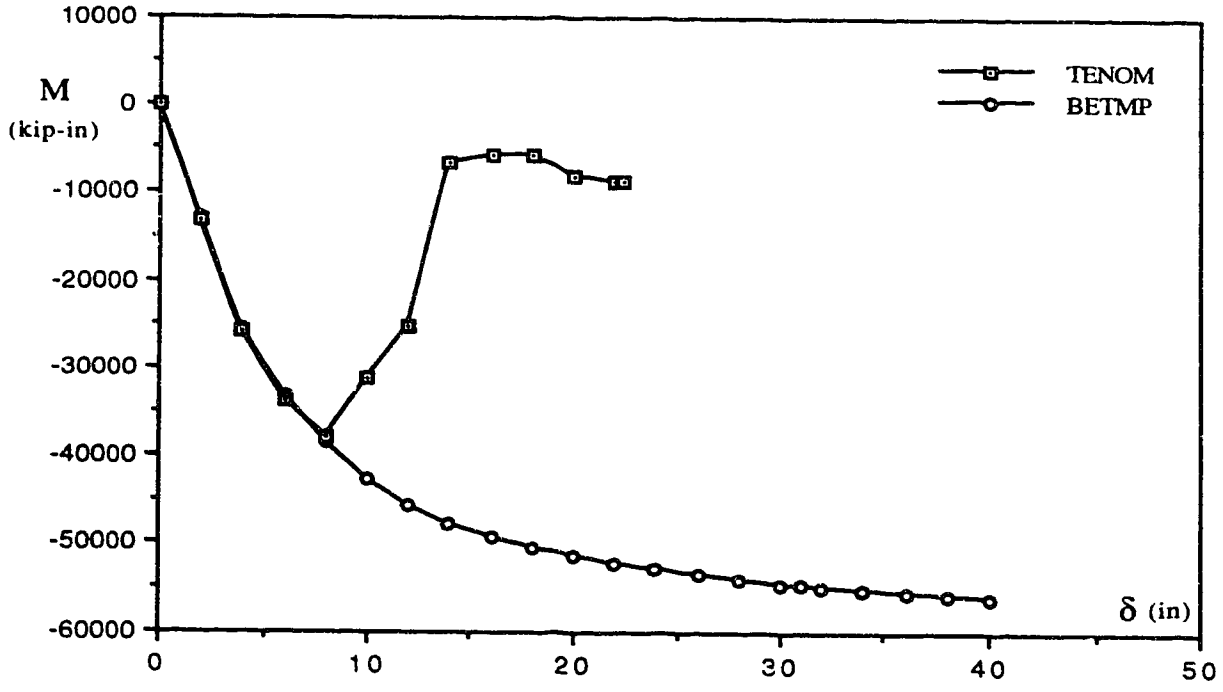

Fig. 7.17 Critical Moment-Settlement Curves in the Stable Zone for Specimens TENOM and BETMP

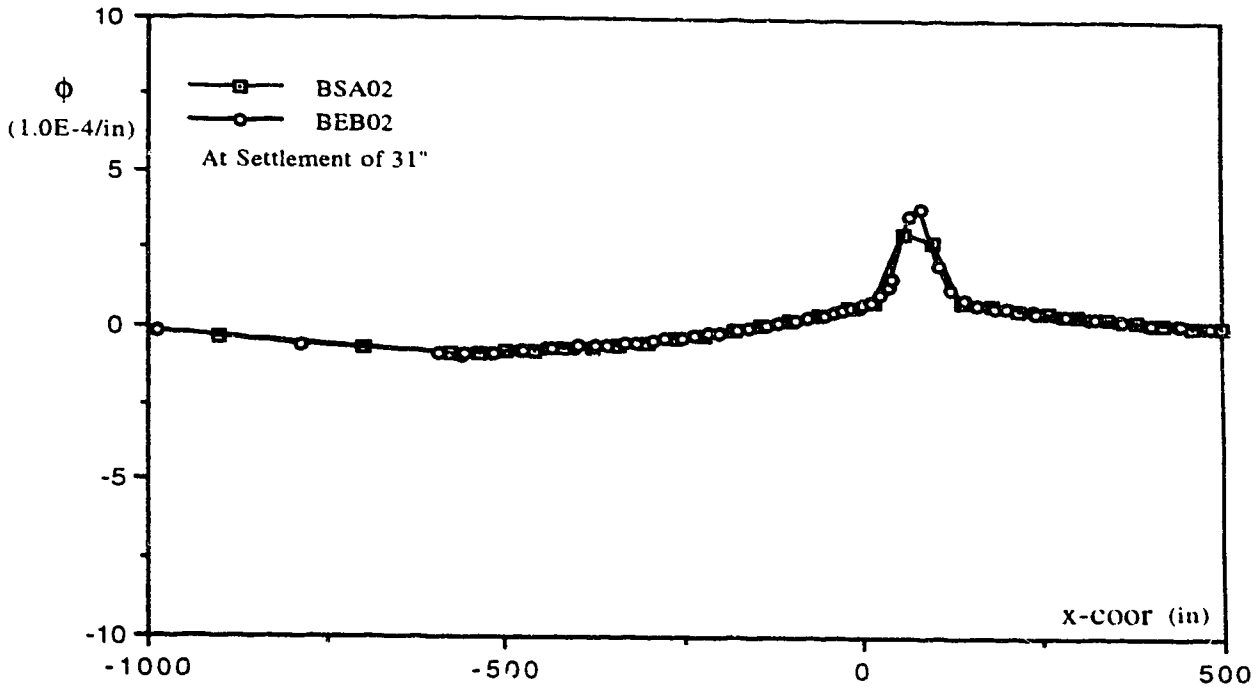

Fig. 7.18 Distributions of Curvature for Specimens BSA02 and BEB02

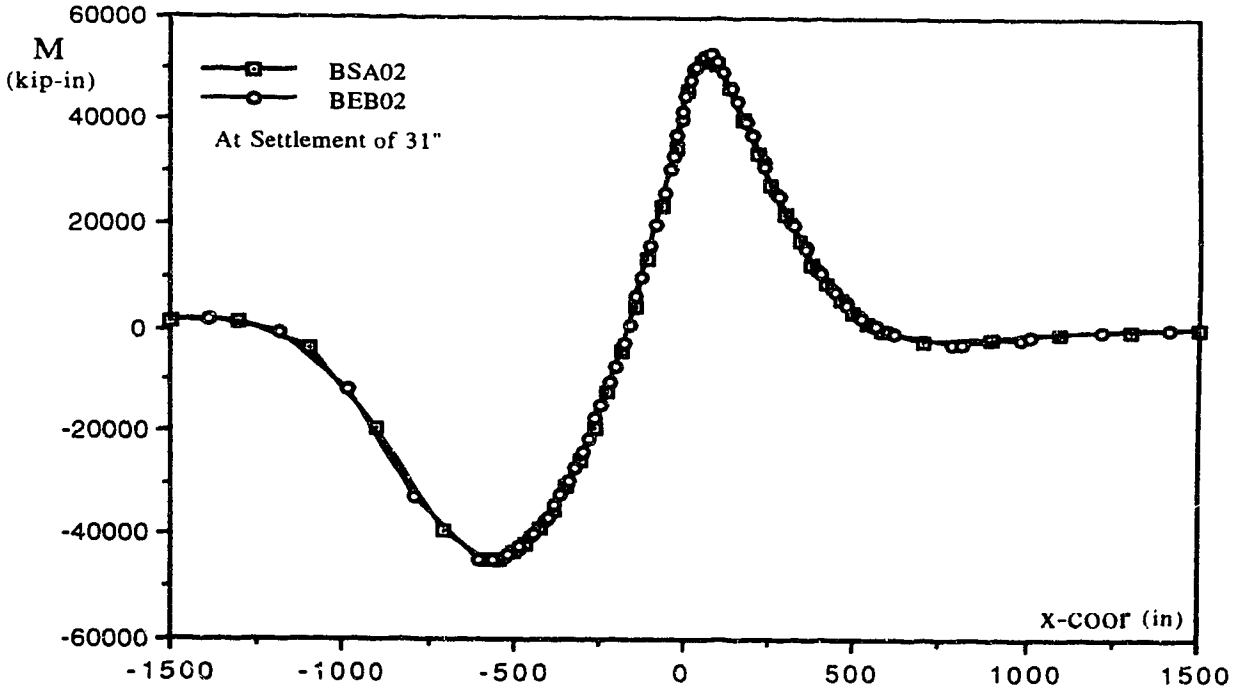

Fig. 7.19 Distributions of Moment for Specimens BSA02 and BEB02

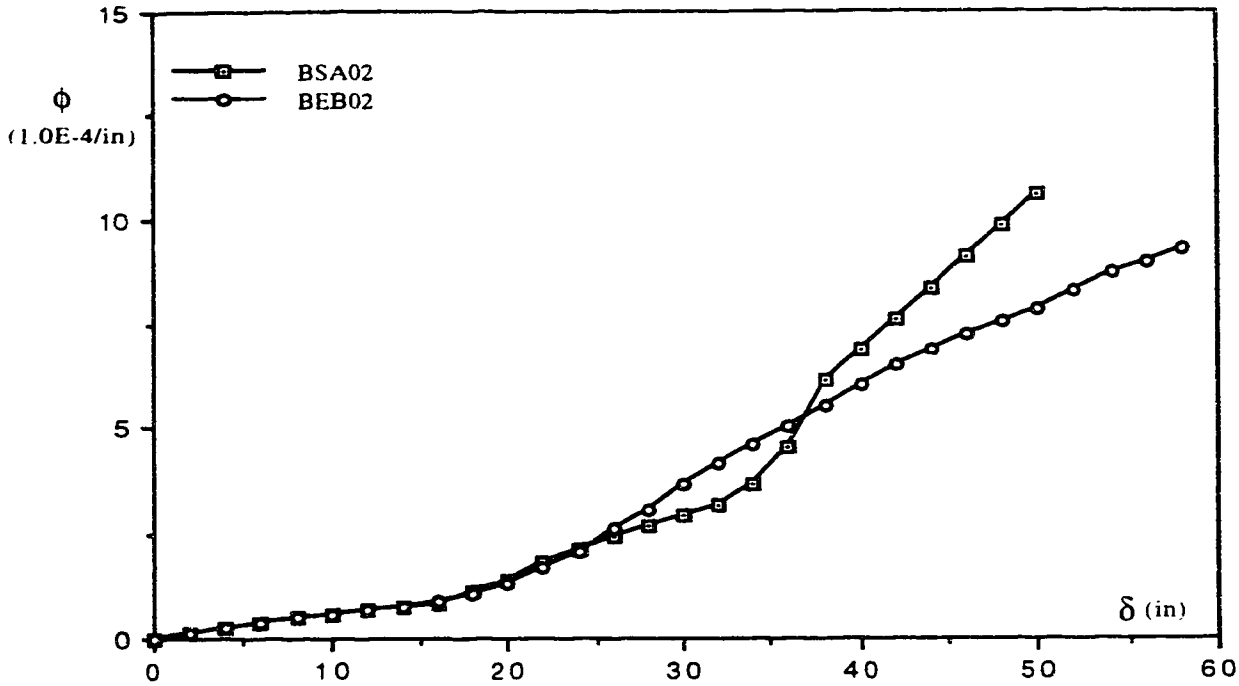

Fig. 7.20 Critical Curvature-Settlement Curves in the Settlement Zone for Specimens BSA02 and BEB02

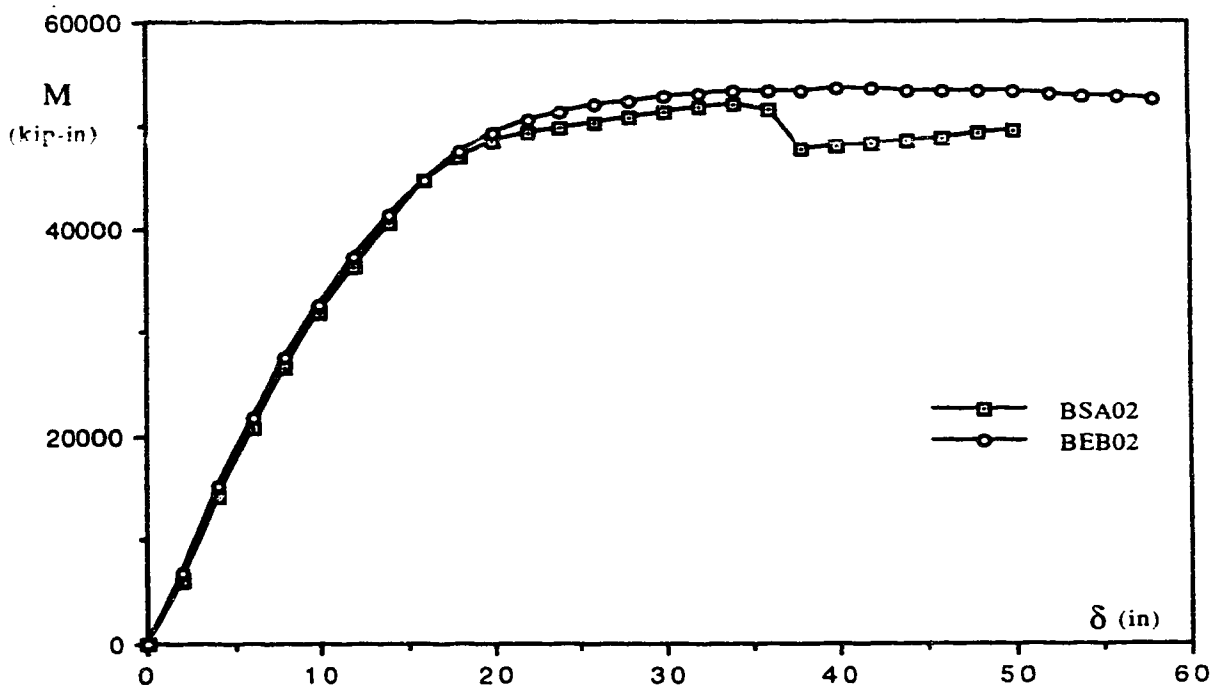

Fig. 7.21 Critical Moment-Settlement Curves in the Settlement Zone for Specimens BSA02 and BEB02

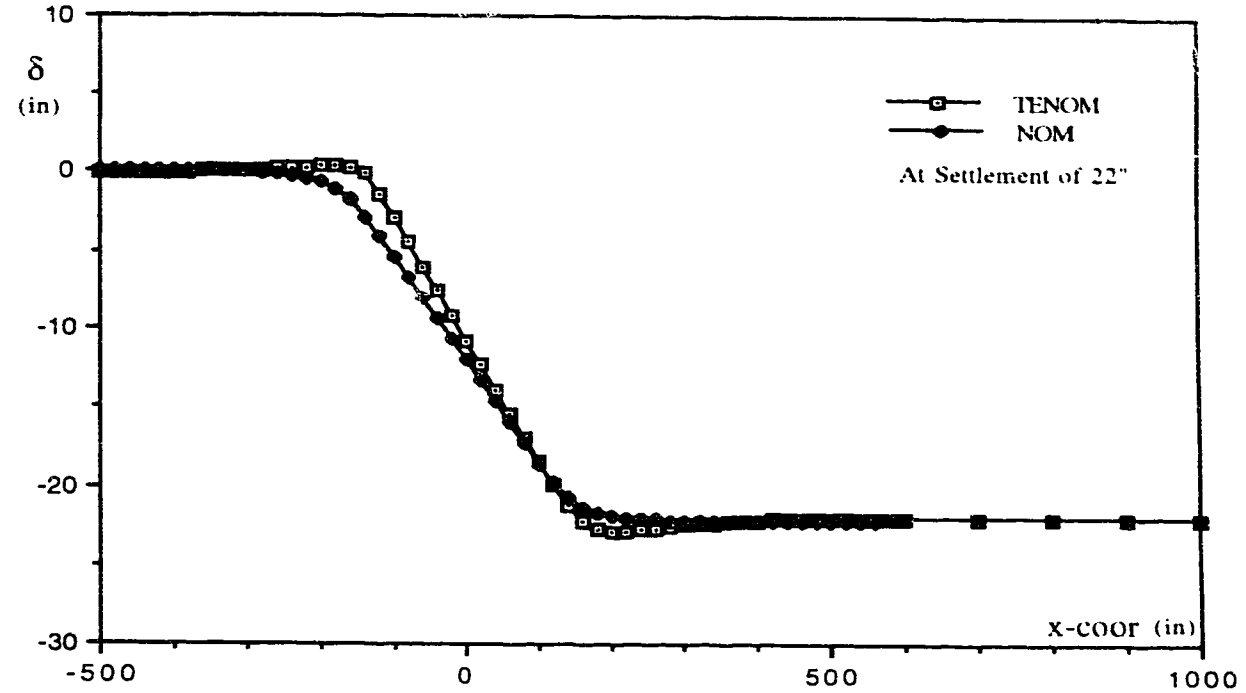

Fig. 7.22 Deformed Configuration for Specimens NOM and TENOM

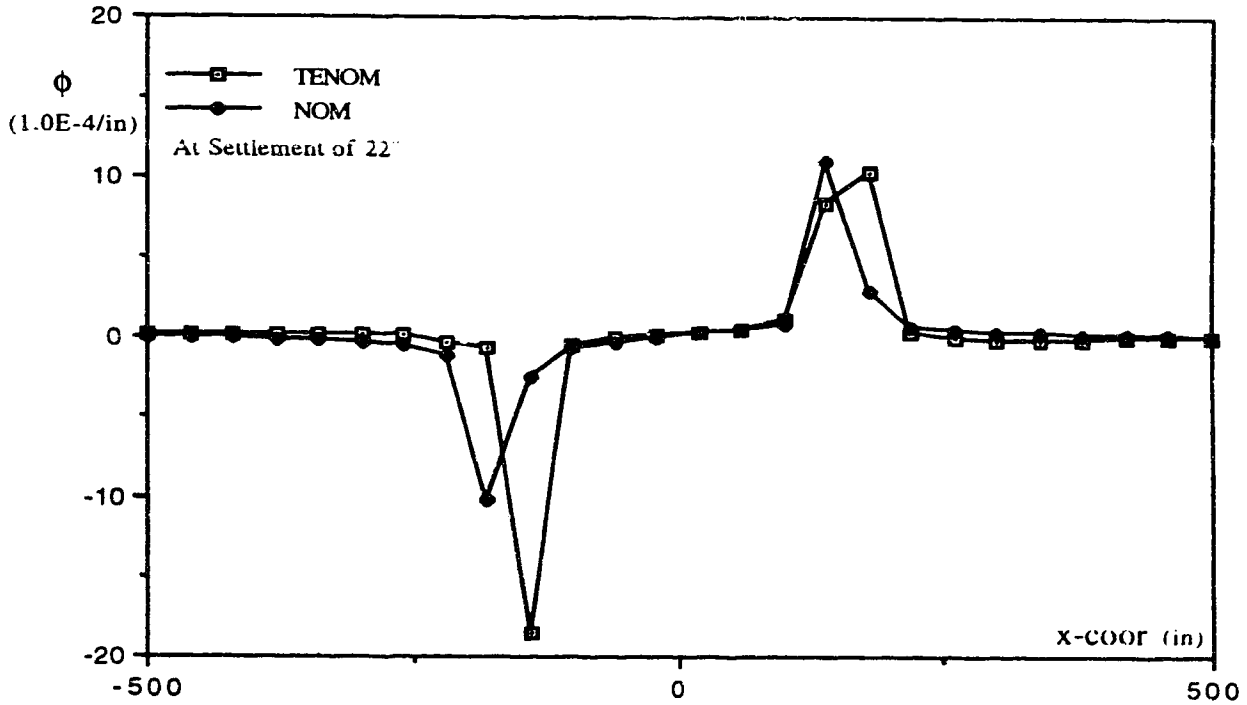

Fig. 7.23 Distributions of Curvature for Specimens NOM and TENOM

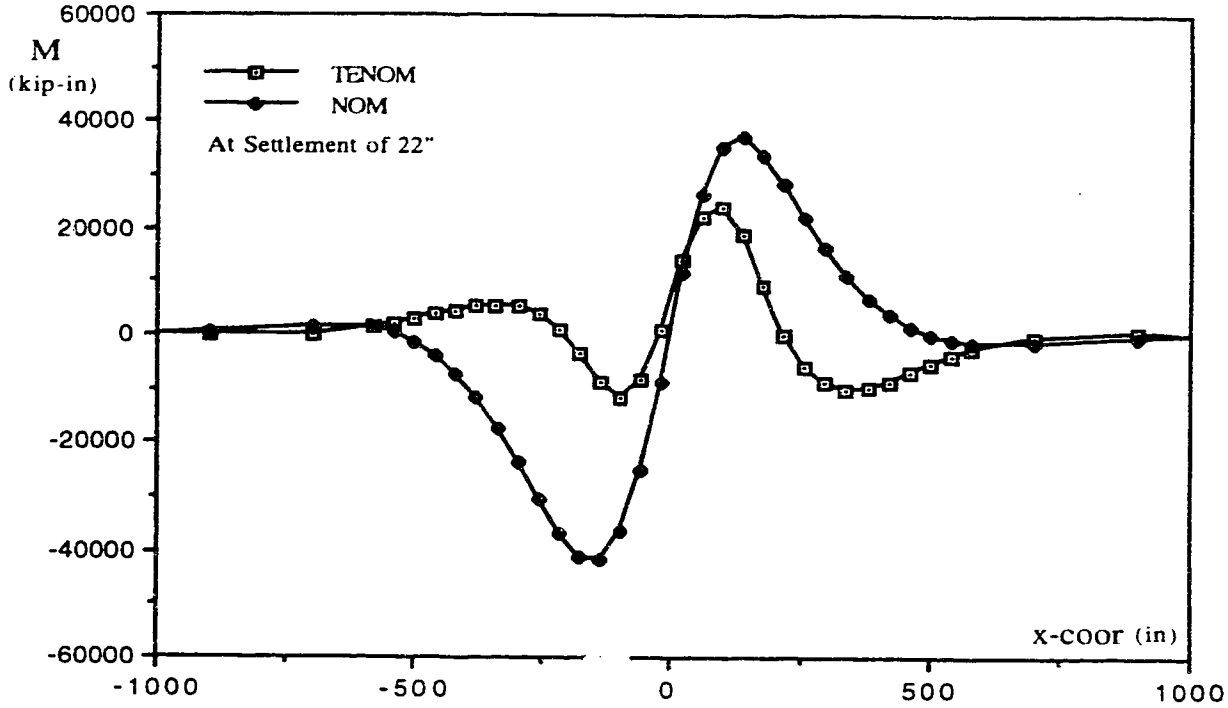

Fig. 7.24 Distributions of Moment for Specimens NOM and TENOM

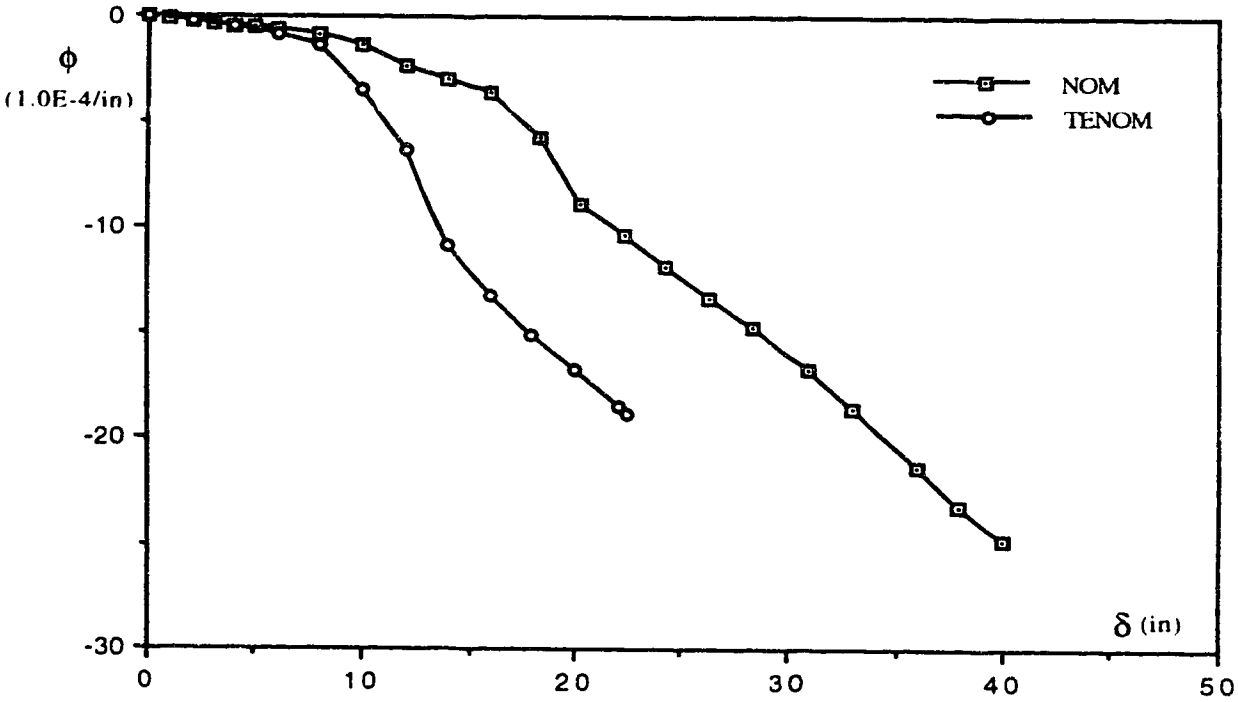

Fig. 7.25 Critical Curvature-Settlement Curves in the Stable Zone for Specimens NOM and TENOM

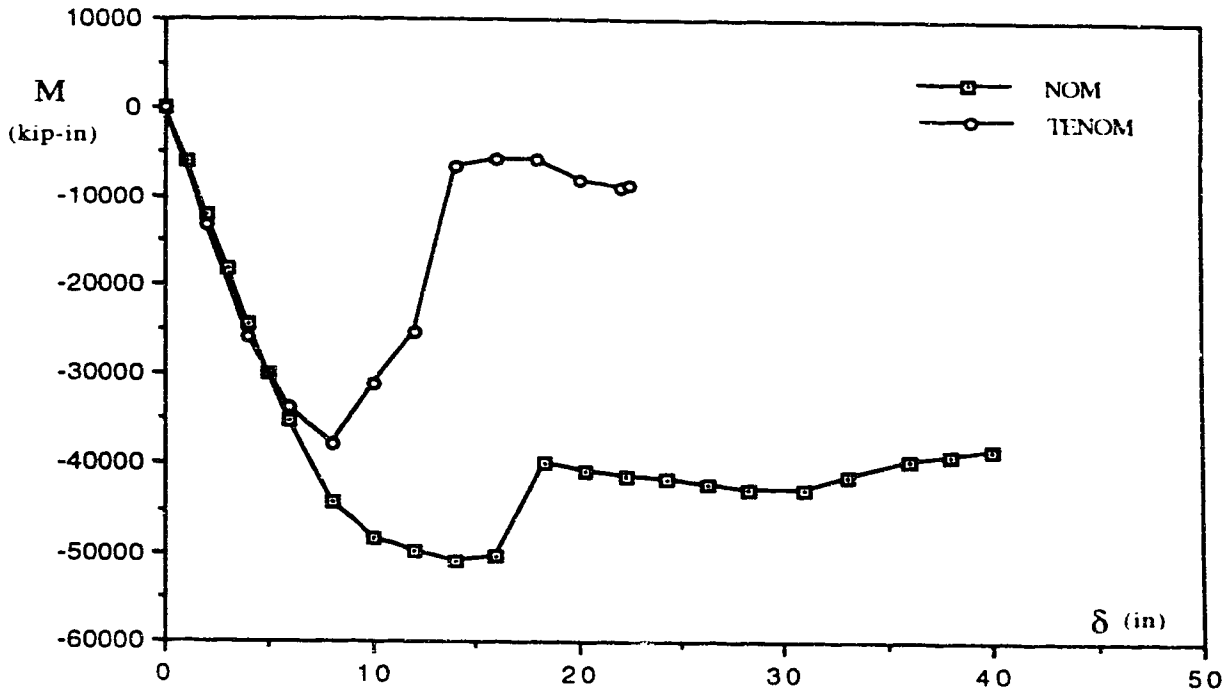

Fig. 7.26 Critical Moment-Settlement Curves in the Stable Zone for Specimens NOM and TENOM

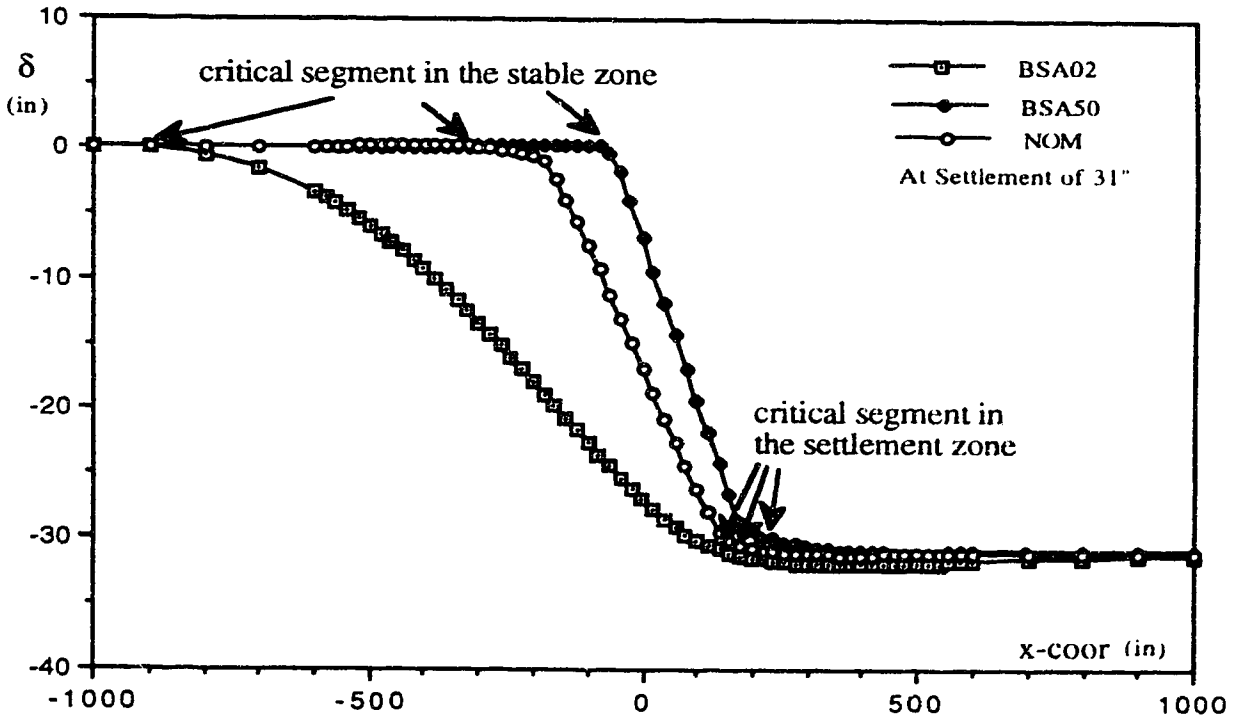

Fig.7.27 Deformed Configuration for Specimens BSA02, BSA50 and NOM

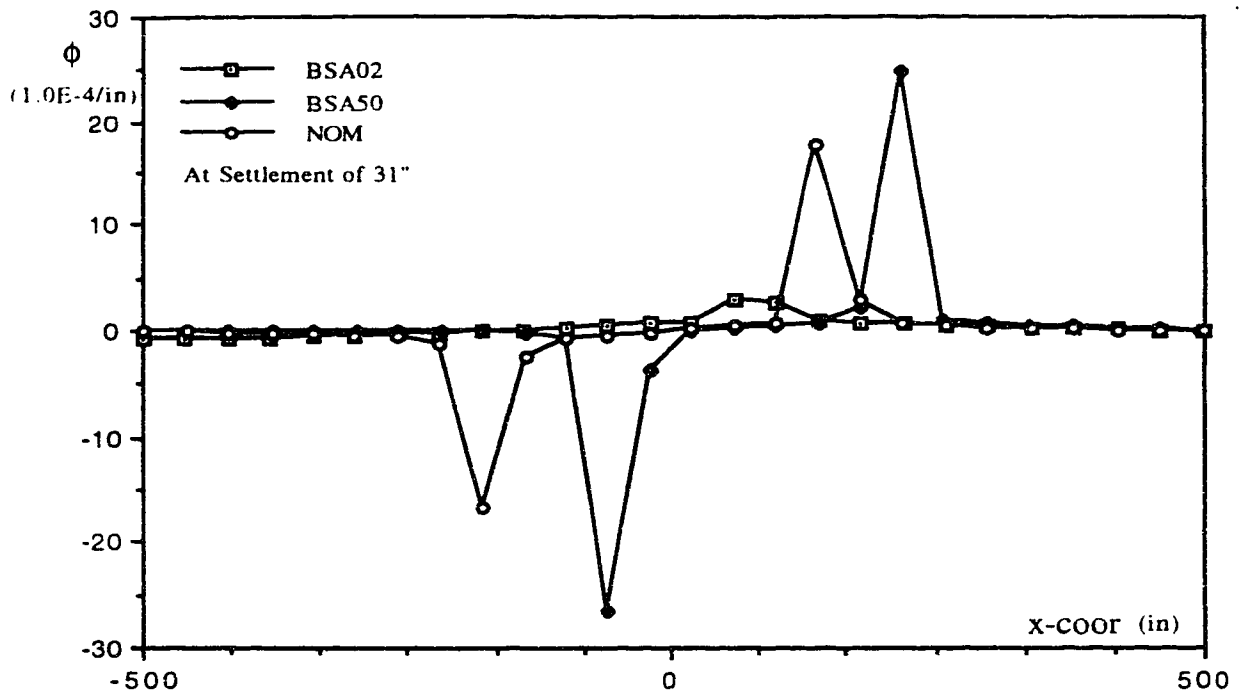

Fig. 7.28 Distributions of Curvature for Specimens BSA02, BSA50 and NOM

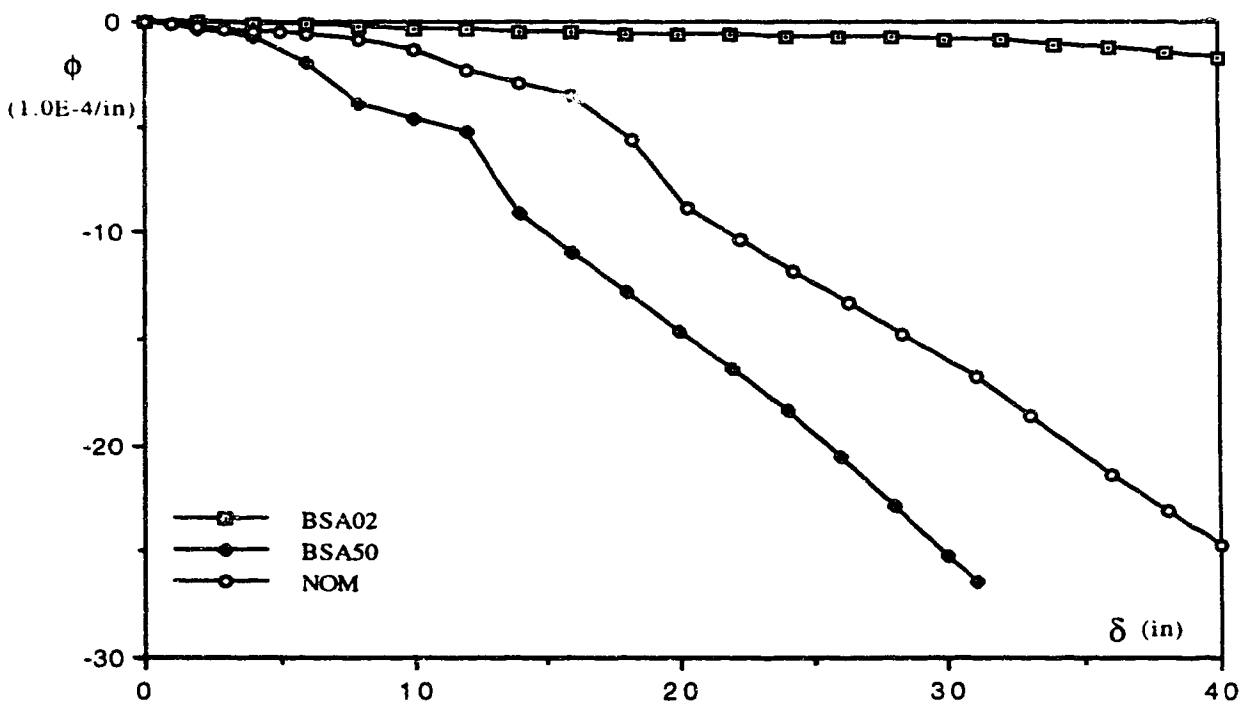

Fig. 7.29 Critical Curvature-Settlement Curve in the Stable Zone for Specimens BSA02, BSA50 and NOM

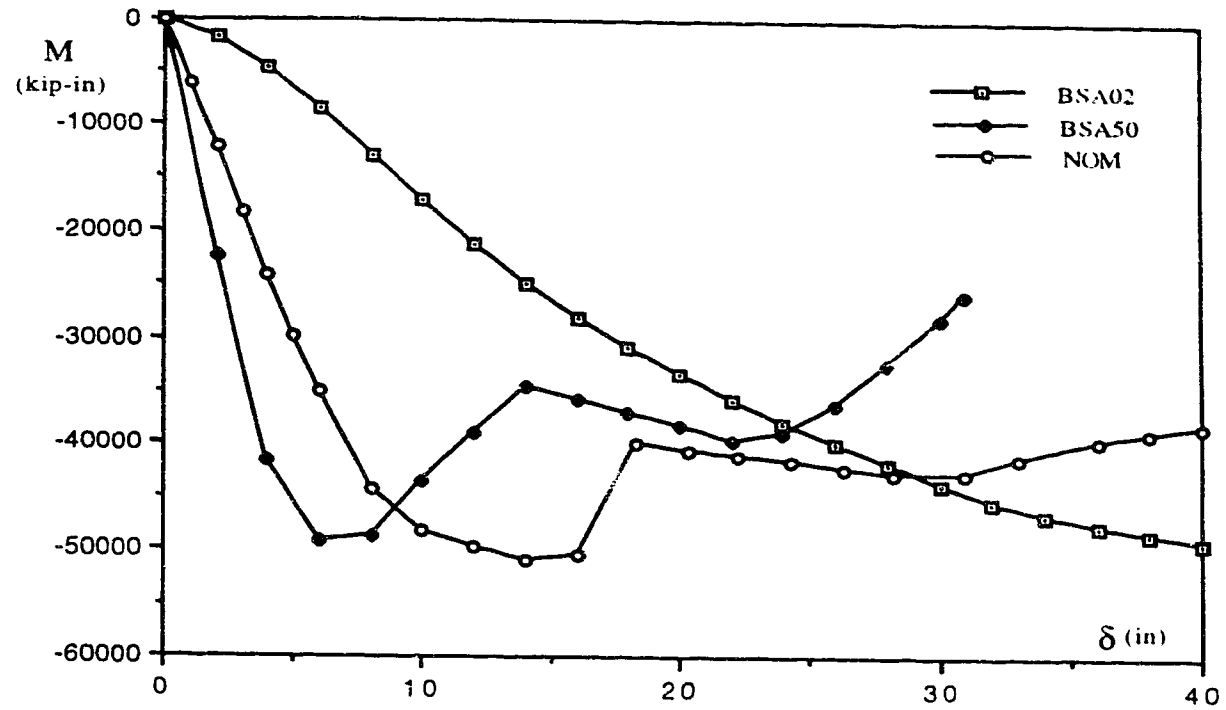

Fig. 7.30 Critical Moment-Settlement Curve in the Stable Zone for Specimens BSA02, BSA50 and NOM

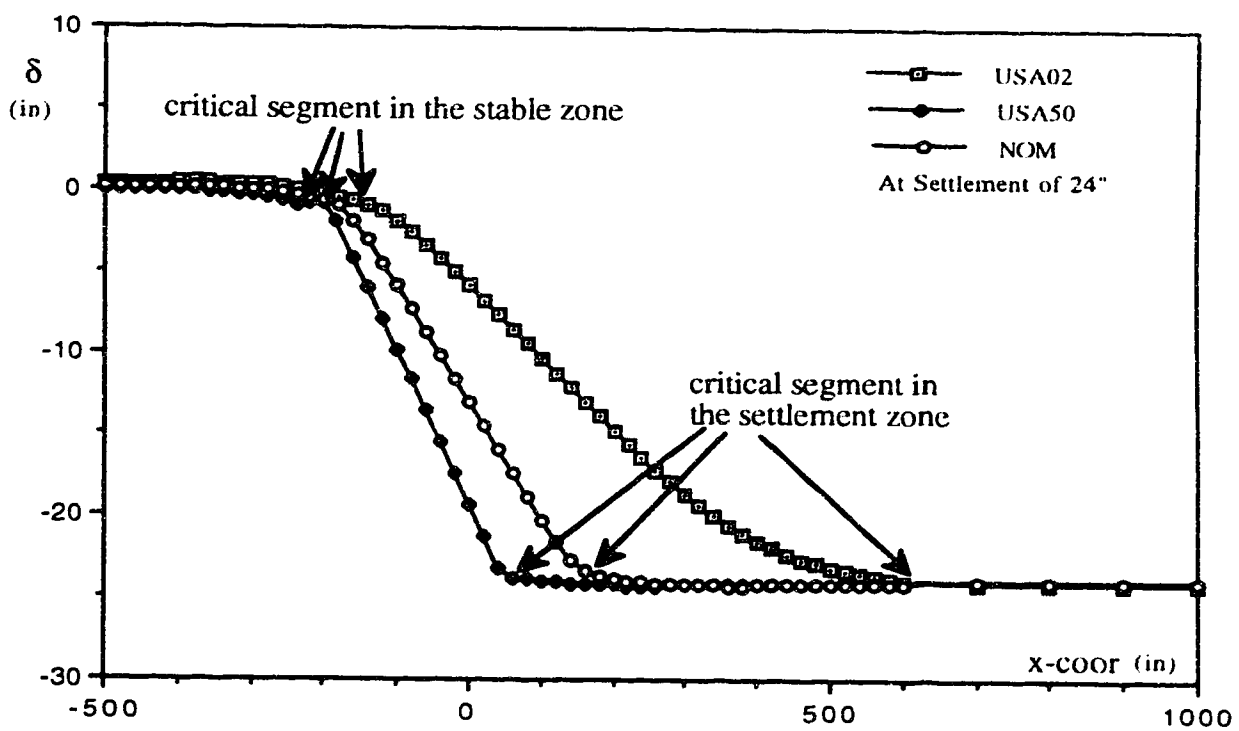

Fig.7.31 Deformed Configuration for Specimens USA02, USA50 and NOM

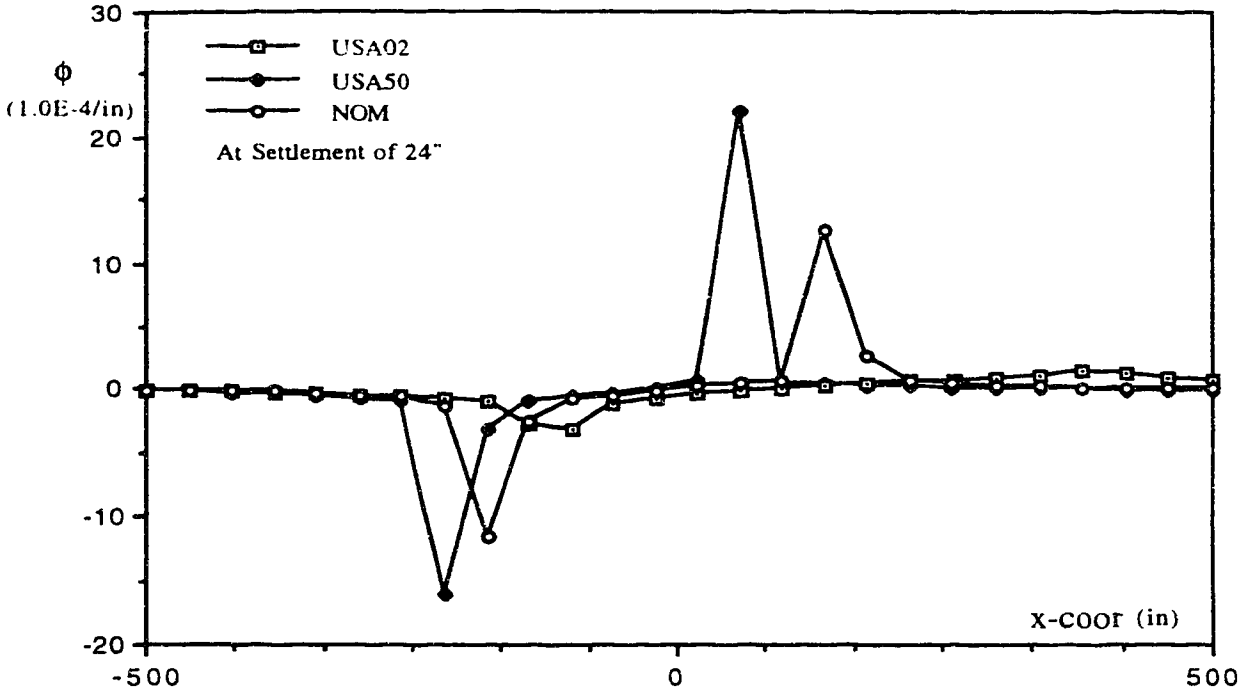

Fig. 7.32 Distributions of Curvature for Specimens USA02, USA50 and NOM

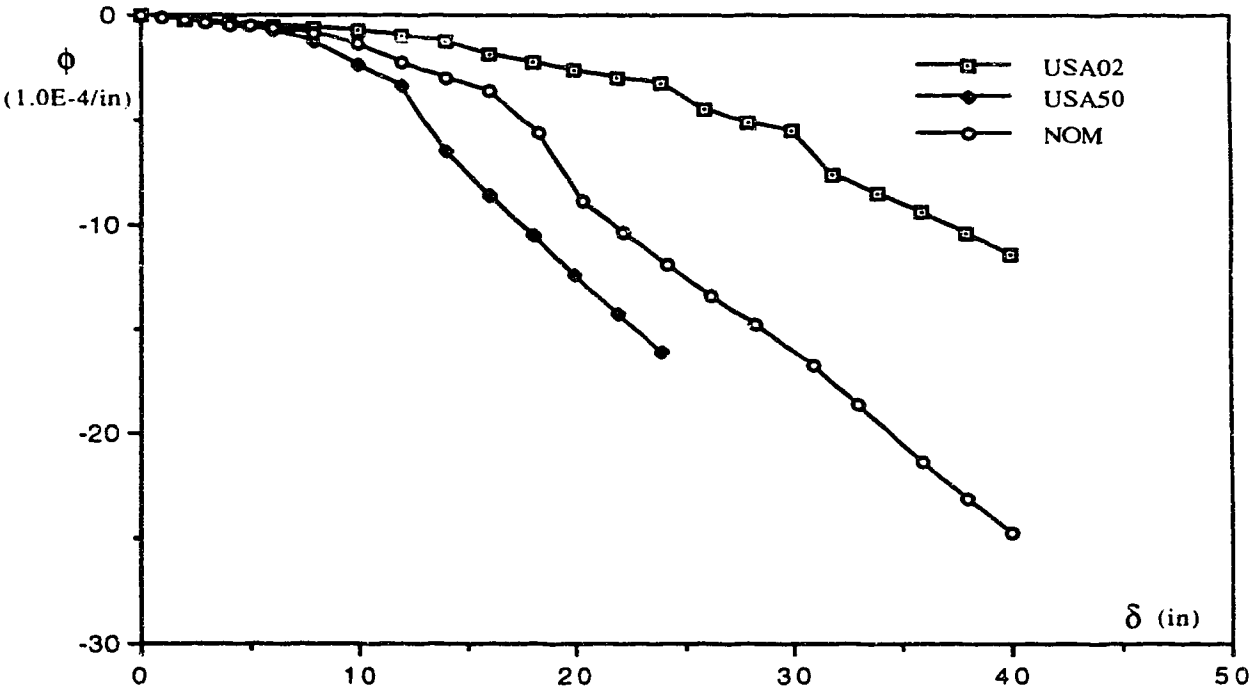

Fig. 7.33 Critical Curvature-Settlement Curve in the Stable Zone for Specimens USA02, USA50 and NOM

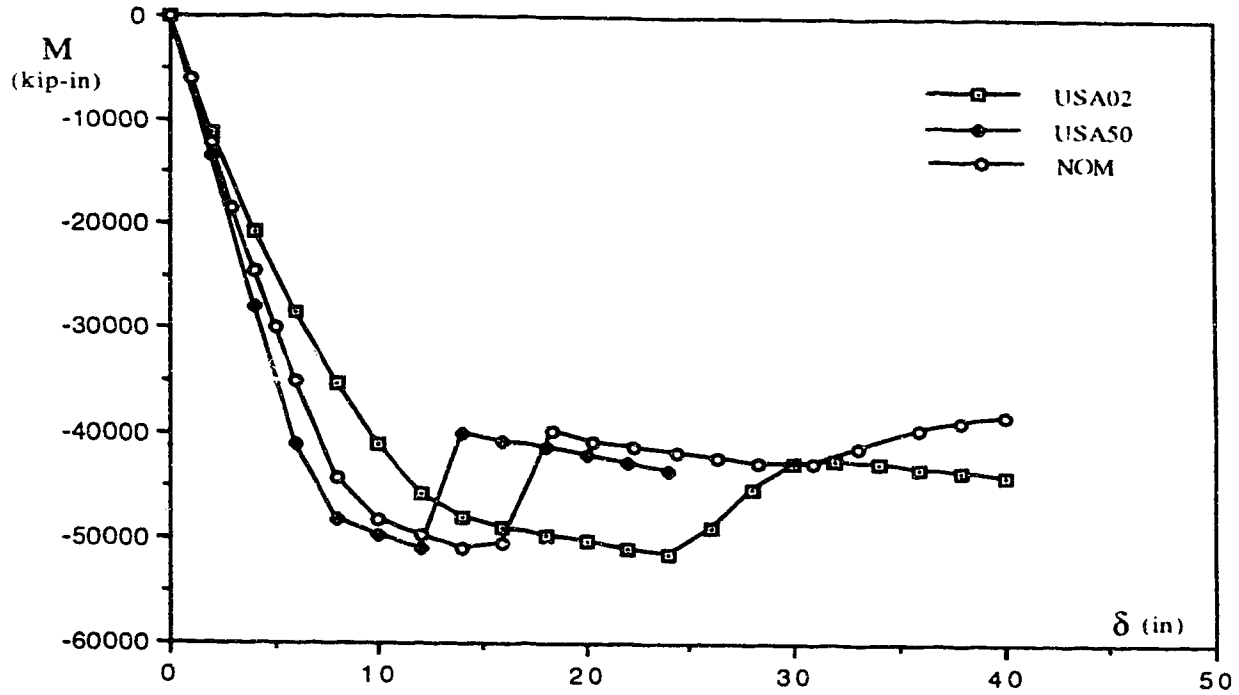

Fig. 7.34 Critical Moment-Settlement Curve in the Stable Zone for Specimens USA02, USA50 and NOM

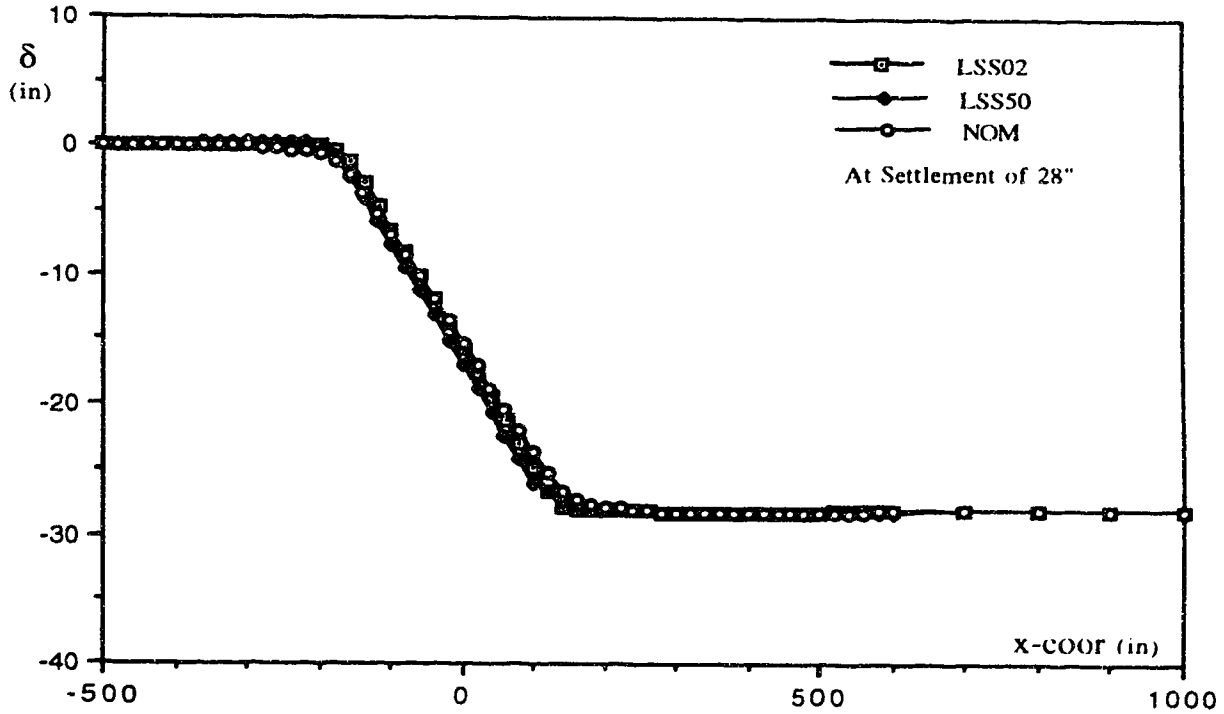

Fig.7.35 Deformed Configuration for Specimens LSS02, LSS50 and NOM

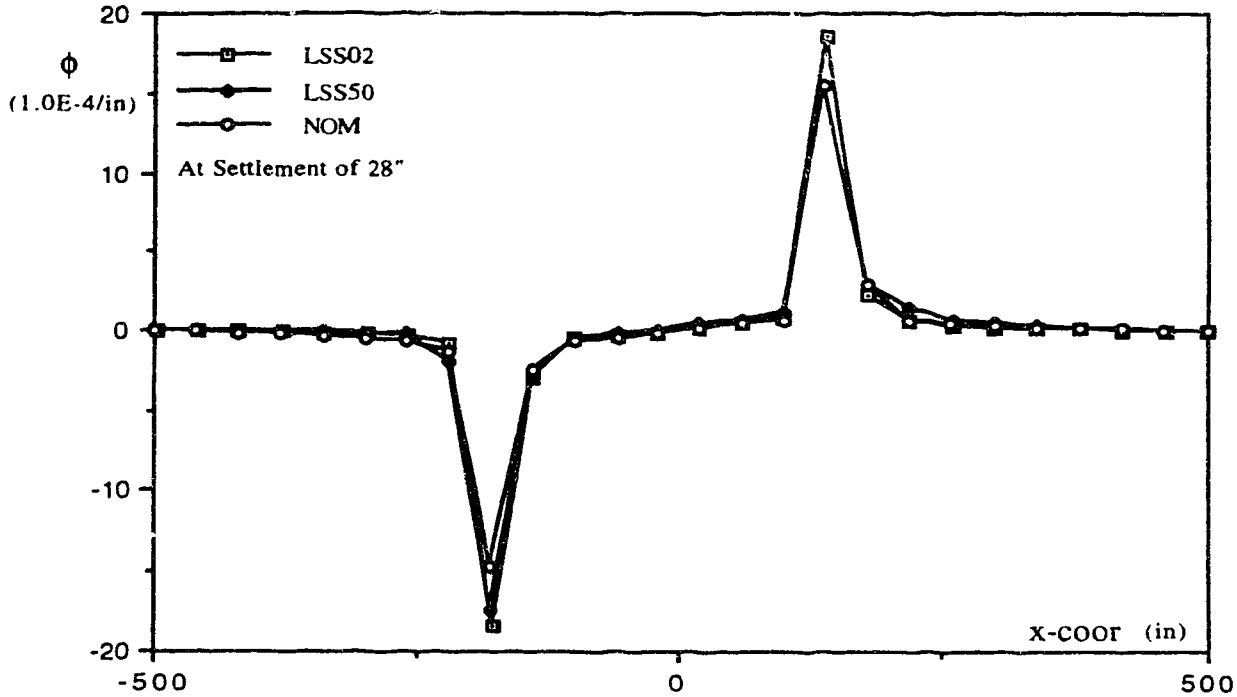

Fig. 7.36 Distributions of Curvature for Specimens LSS02, LSS50 and NOM

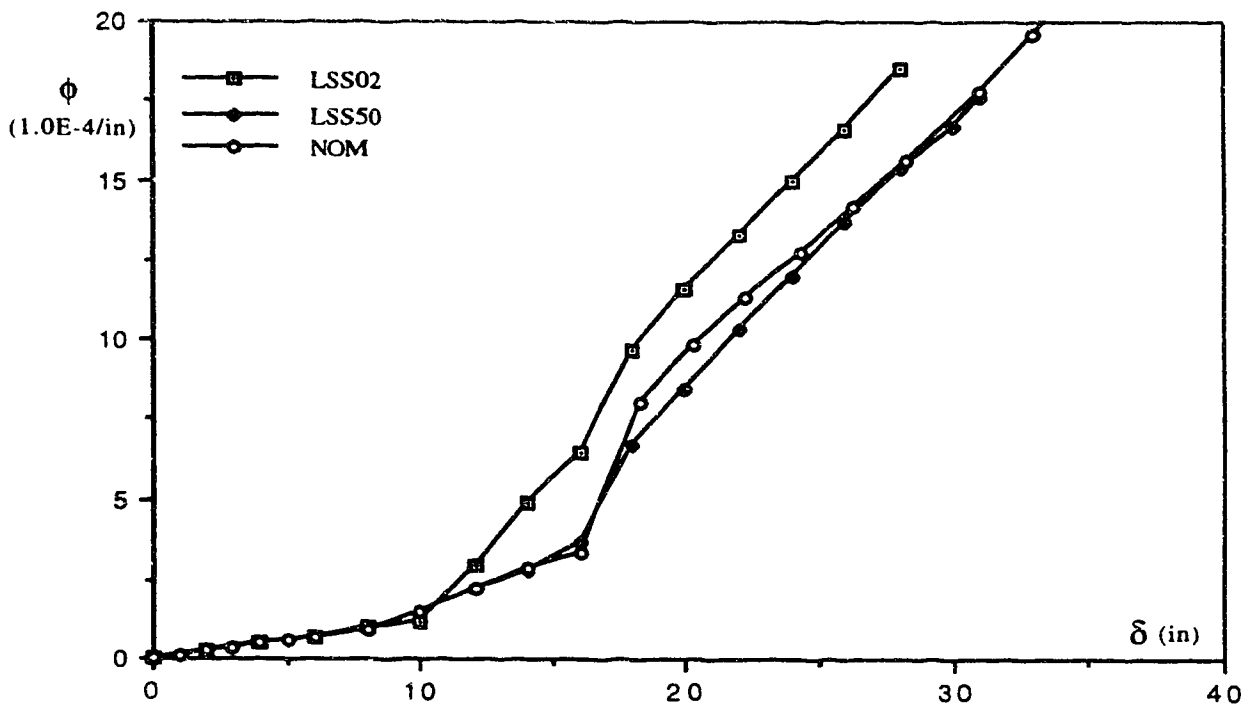

Fig. 7.37 Critical Curvature-Settlement Curve in the Settlement Zone for Specimens LSS02, LSS50 and NOM

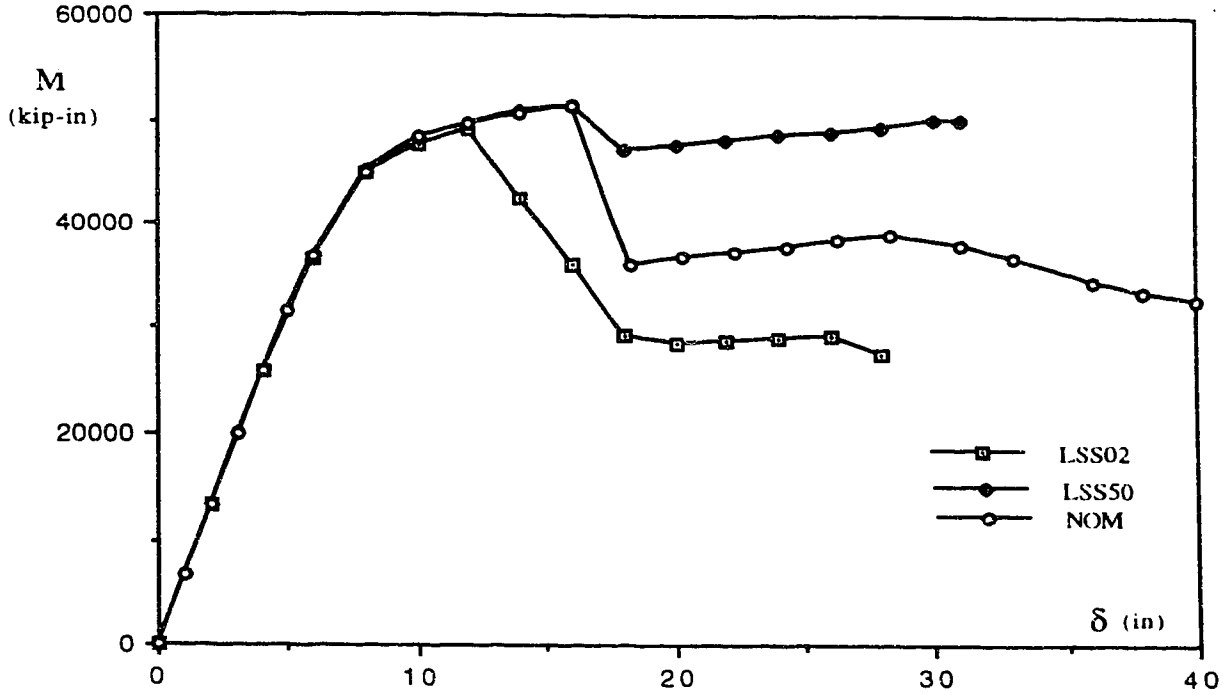

Fig. 7.38 Critical Moment-Settlement Curve in the Settlement Zone for Specimens LSS02, LSS50 and NOM

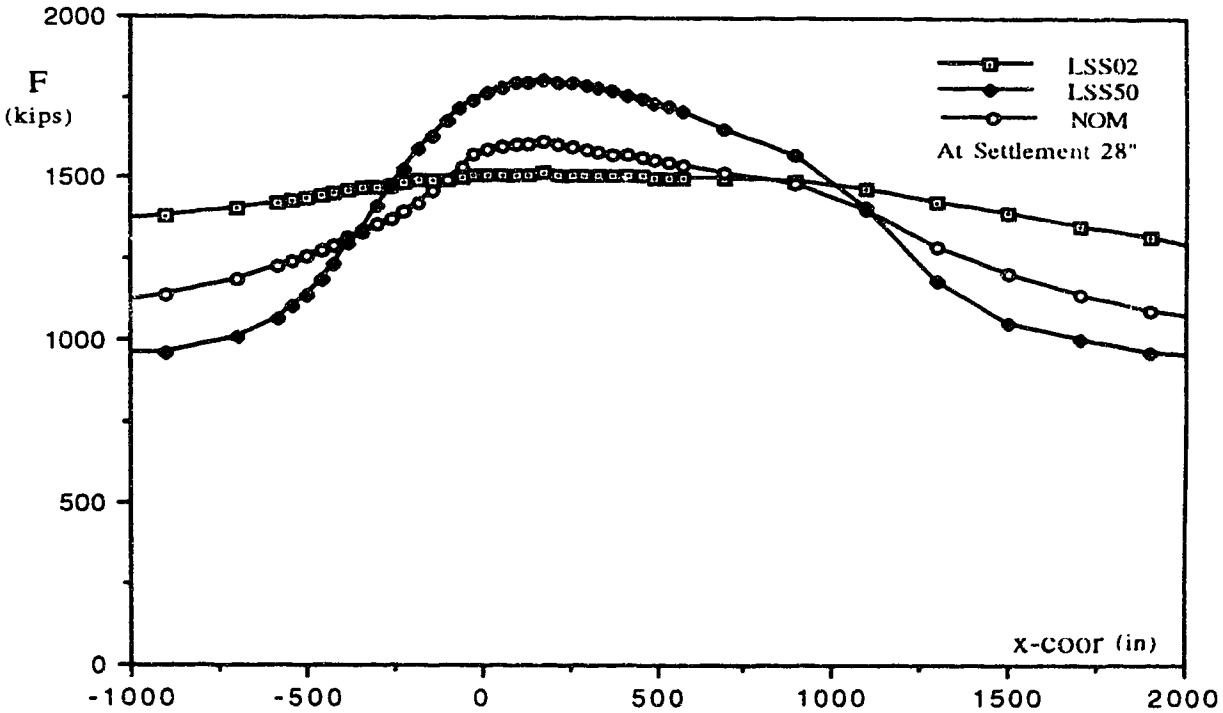

Fig. 7.39 Distributions of Axial Force for Specimens LSS02, LSS50 and NOM

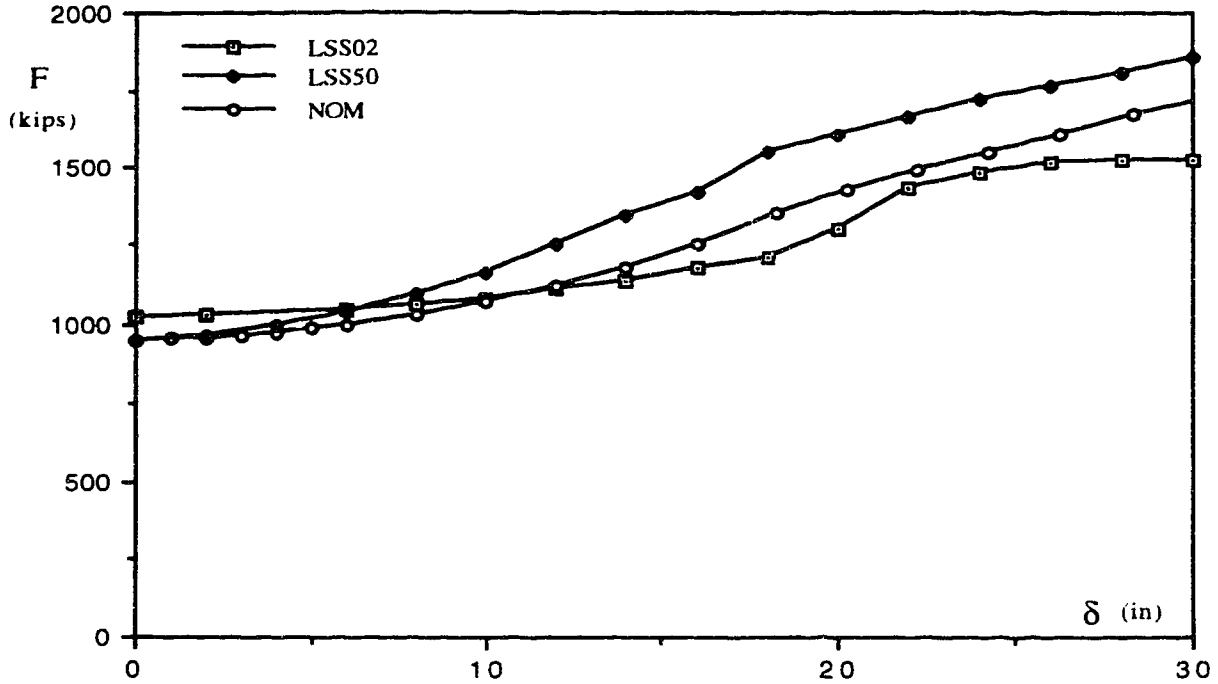

Fig. 7.40 Critical Axial Force-Settlement Curves in the Settlement Zone for Specimens LSS02, LSS50 and NOM

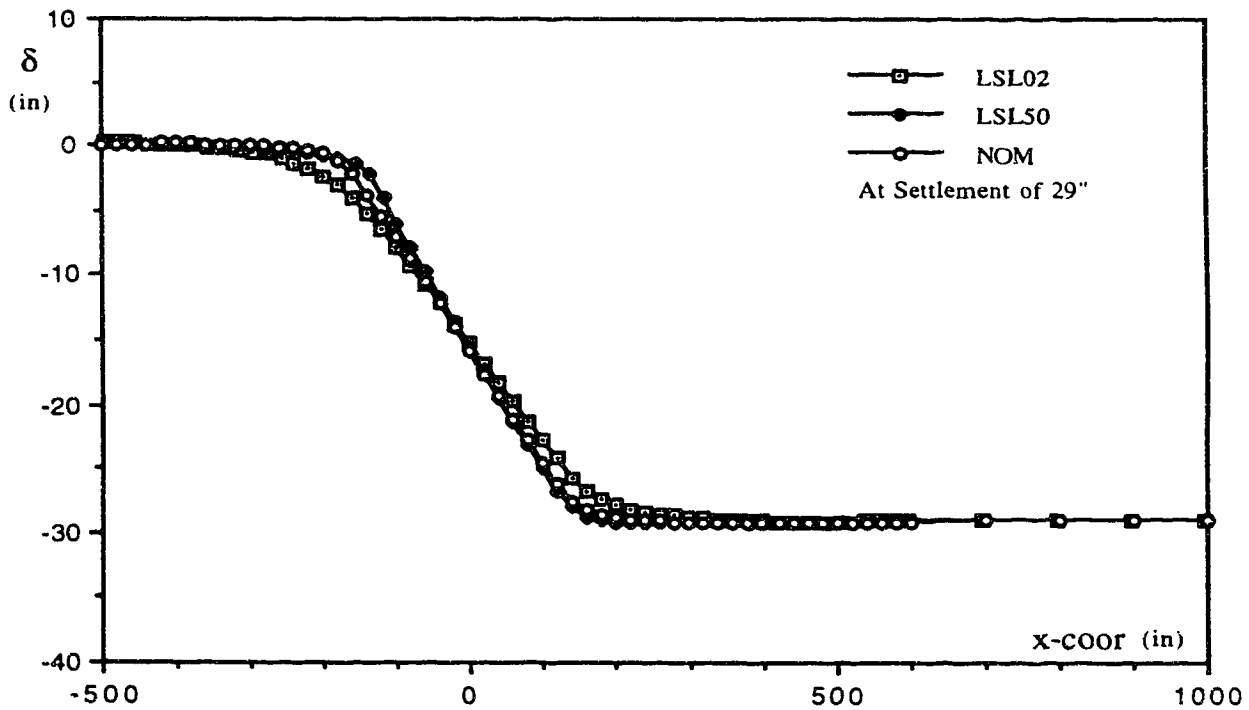

Fig.7.41 Deformed Configuration for Specimens LSL02, LSL50 and NOM

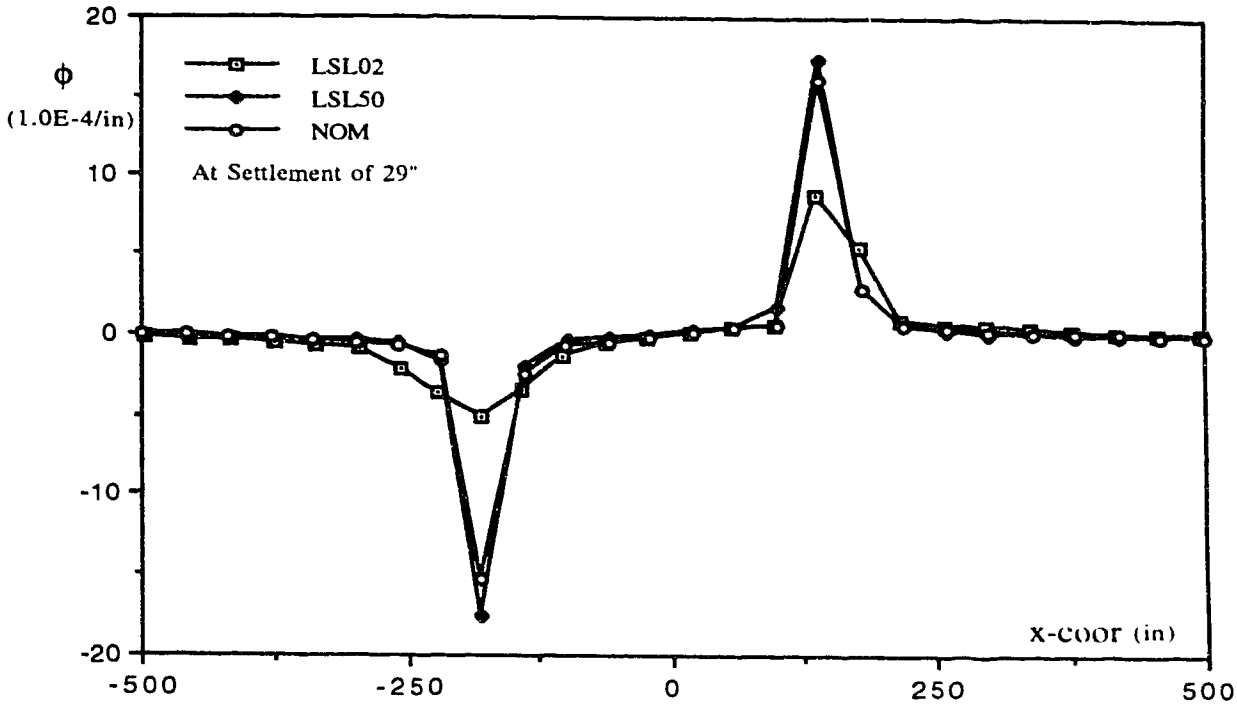

Fig. 7.42 Distributions of Curvature for Specimens LSL02, LSL50 and NOM

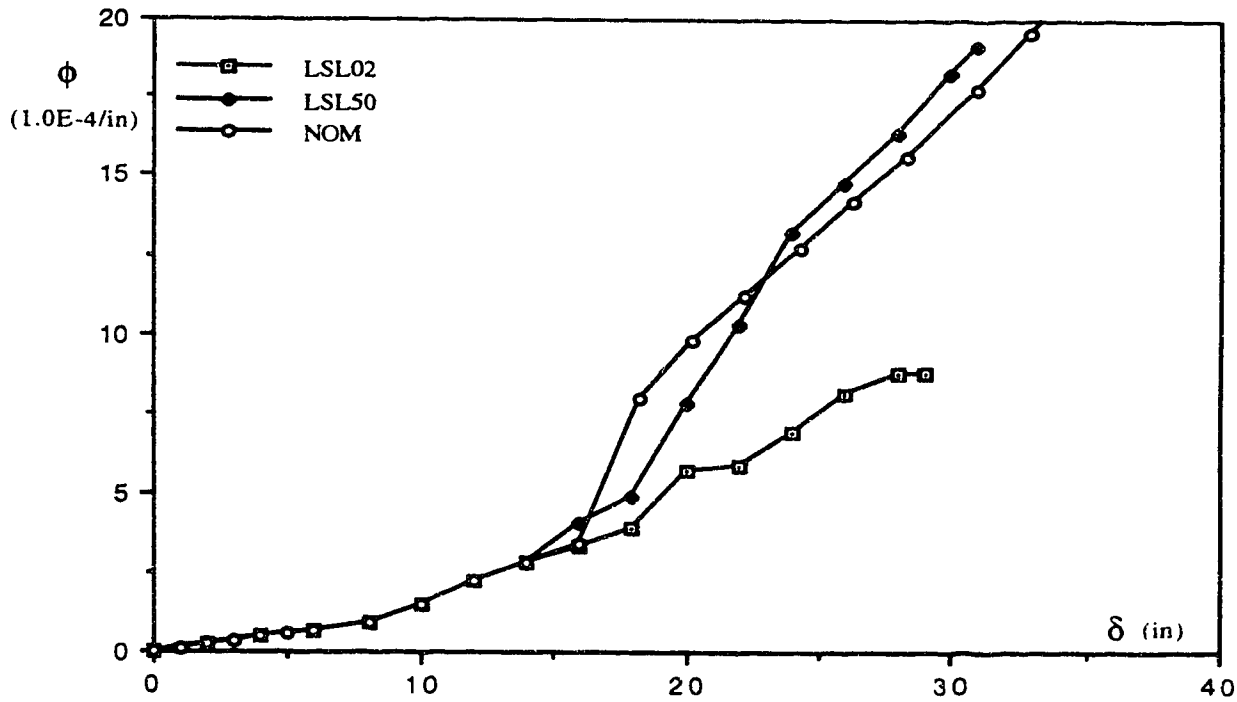

Fig. 7.43 Critical Curvature-Settlement Curve in the Settlement Zone for Specimens LSL02, LSL50 and NOM

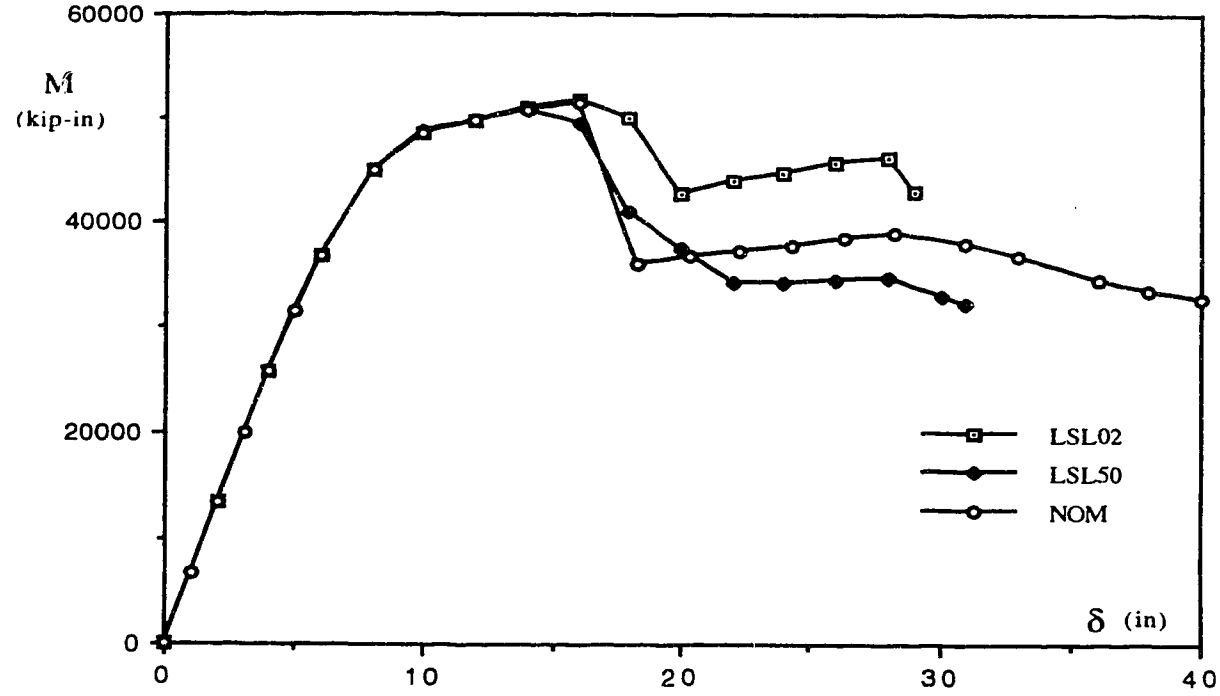

Fig. 7.44 Critical Moment-Settlement Curve in the Settlement Zone for Specimens LSL02, LSL50 and NOM

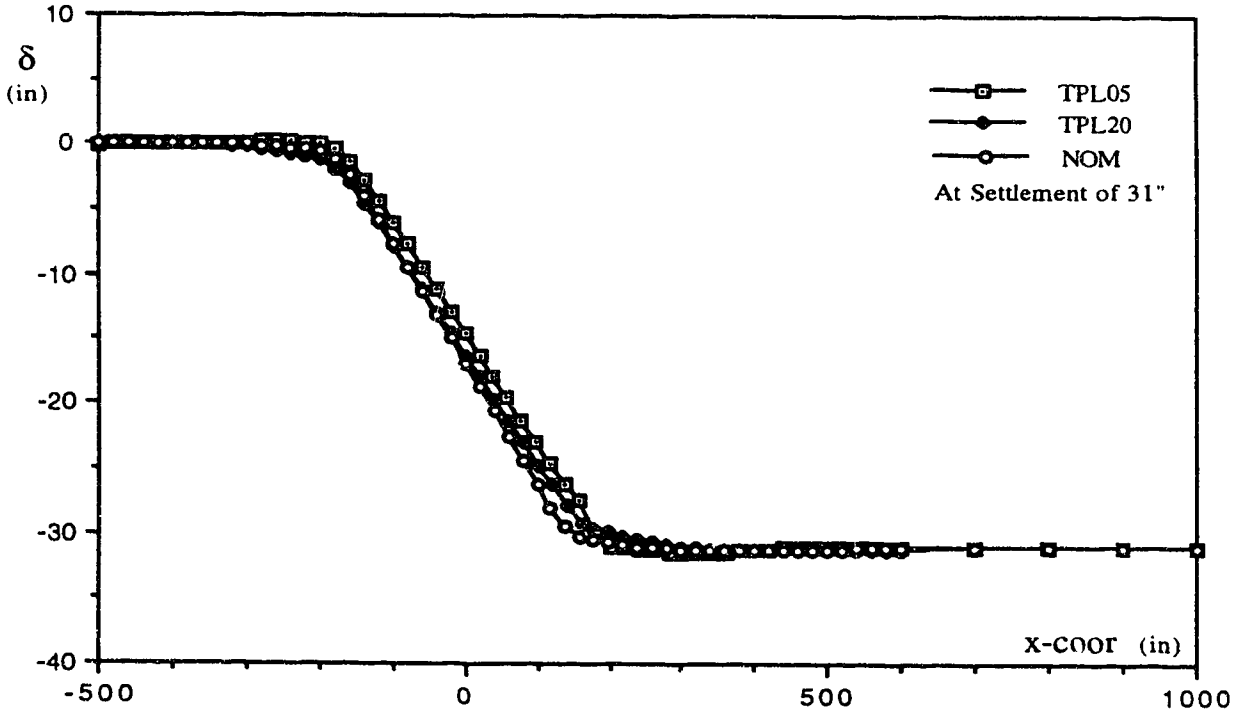

Fig. 7.45 Deformed Configuration for Specimens TPL05, TPL20 and NOM

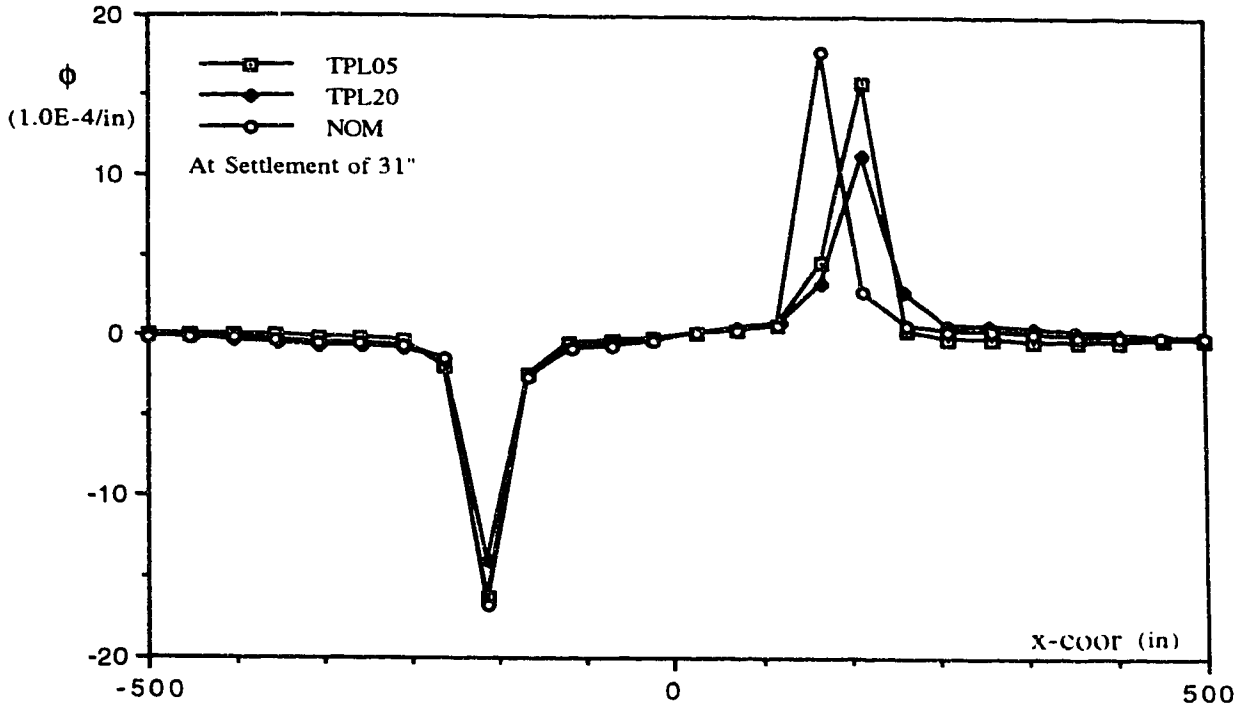

Fig. 7.46 Distributions of Curvature for Specimens TPL05, TPL20 and NOM

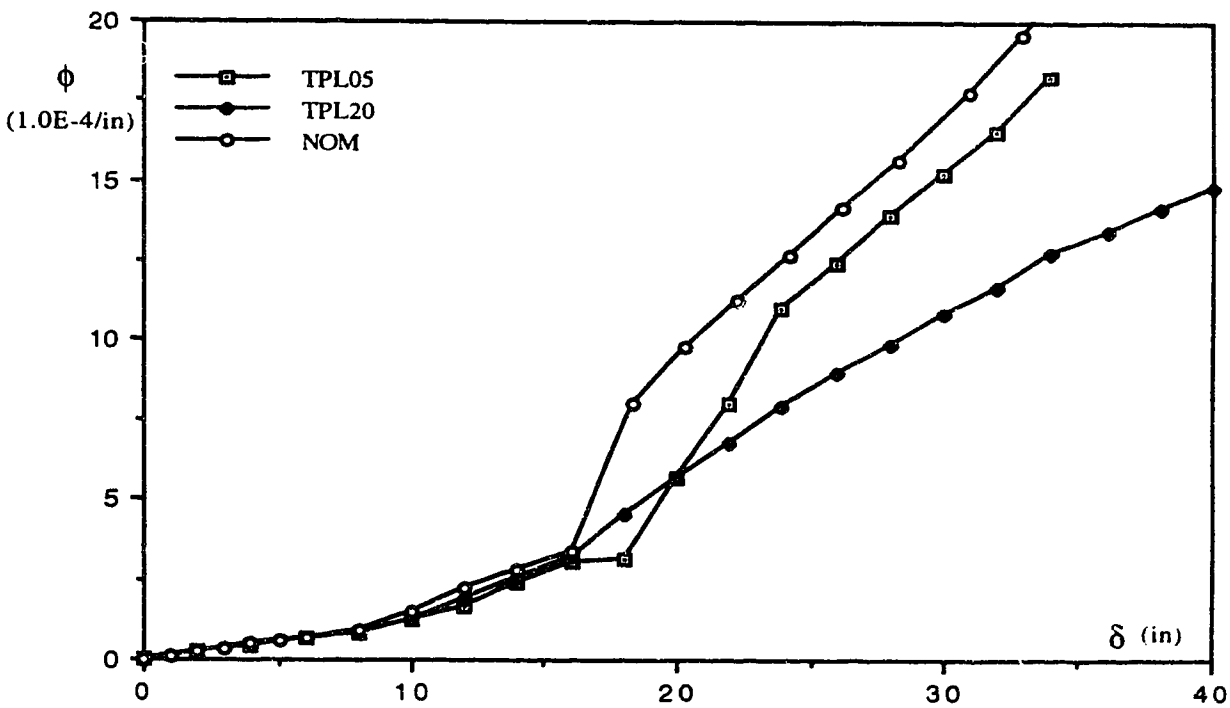

Fig. 7.47 Critical Curvature-Settlement Curve in the Settlement Zone for Specimens TPL05, TPL20 and NOM

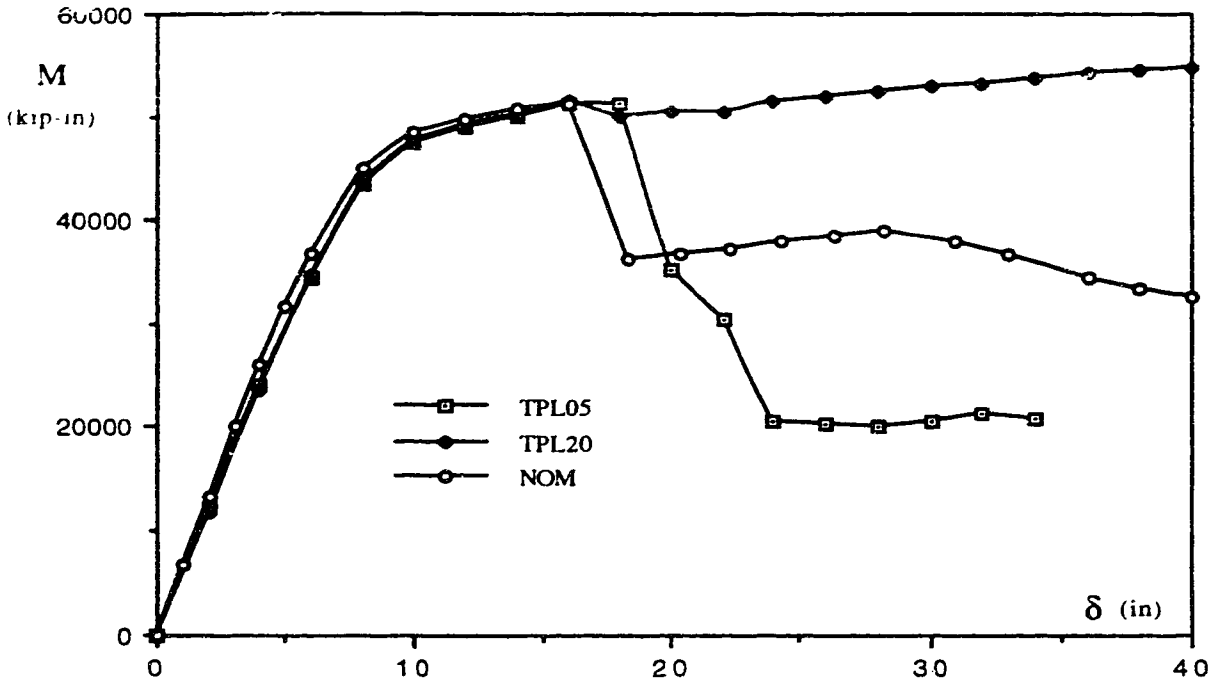

Fig. 7.48 Critical Moment-Settlement Curve in the Settlement Zone for Specimens TPL05, TPL20 and NOM

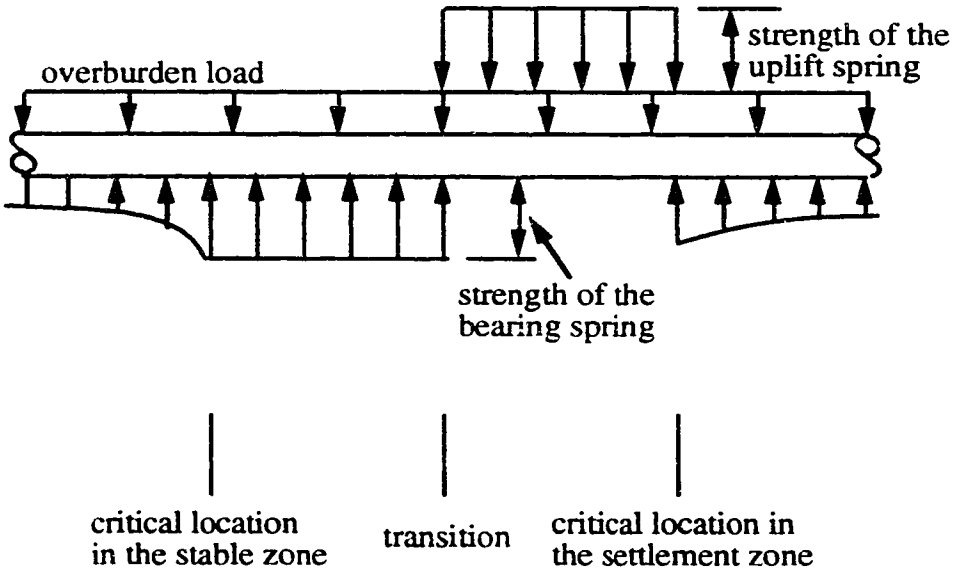

Fig. 7.49 Conceptual Free Body Diagram of Pipelines at the Transition

CHAPTER 8 DEFORMATION DESIGN CRITERIA

The behavior of pipelines, in terms of both the local buckling behavior and the overall performance when they are subject to imposed deformation, has been discussed in the previous chapters. Based on these discussions, design criteria for deformation limit states can be proposed which are believed to have a more rational base than for those used for current practice. In this chapter, discussion is focused on the design and assessment criteria for the deformation limits. The chapter begins with a brief introduction on limit states and the philosophy of limit states design. The details of the proposed design criteria are discussed in the second section. In the third section, the method of applying the proposed design criteria are demonstrated through applications to some of the specimens for settlement analysis in Ch. 7.

8.1 INTRODUCTION

The two principal design philosophies are *working stress design* and *limit states design*. In structural engineering, working stress design principles were almost universally used until about two decades ago when limit states design principles were proposed and adopted in fields such as steel structures for buildings. However, design standards in other fields are still based on working stress design. An example is the Canadian code for oil and gas pipeline systems (Canadian Standards Association, 1986, 1990).

Working stress design appears to be relatively simple in application because it requires only linear elastic analysis to predict the response of structures under specified load conditions. However, it does not directly deal with the failure conditions of structures and it attempts to control undesirable effects indirectly by specifying that under normal operating condition the structure has a factor of safety against yielding of the material. As a result, the design obtained has variable levels of safety for different failure conditions. On the other hand, limit states design is based on a direct evaluation of each of the limit states; and therefore, a more uniform level of safety can be achieved. A safe and economic design can be obtained with greater clarity and rationality with respect to each of the limit states if each unsatisfactory condition be identified as such a state. However, the analytical approach consistent with limit states design should then be able to predict the response of the structure up to all of its limit states. As a result, a rational approach for deformation limit states must be based upon nonlinear analysis including both large displacements and nonlinear material relationships.

In this section, deformation limit states for pipelines are first discussed. This is followed by a brief review of existing design criteria for deformation limit states. The discussions in this, and the following sections, are part of the effort to develop a limit states approach for pipeline design.

8.1.1 Deformation Limit States for Pipelines

Limit states design was introduced into the mainstream of Canadian design practice in 1974 through the 'code' known as Canadian Standards Association Standard S16.1-1974-'Steel Structures for Buildings-Limit States Design'. Since that time it has had a major effect on clarifying and rationalizing the design process for all structural steel buildings and bridges in Canada, and the application of this philosophy has been extended from these types of structures to those constructed of all materials. The limit state philosophy of the Canadian design codes has also had a major impact on the structure of building codes in many other countries around the world.

CSA Standard CAN3-S16.1-M78 (1978) contains the following definition.

> "*Limit States* means those conditions of a structure in which the structure ceases to fulfill the function for which it was designed. Those states concerning safety are called the ultimate limit states and include exceeding of load-carrying capacity, overturning, sliding, fracture and fatigue. Those states which restrict the intended use and occupancy of the structure are called serviceability limit states and include deflection, vibration and permanent deformation."

Because it requires that the designer focus on the specific ways in which structures may fail to perform their function, the limit states philosophy has led to considerable rationalization of the design processes.

It must be recognized that a primary concern of the pipeline industry is to maintain pipeline installations in safe operating conditions over a very extended period of time. Therefore, design-oriented codes which do not explicitly recognize deterioration of the structure, the assessment of safety conditions during the life of the structure, and the effect of organized remedial maintenance on the performance of the structure, are not providing the industry with adequate guidance to address structural performance in the manner which is required. After all, the safety of a structure which is twenty years old is just as important as one which is currently under construction. This implies that for proper guidance of the

industry it would be necessary to extend the limit states philosophy, and recommendations, to deal explicitly with the specification of limit state conditions throughout the life of the structure.

It is the opinion of the author that a proper limit states code for the design of pipelines will require radical surgery on the existing codes, and that there is an urgent need of the industry to recast the present codes into such forms before any major improvements can be made in pipeline engineering design. It has been a fundamental assumption of this work that the industry will be capable of reassessing the performance requirements of their lines in such a way that they can define the conditions under which "the structure ceases to fulfill the function for which it was designed" (CAN3-S16.1-M78). Unfortunately, there does not seem to be much effort to address such issues at this time.

The term 'deformation limit state' is used to distinguish limit states associated with large plastic strains or geometric distortions from those failure states associated with 'brittle' material behavior. Controls for the latter type of failure states have traditionally been based on stress concepts and have tended to dominate the design philosophy relative to pipeline design for most of the last century. However, with the emergence of very high toughness materials, and modern welding technology, it is perhaps time to question this domination. Indeed, the industry appears to be working slowly towards replacing the stress methods for fracture with limiting deformation states.

This study has proceeded on the basis that rational definitions of 'deformation limit states' can be made. In the lack of any industry guidance to the contrary, the assumption is that a deformation limit state exits when either: (a) the cross-sectional dformation of the pipe becomes sufficiently large to interfere with the passage of a pigging device through the pipe; or, (b) the wrinkle becomes sufficiently large that material failure at the wrinkle is imminent. It is not suggested at this time, however, that these states can replace the fracture limits. They should be viewed as complementary to these limits.

Cross-sectional distortion can occur from ovalization or from wrinkling and local buckling. These, in turn, will influence curvature. Consequently, the main thrust of the analyses which have been developed, has been to analyze for the initiation and amplification of local buckling under realistic field conditions. In addition to developing three-dimensional finite element analyses for the analysis of local buckling, this has required the development of methods to predict the concentration of curvatures in regions of softening associated with the local buckling phenomenon.

The first deformation limit state identified above (LS1) is dictated by the passage of pigging devices. A *pigging device* is a type of on-line inspection device for pipelines. It performs various functions, from removal of obstructions to monitoring the geometry and corrosion conditions. In the modern pipeline industry, on-line inspection is believed to be essential for extended life and is as important as the initial design (Price and Anderson, 1991). Consequently, the pigging operation is one of the basic operations to be carried out in pipelines. Typical pigging devices are shown in Figs. 8.1 and 8.2 for small size and large size of pipelines, respectively.

The operational conditions for pigging devices depend upon the purpose of the pigging operation. As discussed by Tiratsoo (1987), the four purposes for pigging operations are : (i) interface separation of fluids; (ii) removal of obstructions; (iii) pipeline maintenance; and (iv) pipeline monitoring. These different purposes lead to different types of pig devices and different requirements on the operational conditions. The basic requirement for all types of pig devices is the passage of the devices, because the pig has to be able to go through the pipeline in order to perform any kind of operation. In addition, a stuck pig can cause a major disruption to the operation of the line. Consequently, any deformation which significantly affects the passage of the pigging operation is a deformation limit state for which rational design, maintenance or repair criteria should be established.

The second deformation limit state identified above (LS2) is associated with the amplitude of the wrinkle. As the wrinkling initiates and develops, the pipe wall starts to fold and large bending deformation is introduced into the pipe wall locally at the wrinkle (see Figs. 4.29(c) to 4.35(c)). The bending deformation at the crease of the wrinkle is particularly large and material failure may be expected when the amplitude of the wrinkle is sufficiently large. Material failure of the pipe wall leads to leakage and rupture. As a result, an ultimate limit state can be established based on the amplitude of the wrinkle. Unfortunately, there is no data available with respect to the amplitude of wrinkle associated with the material failure in the crease of the wrinkle. The determination of this limiting amplitude would require a rational procedure based on the principles of fracture mechanics and this is beyond the scope of this project. However, the reason to consider this as a limit state of deformation is that the material failure condition is the consequence of wrinkling and wrinkling is a deformation dominated phenomenon. It is assumed that the material failure associated with wrinkling can be prevented by limiting the amplitude of wrinkling.

8.1.2 Existing Design Criteria for Deformation

Generally, design criteria for deformations do not exist in the design codes for pipelines, such as the Canadian codes (Canadian Standards Association, 1986, 1990). The existing deformation criteria were developed by the pipeline industry and are summarized well by Price et al. (1978, 1987, 1990 and 1991).

Three measures of deformation have been established. The first is the *longitudinal compressive strain limit* at the onset of local buckling. This is the criterion to prevent the initiation and development of local buckling or wrinkling. The second deformation criterion is the *ovality* of the cross-section. This is designated to prevent excessive denting, or flattening that may be introduced by large reactive forces. The third criterion is the *out-of-roundness*. This is intended, in part, to prevent snap-through collapse. The limiting longitudinal compressive strain has been set from 0.3 percent to 0.8 percent (Price and Barnette, 1987) for pipelines with diameter of 48 inches (1219 mm) to 12 inches (305 mm). This is determined, in general, by experimental measurements and analytical predictions of the strain at the onset of local buckling.

The *ovality* is defined as

$$\text{ovality} = \frac{D - D_{min}}{D} \times 100\% \tag{8.1}$$

where D and D_{min} are the nominal outside diameter and the minimum diametrical measurement, respectively. The ovality has been limited to between 5 to 8 percent in the past (Price, 1990). *Out-of-roundness* has been defined in Eq. (4.1) as

$$\text{out-of-roundness} = \frac{D_{max} - D_{min}}{D} \times 100\% \tag{8.2}$$

where D_{max} is the maximum diametrical measurement. The out-of-roundness has been limited to about 15 percent and 6 percent for pipelines operated at zero and full pressure, respectively (Price and Anderson, 1991). The limit values used for ovality and out-of-roundness have taken the requirement of the passage of pig devices into account. This implies that the experience of the industry is that the passage of pig devices can be guaranteed if the out-of-roundness is less than about 15 percent.

The above three criteria are not based rationally on the deformation limit states of pipelines. The buckling strain limit by itself does not specify a deformation limit state. It is

only if one interprets this limit as an estimate of the conditions under which other distortions become unacceptable that it becomes consistent with limit states philosophy. However, both experimental studies (Bouwkamp and Stephen, 1973) and the analytical studies in this work indicate that at the onset of local buckling the cross-sectional deformation is small and the pipeline can remain fully operational. Hence, the buckling strain criterion can, at most, be considered to be a conservative alternative to a limit states criterion. Because the real behavior of pipelines at deformation limit states is difficult to predict, the buckling strain alternative appears to have been accepted by the pipeline industry even though it may be a poor estimate of true behavior.

The out-of-roundness criterion of Eq. (8.2) is a measure of the cross-sectional distortion. However, it is intended to prevent snap-through collapse which is a load controlled phenomenon. Snap-through collapse is only possible when the load carrying capacity of the pipeline is reached and the rate of reduction of external loads is less than that of the load carrying capacity. For buried pipelines, the major loads are imposed deformations. The basic characteristic of this type of load is that it depends on the stiffness of the pipeline and is applied through the soil-pipeline interaction. As a result, the loads introduced by imposed deformations decrease as the pipeline softens. In addition, as the deformation increases, more support and less load are imposed on the pipeline. Consequently, snap-through collapse is not likely to occur. Furthermore, snap-through collapse is not a failure condition for buried pipelines because the load carrying capacity is not the major concern. Localization of deformation and cross-sectional distortion are associated with the softening behavior of pipeline segments and the failure condition should be determined to rationally establish the deformation limit states.

The ovality criterion of Eq. (8.1) is intended to control dent types of cross-sectional distortion. As far as the deformation for this particular type of the cross-sectional distortion is concerned, this criterion can be replaced by more general deformation criteria based on cross-sectional distortion.

In an effort to review the buckling strain criterion, Lara (1987) studied wrinkle growth after local buckling was initiated. It was concluded that the buckling strain criterion is adequate for pipe segments with low pressure and very conservative for pipe segments with high pressure. Further deformation can be tolerated without risking operational integrity. It was suggested that the compressive strain, at which rapid wrinkle growth begins to occurs is more closely related to the failure condition of pipelines; and therefore, can be used as the deformation limit criterion for design. However, no details were given

with respect to how to determine this critical compressive strain and how to apply it.

8.2 PROPOSED DEFORMATION CRITERIA

To establish rational deformation criteria based on limit states principles is the objective. However, clear guidance from the pipeline industry with respect to the definition of failure in terms of deformation is not available at the present time. Therefore, deformation criteria are established based on the deformation limit states proposed in Sect. 8.1.1. These are associated with the passage of pigging devices and material failure at the crease of the wrinkle. These criteria will be referred as *cross-sectional deformation limit states criteria* and will be discussed in Sect. 8.2.1. Because deformation limit states are not well defined, the applicability of the cross-sectional deformation limit states criteria is restricted and an alternative to them is proposed. It is referred to as the *initiation of softening criterion* which appears to give a good estimation of the deformation limit states. This initiation of softening criterion is discussed in Sect. 8.2.2. For comparison, the *buckling strain criterion*, used currently in the pipeline industry, is also included in Sect. 8.2.3. It is suggested that the buckling strain criterion be replaced by the *initiation of wrinkling criterion* that will be established based on the condition at the initiation of the wrinkling as defined in Ch. 5.

8.2.1 Cross-sectional Deformation Limit States Criteria

The basic assumption for design criteria discussed in this sub-section is that the deformation limit states can be best represented by the deformations which interfere with the passage of pigging devices or cause material failure at the crease of a wrinkle. Experimental studies (Bouwkamp and Stephen, 1973, 1974) and the analytical studies in this project have confirmed that there are essentially two types of buckling modes. They are an inward diamond buckling mode, which occurs at low internal pressure; and, an outward bulging buckling mode which occurs at medium and high internal pressures. The inward buckling mode is likely to affect the passage of the pigging operation because the development of wrinkles in this mode would significantly reduce the diametrical dimension in at least one direction. To the author's knowledge, the outward buckling mode would not interfere with the pigging operation in any significant way. However, it is more likely to cause material failure at the crease. This is because the outward wrinkle tends to have a relatively smaller wavelength than the inward wrinkle, as was discussed in Sect. 4.3.4, and consequently, more bending deformation concentrates on the crease of the wrinkle.

To quantify the deformation with respect to these two deformation limit states and two buckling modes, the diametric differential and diametric expansion, which were defined in Eqs. (4.2) and (4.3), are used to describe the cross-sectional distortion and the amplitude of the wrinkle. Considering the fact that the maximum and minimum diametric dimensions are either the in-plane diameter or the out-of-plane diameter, out-of-roundness is actually the absolute value of the diametric differential. Diametric differential is more informative by differentiating between the two basic buckling models. In general, it is positive and increasing for the inward buckling mode and negative, or close to zero, for the outward buckling mode. When diametric differential is positive, it defines quantitatively the decrease of the in-plane diameter and increase of the out-of-plane diameter. If the deformation of this pattern grows to a certain magnitude, the passage of pigging devices is affected. Consequently, as one of the possible measures, the deformation limit state associated with the passage of pigging devices can be quantitatively defined to be when the diametric differential reaches a limiting value.

At the present time, however, this limiting value of the diametric differential is not available from the pipeline industry. A data base collected from pigging designers and operators is needed to rationally evaluate the limiting value for diametric differential. To illustrate the procedure to establish and apply the limit states criteria for this type of deformation, the limiting value for diametric differential is assumed to be 15 percent. This is based on the fact that out-of-roundness at 15 percent is safe for passage of pigging devices as implied by the criterion presently used in the industry. The deformation criterion can be expressed in equation form as

$$\text{predicted maximum } D_{diff} \leq 15\% \tag{8.3}$$

where D_{diff} is the diametric differential. Since this deformation limit state is considered to be a service limit state, there is no load factor or resistance factor to be applied in the above equation.

The amplitude of the wrinkle for an outward bulging mode is represented by the diametric expansion, which is the average of the maximum and minimum amplitude. Diametric expansion is intended to describe the deformation in the outward buckling mode and the deformation limit state associated with the material failure at the crease of the wrinkle. The amplitude of the inward buckling mode is not properly represented by diametric expansion. However, this pattern of deformation is more likely controlled by the

criterion in Eq. (8.3). As one of the possible measures, the deformation limit state with respect to material failure at the crease of the wrinkle can be quantitatively represented by a limiting value on diametric expansion. Since this limiting value is not available and there is no guidance on what is should be, it is assumed to be 10 percent. The number of 10 percent is believed to be reasonable and conservative. In the test series recently completed in University of Alberta, and the test series currently in progress in the Center for Frontier Engineering Research (C-FER), some specimens have developed wrinkles with an amplitude larger than 10 percent of the pipe diameter. However, no material failure has been observed. The deformation criterion associated with the material failure at the crease of wrinkle is then taken to be

$$\text{predicted maximum } D_{exp} \leq 10\,\% \tag{8.4}$$

where D_{exp} is the diametric expansion. The deformation limit state associated with material failure is considered as an ultimate limit state. Consequently, load factor and resistance factor should be applied to Eq. (8.4) according to the principles of limit states design. Nevertheless, in the demonstration of of application of this criterion to be undertaken in Sect. 8.3, they are neglected for the reasons of simplicity and because no data base is available.

The cross-sectional deformation criteria in Eqs. (8.3) and (8.4) are based on the principles of limit states design, even though the limiting values cannot be firmly established at this time due to lack of the data base to define the limiting conditions. This work focuses on the conceptual approach to be used in the application of such criteria. As more data become available, the limiting values can be revised.

8.2.2 Initiation of Softening Criterion

Because the cross-sectional deformation limit states of pipelines are not well defined, the numerical values for the deformation criteria established in Sect. 8.2.1 have not been validated for the design of pipelines. As a result, an alternative is needed that is more closely related to, and that would improve, the existing criteria. The proposed criterion is based on a lower bound estimation of the cross-sectional deformation limit states and is referred to as the *initiation of softening criterion.*

The behavior of pipelines subjected to differential settlement has been discussed in Sect. 7.2.1. The development of deformation in terms of curvature at the critical segments

has three stages with respect to imposed differential settlement as shown in Figs. 7.10 and 7.12. The third stage is one in which the softening characteristic is implied by the response, and this introduces a much higher growth rate of curvature with respect to settlement. A fundamental assumption adopted here is that any deformation limit state is associated with a curvature that is larger than the curvature at the initiation of the third stage on the critical curvature-settlement curve. This assumption implies that no deformation limit state will be reached until the pipe segment starts to soften. The assumption is conceptually justified by the fact that cross-sectional distortion is mainly introduced by local buckling which is associated with softening behavior of the pipe segment as discussed in Sect. 4.3.5. Based on this assumption, the deformation state at the initiation of the third stage can be taken as a good lower bound estimate for the deformation limit states associated with a larger curvature. This is illustrated in the following by a numerical example.

The critical curvature-settlement curve in the settlement zone for Specimen NOM, which was analyzed in Ch.7, is shown in Fig. 8.3. This curve is identical to that in Fig. 7.12. At the initiation of the third stage, the curvature is 3.3573×10^{-4}/in (1.3218×10^{-5}/mm) and the settlement is 16 inches (406 mm). The curvature increases from 3.3573×10^{-4}/in (1.3218×10^{-5}/mm) to 11.277×10^{-4}/in (4.4398×10^{-5}/mm) while the settlement increases from 16 inches (406 mm) to 22.3 inches (566 mm), i.e. a 236 percent increase in curvature corresponds to a 39 percent increase in settlement. These numbers show that the curvature at a deformation limit state may be significantly larger than the one at the initiation of the third stage. Additional settlement tolerable to the pipeline is, however, not nearly as large as the difference in curvature.

Consequently, the initiation of the third stage on the critical curvature-settlement curve is a reasonable, albeit conservative, estimate to the deformation limit states for the purpose of deformation analysis and design. As discussed in Sect. 7.2.1, the third stage is associated with the softening behavior of pipe segments in the postbuckling region. The initiation of the third stage on the critical curvature-settlement curve corresponds to the "initiation of significant softening" on the moment-curvature curve (compare Fig. 7.10 with 7.11; Fig. 7.12 with Fig. 7.13; Fig. 7.16 with 7.17; Fig. 7.20 with 7.21, etc.). Therefore, if the point of *initiation of significant softening* is defined as the initial point of the first significant softening on the moment-curvature curve, its occurence can be determined directly from the moment-curvature curve by identifying the first segment of softening, or indirectly from the critical curvature-settlement curve by identifying the initial point of the third stage.

Based on the understanding of the behavior of pipelines subjected to differential settlement, the initiation of significant softening on the moment-curvature curve can be established as an alternative to the cross-sectional deformation limit states criteria defined in Eqs. (8.3) and (8.4). Design rules for this point can be translated into the corresponding curvatures or compressive strain at the extreme fiber. As shown in Figs. 4.7 to 4.9, moment-curvature is affected significantly by the internal pressure and the axial load. As a result, the *limiting curvature or compressive strain* established at the initiation of significant softening are dependent on the axial force and internal pressure. This criterion may be symbolically expressed as

$$\text{predicted maximum compressive strain} \leq \text{limiting compressive strain} \qquad (8.5)$$

where the limiting compressive strain could be determined, for example, from the softening points of the curves in Fig. 4.12. Equation (8.5) can be equivalently expressed in terms of curvature.

The initiation of significant softening criterion is not a limit states criterion. However, it appears to be a good alternative until rational deformation limit states can be established, because it is based on the behavior of pipelines subjected to differential settlement and it takes different characteristics of moment-curvature relations into account. Consequently, it is more rational than a criterion based on buckling strain.

8.2.3 Initiation of Wrinkling Criterion

The buckling strain criterion is defined at the onset of local buckling and has been used in industry as the deformation criterion. The criticism of this criterion is the fact that the initiation of local buckling is not significant enough to define the deformation limit states. It appears that, quite generally, more deformation can be tolerated without affecting the integrity and operational condition of pipelines.

Discussions in Sect. 5.1 concluded that wrinkling strain is a better representation than buckling strain for the initiation of local deformation patterns. Based on a similar principle to the buckling strain criterion, which is to prevent any localization of deformation associated with growth of wrinkling, the buckling strain criterion can be replaced by the criterion

$$\text{predicted maximum compressive strain} \leq \text{wrinkling strain} \qquad (8.6)$$

where the wrinkling strain is used to replace the buckling strain. This criterion is referred in the following as *initiation of wrinkling criterion.*

8.3 APPLICATIONS OF DEFORMATION DESIGN CRITERIA

The procedures to apply the deformation criteria established in the previous section are illustrated in this section. The examples used for this purpose are associated with pipelines with a diameter of 48 inches (1219 mm) and thickness of 0.462 inches (11.7 mm) that are subject to internal pressure at a level of 72 percent of the yield pressure. A requirement to apply these criteria is that the predictive approach should be consistent with the deformation criteria to be applied. This means that the predictive approach must have the capability to properly model the softening response of the pipe segments and their interaction with the overall response of the pipeline. This is particularly true for the cross-sectional deformation limit state criteria in Eqs. (8.3) and (8.4) and for the initiation of softening criterion in Eq. (8.5), because the limiting values associated with these criteria will not be reached before the pipe begins to soften.

The following applications of the deformation criteria include generation of design curves and determination of permissible differential settlements. These are discussed in the following sub-sections.

8.3.1 Design Curves

The limiting curvature and compressive strain associated with each of the deformation criteria are dependent on the axial force and internal pressure. For pipelines operating at a specified constant pressure level, they depend only on the axial force. Curves can be plotted in terms of the limit for the compressive strain or the limit for the curvature with respect to axial force. These are referred to as *design curves.* A specific design curve can be generated from each of the three deformation criteria for a given pipeline at a specified pressure level.

Generation of design curves requires shell model analysis of the pipeline segment, as presented in Ch. 4, in order to determine the curvature at which the limit conditions of the design criteria are reached. Each of the design criteria corresponds to its own limit condition. Cross-sectional deformation criteria correspond to the limit condition for which the passage of pigging devices is interfered with, or when material failure in the crease of a wrinkle is inminent. The limit conditions for the initiation of significant softening criterion

and the initiation of wrinkling criterion are established from the shell segment analysis at the points of initiation of significant softening and of the initiation of wrinkling, respectively.

The discussion in this section is confined to a pressure level of 72 percent of the yield pressure. Consequently, the solutions to establish the design curves are those of Specimens PHC40, PHC20, PHC00, PHT20 and PHT40. These solution have been presented and discussed in Ch. 4.

The procedure to determine the limiting curvatures and compressive strains from the cross-sectional deformation limit states criteria in Eqs. (8.3) and (8.4) is relatively straight forward. First the diametric differential and diametric expansion are plotted with respect to the curvature and strain based on the solutions from the shell model analysis. For this group of specimens, examples are shown in Figs. 4.41 and 4.44. If a horizontal line is drawn at 15 percent in Fig. 4.41 and 10 percent in Fig. 4.44, the intersection with each of the curves defines the limiting curvature for the various levels of axial force specified for the corresponding specimens. In general, two values may be obtained from these two figures for a given specimen, the smaller one is used. In fact there are no intersections of the limit condition with the curves in Fig. 4.41 which indicates that the condition of Eq. (8.3) is not of concern for the design of this pipe. The limiting curvatures from Fig. 4.44 are listed in Table 8.2 and plotted with respect to the levels of axial force shown in Fig. 8.5. If diametric differential and diametric expansion are plotted with respect to compressive strain and the similar procedure is applied to these curves, limiting compressive strains can be determined which are listed in Table 8.1 and shown in Fig. 8.4.

For the initiation of softening criterion, the key is to identify the initiation of the first significant softening. From the shell model analysis, the moment-curvature curves and moment-compressive strain curves can be plotted and have been shown in Figs. 4.9 and 4.12. The points of initiation of significant softening are, in general, well defined on these curves and can be identified by observation. Specimen PHC40 is a exception. Because of the high values of pressure and compressive axial load, the moment-carrying capacity is very small. As a result, hardening and softening are not as obvious as for the solutions for other specimens. Under this circumstance, a conservative estimate of the initiation of significant softening can be assumed to be the onset of wrinkling identified as described in Ch. 5. The limiting compressive strains and curvatures for this group of specimens are listed in Tables 8.1 and 8.2 and plotted with respect to the levels of axial load in Figs. 8.4 and 8.5, respectively.

The limiting compressive strains and curvatures for the initiation of wrinkling criterion are defined at the initiation of wrinkling by the procedure of wrinkling analysis discussed in Ch. 5. In the same way as for the other two criteria, determination of limiting strains and curvatures are based on the solutions of shell model analysis. For this group of specimens, the wrinkling strains and curvatures have been listed in Table 5.2. They are repeated in Tables 8.1 and 8.2 and are plotted against the magnitudes of axial force in Figs 8.4 and 8.5, respectively, for comparison with the other two design curves.

Two sets of design curves have been generated in Figs. 8.4 and 8.5. One is in terms of limiting compressive strain and the other is in terms of limiting curvature. It should be pointed out that the design limits for deformation can be equally represented by either limiting compressive strain or limiting curvature provided that the effects of axial force are properly considered. Consequently, only one set of design curves is needed.

The design curves shown in Figs. 8.4 and 8.5 are only applicable to the pressure level of 72 percent. If design curves at a different pressure levels are needed, another set of shell model analyses must be carried out. The generation procedure discussed in this section is then applied to the solutions to obtain the design curves for the specified pressure level.

The design curves in Figs. 8.4 and 8.5 show great differences in the acceptable limits for compressive strain and curvature. The curves derived from the cross-sectional deformation limit states criteria have much greater values in the entire range of axial force considered here. This is to be expected because of the nature of these limit states. However, the magnitude of the difference is directly affected by the arbitrarily assumed limiting values for diametric differential and diametric expansion. The difference between the design curves derived from the initiation of significant softening criterion and initiation of wrinkling criterion is relatively small when the axial force is in compression. This is a reflection of the fact that the significant softening immediately follows the initiation of wrinkling when the axial force is compressive. However, the difference increases rapidly when the axial force becomes tensile. This is due to the influence of tensile axial force on the postbuckling behavior of pipe segments. These observations are based on the design curves in Figs. 8.4 and 8.5 and may not necessarily be valid under other conditions.

8.3.2 Determination of Permissible Settlement

With the design curves established in Sect. 8.3.1, the permissible differential

settlement can be determined by comparing the predicted response of pipelines subjected to differential settlement with the limiting compressive strain or limiting curvature. The analytical approach used to predict pipeline response should be consistent with the way the design curves were established. The approach developed in this project, which is discussed in detail in Ch. 6 and demonstrated in Ch. 7, is consistent for all three design criteria contained in Figs. 8.4 and 8.5 because the local buckling effects are properly included in the line analysis of the pipeline. On the other hand, the conventional elastic-plastic beam analysis is consistent only with the initiation of wrinkling criterion because the effect of local buckling is not included. Considering the fact that the effect of local buckling in the region between the onset of wrinkling and the initiation of the first significant softening is relatively small, the conventional elastic-plastic beam analysis may be used in association with the initiation of significant softening criterion. In the following, two examples are shown to demonstrate the procedure for the determination of permissible differential settlement. All the solutions are obtained by the ISPDR technique developed in this study.

Example 1

The first example is Specimen NOM of Ch. 7. The soil conditions and properties of the pipeline have been defined and the solution has been obtained in Ch. 7 as shown in Figs. 7.7 to 7.13. From the solution, two curves may be plotted. The first is the critical curvature-axial force curve which can be superimposed on the design curves as shown in Fig. 8.6. The intersection with each of the design curves defines a deformation state in terms of curvature where the respective design limit is reached.

The second curve that may be plotted is the critical curvature-settlement curve as shown in Fig. 8.7. Using the limiting values of curvature corresponding to respective deformation criterion which have been obtained in Fig. 8.6, the permissible differential settlement corresponding to each of the deformation criterion can be determined from Fig. 8.7. For Specimen NOM, the value of limiting curvatures are 0.80×10^{-4}/in (3.1496×10^{-6} /mm), 4.48×10^{-4}/in (1.7638×10^{-5} /mm) and 21.08×10^{-4}/in (8.2992×10^{-5} /mm) for the initiation of wrinkling criterion, the initiation of significant softening criterion and the cross-sectional deformation limit states criteria, respectively. Corresponding to these limiting curvatures, the permissible settlements are 7.3 inches (185 mm), 16.24 inches (412 mm) and 34.56 inches (878 mm), respectively. Notice the very large spread of permissible settlements depending on the criterion employed.

Example 2

Applying the same procedure to Specimen TENOM, as shown in Figs. 8.8 and 8.9, the permissible settlements are determined as 7.52 inches (191 mm), 8.26 inches (210 mm) and 22.12 inches (562 mm) corresponding to the initiation of wrinkling criterion, the initiation of significant softening criterion and the cross-sectional deformation limit states criteria, respectively. Specimen TENOM is subject to temperature differential in addition to differential settlement. This reduces the initial tensile axial force of Specimen NOM to a small compressive force. As a result, the limiting curvatures and permissible settlements associated with the initiation of wrinkling and initiation of significant softening criteria are very close. However, they are significantly smaller than those associated with the cross-sectional deformation limit states criteria, as expected. The differences between the limiting curvatures and permissible settlements shown in Figs. 8.7 and 8.9 may not represent the realistic differences because the cross-sectional deformation limit states, on which the limit states criteria herein are based, are not firmly established.

8.4 RECOMMENDATIONS OF PROPOSED DEFORMATION CRITERIA

The initiation of wrinkling criterion is recommended to replace the buckling strain criterion because the initiation of wrinkling is a better initial indication of the localization of deformation which may lead to failure of pipelines to perform their intended functions due to excessive deformation. In addition, the predictive approach for initiation of wrinkling is more consistent and is capable of identifying the onset of wrinkling within acceptable accuracy. Nevertheless, both the buckling strain criterion and the initiation of wrinkling criterion are, in general, overly conservative because the criteria try to exclude the localization of deformation and distortion associated with local buckling and wrinkling.

A better alternative to the buckling strain criterion is the initiation of significant softening criterion. It allows the characteristics of the initial postbuckling response to be considered and utilized. The conventional elastic-plastic beam analysis of pipelines can be approximately used in association with the initiation of significant softening criterion, even though it is conceptually inconsistent with this criterion. In the immediate future, efforts should be made to further rationalize and verify the initiation of significant softening criterion. It has a more rational base and does not rely on a data base to be collected by the industry. Therefore, the initiation of significant softening criterion is recommended for design and assessment of pipelines.

The cross-sectional deformation limit states criteria cannot be applied until the deformation limit states are properly defined. However, there is a real need for these rational criteria to be established if limit states are to be applied effectively to pipeline design. It is recommended that industry begin now to assemble data for the establishment of the rational limit states of deformation.

Specimens	Axial Load F/Fy (%)	Limiting Compressive Strains		
		cross-sectional deformation limit states criteria	initiation of softening criterion	initiation of wrinkling criterion
PHC40	-40	4.52	0.2055	0.2055
PHC20	-20	4.14	0.3616	0.3032
PHC00	0	4.67	0.4579	0.3686
PHT20	20	4.56	0.9538	0.2138
PHT40	40	7.34	4.56	0.1552

Note : the unit for limiting compressive strain is %in/in

Table 8.1 Limiting Compressive Strains for 48" Pipe at High Level of Internal Pressure

Specimens	Axial Load F/Fy (%)	Limiting Curvatures		
		cross-sectional deformation limit states criteria	initiation of softening criterion	initiation of wrinkling criterion
PHC40	-40	7.52	0.16	0.16
PHC20	-20	10.52	0.78	0.66
PHC00	0	10.26	1.29	1.05
PHT20	20	11.19	3.30	0.80
PHT40	40	30.84	18.16	0.85

Note : the unit for limiting curvature is 10^{-4}/in

Table 8.2 Limiting Curvatures for 48" Pipe at High Level of Internal Pressure

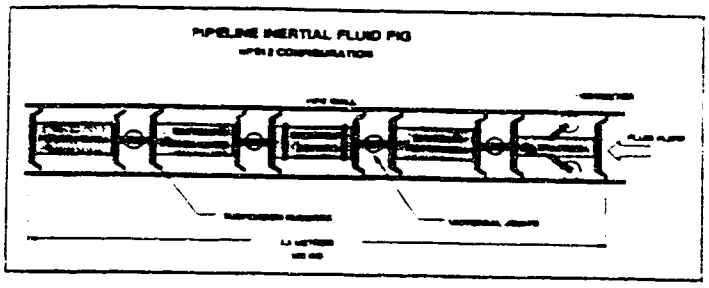

Fig. 8.1 Geometry Pig Train for Small Diameter (12-16 inches) Pipelines

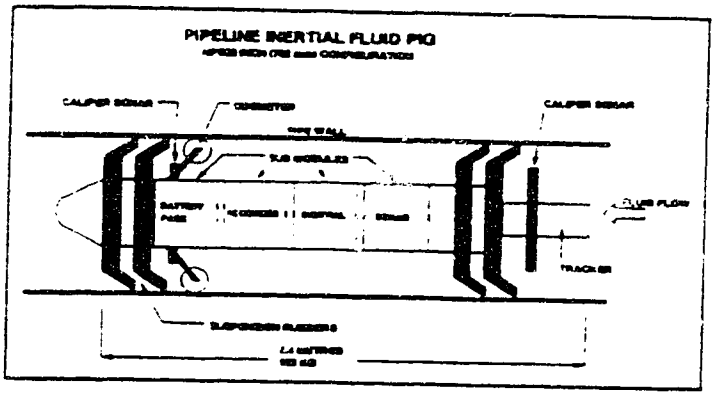

Fig. 8.2 Geometry Pig Train for Large Diameter Pipelines

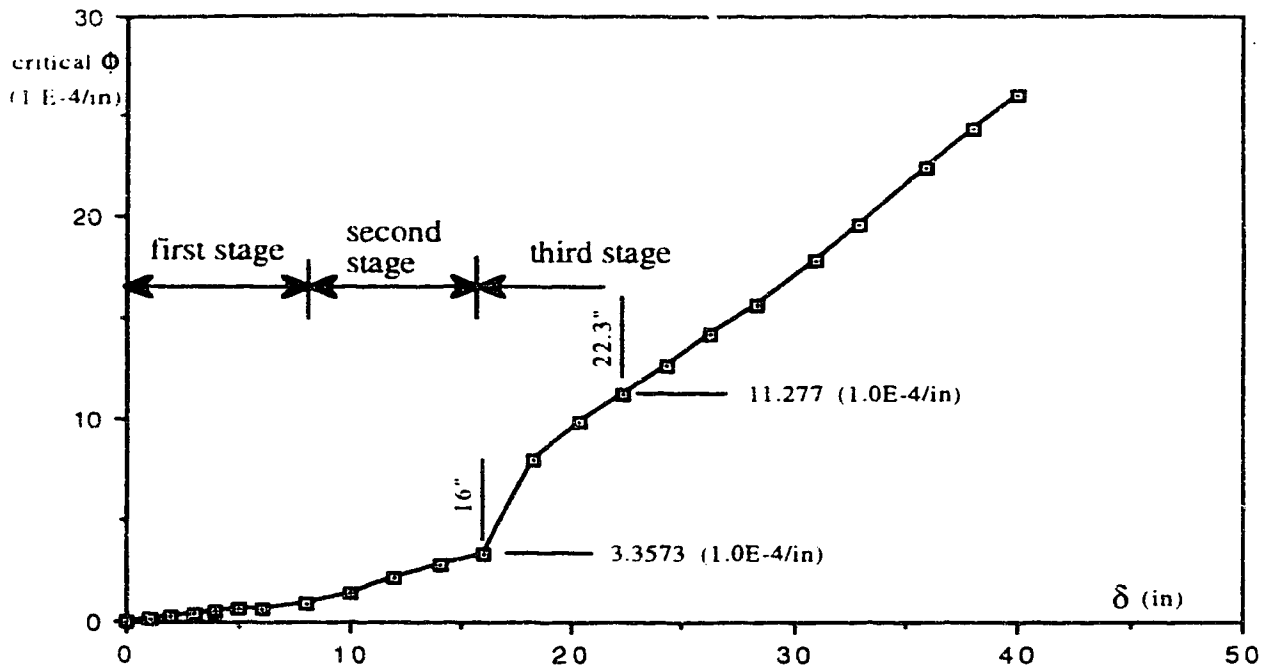

Fig. 8.3 Critical Curvature-Settlement Curve for Specimen NOM

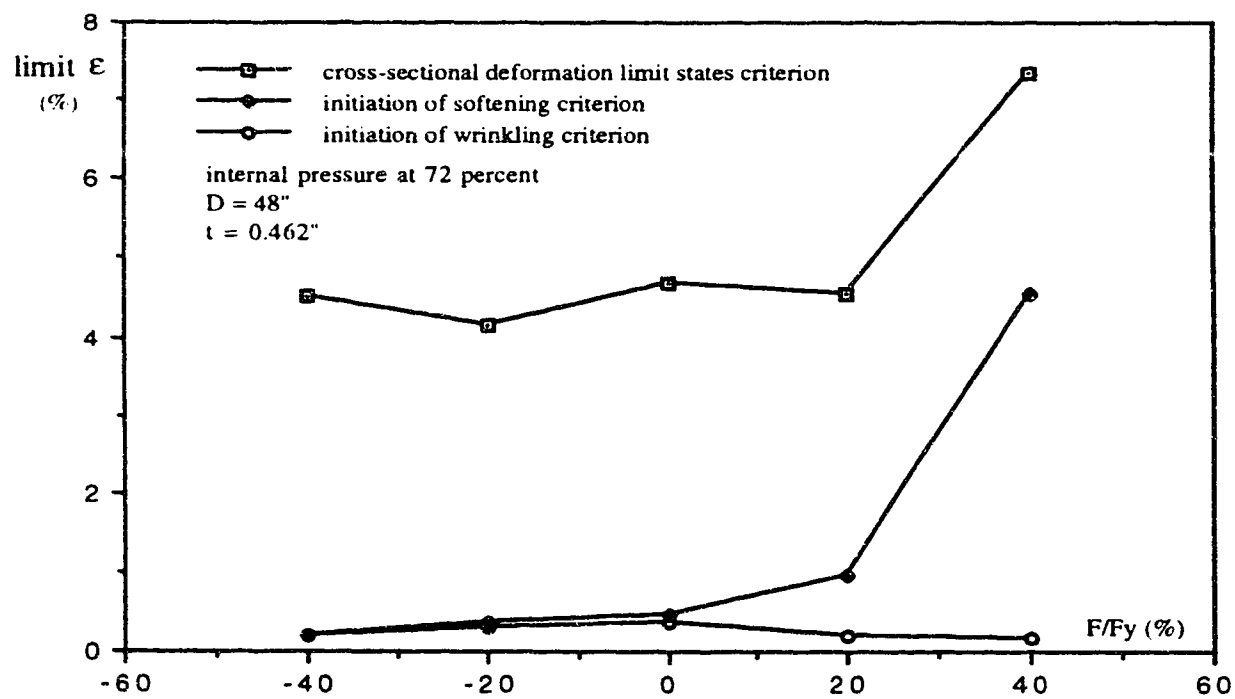

Fig. 8.4 Design Curves in Terms of Limiting Compressive Strain

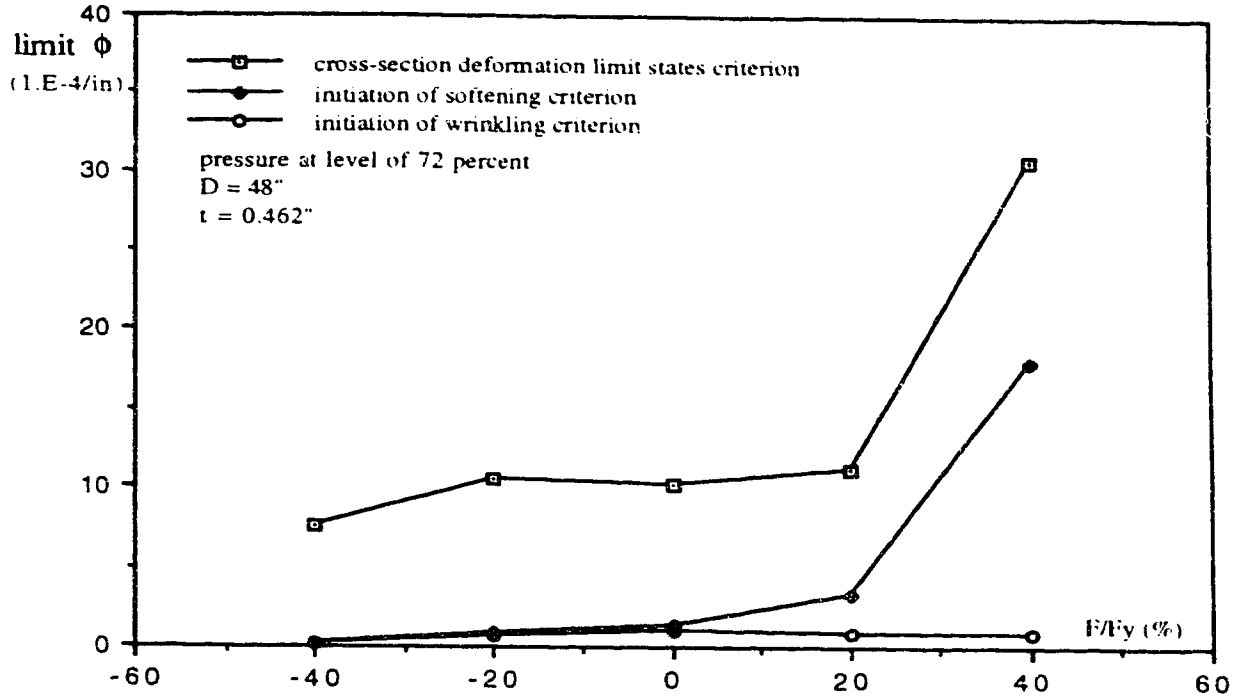

Fig. 8.5 Design Curves in Terms of Limiting Curvature

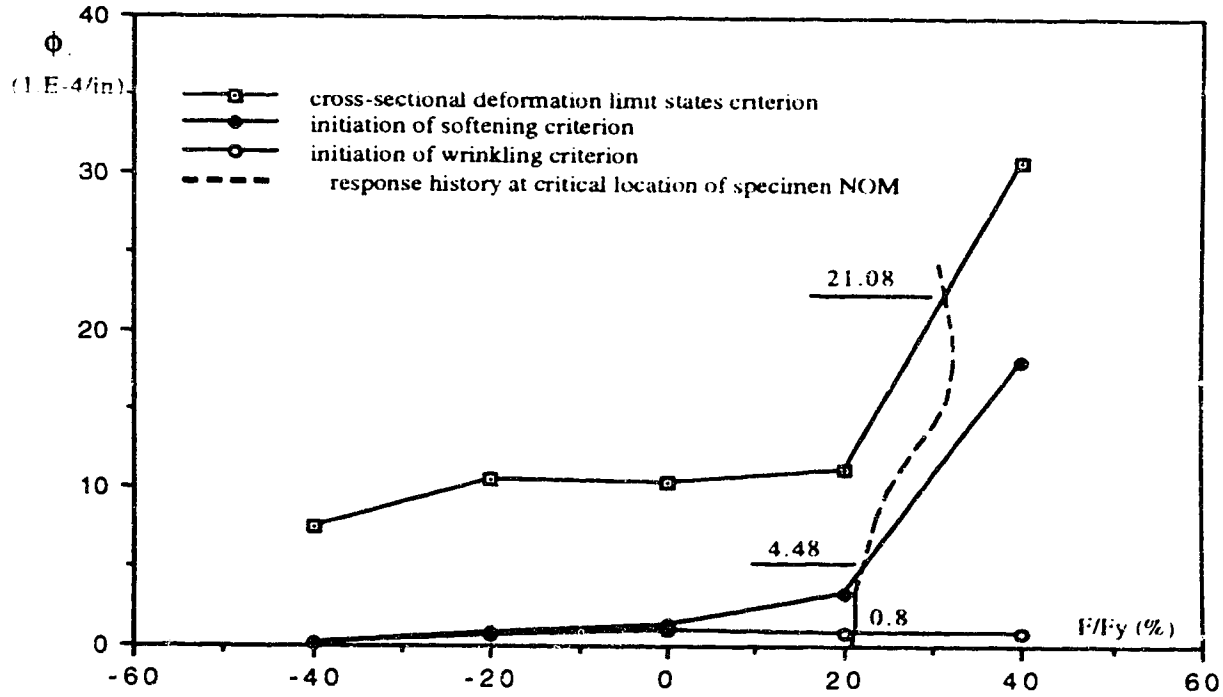

Fig. 8.6 Determination of Limiting Curvatures for Specimen NOM

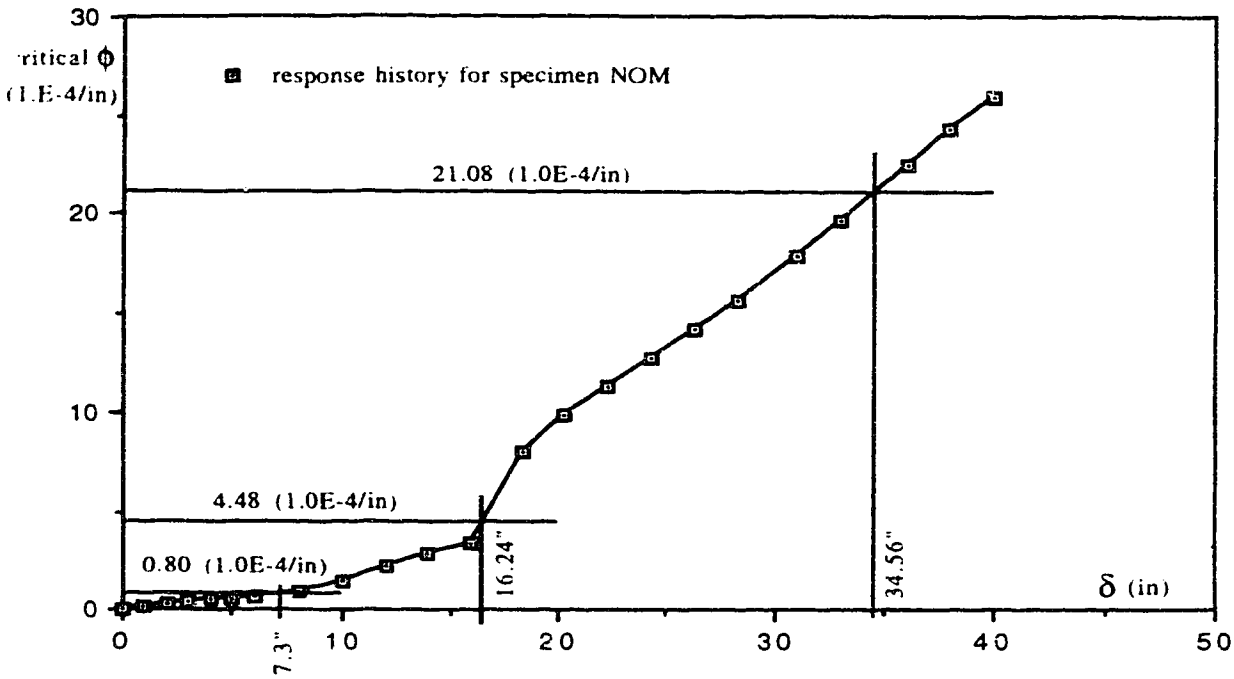

Fig. 8.7 Determination of Permissible Differential Settlements for Specimen NOM

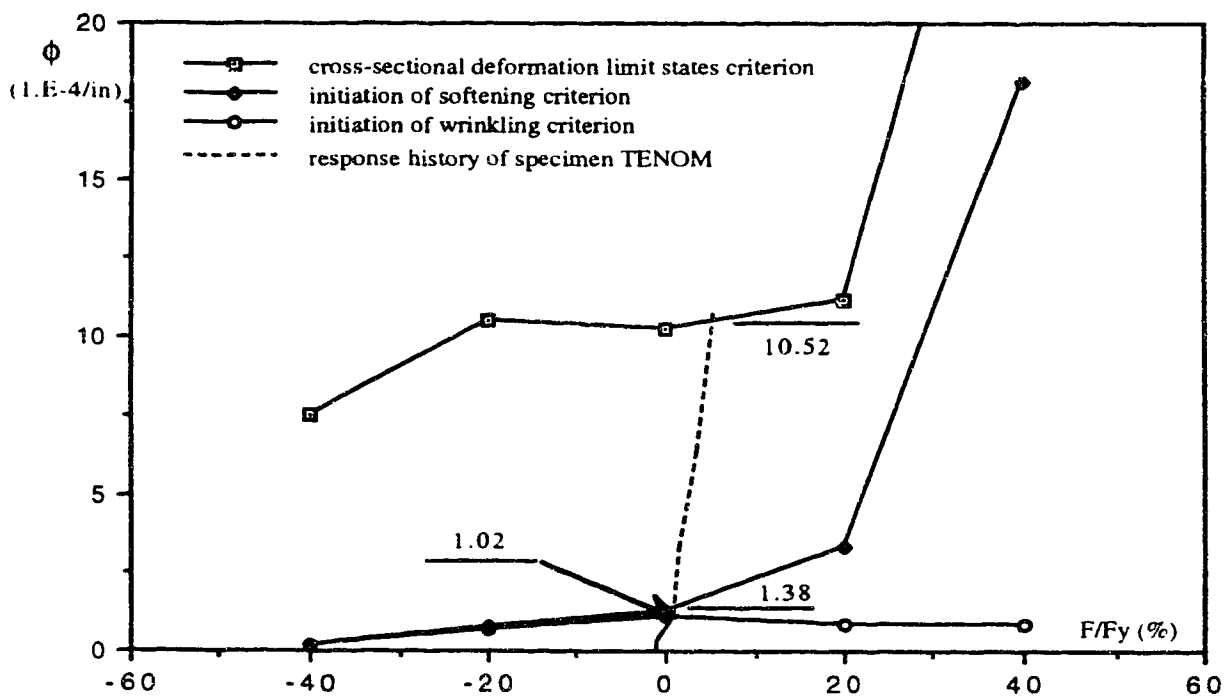

Fig. 8.8 Determination of Limiting Curvatures for Specimen TENOM

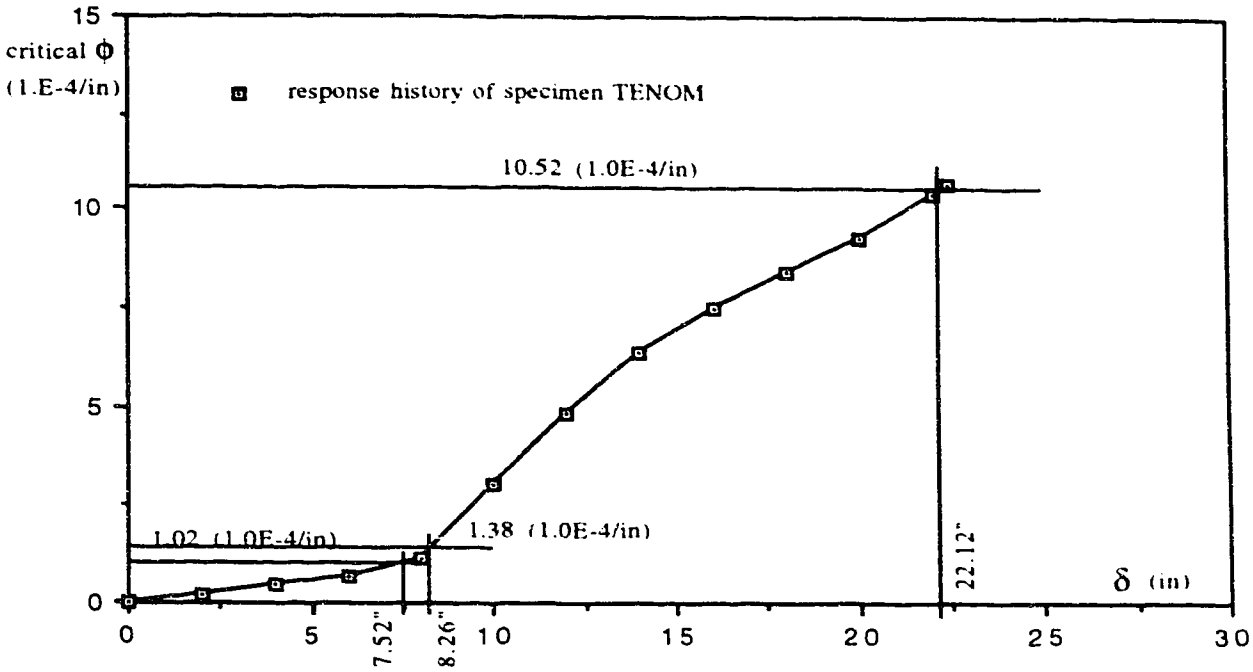

Fig. 8.9 Determination of Permissible Differential Settlements for Specimen TENOM

CHAPTER 9 SUMMARY AND RECOMMENDATIONS

9.1 SUMMARY OF INVESTIGATION

The objective of this work was to study the behavior of buried pipelines and how they respond to large deformations imposed by geotechnical movements. The study has dealt with a number of topics ranging from the prediction of inelastic postbuckling behavior of shells to the application of deformation limit states to pipeline design. In particular, the following have been dealt with.

1. An approach for response prediction of buried pipelines subjected to imposed deformations has been developed. It includes a three-dimensional shell analysis of pipeline segments and a line analysis of the pipeline based on a pipeline-beam element. Pipelines exhibit local buckling behavior. This local behavior and its interaction with the overall performance of the pipeline, as well as the soil-pipeline interaction, are properly integrated into the approach developed herein.

2. A numerical solution technique for nonlinear analysis of unstable postbuckling response of cylindrical shells has been developed. It is based on an improved arc-length control technique. To improve the efficiency of this solution technique, a solution procedure based on the direct search method has been explored and proposed. An example has been included which shows great potential to improve the efficiency over that of the arc-length control technique. Best efficiency is expected to be obtained from the combination of these two solution techniques.

3. Postbuckling analyses have been carried out for a given pipe segment subjected to different loading conditions. Two basic buckling modes, the inward diamond mode and the outward bulging mode, have been predicted. The mode which occurs depends primarily upon the magnitude of the internal pressure. The major effect of the axial load is that it influences the relative significance of the axial deformation component with respect to the flexural deformation component. Deformations have been observed to localize in the buckling segment. The localization of deformation and cross-sectional distortion have been found to be accentuated by the softening behavior of pipeline segments. The postbuckling behavior becomes less unstable with a higher internal pressure and a larger axial load in tension.

4. The concept of initiation of wrinkling has been introduced and an approach to identify the initiation of wrinkling has been developed. The wrinkling analysis has been applied to the given pipeline segment under different loading condition. The results have demonstrated the dependence of the wrinkling strain on both the internal pressure and axial load.The wrinkling strain, in general, decreases as the magnitude of axial load increases, except for the case of compressive axial load combined with zero internal pressure. The internal pressure, in general, increases the wrinkling strain except for cases of internal pressure combined with large compressive axial load. The wrinkling analysis has been applied to pipeline segments with different geometries. The wrinkling strain is found to decrease significantly as the D/t ratio increases but to be insensitive to the diameter of the pipe.

5. A pipeline-beam element has been formulated. The formulation includes large displacements and nonlinear material properties. The soil-pipeline interaction has been modelled by a series of soil springs. The separation of soil from the pipeline is simulated by detaching the soil springs. Stiffness-property-deformation (SPD) relations, that are derivable from postbuckling analyses of cylindrical shells, have been defined and their relationships to cross-sectional stiffness coefficients have been derived. Local buckling behavior is integrated into the line analysis by SPD relations. A program (ABP) has been developed based on the RMDI and ISPDR solution techniques. The effectiveness of this program to predict the response of buried pipelines has been demonstrated.

6. The behavior of buried pipelines subjected to differential settlement has been analyzed. The effects of factors, such as local buckling, temperature differential, and strength and stiffness of the uplift and bearing springs, have been found to significantly influence the response of pipelines. The strength of longitudinal springs and the length of the transition zone are relatively less influential. The rapid growth of localization of deformation has been found to be associated primarily with the softening behavior of the pipeline segment.

7. The author proposes that cross-sectional deformation be the basis for limit states associated with the passage of pigging devices and that material failure at the crease of wrinkles be the basis for an ultimate limit state associated with large deformations. Based on assumed limiting values on the quantitative description of the deformation, as measured by the diametric differential and diametric expansion, cross-sectional deformation limit states criteria have been proposed. Because the limiting values of these limit states criteria cannot be firmly established due to lack of the data base, an alternative criterion, the

initiation of significant softening criterion, has been recommended. It is recommended for use in design and assessment of pipelines in the immediate future until adequate specification of the deformation limit states can be established. It is suggested that the buckling strain criterion, which is currently used in the pipeline industry, be replaced by the initiation of wrinkling criterion.

9.2 RECOMMENDATIONS FOR ADDITIONAL WORK

As with most research projects, although significant progress has been made, important questions remain to be answered and a great deal of development work remains to be done. Some specific recommendations follow.

First, the construction of SPD relations is a major undertaking for a given pipe size and pressure. It is unlikely that design offices will adopt the rational analytical techniques which have been developed herein until it becomes less arduous to construct such curves. Before this can happen it requires still further development in the efficiency of postbuckling shell analysis. It is recommended that the direct search technique of Chapter 3 be further developed as a promising approach to improve the efficiency of the process. Another factor that could greatly reduce the effort required would be for the industry to properly define the limit states. Then much work of determining solutions in the deep postbuckling regions could be curtailed because solutions beyond the limit states are not useful for design or assessment purposes.

Second, this work has concentrated on limit states established with buckling and distortion of the cross-section but has not concerned itself with fracture limit states which have traditionally dominated the thinking associated with pipeline safety. Leaving aside the subject of what constitutes a rational limiting tensile strain which would produce an unacceptable probability of failure, the conditions under which currently acceptable limitations are reached, when rational structural analysis for the behavior of the line is undertaken, could be determined from the same type of analyses as undertaken in this work. It is recommended that this be done.

Third, a generalization of the types of imposed geotechnical movements could be undertaken. For instance, the behavior of the pipe when it is passing through an unstable slope could be assessed. This would give a greater variety of loading conditions and create conditions under which the pipe would be functioning under greater tensile stresses than arise from pure settlements.

Finally, the effects of circumferential welds on the initiation of wrinkles, the localization of deformations, and the initiation of cracks should be investigated.

In addition, it is recommended that the pipeline industry begins now the data collection to qualitatively and quantitatively establish the limits for deformation limit states.

BIBLIOGRAPHY

Almroth, B.O., Brogan, F.A. and Stern, P. (1978), "Automatic Choice of Global Shape Function in Structural Analysis", AIAA Journal, Vol. 16, pp. 525-528

Almroth, B.O. (1966), "Influence of Edge Conditions on the Stability of Axially Compressed Cylindrical Shells", AIAA Journal, Vol. 4, pp. 134-140

Amazigo, J.C. and Budiansky, B. (1972), "Asymtotic Formulas for the Buckling Stresses of Axially Compressed Cylinders with Localized or Random Axisymmetric Imperfections", Journal of Applied Mechanics, Vol. 39, pp. 179-184

Aoki, M. (1971), "Introduction to Optimization Techniques, Fundamentals and Applications of Nonlinear Programming", Macmillan, New York

Arbocz, J. and Babcock, C.D. (1969), "The Effect of General Imperfections on the Buckling of Cylindrical Shells", Journal of Applied Mechanics, Vol. 36, pp. 28-38

Basar, Y. and Kratzig, W.B. (1990), "Introduction into Finite-Rotation Shell Theories and Their Operator Formulation", in Computational Mechanics of Nonlinear Response of Shells, eds. W.B. Kratzig and E. Onate, Springer-Verlag, Germany, pp. 3-30

Bathe, K.J. (1982), "Finite Element Procedures in Engineering Analysis", Prentice-Hall, Inc., Englewood Cliffs, New Jersey, 07632

Batterman, S.C. (1965), "Plastic Buckling of Axially Compressed Cylindical Shells", AIAA Journal, Vol. 3, No. 2, pp. 316-325

Beer, F.P. and Johnston, E. R. Jr. (1985), "Mechanics of Materials", McGraw-Hill Ryerson Limited

Bellini, P.X. and Chulya, A. (1987), "An Improved Automatic Incremental Algorithm for the Efficient Solution of Nonlinear Finite Element Equation", Computer & Structures, Vol. 26, No. 12, pp. 99-110

Bouwkamp, J.G. (1975), "Buckling and Post-Buckling Strength of Circular Tubular Sections", Offshore Technology Conference, Paper No. OTC 2204

Bouwkamp, J.G. and Stephen, R.M. (1974), "Full-Scale Studies on the Structural

Behavior of Large Diameter Pipes under Combined Loading", Report No. UC-SESM 74-1, Dept. of Civil Engineering, University of California-Berkal January

Bouwkamp, J.G., and Stephen, R.M., (1973), "Large Diameter Pipe Under Combined Loading", Transportation Engineering Journal of ASCE , Vol. 99, No. TE3, Proc. Paper No. 9907, pp 521-536

Brazier, L.G. (1926), "On the Flexure of Thin Cylindrical Shells and Other 'Thin' Section", Proc. of the Royal Soc., Series A, Vol. 116, pp. 104-114

Brendel, B. and Ramm, E. (1979), "Linear and Non-Linear Stability Analysis of Cylindrical Shells", Proceeding of International Conference on Engineering Application of the Finite Element Method, Hovik, Norway, May 9-11

Brush, D.O. and Almroth, B.O. (1975), "Buckling of Bars, Plates, and Shells", Publishes by McGraw-Hill Book Company

Bushnell, D. (1985), " Computerized Buckling Analysis of Shells", Martinus Nijhoff Publisher

Bushnell, D. (1984), "Computerized Analysis of Shells - Governing Equations", Computer and Structures, Vol. 18, No. 3, pp. 471-536

Bushnell, D. (1981), "Elastic-Plastic Bending and Buckling of Pipes and Elbows", Computers and Structures, Vol. 13, pp. 241-248

Bushnell, D. (1976), "BOSOR5 - Program for Buckling of Elastic-Plastic Complex Shells of Revolution Including Large Deflections and Creep", Computers and Structures, Vol. 6, pp. 221-239

Bushnell, D. (1974), "Bifurcation Buckling of Shells of Revolution Including Large Deflections, Plasticity and Creep", International Journal of Solids and Structures, Vol. 10, pp. 1287-1305

Canadian Standards Association (1990), "CAN/CSA-Z183-M90 Oil Pipeline Systems", November

Canadian Standards Association (1986), "CAN/CSA-Z184-M86 Gas Pipeline Systems",

September

Canuck Engineering Ltd. (1983), "Norman Wells to Zama Pipeline - Structural Analysis and Soil-Pipe Interaction Study", a report prepared for Interprovincial Pipe Line (NW) Ltd., March

Chajes, A. (1985), "Stability and Collapse Analysis of Axially Compressed Cylindrical Shells", Shell Structures, Stability and Strength, R. Narayanan (ed.), Elsevier Applied Science Publishers, London and New York

Chen, W.F. and Han, D.J. (1988), "Plasticity for Structural Engineering", Springer-Verlag New York Inc.

Croll, J.G. and Walker, A.C. (1972), "Elements of Structural Stability", Halsted Press

de Borst, R. (1988), "Bifurcation in Finite Element Models with a Non-Associated Flow Law", International Journal for Numerical and Analytical Methods in Geomechanics, Vol. 12, pp. 99-116

Dixon, L.C.W. (1972), "Nonlinear Optimization", English Universities Press, London

Donnell, L.H. and Wan, C.C. (1950), "Effects of Imperfections on Buckling of Thin Cylindrical and Columns under Compression", Journal of Applied Mechanics, Vol. 17, pp.73-83

Fox, R.L. (1971), "Optimization Methods for Engineering Design", Addison-Wesley Reading, Mass.

Fung, Y.C. (1965), "Foundations of Solid Mechanics", Prentice-Hall, Inc., Englewood Cliffs, N.J.

Gellin, S. (1979), "Effect of an Axisymmetric Imperfection on the Plastic Buckling of an Axially Compressed Cylindrical Shell", Journal of Applied Mechanics, Vol. 46, pp. 125-131

Harris, L.A., Suer, H.S., and Skene, W.T. (1961), "Model Investigations of Unstiffened and Stiffened Circular Shells", Experimental Mechanics, Vol. 1, No. 7, pp. 1-9

Harris, L.A., Suer, H.S., Skene, W.T. and Benjamin, R.J. (1957), "The Stability of Thin-Walled Unstiffened Circular Cylinders under Axial Compression Includes the

Effects of Internal Pressure", Journal of Aeronautical Sciences, Vol. 24, No. 8, pp. 587-596

Hibbitt, H.D., Karlsson, B.I., and Sorensen, P., (1984) :"ABAQUS Theoretical Manual", Version 4.5, March, 1984

Hoff, N.J., Madsen, W.A. and Mayers, J. (1966), "Postbuckling Equilibrium of Axially Compressed Circular Cylindrical Shells", AIAA Journal, Vol. 4, pp. 126-133

Hutchinson, J.W. (1972), "On the Postbuckling Behavior of Imperfection-Sensitive Structures in the Plastic Range", Journal of Applied Mechanics, Vol. 39, pp. 155-162

Hutchinson, J.W. and Amazigo, J.C. (1967), "Imperfection Sensitivity of Eccentrically Stiffened Cylindrical Shells", AIAA Journal, Vol. 5, pp. 392-401

Hutchinson, J.W. (1965), "Axial Buckling of Pressurized Imperfect Cylindrical Shells", AIAA Journal, Vol. 3, pp. 1461-1466

Iimura, S. and Nishio, N. (1986), "Study of Stress in Buried Pipeline under Thermal Loading", Presented at 1986 International Gas Research Conference, Toronto, Canada, Sept. 8-11, pp. 159-168

Jirsa, J.O., Lee, F.H., Wilhoit, J.C., and Merwin, J.E., (1972) "Ovaling of Pipelines under Pure Bending", Offshore Technology Conference, Paper No. OTC 1569

Koiter, W.T. (1963a), "Elastic Stability and Postbuckling Behavior", Proc. Symp. Nonlinear Problems, R.E. Langer (ed.), University of Wisconsin Press, Madison, pp. 257-275

Koiter, W.T. (1963b), " The Effect of Axisymmetric Imperfections on the Buckling of Cylindrical Shells uner Axial Compression", Kononkl. Ned. Akad. Wetenschap. Proc., B66, pp. 265-279

Koiter, W.T. (1945) "Over de Stabiliteit Van Het Elastich Evenwicht", Delft Thesis, H.J. Paris, Amsterdam, (English Transl.) National Aeronautics and Space Administration, Report TTF-10, 1967

Korol, R.M. (1979) "Critical Buckling Strains of Round Tubes in Flexure", Int. J. Mech.

Sci., Vol. 21, pp 719-730

Lara. P.F. (1987), "Revisiting the Failure Criteria of Buried Pipelines", ASME. Petroleum Division (Publication), PD. Vol. 6, pp. 143-154

Mohareb, M.; Zhou, Z.; Kulak, G.L. and Murray, D.W. (1992), "Preliminary Report on Test Results for 12x0.25 inches X52 Grade Line Pipe", Prepared for Interprovincial Pipe Line Co. Ltd, Edmonton, Alberta, July

Mroz, Z. (1967), "On the Description of Anisotropic Work Hardening", Journal of Mechanical Physics and Solids, Vol. 15, pp. 163-175

Nagy, D.A. and Konig, M. (1979), "Geometrically Nonlinear Behavior Using Buckling Mode Superposition", Computer Methods in Applied Mechanics and Engineering, Vol. 19, pp. 447-484

Napoleao, J., Elwi, A.E. and Murray, D.W. (1991a), "Eigenmode Dominance and Its Application to Structures with Nonlinear Materials", Computers and Structures, Vol. , pp.

Napoleao, J., Elwi, A.E. and Murray, D.W. (1991b), "An Eigenvector-Based Strategy for Analysis of Inelastic Structures", Computer and Structures, Vol. , pp.

Napoleao, J., Elwi, A.E. and Murray, D.W. (1990), "An Eigenvector-Based Strategy for Analysis of Inelastic Structures", Structural Engineering Report No. 166, Department of Civil Engineering, University of Alberta, Edmonton, Canada, T6G 2G7

Noor, A.K. and Peters, J.M. (1981a), "Tracing Post-Limit-Point Paths with Reduced Basis Technique", Computer Methods in Applied Mechanics and Engineering, Vol. 28, pp. 217-240

Noor, A.K. (1981b), "Recent Advances in Reduction Methods for Nonlinear Problems", Computer and Structures, Vol. 13, pp. 31-44

Noor, A.K. and Peters, J.M. (1980), "Reduced Basis Technique for Nonlinear Analysis of Structure", AIAA Journal, Vol. 18, No. 4, pp. 455-462

Nyman, K.J. (1983), "Thaw Settlement Analysis for Buried Pipelines in Permafrost", in

Pipelines in Adverse Environments - II", Edited by Mark B. Pickell, pp. 300-325

Onate, E., Dvorkin, E., Canga, M.E. and Oliver, J. (1990) "On the Option of the Tangent Matrix for Geometrically Nonlinear Analysis Using Continuum Based Beam/Shell Finite Elements", in Computational Mechanics of Nonlinear Response of Shells, eds. W.B. Kratzig and E. Onate, Springer-Verlag, Germany, pp. 83-97

Pinkney, R.B., Stephens, M.J., Murray, D.W. and Kulak, G.L. (1983), "Use of Mearured Imperfections to Predict the Buckling of Axially Loaded Cylindrical Shells", Canadian Journal of Civil Engineering, Vol. 10, No. 4, pp. 662-669

Popov, E.P., Sharifi, P. and Nagarajan, S. (1974), "Inelastic Buckling Analysis of Pipes Subjected to Internal Pressure, Flexure and Axial Loadings", in Pressure Vessels and Piping : Analysis and Computers, edited by I.S. Tuba, R.A. Selby and W.B. Wright, ASME Symposium, Vol. , pp 11-23

Popov, E.P., (1973), "Theoretical Buckling Criteria for 48-inch Steel Pipe", Report to Alyeska Pipeline Service Co., April, 1973

Powell, M.J.D. (1966), "Minimization of Function of Several Variables", in Numerical Analysis : An Introduction, edited by Walsh

Powell, M.J.D. (1964), "An efficient Method for Finding the Minimum of a Function of Several Variables without Calculating Derivatives", Computer Journal, Vol. 7, pp. 155-162

Price, P.St.J. and Anderson, H.A. (1991), "Integrity Monitoring and Maintenance Criteria for New and Existing on Land and Marine Pipelines", Proceeding of the First International Offshore and Polar Engineering Conference, Edinburgh, United Kingdom, 11-16, August

Price, P. St. J. (1990), "Canadian Standards Association Limit States Task Force - State of Practice Review for Pipelines and Representative References", December

Price, P.St.J. and Barnette, J.A. (1987), "Pipeline Codes and Structural Criteria for Pipelines in Arctic and Earthquake Regions", Offshore and Arctic Pipelines, Eds. Jin S. Chung and K. Karal

Price, P. St. J. (1978), "Basis of structural Design Criteria for Buried Gas Transmission

Pipelines", ASME, 78-PET-73

Putot, C. (1988), "Configuration of a Pipeline Deformed by Subsidence", Proceeding of the Seventh International Conference on Offshore Mechanics and Arctic Engineering, Houston, Texas, Feb. 7-12, pp 87-94

Ramm, E. and Matzenmiller, A. (1986), "Large Deformation Shell Analysis Based on the Degeneration Concept", in State-of-the-Art Texts on Finite Element Methods for Plate and Shell Structures, eds. T.J.R. Hughes, E. Hinton, Pineridge Press, Swansea, UK

Ramm, E. (1980), "Strategies for Tracing Nonlinear Response Near Limit Point", in Europe-US Workshop 'Nonlinear Finite Element Analysis in Structural Mechanics', July 28-31, Bochum

Rammerstorfer, F.G. [illegible] K. and Ployer, J., (1989) " Nonlinear Stability Problems Concerning with Buried Pipelines for Hot Water Supply", ASME, Pressure Vessels and Piping Division (Publication), PVP Vol. 169, pp 57-62

Rammerstorfer, F.G., (1982) "Jump Phenomena Associated with the Stability of Geometrically Nonlinear Structures", in : Recent Advances in Nonlinear Computational Mechanics, (Eds. E. Hinton, D.R.J. Owen, and C. Taylor), Pineridge Press Limited, Swansea, U.K., pp 119-153

Reddy, B.D. (1979), "An Experimental Study of the Plastic Buckling of Circular Cylinders in Pure Bending", Int. Journal of Solids and Structures, Vol. 15, pp. 669-683

Riks, E. (1979), "An Incremental Approach to the Solution of Snapping and Buckling Problems", International Journal of Solids and Structures, Vol. 15, pp. 529-551

Riks, E. (1972), "The Application of Newton's Method tothe Problems of Elastic Stability", Journal of Applied Mechanics, Vol. 39, pp. 1060-1066

Row, D.G., Hollings, J.P., Sause, R., Kiureghian, A.Der, (1987), "Design Criteria for offshore Arctic Pipeline", ASME, Petroleum Division (Publication), Pipeline Enginerring Symposium, P.D. Vol.6, pp.171-179

Row, D.G., Powell, G.H., and Morris, G.R., (1983a), "Local Buckling Analysis of Pipelines", Proceedings of the Second International Conference on Offshore

Mechanics and Arctic Engineering, pp. 496-503

Row, D.G., Powell, G.H. and Goodson, N.W. (1983b), "Finite Element Techniques for Pipelines Subjected to Extreme Loads", in Pipelines in Adverse Environments - II", Edited by Mark B. Pickell, pp. 474-485

Selvadurai, A.P.S. (1985), "Numerical Simulation of Soil-Pipeline Interaction in a Ground Subsidence Zone", in Advances in Underground Pipeline Engineering, Edited by Jey K. Jeyapalan, pp. 311-319

Selvadurai, A.P.S., Lee, J.J., Todeschini, R.A.A. and Somes, N.F. (1983), "Lateral Soil Resistance in Soil-Pipe Interaction", in Pipelines in Adverse Environments - II", Edited by Mark B. Pickell, pp. 259-278

Seide, P. and Weingarten, V.I. (1961), "On the Buckling of Circular Cylindrical Shells under Pure Bending", Journal of Applied Mechanics, Vol. 28, pp. 112-116

Selig, E.T. (1988), "Soil Parameters for Design of Buried Pipelines", in Pipeline Infrastructure, Edited by Bruce A. Bennett, pp. 99-116

Sherman, D.R. (1976), "Tests of Circular Steel Tubes in Bending", Journal of the Structural Division, ASCE, Vol. 102, No. ST11, pp. 2181-2195

Stegmuller, Hans (1984), "Non-linear Inelastic Structural Analysis (NISA) - The User Mannual", Institut Fur Banstatik, Univeritat Sttuttgart, Stuttgart, West Germany

Steir E., Gruttmann, F. and Lambertz, K.H. (1990), "Elastic-Plastic Analysis of Thin Shells and Folded Plate Structures with Finite Rotations", in Computational Mechanics of Nonlinear Response of Shells, eds. W.B. Kratzig and E. Onate, Springer-Verlag, Germany, pp. 57-82

Strang, G. (1988), "Linear Algebra and Its Applications", 3rd Edition, Harcourt Brace Jovanich, Publishers, San Diego

Structural Software Development, Inc. (1989), "PIPLIN-III, Computer Program for Stress and Deformation Analysis of Pipelines", 1930 Shattuck Avenue, Berkeley, California 94704, USA

Sultanov, K.S. and Kim, V.Y. (1986), "Experimental Investigations of the Thaw

Governing Longitudinal Interaction Between Elongated Underfround Structures and the Soil", Soviet Mining Science (english translation), Vol. 22, No. 1, pp.50-55

Tennyson, R.C. and Muggeridge, D.B. (1969), "Buckling of Axisymmetric Imperfect Circular Cylindrical Shell under Axial Compression", AIAA Journal, Vol. 7, No. 11, pp. 2127-2131

Wagner, D.A., Murff, J.D., Brennodden, H. and Sveggen, D. (1989), " Pipe-Soil Interaction Model", Journal of Waterway, Port, Coastal, and Ocean Engineering, Vol. 115, No. 2, March, pp. 205-220

Wempner, G.A. (1971), "Discrete Approximations Related to Nonlinear Theories of Solids", International Journal of Solids and Structures, Vol. 7, pp. 1581-1599

Williams, P.J. (1992), "Gas Pipelines and the Challenge of the Cold Regions : An Experimental Study", The International Conference on Pipeline Reliability, Calgary, Canada, June 2-5, pp. **II-2**-1 to **II-2**-12

Wilson, E.L., Ming-Wu, Y. and Dickens, J.M. (1982), "Dynamic Analysis by Direct Superposition of Ritz Vectors", Earthquake Engineering and Structural Dynamics, Vol. 10, pp. 813-821

Wolfe, M.A. (1978), "Numerical Methods for Unconstrained Optimization : An Introduction", Van Nostrand Reinhold, New York

Workman, G.H. (1986), "Structural Response of Buried Northern Gas Pipeline Due to Differential Thaw Settlement", Presented at 1986 International Gas Research Conference, Toronto, Canada, Sept. 8-11, pp. 307-316

Workman, G.H. (1981), "Pipe Wall Stability Analysis of 12.75 in O.D. and 0.25 in W.T. Grade 52 pipe", A Summary Report to CANUCK Engineering Ltd., Applied Mechanics Incorporated, 2121, McCoy Road, Columbus, Ohio, USA 43220

Yen, B.C., Tsao, C.H. and Hinkle, R.D. (1981), "Soil-Pipe Interaction of Heated Oil Pipelines", Transportation Engineering Journal of ASCE, Vol. 107, No. TE1, January, pp. 1-14